

Topics in Mining, Metallurgy and Materials Engineering
Series Editor: Carlos P. Bergmann

Mikhail Gasik
Viktor Dashevskii
Aitber Bizhanov

Ferroalloys

Theory and Practice

 Springer

Topics in Mining, Metallurgy and Materials Engineering

Series Editor

Carlos P. Bergmann, Federal University of Rio Grande do Sul, Porto Alegre,
Rio Grande do Sul, Brazil

“Topics in Mining, Metallurgy and Materials Engineering” welcomes manuscripts in these three main focus areas: Extractive Metallurgy/Mineral Technology; Manufacturing Processes, and Materials Science and Technology. Manuscripts should present scientific solutions for technological problems. The three focus areas have a vertically lined multidisciplinary, starting from mineral assets, their extraction and processing, their transformation into materials useful for the society, and their interaction with the environment.

More information about this series at <http://www.springer.com/series/11054>

Mikhail Gasik · Viktor Dashevskii ·
Aitber Bizhanov


Ferroalloys

Theory and Practice

 Springer

Mikhail Gasik
National Metallurgical Academy
of Ukraine
Dnipro, Ukraine

Viktor Dashevskii
Russian Academy of Sciences
Moscow, Russia

Aitber Bizhanov 
J.C. Steele & Sons Inc
Moscow, Russia

ISSN 2364-3293 ISSN 2364-3307 (electronic)
Topics in Mining, Metallurgy and Materials Engineering
ISBN 978-3-030-57501-4 ISBN 978-3-030-57502-1 (eBook)
<https://doi.org/10.1007/978-3-030-57502-1>

© Springer Nature Switzerland AG 2020

This work is subject to copyright. All rights are reserved by the Publisher, whether the whole or part of the material is concerned, specifically the rights of translation, reprinting, reuse of illustrations, recitation, broadcasting, reproduction on microfilms or in any other physical way, and transmission or information storage and retrieval, electronic adaptation, computer software, or by similar or dissimilar methodology now known or hereafter developed.

The use of general descriptive names, registered names, trademarks, service marks, etc. in this publication does not imply, even in the absence of a specific statement, that such names are exempt from the relevant protective laws and regulations and therefore free for general use.

The publisher, the authors and the editors are safe to assume that the advice and information in this book are believed to be true and accurate at the date of publication. Neither the publisher nor the authors or the editors give a warranty, expressed or implied, with respect to the material contained herein or for any errors or omissions that may have been made. The publisher remains neutral with regard to jurisdictional claims in published maps and institutional affiliations.

This Springer imprint is published by the registered company Springer Nature Switzerland AG
The registered company address is: Gewerbestrasse 11, 6330 Cham, Switzerland

The book is dedicated to our fellow metallurgists victims of the coronavirus pandemic.

Preface

The final stage of the preparation of the manuscript of this book took place in unusual conditions. The COVID-19 pandemic caused by SARS-CoV-2 has hit the world and has already claimed the lives of many, many people around the world and significantly changed our normal lifestyle, filling it with alarming expectations. Although there are a lot of frightening details in the news, there is good news about the progress in finding and creating a vaccine against this dangerous disease. Leading medical research centers and clinics have already begun testing its various modifications.

Such a meaningful and targeted search, based on deep scientific ideas and on the analysis of previous experience, is akin to the approach of ferroalloy scientists to the search for effective ways to give steel the required properties using special alloys—ferroalloys.

In time immemorial, the search for ways to give special properties to steel was based on trial and error. Man learned to use alloying elements to improve the quality of steel and iron products long before he learned about the existence of such elements—even before the beginning of the Iron Age, meteorite iron containing up to 8.5% nickel was used.

Well known are futile attempts by alchemists to find a *philosopher's stone* (lat. *Lapis philosophorum*, aka *masters*, *Rebis*, *elixir of philosophers*, *life elixir*, *red tincture*, *great elixir*, *fifth element*)—a certain reagent necessary for the successful conversion (transmutation) of metals into gold as well as to create the elixir of life.

The first attempts to make conscious use of the properties of alloying elements date back to the Middle Ages, and this happened in the East, famous for its high-quality steel. Held in the 20th century chemical analysis of the steel from which the Japanese weapons of the 11th–13th centuries were made showed the presence of molybdenum in its composition. Today, it is well known that molybdenum alloy steel has high hardness, strength and toughness.

The need to maintain social distancing, unfortunately, did not allow the authors of the book to discuss the contents of this preface in a personal meeting.

I allow myself to take advantage of this circumstance and express my overwhelming surprise to the fact that I have the honor to be a co-author of Profs. Mikhail Gasik and Viktor Dashevskii, from whose books I studied metallurgy and comprehended the basics of the theory of ferroalloy processes. The book is based on the revised and supplemented content of numerous scientific works and textbooks by Mikhail Gasik and Viktor Dashevskii, published many times in the USSR, and then in Russia and Ukraine. Scientific works of Profs. Mikhail Gasik and Viktor Dashevskii formed the basis of almost all projects implemented in the USSR, Russia and Ukraine to create and improve the production of ferroalloys. A chapter has been added devoted to modern methods of preparing raw materials for smelting ferroalloys, in particular, the agglomeration of natural and anthropogenic raw materials in the ferroalloy industry. In particular, attention is paid to the stiff vacuum extrusion technology, which is gaining popularity in briquetting and is based on the scientific results I obtained. The environmental aspects of ferroalloy production are considered.

The content of the book largely fills the gap that exists in the international literature and is associated with insufficient coverage of the contribution of Soviet and Russian scientists to the development of ferroalloy science and technology.

In the sections devoted to fundamental scientific ideas and classical results, there are, with rare exceptions, literary references. In compensation, we provide a recommended list of references. For methodological purposes, we also give examples of calculating fees for the smelting of some ferroalloys, which makes the book interesting for students and graduate students studying metallurgy as well. Metallurgists and ferroalloy engineers will find many useful and important things in the book. Considerable attention is paid to improving the preparation of raw materials for smelting ferroalloys, methods of utilization of waste products and by-products, and environmental issues.

On behalf of my co-authors, I express my gratitude to Prof. Vladimir Zhuchkov (Institute of Metallurgy, Ural Branch of Russian Academy of Sciences) for help in preparing sections related to sintering and pelletizing of manganese ore fines and concentrates.

The authors are especially grateful to the publisher for the goodwill and opportunity to publish this book and the effort to publish it.

Moscow, Russia

Dr. Aitber Bizhanov

Introduction

“Take a new earthen pot, put in it a pound of red copper with half a bottle of Nitric Acid. Boil it for half an hour. Afterwards add three ounces of verdegris (Copper Carbonate), and boil for one hour. Then add two and a half ounces of arsenic, and boil one hour. Add three ounces of oak bark, well pulverized, and let it boil a half hour, add a 64 fluid ounces of rose water boil twelve minutes, then add three ounces of lampblack, and let it boil until the composition is good. To see whether it is cooked enough, dip a nail in it; if it adheres, remove it. It will produce a pound and a half of good gold. If it does not adhere, it is proof that it has not cooked enough; the liquor can serve four times.”

The recipe for a philosopher’s stone. The Great Grimoire. Chapter “Secrets of magic art”

Despite the rapid development of science and technology, all kinds of fashionable definitions of the modern era (*scientific progress, information technology, artificial intelligence*, etc.), humanity still lives in the Iron Age, because the role that iron, and especially its alloy with carbon—steel, plays in the life of modern society is incomparable with any other building and structural material.

Ferrous alloys, in a figurative comparison, are steelmaking *salt* and *pepper*. The use of ferrous alloys as enriching additives for the purpose of deoxidation and alloying improves the physical and mechanical properties and functional characteristics of metal products. Not a ton of steel is smelted without the use of ferrous alloys. The specific and branded assortment of ferrous alloys is extensive. As a rule, separately or in combination, the composition of ferrous alloys includes 20–25 elements of the Periodic system of elements, which differ significantly in physicochemical properties and affect the properties of steel and alloys in different ways.

Ferrous alloys are mainly used in the smelting of steel and cast iron. Some types of ferrous alloys are used in non-ferrous metallurgy, chemical industry, etc. Ferrous alloy production is an integral part of the mining and metallurgical complex, since the essence and main task of the ferrous alloy industry are the primary extraction (recovery) of metals from natural mineral formations mined from the bowels. Ores include nonmetallic minerals, gangue. Therefore, the ore is subjected to enrichment

in one or sequentially in several ways (gravitational, magnetic, electric, flotation, less often—chemical) to obtain concentrates in which the content of the leading metal is significantly higher in comparison with the original ore. The use of concentrates rather than the initial ore allows one to obtain ferroalloys with a high content of the leading (ferroalloy) element, with a lower content of impurity elements (phosphorus, sulfur, non-ferrous metals) and, which should be especially noted, significantly reduce the specific energy consumption.

Historically, the beginning of industrial production and use of ferroalloys date back to the end of the nineteenth century, when melting of carbon ferromanganese and low-grade ferrosilicon in blast furnaces was developed. Ferroalloys with leading metals having a greater chemical affinity for oxygen than iron, as well as ferroalloys with a low carbon content, cannot be obtained by a blast furnace method. The production of ferroalloys of the entire assortment of hardly reducible elements and with low carbon content was successfully mastered in the twentieth century in electric arc furnaces.

The consumption of ferroalloys and, consequently, their production directly depend on the amount of steel smelted. This general position can be somewhat clarified by the specific consumption of ferroalloys per ton of steel in the direction of its decrease in connection with the diversification of methods of steel smelting of various groups and grades, increasing continuous casting, the development of innovative technologies.

In 2013, according to World Steel Association, 1.622 billion tons of steel was produced in the world, of which 779 million tons (48%) in China. According to most forecasts, in 2014 steel production was set at 1.662 billion tons, in 2015 it amounted to 1.635 billion tons, and by 2020, global steel production will increase to 1.814 billion tons (794 million tons will come from China). By 2020, the smelting of alloyed and special, especially corrosion-resistant steels will increase even more significantly. For example, if in 2013, 19 million tons of corrosion-resistant steel was smelted in China (out of 36 million tons of world production), then by 2015 this figure was already 23 million tons (21% more), and by 2020—27.7 million tons (an increase of 8.7 million tons, or 46%, compared with the 2013 figure).

Today, per ton of steel, on average, about 20 kg of various ferroalloys is consumed, of which amount is: ferrochromium of the order of 20%; ferrosilicon—18%, silicomanganese—22%; high-carbon ferromanganese—12%; refined manganese alloys and metallic manganese—5%; ferronickel—4%; and all others—19% in total. At the same time, the smelting of 170 million tons of special steels (20% of world production) required 35% of all consumed ferroalloys, while the melting of 1440 million tons of ordinary grades (respectively 80% of world production) required 65% of all consumed ferroalloys.

The expansion of the assortment of ferroalloy production in relation to meeting the needs of the steel industry is primarily associated with the smelting of ferroalloys of the small tonnage group—alloys of nickel, titanium, niobium, molybdenum, vanadium and ferrovandium, ferrotungsten, etc.

The main producers of niobium alloys are Brazil (about 90% of world production) and Canada. World production and consumption of ferroniobium in 2013 amounted to about 80 thousand tons. In 2014, the increase in ferroniobium smelting was estimated at 83 thousand tons, and over the past five years, the increase has been approximately 4.9% annually.

About 80 thousand tons of tungsten-containing products is sold on the world market (data from 2017), of which about 20% of the ferrotungsten itself falls, i.e., about 16 thousand tons. The largest producers and exporters of ferrotungsten are countries such as China (2.8 thousand tons), Vietnam (2.2 thousand tons), Sweden (0.5 thousand tons). The tungsten content in it is usually 75–85% (in a Swedish-made alloy—more than 90%), and the alloy is supplied in the form of pieces of 80–100 mm, briquettes (40 mm) and pellets (3–10 mm). Tungsten is used for smelting mainly tool steels, including high-speed steels and high-strength carbon steels for various purposes. Along with tungsten, the branded range of these steels also includes molybdenum and chromium. In general, metallurgy absorbs almost 95% of all mined tungsten. World tungsten production is 85–87 thousand tons.

The need for nickel for the smelting of special, primarily corrosion-resistant steels is met mainly by electrolytic nickel produced at non-ferrous metallurgy enterprises. One of the largest producers of ferronickel is Indonesia, where the total ferronickel smelting capacity in Indonesia exceeded 140 thousand tons per year.

World production and consumption of vanadium in the form of ferrovanadium are 86 thousand tons (2013 data). A continuous increase in the production volume of this alloy is noted: It is predicted that by 2020 this figure will increase to 140 thousand tons. The main producers of ferrovanadium (by countries and regions) are: China—49.7% of world production, South Africa—13.9%, Russia—7.8%, Europe—6.7%, North America—4.5%. Forty-six percentage of vanadium produced in the world is consumed in China, 17% in Europe, 13% in North America, 7% in Japan, 6% in the CIS, 3% in India and 8% in other countries. Almost 72% of ferrovanadium is produced from vanadium slag in the world, 19% from primary ore and 9% from secondary vanadium-containing raw materials.

The desire to comply with the high rates of industrialization and growing consumption of steel was not feasible without the significant development of ferroalloy science and technology, which, in turn, is impossible without knowledge of the fundamental principles of the theory of ferroalloy processes.

The book outlines the physical and chemical foundations of high-temperature processes for producing silicon, manganese and chromium ferroalloys, alloys of molybdenum, vanadium, titanium, alkaline earth and rare earth metals, niobium, zirconium, aluminum, boron, nickel, cobalt, phosphorus, selenium and tellurium, iron–carbon alloys by carbon, silicone and aluminothermic methods. The industrial production technologies of these groups of ferroalloys, the characteristics of charge materials and the technological parameters of the melting processes are considered. A description of ferroalloy furnaces is given. Waste recycling, fine agglomeration technologies and environmental issues are considered.

Contents

1	Physicochemical Fundamentals of Ferroalloy Processes	1
1.1	Thermochemistry of Ferroalloy Processes	1
1.2	Thermodynamics of Oxide Formation Reactions	4
1.3	Thermodynamics of Carbide Formation Reactions	11
1.4	Thermokinetics of Ferroalloy Processes	13
1.5	Gibbs Phase Rule	14
2	Phase Equilibria in Metal and Oxide Ferroalloy Systems	15
2.1	General Characteristic of <i>X-T</i> State Diagrams of Systems	15
2.2	Binary Equilibrium Phase Diagrams	16
2.3	Ternary Equilibrium Phase Diagrams	20
	Reference	23
3	Classification of Ferroalloy Processes	25
3.1	Classification of Metals—Leading Ferroalloy Elements	25
3.2	General Requirements for the Quality of Ferroalloys	28
3.3	Classification of Ferroalloy Processes by the Type of Used Reducing Agents	28
3.4	Classification of Ferroalloy Processes by Type of Aggregate	30
3.5	Classification of Ferroalloy Processes by Technological Features	31
4	Metallurgy of Silicon and Silicon Carbide	35
4.1	Properties of Silicon and Its Compounds	35
4.2	Theoretical Foundations of Silicon Reduction by Carbon	42
4.3	The Assortment of Crystalline Silicon and Quality of Raw Charge Materials	43
4.4	The Technology of Crystalline Silicon Smelting	46
4.5	The Technology of Silicon Carbide Production	52
	References	55

5	Metallurgy of Ferrosilicon	57
5.1	Assortment, Microstructure and Properties of Ferrosilicon	57
5.2	Geometric Parameters of Bath and Electrical Characteristics of Electric Furnaces for Ferrosilicon Smelting	64
5.3	The Technology of Ferrosilicon Smelting and Casting	74
	References	92
6	Metallurgy of Manganese Ferroalloys	93
6.1	Properties of Manganese and Its Compounds	93
6.2	Manganese Minerals, Ores and Concentrates	104
6.3	The Technology for High-Carbon Ferromanganese Smelting	105
6.4	The Technology of Ferrosiliconmanganese Smelting	113
6.5	The Technology of Smelting of Metallic Manganese, Low- and Medium-Carbon Ferromanganese	116
6.6	The Technology of Nitrided Manganese and Silicomanganese	123
	References	124
7	Metallurgy of Chromium Ferroalloys	125
7.1	Properties of Chromium and Its Compounds	125
7.2	Chromium Minerals and Ores	132
7.3	The Technology of Obtaining High-Carbon Ferrochromium	134
7.4	The Technology of Obtaining Ferrosilicochromium	137
7.5	The Technology of Obtaining Low-Carbon Ferrochromium	139
7.6	Vacuum Processes of Decarburization and Degassing of Ferrochromium	150
7.7	Oxygen-Converter and Silicothermic Methods of Obtaining Medium-Carbon Ferrochromium	151
7.8	Aluminothermic Method for Producing Metallic Chromium and Ferrochromium	153
7.9	The Technology of Producing Nitrided Ferrochromium	158
8	Metallurgy of Ferrotungsten	161
8.1	Properties of Tungsten and Its Compounds	161
8.2	Tungsten Minerals, Ores and Concentrates	164
8.3	The Technology of Obtaining of Ferrotungsten by Carbon-Silicothermic Method	165
8.4	The Technology of Ferrotungsten Production by Aluminothermic Method	170
9	Metallurgy of Ferromolybdenum	171
9.1	Properties of Molybdenum and Its Compounds	171
9.2	Molybdenum Minerals, Ores and Concentrates	176

9.3	Oxidative Firing of Molybdenum Concentrate	176
9.4	The Technology of Producing Ferromolybdenum by an Out-of-Furnace Silicoaluminothermic Method	177
10	Metallurgy of Ferrovanadium	183
10.1	Properties of Vanadium and Its Compounds	183
10.2	Vanadium Minerals, Ores and Concentrates	187
10.3	Technology of Metallurgical Processing of Vanadium-Containing Concentrates	189
10.4	The Technology of Chemical Processing of Vanadium-Containing Slag	191
10.5	Thermodynamics of Vanadium Reduction from Oxides	194
10.6	The Technology of Producing Ferrovanadium by Silicoaluminothermic Method	195
10.7	The Technology for Production of Ferrovanadium by the Aluminothermic Method	197
10.8	Ferrosilicovanadium Production Technology	198
10.9	The Technology of Production of Nitrided Ferrovanadium	199
11	Metallurgy of Ferrotitanium	201
11.1	Properties of Titanium and Its Compounds	202
11.2	Titanium Minerals, Ores and Concentrates	207
11.3	Thermodynamics of Titanium Oxides Reduction	208
11.4	Oxidative Firing of Titanium Concentrates	210
11.5	The Technology of Ferrotitanium Production by Aluminothermic Method	210
11.6	The Technology of Producing Metallic Titanium with Magnesium-Thermic Reduction	214
12	Alkaline Earth Metal Ferroalloys	219
12.1	Calcium Carbide and Silicocalcium	219
12.1.1	Properties of Calcium and Its Compounds	220
12.1.2	Calcium Carbide Smelting Technology	223
12.1.3	Silicocalcium Smelting Technology	227
12.2	Ferrosilicobarium and Aluminobarium	231
12.2.1	Properties of Barium and Its Compounds	231
12.2.2	Ferrosilicobarium Smelting Technology	236
12.2.3	Aluminobarium Smelting Technology	238
12.3	Ferrosilicostrontium	238
12.3.1	Properties of Strontium and Its Compounds	239
12.3.2	Minerals and Ores of Strontium	242
12.3.3	Ferrosilicostrontium Smelting Technology	243

12.4	Ferrosilicon Magnesium	243
12.4.1	Properties of Magnesium and Its Compounds.	244
12.4.2	Minerals and Ores of Magnesium	245
12.4.3	Technology for Producing Magnesium and Magnesium Ferroalloys	246
12.5	Beryllium	248
12.5.1	Properties of Beryllium and Its Compounds	248
12.5.2	Beryllium Minerals and Ores	249
12.5.3	Beryllium Production Technology	249
13	Metallurgy of Ferroniobium	251
13.1	Properties of Niobium and Its Compounds	251
13.2	Niobium Minerals and Ores.	256
13.3	Thermodynamics of Niobium Reduction Reactions	257
13.4	The Technology for Producing Ferroniobium by Aluminothermic Method.	258
	Reference	261
14	Ferrosilicozirconium and Ferro-Alumino-Zirconium	263
14.1	Properties of Zirconium and Its Compounds	263
14.2	Zirconium Minerals, Ores and Concentrates	266
14.3	Thermodynamics of Zirconium Reduction Reactions.	269
14.4	The Technology for Producing Ferrosilicozirconium by Aluminothermic Method.	269
14.5	The Technology for Producing Ferro-Alumino-Zirconium by Aluminothermic Method.	272
15	Ferroaluminum and Silicoaluminum	275
15.1	Properties of Aluminum and Its Compounds	275
15.2	Aluminum Minerals and Ores	280
15.3	Ferroaluminum Production Technology	280
15.4	Silicoaluminum Production Technology	281
16	Ferroboron and Boron Carbide	285
16.1	Properties of Boron and Its Compounds	285
16.2	Boron Minerals and Ores	287
16.3	Thermodynamics of Boron Reduction Reactions.	289
16.4	The Technology of Ferroboron Production	290
16.5	The Technology of Boron Carbide Production	292
17	Ferroalloys with Rare-Earth Metals	297
17.1	Properties of Rare-Earth Metals and Their Compounds	297
17.2	Minerals, Ores and Concentrates of Rare-Earth Metals	300
17.3	The Technology for Producing Ferroalloys with Rare-Earth Metals	304

18	Iron–Carbon Alloys	307
18.1	Properties of Iron and Its Compounds	307
18.2	Reduction of Iron by Carbon and Gases	310
18.3	Cast Iron Electrothermics	312
19	Metallurgy of Ferronickel	317
19.1	Properties of Nickel and Its Compounds	317
19.2	Nickel Minerals and Ores	321
19.3	The Technology of Production and Refining Ferronickel	324
20	Metallurgy of Cobalt	329
20.1	Properties of Cobalt and Its Compounds	329
20.2	Cobalt Minerals and Ores	333
20.3	The Technology of Cobalt Production	334
21	Metallurgy of Ferrophosphorus	339
21.1	Properties of Phosphorus and Its Compounds	339
21.2	Minerals and Ores of Phosphorus	342
21.3	Thermodynamics of Phosphorus Reduction Reactions	343
21.4	Preparation of Phosphorites for Electrofusion	344
21.5	Electric Furnaces for Phosphorus Reduction	345
21.6	Phosphorus Electrothermics	346
22	Ferroselenium and Ferrotellurium	349
22.1	Properties of Selenium, Tellurium and Their Compounds	349
22.2	Selenium and Tellurium Ores	351
22.3	Alloying Steel with Selenium and Tellurium	352
23	Metallurgy of Electrocorundum	355
23.1	Corundum Properties	355
23.2	Electrocorundum Technology	356
23.3	Normal Corundum Technology	357
24	Electrofused Fluxes	363
24.1	Requirements for Fluxes and Methods for Their Preparation	363
24.2	Flux Electrofusion	365
24.3	Impurities Behavior in Flux Electrofusion	366
25	Preparation of Charge Materials for Ferroalloys Smelting	369
25.1	Drying Manganese Concentrates	369
25.2	Sinter Production	370
25.2.1	Manganese Ore Sintering	370
25.2.2	Chromium Ore Sintering	383
25.3	Pelletizing	385
25.3.1	Cold Bonded Pellets (CBP)	392
25.4	Briquetting	397
25.4.1	Basic Industrial Technologies of Briquetting in Ferrous Metallurgy	397

25.4.2	Metallurgical Properties of Brex on the Basis of Manganese Ore Concentrate	415
25.4.3	Metallurgical Properties of Brex Based on Manganese Ore Concentrate and Baghouse Dusts of Silicomanganese Production	417
25.4.4	Full-Scale Testing of Silicomanganese Smelting with Brex in the Charge of Submerged EAF	425
25.4.5	Metallurgical Properties of Briquettes Based on Chromium-Containing Materials	430
25.5	Charge Preheating	438
25.6	Charge Prereduction	441
25.7	Firing Carbonate Manganese Concentrates	444
25.8	Wastes and by-Products Processing	448
	References	452
26	Ferrous Furnaces	457
26.1	Electric Ore-Smelting Furnaces	459
26.2	Refining Electric Furnaces	469
27	Self-baking Electrodes	477
27.1	Self-baking Electrodes Design	477
27.2	Electrode Mass	478
27.3	Electrode Mass Production Technology	483
27.4	The Processes Occurring During Firing of the Electrode Mass	484
28	Ferrous Dispersion (Atomizing)	489
29	Environmental Protection in Ferrous Industry	493
29.1	Basic Principles	493
29.2	Characterization of Harmful Emissions in Ferrous Production	494
	References	497
Appendix A: Calculation of the Charge for Smelting High-Carbon Ferrous by Flux Method		499
Appendix B: Calculation of the Charge for Smelting Ferrosilicomanganese		509
Appendix C: The Charge Calculation for Smelting High-Carbon Ferrochromium		519
Recommended Bibliography		527

About the Authors

Mikhail Gasik was born on June 30, 1929. He is Doctor of Technical Sciences (1969) and holds positions as Professor (1971), Academician of the National Academy of Sciences of Ukraine (1990), Honored Foreign Member of the Russian Academy of Sciences (2004), Foreign Member of the Georgian Academy of Sciences (2005) and Honorary Member of the Academy of Sciences of the Republic of Kazakhstan (2006). He has been awarded numerous prizes such as Laureate of the State Prize of the Ukrainian SSR (1977), Prize of the Council of Ministers of the USSR (1990), E.O. Paton Prize of the National Academy of Sciences of Ukraine (1995), State Prizes of Ukraine (1998, 2004), and Prizes named after Yaroslav the Wise of the Academy of Sciences of the Higher School of Ukraine (2002) and Prizes named after Z. I. Nekrasov National Academy of Sciences of Ukraine (2006). The main areas of scientific and scientific–pedagogical activity are as follows: fundamental studies of the problems of physical chemistry of high-temperature interaction processes in metal and oxide systems based on manganese, silicon, chromium, aluminum. He has published number of scientific papers—over 420, including 21 scientific monographs and 5 textbooks for universities.

Viktor Dashevskii was born on October 13, 1933. He is Doctor of Technical Sciences and holds positions as Professor of the National Research University “Moscow Institute of Steel and Alloys,” Head of the Laboratory of the Institute of Metallurgy and Material Sciences named after A. A. Baykov, Russian Academy of Sciences, Council of Ministers of the USSR Prize Winner, Russian Government Prize Winner, I. P. Bardin Prize of Russian Academy of Sciences Winner. He is a well-known specialist in physical chemistry of the metallurgical and oxide smelts, theory and practice of the ferroalloy electrothermal production. He is Author of a big amount of pioneer’s scientific researches. Scientific Society estimated highly contribution of him into the metallurgical science—he had been chosen as Member–Correspondent of Russian Academy of Natural Sciences and Acting Member of the New York Academy of Sciences (USA). He has been included in Marquis Who’s Who in 1999.

Aitber Bizhanov was born on October 6, 1956. He has a Ph.D. degree in the agglomeration of natural and anthropogenic materials in metallurgy. He graduated from Moscow Physical Technical Institute in 1979, background—applied mathematics. Since 1981 to 1992, he was Researcher in the Institute for High Temperatures of Russian Academy of Sciences. Since 1992, he is being involved in activities related to recycling of metallurgical wastes. He is Author of more than 70 publications including four books (two of them published by Springer) and is owner and Co-author of 15 Russian patents in the field. He is Author and owner of the “BREX” trademark. With his personal participation, projects of briquetting of natural and anthropogenic raw materials of ferrous metallurgy were successfully implemented in a number of countries. He is Member of Institute for Briquetting and Agglomeration (IBA) since 2011. He has been included in Marquis Who’s Who on September 19, 2019.

Chapter 1

Physicochemical Fundamentals of Ferroalloy Processes



1.1 Thermochemistry of Ferroalloy Processes

Ferroalloy processes are based on the laws of physical chemistry, and more specifically, on the laws of chemical thermodynamics (thermochemistry) and chemical kinetics (thermokinetics). The laws of chemical thermodynamics with the help of a mathematical apparatus allow us to solve problems and get answers to questions: can this or that reaction proceed at specific given process parameters (temperature T and pressure P) and, if so, in which direction it will go. Thus, the laws of chemical thermodynamics determine the possibility and direction of a chemical reaction at given process parameters. The laws of chemical kinetics make it possible to estimate, according to well-known analytical dependencies, the time during which a given reaction can change from a non-equilibrium to an equilibrium state when the process parameters (T , P) change.

Thermochemistry is a section of chemical thermodynamics as applied to high-temperature chemical (metallurgical) processes. The possibility and direction of reactions in thermochemical processes is determined by a thermodynamic quantity—a change in Gibbs energy (ΔG_{298}°):

for standard state ($T = 298\text{ K}$, $P = 101.3\text{ kPa}$) function ΔG_{298}° has the form of a straight line

$$y = b - kx;$$

$\Delta G_{298}^{\circ} = \Delta H_{298}^{\circ} - T \Delta S_{298}^{\circ}$, where ΔH_{298}° —enthalpy change, a ΔS_{298}° —change in the entropy of the reaction.

The values included in this formula have the following dimension: ΔG_{298}° —J/mol; ΔH_{298}° —J/mol; ΔS_{298}° —J/(mol K); T —K.

The ferroalloy process with the participation of multicomponent charge materials can be reduced to a single reaction that determines the purpose and task of the process and can be written as follows:



The equilibrium constant (K_P) of the reaction, which is a mathematical expression of the *law of acting masses*, has the form:

$$K_P = \frac{a_C^c \cdot a_D^d}{a_A^a \cdot a_B^b} = \frac{x_C^c f_C^c \cdot x_D^d f_D^d}{x_A^a f_A^a \cdot x_B^b f_B^b},$$

where a is the activity of the components involved in the reaction; x is the mole fraction of the corresponding component; f are the activity coefficients of these components.

At temperatures of ferroalloy processes, the possibility and direction of reactions are evaluated by

$$\Delta G_T^0 = \Delta H_T^0 - \Delta S \cdot T.$$

An analytical study of the function $\Delta G_T^0(T)$ indicates that ΔG_T^0 can take three values:

(1) $\Delta G_T^0 < 0$; (2) $\Delta G_T^0 > 0$; (3) $\Delta G_T^0 = 0$. In physical chemistry, it is accepted that if $\Delta G_T^0 < 0$, the reaction for the given conditions (T, P) proceeds in the forward direction (i.e., toward the formation of reaction products); if $\Delta G_T^0 > 0$, the reaction, if it was in equilibrium, with a change in T, P should shift toward the original components and, if $\Delta G_T^0 = 0$, the reaction is in equilibrium. In the educational, and sometimes in the scientific literature, very often the conditions $\Delta G_T^0 > 0$ are not interpreted quite correctly. It is indicated that under this condition, the initial components of the reaction will not interact. It should be borne in mind that at $\Delta G_T^0 > 0$ and certain parameters (T, P), the reaction can proceed; however, the yield of reaction products will not be complete; if the reaction was in equilibrium, and the conditions changed so that the ΔG_T^0 value became greater than zero, then the reaction will shift toward the starting components and the yield of reaction products will decrease.

In the theory of metallurgical (ferroalloy) processes, the temperature corresponding to the condition $\Delta G_T^0 = 0$ is taken as the temperature of the onset of a chemical reaction, although, as indicated above, the reaction under the condition $\Delta G_T^0 > 0$ can proceed, but with a lower yield of products than under the condition $\Delta G_T^0 < 0$. Since ΔG_T^0 and the equilibrium constant of the reaction K_P are interconnected by the relation:

$$\Delta G_T^0 = -RT \ln K_P,$$

The conditions $\Delta G_T^0 < 0$ correspond to $K_P > 1$; $\Delta G_T^0 > 0$, $K_P < 1$ and $\Delta G_T^0 = 0$ at $K_P = 1$.

For most individual substances and chemical reactions occurring in ferroalloy processes, thermodynamic functions are given for standard conditions. Under real conditions, these processes occur at high and very high temperatures. With a complete

description of the thermodynamics of the reactions, $\Delta G_T^\circ(T)$ is calculated for any given high temperature. To do this, precalculate

$\Delta H_T^\circ(T)$ and $\Delta S_T^\circ(T)$:

$$\Delta H_T^\circ(T) = \Delta H_{298}^\circ + \int_{298}^T \Delta C_p dT,$$

$$\Delta S_T^\circ(T) = \Delta S_{298}^\circ + \int_{298}^T \frac{\Delta C_p}{T} dT.$$

Many components involved in the reactions of ferroalloy processes undergo phase transformations, accompanied by a change in their crystal chemical structures and state of aggregation. These transformations are associated with a change in energy in reacting systems, which should be taken into account in more accurate thermodynamic calculations of $\Delta H_T^\circ(T)$ and $\Delta S_T^\circ(T)$ according to the formulas below:

$$\Delta H_T^\circ = \Delta H_{298}^\circ + \int_{298}^{T_c} \Delta C_{p1} dT + \Delta H_c + \int_{T_c}^{T_m} \Delta C_{p2} + \lambda_m + \int_{T_m}^T \Delta C_{p3} dT,$$

$$\Delta S_T^\circ = \Delta S_{298}^\circ + \int_{298}^{T_c} \frac{\Delta C_{p1}}{T_c} dT + \frac{\Delta H_c}{T_c} + \int_{T_c}^{T_m} \frac{\Delta C_{p2}}{T_m} + \frac{\lambda_m}{T_m} + \int_{T_m}^{T_i} \frac{C_{p3}}{T_i} dT,$$

where ΔC_p —change in heat capacity of substances, J/(mol K); ΔH_c and λ_m —enthalpy of conversion of components and heat of fusion of substances, respectively. The possibility and direction of the reaction can be estimated by the value of the equilibrium constant. The condition $K_p = 1$ corresponds to the equilibrium of the reaction, $K_p > 1$ —the reaction proceeds toward the formation of reaction products and $K_p < 1$ —the yield of reaction products decreases.

Since $\Delta G_T^\circ = -RT \ln K_p = \Delta H_T^\circ - \Delta S_T^\circ T$, then $\ln K_p = -\Delta H_T^\circ/RT + \Delta S_T^\circ/RT$; denoting $-\Delta H_T^\circ/R = -A$ and $\Delta S_T^\circ/R = B$, we obtain the dependence $K_p(T)$ (Arrhenius formula):

$$\ln K_p = -A/T + B.$$

Thus, the equilibrium constant of the reaction depends on temperature (at constant pressure) and does not depend on the activity (concentration) of the components involved in the reaction. If there are condensed and gaseous components in the system, the equilibrium constant is a function of temperature and pressure.

In ferroalloy processes, reactions can be endothermic (carbothermic processes involving solid carbon) and exothermic (metallothermic processes). In some cases, it is important to evaluate the effect of temperature (pressure) on the direction of the reaction. External impact can be estimated using Le Chatelier's theorem (principle): "When any system at equilibrium for a long period of time is subjected to a change in concentration, temperature, volume, or pressure, (1) the system changes to a new equilibrium, and (2) this change partly counteracts the applied change".

According to the van't Hoff equation, the equilibrium constant is associated with a change in the reaction enthalpy of isobar

$$\Delta H_T^0 = RT^2(d \ln K_P/dT).$$

A quantitative expression of Le Chatelier's theorem is given by the Clausius–Clapeyron equation

$$dP/dT = Q/T \Delta V,$$

where dP/dT —pressure change with temperature T ; Q —heat absorbed or released by a gram of substance; ΔV is the change in the specific volume accompanying the reaction.

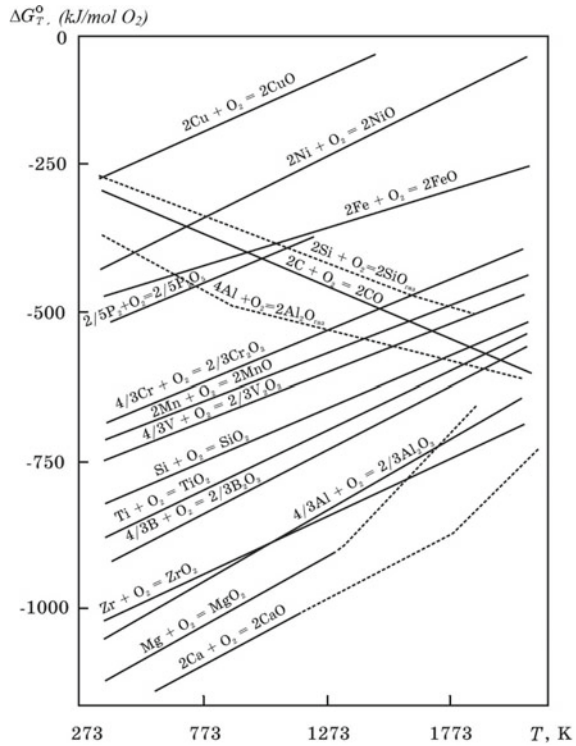
1.2 Thermodynamics of Oxide Formation Reactions

Ferroalloys are produced using oxygen compounds of ferroalloy elements as charge materials, i.e., ores and concentrates in which elements (metals) are contained in the form of oxides (oxide minerals). Upon receipt of a molybdenum sulfide concentrate at the ferroalloy plant, it must be preliminarily subjected to oxidative firing to convert molybdenum sulfide (MoS_2) to the oxides MoO_2 and MoO_3 . Carbonate types of raw materials (limestone, manganocalcite manganese concentrates) are also fired. During smelting of silicocalcium, a charge containing CaCO_3 or lime (CaO), which is obtained by preliminary firing of limestone, is loaded into an electric furnace. Therefore, in the thermodynamic analysis of the reduction reactions occurring in the baths of ferroalloy electric furnaces, the reactions of the interaction of *oxides* with a reducing agent (carbon, silicon or aluminum) are considered.

Using the tabular standard values of the thermodynamic constants of substances (heats of chemical reactions of the formation of compounds (oxides) from components ΔH_T^0 , heats of phase transitions of elements and chemical compounds ΔH_c , entropy of elements and chemical compounds S_{298}^0 , change in entropy during phase transitions and chemical reactions), one can obtain $\Delta G_T^0(T)$ dependence for the reactions of the interaction of elements with molecular oxygen for a wide temperature range.

Since the function $\Delta G_T^0 = \Delta H_T^0 - \Delta S_T^0 T$ has the form of a straight line (equation $y = b - kx$), kinks are observed at the points of phase transitions of the function

Fig. 1.1 Diagram of the chemical affinity of elements for oxygen



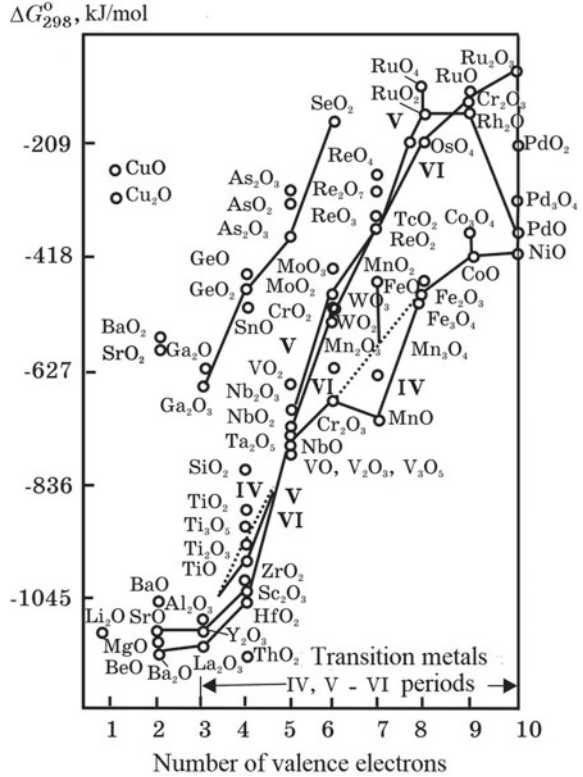
$\Delta G_T^0(T)$. The dependence $\Delta G_T^0(T)$ has the form of a broken line, which is shown for some reactions in a diagram called a diagram of the chemical affinity of elements for oxygen (Fig. 1.1).

The physicochemical interpretation of the graphical representation of the $\Delta G_T^0(T)$ function for reactions in *element—oxygen* systems allows us to note several fundamental conclusions. With an increase in the number of valence electrons of an isolated atom of an element, the thermodynamic strength of the oxide decreases (Fig. 1.2).

The smaller the ΔG_T^0 ($\Delta G_T^0 < 0$), the greater the chemical affinity of the element for oxygen; conditions $\Delta G_T^0 = 0$ —mean the equilibrium of the reaction of interaction of a different element with oxygen, and for $\Delta G_T^0 > 0$ —thermal dissociation of the oxide.

1. An analysis of the position on the $\Delta G_T^0(T)$ line diagram indicates that all elements have different chemical affinities for oxygen. To increase the thermodynamic strength of the formed oxides, the elements are arranged in a row (at 1600 °C): Cu, Ni, Co, W, Mo, Fe, P, Cr, Mn, V, Nb, Si, Ti, B, Al, Zr, Mg, Ca. A kink on the straight lines $\Delta G_T^0(T)$ takes place at phase transition temperatures.
2. The chemical affinity of elements to oxygen decreases with increasing temperature, i.e., the higher the temperature, the lower the thermodynamic strength of the oxides.

Fig. 1.2 Dependence of the thermodynamic strength of element oxides on the number of valence electrons of an isolated atom of an element



- The chemical affinity of carbon to oxygen by the reaction $2C + O_2 = 2CO$ with the formation of gaseous oxide of CO increases with increasing temperature, but not decreases, as is typical for most other elements. When solid carbon interacts with molecular oxygen to form CO_2 , the thermodynamic strength of CO_2 oxide weakly depends on temperature.
- The point of intersection of the $\Delta G_T^0(T)$ line of a certain element with the $\Delta G = 0$ line corresponds to the equilibrium temperature of the reaction of the element interacting with oxygen.
- The temperature corresponding to $\Delta G_T^0 = 0$ is conventionally taken as the temperature of the onset of thermal dissociation of the oxide. For most oxides, these temperatures exceed several thousand degrees. This is one of the main reasons why ferroalloy elements (ferroalloys) are not obtained by simply heating the oxides, and all ferroalloy processes are based on the reduction of elements from their oxides with appropriate reducing agents (carbon, silicon or aluminum).
- The point of intersection of the $\Delta G_T^0(T)$ line of carbon for the $C + O_2 = 2CO$ reaction with the $\Delta G_T^0(T)$ line of the corresponding element means the chemical affinity of carbon and this element to oxygen is equal. An increase in temperature promotes an increase in the chemical affinity of carbon for oxygen and,

conversely, a decrease in the affinity of the corresponding element for oxygen. In this aspect, carbon is a “universal” reducing agent capable of reducing any element from its oxide if the necessary temperature conditions are created.

7. The position of carbon in the above series of chemical affinity of elements to oxygen is determined by temperature. At low temperatures, carbon is in the extreme left position, and at high temperatures, it is in the extreme right. With increasing temperature, the carbon will gradually move from left to right, occupying an intermediate position between the elements in the above row.
8. A comparison of the positions of the lines of the three reducing elements used in the production of ferroalloys (C, Si and Al) shows that at moderate temperatures, aluminum and silicon are characterized by a higher reducing ability than carbon. However, at high temperatures, carbon is a stronger reducing agent.

These main points, arising from the analysis of the chemical affinity diagram of elements for oxygen, help to find out other features of redox processes that occur in ferroalloy furnaces in the smelting of ferroalloys and their refining from harmful impurities.

In some textbooks and teaching aids, the position of carbon lines (its oxidation to CO and CO₂) does not find a physicochemical explanation but is usually interpreted as the “universality” of carbon properties. Such a “fetishization” of carbon made it necessary to reveal the essence of this “paradox” and to show that carbon is not an exception in this aspect, but the most typical example of the well-known in physical chemistry position on the nature of the $\Delta G_T^0(T)$ function of reactions involving condensed and gaseous components (substances).

Let us turn to an analytical study of the function $\Delta G_T^0 = \Delta H_T^0 - \Delta S_T^0 T$. In the case of the oxidation of elements with oxygen, ΔH_T^0 always has a negative value ($-\Delta H_T^0 = +Q_T^0$), since oxidation is accompanied by heat generation. Therefore, the position (slope) of the straight line $\Delta G_T^0(T)$ in the diagram is determined by the value of ΔS_T^0 and its sign.

The change in the entropy of the reaction of the interaction of elements with oxygen is calculated as the algebraic sum of the entropy of the reaction products minus the sum of the entropy of the starting components. It is known that the entropies of gaseous substances (oxides O₂, CO₂, CO, SiO_g, Al₂O_g) are significantly higher than the entropies of condensed substances (C_s, Si_s, SiO_{2s}, Al_s, Al₂O_{3g}). Calculations show that for reactions accompanied by an increase in the number of moles of gaseous substances, which is observed in the reaction $2C + O_2 = 2CO$, the change in the entropy ΔS_T^0 will always be positive. Then in the expression $\Delta G_T^0(T) = \Delta H_T^0 - \Delta S_T^0 T$, both terms will be with a minus sign. Therefore, an increase in temperature leads to a decrease in ΔG_T^0 , i.e., increase the thermodynamic strength of CO oxide. In the case of the reaction $C + O_2 = CO_2$, the number of moles of gaseous substances does not change, and therefore, the reaction weakly depends on temperature.

If the interaction of other elements with molecular oxygen proceeds under conditions when the formation of gaseous oxides (SiO_g, Al₂O_g, etc.) is possible, an increase

in temperature increases the thermodynamic strength of these oxides. The above provisions are illustrated by the calculated data.

Conditions of the problem. Using tabular data, make the equation $\Delta G_{298}^{\circ}(T)$ for the following reactions:



and analyze the effect of temperature on the conditions for the formation of oxides (thermodynamic strength of oxides).

The tabular values of ΔH_{298}° and S_{298}° for the components involved in the reaction are as follows:

Parameter	C _s	Si _s	Ca _s	O _{2g}	CO _{2g}	CO _g	SiO _g	CaO _s	SiO _{2s}
$-\Delta H_{298}^{\circ}$ kJ/mol	0	0	0	0	393.1	102.1	98.2	633.7	909.5
S_{298}° J/mol K	5.7	18.8	41.6	204.8	217.2	197.4	231.9	39.7	41.4

The change in the enthalpy of reaction (A) is:

$$\begin{aligned} \Delta H_{298}^{\circ}(A) &= 2\Delta H_{298}^{\circ}(CO_g) - 2\Delta H_{298}^{\circ}(C_s) \\ &\quad - \Delta H_{298}^{\circ}(O_2) = -2 \cdot 102.1 = -204.2 \text{ kJ/mol.} \end{aligned}$$

The change in the entropy of reaction (A) is

$$\begin{aligned} \Delta S_{298}^{\circ} &= 2S_{298}^{\circ}(CO_g) - 2S_{298}^{\circ}(C_s) - S_{298}^{\circ}(O_{2g}) = 2 \cdot 197.4 - 2 \cdot 5.7 \\ &\quad - 204.8 = +178.6 \text{ J/(mol K).} \end{aligned}$$

Having performed the corresponding calculations for the remaining reactions, we obtain the expression $\Delta G_{298}^{\circ}(T)$ for all reactions (A)–(E) in J/mol O₂:

$$\Delta G_T^{\circ}(A) = -204,200 - 178.6T;$$

$$\Delta G_T^{\circ}(B) = -393,100 - 6.7T;$$

$$\Delta G_T^{\circ}(\text{C}) = -909,500 + 182.2T;$$

$$\Delta G_T^{\circ}(\text{D}) = -196,400 - 221.4T;$$

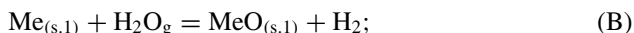
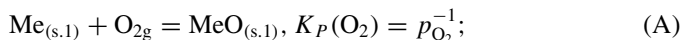
$$\Delta G_T^{\circ}(\text{E}) = -1,267,400 + 208.6T.$$

Thus, the thermodynamic probability of reactions with the formation of gaseous oxides of CO_g and SiO_g increases with increasing temperature. This relationship is weakly manifested for reaction (B) with the formation of CO_2 .

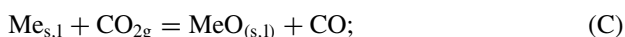
The thermodynamic conditions of reactions (C) and (E) with the formation of oxides SiO_2 and CaO_s in the condensed state worsen with increasing temperature. Note that both of these reactions proceed with the disappearance of the gaseous component (O_2).

The possibility of oxidation (reduction) of metals (elements) is characterized by the redox potential of the gas phase, which means the value of the partial pressure of oxygen (for the $\text{Me}-\text{MeO}-\text{O}_2$ system) or the ratio $p_{\text{H}_2}/p_{\text{H}_2\text{O}}$ and $p_{\text{CO}}/p_{\text{CO}_2}$ or $\lg \text{H}_2/\text{H}_2\text{O}$; $\lg \text{CO}/\text{CO}_2$ (Fig. 1.3).

The interaction of metals with oxygen and gas mixtures of $\text{H}_2\text{O}-\text{H}_2$ and CO_2-CO with the formation of oxides is described by the reactions:



$$K_R(\text{H}_2\text{O}) = p_{\text{H}_2}/p_{\text{H}_2\text{O}}$$



$$K_P(\text{CO}_2) = p_{\text{CO}}/p_{\text{CO}_2}$$

The functional dependence $\Delta G_T^{\circ}(T)$ of reaction (A) can be quite graphically interpreted by representing the function $\Delta G_T^{\circ}(T)$ in the $T-\Delta G^{\circ}$ coordinates. From the position of the lines characterizing the change in the Gibbs energy of the reactions of oxide formation, it is possible to evaluate the possibility and direction of any reaction. Richardson and Jeffez supplemented this generally accepted form of the graphical representation of the $\Delta G(T)$ function with nomographic scales (Fig. 1.3), which make it possible to find the graphical analytical method for the pressure of dissociation of oxides and the equilibrium ratios of $\text{H}_2/\text{H}_2\text{O}$ and CO/CO_2 in gas mixtures for given temperatures. The procedure for finding the desired values of p_{O_2} , $\text{H}_2/\text{H}_2\text{O}$ and CO/CO_2 is as follows. On the nomographic vertical line located to the left of the diagram, three points x , y and z are indicated. The three scales on the

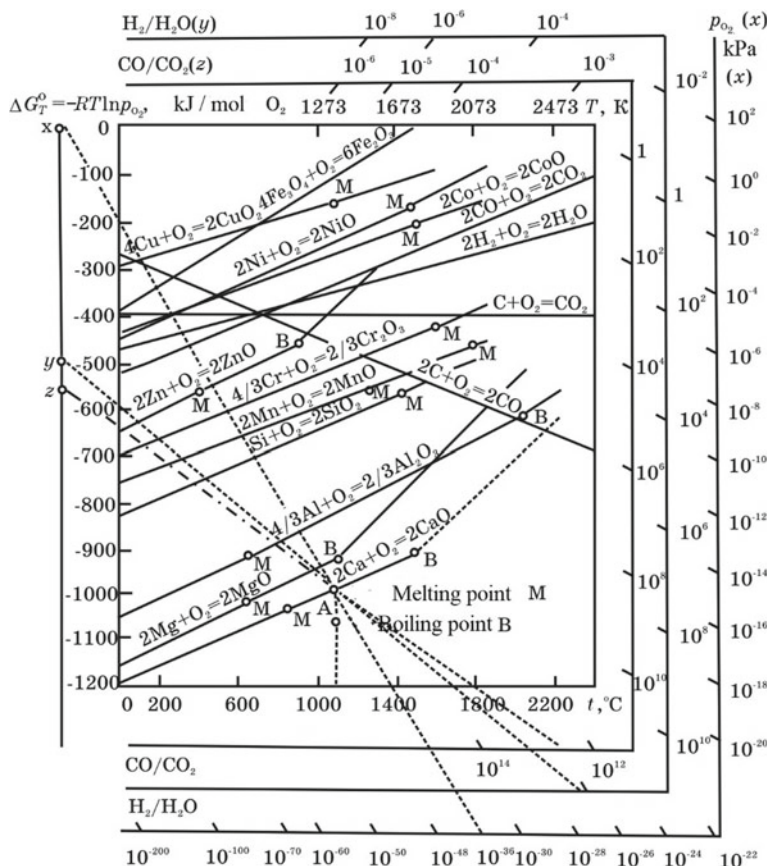


Fig. 1.3 Ellingham–Richardson–Jeffez diagrams for metal–metal oxide equilibria: points M and B are the temperatures of phase transformations of elements

right side of the diagram show numerical values of p_{O_2} (x scale), H_2/H_2O ratios (y scale) and CO/CO_2 (z scale).

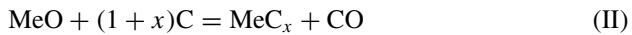
The determination of the desired value of p_{O_2} for the reaction of thermal dissociation of an oxide, for example CaO , is carried out as follows. Initially, on the temperature scale, we mark the temperature of interest (we take 1273 K) and draw a vertical line until it intersects with the characteristic line for the reaction $2Ca + O_2 = 2CaO$. We denote the intersection point of these two lines A. Then, through the points x and A we draw a straight line until it intersects with the scale p_{O_2} (x scale). The value p_{O_2} indicated on this scale will be the oxide dissociation pressure equal to 10^{-34} kPa. To find the H_2/H_2O ratio in the gas mixture corresponding to the dissociation pressure $p_{O_2} = 10^{-34}$ kPa, we draw a straight line through the points y and A to the intersection with the H_2/H_2O scale (y scale). We find that the dissociation pressures for CaO $p_{O_2} = 10^{-34}$ kPa correspond to the ratio $H_2:H_2O = 10^{12}$.

Therefore, even a small amount of H_2O in the gas mixture characterizes it as very oxidizing, leading to the oxidation of metallic calcium to CaO . The procedure for determining the CO/CO_2 ratio is similar to the previous one, with the only difference being that we draw a straight line through points z and A until it intersects with the CO/CO_2 scale (z scale). Found CO/CO_2 ratio corresponding to the dissociation pressure of CaO oxide $p_{\text{O}_2} = 10^{-34}\text{kPa}$.

Thus, the Ellingham–Richardson–Jefez diagram allows a graphical method to determine the dissociation pressure of the oxide formed by the reactions presented on it, as well as to find the $\text{H}_2/\text{H}_2\text{O}$ and CO/CO_2 ratios corresponding to a specific value of the dissociation pressure of each oxide at a given temperature.

1.3 Thermodynamics of Carbide Formation Reactions

The high chemical affinity of most elements to carbon is due to the formation of not pure metals, but their carbides, when reducing metals from their oxides with carbon. Thermodynamic analysis of reactions



confirms the preference for the occurrence of reaction II due to the formation of MeC_x carbide.

Carbides of elements are formed by exothermic reactions.



that, *ceteris paribus*, according to Le Chatelier's principle, provides the reaction II.

Large-scale production of ferroalloys is based on the use of metals from their oxides with carbon as a reducing agent. Therefore, it is very important to know the thermodynamic constants of simple and complex carbides and their behavior at high temperatures of ferroalloy processes. In the subsequent chapters, when analyzing the reactions of metal reduction with carbon, the numerical values of the enthalpies and changes in entropy included in the expression $\Delta G(T)$ are given. The following are some of the thermodynamic constants of the individual properties of carbides to identify the features of the interaction of elements of certain groups of the Periodic system of elements with carbon (Table. 1.1).

Thus, group IVa carbides have the highest formation enthalpies. Moreover, the heat of formation increases in the series $\text{TiC} \rightarrow \text{ZrC} \rightarrow \text{HfC}$, i.e., the thermodynamic strength of carbides of the IVa—group increases with increasing atomic number of the element. A similar pattern is observed in the Va group of elements, where the absolute value of ΔH_{298}^0 increases in the series $\text{VC} \rightarrow \text{NbC} \rightarrow \text{TaC}$.

Table 1.1 Standard enthalpies of formation and entropy of carbides of ferroalloy elements

Carbide	$-\Delta H_{298}^{\circ}$, kJ/mol	S_{298}° , J/mol	Carbide	$-\Delta H_{298}^{\circ}$, kJ/mol	S_{298}° , J/mol
CaC ₂	58.9	70.2	VC _{0.88}	101.6	27.6
SrC ₂	84.4	71.0	NbC	137.9	35.1
BaC ₂	73.9	87.7	TaC	143.2	42.4
Be ₂ C	117.6	16.30	Cr ₂₃ C ₆	98.2	105.7
MgC ₂	50.5	58.5	Cr ₇ C ₃	227.8	200.6
B ₄ C	46.4	27.1	Cr ₃ C ₂	109.5	85.3
SiC	66.8	16.5	CeC ₂	96.9	73.9
TiC	183.5	24.2	Fe ₃ C	25.0	105.1
ZrC	201.4	33.14	Mn ₇ C ₃	108.6	238.6
HfC	218.3	39.5	WC	38.0	41.8
			Mo ₂ C	45.9	65.6

Alkaline earth metals (IIa group) form MeC₂ type carbides. In this group of metals, the heat of formation of carbides also increases with increasing element number, i.e., in a row MgC₂ → CaC₂ → BaC₂.

Alkali metals (Ia group) form carbides of the Me₂C₂ type. The enthalpy of formation of Li₂C₂ is -59.3 kJ/mol, Na₂C₂ -18.4 kJ/mol.

A more complete assessment of the thermodynamic strength of carbides is provided by an analysis of the expressions of the change in Gibbs energy as a function of temperature. So, the functions $\Delta G_T^{\circ}(T)$ for carbides NbC and TiC have the form (J/mol):

$$\text{Nb}_s + \text{C}_s = \text{NbC}_s; \Delta G_T^{\circ}(\text{NbC}) = -130,200 + 1.77T,$$

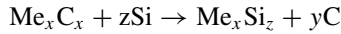
$$\text{Ti}_s + \text{C}_s = \text{TiC}_s; \Delta G_T^{\circ}(\text{TiC}) = -185,870 + 13.24T.$$

Carbides of ferroalloy elements have different congruent melting and decomposition temperatures (according to peritectic reactions). As follows from the Table. 1.2, the most refractory is hafnium carbide HfC ($T_m = 4163$ K).

Table 1.2 Melting points of ferroalloy carbides

Carbide	T_m , K	Carbide	T_m , K	Carbide	T_m , K
HfC	4163	VC	3100	CaC ₂	2573
TaC	4153	W ₂ C	3003	BaC ₂	2053
NbC	3773	MoC	2973	Fe ₃ C	1923
ZrC	3803	ThC	2900	Cr ₂₃ C ₆	1823
TiC	3523	UC	2623	Mn ₇ C ₃	1673

Despite the relatively large thermodynamic strength of carbides in the presence of liquid silicon, they interact by reaction



with the formation of chemical compounds—silicides, since the thermodynamic strength of the latter is higher than carbides. Due to this, it is possible to produce silicon ferroalloys with a low carbon content, using metallurgical coke as a reducing agent.

1.4 Thermokinetics of Ferroalloy Processes

Thermokinetics is a section of chemical kinetics devoted to the presentation of the laws governing the progress of ferroalloy processes (chemical reactions) in time. The main postulate of chemical kinetics is the expression of the dependence of the reaction rate on the concentration (activity) of reacting substances. Actually, the rate of a chemical reaction is the number of molecules (atoms) of a given species reacting per unit time, and for the reversible reaction, $aA + bB \leftrightarrow cC + dD$ has the form in the forward direction $w_1 = k_1 x_A^a x_B^b$ and in the opposite direction $w_2 = k_2 x_C^c x_D^d$, where x is the molar component fraction.

The physical meaning of the constant coefficients k_1 and k_2 is found by assuming that the concentrations of all components are equal to unity. Then, $w_1 = k_1$ and $w_2 = k_2$. Reaction rate is a function of time

$$w = -dx_i/dt.$$

The effect of temperature on the reaction rate. In accordance with Le Chatelier's theorem, an increase in temperature for endothermic reactions creates thermodynamic conditions for the reaction to proceed in the direction of increasing the yield of products and accelerates the reaction. For exothermic reactions, the temperature increase according to Le Chatelier's theorem counteracts the development of the reaction in the forward direction, the degree of completion of the reaction decreases. In this aspect, it would seem rational to lower the temperature. However, it is necessary to choose an optimally moderate temperature for each exothermally proceeding process, since at low temperatures, diffusion processes in the reducing agent—slag ore melt—ferroalloy system are significantly slowed down.

The dependence of the rate constant of the endo- or exothermic reaction on temperature is described by the Arrhenius equation, which has the form

$$d \ln k/dT = A/(RT^2).$$

The value of A has a dimension (J/mol) and is called *the activation energy*. Integrating this expression, we get:

$$\ln k = [-A/RT] + \ln c,$$

where c is the integration constant. In the coordinates $\ln k(1/T)$, the function $\ln k = f(1/T)$ represents the equation of a straight line. Therefore, the $-A/R$ ratio is $\text{tg}\alpha$, and $\ln c$ is the segment b along the y -axis.

The function $\ln k(1/T)$ can be written as $k = c \cdot e^{-A/(RT)}$

An analysis of this equation shows that for a given c , the chemical reaction rate (k) will be the greater, the lower the activation energy (A).

1.5 Gibbs Phase Rule

The *phase rule* is a thermodynamic law that relates the number of phases (P) in thermodynamic equilibrium with the number of components (C) of the system, the number of its degrees of freedom (F) and the number of external parameters that determine the state of the system.

The number of components (C) of a system is the smallest number of starting materials sufficient for the formation of all phases of a given system. The number of components is equal to the number of starting materials if in the system the starting materials do not enter into chemical reactions with each other.

By the *number of degrees of freedom* (or variability) (F) of a system is understood the number of thermodynamically independent state parameters, such as pressure, temperature, concentration of substances (x), which can be changed in a certain interval independently of each other without changing the number of phases (P).

Usually, the effect on the system of only two parameters is taken into account—temperature and pressure. In this case, the phase rule, called the Gibbs phase rule, is written as:

$$F = C - P + 2$$

The phase rule is of great importance in the analysis of phase equilibrium diagrams, equilibria of the totality of chemical reactions for producing electro ferroalloys.

The law of distribution of impurities. The distribution of components between the phases of the system at phase equilibrium is described by the distribution law, which establishes that the ratio of the thermodynamic activities of the impurity in two phases at phase equilibrium is a constant value. In a first approximation, the activity of the components can be replaced by concentration. The ratio of component activities is called the *distribution coefficient*.

Chapter 2

Phase Equilibria in Metal and Oxide Ferroalloy Systems



2.1 General Characteristic of X - T State Diagrams of Systems

When developing new and improving existing technological processes for the production of ferroalloys, data on phase equilibria in binary, ternary and more complex systems of metals, oxides, nitrides and others are important. In some cases, this information is crucial. A study of the position of the boundary lines that outline the concentration fields of the equilibrium state of phases, their aggregate transformation, allows some thermodynamic calculations to be performed. These questions are studied by *geometric thermodynamics*.

It is important to understand why, when forming the brand composition of ferroalloys, normative documents indicate quite definite concentration ranges for the content of one or another element. A deeper knowledge of the features of the state diagrams of oxide and other systems also makes it possible to reasonably perceive the patterns of changes in the whole complex of physical and physicochemical properties of ferroalloys, slags, fluxes in relation to changes in chemical composition and temperature.

In ferroalloy theory, diagrams with complex phase equilibria are used even when the number of components does not exceed two. Understanding complex systems requires knowledge of phase equilibria in simpler systems, which are, as it were, “bricks” for constructing complex diagrams.

A hypothetical complex two-component diagram of phase transformations according to F. Raines [1] with an indication of all possible phase transformations and critical points is presented in Fig. 2.1.

Two types of three-phase equilibria should be distinguished: eutectic and peritectic, in which the following transformations exist:

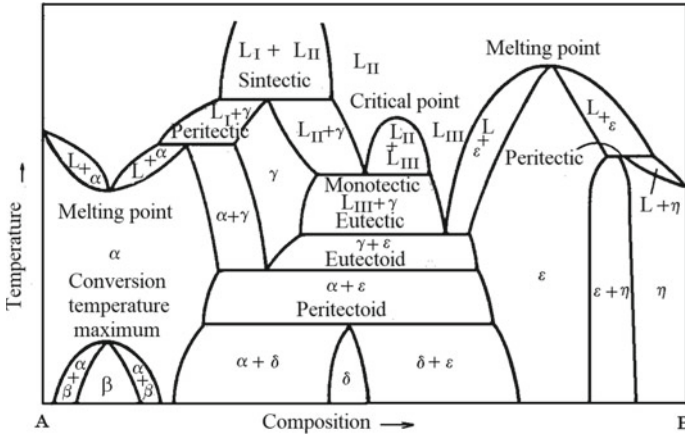
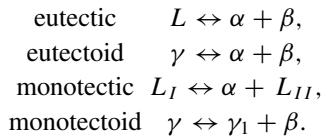
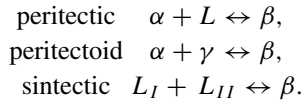


Fig. 2.1 Hypothetical phase equilibrium diagram in two-component system

Eutectic type:



Peritectic type:



The eutectic type also includes the *catatectic* transformation, in which the solid phase turns into a liquid and a new solid phase $\gamma \leftrightarrow L_I + \beta$.

2.2 Binary Equilibrium Phase Diagrams

Isomorphic systems. In these systems, components A and B are mutually soluble in solid and liquid states and the two-phase liquid + α -phase region has the form of a “lens” (Fig. 2.2).

Eutectic and eutectoid systems.

Eutectic systems. The phase equilibrium diagram of the eutectic system is shown in Fig. 2.3. Features of the eutectic system, consisting of two components A and B, are as follows. Adding the first quantities of component A(B) to component B(A)

Fig. 2.2 Isomorphous two-component system of phase equilibria

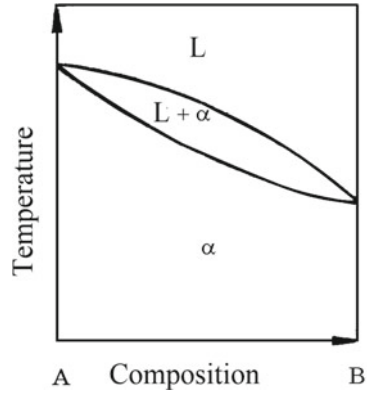
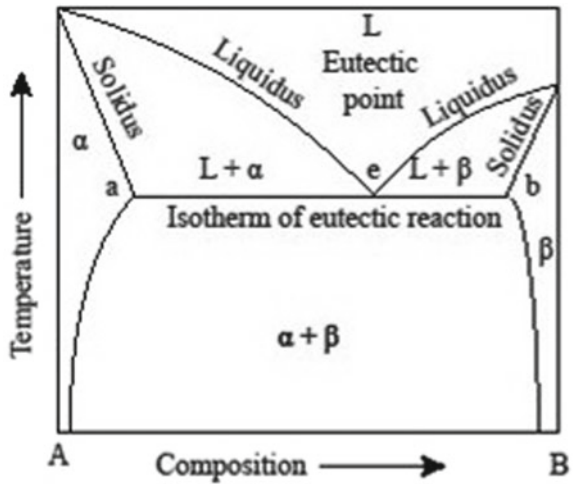
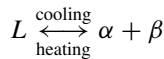


Fig. 2.3 A two-component eutectic-type phase equilibrium diagram



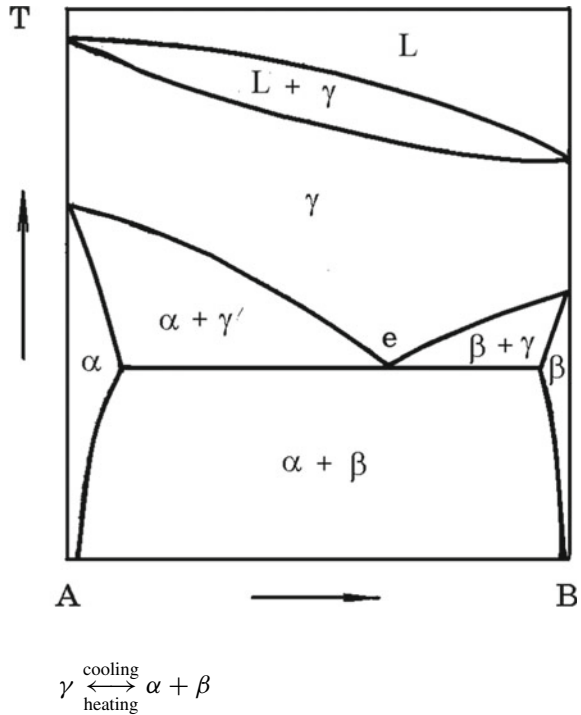
reduces the liquidus curve to a eutectic composition. At the eutectic point e , the liquid coexists with the α -phases and β -phases. Components A and B in the liquid state dissolve indefinitely, and in the solid state it is limited. Upon cooling, the eutectic composition liquid decomposes into two phases α and β by reaction



The maximum solubility of component $A(B)$ in $B(A)$ corresponds to the eutectic temperature.

Eutectoid systems. Systems of this type are similar to the eutectic systems considered above. Three solid cooling phases are involved in the eutectoid reaction

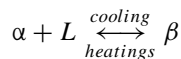
Fig. 2.4 Two-component eutectoid phase equilibrium diagram



One of the differences between a eutectoid and a eutectic system is the absence of a liquid phase in the eutectoid reaction. From the given diagrams in Fig. 2.4 with a eutectoid transformation, it follows that both components A and B have allotropic (polymorphic for oxide systems) transformations, although eutectoid reactions can proceed without these transformations. An illustration of a diagram with a eutectoid reaction is the well-known equilibrium diagram of the Fe–C system. The eutectoid point (point *c*) corresponds to 0.8% C and a temperature of 738°C. Component A (Fe) undergoes allotropic transformations of $\alpha\text{-Fe} \leftrightarrow \gamma\text{-Fe}$ at 911°C and $\gamma\text{-Fe} \leftrightarrow \delta\text{-Fe}$ at 1392°C. Eutectoid transformation is inherent in a number of binary metallic and oxide systems of ferroalloy production.

Peritectic and peritectoid systems.

Peritectic systems. A peritectic transformation takes place upon heating and involves the decay of one solid phase into a liquid and a new solid phase; i.e., the solid phase melts incongruently (with decay) (Fig. 2.5):



Peritectoid systems. The basis for the interpretation of transformation as a peritectoid is the reaction

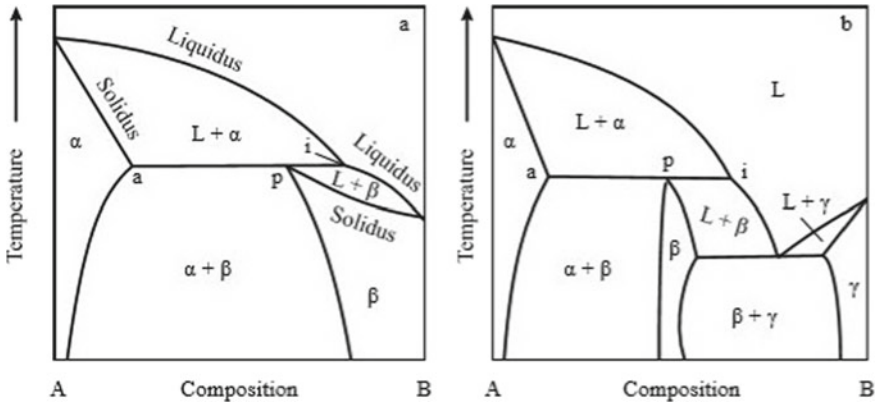
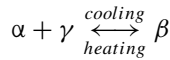


Fig. 2.5 Two-component phase equilibrium diagram with peritectic (a) and peritectic and eutectic transformations (b)



in which the solid phase β breaks up into two new solid phases α and γ (Fig. 2.6).

Monotectic systems. The general view of the diagram with monotectic transformation is shown in Fig. 2.7. Monotectic three-phase reaction

Fig. 2.6 Two-component phase equilibrium diagram with peritectoid transformation

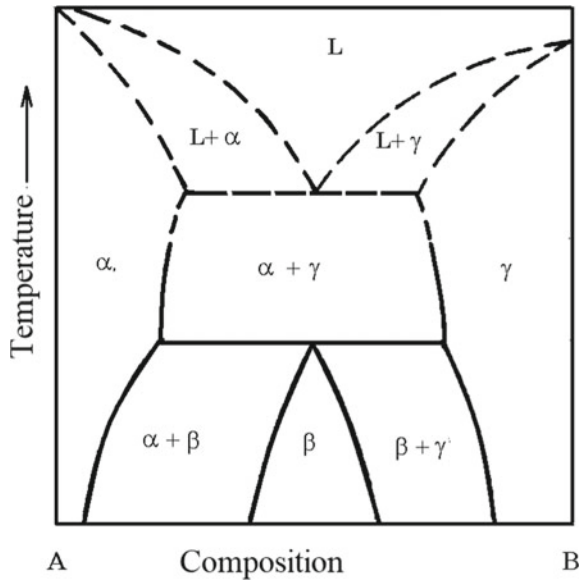
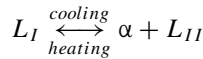
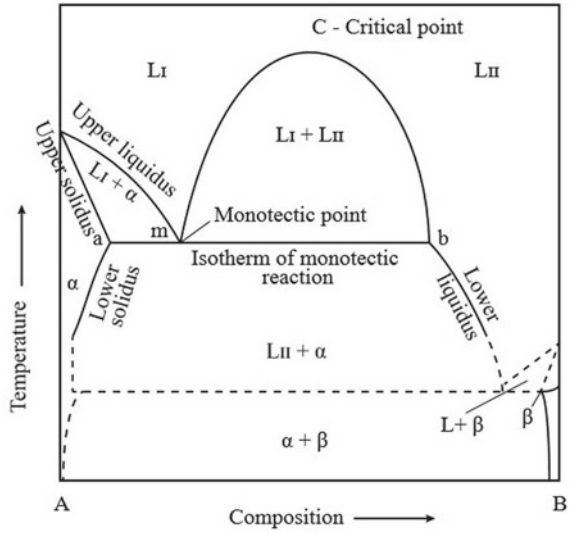


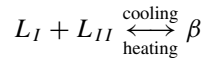
Fig. 2.7 Two-component phase equilibrium diagram with monotectic transformation



belongs to the eutectic class.

With decreasing temperature, the liquid phase L_I decomposes into a solid phase and a new liquid L_{II} . There is an area where the liquid phases L_I and L_{II} do not mix.

Dual syntectic systems. A syntectic reaction is a type of peritectic transformation and represents the decomposition of the solid phase β when heated into two liquids



In the diagram, the region of existence of two liquids L_I and L_{II} is limited by the field of two liquids with an upper critical point (Fig. 2.8). Among technical alloys, no syntactic reactions were observed.

2.3 Ternary Equilibrium Phase Diagrams

The $X-T$ diagram of a system consisting of three components is graphically displayed in volume so that the composition is applied on the horizontal plane, and the temperature is applied vertically. The three-phase equilibrium in the spatial model for two eutectic systems and one isomorphous binary system is shown in Fig. 2.9.

In the spatial image of the phase equilibrium in the $MnO-FeO-SiO_2$ system (Fig. 2.10), the dashed line shows the region of existence of two immiscible liquids.

Fig. 2.8 Two-component phase equilibrium diagram with syntectic reaction

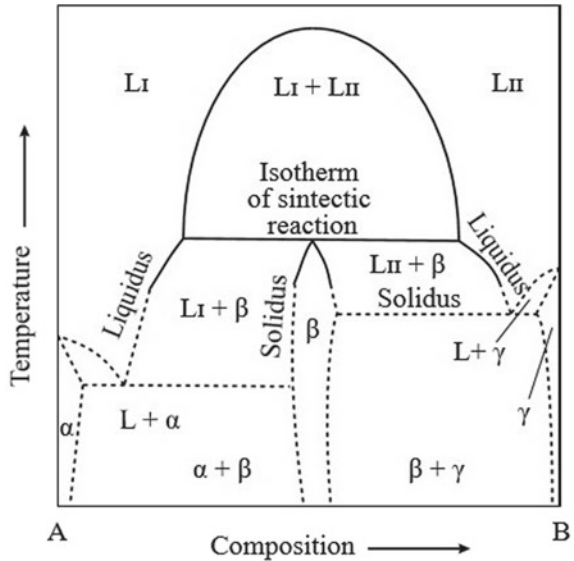
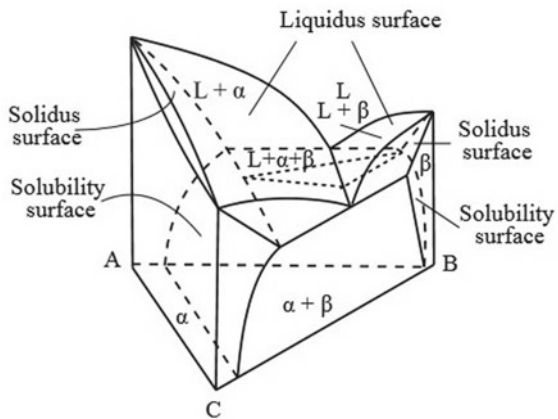


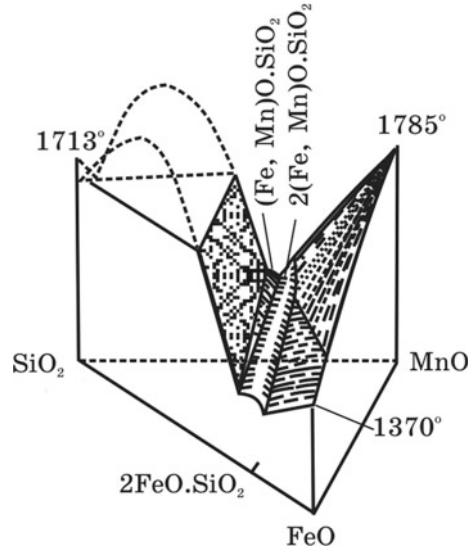
Fig. 2.9 Three-phase equilibrium in a simple ternary system



To display phase equilibria in a triple condensed system, the Gibbs triangle is used. Pure components (100%) are located at the vertices of the triangle, double compositions on its sides and triple components inside the triangle. The trigonal prism can be dissected by horizontal or vertical planes and obtain an isothermal or isopleth (vertical section of the phase equilibrium diagram; poythermal) section on the plane.

To calculate the composition of the alloy inside the triangle, it is necessary to draw three lines parallel to its sides through a given point. The straight-line segments cut off by their intersection point and removed from the top of the triangle (the content of

Fig. 2.10 Spatial model of MnO–FeO–SiO₂ system state



pure components) will characterize the percentage of each component in the ternary alloy.

Multicomponent systems. The phase equilibrium diagrams of systems containing four or more components are very complex. Thus, a temperature–composition diagram for a four-component system would require four measurements. Therefore, isobaric or isopleth sections are used. To find the composition in a four-component system, use the correct tetrahedron, which has the same properties as an equilateral triangle.

The total length of line segments drawn through a given point parallel to four edges to the intersection with the corresponding faces is equal to the length of any edge taken as 100%.

Conode triangles. To characterize three-phase equilibrium in a diagram, it is necessary to use such an element of the diagram that each selected temperature would show the composition of three conjugate phases. According to F. Raines, such an element is a triangle composed of conodes (Fig. 2.11).

When any three ternary alloys are mixed, the composition of the formed new alloy P will be inside the triangle RSL . An example of calculating the composition of alloy R . Three compositions of R, S and L are known (Fig. 2.11):

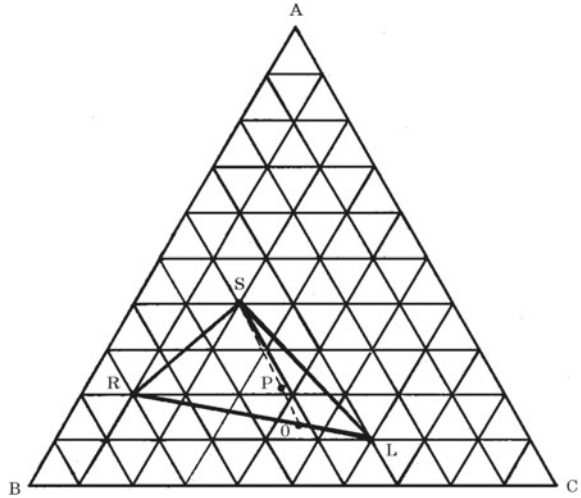
$$R = 20\%A + 70\%B + 10\%C;$$

$$S = 40\%A + 40\%B + 20\%C;$$

$$L = 10\%A + 30\%B + 60\%C.$$

When mixing two parts of an alloy of composition R with three parts of alloy S and five parts of alloy L , we obtain the composition of alloy P :

Fig. 2.11 Conodal triangle analysis



$$0.2 \times 20 + 0.3 \times 40 + 0.5 \times 10 = 21\%A$$

$$0.2 \times 70 + 0.3 \times 40 + 0.5 \times 30 = 41\%B$$

$$0.2 \times 10 + 0.3 \times 20 + 0.5 \times 60 = 38\%C$$

Therefore, the composition of alloy P (21%A + 41%B + 38%C) will be inside the triangle RLS, at point P (Fig. 2.11). The rule of the conodal triangle remains true no matter in what proportion the three alloys of compositions R, S and L were taken.

Reference

1. Raines F (1960) Phase equilibrium diagrams in metallurgy. Metallurgizdat, p 376. (in Russian)

Chapter 3

Classification of Ferroalloy Processes



3.1 Classification of Metals—Leading Ferroalloy Elements

According to the modern classification, metals are divided into two main groups: ferrous and non-ferrous. The first group includes iron in the entire variety of products, where it is the main metal—cast iron, steel of various chemical compositions and ferroalloys. The second group unites almost all known metals. Depending on the physicochemical properties, metals are divided into the following groups: (1) light (Al, Ba, Be, K, Ca, Li, Mg, Na, Rb, Si, Sr, Tl, Cs); (2) rare (V, W, Ga, Hf, Y, Ge, Mo, Re, REM (rare earth metals), Se, Ta, Ti, Te, Zr); (3) heavy (As, Bi, Cd, Co, Cu, Cr, Mn, Hg, Ni, Sb, Sn, Pb); (4) noble (Au, Ag, Ir, Os, Pt, Rd, Rh, Ru) and radioactive (Pu, Po, Ra, Np, Th, U).

A number of elements belonging to the group of non-ferrous metals are the basis of alloys called ferroalloys and are two-component or more complex compositions of the corresponding metals and non-metals with iron. Conventionally, the metals and non-metals that make up the basis of ferroalloys can be called ferroalloy elements. These include elements: Mn, Si, Cr, Ca, Al, Ba, Sr, Mg, Ti, V, W, Mo, Nb, REM, Se, Ta, Te, Zr, Ni, B. In ferroalloys in large or smaller amounts of impurity elements are present: S, P, Cu, Sn, Sb, Bi, O, H, N, etc.

A comparative diagram of the prevalence of these elements in nature is presented in Fig. 3.1.

Two groups of ferroalloys are distinguished—bulk (major) and minor.

The group of *bulk (major) ferroalloys* (production volume millions of tons) includes silicon ferroalloys (ferrosilicon of all grades, crystalline silicon); manganese ferroalloys (high-carbon, medium-carbon and low-carbon ferromanganese, silicomanganese, metallic manganese, nitrided manganese, manganese ligatures); chromium ferroalloys (high-carbon, medium-carbon and low-carbonaceous ferrochromium, ferrosilicochromium, metallic chromium, nitrided ferrochromium, ligatures of complex compounds).

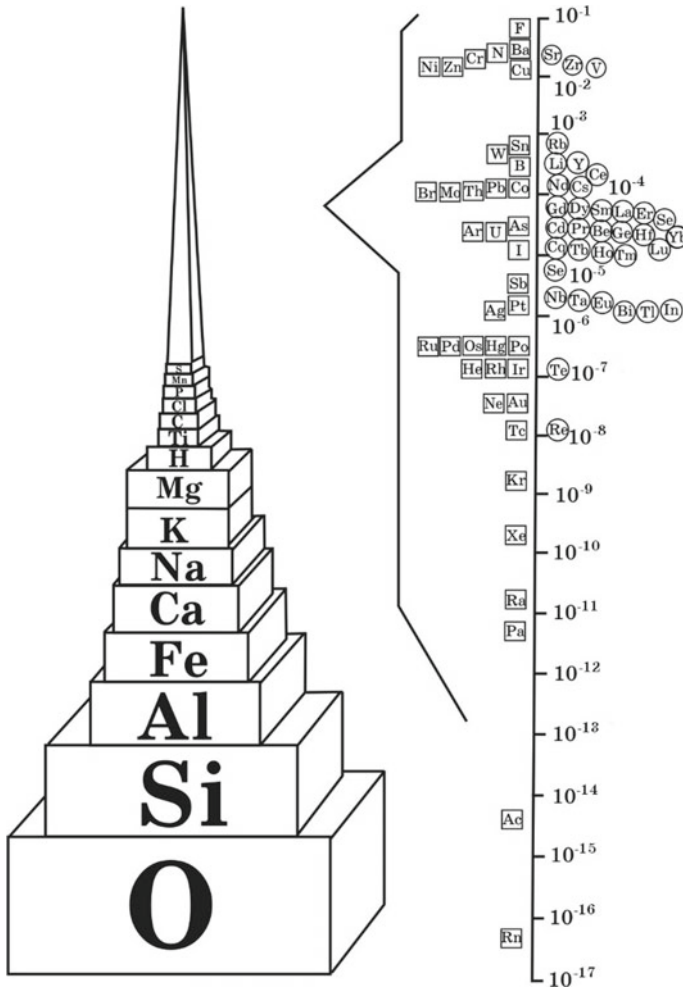


Fig. 3.1 Prevalence of elements in the earth's crust, % mass

The group of *minor ferroalloys* (production volume of tens and hundreds of thousands of tons) includes: ferrotungsten; ferromolybdenum; ferrovandium; ferrotitanium and alloys systems Fe–Si–Ti, Ti–Cr–Al; Ti–Cr–Al–Fe, Ti–Ni; ferroniobium and alloys of the Ni–Nb, Nb–Ta–Fe systems; Nb–Ta–Mn–Al–Si–Ti; Nb–Ta–Al; ferrosilicozirconium and ferro-alumo-zirconium; ferronickel and ferrocobalt; alloys with aluminum (silicoaluminum, ferroaluminum, aluminum ferrosilicon, alloys of the Fe–Al–Mn–Si, Fe–Mn–Al systems); alloys of alkaline-earth metals (silico-calcium, silicobarium, silicomagnesium, strontium silicon, complex alloys of the systems Fe–Si–Mg–Ca; Si–Ca–Ba–Fe; Si–Ba–Fe; Si–Ba–Sr and others); ferroboron, ferboral and ligatures with boron (Ni–B, Cr–B, B–Si–Al–Ti–Zr); alloys with rare

earth metals (REM) of REM–Si systems; Ce–Si–Fe; REM–Al–Si; phosphorus and ferrophosphorus; ferroselenium and ferrotelurium.

The main components of ferroalloys are called leading elements. The degree of reduction and transition of an element to metal or extraction of a leading element determines the technical and economic efficiency and feasibility of the technology used. Analysis and comparison of production indicators of ferroalloys from raw materials of various compositions and methods of their production in furnaces of various designs and capacities are carried out under the condition that the number of ferroalloys is calculated in base tons. Base ton—1 ton of ferroalloy, ore, concentrate with a strictly defined content of the leading element or its compounds. For example, in accordance with the FS45 grade ferrosilicon standard, it may contain 41–47% Si, and 1 ton of alloy with 45% Si is taken as the base ton.

The properties of ferroalloys largely depend on the physicochemical properties of the leading elements, which are the metals of the first three large periods, more precisely, the transition metals of the first (Sc, Ti, V, Cr, Mn, Fe, Co, Ni), the second (Y, Zr, Nb, Mo), third (La, Ta, W) periods, as well as metals at the beginning of large periods (Mg, Ca, Sr and Ba) of the Periodic Table of D.I. Mendeleev. The properties of metals are determined by the structure of s-electron, p-electron, d-electron and f-electron shells. The designation of electronic shells comes from the first letters of the corresponding words: s—sharp; p—principal; d—diffuse; f—fundamental.

In accordance with a change in the electronic configuration of metals, their properties naturally change. For example, the melting temperature of metals, as a characteristic of the resistance of the crystal lattice to thermal fluctuations, rises in each large period as the levels are filled with electrons, reaching maximum values for chromium (first period), molybdenum (second period) and tungsten (third period), and then decreases. The same character is observed for the boiling temperature of metals, as a measure of the energy of the atomic bonding, the heat of vaporization, valency and some other properties of the elements.

The majority of ferroalloys are used in steelmaking for alloying and deoxidizing steel, as well as for alloying and modifying cast iron and alloys, the manufacture of welding electrodes, the production of chemical compounds, as a starting material for protective coatings on metal structures and devices, in the enrichment of minerals. Ferroalloys also serve as feedstock for the preparation of highly pure substances (elements and compounds) and are widely used as reducing agents in metallothermic processes.

Most ferroalloys contain a relatively large amount of iron. This is because in the feedstock, along with the oxides of the leading element, iron oxides are always present, which are not a harmful impurity for most ferroalloys. Moreover, iron, dissolving the reduced leading element, reduces the activity of the latter and the melting point of ferroalloys, increases the density of a number of ferroalloys and increases the useful use of leading elements in the deoxidation and alloying of steel and alloys. The formation of metal solutions of reduced elements in iron by reducing the activity of the leading element in the solution decreases the Gibbs energy of the reduction process. Thus, during the formation of iron-based solutions, the reduction

of the leading element is possible at lower temperatures with higher recovery; therefore, iron is often specially introduced into charge materials (in the form of chips, less often in the form of oxides). The cost of reduced elements in ferroalloys is lower than pure ones.

3.2 General Requirements for the Quality of Ferroalloys

The quality of ferroalloys is characterized by the content and limits of variations of the leading element, the concentration of regulated accompanying impurities (C, P, S, non-ferrous metals, N, H, O, etc.), particle size distribution, density, state of the surface of the pieces, melting point, the content of non-metallic inclusions and inclusions of slag.

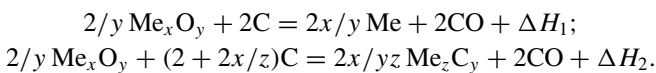
Chemical composition. The main indicator of the quality of a ferroalloy is its chemical composition and, above all, the content of the leading element in it. In this case, it is important that the content of the alloying element in the ferroalloy of individual smelting be combined in one batch.

Granulometric composition. An important characteristic of the quality of a ferroalloy is its particle size distribution, since with the right choice, the process of dissolution melting is accelerated, and high absorption of the alloying element in the steel bath is ensured. At the request of consumers, ferroalloys are delivered with a strictly specified particle size distribution. The mechanical properties of ferroalloys are also important, since the choice of crushing devices for producing alloys of a given particle size distribution depends on them.

3.3 Classification of Ferroalloy Processes by the Type of Used Reducing Agents

This feature is the main one, since not only the physicochemical processes that determine the essence of the technology of various ferroalloys depend on the type of reducing agent, but also practical methods of conducting the process, the type of furnace unit used, the chemical composition of the resulting alloy and the area of its use. According to this criterion, the processes of production of ferroalloys are classified into *carbothermic*, *silicothermic* and *aluminothermic*. Calcium-thermic and magnesium-thermic processes are not used in metallurgy of ferroalloys.

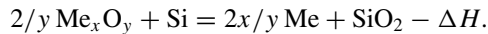
Carbothermic processes. In carbothermic processes, a solid carbon is a reducing agent for oxides. In general terms, total reactions can be represented as follows:



The main feature of these processes is that one of the reduction products is carbon monoxide, the removal of which from the bath ensures irreversibility of the reactions. By carbon, all elements from their oxides can be reduced at high process temperatures, since the chemical affinity of carbon to oxygen increases with increasing temperature. Carbon has a low cost, and carbon materials of various quality can be used.

The disadvantages of carbon as a reducing agent include the following: (1) during the reduction of oxides, carbides are formed; with increasing silicon content in the alloy, the carbon concentration decreases; (2) oxides reduction reactions occur with the absorption of a large amount of heat ($\Delta H \gg 0$); therefore, as a rule, the use of high-power electric arc furnaces is required.

Silicothermic processes. Silicothermic reduction of metals from oxides occurs by reaction



The reduction of silicon oxides is carried out using complex high-silicon ferroalloys of the Me–Fe–Si type, where Me is Mn, Cr, which are preliminarily obtained by the reduction of silica (as well as manganese and chromium oxides) with carbon. Therefore, the technological scheme for the production of low-carbon ferroalloys includes the stage of smelting of the alloys for further processing: ferrosiliconmanganese and ferrosilicochromium. In some cases, ferrosilicon of the FS75 or FS65 grades is used as a reducing agent in the silicothermic process (smelting of ferrotungsten, ferromolybdenum, ferrovanadium, etc.). Because of silicon oxide reduction, the slag is enriched with silica. A high degree of reduction of the leading element is achieved by reducing the activity of SiO_2 in the slag; therefore, melting is carried out by the flux method using lime (CaO) as a flux. Silicon can also be used as a reducing agent in the reduction of oxides of elements with a higher chemical affinity for oxygen than silicon. In this case, a satisfactory removal of the leading element is achieved by introducing an excess amount of silicon into the charge. The final product is obtained with a high concentration of silicon (silicothermic silicocalcium, etc.).

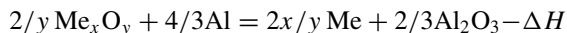
Silicon has a high chemical affinity for oxygen; therefore, it can serve as a reducing agent for elements from oxides such as Cr_2O_3 , MnO , MoO_3 , WO_3 and V_2O_5 . The reduction of oxides with silicon is accompanied by the release of heat, which, as a rule, is insufficient to conduct out-of-furnace silicothermic process, so the process is conducted in electric furnaces of relatively low power (2.5–7 MV · A).

Silicon as a reducing agent has the following disadvantages:

- (1) due to the formation of silica, the amount of slag increases, in which strong silicates of the lower oxides of the leading element are formed; further reduction of the leading element is possible when oxides with high basic properties are introduced into the slag (charge) (CaO , MgO).
- (2) at temperatures of smelting of ferroalloys, silicon forms solutions with metals that are characterized by significant negative deviations from ideal behavior,

which indicates the strength of the Me–Si bond and makes it difficult to obtain alloys with a low silicon concentration.

Aluminothermic processes. Aluminothermic reduction of metals from oxides proceeds by reaction



and is characterized by significant negative Gibbs energy, so the process proceeds with a high useful extraction of the leading element. The main features of the aluminothermic process: the release of a significant amount of heat as a result of the course of the reduction reaction and the possibility of carrying out processes outside the furnace. In this case, high temperatures (2400–2800 K) are achieved, which ensure the production of slag and metal with a temperature exceeding the onset of crystallization, good separation of the metal and slag phases, and a high process speed. In aluminothermic processes, the recovery of metals from oxides does not require additional heat supply (use of an electric furnace), with the exception of extra strong oxides (for example, production of ferrosilicozirconium), when they are melted in an electric arc furnace.

The advantage of aluminothermic processes is: (1) the ability to reduce a wider range of elements with a chemical affinity for oxygen less than that of aluminum; (2) reduction of oxides and production of alloys and technically pure metals with a low concentration of carbon and impurities of non-ferrous metals; (3) the simplicity of the hardware design process, low capital costs; (4) process management in the leaning furnace with the release of slag and metal; (5) the possibility of preliminary melting of oxides and fluxes in an electric furnace, which can significantly intensify the process and reduce the consumption of aluminum; (6) the use of high-alumina slag for the production of synthetic slag, as well as high-alumina cement.

The disadvantages of the aluminothermic process include: (1) the high cost and scarcity of aluminum; (2) the possibility of the formation of lower oxides of the leading metals, a decrease in the thermodynamic probability of the reduction of these oxides and the reduction of metals from the charge; (3) the formation of high-alumina slag with a high viscosity, causing loss of reduced metal in the form of metal shots.

3.4 Classification of Ferroalloy Processes by Type of Aggregate

The main methods for the production of ferroalloys that currently exist are electric furnace, metallothermic, blast furnace, electrolytic and special methods.

The electric furnace method is based on the use of electric arc furnaces, in which heat is released when current passes through the gas gap and charge materials with a sufficiently high electrical resistance. The processes are characterized by obtaining

high temperatures in the area of combustion of electric arcs, carrying out processes with any composition of the gas phase (reducing, oxidizing, neutral) and in vacuum. It is possible to easily and quickly change the power of a furnace plant with full automation of its operation.

The metallothermic method is based on the use of heat from chemical reactions for the reduction of element oxides with aluminum and silicon. These processes can be carried out without the supply of electrical energy, although in recent years most technologies have provided for the preliminary melting of charge materials in electric arc furnaces to intensify the process, save expensive reducers and more fully remove the leading elements from the charge into metal.

The blast furnace method allowed for the first time to obtain ferroalloys containing silicon, manganese and chromium, but this method requires a significant consumption of high-quality coke, and the resulting alloys contain carbon at the saturation limit, so it is impossible to obtain low-carbon ferroalloys in a blast furnace. So, in the smelting of high-carbon ferromanganese in a blast furnace, the coke consumption per 1 ton of alloy is 1700–1800 kg, while in the smelting of this alloy in an ore-smelting electric furnace, the coke consumption is not more than 450–500 kg/t, which determines a lower the cost of the alloy melted electrochemically. In a blast furnace, it is impossible to create temperature conditions for obtaining ferroalloys containing metals having a greater chemical affinity for oxygen than iron, as well as refractory metals.

The electrolytic method is based on the electrolysis of aqueous solutions or molten salts and is used to produce highly pure metals. This method is associated with significant energy consumption and the need to use especially pure raw materials.

Special methods are used to obtain and refine alloys in vacuum resistance furnaces, induction furnaces and in converters, which makes it possible to produce ferroalloys and pure metals with a very low content of carbon, oxygen, hydrogen, non-metallic inclusions, as well as nitrided ones.

3.5 Classification of Ferroalloy Processes by Technological Features

The variety of reducing agents used determines a number of features of ferroalloy processes, which are the basis for their classification according to various technological characteristics.

Continuous and batch processes. Ferroalloy processes are divided into *continuous* and *batch*. Continuous processes are conducted in stationary ore-smelting electric furnaces. Furnaces can be single-phase (with one or two electrodes) and three-phase with three or with a large number of electrodes, a multiple of three. The furnaces are powered by an alternating current of industrial frequency (50 Hz) and can have a round or rectangular bath. Furnaces with a round bathtub are equipped with electrodes of circular cross section; furnaces with a rectangular bathtub can have both round and flat (rectangular, oval) electrodes. In furnaces with a round bath, the electrodes are

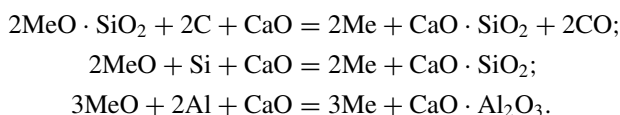
located at the vertices of an equilateral triangle; in furnaces with a rectangular bath, the electrodes are located in one line. Continuous processes are characterized by continuous loading of the charge into an ore-smelting electric furnace with a closed top. The mixture is located in the furnace at a certain level throughout the process. The electrodes are constantly immersed in the charge, and the release of metal and slag is carried out periodically or continuously. In this case, furnaces of large unit electric power (16.5–100 MV · A) are used, and carbon-containing materials (coke, semi-coke, less often anthracite, coal) are used as reducing agent.

Periodic processes are carried out using a certain amount of charge materials intended for one heat. The charge loaded into the furnace is completely melted with the reduction of the oxides of the leading elements. Melting is carried out in steel-type arc electric furnaces with a capacity of 5–8 MV · A (silicothermic processes) or in melting furnaces (aluminothermic processes). The release of melting products (metal and slag) is carried out periodically; most often, they release metal and slag from the furnace at the same time.

Slag-free and slag processes. Slag-free processes include ferroalloy smelting, in which the amount of slag is insignificant and amounts to 3–5% of the mass of the metal (e.g., smelting of crystalline silicon, ferrosilicon and ferrosilicochromium). In slag-free processes, slag is formed by oxides contained in small quantities in ores, concentrates, coke ash, and not recovered during smelting.

Slag processes are accompanied by the formation of a significant amount of slag. The slag ratio can be 1.2–1.5 (e.g., in the smelting of high-carbon ferromanganese and ferrosiliconmanganese) and 2.0–3.5 (e.g., in the production of low-carbon ferrosilicochromium and manganese metal by the silicothermic method).

Flux and flux-free processes. Ferroalloys smelting in a batch process is most often carried out by a flux method, although flux-free melting is advisable under certain conditions. With the flux method, the reduction of the oxides of the leading element occurs according to the reactions:



The introduction of flux reduces the activity of SiO_2 and Al_2O_3 in the slag, which is accompanied by an increase in the yield of the reduced metal. As fluxes, materials containing CaO , MgO and other components that form the most durable chemical compounds with oxides—products of reduction reactions—are used. At the same time, the viscosity of the slag decreases, the melting temperature of the slag decreases (or increases), and the concentration of impurities in the ferroalloy decreases, which leads to a more complete extraction of the lead element and an increase in the quality of the ferroalloy.

Electric melting and melting without flux are possible. At the same time, energy consumption is reduced and furnace productivity is increased, but the degree of reduction of the leading element is decreased. Slag contains a significant amount

of oxides of the leading element, and it is usually used for smelting ferroalloys. At the same time, the consumption of flux decreases and the through use of the leading element increases. However, the flux-free method can be carried out using high-quality ores and concentrates with a low content of phosphorus and other impurities. The choice of a technology for melting with the introduction of flux into the mixture or melting without flux is determined by the quality of the obtained ferroalloy, its economy and the possibility of increasing the productivity of the furnace.

Chapter 4

Metallurgy of Silicon and Silicon Carbide



4.1 Properties of Silicon and Its Compounds

Silicon belongs to VIA group of the Periodic Table of Elements, atomic number 14, atomic mass 28.08, electron shell configuration $3s^2 3p^2$, exhibits oxidation state +4 (the most stable), +3, +2 and +1. The melting point of silicon is 1415 °C; the boiling point is 3250 °C. The silicon crystal lattice is cubic, face-centered diamond type. The affinity of the silicon atom to the electron is 1.22 eV, Pauling electronegativity is 1.8, the atomic radius is 0.133 nm, and the ionic radius is Si^{4+} 0.040 nm (coordination number 4), covalent radius 0.1175 nm.

Table 4.1 shows the thermodynamic constants of silicon and some of its compounds.

Silicon melts with a decrease in volume of 9%. The density of silicon is 2.33 g/cm³. In the range 1687–1973 K, the dependence of density on temperature is described by the expression (g/cm³):

$$d_{\text{si}} = 2.49 - 2.722 \cdot 10^{-4}(T - 1687).$$

Si–O system (Fig. 4.1). The solubility of oxygen in solid silicon is very small; therefore, this region is not shown in the state diagram. The temperature dependence of soluble oxygen in liquid silicon has the form:

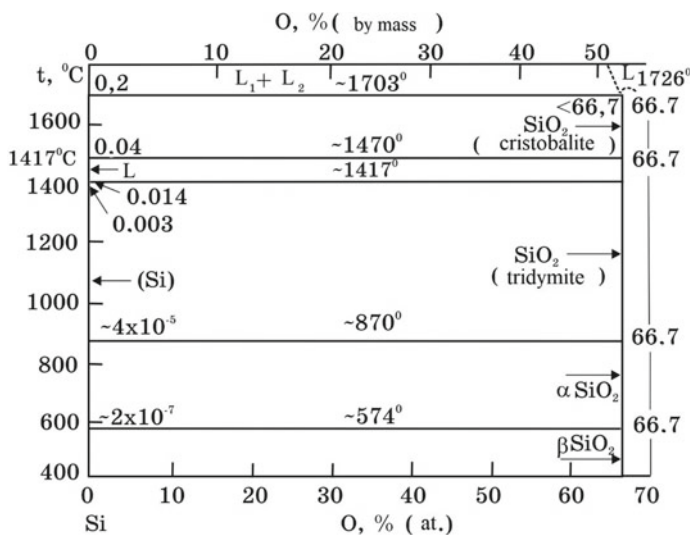
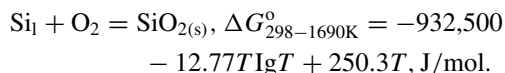
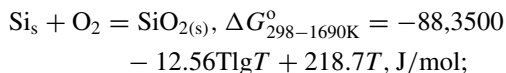
$$\lg[\%O]_{\text{si}} = -6975/T + 1.5205.$$

The change in the Gibbs energy of the reaction of dissolution of molecular oxygen in liquid silicon is described by the equation: $\Delta G_T^{\circ} = -339,663 + 69.9T$, (J/mol $\frac{1}{2}\text{O}_2$).

The change in the Gibbs energy of the reactions of formation of silica taking into account the state of aggregation of silicon is characterized by the following equations:

Table 4.1 Thermodynamic constants of silicon and some of its compounds

Substances formula	ΔH_{298}° , kJ/mol	ΔG_{298}° , kJ/mol	S_{298}° , J/(mol K)	C_{p298}° , J/(mol K)
Si	–	–	18.84	20.06
Si _{Fas}	452.2	407.9	167.98	22.27
SiO ₂ (α -quartz)	–911.59	–857.49	41.89	44.47
SiO _{gas}	–103.42	–130.299	211.61	29.89
SiC-cubic	–66.15	–63.768	16.62	26.88
SiC-hexagonal	–62.81	–60.377	16.497	28.81

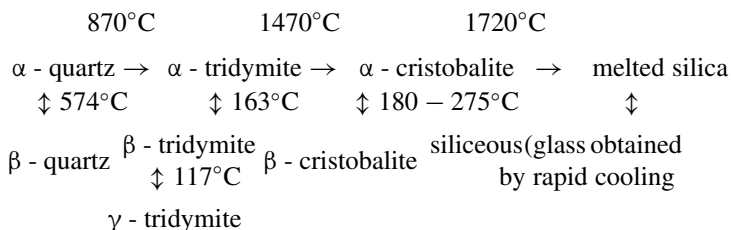
**Fig. 4.1** Equilibrium state diagram of the Si–O system

The most stable phase is SiO₂ (quartz), melting point $t_m = 1726$ °C and boiling point $t_b = 2275$ °C, silica has several modifications that are stable in certain temperature ranges (Table 4.2).

The transformation of quartz during heating (cooling) is accompanied by a relatively large change in volume, sometimes leading to cracking of quartz (quartzite), as a component of the charge, on the furnace top. The sequence of phase transitions of quartz is presented in the diagram below:

Table 4.2 Characterization of the main phase transformations of silica at $p_{O_2} = 100$ kPa (Q_f —heat of phase transformation)

Transformation	$t, ^\circ\text{C}$	$\Delta V, \%$	$-Q_f, \text{J/mol}$
β -quartz \rightarrow α -quartz	574	0.80	1047
α -quartz \rightarrow α -tridymite	870	14.70	502
α -quartz \rightarrow α -cristobalite	1050	14.70	837
α -cristobalite \rightarrow melt	1726	1260	1793



Not all silica modifications have the same value for characterizing the behavior of quartzite in the smelting of ferrosilicon and other silicon ferroalloys.

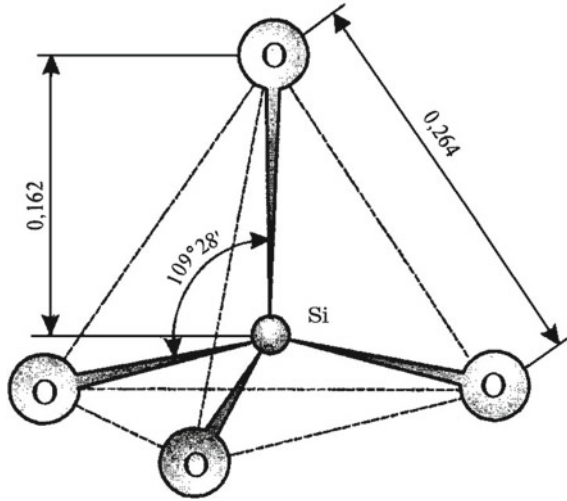
According to the rate of modification transformations of quartz, two groups of transitions are distinguished. The first group includes fast transitions in any main form of SiO_2 , and in two directions, i.e., enantiotropically. In the diagram, they are indicated by vertical arrows indicating temperatures. The high rate of these transitions is explained by small changes in the lattice parameters. Therefore, with the β -quartz \rightarrow α -quartz transition, the volume increases by only + 0.8%, while the α -quartz \rightarrow α -tridymite transition is accompanied by a change in volume by + 14.7%.

The second group of transitions proceeding slowly is located in a horizontal row due to the deep rearrangement of the crystal lattices. For example, α -quartz can be melted while in an unstable state. Under ordinary conditions, β -quartz is a stable form (see the scheme), therefore in nature, there are quartz, and many varieties of quartz minerals are in the β -form (rock crystal, gangue quartz, quartz sands, sandstones, quartzite, chalcedony, flint, etc.)

The main crystal-chemical structural unit of quartz is the silicon-oxygen tetrahedron $[\text{SiO}_4]^{4-}$ (Fig. 4.2), in which the silicon atom is located in the center of the tetrahedron and at its vertices. The distance between the silicon atoms and Si–O oxygen is equal to the distance of 0.162 nm, the nearest oxygen atoms are 0.264 nm from each other, and the angle of the OSiO is $109^{\circ}28'$. The charge of the tetrahedron is -4 . $[\text{SiO}_4]^{4-}$ tetrahedra can be in contact, forming various more complex structural configurations.

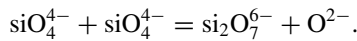
Modern ideas about the melts of silicates. Binary and more complex silicates according to [1] are polyanionic liquids represented by a set of $\text{Si}_j\text{O}_y^{z-}$ anions (where $z = 2y - 4i$) in chemical equilibrium. At the first stages of the study, it was assumed that in the MeO-SiO_2 binary system, both $\text{Si}_j\text{O}_y^{z-}$ and O^{2-} ions are separated by cation shells. Later, an approach was substantiated to develop a theory of the structure

Fig. 4.2 Scheme of elementary tetrahedron SiO_4^{4-} (distances in nm)

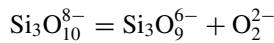


of silicates and slags, according to which the melt structure is determined by the equilibrium of three forms of the oxygen atom: one-, two-bound and free $2\text{O}^- = \text{O}^0 + \text{O}^{2-}$.

According to the polymer model, two SiO_4^{4-} monomers can form a complicated anion-dimer according to the scheme



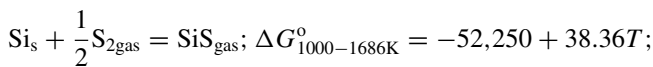
According to the model, the $\text{Si}_3\text{O}_{10}^{8-}$ trimer, with one self-closure, cleaves the O^{2-} ion according to the scheme



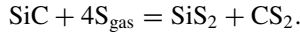
and becomes ring-shaped. When quantitatively processing the model, isomers were not taken into account, and therefore, an interpretation of the general model, including all kinds of anion structures and their isomeric forms, was given.

Si-S system. The solubility of sulfur in solid silicon at a temperature close to the melting point is very low and is characterized by the following data: at 1573 K – $4 \times 10^{-8}\%$ (at), at 1673 K, it increases to $6 \times 10^{-8}\%$ (at). Silicon with sulfur forms sulfides SiS_{gas} and $\text{SiS}_{2(\text{gas})}$.

The temperature dependence of the Gibbs energy change of the reaction of formation of sulfur sulfide is represented by the equation:



Sulfur vapor at a temperature above 900 °C interacts with SiC by the reaction:



The reactions considered are important for interpreting the behavior of sulfur contained in charge materials and, first of all, in coke (up to 2%), during the smelting of crystalline silicon, silicon carbide SiC and other silicon ferroalloys.

Carbon properties. The atomic number of carbon is 6, and the atomic mass is 12.011. Carbon does not melt under normal pressure.

The transition of carbon into a liquid state requires high temperatures and pressures. As follows from Fig. 4.3, equilibrium conditions for the transition of carbon solid \leftrightarrow liquid state are determined by the line delimiting regions 1 and 2. For example, to obtain carbon in liquid form at 3000 K, a pressure > 400 GPa is required.

C–O system. The interaction of carbon and oxygen under certain conditions can lead to the formation of CO and CO₂. For the reaction $2\text{C} + \text{O}_2 = 2\text{CO}$, the equilibrium constant has the form:

$$K_P = p_{\text{CO}}^2 / (a_{\text{C}}^2 - p_{\text{O}_2}), \tag{4.1}$$

at $a_{\text{C}} = 1$, $K_P = p_{\text{CO}}^2 / p_{\text{O}_2}$.

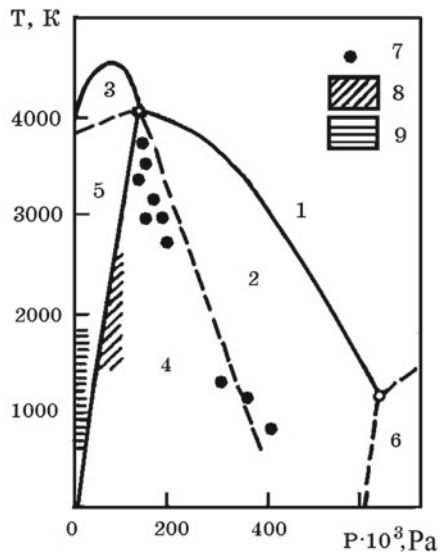
The temperature dependence of $\lg K_P$ is determined by the equation $\lg K_P = 56,324/T + 36.89$ and $\Delta G_T^\circ = -236,000 - 168.8T$, J/mol O₂.

For the reaction $\text{C} + \text{O}_2 = \text{CO}_2$, the equilibrium constant is

$$K_P = p_{\text{CO}_2} / (a_{\text{C}} - p_{\text{O}_2}), \tag{4.2}$$

at $a_{\text{C}} = 1$, $K_P = p_{\text{CO}_2} / p_{\text{O}_2}$, $\lg K_P = 86,255/T + 0.184$,

Fig. 4.3 Carbon state diagram: 1—liquid; 2—stable diamond; 3—stable graphite; 4—stable diamond and metastable graphite; 5—stable graphite and metastable diamond; 6—is a hypothetical region of other solid carbon modifications; 7—points corresponding to the conditions for the direct transformation of graphite into diamond; 8—areas of diamond formation using metals; 9—field of experiments on the formation of diamond at low pressure



$$\Delta G_T^\circ = -394,210 - 0.842T, \text{ J/mol O}_2.$$

Carbon monoxide CO can interact with oxygen by the reaction $2\text{CO} + \text{O}_2 = 2\text{CO}_2$, the equilibrium constant of which

$$\lg K_P = p_{\text{CO}_2}^2 / (p_{\text{CO}}^2 p_{\text{O}_2}) \quad (4.3)$$

$$\lg K_P = 123,520/T - 41.5,$$

$$\Delta G_T^\circ = -565,000 + 189.86T, \text{ J/mol.}$$

Carbon and carbon dioxide can interact by the reaction $\text{CO}_2 + \text{C} = 2\text{CO}$, the equilibrium constant of which

$$K_P = p_{\text{CO}}^2 / (p_{\text{CO}_2} - a_C) \quad (4.4)$$

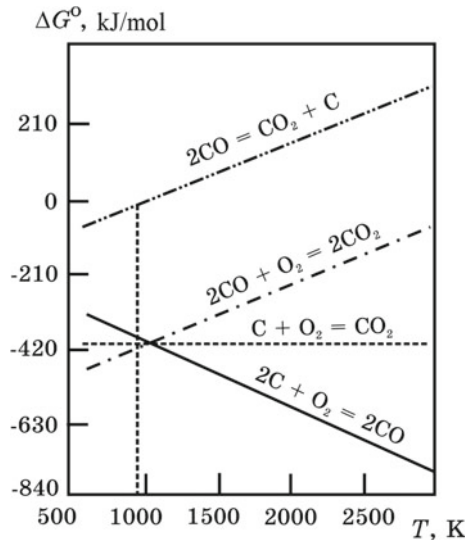
$$\lg K_P = -37,330/T + 38.160,$$

$$\Delta G_T^\circ = 170,780 - 174.58T, \text{ J/mol.}$$

Figure 4.4 shows the dependence $\Delta G_T^\circ (T)$ for the reaction (4.1)–(4.4).

An analysis of the equations shows that the thermodynamic probability of the reaction (4.3) decreases and for the reaction (4.1), increases with increasing temperature. A change in temperature due to a slight change in the entropy of the reaction

Fig. 4.4 Dependence of the change in Gibbs energy on the temperature of reactions in the C–O system



weakly affects the thermodynamic probability of the reaction (4.2). The straight lines $\Delta G_T^0 = f(T)$ in Fig. 4.4 for reactions (4.1), (4.2) and (4.3) intersect at a point corresponding to a temperature of 976 K. Under conditions of excess carbon and at $T > 1300$ K, the only product of the interaction of carbon with oxygen is CO. With an excess of oxygen, carbon and CO are oxidized to CO_2 .

Si–C system. The state diagram of the Si–C system is presented in Fig. 4.5. The solubility of carbon in solid silicon is very low, and in the liquid state increases significantly. The dependence $[\%C] = f(1/T)$ has the form [2]

$$[\%C] = 3359 \cdot \exp(22147/T).$$

In this system, SiC carbide with a composition of 70% Si and 30% C is formed, which at 2545 °C is converted by a peritectic reaction.

The reaction of solid silicon with carbon $\text{Si}_s + \text{C}_s = \text{SiC}_s$ is characterized by a change in Gibbs energy $\Delta G_{298-1683\text{K}}^0 = -53,510 + 69.5T$ and for a reaction involving liquid silicon

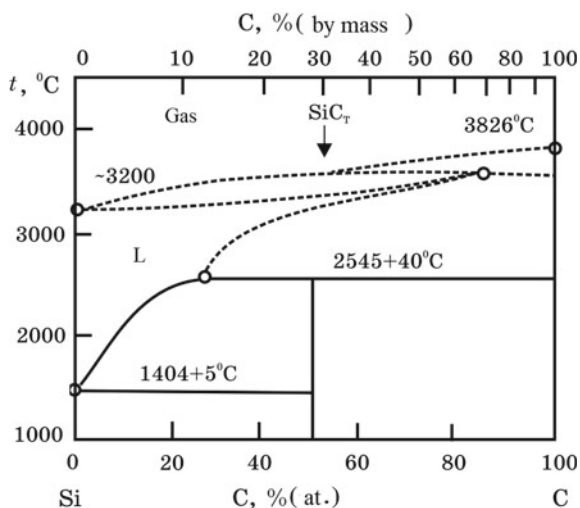


Gibbs energy change equation has the form: $\Delta G_T^0 = -100,600 + 34.9T$. The gas phase above SiC carbide has a complex composition that is temperature dependent. So, at 2000 K, the gas phase contains% (vol.): 86.5 Si; 6.1 SiC_2 ; 7.4 SiC.

The density of silicon carbide is 3.22 g/cm³.

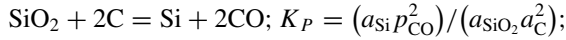
The specific electrical resistance of silicon carbide at temperatures up to 1273 K is 1.3 Ω·m. Silicon carbide is colorless; the presence of impurities stains it in green or black.

Fig. 4.5 Equilibrium state diagram of the Si–C system



4.2 Theoretical Foundations of Silicon Reduction by Carbon

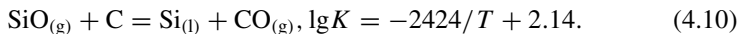
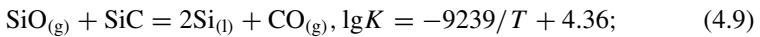
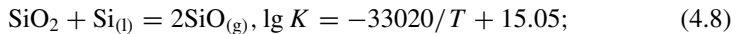
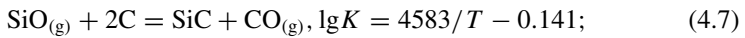
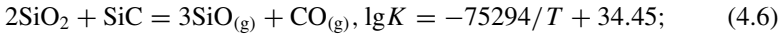
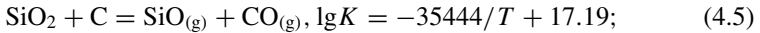
The balance reaction characterizing the process of reducing silicon from silica to carbon in the preparation of crystalline silicon can be described by the equation



$$\Delta G_T^\circ = 697390 - 359.07T, \text{ J/mol.}$$

The theoretical temperature of the onset of the reaction ($\Delta G_T^\circ = 0$) is 1942 K. However, in reality, the process of silicon reduction with carbon at various temperatures proceeds through the stages of the formation of intermediate products $\text{SiO}_{(\text{g})}$ and SiC , which must be taken into account in thermodynamic analysis to correctly predict the parameters of the technology for smelting crystalline silicon. Thus, a thermodynamic analysis of the reactions of reduction of Si from SiO_2 by carbon can consist in revealing the features of phase equilibria in the Si–O–C system.

In [3–5], a model for thermodynamic analysis of the dominant phase equilibria in the Si–O–C system was based on the minimum number of reactions chosen and the minimum number of possible components in the system (condensed SiO_2 , SiC , Si, C and gaseous SiO_{gas} and CO). The following six basic reactions were taken into account:



An analysis of the calculations of the phase equilibria in the Si–O–C system using the six reaction model and the interpretation of the results presented in the $\log(p_{\text{SiO}}/p_{\text{CO}}) - 1/T$ coordinates shows that this thermodynamic model is inadequate [6]. It is known that the components of the coordinate axes cannot contain the dominant element (in our case, silicon), since, upon calculations, the Gibbs phase equilibrium rule $F = C - P + 2$ (Sect. 1.5) will not be satisfied.

The *six reaction* model calculates the equilibria in the Si–O–C system only for four condensed phases and only takes into account the partial pressures of SiO and CO, and the components with lower pressures are not included. The forced restriction of the total partial pressure of the components $p_{\text{SiO}} + p_{\text{CO}} = 1$ atm is contradictory to, e.g., the possibility of reaction (1) ($\text{SiO}_2 + \text{C} = \text{SiO} + \text{CO}$). The equilibrium constant of the reaction is 2.22 at 1800 K.

At 1800 K, the change in the Gibbs energy of the reaction at conditions $p_{\text{tot}} = p_{\text{SiO}} + p_{\text{CO}} = 1$ atm calculated with new thermodynamic data is 13,763 J/mol. The equation $p_{\text{SiO}}(1 - p_{\text{SiO}}) = 2.22$ has no real solutions, since the partial pressures p_{SiO} and p_{CO} are complex numbers, $0.5 \pm 1.404i$. Thus, in this approximation, the system cannot physically exist, although it is reliably known that the reaction can occur.

Another peculiarity of the additional restriction $p_{\text{SiO}} + p_{\text{CO}} = 1$ atm should be taken into account. On this basis, the $p_{\text{SiO}}p_{\text{CO}}$ product should always be smaller than or equal to 0.25, since the maximum (0.25) is achieved at $p_{\text{SiO}} = p_{\text{CO}} = 0.5$. In a similar manner, the equilibrium constant of reaction (4.4) ($\text{SiO}_2 + \text{Si} = 2\text{SiO}$) is 2.4 at 2200 K, and this means that $p_{\text{SiO}} = 1.55$ and $p_{\text{CO}} = 1 - 1.55 = -0.55$ atm, which has no physical sense. These data confirm that, under the condition $p_{\text{SiO}} + p_{\text{CO}} = 1$ atm, the equilibria of reactions (4.5), (4.6) and (4.8) have no solutions in the region of elevated temperatures if we use only the six chosen reactions.

4.3 The Assortment of Crystalline Silicon and Quality of Raw Charge Materials

Silicon assortment. Silicon of technical purity (96–99%) (Table 4.3), called *crystalline*, is obtained by reducing it from quartz or quartzite by carbon in ore-smelting electric furnaces using alternating or direct (less often) current. The balance reaction for producing silicon can be represented in the following form (in J/mol):

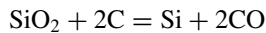


Table 4.3 Chemical composition of crystalline silicon

Silicon grade	The content of elements, % (by weight)				
	Si, no less	Impurities, no more			
		Fe	Al	Ca	Fe + Al + Ca, no more
Si00	99.0	0.4	0.4	0.4	1.0
Si0	98.8	0.5	0.6	0.4	1.2
Si1	98.0	0.7	0.7	0.6	2.0
Si2	97.0	1.0	1.2	0.8	3.0
Si3	96.0	1.5	1.5	1.5	4.0

$$\Delta G_7^0 = 697,390 - 359.07T.$$

The theoretical temperature of the onset of this reaction, as noted above, is 1942 K (1669 °C).

Applications for crystalline silicon. Crystalline silicon has a wide range of applications: for smelting silicon–copper alloys; synthetic aluminosilicon alloys (*silumins*) alloyed with other metals of silicon bronze, obtaining organosilicon compounds, and is also used in ferrous metallurgy for deoxidation and alloying of special steels and alloys. The highest quality grades of silicon can be used as a starting material for the production of silicon of solar and semiconductor purity.

The chemical industry consumes 44% of the crystalline silicon produced. The annual growth in silicon consumption in this industry has reached 6%. About half of the volume of smelted silicon is spent on obtaining aluminum–silicon cast alloys (*silumins*) for the engineering industry.

With increasing energy consumption and environmental requirements, high-purity silicon has become the focus of attention of scientists and specialists involved in renewable energy sources and, above all, solar energy.

Quality of quartzite for smelting crystalline silicon. Quartzite represents a rock composed of quartz cemented by quartz material. In geological practice, quartzite is a dense and strong rock consisting of quartz grains and cemented by a silica binder, which together with quartz grains represents an *opal—chalcedony—quartz system*. The fibrous structure of chalcedony includes water-containing opal secreted between the fibers.

Quartzite–sandstones, mainly consisting of quartz, are also distinguished in the geological literature, the color is absent, the color is light, gray-white, sometimes it contains hematite pigment and is painted in pink and red tones, and even less often, they contain highly metamorphosed carbonaceous matter, coloring them in dark gray tones.

For the smelting of crystalline silicon at the Zaporizhzhya Aluminum Plant (OJSC ZALK), high-purity quartzite is used for impurity oxides of the Banichsky deposit (Ukraine). The following quality indicators are regulated in Banichsky quartzite: not less than 99.0% SiO₂ and not more than 0.25% Al₂O₃, 0.15% Fe₂O₃ and 0.025% CaO. The bulk weight of quartzite is 1.4 t/m³, and the size of pieces is 20–90 mm. Due to the higher cost and relatively smaller production of Banichsky quartzite in comparison with the quartzite of the Ovruch deposit (Ukraine), it is used for the smelting of crystalline silicon and high-silicon ferrosilicon with a low aluminum content.

It is important to note that the suitability of quartzite of each deposit is determined not only by its chemical composition, but also by its behavior in ore-smelting electric furnaces due to cracking and other factors. The suitability of quartzite for the smelting of silicon, ferrosilicon and other silicon ferroalloys should be confirmed by lengthy industrial tests of their electrometallurgical properties.

Quality of carbon reducing agents. The basic requirements for the quality of carbonaceous reducing agents are different for each group of ferroalloys and include

monitoring of the following indicators: (1) the content of solid (nonvolatile) carbon, volatile substances, working moisture and sulfur; (2) the amount and chemical composition of the ash; (3) electrical resistivity; (4) porosity; (5) physical and mechanical properties (particle size distribution, strength characteristics); (6) the reducing ability with respect to the oxides of the reduced element. But under the real conditions of the ferroalloy process (high temperatures, a low charge column in a ferroalloy furnace, the inevitable process of the formation of metal carbides and gaseous lower metal oxides, etc.), one of the most important characteristics of carbon reducing agents is the reducing ability of the carbon material, taking into account its electrical resistance and other parameters. Table 4.4 shows the compositions and properties of the most widely used reducing agents.

The possibility and feasibility of using a specific reducing agent to obtain a certain type of ferroalloy are determined during testing in industrial conditions.

Table 4.4 Comparative characteristics and quality of carbon reducing agents

Parameter	Metallurgical coke	Coke breeze	Semi-coke	Petroleum coke	Charcoal
<i>Technical analysis content, %</i>					
A^d (ash)	10.65	10.80	27.00	0.71	1.45
V^{daf} (volatile)	1.44	1.20	5.60	8.08	14.54
W^p (moisture)	0.44	1.30	1.90	0.80	2.10
S_t^d (sulfur)	0.89	1.34	0.91	4.23	0.04
C_s (carbon)	87.02	86.66	71.49	86.98	83.97
Reactivity at 1323 K, ml/(g s)	0.69	0.92	8.00	0.42	11.1
ρ_{spec} , Ohm m (fraction 3–6 mm)	1.21	1.48	7500	3×10^6	2×10^6
Structural strength, %	83.0	85.0	63.7	64.3	39.0
<i>Density, g/cm³</i>					
True	1.82	1.95	1.58	1.41	1.40
Apparent	0.91	0.93	0.93	1.12	0.40
Porosity, % (cm ³ /g)	53.1 (0.49)	49.7 (0.51)	55.0 (0.67)	20.1 (0.18)	63.8 (1.1)
<i>Ash content, %</i>					
SiO ₂	35.4	36.5	75.7	46.3	1.90
Al ₂ O ₃	23.3	22.2	11.2	24.3	3.40
CaO + MgO	3.8	3.9	3.0	10.5	41.1
Fe ₂ O ₃	33.8	33.7	7.6	14.2	0.85
P ₂ O ₅	0.24	0.24	0.03	0.75	5.12
K ₂ O + Na ₂ O	2.13	2.64	1.18	0.13	0.29

The tendency of carbon materials to graphitization is of negative importance. Graphitization causes a decrease in the chemical activity of carbon, electrical resistance and specific surface, which impairs the ability of a carbon material to reduce metals from oxides.

The electrical resistance of the charge mixtures. An important property of a charge for producing ferroalloys by a carbothermic process with electrodes immersed in a charge is its specific electrical resistance ρ , which, all other things being equal, depends on the amount and particle size distribution of coke, quartzite and other charge components.

With a decrease in the size of pieces of coke and quartzite, the value of ρ increases. Excessive reduction in the size of the pieces reduces the gas permeability of the charge column in the furnace bath, which leads to a drop in productivity and technical and economic indicators of smelting ferroalloys. In practice, the calculation of the particle size distribution of the charge is checked by examining the operation of furnaces on the charge of various particle size distribution.

The desire of ferroalloys technologists to maximize the electrical resistance of the mixture during alloy melting by a continuous process is explained by the need to reduce the fraction of the charge conduction current and increase the proportion of the current passing through the electric arc—a high-temperature heat source.

Crystalline silicon of high purity in terms of the content of impurities for special purposes can be obtained by a two-stage technology. At the first stage, it is necessary to produce silicon carbide in industrial resistance electric furnaces, the content of impurity elements in which is always lower than in the quartz (quartzite) used. In the second stage, from a mixture of silicon carbide and quartz (quartzite) of high purity in an electric arc furnace, crystalline silicon can be obtained by the reaction $\text{SiO}_2 + 2\text{SiC} = 3\text{Si} + 2\text{CO}$. Two-stage technology has not received industrial application.

4.4 The Technology of Crystalline Silicon Smelting

Crystalline silicon (Table 4.3) is used in the production of foundry silicon–aluminum alloys (such as silumins), the chemical and electronic industries (after additional purification of technical silicon from impurities) and other branches of technology.

Silicon is obtained by reducing SiO_2 with carbon. The main reactions by which silicon is obtained have been considered above.

General characteristics of alternating current silicon smelting technology. The technological scheme of silicon production is shown in Fig. 4.6. Quartzite (less commonly quartz) and carbon reducing agents are used as charge materials for silicon smelting; strict quality requirements are imposed on the content of harmful impurities, particle size distribution, electrical resistivity, etc. The impurity minerals contained in quartzite, reducing agent ash, and electrodes are source of iron, aluminum, calcium and other elements in silicon. Unreduced impurity oxides are slagged with silica, as a result of which a small amount of acidic slag is formed, which wets liquid silicon well.

The natural forms of silica are represented by the mineral quartz or rocks almost completely composed by it—quartzite, quartzite–sandstones, etc. The density of

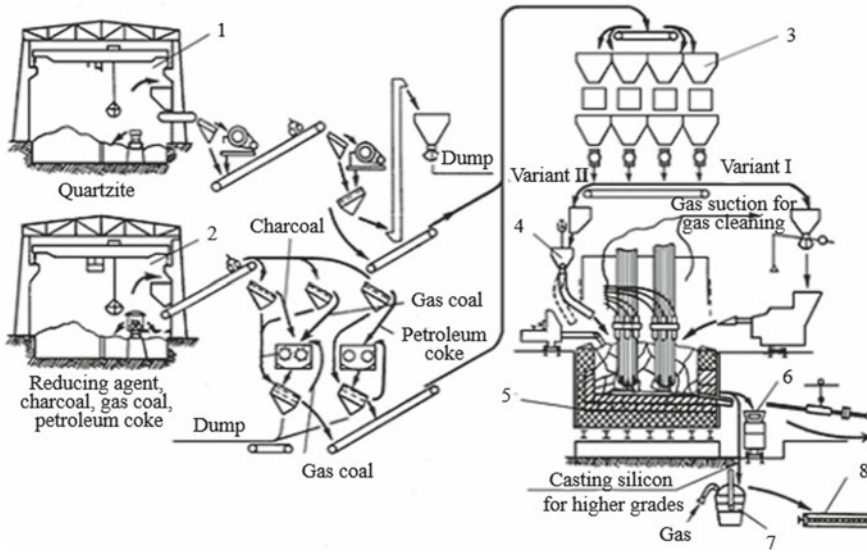


Fig. 4.6 Schematic diagram of the production of crystalline silicon in a single-phase electric furnace with a capacity of 6.5 MV A with two electrodes. 1—warehouse of quartzite; 2—a warehouse of carbonaceous reducing agents; 3—silos for technological materials; 4—furnace bunkers; 5—single-phase arc electric furnace with two graphite electrodes; 6—mold for liquid silicon; 7—a ladle for refining silicon; 8—mold for casting silicon; option I—loading the mixture using a machine; option II—on the ducts

quartz is 2.59–2.65 g/cm³, and the hardness is ~7 on the Mohs scale. Depending on the amount of impurities, the color and hardness of quartz change. When quartzite is crushed, part of the impurities is removed with fines. After crushing, quartzite is washed to remove clay, dust deposits and brittle inclusions. Quartzite should have high heat resistance, crack slightly when heated, have a small apparent porosity (<2%), low moisture absorption (0.1–0.5%). Below are the technical requirements for quartzite intended for the smelting of crystalline silicon:

Field	Pervouralskoye (Russia)	Banichskoe (Ukraine)
<i>Composition, %</i>		
SiO ₂ , no less	98.0	98.0
Fe ₂ O ₃ , no more	0.25	0.15
Al ₂ O ₃ , no more	0.60	0.25
CaO, no more	0.25	0.15
Fraction, mm	10–250	40–250

Silicon is smelted in three-phase open ore-smelting electric furnaces with a capacity of 6.5; 16.5 and 22.5 MV A alternating current continuous process with a constant release of the melt. The bathtubs of the furnaces are lined with carbon blocks. Electrodes are graphitized. Self-baking continuous electrodes are of limited use because they contribute iron through a steel casing. For smelting, quartzite with a grain size of 20–50 mm, charcoal—10–80 mm, petroleum coke and gas coal—5–15 mm are used. The mixed charge coming from the furnace bins is loaded into the furnace by a filling machine. The mixture is introduced so that cones <0.5 m high are constantly supported at the electrodes.

The release of silicon is carried out continuously, which is caused by the need to reduce the duration of stay of the melt in the atmosphere of the furnace gas due to the development of secondary carbide formation. Since the density of silicon (2.2 g/cm³ at 1600 °C) is less than the density of the slag melt (2.6–2.8 g/cm³) having a high viscosity (1.0–1.5 Pa s at 1700 °C), continuous release contributes to the exit of slag melt, which facilitates furnace maintenance and reduces deviations in the electric melting mode.

The normal operation of the furnace is characterized by a stable and deep landing of the electrodes, a uniform release of gas over the upper surface, the absence of darkened areas of sintering of the top and local gas emissions—fistulas, the mixture is lowered without collapses, the release of silicon and slag is constant in quantity; the current load on the electrodes is stable and corresponds to the specified. A diagram of the structure of the bath of a furnace melting silicon is shown in Fig. 4.7.

In the process of silicon reduction by carbon, the reaction product is also CO burning on the top.

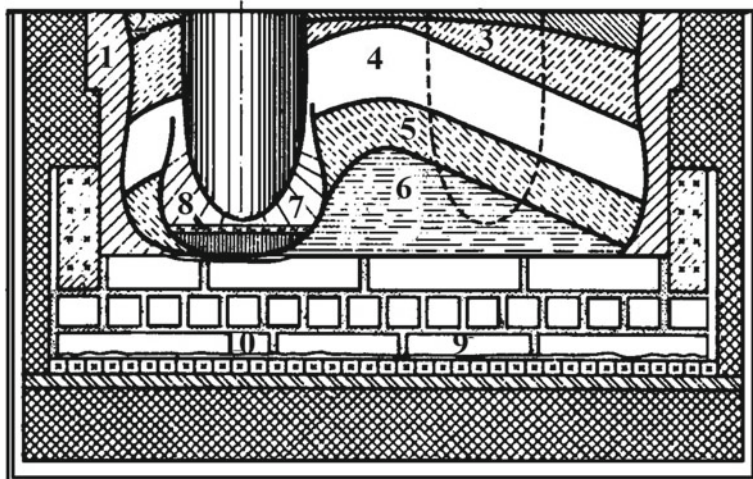


Fig. 4.7 Structure of the bath of the ore-smelting furnace for smelting crystalline silicon. 1—skull; 2—layer of the initial charge; 3—layer of hot charge; 4—a layer of softened charge; 5—restoration zone; 6—metal carbide coating; 7—subelectrode cavity; 8—silicon melt; 9, 10—carbon blocks

When smelting silicon under alternating current in a furnace with a capacity of 16.5 MV A, 2540 kg of quartzite, 1310 kg of charcoal, 150 kg of petroleum coke, 240 kg of gas coal are consumed per 1 ton of silicon at an electric power consumption of 11,200–12,200 kWh.

The extraction of silicon is 78–85%; 0.5% of reduced silicon is lost with slag. Passes to silicon from the mixture, %: 50–55 Al; 35–40 Ca; 30–35 Mg; 95–98 Fe. The resulting silicon has the composition shown in Table 4.5.

During operation of the alternating current furnace with a capacity of 22.5 MV A, gas is generated (~120 thousand m³/day) of the following composition, %: 80–85 CO; 4–8 CO₂; 1–3 CH₄; 0.1–1 H₂O; 1–4 N₂; 1–3 H₂, which before cleaning contains 1.2–2 g/m³ of dust composition, %: 80 SiO₂; 2–4 Al₂O₃; 0.1–0.2 Fe₂O₃; 1–2 CaO; 7–8 C.

During the operation of the furnace, ~82% of the heat is introduced with electricity, ~17% is introduced as a result of carbon combustion, and 1% is the physical heat of the mixture and the formation of compounds in the slag. The consumable part consists of the following articles: heat for reduction of oxides 69–72%, losses with exhaust gases 4–9%, heat carried away by metal 4–6% and slag 0.2–0.3%, heat losses by masonry of the furnace and through the casing 2–4%, heat loss through the top of the furnace 9–12% and with cooling water 1–5%, electrical losses 10%.

After the mold is filled with silicon, which is continuously discharged from the furnace, the melt crystallizes. Then, the ingot is crushed, the slag is separated, and the finished products are sent to the consumer. In some plants, silicon is released into carbonaceous molds, where it settles to separate slag. Release can be carried out in settlers with refining the melt from aluminum and calcium impurities by blowing gases (chlorine, oxygen, argon). Silicon is also refined in heated ladles with fluxes from alkali metal salts (NaCl, Na₃AlF₆, etc.). In the process of refining, the aluminum content decreases from 0.30–0.45 to 0.10–0.20% and calcium from 0.6–1.0 to 0.2–0.4% and the amount of slag, oxide and carbide inclusions. During silicon smelting, 3–8% of slag is formed from the mass of the alloy of the following composition, %: 30–50 SiO₂; 10–30 Si; 8–15 SiO; 10–40 SiC; 0.5–1.0 Fe₂O₃; 12–15 Al₂O₃; 20–30 CaO. This slag can be used for the deoxidation of steel in a furnace, ladle or molds, as well as in the smelting of ferroalloys with silicon.

Features of silicon smelting technology in a direct current arc furnace. The technology of smelting silicon, as well as other ferroalloys in ore-smelting electric furnaces with alternating current, along with many positive parameters, has some drawbacks, which is associated with a number of specific effects characteristic of using a three-phase system of high alternating currents.

Table 4.5 Chemical composition of crystalline silicon, %

Smelter	Si	Fe	Al	Ca	Mg
1	98.3–97.5	0.54–0.84	0.52–0.66	0.39–0.70	0.01–0.05
2	99.20–97.84	0.39–0.80	0.25–0.45	0.32–0.54	0.01–0.012
3	99.06–98.98	0.27–0.40	0.25–0.30	0.30–0.38	n/a

Among the main ones, the inductive resistance of individual conductors and the entire electric furnace circuit with respect to active resistance is of great importance. With alternating current, in the presence of inductive resistance, the current and voltage do not coincide in phase, and therefore, the active power P_a entering the furnace is

$$IP_a = UI \cos \varphi.$$

In this case, the power factor

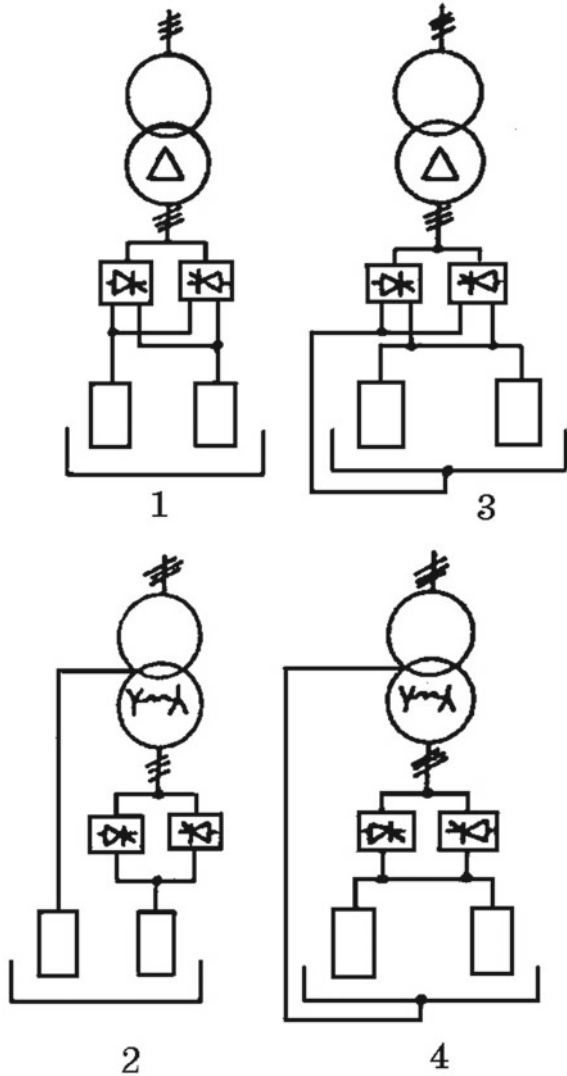
$$\cos \varphi = \frac{P_a}{UI} = \frac{r}{z} = \frac{r}{\sqrt{r^2 + x^2}},$$

where r is the active electrical resistance of the conductor; x is the inductive resistance. In this connection, the natural coefficient of electric power of medium-power arc ferroalloy furnaces is 0.80–0.85, and for furnaces of large unit capacity (20–30 MV A), it decreases to 0.6–0.7. In furnaces operating on alternating current, the surface effect and the proximity effect of the location of the short-circuit conductors cause additional losses of electrical energy, which are supplemented by electromagnetic energy losses in the metal structures surrounding the alternating current conductors. The smelting of silicon and other ferroalloys, regardless of the type of current (AC or DC), is carried out with the working ends of the electrodes immersed in the charge. In the case of alternating current, charge conduction currents that are closed between the electrodes of various phases in the upper horizons of the furnace bath cause heating of the charge materials on the furnace top and worsen the gas-dynamic and electrical conditions of the furnace. When using alternating current, the electric arc extinguishes and ignites twice during the period, which reduces the stability of the arc discharge. The above and other disadvantages of using alternating current and, consequently, the operation of ore-smelting electric furnaces in the production of silicon, ferrosilicon and other ferroalloys led to extensive research and development work on the use of various rectifier circuits and the creation of furnaces and technology for smelting with direct current.

Figure 4.8 shows possible DC power schemes for a two-electrode ore-reduction furnace for silicon smelting at OJSC ZALK. The circuit implemented during the reconstruction of the furnace consists of two rectifier units, each of which consists of a transformer unit and a reversible rectifier structurally combined with it. The power source of the combined *thyristoformer*-type furnace made it possible to compactly place the electric furnace in the same production areas of the existing workshop as the alternating current furnace.

As follows from Fig. 4.8, the furnace's power supply is possible both according to the scheme with voltage supply between the electrodes and according to the scheme of independent supply of each electrode from its rectifier. A carbon hearth is created in the furnace, and the electrical leads are connected using a copper current lead to the leads of the rectifier.

Fig. 4.8 Power circuits for direct current power supply of a single-phase two-electrode furnace with a capacity of 6.5 MV A for silicon smelting: 1–4—various schemes for connecting the electrodes to the furnace transformer



A single-phase, two-electrode furnace on rectified electric current for silicon smelting was commissioned in 1997 at OJSC ZALK with an oval bath, and the technical characteristics of this furnace are as follows:

Active power, MW	6.4
Supply voltage, kV	10
Diameter of electrodes, mm	710
Type of electrodes	graphitized
Capacity, t/year	4000

The power supply of the furnace according to the “electrodes—hearth” scheme provides greater efficiency of power distribution in the furnace bath compared to alternating current. The advantages of direct current furnace operation: The specific consumption of expensive graphitized electrodes is reduced by 15–20%, the specific energy consumption is reduced by reducing reactive power, conditions are created to reduce scarce wood chips, and the quality of marketable silicon is improved, improving working conditions for staff.

The cost estimate of the efficiency of resource savings in the smelting of silicon in a DC furnace is a 5–15% reduction in the cost of silicon, taking into account the depreciation of the additional costs of reconstruction of the furnace as a whole.

4.5 The Technology of Silicon Carbide Production

Silicon carbide (carborundum)—SiC is widely used as an artificial abrasive material with high microhardness. An abrasive tool made of silicon carbide is used in the metalworking and metallurgical industries to clean metal products. High thermal and chemical resistance allows it to be used for the manufacture of refractories. In combination with aluminosilicate fibers, SiC and SiO₂ are part of composite materials. In the electrometallurgy of silicon and silicon ferroalloys, carborundum is also of interest as an intermediate product in the complex physicochemical process of smelting silicon of technical purity, silicocalcium, ferrosilicon, silicoaluminium and other silicon-containing ferroalloys.

In nature, silicon carbide is found in the form of the mineral moissanite (SiC), which was discovered in the Irkutsk region in 1956 and in the sands of the Dnieper-Donets Depression in 1965. The density of SiC is 3.22 g/cm³, the decomposition temperature is 2880 K, the heat of formation $\Delta H_{298}^{\circ} = 66.16$ kJ/mol. Artificial silicon carbide is obtained by reduction of SiO₂ with carbon



Reaction start temperature ($\Delta G_T^{\circ} = 0$) 1725 K at $p_{\text{CO}} = 100$ kPa.

Distinguish between black and green carborundum. Both types of industrial product are obtained in electric resistance furnaces, in which the working resistance is a layer of coke and the mixture itself, consisting of carbonaceous reducing agent and silica sand.

At high temperatures, Al₄SiC₄ can dissociate with the formation of SiC, Al_g and C_s. The vapor pressure Al_g over the Al₄SiC₄–SiC–C_s system depends on temperature according to the expression $\lg p(\text{Pa}) = -1856/T + 12,143$.

To obtain green silicon carbide, sodium chloride is added to the mixture, which reduces the harmful effect of some charge impurities. Alumina has a harmful effect in quartz sand. Therefore, quartz sands are thoroughly washed. However, it is possible that the remaining clay sticks, as well as the ashes of reducing agents under reducing conditions, can form complex carbides of the type Al₄SiC and Al₄CSi₄, which have

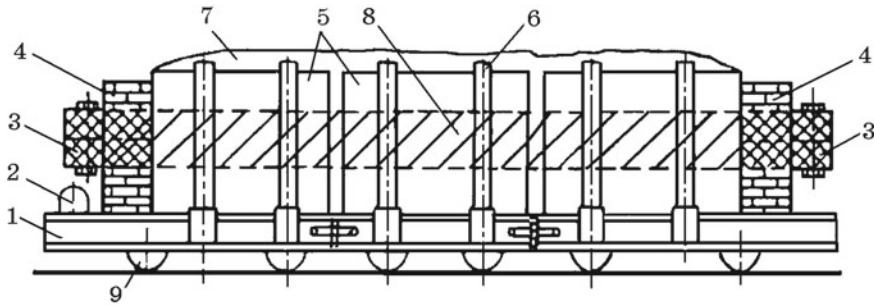


Fig. 4.9 Self-propelled resistance electric furnace for silicon carbide production. 1—trolley; 2—the mechanism of movement of the furnace; 3—current lead assembly; 4—end walls; 5—removable shields; 6—persistent racks; 7—charge; 8—core; 9—wheel sets

different stability. According to some data, the supposedly black color of industrial silicon carbide is due to the presence of aluminum. Salt eliminates this effect.

The unit capacity of the resistance furnace is 4000–4500 kV A. The furnace is a self-propelled platform, at the ends of which there are current-carrying carbon electrodes. Return to the bottom of the platform, quartz sand, and then lay out core from lump of petroleum coke, which is the working resistance in the initial period of the process. A reaction mixture is poured on top of the core (Fig. 4.9). Below is the specific consumption of charge materials and electricity in the production of black (numerator) and green (denominator) silicon carbide:

Consumption of materials, kg/ t:

quartz sand	1750/2000
anthracite	900/700
petroleum coke	300/600
wood sawdust	170/370
salt (NaCl)	—/230
Electricity consumption, kWh/t	8200/10000

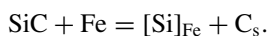
Quartz sand should be used pure by impurities (99.6% SiO₂; 0.3% FeO; 0.07% Al₂O₃; 0.04% CaO; 0.03% MgO; 0.02% TiO₂). As a reducing agent, only low-ash carbon materials can be used: anthracite (3% ash, 93% of C_s); petroleum coke (0.8% ash, 94% St, 5% volatiles, 3% moisture). 50–65 tons of the charge and 3200–4500 kg of core are loaded into the furnace, and then, it is connected to the furnace transformer. The process of producing carborundum is controlled mainly by the consumption of electricity.

For a furnace with an installed transformer capacity of 3.5 MW, the process is considered complete if the energy consumption is 65–70 MWh. The furnace is cooled for 24–32 h, and then, its contents are disassembled. The composition of the products is given in Table 4.6.

Table 4.6 Chemical composition of the products of green carborundum, %

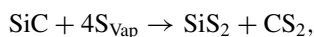
Product	Si	SiO ₂	SiC	Al ₂ O ₃	Fe ₂ O ₃
SiC (lumps)	0.17	0.12	97.82	0.92	0.48
Amorphous	0.16	9.21	71.54	0.78	0.82
Splices	–	13.45	70.11	1.33	0.69
Charge	–	45.40	11.14	0.30	0.55
Siloxicon	–	35.14	36.50	3.60	0.52
Cakes	–	42.14	5.32	0.58	0.41
Product	CaO	MgO	C	NaCl	LOI
SiC (lumps)	0.30	0.26	–	–	–
Amorphous	0.74	0.47	15.15	0.55	0.50
Splices	4.60	0.26	0.03	0.46	–
Charge	1.00	0.47	31.50	8.78	0.80
Siloxicon	2.30	0.30	14.65	6.98	–
Cakes	0.35	0.19	19.50	20.0	–

Lump SiC is sent for further processing to obtain abrasive grains of various classes, and “splices” containing up to 70% SiC are used in the smelting of ferrosilicon, in the production of refractory masses, as part of carbon masses for self-baking electrodes and other purposes. Silicon carbide introduced into the charge for smelting ferrosilicon is relatively easily destroyed by metallic iron by the reaction:



This reaction can proceed until the silicon content in the alloy reaches 23–24% with the formation of silicocarbide $\text{Fe}_5\text{Si}_3\text{C}_x$, which is in equilibrium with silicon carbide.

The industrial production of silicon carbide is accompanied by the release of a large volume of gaseous products of chemical reactions. In accordance with the design of the furnace and the method of loading CO, the $\text{SiO}_2 + 3\text{C} = \text{SiC} + 2\text{CO}$ formed by the reaction should burn out to CO_2 . However, for some reasons, incomplete oxidation of CO to CO_2 takes place, and part of the CO enters the environment. Sulfur contained in carbon reducing agents passes into the gaseous phase in the form of various compounds. At $t > 900^\circ\text{C}$, SiC can interact with sulfur vapors by reaction



as well as with halogens to form harmful compounds.

The above requires the creation of systems for collecting and cleaning dust and gas emissions, which is implemented in industry.

References

1. Esin OA (1974) Equations of the polymer model of molten silicates in the approximation of regular solutions. *Russ J Inorg Chem* 48(2108) (in Russian)
2. Klevan OS, Engh TA (1995) INFACON 7. pp 441–450
3. Ryabchikov IV (1966) Thermodynamic study of the Si–O–C system at high temperatures. *Russ Metall (Metally)* 2:14–19 (in Russian)
4. Tolstoguzov NV (1992) Theoretical fundamentals and technology of melting of silicon and manganese alloys. *Metallurgiya, Moscow* (in Russian)
5. Tolstoguzov NV (1990) Diagram of the Fe–Si–O–C System. *Izvestiya VUZov. Ferrous Metall* 12:14–18 (in Russian)
6. Gasik MM, Gasik MI (2010) Thermodynamic analysis of the dominant phase equilibria in M(Si, Cr, Al)–O–C Systems. *Russ Metall (Metally)* 2010(6):548–556 (in Russian)

Chapter 5

Metallurgy of Ferrosilicon



5.1 Assortment, Microstructure and Properties of Ferrosilicon

Ferrosilicon assortment. Ferrosilicon is a large group of alloys of the iron–silicon system and is intended for deoxidation and alloying of steel. It is widely used in the foundry industry in the production of castings from iron and steel. In accordance with Russian Standard GOST 1415-78, 20 grades of ferrosilicon can be produced taking into account the functional purpose of each grade (Table 5.1).

So, for example, an alloy of the FS75 (el.) grade is intended for alloying electrical steel; FS20 (I), FS45 (I), FS65 (I) and FS75 (I)—for use in the manufacture of cast products.

In 1993, the State Standard of Russia and the Interstate Council for Standardization, Metrology and Certification adopted the ferrosilicon standard (GOST 1415-93) by direct application of the ISO 5445-80 standard. In Russia, GOST 1415-93 was put into effect directly as the state standard of the Russian Federation from 01.01.1997 (Table 5.2).

GOST 1415-93 also recommended the branded and chemical compositions of ferrosilicon with the accepted international designation of alloy grades from FeSi10 to FeSi90A12 (Table 5.3).

In accordance with the Ukrainian standard DSTU 4127-2002 (Table 5.4), nine grades of ferrosilicon can be produced from FS10 (8–14% Si) to (inclusive) FS90 (87–95% Si).

The standard Ukrainian DSTU 4197-2002 permits the production and supply of ferrosilicon in accordance with the international standard ISO 5445: 1980 (Table 5.4).

Fe-Si system. Silicon belongs to ferrite-forming elements and therefore narrows the γ -Fe region (Fig. 5.1). The maximum solubility of silicon in γ -Fe is 1.63% Si. The biphasic region ($\alpha + \gamma$) extends to 1.94% Si. There are a number of silicides in the Fe-Si system: Fe₃Si (14.28% Si), Fe₂Si (20.0% Si), Fe₅Si₃ (23.18% Si), FeSi (33.46%) and FeSi₂ (50.15% Si).

Table 5.1 Chemical composition, %, ferrosilicon (GOST 1415-78)

Grade	Si	C	S	P	Al	Mn	Cr	Ti	Cs
		No more							
1	2	3	4	5	6	7	8	9	10
FS92	No less 92	–	0.02	0.03	2.5	0.2	0.2	–	0.5
FS90	No less 89	–	0.02	0.03	3.5	0.2	0.2	–	–
FS90A2,5	No less 89	0.1	0.02	0.03	2.5	0.2	0.2	–	–
FS75	Over 74 to 80	–	0.02	0.05	–	0.4	0.4	–	–
FS75A2,5	Over 74 to 80	–	0.02	0.05	2.5	0.4	0.3	–	–
FS75(f)	Over 74 to 80	0.1	0.02	0.04	1.5	0.3	0.3	–	–
FS75(e)	Over 74 to 80	0.1	0.02	0.04	0.1	0.3	0.2	0.05	0.1
FS70	68–74	–	0.02	0.05	2.0	0.4	0.4	–	–
FS70A1(e)	68–74	0.1	0.02	0.04	1.0	0.3	0.3	0.1	–
FS70(e)	68–74	0.1	0.02	0.04	0.1	0.3	0.3	0.04	0.1
FS65	63–68	–	0.02	0.05	2.5	0.4	0.4	–	–
FS65A2	63–68	–	0.02	0.05	2.0	0.4	0.4	–	–
FS65(f)	63–68	0.1	0.02	0.04	1.6	0.4	0.4	–	–
FS65(e)	63–68	0.1	0.02	0.04	1.2	0.3	0.03	0.05	0.5
FS45	41–47	–	0.02	0.05	2.0	0.6	0.5	–	–
FS45(f)	41–47	0.2	0.02	0.05	1.5	0.6	0.5	–	–
FS25	23–27	0.6	0.02	0.06	1.0	0.8	1.0	–	–
FS25U0,8	23–27	0.8	0.02	0.06	1.0	0.9	1.0	–	–
FS20	20–23	1.0	0.02	0.10	1.0	1.0	–	–	–
FS20(f)	19–23	1.0	0.02	0.20	1.0	1.0	0.3	–	–

Note In the designation of ferrosilicon brands, lowercase letters indicate the main purpose: *f*—for foundry; *e*—for smelting electrical steel

Table 5.2 Grades and chemical composition of ferrosilicon in accordance with GOST1415-93

Grade	Mass fraction, %						
	Si	C	S	P	Al	Mn	Cr
		No more					
FS90	over 78 to 95	0.1	0.02	0.03	3.5	0.3	0.2
FS75	» 74 » 80	0.1	0.02	0.04	3.0	0.4	0.3
FS70	» 68 » 74	0.1	0.02	0.04	2.0	0.4	0.4
FS70A1	» 68 » 74	0.1	0.02	0.04	1.0	0.3	0.3
FS65	» 63 » 68	0.1	0.02	0.05	2.5	0.4	0.4
FS50	» 47 » 52	0.1	0.02	0.05	1.8	0.6	0.5
FS45	» 41 » 47	0.2	0.02	0.05	2.0	1.0	0.5
FS25	» 23 » 29	0.8	0.02	0.06	1.0	1.0	0.8
FS20	» 19 » 23	1.0	0.02	0.10	1.0	1.0	0.8

Table 5.3 Grades and chemical composition of ferrosilicon according to ISO 5445: 1980

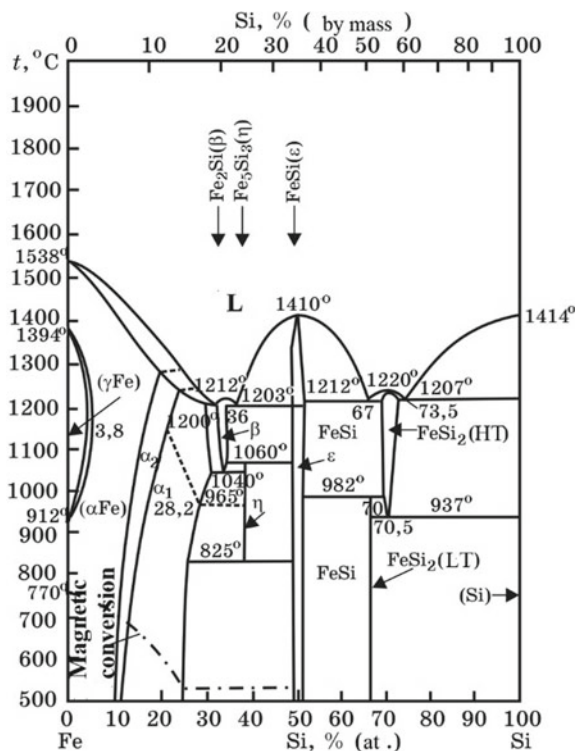
Grade	Mass fraction of the element, %										
	Silicon		Aluminum		Phosphorus	Sulfur	Carbon	Manganese ^a	Chromium ^a	Titanium ^a	
	More	Up to and including	More	Up to and including							
FeSi10	8.0	13.0	-	0.2	0.15	0.06	2.0	3.0	0.8	0.30	
FeSi15	14.0	20.0	-	1.0	0.15	0.06	1.5	1.5	0.8	0.30	
FeSi25	20.0	30.0	-	1.5	0.15	0.06	1.0	1.0	0.8	0.30	
FeSi45	41.0	47.0	-	2.0	0.05	0.05	0.20	1.0	0.5	0.30	
FeSi50	47.0	51.0	-	1.5	0.05	0.05	0.20	0.8	0.5	0.30	
FeSi65	63.0	68.0	-	2.0	0.05	0.04	0.20	0.4	0.4	0.30	
FeSi75A11	72.0	80.0	-	1.0	0.05	0.04	0.15	0.5	0.3	0.20	
FeSi75A11,5	72.0	80.0	1.0	1.5	0.05	0.04	0.15	0.5	0.3	0.20	
FeSi75A12	72.0	80.0	1.5	2.0	0.05	0.04	0.20	0.5	0.3	0.30	
FeSi75A13	72.0	80.0	2.0	3.0	0.05	0.04	0.20	0.5	0.5	0.30	
FeSi90A11	87.0	95.0	-	1.5	0.04	0.04	0.15	0.5	0.2	0.30	
FeSi90A12	87.0	95.0	1.5	3.0	0.04	0.04	0.15	0.5	0.2	0.30	

^aThe maximum values shown are for information only

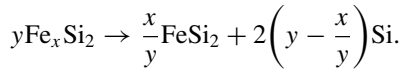
Table 5.4 Chemical composition of ferrosilicon DSTU 4127-2002

Alloy grade	Mass fraction of the element, %						
	silicon	C	S	P	Al	Mn	Cr
		No more					
FS90	from 87 to 95 incl.	0.2	0.02	0.04	3.5	0.5	0.2
FS75	over 74 » 80 »	0.2	0.02	0.05	3.0	0.5	0.5
FS70	» 68 » 74 »	0.2	0.02	0.05	2.5	0.5	0.5
FS65	от 63 » 68 »	0.2	0.02	0.05	2.5	0.5	0.5
FS45	» 41 » 47 »	0.2	0.02	0.05	2.0	1.0	0.5
FS25	over.23 » 29 »	0.8	0.02	0.10	1.0	1.0	0.8
FS20	» 19 » 23 »	1.0	0.02	0.10	1.0	1.0	0.8
FS15	» 14 » 19 »	1.5	0.02	0.15	1.0	1.5	0.8
FS10	from 8 » 14 »	2.0	0.02	0.15	0.2	3.0	0.8

Note The letters and numbers in the designation of the brand of ferrosilicon mean: FS—ferrosilicon; numbers following letters—mass fraction of silicon

Fig. 5.1 State diagram of the Fe-Si system

Bisilicide FeSi_2 exists in two versions: high-temperature FeSi_2 (HT) in the range of 937–1220 °C and low-temperature FeSi_2 (LT) below 937 °C. High-temperature modification is a non-stoichiometric compound that exists in a certain range of silicon concentration. In the literature, this silicide is described by the formula $\text{FeSi}_{2,3}$, i.e., as a phase with excess silicon. Precision studies performed in the 90s found that bisilicide is a compound with a deficiency of iron atoms, i.e., Fe_xSi_2 , which at 937 °C is eutectoid converted to stoichiometric silicide FeSi_2 and silicon by reaction



Thermodynamic properties of alloys of the Fe-Si system. Thermodynamic properties of liquid and solid alloys of the Fe-Si system by combining the Knudsen effusion method and mass spectrometry in the temperature range 1078–1509 °C and a composition range of 9.2–82.2 at. % Fe were studied in [1].

The vapor pressure of iron and silicon over alloys was measured, the chemical compositions of which corresponded to the concentration regions of two-phase equilibria: Fe_2Si (20 at.% Si) + FeSi (33.3 at.% Si), FeSi (33.3 at.% Si) + FeSi_2 (50 at.% Si), as well as temperature–concentration fields of equilibrium of silicide with liquid.

It has been established that *associative reactions* occur in melts of the Fe-Si system in a wide range of chemical composition with the formation of liquid Fe_3Si groups; Fe_2Si ; FeSi and FeSi_2 . For these groups, the calculated values ΔH_T° and S_T° :

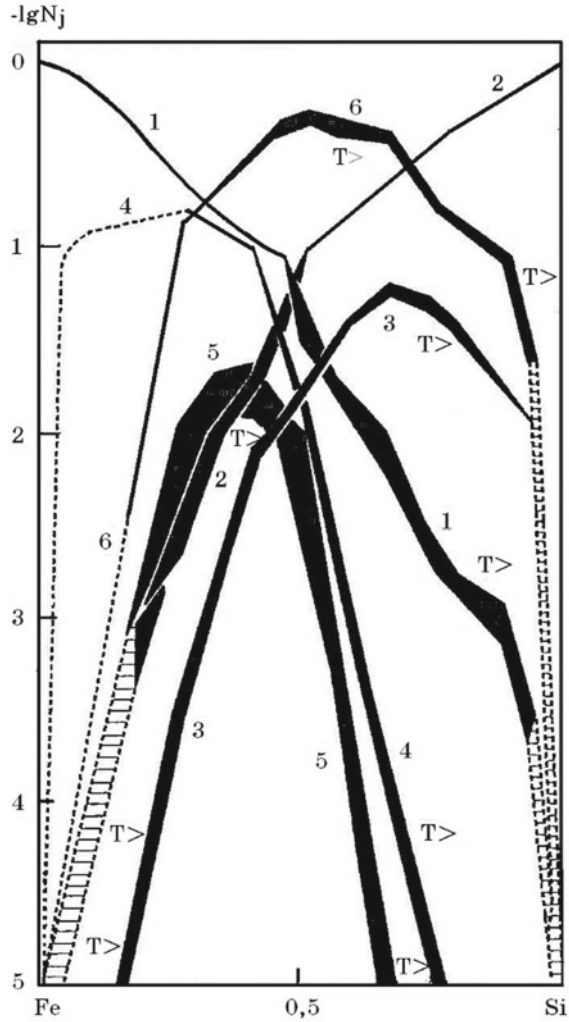
Grouping	$-\Delta H_T^\circ$, J/mol	S_T° , J/(mol·K)
Fe_3Si	143,673	28.63
Fe_2Si	110,360	16.28
FeSi	99,814	23.70
FeSi_2	101,345	29.37

With an increase in the atomic fraction of silicon in the composition of the Fe-Si system melts, the concentration of conditionally “free” silicon increases (Fig. 5.2, curve 2), while the “free” iron decreases (curve 1).

With a change in the atomic fraction of silicon in the groups (associates) $[\text{Fe}_x\text{Si}_y]$, non-monotonic dependences are observed with maxima of their concentrations at certain atomic ratios of silicon and iron. Moreover, the thermodynamic stability of groups (associates, clusters) is different and it is accepted proportional to the maximum concentration of clusters. For 1600 °C, the thermodynamic strength of the $[\text{FeSi}]$, $[\text{Fe}_3\text{Si}]$, $[\text{FeSi}_2]$ and $[\text{Fe}_5\text{Si}_3]$ clusters correlates as 17.2:6.6:1.9:1.0, respectively. The most thermodynamically stable (strong) are clusters of congruently melting (without decomposition) chemical compound (monosilicide) FeSi .

The activity of silicon in melts of the Fe-Si system increases with increasing silicon concentration, which is illustrated by the data in Fig. 5.3. With an increase in the activity of silicon, the activity of iron decreases. The intersection of the a_S and

Fig. 5.2 Melt composition Fe-S: 1—[Fe]; 2—[Si]; 3—[FeSi₂]; 4—[Fe₃Si]; 5—[Fe₅Si₃]; 6— [FeSi]. The sign “T>” corresponds to the area of composition change $T = 2003$ K; the other border ($T = 1873$ K) is not indicated

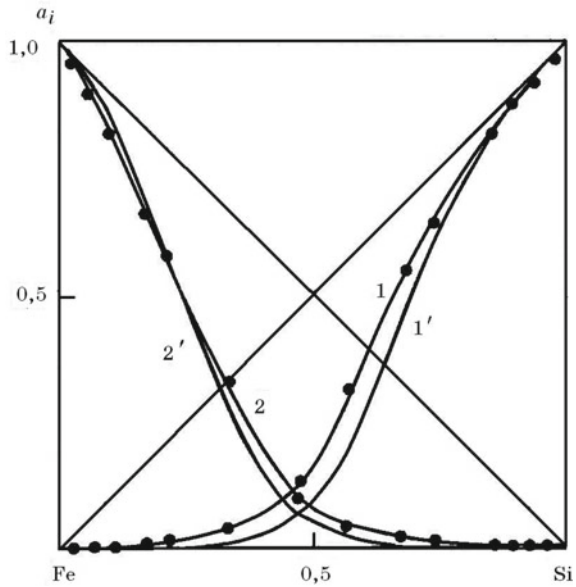


a_{Fe} lines corresponds to the atomic concentration of silicon in the 0.48 alloy, and not to the eutectic composition.

The thermodynamic functions $\Delta G_T^0(T)$ of iron silicide formation reactions were calculated in [2] using the following equations (in J/mol):

$$\begin{aligned}\Delta G_T^0(\text{Fe}_2\text{Si}) &= -129028 + 2.52T, \\ \Delta G_T^0(\text{FeSi}) &= -163132 + 1.79T, \\ \Delta G_T^0(\text{FeSi}_2) &= -121842 + 7.18T.\end{aligned}$$

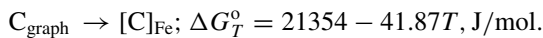
Fig. 5.3 Activities of silicon a_{Si} and a_{Si}' and iron a_{Fe} and a_{Fe}' in solutions of the Fe-Si system at 1600 °C; a_{Si} and a_{Fe} —calculated; a_{Si}' and a_{Fe}' —experimental data



The change in the integral and partial excess Gibbs energies of the melts of the Fe-Si system depending on the molar concentration of silicon is shown in Fig. 5.4.

Figure 5.4 confirms that silicon and iron form thermodynamically strong compounds (silicides in the solid state) and associates (in the liquid state), which is accompanied by a decrease in the activity of silicon in industrial ferrosilicon and improves the thermodynamic conditions for the reduction of silicon from silica by carbon in the presence of iron.

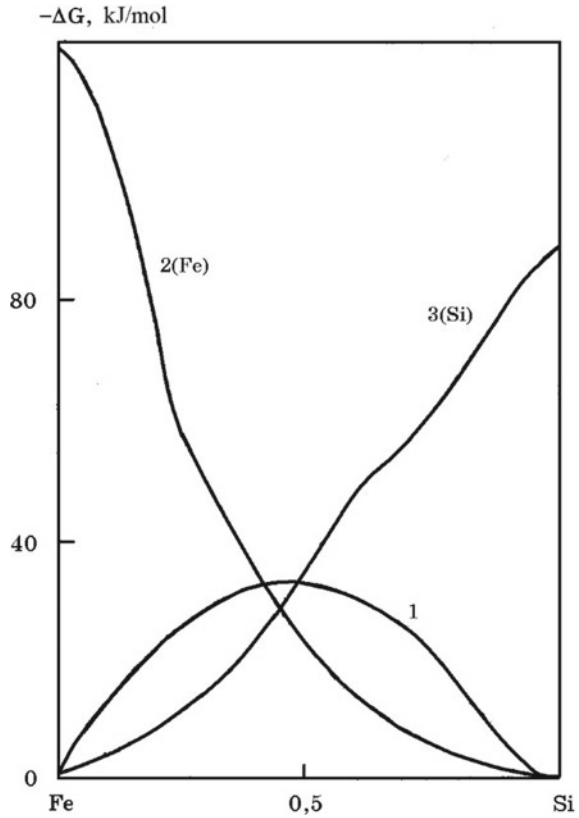
Fe-Si-C system (Fig. 5.5). The solubility of carbon in pure iron depends on temperature $[\%C]_{Fe} = 1.30 + 2.5 \times 10^3 t, \text{ } ^\circ\text{C}$. The process of graphite dissolution in iron is characterized by a change in Gibbs energy:



The addition of silicon to a saturated iron–carbon melt reduces the solubility of carbon in it in a complex manner. In the range of silicon concentrations 0–23.18% Si, the $[\%C] = f [\%Si]$ bond is close to straight (Fig. 5.5). At a silicon content corresponding to Fe_5Si_3 silicide, a bend is marked on the curve. With a further increase in the silicon concentration in the alloy, the curve section asymptotically approaches the axis of silicon concentrations. Alloys with 0–23.18% Si are in equilibrium with pure graphite, and with a higher silicon content, they are in equilibrium with silicon carbide.

The effect of silicon on the solubility of carbon in alloys of the Fe-Si system is reflected in the standards for ferrosilicon (Tables 5.1, 5.2, 5.3 and 5.4). The solubility of carbon in alloys of the Fe-Si system increases with increasing temperature. Alloys

Fig. 5.4 Integral 1 and partial 2(Fe), 3(Si) excess Gibbs energies of solutions of the Fe-Si system at 1600 °C

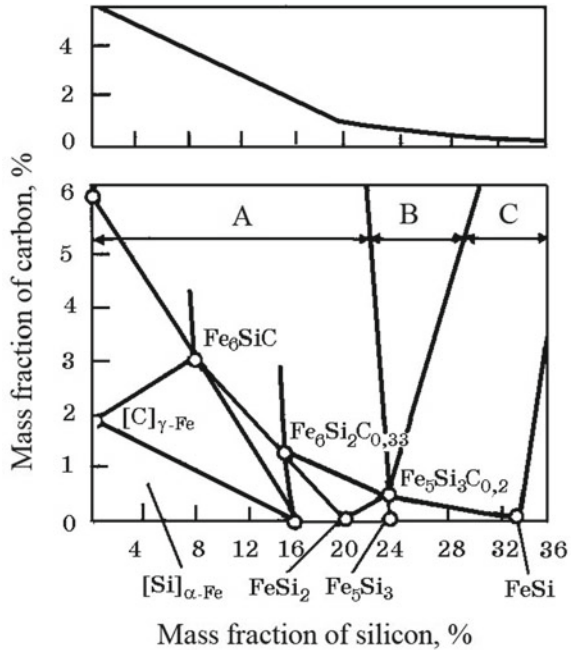


of various grades released from the furnace have a relatively high temperature (1600–1800 °C). In the process of lowering the temperature of the alloy in the ladle in liquid ferrosilicon, the solubility of carbon decreases, which leads to the release of graphite in alloys containing up to 22–24% Si, or silicon carbide in alloys with a silicon content of more than 22–24%. To improve the floating conditions of the precipitated particles of graphite or silicon carbide, liquid ferrosilicon is kept in a ladle before casting.

5.2 Geometric Parameters of Bath and Electrical Characteristics of Electric Furnaces for Ferrosilicon Smelting

Ore-smelting furnaces, unlike steelmaking furnaces, are characterized not by the capacity of liquid metal, but by the electric power of furnace transformers.

Fig. 5.5 Influence of the mass concentration of Si on the solubility of carbon in Fe-Si_{sat} alloys equilibrium with graphite (region A), graphite and silicon carbide (region B) and silicon carbide (region C), at 1760 °C



The net power of the ferroalloy arc furnace (P_n) is calculated by the expression $P_n = (GW)/(365 \cdot 24 K_t K_{max})$, where G is the specified furnace capacity, t/year; W —specific energy consumption for the smelting of this type of ferroalloys, kWh/year; 365·24—the number of hours per year, h; K_t —coefficient of use of calendar time (take $K_t = 0.80-0.95$); K_{max} —utilization of the maximum power of the furnace.

The full power of the furnace transformer is called the *rated power* (S_r). The full operating power of the furnace transformer S is defined as $S = 3 \cdot I_{el} \cdot U_1$ and characterizes the load on the supply network. The power introduced into the furnace bath is called active power and is denoted by P_a . Active power is always lower than the full operating power by the value of the power factor $\cos\varphi$, less than unity and $\cos\varphi$ the less, the greater the rated power of the furnace transformer and, therefore, the geometric parameters of the furnace bath. The lack of reliable theoretical methods for determining the geometric parameters of ore-smelting furnace forces them to be selected by analogy with well-functioning furnaces according to empirical formulas. The main parameters characterizing the OSF bath (working space) are the diameter of the electrode, the diameter of the electrodes cycle, the diameter and depth of the bath. Of these, most attention is traditionally paid to the diameter of the electrodes cycle; it is believed that possible errors in determining the remaining parameters can be easily eliminated by changing the design of the lining and the level of the top. In [3], data were analyzed on the influence of such parameters on the active power of furnaces using 118 ore-smelting furnaces of various ferroalloy plants as an example. The following are the results obtained in this work.

The diameter of the electrodes. First, it can be noted the good agreement between the change in the diameter of the electrodes D_e of the ore-smelting furnace with the dependence $D_e-S^{1/3}$ (where S is the nominal installed power of the furnace transformer, $MV \cdot A$), which follows from the theory of similarity. The same dependence can be obtained in another way, namely from the thermal balance of the electrode. The condition of thermal equilibrium is observed when the powers are equal: the power released by the electrode during the passage of current and the power transmitted by the electrode to the environment

$$4\rho I_e^2 k_a / \pi D_e^2 = q\pi D_e, \quad (5.1)$$

where from

$$D_e = [4\rho I_e^2 k_a / \pi^2 q]^{1/3} = G(\rho I_e)^{1/3}; \quad D_e \sim \rho^{1/3}. \quad (5.2)$$

where ρ is the electrical resistivity of the electrode material; q is a coefficient characterizing the density of the heat flux of heat transfer from a unit of its surface; I_e is the current in the electrode; k_a is the coefficient of increase in the active resistance of the electrode when the furnace is supplied with alternating current. If we take into account that the active net power $P_n = \cos\varphi S\eta$ (here η is the electrical efficiency), then for $\cos\varphi\eta = \text{const}$ the dependence $D_e-S^{1/3}$ is observed. Numerical processing of the data shown in Fig. 5.6 gives:

$$D_e = 466 S^{1/3}. \quad (5.3)$$

Electrode cycle diameter. The current spreading in the ore-smelting furnace bath is possible in several ways: electrode–electrode according to the “triangle” scheme, electrode–hearth and electrode–conductive lining of the walls according to the “star” scheme. The diameter of the electrodes cycle D_c should be chosen so that the main part of the power introduced into the bath is allocated under the ends of the electrodes (current spreading according to the “star” electrode scheme is under), i.e., observance of conditions $E_{e,e} < E_{e,h}$, where $E_{e,e}$ and $E_{e,h}$ —average electric field strengths in the areas of the electrode–electrode and electrode–hearth, respectively. Given the geometry of the bathtub of round three-electrode furnaces, we can write:

$$\begin{aligned} U_{e,h}/h_0 &> U_{e,e}/[D_c \cos(\pi/6) - D_e], \\ U_p/h_0 &> 3^{1/2}U_p/[D_c \cos(\pi/6) - D_e]. \end{aligned} \quad (5.4)$$

where $U_{e,h}$, $U_{e,e}$, U_p —voltage at the electrode–hearth, electrode–electrode sections and phase voltage, respectively, where from

$$\begin{aligned} D_c &\geq (3^{1/2}h_0 + D_e)/\cos(\pi/6), \\ D_c &\geq (2.55 - 2.95)D_e, \end{aligned} \quad (5.5)$$

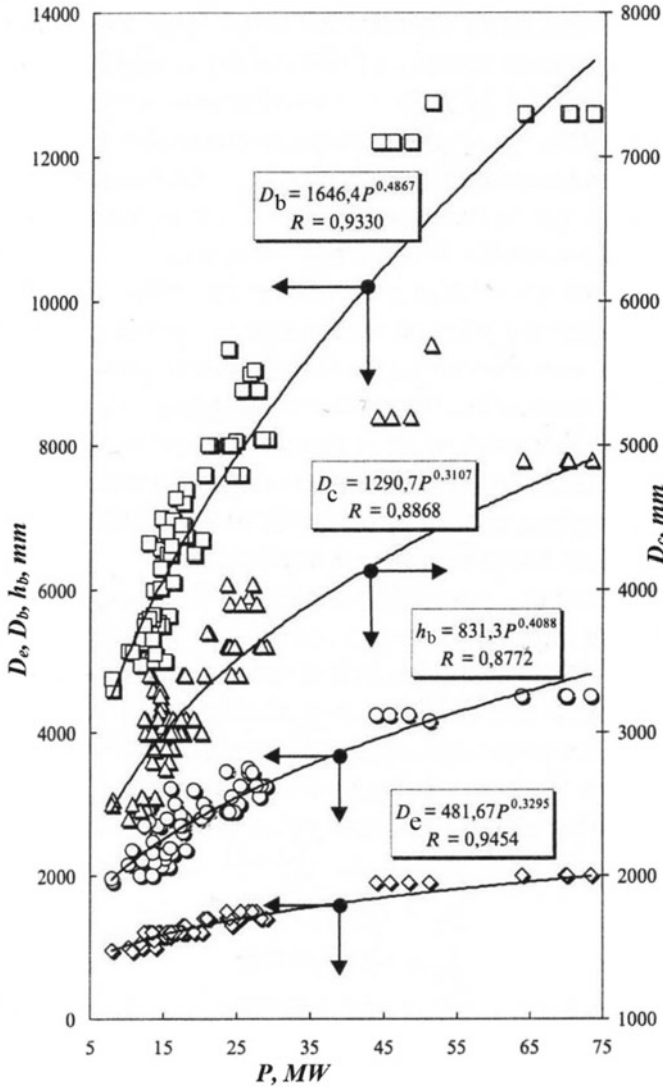


Fig. 5.6 Correlation between the geometric parameters of bathtubs of ferroalloy furnaces and their active power: points—actual data (\square — D_b , Δ — D_c , \circ — h_b , \diamond — D_e); lines—regression curves

where h_0 is the distance from the end of the electrode to the hearth; in inequality (5.5), it is taken into account that in order to ensure the normal operation of the ore-smelting furnace, h_0 must be chosen within the limits of $(0.7-0.9)D_e$.

Larger values of D_c/D_e are characteristic for closed furnaces, lower values—for open ones. The value of h_0 is taken for furnaces smelting silicon alloys; for furnaces operating with a slag process, in view of the structural features of their working

space (a large proportion of the lined part of the electrode is placed in the slag, whose electrical resistivity is higher than that of a heated mixture), the inequality $E_{e,e} < E_{e,h}$ is satisfied when $h_0 = (1.2-1.4)D_e$.

Since the thermal situation of the periphery of the bath has little effect on the temperature field of the reaction zones where the bulk of the furnace current flows, the dependence of the diameter of the electrodes cycle on the power of the transformer should be weak.

Based on the above considerations, the following formula was proposed for determining the reduced diameter of the electrodes cycle:

$$D_c/D_e = 2.4S^{1/20}. \quad (5.6)$$

Numerical processing of the data shown in Fig. 5.6 gives:

$$D_c/D_e = 2.236S^{0.049}. \quad (5.7)$$

Bath diameter. In contrast to the diameter of the electrodes cycle, the diameter of the bath should substantially depend on the power of the furnace transformer. Indeed, while maintaining the numerical values of the specific volumetric capacities of the model and designed furnaces, the volumes of the working space in which these capacities are allocated grow as a cube of linear dimensions, and the heat-transfer surface of the periphery of the bath is proportional to the square of linear dimensions. It is also necessary to take into account the increase in the heat flux from the internal volumes of the bath into the environment. Therefore, with increasing furnace power, the relative diameter of the bathtub ((D_b/D_e)) should increase so as to ensure the creation of a skull layer:

$$D_b/D_e = 3.75S^{1/8} \quad (5.8)$$

The empirical dependence found (according to Fig. 5.6) has the form:

$$D_b/D_e = 3.717S^{0.125}. \quad (5.9)$$

Bath depth. Studying the influence of the degree of loading the bath with charge materials on the electrotechnological modes of operation of the furnace showed that the normal course of the technological process is ensured when choosing the depth of the bath (from the middle level of the top to the hearth) from the ratio:

$$H_b/D_e = (1.8 - 2.0)S^{1/30}. \quad (5.10)$$

It should be noted that relation (5.10) gives good results for small- and medium-power furnaces equipped with electrodes with a diameter of up to 1500 mm. For more powerful furnaces, the bath depth can also be selected from design considerations and the technical feasibility of trouble-free operation of large-diameter self-baking electrodes. The fact is that the formation and operation of such electrodes are a

complex scientific and technical task that has not yet received its final solution. The difficulties in the formation of large-diameter electrodes are mainly due to the fact that with an increase in the transverse dimensions of the coal block, the relative penetration depth of the alternating current flowing through the electrode decreases (therefore, the conditions for its formation worsen). So, with a specific electric resistance of 62–64 $\mu\Omega$, the depth of current penetration at a frequency of 50 Hz in the coking zone is 560–570 mm, which is less than half the electrode diameter for $D_e > 1200$ mm. Electrodes with a diameter of more than 1500 mm have a linear mass larger than 2.6 t/m (for a 1900 mm electrode—4.3 t/m) at $\sigma_e = 6.2\text{--}17.3$ MPa. Thus, for given electrode length l_e and distance from the lower edge of the electrical contact node to the average level of the top of the furnace l_t , the depth of immersion of the electrode in the charge $h_e = l_e - l_t$; having accepted the gap between the end of the electrode and the bottom $h_0 = (0.7\text{--}0.9) D_e$, we determine the depth of the bath:

$$H_b = h_e + h_0 \leq l_e + 0.9D_e. \quad (5.11)$$

For furnaces operating with a slag process, h_0 can be taken equal to $(1.0\text{--}1.1)D_e$, thus:

$$H_b \leq l_e - l_t + 1.1D_e. \quad (5.12)$$

The method by which the above equations are obtained is largely heuristic, at least in that part where it became necessary to justify the laws of development of the ore-smelting furnace as a technical object and to formulate a promising direction for improving their parameters and the conditions for terminating the search in the extremum region. The obtained dependences are unlikely to give a final solution to the problem of optimizing the geometric parameters of the furnaces, but along with this in the current situation they serve as a good working tool that can be used to create more reliable design methods for the construction and reconstruction of existing furnaces, moreover, a quite satisfactory agreement of the geometric parameters of well-functioning furnaces with the calculation according to formulas (5.3), (5.6)–(5.12) is observed.

At the very first stage, it seems logical to limit ourselves to identifying common correlations that can be useful and reliable in the sense that they are a generalization of the vast accumulated experience of real production. In essence, currently operating furnaces are the result of deliberate evolution, in the known sense of even “selective choice” according to the criterion of increasing their technical and economic indicators: perhaps it is impossible to find a single ferroalloy furnace from the presented sample that has retained its original “design” sizes. In the same way, it is difficult to detect two furnaces that are absolutely identical in geometric parameters (at a given power), which, on the one hand, reflects the most significant feature of any evolutionary process—its dynamism and incompleteness, at least with respect to objects of recent generations, and on the other hand, the lack of unity of opinion, which could be concentrated in the concept of a “well-functioning furnace” (a typical example of a fuzzy set), has already been noted. In fact, taking into account possible

and unavoidable for practical data variations, the statistical selection, including the geometric parameters of the baths of the existing ferroalloy furnaces, seems representative enough to ensure the reliability and correctness of the correlation dependencies obtained by regression analysis.

Since the energy introduced into the furnace bath is ultimately determined (and first of all) by the active power, it was reasonable to construct the correlation dependencies of the geometrical parameters of the baths on P (power) (Fig. 5.6). The regression equations obtained by statistical processing of the entire set of data (regardless of the type of smelted alloy) have the form:

$$D_b = 1646.4P^{0.4867}, \quad (5.13)$$

$$D_c = 1290.7P^{0.3107}, \quad (5.14)$$

$$H_b = 831.3P^{0.4088}, \quad (5.15)$$

$$D_e = 481.7P^{0.3295}. \quad (5.16)$$

To identify the features inherent in ferrosilicon-smelting furnaces, a “truncated” sample was also processed, including only ferrosilicon furnaces (Fig. 5.7). At the same time, the results concerning furnaces with transformers with a capacity of 33 and 63 MV•A, as well as the features of furnaces operating with a low level of the top, were taken into account. The correlation dependencies of the parameters of baths of ferrosilicon furnaces on active power are described by the following equations:

$$D_b = 1725.64P^{0.4782}, \quad (5.17)$$

$$D_c = 1184.8P^{0.337}, \quad (5.18)$$

$$h_b = 761.39P^{0.4305}, \quad (5.19)$$

$$D_e = 483.4P^{0.3257}. \quad (5.20)$$

A comparison of the corresponding correlation Eqs. (5.13)–(5.16) and (5.17)–(5.20) shows their insignificant differences (no more than 2% even for high-power furnaces), which indicates the possibility of choosing the geometric parameters of the furnace baths regardless of their specialization in the type of alloy to be smelted (at least within the range of variations for the fleet of furnaces in operation).

The ore-smelting furnace passport parameter, however, is the installed capacity of the furnace transformer S , and it seems necessary to choose the parameters of the furnace bath depending on this indicator. The relationship of the active power of the furnace with the installed power of the furnace transformer is illustrated in Fig. 5.8.

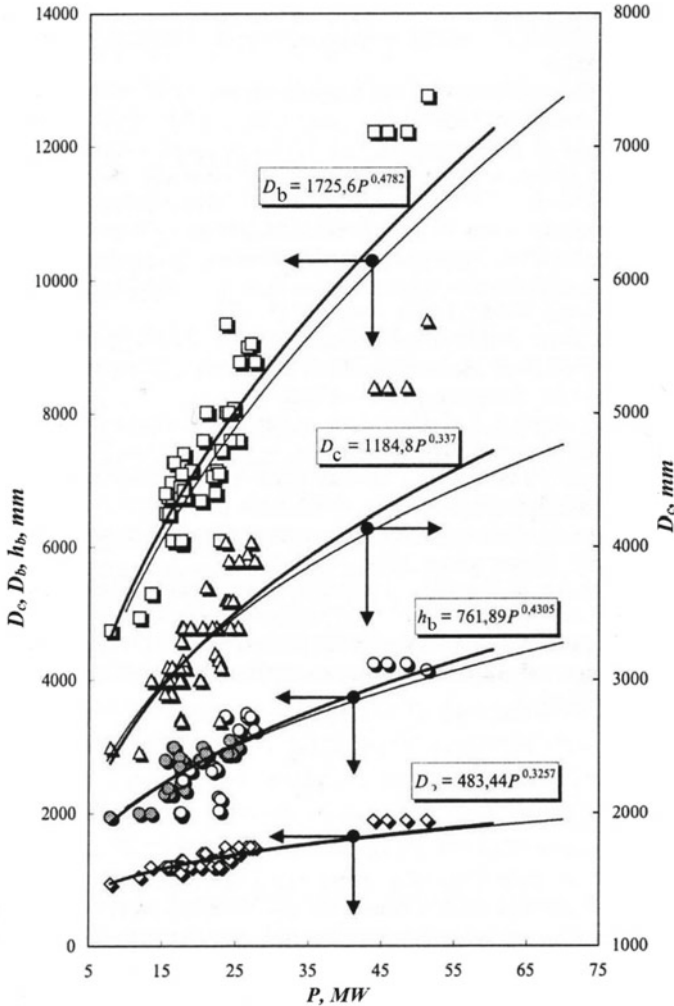


Fig. 5.7 Correlation between the geometric parameters of bathtubs of ferrosilicon furnaces with their active power: points—actual data (designations—according to Fig. 5.6); thin lines—regression curves according to (5.13)–(5.16); thick lines—regression curves according to (5.17)–(5.20)

A reliable correlation dependence ($R = 0.9842$) is established for $P = f(S)$, but at the same time, the P/S ratio (sometimes interpreted as a power utilization coefficient) cannot be considered indicative.

Correlations between the geometric parameters of the ore-smelting furnace and the installed capacity of furnace transformers are presented in Fig. 5.9. The regression equations obtained by processing the data on furnaces smelting the entire spectrum of ferroalloys have the form:

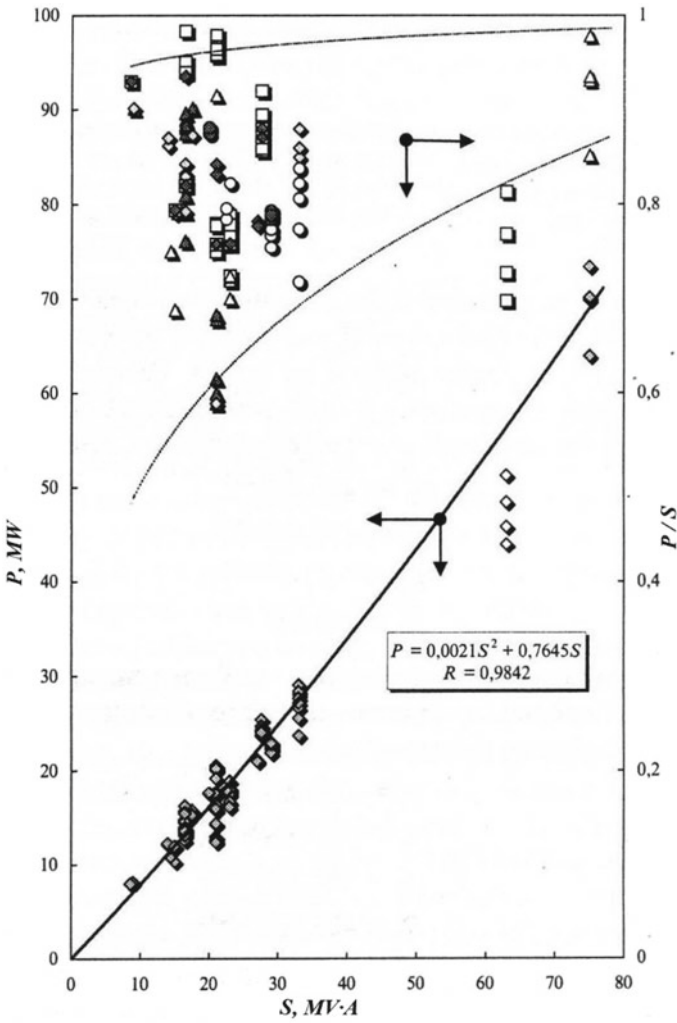


Fig. 5.8 Dependences of the active power of the furnace (thick line) and the power utilization factor P/S (thin dashed lines) on the power of furnace transformers; points—actual data

$$D_B = 1466.2P^{0.4937}, \tag{5.21}$$

$$D_p = 1190.9P^{0.3173}, \tag{5.22}$$

$$h_B = 741.3P^{0.4305182}, \tag{5.23}$$

$$D_s = 441.6P^{0.3371}. \tag{5.24}$$

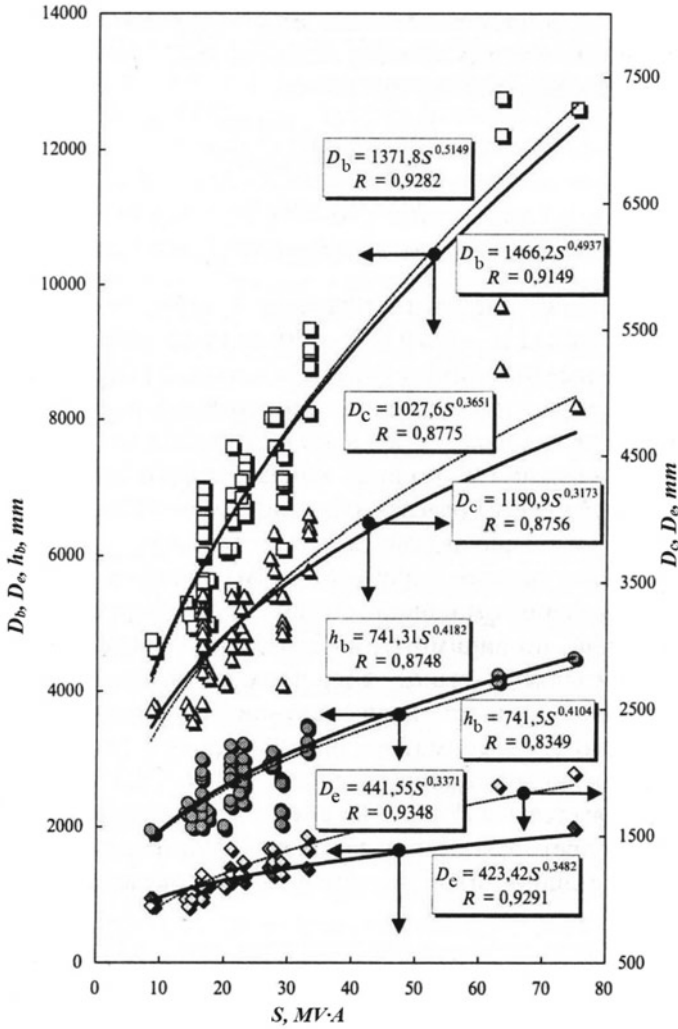


Fig. 5.9 Correlation between the geometric parameters of bathtubs of ferroalloy furnaces and the power of furnace transformers: points—actual data (designations—according to Fig. 5.6); thick lines—regression curves according to (5.21)–(5.24), thin dashed lines—the same according to (5.25)–(5.28)

Similar regressions for a sample that includes only specialized ferrosilicon furnaces are described by the equations:

$$D_b = 1371.8P^{0.5149}, \tag{5.25}$$

$$D_c = 1027.6 \cdot P^{0.6351}, \tag{5.26}$$

$$h_b = 741.5P^{0.4104}, \quad (5.27)$$

$$D_e = 423.42P^{0.3482}. \quad (5.28)$$

The coupling tightness coefficients of Eqs. (5.21)–(5.28) are slightly higher than when describing the correlation relationships of bath parameters with active power, which is not surprising, since during design it is the installed power of furnace transformers that is taken as the determining one. The discrepancies in the values of the parameters determined by Eqs. (5.21)–(5.24) and the corresponding Eqs. (5.25)–(5.28) are also small and do not exceed 3–5% within the capacities up to 63 MB•A, which is quite acceptable for practice.

Thus, the performed correlation and regression analysis of the geometric parameters of the baths of ferrosilicon furnaces not only allowed us to determine their quantitative relationships with the installed capacity of furnace transformers, but also showed the reliability of these connections and the possibility of their use in the practice of designing electric furnaces and predicting the development of furnace construction.

5.3 The Technology of Ferrosilicon Smelting and Casting

Ferrosilicon is smelted in ore-smelting furnaces (Fig. 5.10) with a capacity of 22.5–63 MV•A (Table 5.5). The location of the furnace and processing equipment is shown in Fig. 5.11.

The raw materials for producing ferrosilicon is quartzite with a particle size of 20–80 mm. Usually they are pre-washed, crushed and sorted. Quartzite suitable for smelting ferrosilicon should contain not less than 97% SiO₂ and not more than 1.5% Al₂O₃.

In the smelting of ferrosilicon, metallurgical coke (coke nut) 5–20 mm in size is mainly used. The reducing agent must have high electrical resistance and reactivity with respect to silicon oxide and must have constant moisture content.

Power factor $\cos\varphi$ equals:

$$\cos\varphi = \sqrt{1 - (I_{el}x/U_p)^2}.$$

Knowing $\cos\varphi$, the full working power of the stove transformer is $S = 3 P_d/\cos\varphi$.

In the technology of ferroalloy processes, it is important to know the relationship between the resistance of the bath (r_b) of the furnace and its dimensions.

A ferroalloy furnace, as a powerful electric receiver, generally obeys the laws of an electrical conductor. The larger the furnace bath, the lower its active electrical resistance. Even with a significant fraction of the arc discharge, the electric circuit of the furnace obeys Ohm's law.

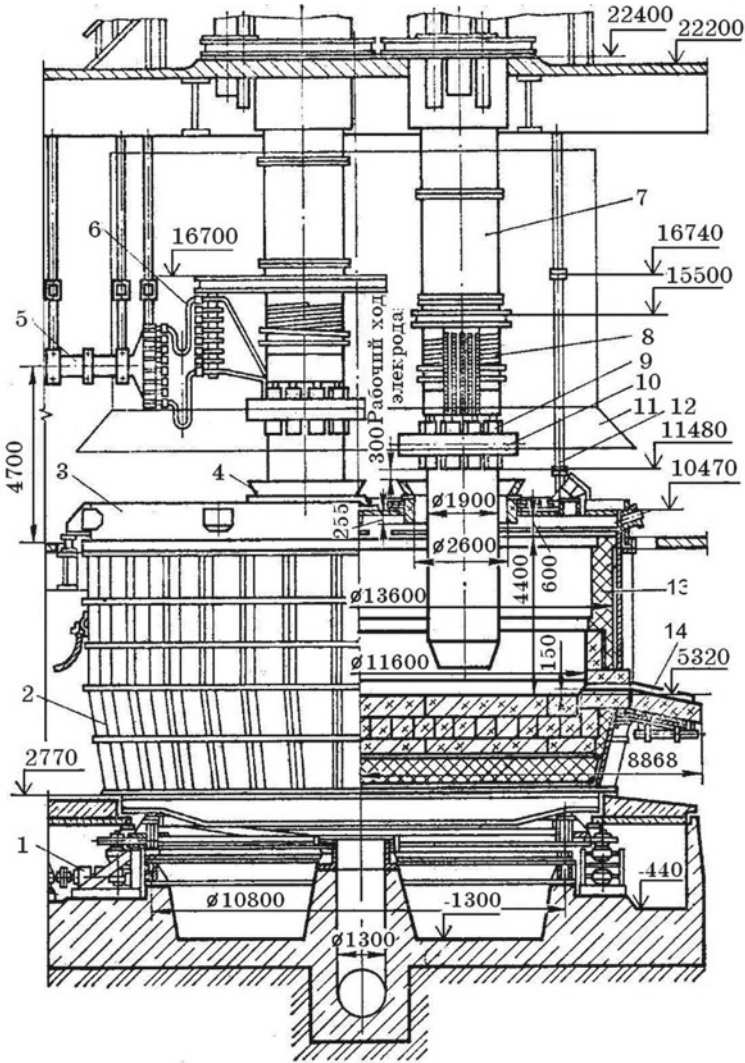
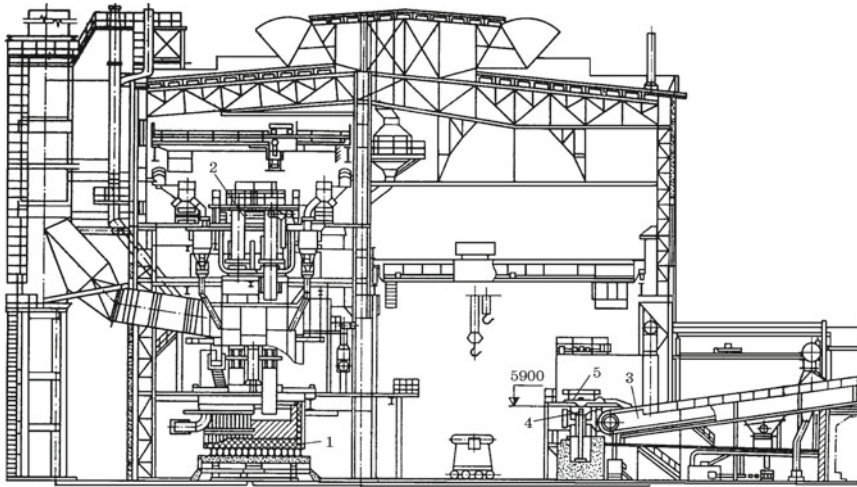


Fig. 5.10 Round closed ore-smelting electric furnace: 1—bath rotation mechanism; 2—furnace casing; 3—arch of the furnace; 4—funnel; 5—short network; 6—flexible cables of the secondary current supply; 7—bearing casing of the electrode; 8—secondary current supply; 9—contact cheeks; 10—pressure ring; 11—an umbrella; 12—suspension of the arch; 13—lining of the bath; 14—notch

From the presented in Fig. 5.12 of the I_{el} electrode current distribution scheme it follows that part of it passes through an arc discharge (I_a), the second part (I_c) passes through a charge at the electrode-charge-electrode and electrode-charge-bath lining-charge-electrode sections. The corresponding resistances are indicated as follows: arcs— r_a ; connected in series with r_a the melt resistance r_m ; charge

Table 5.5 Parameters of closed ore-smelting electric furnaces for smelting ferrosilicon

Parameter	Furnace 1	Furnace 2	Furnace 3
Bath depth, mm	2900	3500	5000
Diameter of a bath, mm	6800	8700	11,600
Diameter of electrodes, mm	1400	1500	1900
High side voltage, kV	10	110	220
Rated voltage of the working stage of the transformer, V	188	224	268.8
Full power, MV·A	22.6	40	80
Current in electrodes, kA	84.6	103	171.8
Power, MW: network consumption net			
	25.0	36.9	74.2
	23.5	33.7	66.2
Useful voltage, V	92.4	109	128.3
Power of Longitudinal compensation device MV·A	14.0	22.4	82.5
Power coefficient:			
Actual	0.70	0.65	0.50
With Longitudinal compensation device	0.937	0.921	0.926
Electric efficiency	0.908	0.915	0.892

**Fig. 5.11** Unit for smelting silicon alloys with round closed furnaces with a capacity of up to 30 MVA: 1—electric furnace; 2—electrodes; 3—filling machine; 4—filter; 5—bucket

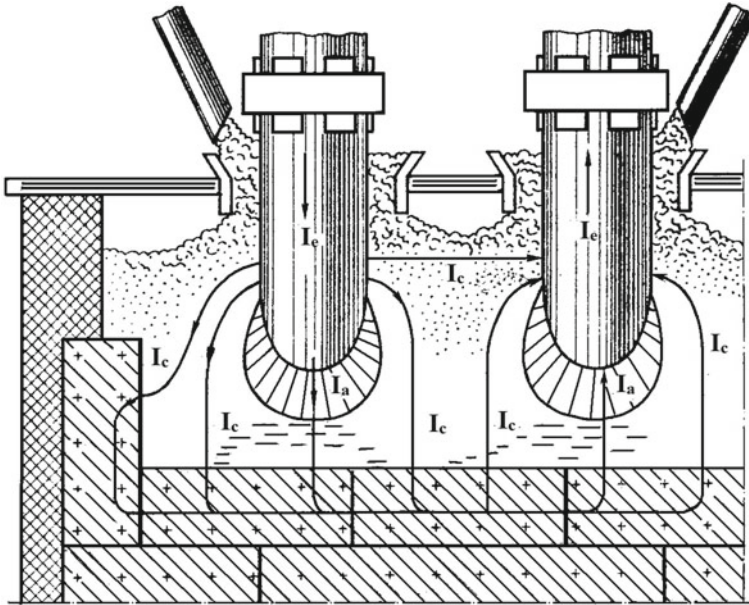


Fig. 5.12 Scheme of current distribution of the electrode I_{el} in the bath of ferroalloy furnace

resistance, on the electrode–charge–electrode section, shunting the arc according to the triangle scheme and resistance, electrode–charge–lining—charge–electrode, shunting the arc according to the star scheme— r_s . Then, the bath conductivity $1/r_b$ as the reciprocal of the resistance will be equal to the sum of the conductivity of its individual sections: $1/r_b = 1/(r_a + r_m) + 1/r_s$.

Thus, the conductivity of the bath is influenced by factors that should be taken into account both in the design of furnaces and in the process control.

The most important parameter is the useful phase voltage U_{use} which depends on the net power per one electrode $P_{u,e}$, and this relationship has the form $U_{use} = CP_{u,e}^n$, where C and n are constant values for this type of process and the type of smelted ferroalloy. For slag-free processes (production of ferrosilicon), $n = 0.33$, and for slag processes (production of ferrosiliconmanganese, ferromanganese), $n = 0.25$. Coefficient C also depends on the type of ferroalloy process, the type of melted alloy and is numerically equal: upon receipt of FS75 3.4–3.7; FS45 3.2–3.6; ferrosiliconmanganese 5.1–6.5; silicocalcium 5.7–6.0; electrocorundum 9.8–10.2; calcium carbide 2.6–3.0.

The working current in the electrode I_{el} (A) and the linear operating voltage U_1 (V) are calculated by the formulas:

$$I_{el} = P_{u,e}/U_{use} \text{ and } U_1 = \sqrt{3}I_{el}\sqrt{x^2 + r^2},$$

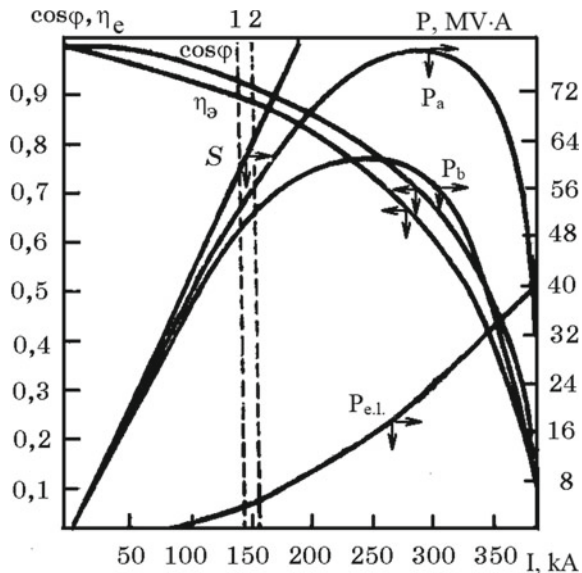
where x and r are the inductive and Ohmic resistance of the furnace installation (bathtub, short circuit and transformer).

The full operating power of the furnace transformer is indicated as S (MV·A), the active power consumed by the furnace from the mains P_a (MW), the useful power of the bath P_b (MW), power loss $P_{e.l.}$ (MW), power factor $\cos\varphi$ and electrical efficiency η_e . Using the known analytical dependences of these values on the electrode current I_{el} (kA), specific values of the electrical characteristics are calculated and their graphical dependence on the current is constructed (Fig. 5.13).

As follows from the data in Fig. 5.13, when the electrode current increases, the values of P_a and P_b increase, reach extreme values at certain current values and then decrease, despite a further increase in the electrode current. Losses of electric power increase with increasing current in the entire range of its values. Power factors $\cos\varphi$ and electrical efficiency η_e decrease significantly with increasing current. If we optimize the smelting process according to the maximum power of the bath P_b , then there would be large losses of electric power and low values of $\cos\varphi$ and η_e . In practice, the electric mode is optimized not by the maximum value of P_b , but by the minimum specific energy consumption and rational technical and economic indicators leading to the production of ferroalloy products with the lowest cost. This corresponds to the regime in the ascending section of the curve $P_b = f(I_{el})$. Two vertical dashed lines show the range of electrode current values that allow you to have the best furnace performance when smelting ferrosilicon grades FS45 (line 1) and FS65 (line 2). The electric mode of operation of the furnaces is maintained automatically by the value of the rated current by vertical movement of the electrodes.

Since the electrical and geometric parameters of each ore-smelting furnace, including a ferrosilicon furnace, are interconnected, one of the important factors

Fig. 5.13 Change in electrical characteristics depending on the electrode current of the RKZ-63 ferroalloy furnace with installed furnace transformer power of 81 MV·A in the smelting of ferrosilicon FS45 and FS65



by which the furnace maintenance personnel can control the process is the electrode landing depth (it can change under the influence of switching voltage steps and changing the charge composition). Excess carbon reducing agent leads to a decrease in the electrical resistance of the bath; therefore, the depth of immersion of the electrodes in the mixture decreases. The lack of a reducing agent increases the electrical resistance of the bath and leads to the displacement of the electrodes downward, i.e., to a deeper fit of the electrodes. A significant deviation of the electrode immersion depth from the optimal one is evidence of violation of the furnace course and requires the adoption of the necessary measures for recovery by adjusting the charge or changing the voltage level.

The mixture is loaded into the furnace through pipe-chute through the funnels around the electrodes on the stoves with a closed arch with the capture of exhaust flue gases (90% CO) or filling machine (on open furnaces).

The gas exhaust system and gas purification consist of two parallel lines working alternately. Gas enters the inclined gas-irrigated duct and the scrubber, where it is preliminarily cleaned of dust. Then, the gas is sent to a Venturi pipe (fine gas purification) and sequentially to a droplet separator to separate the moisture.

Pure gas is supplied to the consumer. The necessary vacuum in the system is created by turbo-gas blowing. The sludge released in the system goes to the sludge collector. The pressure under the arch is 2.0–5.0 Pa, and the gas temperature is 500–600 °C.

Main malfunctions during operation of the furnaces. With a lack of a reducing agent, current fluctuations are observed, the electrodes in the charge are unstable, gas evolution is concentrated near the electrodes, the sintering of the charge is increased and the number of fistulas increases, and viscous slag and furnace gases flow through the notch. The diameter and length of the working ends of the electrodes are reduced, the temperature at the top increases from 500–600 °C to 1000–1200 °C with an increase in silicon losses due to evaporation and entrainment of dust. With prolonged violations of this type, the output of slag ceases, the notch closes poorly. To correct the operation of the furnace, it is necessary to restore the correct composition of the mixture and simultaneously introduce a “light” charge under the electrodes (with an excess of reducing agent) or change the operating voltage. With an excess of reducing agent, the electrodes rise, the crucibles become narrow, there is a collapse of the charge at the electrodes, the operation of electric arcs is audible, slag and alloy do not leave the furnace well, which is associated with an increase in the amount of silicon carbide in the bath. At the same time, work on short electrodes may be a possible cause of violations.

Signs of good furnace running are: (1) uniform burden descent in all funnels without sections of the sintered charge; (2) deep immersion of electrodes; (3) overpressure under the arch of 2.0–5.0 Pa; (4) temperature under the arch <500–600 °C; (5) the hydrogen content in the top gas <5%, oxygen <1%; and (6) the amount of exhaust gas is constant. The increase in pressure under the arch is often a consequence of the lack of a reducing agent and the formation of large quantities of SiO_{gas}.

Composition and properties of slag. Ferrosilicon smelting refers to slag-free processes, since the amount of slag (its silicate base) does not exceed 3–5%. However,

the course of the furnace and the release of ferrosilicon and slag (through the same notch) are complicated due to a change in the composition of the slag. By their composition, the slags represent a *heterogeneous* phase consisting of a silicate base (48–50% SiO_2 , 20–25% Al_2O_3 , 15–18% CaO), silicon carbide (10–15%) and inclusions of ferrosilicon. The silicate component is formed from silica of quartzite and impurity oxides (Al_2O_3 , CaO , MgO) contained in quartzite and coke ash. Silicon carbide is an intermediate compound of the reduction reactions of silicon quartzite with carbon. Depending on the chemical composition of the silicate part, furnace slag can crystallize in the concentration fields of anorthite ($\text{CaO}\cdot\text{Al}_2\text{O}_3\cdot 2\text{SiO}_2$) or gehlenite ($2\text{CaO}\cdot\text{Al}_2\text{O}_3\cdot\text{SiO}_2$) of the $\text{CaO}\text{-Al}_2\text{O}_3\text{-SiO}_2$ system (Fig. 5.14). Slags of anorthite composition, taking into account the presence of SiC in them, are characterized by low processability. To improve technological characteristics (increase fluidity), limestone is periodically planted in the mixture, which allows the furnace bath to be freed from viscous heterogeneous slag.

Ferrosilicon production and casting technology. Reducing smelting products—ferrosilicon and slag (3–5% of the mass of the alloy)—are discharged from the furnace into the ladle through one notch hole (taphole), which, after the previous melting is released, is closed with a taphole clay (“cone”), consisting of refractory

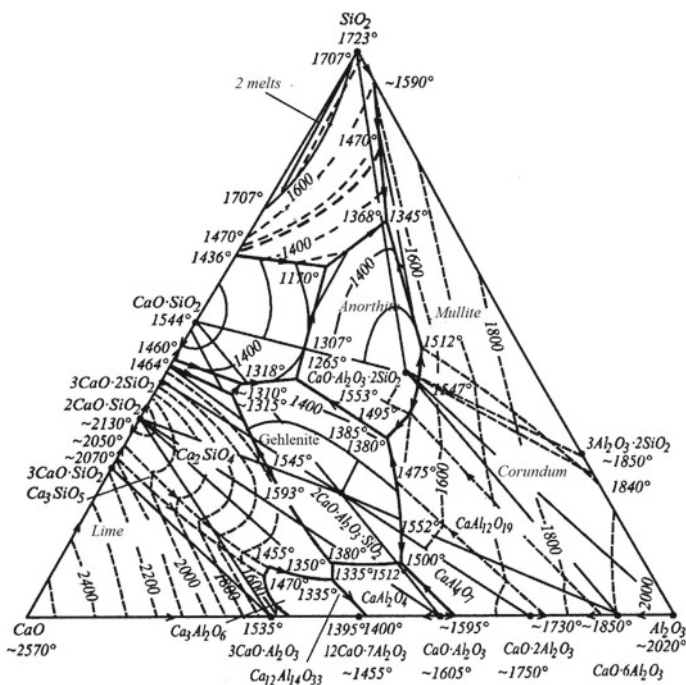


Fig. 5.14 Diagram of phase equilibria in the $\text{CaO}\text{-Al}_2\text{O}_3\text{-SiO}_2$ system. Solid lines—boundaries of coexisting mineral phases (anorthite $\text{CaO}\cdot\text{Al}_2\text{O}_3\cdot 2\text{SiO}_2$, $t_m = 1553^\circ\text{C}$; gehlenite $2\text{CaO}\cdot\text{Al}_2\text{O}_3\cdot\text{SiO}_2$, $t_m = 1545^\circ\text{C}$)

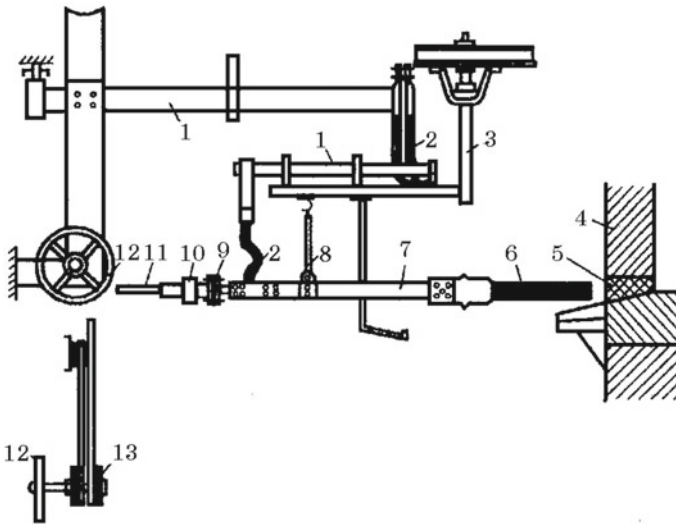


Fig. 5.15 The scheme of the device for burning tapholes: 1—one of the phases of the busbar; 2—flexible cable; 3—bracket; 4—carbon lining; 5—notch; 6—electrode for burning tapholes; 7—electrode holder; 8—suspension of the electrode holder; 9—counterweight; 10—clamp; 11—handle; 12—helm; 13—shunt connected to one of the phases of the electric furnace

clay (50% SiO₂, 35% Al₂O₃, 1.5% TiO₂, 0.5% CaO, residual H₂O) with coke or able to coking carbon mass. During the period between two successive releases of ferrosilicon, the taphole clay (“cone”) is fired. To open the taphole, the “cone” is melted (burned) using an electric firing device (Fig. 5.15). The notch hole should be 160–120 mm in diameter, which provides a good yield of ferrosilicon and slag. At the end of the release, the notch is cleaned of slag deposits and closed with a taphole clay (“cone”).

According to established practice, the number of ferrosilicon releases depends on the specific energy consumption per ton of alloy, that is, on the grade of ferrosilicon:

Ferrosilicon grade	FS20	FS25	FS45	FS65	FS75
Specific power consumption, kWh/t	2180	2820	4700–5200	7500–8000	8800–9500
Number of releases per shift (8 h)	6–8	6–8	5–6	4–5	4–5

Specific electrical resistivity of ferrosilicon (liquid). For the calculation of the electrical circuit of ferrosilicon furnaces and the selection of rational electrical modes for its smelting, data on the specific electrical resistivity (SER) of various types of liquid ferrosilicon are important. Ferrosilicon of industrial smelting by the content of impurity elements (Al, Ca, Ti, Mn, Cr, Mg, P, As, S, C) differs significantly from model silicon–silicon alloys, usually used for experimental determination of SER of liquid and solid binary alloys of the iron–silicon system.

The SER measurements were carried out under industrial conditions on a jet of liquid ferrosilicon with its free outflow from the notch of the furnace bath through an intermediate graphite crucible funnel (Fig. 5.16).

The SER of the jet (ρ) of liquid ferrosilicon flowing out of the furnace bath through the chute into the ladle was measured. A diagram of a device for measuring the resistivity of liquid ferrosilicon is shown in Fig. 5.16. The value of ρ is calculated by the formula:

$$\rho = \frac{\Delta U \cdot S_{av}}{L_j I},$$

where ΔU is the voltage drop along the length of the section, V ; I is the current flowing along the stream, A ; S_{av} —the average cross section of a jet of liquid ferrosilicon; L_j —the length of the jet.

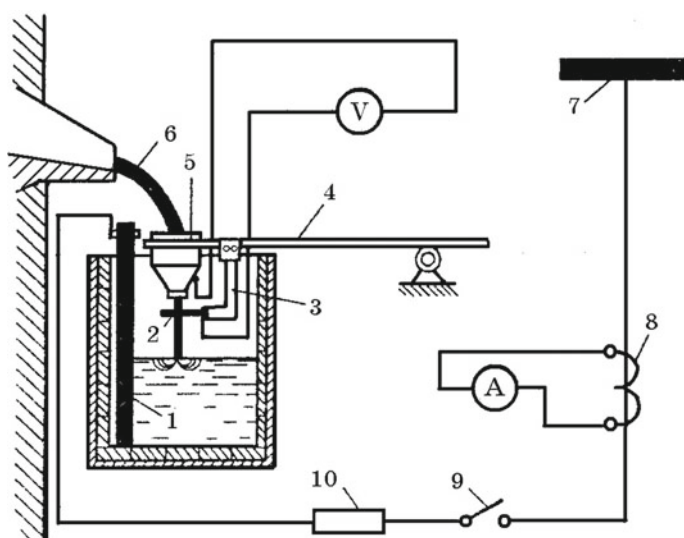


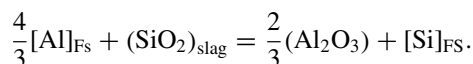
Fig. 5.16 Schematic diagram of the electrical circuit for measuring the electrical conductivity of liquid ferrosilicon: 1—graphite rod; 2—ring graphitized electrode; 3—a bracket made of a steel pipe into which a graphitized electrode is inserted; 4—rod holder graphite funnel; 5—graphitized funnel; 6—a jet of ferrosilicon discharged from the furnace bath; 7—bus for connecting the burner; 8—current transformer; 9—breaker; 10—resistance box

The average value of SER in the range of 1700–1720 °C for ferrosilicon of various grades was:

Ferrosilicon grade	FS25	FS45	FS75
ρ , Ohm·m	21.7×10^{-8}	25.5×10^{-8}	30.6×10^{-8}

Ferrosilicon refining from aluminum. In accordance with the international standard GOST 1415-93, the aluminum content in the high-silicon ferrosilicon grade FS70A1 should not exceed 1%. In the former GOST 1415-78 and in regulatory documents of foreign companies, the aluminum content in FS75(e) ferrosilicon, intended for use in the smelting of electrical steel, should not exceed 0.1%, and in FS75 (l) grade ferrosilicon to produce cast steel no more than 1.5%. At the same time, the industrial practice of smelting ferrosilicon using quartzite and metallurgical coke shows that the actual aluminum content in ferrosilicon grades FS65, FS70 and FS75 exceeds 1.5% and ranges from 1.8 to 2.5%.

High-silicon ferrosilicon should be refined from aluminum, and sometimes from other impurities (Ca, Ti, Cr). There are two groups of methods for reducing the aluminum content in ferrosilicon. The essence of the methods of the first group consists of refining liquid ferrosilicon in arc (less often induction) electric furnaces under the slag of the CaO–SiO₂ system, which is enriched with alumina as aluminum is oxidized by the reaction



Therefore, equilibrium in the ferrosilicon–slag system occurs when a certain content of aluminum in the alloy and alumina in the slag of triple composition CaO–Al₂O₃–SiO₂ are reached. Slag in its composition and fusibility is in the system SiO₂–CaO–SiO₂–CaO·Al₂O₃·SiO₂ (anorthite) (Fig. 5.14). With a decrease in aluminum concentration during the refining process, its activity decreases, which necessitates the maintenance of a lower content of Al₂O₃ in the slag. To achieve 0.1% Al in ferrosilicon, twofold and threefold treatment with “fresh” slag mixtures is carried out.

The disadvantages of the furnace refining method (both out-of-furnace and ladle methods) are a decrease in the silicon content (fumes in the form of SiO_{gas}), as well as a relatively high specific energy consumption of 1400–1500 kWh/t. When refining ferrosilicon with a double formation of slag, the aluminum content decreases to a greater extent, but silicon losses increase and energy consumption increases.

The essence of the second group of ferrosilicon refining methods consists in treating liquid ferrosilicon in a ladle with slag-forming mixtures consisting of lime, quartz sand using diluent additives (or without them), but with melt blowing in the ladle with air, technically pure oxygen, nitrogen or mixtures thereof. As a slag-forming mixture, lime, quartz sand, iron ore and fluorspar (CaF₂) are used.

In the ladle, from this mixture of components, a slag is formed having oxidizing ability, primarily with respect to aluminum, although silicon is partially oxidized.

The acceleration of the refining process is achieved by blowing the melt in the ladle with gaseous energy carriers (air, oxygen, nitrogen or their mixtures) using lances immersed in the melt.

Siderite—iron carbonate is used as a refining component. When heated, siderite thermally dissociates $\text{FeCO}_3 \rightarrow \text{FeO} + \text{CO}_2$, and the iron oxide formed interacts with ferrosilicon aluminum.

The CO_2 gas released in this process helps melt the melt. A higher degree of aluminum removal is achieved when using fluorspar with siderite with twofold and threefold updating of slag in the ladle during refining.

The microstructure of ferrosilicon. The microstructure of ferrosilicon ingots of the FS45 grade is represented by the FeSi phase, Fe_xSi_2 non-stoichiometric silicide, the FS65 and FS75 grades by Fe_xSi_2 silicide and the pure silicon phase. At temperatures below 937 °C, Fe_xSi_2 silicide is converted to FeSi_2 and the phase of secondary pure silicon. Numerous impurity elements form the so-called excess precipitation phases, which have a complex chemical composition, crystallize in intergranular precipitates of the main phases (iron silicides). As an example Fig. 5.17 shows the energy spectra of the elements of the main and excess phases on the freshly formed fracture surfaces of ferrosilicon samples of various grades FS75, FS65 and FS45.

In the upper right corner of the spectrograms are the tables of the results of quantitative processing, where the first column of numbers (S) is the intensity of the analytical line (peak area in pulses), which directly reflects the content of this element in the analyzed microvolume. The second column (dS) is the error of the found area value, determined by the residual mismatch between the modular and the desired working part of the spectrum. The third column ($S, \%$) is the fraction of the peak area in the sum of the areas of all peaks in the spectrogram in relative percentages. From an analysis of the spectrogram data, it follows that microprobe excess phases of evolution on the surface of freshly formed fractures have a very complex chemical composition, and some of them contain phosphorus and arsenic. No phosphorus and arsenic were found on the polished sections of the samples of the corresponding melts due to their interaction in the process of manufacturing polished sections with reagents water with the formation of gaseous phosphine PH_3 and arsine AsH_3 —industrial poisons. Microprobing confirmed the presence of basic silicide structures and the phase of pure silicon.

As an example, the diversity of the composition of the excess release phases in the structure of the FS65 ferrosilicon ingot in Table 5.6 shows data on the chemical composition of the phase of pure silicon, silicides and excess phases of selection.

Fractionation of ferrosilicon ingots. The competitiveness of ferrosilicon, as well as other ferroalloys in the markets of ferroalloy products, along with the regulated standard of chemical compositions, is also determined by the size class (Table 5.7).

In this regard, ferrosilicon ingots of machine casting are subjected to fractionation by crushing and sieving, accompanied by the formation of small fractions.

The presence in the ingots of porosity and many excess phases of precipitation leads to a decrease in the mechanical strength of the ingots, which is enhanced by the phase transformation of $\text{Fe}_x\text{Si}_2 \rightarrow \text{FeSi}_2 + \text{Si}$. It was experimentally established that

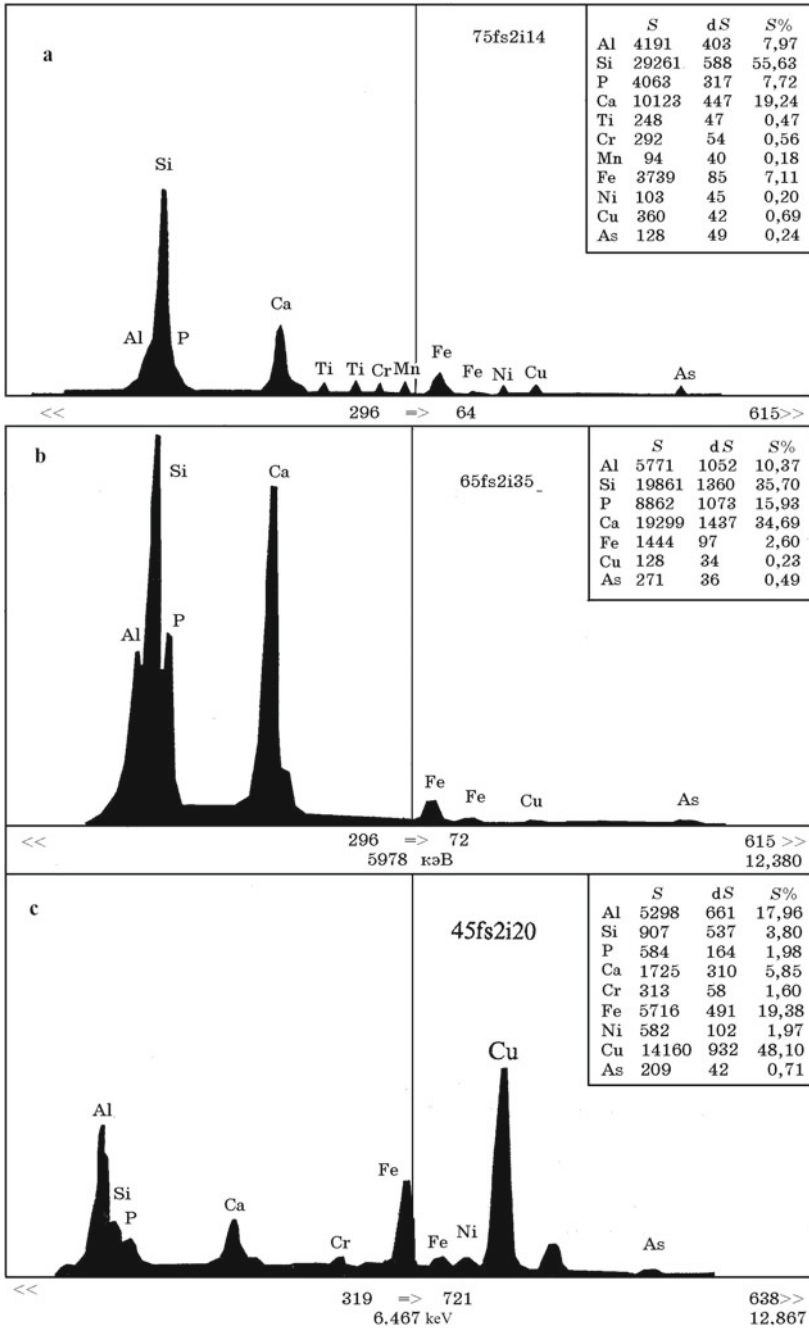


Fig. 5.17 Energy spectra of elements in excess phases of the release of a “fresh” fracture of a sample of ferrosilicon FS75 (a), FS65 (b) and FS45 (c)

Table 5.6 Chemical composition of the main structural components and the excess phases of precipitation in the microstructure of an FS65 ferrosilicon ingot of machine casting

Phase number	The content of elements, %										
	Si	Al	Fe	Cu	P	As	Ti	Cr	Mn	Ni	Cu
1	99.4	–	0.6	–	–	–	–	–	–	–	–
2	98.5	–	0.9	0.4	–	–	0.2	–	–	–	–
3	97.7	–	0.5	0.8	–	–	–	–	–	–	–4
4	84.5	1.8	13.2	–	–	–	–	0.2	0.1	0.1	0.1
5	61.4	11.1	4.6	15.2	6.1	–	0.6	0.4	–	0.1	0.5
6	61.0	–	30.0	2.6	–	–	2.6	0.3	–	–	–
7	57.1	14.0	11.3	9.0	3.8	–	0.9	1.0	0.4	0.6	1.9
8	54.8	20.0	2.6	10.1			2.6	7.3	2.0		0.7
9	52.7	18.1	23.0	4.4	–	–	0.7	0.3	0.1	0.3	0.5
10	51.6	15	28.1	4.0	–	–	–	–	0.3	0.3	0.5
11	45.4	16.1	13.5	14.2	–	–	1.0	–	–	0.8	7.6
12	40.2	6.6	10.8	–	–	–	10.8	5.6	–	–	0.2
13	35.7	10.4	2.6	34.7	15.9	0.5	–	–	–	–	0.2
14	34.8	24.2	2.0	35.1	–	–	–	–	–	0.6	3.3
15	30.7	–	9.7	–	–	0.5	20.0	6.5	–	–	0.4

Table 5.7 Grain sizes of ferrosilicon

Class	Particle size range, mm	Undersize product, % by weight		Oversize product, % by weight
		total	less than 3.15 mm	
1	100–325	20	6	No piece should exceed more than 1.5 times the limit of the specified size range in two or three dimensions
2	75–200	20	6	
3	35–100	18	6	
4	10–75	18	7	
5	3.15–35	8		
6	3.15–10	10		
7	3.15–6.3	10		
8	No more than 3.15	–		

with an increase in the silicon content in ferrosilicon of industrial smelting from 25 to 90%, the temporary compressive strength (σ_{com}) decreases from 10.7 to 2.8 kg/mm² (Table 5.8).

The dependence $\sigma_{\text{com}} = f[\%Si]$ is represented by the equation:

$$\sigma_{\text{com}} = -0.14[\%Si] + 14.12, \text{ kg/mm}^2.$$

Table 5.8 Temporary compressive strength and hardness of ferrosilicon samples of various grades

Alloy grade	The content of elements, %			σ_{com} , kg/mm ²	Hardness, HV
	Si	C	P		
FS25	26.3	0.28	0.04	10.7	420
FS45	44.7	0.1	0.05	8.1	370
FS65	66.3	0.1	0.05	5.0	350
FS75	79.1	0.1	0.03	4.7	350
FS90	89.7	0.1	0.03	2.8	320

In technological schemes for the production of ferrosilicon, a stage for crushing ingots and sieving the resulting product into size classes is provided. Crushing and screening complexes in ferrosilicon shops are the same necessary mechanical and technological equipment, as, for example, filling machines.

Density of ferrosilicon. Due to the significant difference in the density of iron and silicon, there is an inverse relationship between the density of ferrosilicon and its silicon content:

Ferrosilicon	FS20	FS25	FS45	FS65	FS75	FS90
Mass content of Si, %	19–23	23–27	41–47	63–68	74–80	89
Apparent density, g/cm ³	6.7	5.2–6.5	4.9–5.4	3.1–3.5	2.8–3.1	2.4–2.5

This relationship is used for rapid determination of silicon content in the conditions of ferrosilicon shops. The essence of the method is as follows. The ferrosilicon sample is crushed and a weighed sample of an alloy of a fraction of 1–3 mm weighing 100 g is sieved. The sample is poured into a volumetric flask with kerosene, and its bulk density is determined (cm³/100 g). The tabulated data determine the silicon content in a particular smelting of ferrosilicon.

By processing the tabulated data used in the express laboratories of ferrosilicon shops, the dependences of the silicon content in ferrosilicon of various grades on its bulk density (cm³/100 g) for various alloy grades are obtained:

$$\text{FS25 } [\% \text{Si}]_{\text{FS25}} = 7.5878V_{\text{FS25}} - 94.724;$$

$$\text{FS45 } [\% \text{Si}]_{\text{FS45}} = 3.1335V_{\text{FS45}} - 20.435;$$

$$\text{FS65 } [\% \text{Si}]_{\text{FS65}} = 2.0236V_{\text{FS65}} - 85.586.$$

Since in the range of silicon concentrations in ferrosilicon 25–65% the tabulated values of $[\% \text{Si}]_{\text{FS}}$ and V_{FS} , cm³/100 g do not lie on a straight line, an equation of the second degree is obtained:

$$[\% \text{Si}]_{\text{FS}} = -0,1807V_{\text{FS}}^2 + 11.395V_{\text{FS}} - 110.43.$$

The deviation from the additivity of the density of ferrosilicon grades FS25, FS45 and FS65 is due to the structural features of the alloys, as well as different contents of impurity elements.

Specific consumption of charge materials and electricity. Below are the specific consumption of materials and electricity in the smelting of ferrosilicon in closed electric furnaces of various grades:

Ferrosilicon	FS20	FS25	FS45	FS65	FS75
Material consumption, kg:					
Quartzite	370	552	931	1568	1930
Iron shavings	810	780	658	343	250
Coke breeze	200	280	438	720	845
Electrode mass	10	8	16	43.3	54
Power consumption, kW-h/t	2100	2750	4800	7410	8800
Silicon recovery, %	94.3	98.5	98.2	92.1	91.8

Properties of silica dust and its utilization. The flue furnace gases of ferrosilicon furnaces have a high content of siliceous dust and therefore are cleaned. Caught by dry gas cleaning dust has a chemical composition, % (by weight):

SiO ₂	Al ₂ O ₃	CaO	MgO	Fe ₂ O ₃	LOI.
80–95	1.8–8.6	0.4–2.6	5.1–1.3	0.2–0.4	0.8–1.7

Dust is a fine material with a bulk density of 0.18–0.23 t/m³ and a particle size of 5 μ. The specific dust surface averages 2000 m²/kg. Dust and gas formations account for the bulk of the loss of silicon, which amounts to 10–15% when smelting ferrosilicon grade FS75. The rational use of siliceous dust trapped in gas purification is one of the urgent tasks of ferrosilicon production—saving material resources and increasing the efficiency of solving the environmental protection problem. Among the many directions of methods for the utilization of siliceous dust, the possibility of using it as part of building cement, in which it exhibits *pozzolanic* properties, is noted, upon receipt of liquid glass by the “wet” method by converting silica into sodium silicate by treating it with an aqueous solution of caustic alkali, as well as obtaining ceramics, sorbents, silicon tetrachloride SiCl₄, SiC carbide, Si₃N₄ nitride, reinforcement of elastomers (rubber products), etc.

The composition and properties of shungite. Shungite (shungite rock) is an ancient Precambrian formation, a fossil natural substance consisting of carbon substance, silica and impurity oxides and therefore is considered as a possible initial component of the charge for smelting ferrosilicon and other silicon ferroalloys. The only shungite field identified is located in Karelia (Russia). Shungite received its name from the village of Shunga, located in this field. The carbon substance has the formula C₇₉H₁₉O₁₅N_{0.3} and is highly metamorphosed caustobiolite, containing mainly amorphous carbon of a disordered structure. Shungite rocks make up thick layers. The

composition and properties of shungite rock from various widespread areas of the deposit vary significantly in the content of carbonic substance, the amount and chemical composition of the siliceous component.

The carbonic substance has a chemical composition (wt%):

C	H	N	O	S	H ₂ O ^a
93.45	0.99	0.70	4.86	0.54	6.53
93.13	0.73	0.99	2.72	0.43	7.49

^a(above 100%)

The siliceous component of shungite rocks is represented by fine-crystalline inclusions of quartz (chalcedony) and fine-crystalline seericite (finely scaled muscovite $KAl_2 \cdot [(OH, F)_2AlSi_3O_{10}]$). The silica grains have an isometric shape and the sinuous constituent of the following C% is silica in %):

SiO ₂	TiO ₂	Al ₂ O ₃	Fe ₂ O ₃	MgO	CaO	Na ₂ O	K ₂ O
83.0	0.58	7.50	3.46	0.24	0.30	0.19	2.20

According to the composition of the mineral base, shungite rocks are divided into three types: A—high siliceous, B—medium siliceous and C—low siliceous.

Shungite has a density of 1.75–1.80 g/cm³. The electrical resistivity of shungite rocks depends on the carbon content in them, which varies widely and this relationship is described by the equation:

$$\rho = 0.0162 \cdot C^{-1.72} \Omega \cdot \text{cm},$$

where C is the mass fraction of carbon, %.

Carbon substance has a different electrical resistivity, which is determined by its structure. The beginning of the study of shungite was devoted to the study of their combustible properties, which is explained by the desire to find “northern anthracite” in shungite. The calorific value of low-ash shungite is close to that for anthracite. According to the structural characteristics and properties, the carbonaceous substance of shungite rocks is a natural analogue not of anthracite, but of artificial *glassy carbon*, a product of heat treatment of some carbonaceous substances, which are converted into carbonized products by pyrolysis, *bypassing the liquid phase*.

The most promising for involvement in the production of ferroalloys are shungite rocks with a high siliceous base of groups IIa and IIIa (83.0–86.7% SiO₂) (Table 5.9). Rocks with a high alumina content can be used for the production of silicon alloys with aluminum and manganese with a partial replacement of coke and quartz. Shungite rocks of the II and III varieties are practically non-porous, with a density of 2.2–2.5 kg/m³. Most of them belong to thermally stable rocks.

Differential curves of thermal analysis of shungite rock indicate a strong endothermic effect, starting from a temperature of 1200–1300 °C, indicating the beginning of the interaction of silicon with carbon. Petrographic studies have shown

Table 5.9 Chemical composition of shungite rocks of groups II A and III A

Group	Content, %									
	SiO ₂	TiO ₂	Al ₂ O ₃	FeO	MgO	CaO	Na ₂ O	K ₂ O	C	
<i>Content limit</i>										
II A	36.40–56.60	0.17–0.67	2.79–6.50	0.14–2.25	0.41–0.85	0.06–0.32	0.02–0.30	0.05–2.21	37.0–55.0	
III A	55.0–71.3	0.11–0.44	2.24–5.53	1.00–5.10	0.40–1.90	С.п.	С.п.	0.60–2.30	22.0–31.0	
					0.76		1.00			
<i>Group average component content</i>										
II A	47.50	0.33	4.30	1.98	0.70	0.17	0.11	0.31	43.0	
III A	62.90	0.24	4.16	2.39	0.75	0.33	0.20	1.47	27.6	
<i>The average content of components in the silicate part of the rocks</i>										
II A	83.0	0.58	7.50	3.46	1.24	0.30	0.19	2.20	–	
III A	86.7	0.33	5.75	3.30	1.04	0.45	0.28	2.03	–	

that the endothermic effect is associated with the formation of silicon monoxide SiO. At higher temperatures, silicon carbide of cubic modification β -SiC is formed.

Shungite rock in the mixture for the smelting of ferrosilicon FS45 and ferrosilicon-manganese FeSiMn17 increases their electrical resistivity to temperatures of 1000–1200 °C, which positively characterizes the rock as a possible component of charge mixtures to replace part of coke and quartzite. However, industrial experiments have shown that the use of shungite rock (47–62% SiO₂, 27–40% C and 4–5% Al₂O₃) in a charge for smelting ferrosilicon significantly increases the aluminum content in it. Shungite rock can be considered as a component of the mixture for smelting ferrosilicon aluminum and ferrosiliconmanganese, although large-scale industrial tests are necessary to confirm its effectiveness.

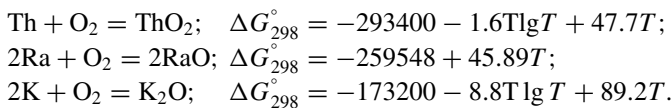
Natural radioactivity of charge materials, ferrosilicon and slag. Mineral types of raw materials and carbonaceous reducing agents entering the plants for smelting ferrosilicon contain various amounts *radioactive elements* (radionuclides) of natural origin, most notably $^{226}_{88}\text{Ra}$, $^{232}_{90}\text{Th}$, the radioactive isotope of potassium $^{40}_{19}\text{K}$. Among the mining and metallurgical raw materials, fossil coals, the highest natural radioactivity is in acidic species containing uranium (3.5–10⁻⁴%) and thorium (1.8–10⁻³%), and the smallest are ultrabasic species containing uranium 3.0 × 10⁻⁷% and thorium 5 × 10⁻⁷%. In crystalline rocks (ores), radioactive elements are often found in accessory minerals, for example, zircon ZrO₂·SiO₂, monazite (Ce, La, Nd, Th) [PO₄], brannerite (U, Ca, Th, V) (Ti, Fe)₂O₆ and others. Relatively many radioactive elements are found in organogenic deposits, which are caused by the presence of carbon of organic origin.

The half-life of the thorium radionuclide $^{232}_{90}\text{Th}$ is $T_{1/2} = 1.41 \times 10^{10}$ years, radium $^{226}_{88}\text{Ra}$ —1600 years. In the quantitative assessment of the radioactivity of materials, the contribution of the radioactive potassium isotope $^{40}_{19}\text{K}$ ($T_{1/2} = 1.32 \cdot 10^9$ years), the content of which is 0.012% in nature, is taken into account.

Radioactive elements are contained in fossil materials mainly in the form of oxides RaO, ThO₂, the thermodynamic characteristics of which are given below:

Oxides	$-\Delta H_{\text{gen}}^{\circ}$, kJ/mol	S_{298}° , J/(mol·K)	C_p , J/(mol·K)	t_m , °C
RaO	515.4	84.0	48.2	
ThO ₂	1226.4	65.23	61.76	3350

Changes in the Gibbs energy of the reactions of the formation of oxides ThO₂, RaO and K₂O are described by the following equations (cal/mol O₂):



Due to the high thermodynamic strength, the oxides Ra, Th and to a lesser extent K during ferrosilicon smelting are only partially reduced by carbon and are mainly concentrated in the silicate part of heterogeneous furnace slag. In this case, the

equivalent radioactivity of the slag is significantly increased in comparison with the starting materials. To ensure safe operation, the radioactive safety standards NRB-96 (Russia) and NRBU-97 (Ukraine) were introduced, according to which the equivalent radioactivity of materials should not exceed 370 Bq/kg. The mass of the radionuclide in raw materials and its activity are interconnected and this dependence is expressed by the equation:

$$m = \frac{A \cdot T_{1/2}}{0,693} \cdot \frac{A_0}{N_A},$$

where A —activity, Bq/kg; m —mass, g; A_0 —atomic mass; N_A — $6022 \cdot 10^{23} \text{ mol}^{-1}$ —Avogadro number; $T_{1/2}$ —half-life, sec.

The equivalent radioactivity of a specific charge material A_{eq} is calculated as the sum of the effective radioactivity of the radium, thorium and potassium isotope nuclides:

$$A_{\text{eq}} = A_{\text{Ra}} + 1.25A_{\text{Th}} + 0.08A_{\text{K}}.$$

The results of a study of the radioactivity of charge materials indicate that the activity of quartzites varies from 15 to 30 Bq/kg, coke breeze from 40 to 60 Bq/kg and steel chips from 5 to 7 Bq/kg. Due to the concentration of Ra, Th and K oxides in the silicate part of the heterogeneous furnace slag, its activity significantly exceeds 370 Bq/kg. The activity of FS45 grade ferrosilicon is not higher than 7 Bq/kg, and that of FS65 and FS75 grades 41–46 Bq/kg. Due to dilution of the silicate part of the furnace slag with silicon carbide with low activity, as well as ferrosilicon inclusions, the radioactivity of ladle slag ferrosilicon of high silicon grades is about 370 Bq/kg and the lower the more ferrosilicon inclusions in samples of heterogeneous slag. Data on the natural radioactivity of the starting charge components and ferrosilicon smelting products make it possible to calculate the actual amount of the silicate part of the heterogeneous furnace slag. The results of the balance calculations show that the amount of silicate part of the slag varies in a small range from 2.5 to 4.7%, while the mass of ladle slag with inclusions of ferrosilicon and silicon carbide reaches 7–10% or more.

References

1. Moiseev GK, Vatolin NA et al (1994) J Phys Chem 337(6):775–778 (in Russian)
2. Zaitsev AI, Zemchenko MA, Mogutnov BM (1991) Thermodynamic properties and phase equilibria in the Fe-Si system (RZHM Metallurgy. 1991. 10A53) (in Russian)
3. Polyakov OI, Zubov VL, Gasik MI (2000) Rational geometric parameters of baths of ferrosilicon furnaces. Steel 4:37–42 (in Russian)

Chapter 6

Metallurgy of Manganese Ferroalloys



6.1 Properties of Manganese and Its Compounds

Manganese—element of the VIIIb group of the Periodic system of elements. Atomic number of manganese 25, atomic mass 54.93, configuration of the outer electron shell of the atom $3d^54s^2$, oxidation state from 2 to 7, the most stable are Mn^{2+} and Mn^{4+} . Four cubic crystalline modifications of manganese are known: α -Mn modification, density 7.44 g/cm^3 , is stable below $710\text{ }^\circ\text{C}$; at 727 – $1090\text{ }^\circ\text{C}$ — β -Mn, density 7.29 g/cm^3 ; at 1090 – $1138\text{ }^\circ\text{C}$ — γ -Mn, density 6.37 g/cm^3 ; above $1138\text{ }^\circ\text{C}$ — δ -Mn, density 6.28 g/cm^3 . The melting point of manganese is $1244\text{ }^\circ\text{C}$, and the boiling point is $2150\text{ }^\circ\text{C}$. Manganese has an abnormally high vapor pressure. The temperature dependence of manganese vapor pressure is described by the equations:

$$\lg P_{Mn}(\text{Pa}) = 10.8828 - 13,625/T \quad (1043 \leq T \leq 1158\text{ K}),$$

$$\lg P_{Mn}(\text{Pa}) = 20.005 - 14,850/T + 2.52 \lg T \quad (1518 \leq T \leq 2353\text{ K}).$$

Mn–Fe system (Fig. 6.1). In the Mn–Fe system, there exists a large region of solid solution based on γ -Fe and γ -Mn. α -Mn and β -Mn solutions are formed at a concentration of >68 – 70% Mn.

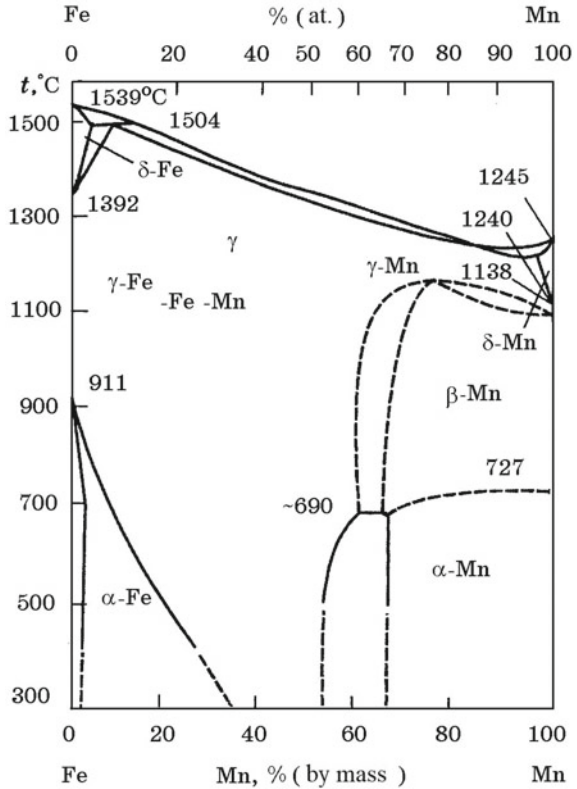
The low melting point of alloys in the Mn–Fe system is $1232\text{ }^\circ\text{C}$ with an atomic manganese content of 87% .

The integral enthalpy of mixing reaches a maximum of -8360 J/mol at $x_{Mn} = 0.7$.

Mn–C system (Fig. 6.2). In the Mn–C system, carbides were identified: $Mn_{23}C_6$ (5.38% C), Mn_3C (6.77% C), Mn_5C_2 (8.03% C), Mn_7C_3 (8.57% C). The liquidus curve in the Mn–C state diagram can be described by the equation

$$\lg[\text{C, \% at.}] = -375.8/T - 0.347.$$

Fig. 6.1 Equilibrium state diagram of the Fe–Mn system



The dependence $\Delta G_T^0(T)$ for the reaction of graphite dissolution in liquid manganese $\text{C}_s + \text{Mn}_l = [\text{C}]_{\text{Mn}}$ has the form:

$$\Delta G_T^0 = 17,600 - 25.64T, \text{ J/mol.}$$

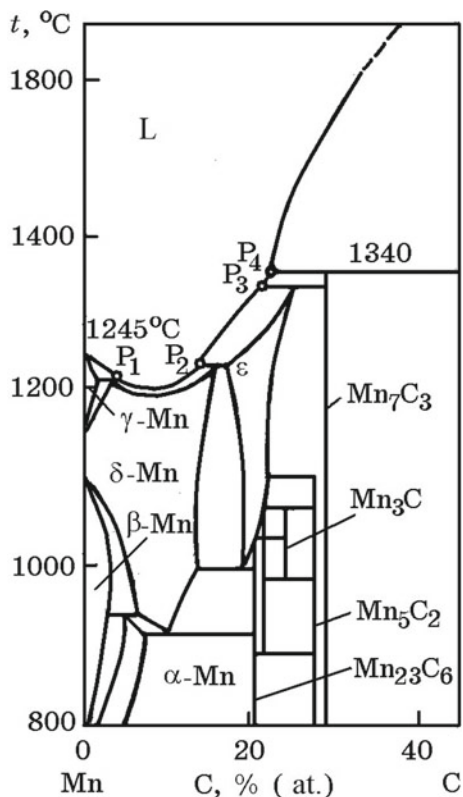
The temperature dependence of the change in the Gibbs energy of the reaction for the formation of higher manganese carbide Mn_7C_3 from the elements $7\text{Mn} + 3\text{C} = \text{Mn}_7\text{C}_3$ is described by the equation:

$$\Delta G_T^0 = 66,155 - 58.24T, \text{ J/mol.}$$

Mn–Si system (Fig. 6.3). The system state diagram is constructed taking into account the existence of 7 manganese silicides and solid solutions of silicon in manganese.

The heats of formation of manganese silicides Mn_3Si , Mn_5Si_3 , MnSi and $\text{MnSi}_{1.7}$ are, respectively, 17, 24.85, 30.5 and 28.15 kJ/mol. The density of liquid alloys of the Mn–Si system decreases with increasing silicon concentration. At 1500 K and a silicon content of 30% and 60% (at.), the density of the alloys is 5.31 and 4.35 g/cm³

Fig. 6.2 Equilibrium state diagram of the Mn–C system



(6.37 and 2.32 g/cm³ for pure manganese and silicon). The activity of manganese and silicon in Mn–Si melts depends on the alloy composition and temperature. The curves a_{Mn} and a_{Si} (Fig. 6.4) intersect.

The structural units of the Mn–Si system melts in the aspect of the model of associated solutions are Mn and Si and three associates Mn₃Si, Mn₂Si and MnSi. Using the optimization procedure, enthalpy values and entropy changes that accompany the association processes in the Mn–Si system were calculated ([1], Fig. 6.5):

Associates	$-\Delta H^{\circ}$, J/mol	ΔS° , J/(mol K)
Mn ₃ Si	3553	-18.48
Mn ₂ Si	101,066	-15.15
MnSi	93,567	-22.53

As follows from the data in Fig. 6.5, the largest fraction in Mn–Si melts at 1873 K is represented by MnSi associates.

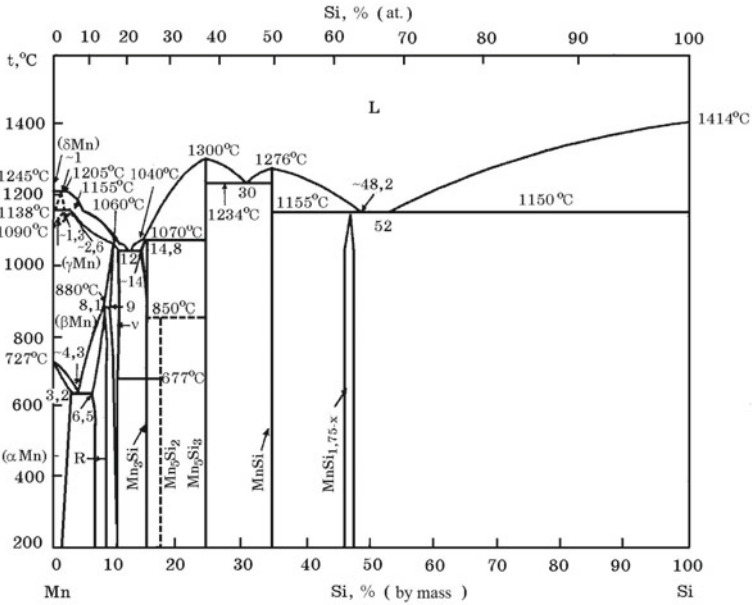
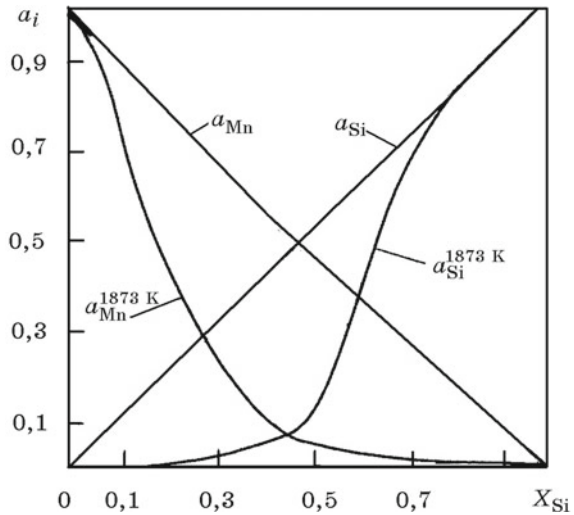


Fig. 6.3 Equilibrium state diagram of the Mn-Si system

Fig. 6.4 Manganese and silicon activity in alloys of Mn-Si system at 1873 K (a_{Mn} and a_{Si} —for a hypothetical ideal, a_{Mn}^{1600} and a_{Si}^{1600} —for model solutions)



Mn-Si-C system (Fig. 6.6). The solubility and activity of carbon in the melts of the Mn-Si-C system decrease with increasing silicon content, which is explained by the higher thermodynamic strength of the chemical bonds of manganese atoms with silicon than with carbon. This position is common for melts of the Fe-Si-C,

Fig. 6.5 Silicocarbide phases in the Mn–Si–C system

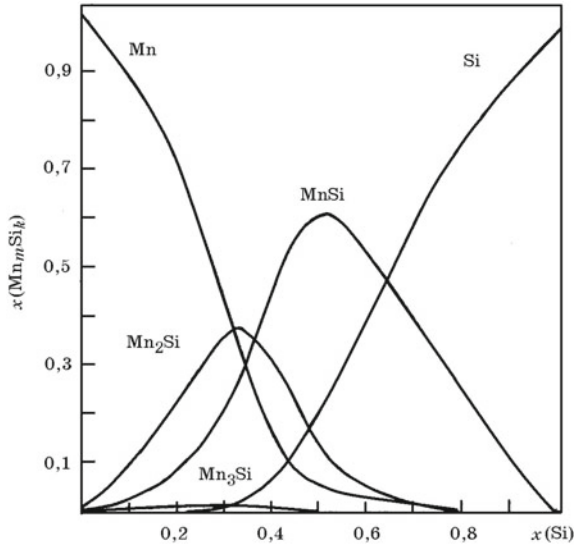
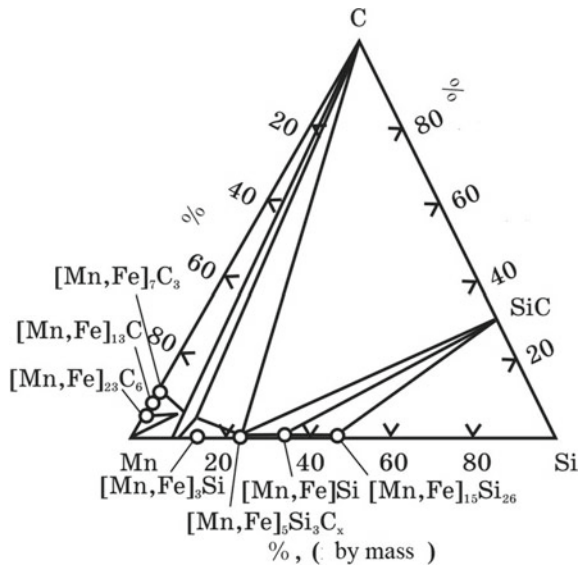


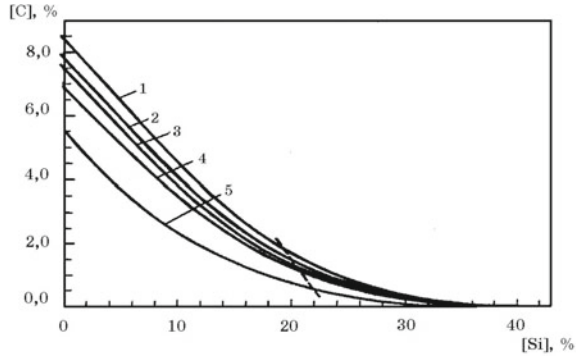
Fig. 6.6 Equilibrium state diagram of the Mn–Si–C system



Mn–Si–C and Cr–Si–C systems, as well as for melts of the (Mn, Fe)–Si–C, (Cr, Fe)–Si–systems C and (Cr, Mn)–Si–C. Figure 6.5 shows the dependences of the equilibrium carbon contents on the silicon concentration in melts of the Mn–Si–C, (Mn, Fe)–Si–C and Fe–Si–C systems at 1600 °C (Fig. 6.7).

The highest solubility of carbon occurs in the Mn–Si–C system, and the lowest in the Fe–Si–C system. As the % Mn/% Fe ratio decreases, the equilibrium solubility of

Fig. 6.7 Equilibrium carbon contents depending on the concentration of silicon in the systems: 1—Mn–Si–C_{sat}; 2—Mn–Fe–Si–C_{sat} at.% Mn/% Fe = 4; 3—Mn–Fe–Si–C_{sat} at.% Mn/% Fe = 2; 4—Mn–Fe–Si–C_{sat} at.% Mn/% Fe = 1; and 5—Fe–Si–C_{sat}



carbon decreases. A significant difference in the solubility of carbon in the systems under consideration when the silicon content is up to ~10–15% gradually decreases, and over 23–25% of the curves merge. It is important to note that with an increase in the silicon content to 23–25%, the equilibrium phase is graphite. In the concentration range of silicon content of more than 23–25%, the melts are in equilibrium with silicon carbide. For the Mn–Si–C system, the limiting value of the silicon content at which carbon can coexist with silicon carbide is 23.48% Si, which corresponds to the composition of the Novotny phase $Mn_5Si_3C_x$.

Figure 6.8 shows the manganese corner of the ternary diagram [Mn, Fe]–Si–C with the ratio %Mn/%Fe = 4. The presence of iron–manganese silicocarbitides $[Mn, Fe]_{17}Si_4C_3$, $[Mn, Fe]_3SiC$ in equilibrium is noteworthy with graphite and manganese silicocarbide $Mn_5Si_3C_x$ in equilibrium with SiC. The position of the carbon solubility isotherms in the melts of the [Mn, Fe]–Si–C system at.% Mn/% Fe = 4 indicates that with decreasing temperature the equilibrium carbon content decreases and the process is accompanied by the release of graphite or silicon carbide.

In commodity grades of ferrosiliconmanganese, depending on the alloy grade, up to 15–20% Fe can be contained at 65% Mn. Figure 6.8 shows the manganese corner of the ternary diagram [Mn, Fe]–Si–C with the ratio % Mn/% Fe = 4. The presence of iron–manganese silicocarbitides $[Mn, Fe]_{17}Si_4C_3$, $[Mn, Fe]_3SiC$ in equilibrium with graphite is noteworthy and manganese silicocarbide $Mn_5Si_3C_x$ in equilibrium with SiC. The position of the carbon solubility isotherms in the melts of the [Mn, Fe]–Si–C system at.% Mn/% Fe = 4 indicates that with decreasing temperature the equilibrium carbon content decreases and the process is accompanied by the release of graphite or silicon carbide.

The equilibrium boundary between carbo-silicidal phases and Mn–Fe–Si–C melts with graphite and SiC in Fig. 6.8 is represented by a broken line.

Mn–P system (Fig. 6.9). Phosphorus does not form solid solutions in manganese, but a number of manganese phosphides Mn_3P , Mn_2P , Mn_3P_2 , MnP are known (Table 6.1).

In the melts of the Mn–P system, there is a strong interparticle interaction of manganese with phosphorus, characterized by a significant negative deviation from Raoult’s law.

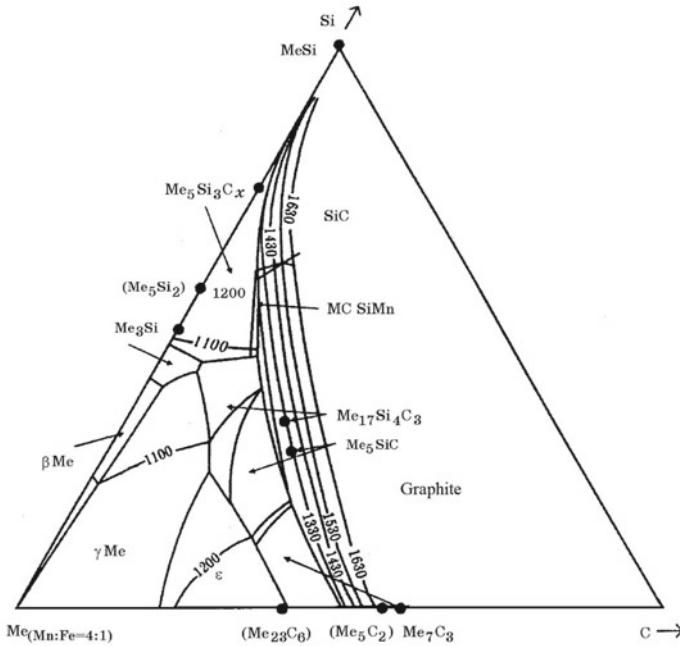


Fig. 6.8 Phase equilibria in the manganese corner of the Me (Mn: Fe = 4: 1)–Si–C diagram indicating the alloy composition regions in equilibrium with SiC and graphite; isotherms in °C

Mn–S system (Fig. 6.10). Manganese with sulfur forms thermodynamically strong manganese sulfides MnS and MnS₂. MnS sulfide melts at 1610 °C. A change in the thermodynamic potential of the sulfide formation reaction $\text{Mn}_T + \frac{1}{2}\text{S}_s = \text{MnS}_s$ in the range of 973–1573 K is described by the expression $\Delta G = \Delta G_T^0 = -296520 + 76.73T$, J/mol.

Mn–O system (Fig. 6.11). The equation for calculating the solubility of oxygen in liquid manganese at $a_{\text{MnO}} = 1$ has the form: $\log[\text{O}]\text{Mn} = -4823/T + 1.159$. An eutectic at 1245 °C corresponds to an oxygen content of 0.0095%.

For metallurgy of manganese, it is of great interest to know the properties of manganese oxides MnO₂, Mn₂O₃, Mn₃O₄ and MnO (Table 6.2).

Thermal Dissociation of Manganese Oxides. Mass spectroscopic methods were used to determine oxygen pressures and the composition of the vapor phase over MnO₂, Mn₂O₃, Mn₃O₄ and MnO (Table 6.3).

Thermal dissociation of the lower manganese oxides Mn₃O₄ and MnO occurs according to reactions 3 and 4 (see Table 6.3), and the dissociation pressure depends only on temperature, since Mn₃O₄ has practically no homogeneity region (Fig. 6.11).

During the evaporation of MnO, the vapor-gas phase consists of Mn⁺, MnO⁺, O ions; the intensity of the MnO⁺ and O⁺ ions is negligible.

Fig. 6.9 Equilibrium state diagram of the Mn–P system: **a** according to experimental data and **b** according to the results of thermodynamic calculation

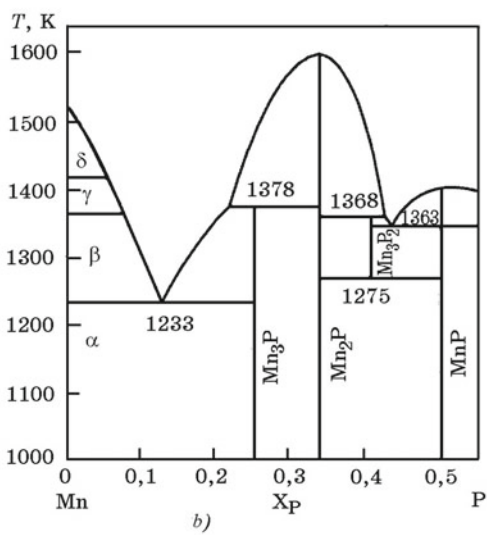
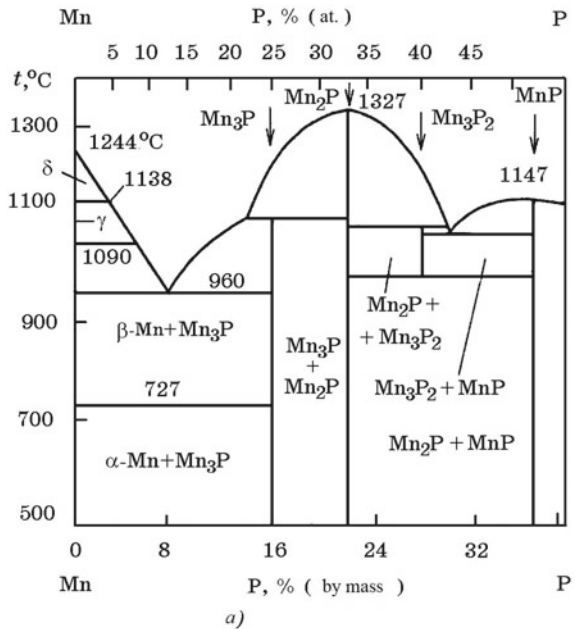


Table 6.1 Enthalpy and entropy of manganese phosphides

Phosphide	$-\Delta H_{298}^{\circ}$, kJ/mol	S_{298}° , J/(mol K)
Mn ₃ P	161	89.0
Mn ₂ P	150	76.0
MnP	96	49.2

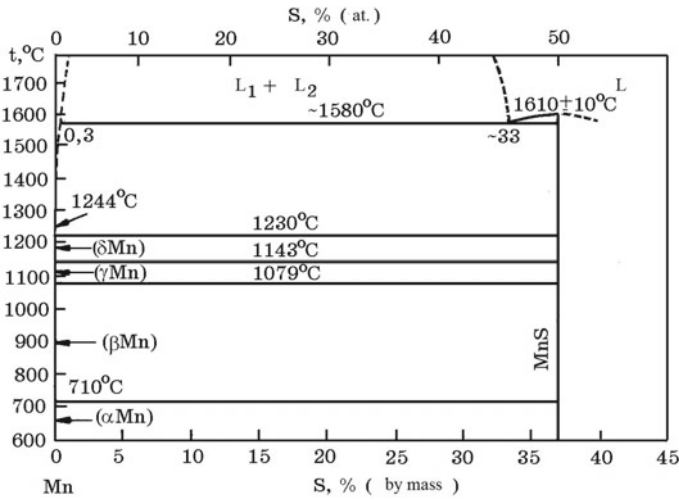


Fig. 6.10 Equilibrium state diagram of the Mn-S system

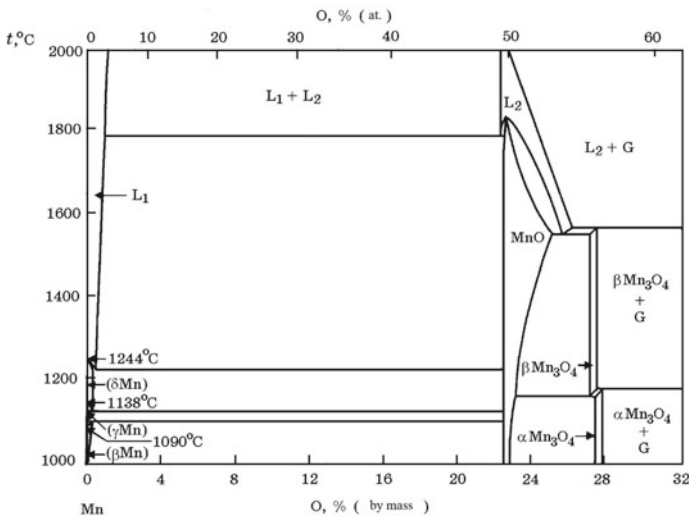


Fig. 6.11 Equilibrium state diagram of the Mn-O system

MnO-CO₂ system. Manganese carbonate MnCO₃ (rhodochrosite) is formed in this system. When heating MnCO₃ in the range of 620–690 °C, the carbonate dissociates by the reaction: MnCO₃ = MnO + CO₂. The mechanism of MnCO₃ dissociation is complex.

MnO-SiO₂ system (Fig. 6.12). Manganese oxide MnO with silica forms two compounds: tephroite (Mn₂SiO₄, 70.92% MnO) and rhodonite (MnSiO₃, 54.19%

Table 6.2 Physicochemical properties of manganese oxides

Parameters	MnO	Mn ₃ O ₄	Mn ₂ O ₃	MnO ₂
Relative molecular weight	70.93	228.81	157.87	86.93
<i>The oxygen content, %</i>				
Atomic	50	57.12	60	66.67
Mass	22.55	27.97	30.40	36.80
Density, g/cm ³	5.18	4.70	4.94	5.026
The heat of formation $-\Delta H_{298}^{\circ}$, kJ/mol	385.186	1387.5	971.75	521.257
Standard entropy S_{298}° , J/(mol K)	61.5	148.63	110.53	53.172
Gibbs energy change $-\Delta G_{298}^{\circ}$, kJ/mol	363.41	1281.16	882.0	466.409
The melting temperature, °C	1845	1590	1350	850

Table 6.3 Thermodynamic data of reactions of thermal dissociation of oxygen compounds of manganese according to the results of mass spectroscopic studies

Reaction	$\lg p_{O_2} = A/T + B(\text{Pa})$	T, K
$4\text{MnO}_{2(s)} = 2\text{Mn}_2\text{O}_{3(s)} + \text{O}_{2(\text{gas})}$	$\lg p_{O_2} = -9860/T + 15.98$	560–640
$6\text{Mn}_2\text{O}_{3(s)} = 4\text{Mn}_3\text{O}_{4(s)} + \text{O}_{2(\text{gas})}$	$\lg p_{O_2} = -11740/T + 13.92$	810–910
$2\text{Mn}_3\text{O}_{4(s)} = 6\text{MnO} + \text{O}_{2(\text{gas})}$	$\lg p_{O_2} = -23910/T + 17.73$	1270–1350
$2\text{MnO}_s = 2\text{Mn}_{\text{gas}} + \text{O}_{2(\text{gas})}$	$\lg p_{O_2} = -24730/T + 14.00$	1602–1747

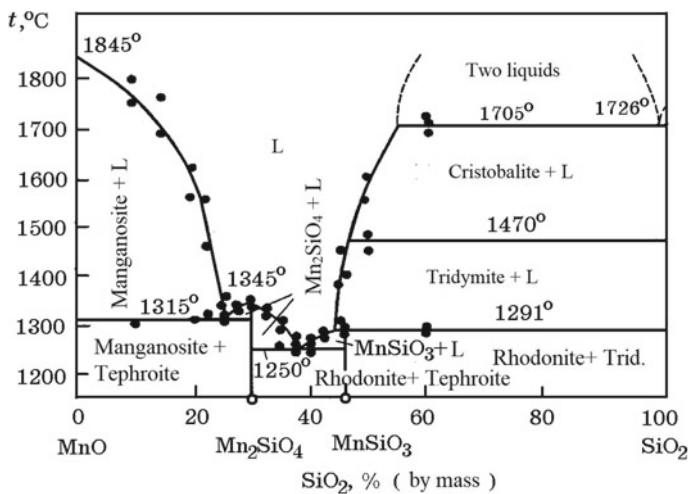


Fig. 6.12 Equilibrium state diagram of the Mn-SiO₂ system

MnO). Tephroite is stable up to a melting point of 1345 °C; rhodonite decomposes *peritectically* at 1291 °C. There are two eutectics in the system, which correspond to temperatures of 1315 and 1251 °C.

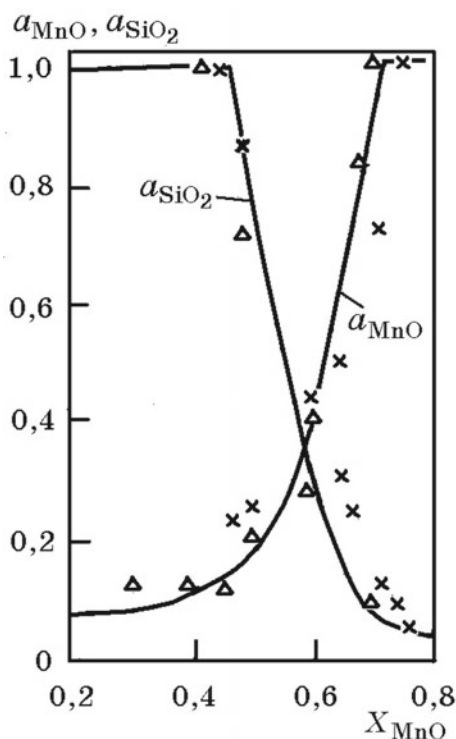
Tephroite (orthosilicate) and rhodonite (metasilicate) are formed from oxides by the reactions: $2\text{MnO} + \text{SiO}_2 = \text{MnSiO}_3$, $\Delta H = -59,440 \text{ J/mol}$ and $\text{MnO} + \text{SiO}_2 = \text{MnSiO}_3$, $\Delta H = -29,220 \text{ J/mol}$.

The activities of MnO and SiO₂ in the two-phase temperature–concentration regions of MnO + L and SiO₂ + L of the MnO–SiO₂ state diagram (Fig. 6.12) are equal to unity. In the single-phase region, the existence of the melt (L) of the activity of MnO and SiO₂ changes; with an increase in the fraction of MnO, its activity increases, and the activity of SiO₂ decreases (Fig. 6.13). When choosing pure solid oxides MnO and SiO₂ as the standard state, the dependence of the logarithm of the activity coefficient of MnO and SiO₂ on their molar fractions has the form:

$$\lg f_{\text{MnO}} = -3.123(1 - x_{\text{MnO}})^2 + 0.348;$$

$$\lg f_{\text{SiO}_2} = -3.123(1 - x_{\text{SiO}_2})^2 + 1.188.$$

Fig. 6.13 Activity of manganese oxide a_{MnO} and a_{SiO_2} in the MnO–SiO₂ system at 1600 °C



The results of calculating the activity and activity coefficients of MnO and SiO₂ according to [2] are given below:

x_{MnO}	0.526	0.550	0.600	0.650	0.700	0.737
x_{SiO_2}	0.474	0.450	0.400	0.350	0.300	0.263
f_{MnO}	0.443	0.520	0.705	0.923	1.256	1.355
f_{SiO_2}	2.108	1.751	1.158	0.739	0.455	0.310
a_{MnO}	0.233	0.286	0.423	0.600	0.879	1.000
a_{SiO_2}	1.000	0.788	0.463	0.258	0.136	0.082

6.2 Manganese Minerals, Ores and Concentrates

The explored reserves of manganese ores on the continents are extremely uneven: South Africa 57%, Ukraine 21%, Gabon 7%, Australia 4%, other countries 11%.

Significant reserves of manganese are concentrated on the bottom of the oceans in the form of iron–manganese nodules containing non-ferrous metals Cu, Ni, Co, Mo, etc.

The most common manganese minerals are: pyrolusite MnO₂, Hausmannite Mn₃O₄, manganite MnO(OH), psilomelane MnO·MnO₂·nH₂O, manganocalcite (Mn, Ca)CO₃, etc.

Deposits of manganese ores are unevenly located on the territory of the former USSR. In Russia, 6.1% of the reserves of manganese ores of the former USSR have been explored, 82.4% in Ukraine, 8.9% in Georgia and 2.6% in Kazakhstan.

The majority of manganese ores are mined in Nikopol (~80%) and Chiatura (~20%) manganese ore basins.

The most common are carbonate and mixed manganese ores (70.3% of the total reserves); oxide constitutes 28.3%. The reserves of oxidized ores (1.1%) and iron–manganese (0.3%) are limited.

Manganese ore minerals, like concentrates, are complex mineral raw materials. Manganese ores of the main deposits of the CIS countries are characterized by a relatively high phosphorus content (0.2–0.3%). The occurring isolated phosphorus-containing minerals are represented by the kurskite Ca₃(PO₄)·CaO₃, francolite Ca₁₀F₂CO₃O₂₄·H₂O, vivianite (FeO₄) and other phosphates.

According to the content of ore-forming minerals, oxidized ores are divided into manganite-psilomelanic with an admixture of pyrolusite; pyrolusite-psilomelanic with an admixture of manganite; and pyrolusite-psilomelanic. Carbonate ores belong to the isomorphic series of manganocalcite–calcium rhodochrosite. The latter contains an average of 80–86% MnCO₃; 14–20% CaCO₃; and 39.8–42% Mn. Manganocalcite has a variable composition%: 28–58 MnCO₃; 42–56 CaCO₃; and 13–30 Mn.

Nonmetallic minerals in manganese ores are represented by quartz, feldspar, opal, chalcedony, glauconite $(K,Na,Ca)_{<1}(Al, Fe^{2+}, Fe^{3+}, Mg)_2 \cdot [(OH)_2Al_{0,5}Si_{3,65}O_{10}]$. Manganese ore mined from the bowels is subjected to enrichment using complex methods and technological schemes (washing, gravity, electromagnetic, flotation, etc.) (Fig. 6.14a).

Quality Requirements for Manganese Concentrates. The chemical composition of manganese concentrates in the Nikopol basin is governed by the content of manganese and silicon dioxide, as well as the amount of moisture (Table 6.4), and the particle size distribution—by the fractions shown in Table 6.5.

6.3 The Technology for High-Carbon Ferromanganese Smelting

Dephosphorization of Manganese Concentrates. Manganese ore mined from the bowels has a high content of harmful impurities—phosphorus 0.18–0.22%. When manganese ore is enriched by mechanical methods, phosphorus is not removed and passes into manganese concentrates. For the smelting of manganese ferroalloys with a low phosphorous content, part of the concentrates is subjected to dephosphorization by the electrometallurgical method.

The essence of the method consists in the selective reduction of phosphorus and iron by carbon with their conversion to associated high-phosphorus ferromanganese. For this, manganese concentrates in a mixture with a small amount of coke are melted in a ferroalloy electric furnace (Fig. 6.15).

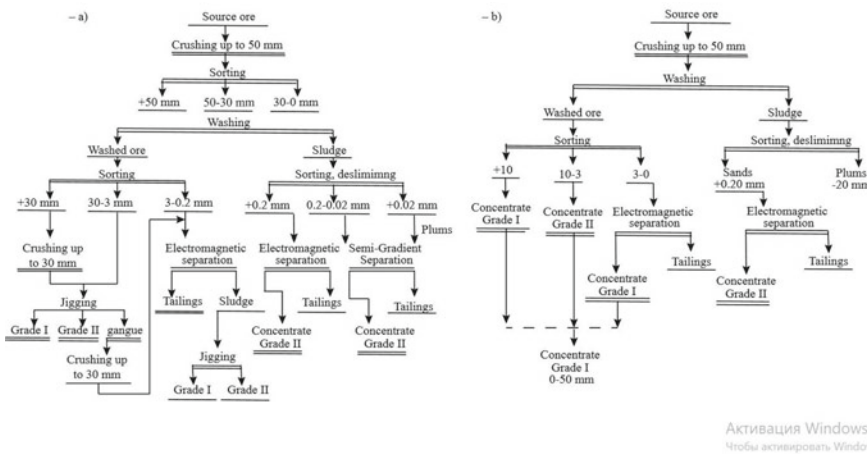


Fig. 6.14 Schematic diagram of the enrichment of manganese ores in the Nikopol basin: **a** oxide ores and **b** carbonate ores

Table 6.4 Requirements of technical conditions for the quality of manganese concentrates of the Nikopol basin

Concentrates	Grade	Content, %		
		Mn	Moisture	LOI
Manganese oxide (O)	I	43.1/43.0 ^a	16.0	–
	IB	– /41.0	16.0	–
	II	– /34.0	22.0	–
	III	– /25.0	23.0	–
Manganese oxide-carbonate (OC)	I	26.5/26.0	18.0	17.0
	II	– /23.0	20.0	14.0
Manganese flotation oxide (FO)	I	– /43.0	27.0	–
	II	– 34.0	27.0	–
Manganese flotation oxide-carbonate (FOC)	I	– /26.0	27.0	17.0
	II	– /23.0	27.0	14.0

^a The numerator is the highest, and the denominator is the first category of quality

Table 6.5 Granulometric composition of manganese concentrates in the Nikopol basin

Fraction, mm	Oxide concentrate (gravity)			Oxide-carbonate concentrate I grade
	Grade			
	A	I	II	
More than 25	2.49	10.76	8.66	–
25–8	32.33	17.89	10.02	–
8–5	26.62	35.96	15.33	–
5–3	19.87	5.06	6.90	–
3–0.5	13.81	22.67	41.85	65.92
0.5–0.2	4.88	5.28	13.85	18.46
0.2–0.1	–	2.38	–	–
Less than 0.1	–	–	3.40	15.62

The process is conducted continuously, and melting products are released periodically. The resulting slag contains 38–40% Mn and not more than 0.012–0.017% P, the associated phosphorous alloy contains 50–55% Mn and 1.5–2.5% Si, and the rest is Fe, C, etc.

High-Carbon Ferromanganese Assortment. The chemical composition of electrothermic high-carbon ferromanganese is regulated by GOST 4755-80 (Table 6.6) (Russia) and DSTU 3547-97 (Table 6.7) (Ukraine).

Ore-smelting electric furnaces. High-carbon ferromanganese with a phosphorus content of $\leq 0.35\%$ and $\leq 0.6\%$ is smelted in RPZ-63 closed-type ore-smelting electric furnaces (Fig. 6.16) and RKG-81 (Fig. 6.17).

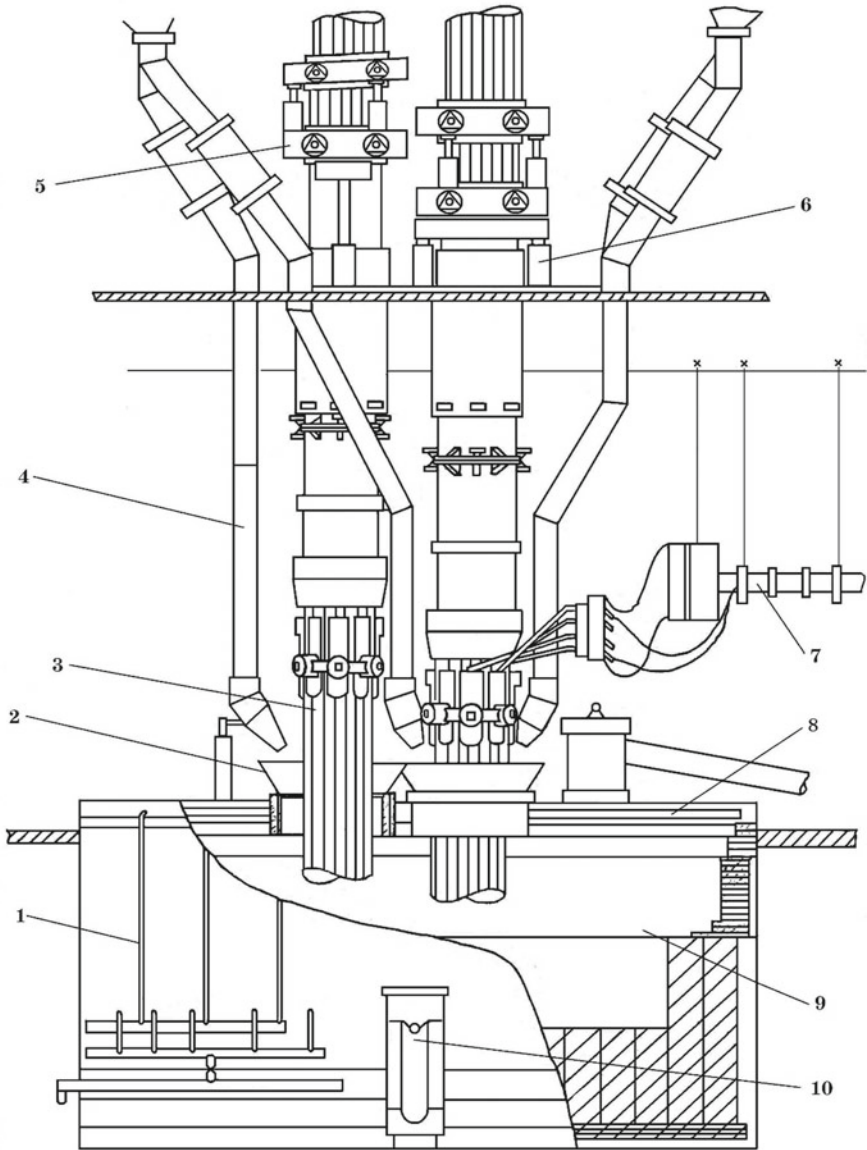


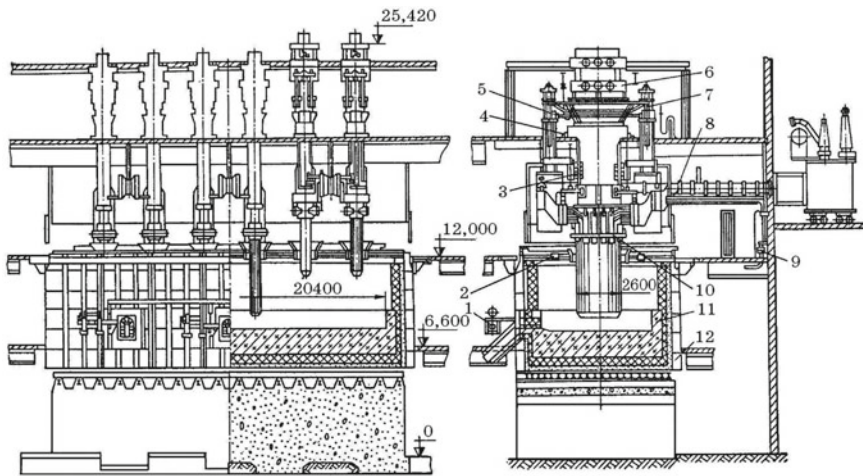
Fig. 6.15 Ore-smelting electric furnace for smelting low phosphorous slag 1—casing of the furnace bath; 2—loading funnel for feeding the mixture into the furnace bath; 3—continuous self-baking electrodes; 4—tubes for feeding the mixture into the funnel; 5—a system for holding and bypassing electrodes; 6—hydraulic cylinders for moving electrodes; 7—packages of a short power supply network of the furnace from the furnace transformer; 8—furnace arch; 9—bath furnace; and 10— notch and exhaust trough

Table 6.6 Chemical composition (%) of high-carbon ferromanganese produced by electrothermic method (GOST 4755-80)

Grade (GOST 4755-80)	Mn, no less	C	Si	P	S
		No more			
FeMn78A	78–82	7	2	0.05	0.03
FeMn 78K	78–82	7	1	0.35	0.03
FeMn 78	78–82	7	2	0.35	0.03
FeMn 75AC6	75	7	6	0.05	0.03
FeMn 75C4	75	7	4	0.45	0.03
FeMn 75C9	75	6	9	0.45	0.03
FeMn 75	75	7	1	0.45	0.03
FeMn 70	70	7	6	0.60	0.03

Table 6.7 Chemical composition (%) of high-carbon ferromanganese (DSTU 3547-97)

Grade	Mn	C, max	Si, max	P, max	S, max
FeMn78A	75–82	7.0	6.0	0.10	0.03
FeMn78B	75–82	7.0	6.0	0.70	0.03

**Fig. 6.16** Ore-smelting rectangular closed electric furnace of RPZ-63 type with a capacity of 63 MV A for smelting manganese ferroalloys: 1—devices for notch burning; 2—arch; 3—a device for fixing the electrode holder; 4—seals; 5—hydraulic drive system; 6—device for bypassing the electrodes; 7—hydraulic lift; 8—short network; 9—water cooling system; 10—electrode holder; and 11—lining; 12—casing

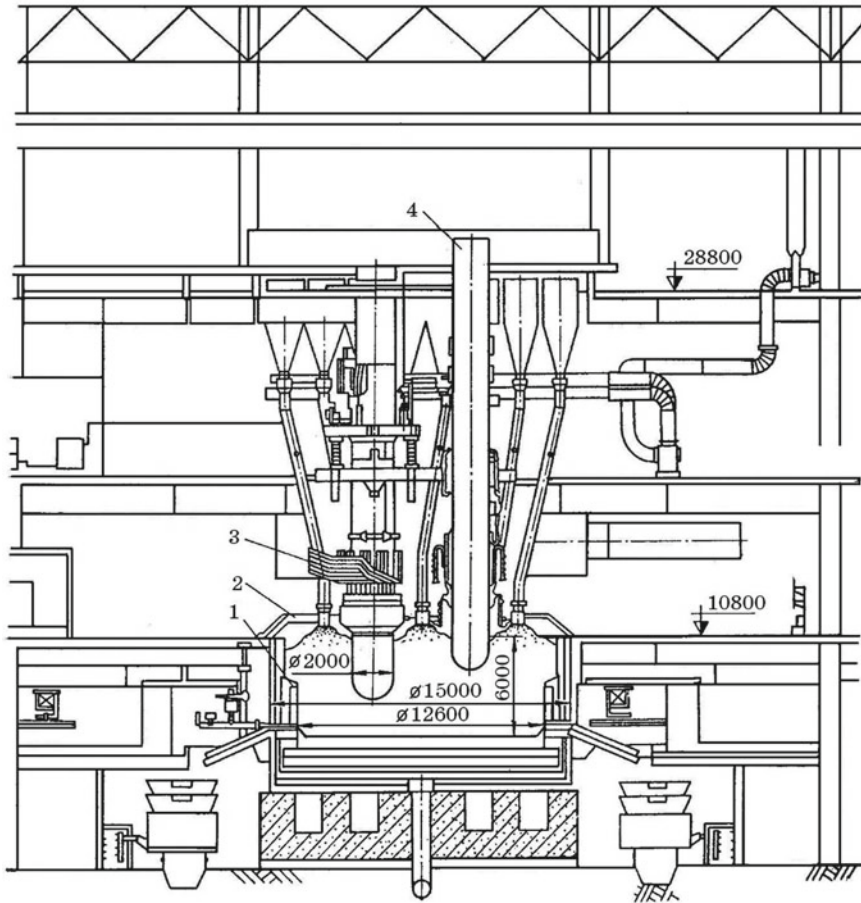


Fig. 6.17 Ore-smelting round sealed electric furnace with capacity 81 MV A for smelting manganese alloys: 1—carbon blocks of the walls of the furnace; 2—arch; 3—short network; and 4—electrode

Below are the technical characteristics of electric furnaces with rectangular (RPZ-63) and round (RKG-81) bathtubs for smelting high-carbon ferromanganese (self-baking electrodes):

Furnace type	RPZ3-63	RKG-81
Installed capacity of the furnace transformer, MV A	63 (3 × 21)	81 (3 × 27)
High side voltage, kV	154	154
Secondary voltage limits, V	238.5–137.0	340–180
Maximum current in phase, kA	112	160
Power factor	0.91	0.92

(continued)

(continued)

Furnace type	RPZ-63	RKG-81
Electrode dimensions in cross section, mm	3000 × 750	Diameter 2000
The distance between the electrodes, mm	3300	4300
Average electrode travel speed, m/min	0.5	2
Electrode stroke, mm	1200	1600
<i>Dimensions of the melting space, mm</i>		
Length/diameter	20,340	15,000
Width	6000	–
Height	3190	7300
Number of notches	3	2

RPZ-63 electric furnaces are equipped with three single-phase transformers, each having 23 voltage levels.

The energy and structural characteristics of the RPZ-63 and RKG-81 furnaces are given below:

Furnace	RPZ-63	RKG-81
The current density in the cross section of the electrode, A/cm ²	5.30	5.13
Power density in the cross section of the electrode, W/cm ²	413.8	478.5
Specific power in the volume of the bath, kW/m ²	65.8	72.4
Specific active power on the area of the electrode cycle, kW/m ²	2200	1800
The cross-sectional area of the electrode, m ²	2.25	2.14
Hearth area, m ²	188.6	124.6

The optimal active power of the RKG-81 furnace is 45–47 MW. High performance of a round furnace is guaranteed under the condition of using a manganese sinter fraction of 20–100 mm and a content of $\leq 14\%$ SiO₂, a manganese concentrate of a fraction of 10–30 mm and a content of $\leq 112\%$ SiO₂.

RPZ-63 electric furnaces are equipped with a longitudinal-capacitive compensation unit, which provides an increase in power factor up to 0.90–0.92.

The gas treatment system of the furnace consists of six typical independent lines with one backup. At the outlet of the gas treatment system, the gas contains less than 20 mg/m³ of dust, which allows it to be burned in boiler furnaces and used for the sintering of manganese concentrates. Deepening the furnace bath from 2.85 m according to the design to 4.5 m allowed to reduce the dust content of flue gas by 2–2.5 times.

Ore-smelting electric furnaces are equipped with continuous self-baking electrodes, the use of which ensures the continuity of the process without stopping the furnaces to build up electrodes.

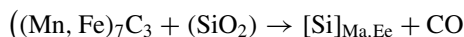
Physicochemistry of the process. Theoretical temperature of the beginning of manganese reduction to MnC_x carbide by reaction



$$\Delta G_T^0 = 196,293 - 123T$$

equal to 1597 K (1324 °C). Since ferromanganese contains ~7% C, in a first approximation we can assume that the alloy is mainly represented by carbides Mn_7C_3 and $(\text{Mn}, \text{Fe})_7\text{C}_3$.

The temperatures of the beginning of reduction and melting of ferromanganese are close; therefore, liquid droplets of carbon-saturated metal, deposited on the bottom of the furnace, interact with coke and with slag melt, which leads to the reduction of silicon according to the scheme:



High-carbon ferromanganese FMN78 (up to 0.7% P) is smelted mainly by an economical flux-free process. The resulting high-manganese slag (38% Mn) is used as the initial component of the charge for smelting silicomanganese with a low phosphorus content, which increases the extraction of manganese and reduces the consumption of charge materials.

In the flux method, high-carbon ferromanganese is smelted using starting concentrates, coke and limestone. To achieve a lower phosphorus content in the charge, the calculated amount of high-manganese low-phosphorous slag (HMLPS) is used. The process leads to a more complete reduction of manganese and the production of waste slag with a basicity of %CaO/%SiO₂ 1.0–1.2 and a MnO content of 10–14%. Calculation of the charge for smelting high-carbon ferromanganese flux method is given in Appendix A.

The flux method is less economical in comparison with the flux-free method (Table 6.8). Regardless of the method of smelting ferromanganese, the release of the alloy and slag from the six-electrode RPZ-63 furnaces is made from three notches of the furnace in turn into the ladle. The taphole is opened with a machine that can move along the guides, drill the taphole, clean the front wall of the furnace in the taphole zone, knock out the cork of the remaining drill hole in the taphole and return to its original position.

After the release of the melting products, the trolley with the ladle is fed into the casting span. The slag is poured into the bowl, and the slag remaining in the ladle is thickened with sand to prevent it from falling onto the ingots. Then, the ladle with ferromanganese is fed to the filling machine, and the slag is taken out for slag processing or dump. Ferromanganese is poured on belt machines with cast iron molds.

The filling machine is intended for casting ferroalloys into molds, cooling, forming ingots and transporting them to the finished goods warehouse. It is a closed two-belt conveyor with a length of 70 m. The main technical data of the filling machine are given in Table 6.9. The optimum temperature for casting ferromanganese is 1380–1340 °C, and the ingot thickness in the mold is 85 mm.

Table 6.8 Main technical and economic indicators of smelting high-carbon ferromanganese

Parameters	Smelting method	
	Flux	Non-flux
<i>Specific consumption, kg/b.t</i>		
Manganese raw material (48% Mn)	2060	2971
Coke	580	415
Pellets	110	85
Limestone	700	–
Electrode mass	21	22.4
Specific power consumption, kWh/b.t	4290	3498
Slag (HMLPS) yield (48% Mn), kg/b.t	–	1353
Mn in slag, %	14.2	35.8
Slag ratio	1.2	0.88
Extraction of Mn, %	78–82	98.8

Table 6.9 Technical characteristics of the casting machine MPF-4-722-270

Parameter	Design values
<i>The capacity of the casting, t/h</i>	
Low-phosphorous slag	24
Silicomanganese	48
Ferromanganese	60
Conveyor speed, m/min	3.25; 5; 6.5; 10
The total number of molds, pcs	726
Type of tilting device	Hydraulic lifts
Bucket tilt angle, degrees	100
Conveyor tilt angle, degrees	8°30'
Bucket capacity, m ³	8
Drive power, kW	50
Mold weight, kg	370
Machine weight, t	504
<i>Dimensions, mm</i>	
Length	79,500
Width	12,200
Height	9950

Fractionation of ferroalloys at the NZF is carried out by a crushing and screening complex, which includes: «KueKen» jaw crusher equipped with a device for regulating the output gap from 50 to 150 mm and providing crushing of metal without friction, vibration screening of the «Seko» company, consisting of a box assembly with three removable screens and feeder P1-1211.

Depending on the required size class of finished products, a certain exit slit is installed on the crusher, and the necessary sieves with mesh sizes of 80×80 , 70×70 , 50×50 , 20×20 , 10×10 and 5×5 mm are installed on the crusher. Productivity of crushing and screening complex is 120–150 thousand tons/year depending on the fraction.

Along with the production of high-carbon ferromanganese in electric furnaces, in modern conditions its production in blast furnaces has partially been restored. At the Kosaya Gora Iron Works (Russia), ferromanganese is smelted in three blast furnaces with volumes of 880, 706 and 408 m³.

From the technological point of view, ferromanganese blast furnace smelting is characterized by a number of progressive measures aimed at increasing smelting efficiency: increasing blast temperature, increasing blast furnace gas pressure, using basic magnesia slags, involving lumpy naturally fluxed carbonate manganese ore, iron–manganese low-phosphorous ore from Kazakhstan, manganese sinter and high-basicity sinter (*iron flux*). An increase in the temperature of the blast leads to a rational distribution of heat in the furnace and favorably affects the restoration of manganese. An increase in the temperature of the blast by 100 °C gives a coke saving of 6–8%. With this in mind, two high-temperature small-sized air heaters with a corundum ball nozzle with blast heating up to 1400 °C were built at the plant. Favorable conditions for the restoration of manganese create the main slag. The optimum basicity should be considered the CaO/SiO₂ ratio, equal to 1.2–1.3 with a content of 6–8% MgO. When using carbonate ore, the gas permeability of the mixture improves, the top temperature decreases, the consumption of raw fluxes decreases, and the utilization of manganese increases.

The proportion of carbonate ore in the mixture is limited by its high phosphorus content. This shortcoming was offset by the development of the Ushkatynsk manganese ore in production. In recent years, the plant has been working to involve in the production of iron flux basicity of 3.5. Its use made it possible to exclude expensive metal additives from the charge and sharply reduce the consumption of raw fluxes.

At OJSC Magnitogorsk Iron and Steel Works, ferromanganese is smelted in a blast furnace using manganese ore from the Zhairemsky deposit. The specific consumption of charge materials is determined by solving a system of three equations: for manganese, slag basicity and magnesia content. The slag yield is 1150 kg/t of alloy. Tuyere gas has the composition: 34.8% CO, 2.7% H₂, 62.5% N₂. In the blast flow 30 m³/t of process oxygen and 60 m³/t of natural gas. The temperature of the air heater is 1250 °C. The composition of blast furnace gas is: 9.5% CO₂, 31.4% CO, 2.0% H₂ and 57.1% N₂.

6.4 The Technology of Ferrosiliconmanganese Smelting

Ferrosiliconmanganese is used for deoxidation and alloying of steel, alloys, cast iron, production of refined manganese alloys in the metallurgical industry. This is a ferroalloy, the basis of which is manganese with a mass fraction of at least 60%

and silicon with a mass fraction of 10–35%, and the alloy also contains phosphorus, sulfur and carbon with limited upper mass fractions (Table 6.10). The calculation of the charge for smelting ferrosiliconmanganese is given in Appendix B.

Depending on the mass fraction of phosphorus (P), ferrosiliconmanganese is divided into groups A and B, and by size of pieces—into size classes 1, 2, 3, 4, 5.

The carbon content in the alloy depends on the concentration of silicon: The more silicon in the alloy, the lower the solubility of carbon in it, since the chemical bond of Mn–Si is higher than Mn–C.

The process of forming silicomanganese consists of the following stages. The process of forming silicomanganese consists of the following stages. Initially, the processes of reduction of higher manganese oxides MnO_2 , Mn_2O_3 and Mn_3O_4 develop with the participation of CO and then MnO according to the direct reduction reaction to carbide: $(\text{MnO}) + (1 + x)\text{C} \rightarrow \text{MnC}_x + \text{CO}$. In the zone of high temperatures, the reaction of silica reduction is noticeably developing. The presence of a metal melt thermodynamically facilitates the process of silicon reduction with the formation of ferrosiliconmanganese $(\text{SiO}_2) + 2\text{C} + \text{MnC}_x = [\text{Mn-Si-C}_x] + 2\text{CO}$.

Ferrosiliconmanganese in the conditions of OJSC “NZF” is smelted in electric furnaces with rectangular baths (RPZ-63), with round baths (RKZ-75, RKZ-27). The charge uses manganese sinter AMNV-2 (manganese content not less than 37%) and AMNV-1 (not less than 47.5% Mn) with a grain size of 5–200 mm, produced on sintering machines of the NZF. In order to reduce the phosphorus content in ferrosiliconmanganese from 0.60 to 0.50%, 0.35, 0.25 and 0.15% manganese slag is used in the charge (fraction 0–150 mm). Along with Nikopol manganese concentrate, imported high-manganese low-phosphorous manganese ores from the deposits of Ghana, Gabon and Australia are used.

As a silica-containing component, quartzite (not less than 96% SiO_2 and not more than 1.8% Al_2O_3) with a grain size of 25–80 mm is used, and reducing agents—coke—sorted fractions of 5–25 mm and anthracite. For the formation of furnace slag of a certain basicity, limestone is used (the sum of % CaO + % MnO is not less than

Table 6.10 Chemical composition of ferrosiliconmanganese

Alloy grade	Mass share of element, %					
	Si	Mn, no less	C	P		S
				A	B	
			No more			
SiMn25	From 25.0 to 35.0 incl.	60.0	0.5	0.05	0.25	0.03
SiMn 22	«20» 25.0 «	65.0	1.0	0.10	0.35	0.03
SiMn 17	«15» 20.0 «	65.0	2.5	0.10	0.60	0.03
SiMn 12	«10.0» 15.0 «	65.0	3.5	0.20	0.60	0.03

Note The letters and numbers in the designation of the brand of the base alloy of ferrosiliconmanganese mean: Mn—manganese, Si—silicon; the numbers following the letter are the average mass fraction of silicon in whole units

51.5%). The ratio of C_s/Mn in the charge should be 0.38–0.47 (RPZ-63 furnace) and 0.38–0.4 (RKZ-75 furnace); the ratio $C/(Mn + SiO_2)$ in the range of 0.19–0.25; and SiO_2/Mn no more.

The normal technological process of smelting ferrosiliconmanganese is characterized by a uniform charge flow, top gas pressure under the arch of 1–3 Pa (closed RPZ-63 furnaces), 5–20 Pa (RPG-63 sealed furnaces) and 20–50 Pa (RKG-75 furnaces). The gas temperature in the under-arch space should not exceed 400 °C (RPZ-63 furnaces) and 200 °C (RKG-75 furnaces). Top gas contains up to 85% CO. The content of oxygen and hydrogen in the top gas should not exceed 1.0 and 8%, respectively.

For the smelting of ferrosiliconmanganese with a low phosphorous content, charges with various amounts of low-phosphorous manganese ore components are used (Table 6.11).

With a decrease in the phosphorus content in ferrosiliconmanganese (i.e., with an increase in the fraction of slag), the specific energy consumption significantly increases, the slag multiplicity increases, and the useful manganese extraction decreases (Table 6.12).

Ferrosiliconmanganese and slag from the RPZ-63 furnace are released after 2 h (after the next release) into cascaded ladles (one for metal and two for slag). Notches are opened by the car. Ladles for receiving the alloy lined with bold sand using the SB-50 sandblast.

Slag (47–40% SiO_2 , 13–15% Mn, 12–13% CaO, 5–7% Al_2O_3 , 2.9–3.1% MgO) is discharged into steel buckets with a capacity of 11 m³. Duration of release is 20–40 min. Notches are covered with carbon mass. Ladles with metal and slag are rolled out into the casting span.

Ferrosiliconmanganese is poured on a filling machine, which has the following characteristics: number of conveyors 2; conveyor speed 3.25; 5; 7; 10 m/min; length 70.4 m; total number of molds 725; and tilt angle of the tilter 100°.

Table 6.11 Compositions of the charges for smelting ferrosiliconmanganese with different phosphorous contents

Charge component	Phosphorus content in ferrosiliconmanganese, %				
	0.15	0.25	0.35	0.50	0.60
Sinter	–	500	940	1370	1660
Manganese slag	900	730	360	180	–
Manganese ore (Australia)	680	400	340	140	–
Coke	310	310	320	320	320
Quartzite	250	260	260	260	260
Limestone	60	–	–	–	–
Iron ore pellets	55	65	50	50	50
Secondary manganese raw materials (waste)	200	300	300	400	400

Table 6.12 Technical and economic indicators of smelting ferrosiliconmanganese with different phosphorus contents

Parameters	Phosphorus content, %			
	0.20	0.35	0.50	0.60
<i>Specific consumption, kg/t</i>				
Manganese raw materials (48% Mn)	1843	1728	1700	1674
Coke	415	425	410	395
Quartzite	285	333	305	294
Limestone	100	–	–	–
Recyclable waste	163	234	251	217
Secondary manganese raw materials	–	208	194	153
Electrode mass	28.5	24.6	24.2	24.0
Specific power consumption, kWh/t	4191	4088	3930	3840
Mn content in slag, %	11.7	12.4	12.6	12.5
Slag ratio	1.6	1.5	1.4	1.3
Extraction	75.26	79.9	81.5	82.2

The gas cleaning system of the RPZ-63 furnace consists of six standard independent lines and one common gas blower. Up to 50 m³/h of water is consumed for cooling and wet gas purification. Usually, five lines work with one backup. At the exit of the gas treatment system, the gas contains up to 20 mg/m³ of dust, which allows it to be burned in boiler furnaces.

6.5 The Technology of Smelting of Metallic Manganese, Low- and Medium-Carbon Ferromanganese

Metallic Manganese. Manganese of technical purity (95–99.8% Mn), called metallic (Table 6.13), is obtained by silicothermic and electrolytic methods. In some countries, manganese metal is produced by the aluminothermic method.

Table 6.13 Chemical composition of metallic manganese, % (GOST 6008-90)

Grade	Production method	Mn, no less	C	Si	P	S
			No more			
Mn998	Electrolytic	99.8	0.04	–	0.003	0.003
Mn997		99.7	0.06	–	0.05	0.10
Mn965	Electrothermic	96.5	0.10	0.8	0.05	0.05
Mn95		95.0	0.20	1.8	0.07	0.05

Silicothermic Metallic Manganese Technology. The silicothermic process for the production of manganese ferroalloys is based on the reaction of reduction of MnO by silicon of silicomanganese. The technology of metallic manganese includes three stages (Fig. 6.18): I—smelting of low-phosphorous high-manganese slag; II—smelting silicomanganese with high silicon content; and III—obtaining metal manganese.

Smelting of low-phosphorous charge slag (LPCS; “charge” means purposed for further processing). The mixture for the smelting of the low-phosphorous charge

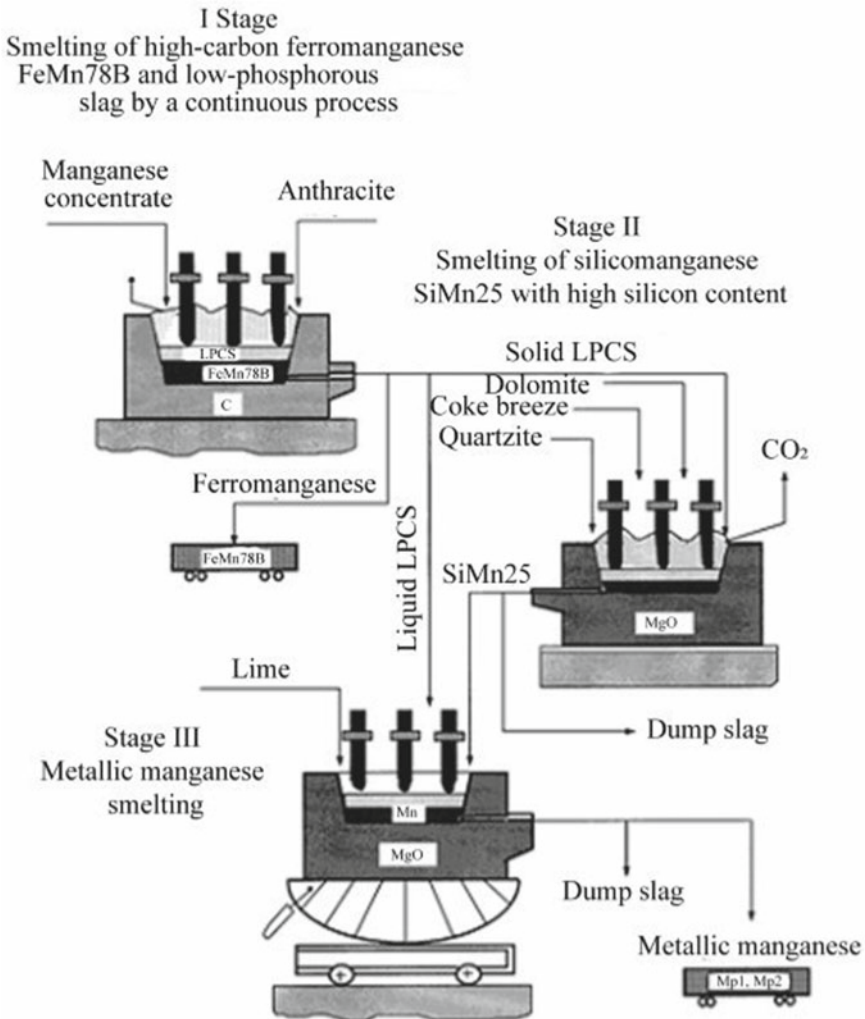


Fig. 6.18 Three-stage technological scheme for the production of metallic manganese with the preparation of FMn78B ferromanganese in the first stage and low-phosphorous charge slag (LPCS)

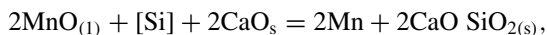
slag consists of manganese concentrate, dump slag of commercial ferrosilicomanganese and coke, the amount of which is determined from the calculation of the reduction of iron, phosphorus and partially manganese. Previously, slag was smelted by the carbothermic method in inclined arc furnaces with a capacity of 5 MV A with magnesite lining (Fig. 6.15) by a batch process. The disadvantage of the previously used technological scheme is the formation at the first stage of an associated phosphorous alloy containing, %: 45–55 Mn; 30–45 Fe; 1.5–3 P; 0.1–0.3 Si; 3.5–5 C, which did not have a wide industrial use and which led to a decrease in the beneficial use of manganese. In order to increase the beneficial use of manganese in the first stage according to the current technological scheme, the slag is smelted by a continuous process (Fig. 6.18); along with slag, not an associated phosphorous alloy is produced, but commercial high-carbon ferromanganese FeMn78B grade (up to 0.7% P) due to the greater amount of reduced manganese. This required the adjustment of the technology for smelting silicomanganese with high silicon content and metallic manganese, as the first stage slag began to contain 36–38% Mn against 42–44% according to the previously used technological scheme.

Smelting of silicomanganese with high silicon content (“foundry” silicomanganese). Silicomanganese with high silicon content is obtained in ore-smelting furnaces by co-reducing manganese and silicon from a charge consisting of redox phosphoric manganese slag, quartzite and coke. Silicomanganese is smelted in furnaces with a capacity of 16.5 MV A by a continuous process with periodic production of alloy and slag. The normal course of the furnace is characterized by a stable immersion of electrodes in the charge and a uniform release of metal and slag from the furnace. To obtain silicomanganese with a low iron content, graphitized electrodes with a diameter of 450 mm are used; 83.7% Mn and ~60% Si go into the alloy. The carbon content in the alloy is 0.08–0.1% at a silicon concentration of 27–29%. The chemical composition of the dump slag of silicomanganese is, %: 8.6 Mn (11.09 MnO); 46.8 SiO₂; 18.8 CaO; 10.0 MgO; 9.9 Al₂O₃; 0.002 P; and 1.7 S. The slag ratio is 0.8–1.

Smelting of metallic manganese. The process of reduction of MnO by silicon of converted silicomanganese can be represented by the reaction



The introduction of calcium oxide improves the thermodynamic conditions of the process, shifting it toward a more complete extraction of manganese and metal yield. For the reaction



$$\Delta G_{1773-1873\text{K}}^0 = 18480 + 86.47T, \text{ J/mol.}$$

The addition of CaO to the MnO–SiO₂ system increases the thermal effect of the Mn reduction reaction by silicon. Melting is carried out using liquid low-phosphorous

manganese slag in open inclined arc furnaces with a capacity of 5 and 7 MV A (Fig. 6.19). The furnace bath is lined with magnesite brick. Lime is used as a flux, %: 93.2 CaO; 0.3–0.5 SiO₂; 0.04 FeO; 0.1 Al₂O₃; 0.5 MgO; 0.03 S; 0.005 P; and 7.5–7.8 LOI. The reducing agent is crushed (granular) silicomanganese. The total melting time is 3–3.5 h. Specific consumption of charge materials and electric energy per 1 t of manganese metal is: 2087 kg of low-phosphorous slag (48% Mn), 650 kg of silicomanganese, 1631 kg of lime, 2590 kWh/t electricity. The slag ratio reaches 3.6–4.0, depending on the brand of smelted metallic manganese.

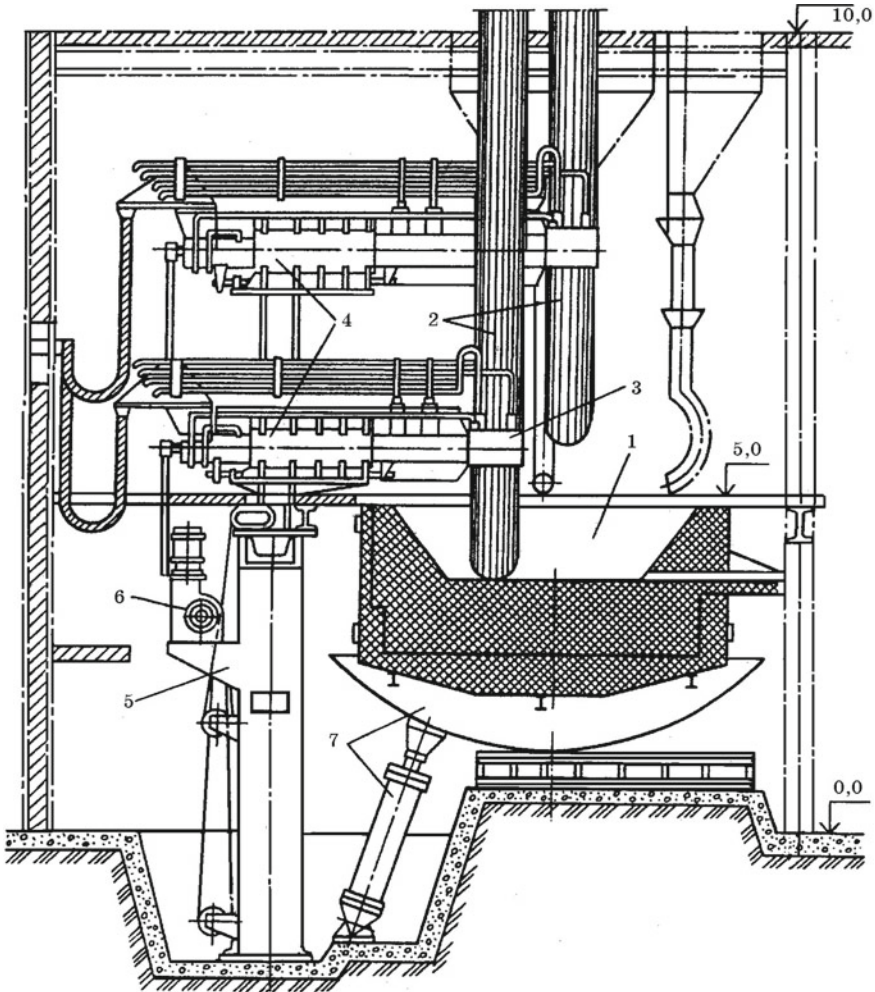


Fig. 6.19 General view of a ferroalloy refining furnace: 1—bath; 2—electrodes; 3—contact node; 4—electrode holder sleeve; 5—telescopic stand; 6—lifting mechanism; and 7—cradle and tilt mechanism

Table 6.14 Chemical composition of metallic manganese, %

Shot	Mn	C	Si	Fe	Al	Ca	Mg	P	S
1	96.3	0.12	1.2	1.9	0.054	0.03	0.009	0.05	0.02
2	96.6	0.13	1.4	2.0	0.08	0.04	0.012	0.05	0.012
3	96.0	0.14	1.2	2.1	0.09	0.04	0.012	0.06	0.015

Table 6.15 Chemical composition of dump slag of metallic manganese, %

Shot	Mn	SiO ₂	CaO	MgO	Al ₂ O ₃	FeO	P	C	S
1	13.7	29.0	45.4	3.3	3.5	0.20	0.003	0.23	0.34
2	15.4	28.9	44.2	3.1	1.8	0.18	0.003	0.12	0.08
3	14.6	27.9	44.4	3.0	2.1	0.15	0.005	0.17	0.15

Metallic manganese of the grade better in terms of Si, P and C content can be obtained under the condition of higher material costs and, therefore, at lower economic indicators. During cooling, the waste slag of metallic manganese is scattered into a fine powder due to the conversion of β -2CaO·SiO₂ to γ -2CaO·SiO₂, which is accompanied by a 12% increase in volume. The actual chemical composition of manganese metal is given in Table 6.14 and dump slag in Table 6.15.

A feature of the technology for producing metallic manganese is the relatively low through beneficial use of manganese, not exceeding 50–52% of the specified value, which is the main reason for the high specific consumption of electricity, charge materials and the relatively high prime cost of manganese. The low extraction of manganese from concentrates into the commodity metal is explained by the large losses of manganese with waste slag, mainly at stage III of the process, which explains the fact that the transition of manganese to the commodity metal at this stage does not exceed 60–63%.

Electrolytic production of metallic manganese. The raw materials for producing electrolytic manganese are oxide ores and concentrates (peroxide version) or carbonate concentrates (carbonate variant). The technology includes the following main stages: (1) reducing firing of ore and concentrates at 700 °C; (2) leaching; (3) purification of solutions from impurities; and (4) electrolysis. The calcined ore and concentrates are leached with reverse analyte (15–17 g/l): 135–145 g/l (NH₄)₂SO₄, 20–25 g/l H₂SO₄. Sulfuric acid and ammonium sulfate are added to the leach solution, as a result of which the concentration of H₂SO₄ increases to 45–40 g/l, (NH₄)₂SO₄ to 150–165 g/l. The leaching process leads to complete neutralization of the analyte (pH 3.5–4.5), while the concentration of manganese in the solution rises to 40 g/l and the content of (NH₄)₂SO₄ to 180 g/l. The solution is purified from impurities (Fe, Ni, Al, Co, Mg, Cu, P, etc.) with the help of ammonium sulfide (NH₄)₂S contained in ammonia water of coke production. After purification, the solution (33–35 g/l manganese and 145 g/l ammonium sulfate, pH 7–7.5) is fed into the cathode space from the end of the bath made of vinyl plastic. The anode solution is removed from the other end of the bath. The exchange rate of the solution

is 30 ml/h per 1 A. The electrolysis is carried out at a current strength of 2000 A, which ensures a current density of 300–350 A/m² at the cathode and 700 A/m² at the anode (electrolysis temperature 35–38 °C, duration 24 h). Manganese deposited on the cathode is removed in the form of ingots and smelted in induction furnaces. The production of 1 ton of manganese consumes 4000–4200 kg of manganese concentrate (48% Mn), 1300–1500 kg of sulfuric acid (75% H₂SO₄), 1600–1900 kg of ammonium sulfate, 500–550 kg of ammonia water, 450–500 kg of standard fuel and 10,500–12,000 kWh of electric energy. The structure of the production cost of 1 ton of electrolytic manganese is as follows: raw materials—29.6%; electricity—22.5%; and processing costs and other—49.1%. The cost of electrolytic manganese is 3 times higher than the cost of metal manganese electrosilicothermic production.

Smelting of low- and medium-carbon ferromanganese. Low- and medium-carbon ferromanganese (Table 6.16) is smelted in an electric arc furnace with a capacity of 5 MV A using the silicothermic method by a batch process. Slag basicity is 1.3–1.4.

Medium-carbon ferromanganese with a phosphorus content of 0.10% is obtained by the silicothermic method according to the three-stage scheme (Fig. 6.18). The composition of the charge includes low-phosphorous manganese slag of flux-free smelting of ferromanganese, silicomanganese with a high silicon content and lime (Table 6.17, option 1). When smelting low- and medium-carbon ferromanganese with a higher phosphorus content (0.30 and 0.35%), the charge can consist of charge manganese slag, Nikopol manganese concentrate of the first grade, silicomanganese as a reducing agent (screenings of fractionated SiMn17 ingots) and lime (Table 6.17, option 2).

Technical and economic indicators of smelting medium-carbon ferromanganese with different phosphorus contents are given in Table 6.18, from which it follows that with a decrease in the phosphorus content in medium-carbon ferromanganese, the extraction of manganese into a metal decreases from 63.2% for an alloy from 0.40% P to 57.1% for an alloy with 0.1% P; correspondingly, the specific consumption increases electricity by 32.2%.

Table 6.16 Chemical composition of low- and medium-carbon ferromanganese, %

Grade	Mn, no less	C	Si	P	S
		No more			
<i>Low-carbon ferromanganese</i>					
FeMn0.5	85	0.5	2.0	0.30	0.03
<i>Medium-carbon ferromanganese</i>					
FeMn 1.0A	85	1.0	1.5	0.10	0.03
FeMn 1.0	85	1.0	2.0	0.30	0.03
FeMn 1.5	85	1.5	2.5	0.30	0.03
FeMn 2.0	75	2.0	2.0	0.35	0.03

Table 6.17 Technical and economic indicators of production of medium-carbon ferromanganese

Parameter	Technology options	
	1	2
<i>Specific consumption of materials, kg/base t</i>		
SiMn17 fractionation screenings	1395	1500
Manganese slag	1115	–
Grade I oxide concentrate	–	850
Total manganese raw materials (48% Mn)	2510	2350
Lime	950	640
Fluorite concentrate	30	20
Graphite electrodes	30	18
Specific energy consumption, kWh/base t	2550	1530
The manganese content in the slag, %	13.5	13.2
Slag ratio	2.25	1.7
<i>Manganese distribution, %</i>		
In metal	66.5	70.9
In slag	21.4	14.7
In screenings	3.0	3.1
Lost	9.1	11.3

Table 6.18 Technical and economic indicators of smelting medium-carbon ferromanganese with different phosphorus contents

Parameter	FeMn88P40	FeMn88P30	FeMn88P10
Actual furnace power, kW	2958	2565	2899
<i>Material consumed, kg/t</i>			
Commodity silicomanganese	773	440	–
Low-phosphorous slag (48% Mn)	1558	1800	1970
Silicomanganese with high silicon content	169	235	692
Lime	1204	1230	1670
Graphite electrodes	12.1	13.9	12.5
Magnesite brick	70.0	76.0	70..3
Electric power consumption, kWh/t	1971	2265	2606
Manganese extraction, %	63.2	61.1	57.1
Through consumption of electricity, kWh/t	9163	8748	10,999

6.6 The Technology of Nitrided Manganese and Silicomanganese

Nitrided manganese (2–6% N) (Table 6.19) is used in the production of many steel grades. When smelting corrosion-resistant steels of the austenitic class, nitrogen is introduced as a substitute for a part of nickel; the nitrogen content reaches 0.5–0.6%. Nitrided metal manganese is a two-component Mn–N system (Fig. 6.20), in which nitrides are formed: Mn_4N (5.99% N), Mn_5N_2 (9.2–11.92% N), Mn_3N_2 (13.5–15% N) and others. When nitriding liquid manganese with molecular nitrogen, the solubility of nitrogen decreases with increasing temperature due to the exothermicity of the reaction. Therefore, a solid-phase process for producing manganese nitrides has been developed.

Table 6.19 Chemical composition of nitrided manganese, % (GOST 6008-90)

Grade	Source manganese	Mn, no less	C	Si	P	S	N, no less
			No more				
Mn92H6	Electrolytic	92.0	0.10	–	0.005	0.10	6.0
Mn87H6	Silicothermic	87.0	0.20	1.8	0.07	0.05	6.0
Mn89H4		89.0	0.20	1.8	0.07	0.05	4.0
Mn91H2		91.0	0.20	1.8	0.07	0.05	2.0

Fig. 6.20 Equilibrium state diagram of the Mn–N system

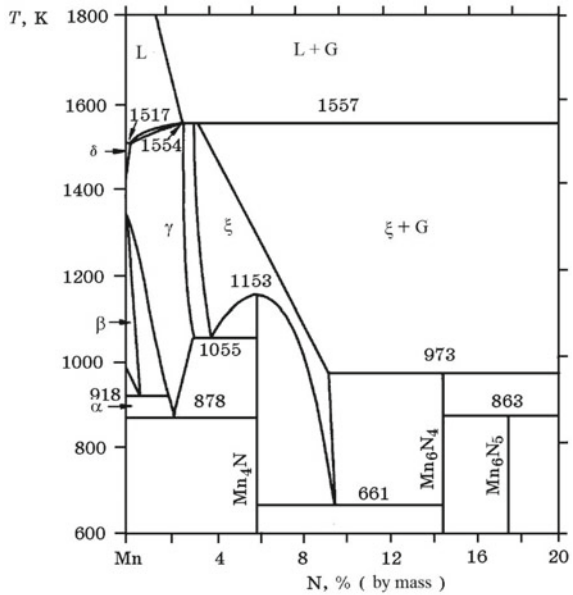


Table 6.20 Chemical composition of nitrided ferrosiliconmanganese, %

Grade	Mn, no less	N	Si	C, no more
SiMn7H	60.0	7.1	9–17	3.5
SiMn5H	60.0	4.0–7.0	9–17	3.5

The production technology of nitrided manganese by the solid-phase process is as follows. Manganese powder (fraction ≤ 2 mm) obtained in a ball mill in a nitrogen atmosphere is poured into trays and placed in vacuum furnaces at a temperature of ≤ 200 °C. After creating a vacuum of ≤ 133.3 Pa and subsequent heating to 800 °C, molecular nitrogen with a purity of 99% N₂ is supplied to the furnace. The temperature of the isothermal extract is 900–950 °C.

Due to the exothermicity of the process, the powder is sintered into strong cakes. Charge is cooled in a nitrogen atmosphere; the total duration of the process is 70 h. The strength of the cakes is satisfactory if nitriding is carried out at 750–900 °C. The density of the cake is 5.9–6.4 g/cm³. When creating a vacuum at the first stage of the process, a layer of manganese powder is loosened by hydrogen released from it (140–250 cm³/100 g), which facilitates the access of nitrogen during nitriding. To obtain 1 t of marketable nitrided manganese, 1030 kg of metallic manganese, 150 m³ of nitrogen and 1180 kWh of electricity are consumed. The beneficial use of manganese is 97%.

Ferrosiliconmanganese can also be nitrided (Table 6.20). During nitridation of ferrosiliconmanganese, a phase of the Mn_{5-x}Si_{3-y}N_{x+y} type and carbide (Mn, Fe)₃₂C₆ are formed. Regardless of the final nitrogen content (<9%), $x = 2.95$ and $y = 0.65$.

The solid-phase method for producing nitrided ferroalloys is characterized by versatility and can be used to produce nitrided high-carbon ferromanganese with vanadium and other alloys.

References

1. Shchelkova NE, Zaitsev AI, Mogutnov BM (1999) Rasplavy 1999(3):35–43 (in Russian)
2. Burylev BP, Moisev LP (2001) Izvestiya VUZov. Ferrous Metall 2001(8):3–5 (in Russian)

Chapter 7

Metallurgy of Chromium Ferroalloys



7.1 Properties of Chromium and Its Compounds

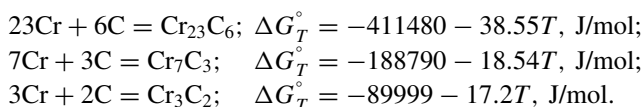
Chromium—element of the VIb group of the Periodic system of elements. Atomic number 24; atomic mass 51.996; electronic configuration $3d^5 4s^1$; melting point 1907 °C and boiling point 2671 °C; density 7.19 g/cm³; oxidation state 2, 3 and 6. Chromium has a body-centered cubic lattice and does not have allotropy. Liquid and solid chromium has a relatively high vapor pressure

$$\lg P_{\text{Cr}} = -20,380/T + 12.46, \quad \text{at } 1800 \text{ K} \quad P_{\text{Cr}} = 13.7 \text{ Pa.}$$

Cr–Fe system. Chromium forms a continuous series of solid and liquid solutions with iron (Fig. 7.1). The region of the γ -phase completely “closes” at 13% Cr. At a temperature of ≤ 820 °C in the range of 30–60% Cr, there is a solid and brittle σ -phase. Chromium solutions in iron-based melts are close to ideal, at 1600 °C $\gamma_{\text{Cr(Fe)}}^\circ = 1$

Cr–C system (Figs. 7.2 and 7.3). Chromium with carbon forms carbides Cr₂₃C₆, Cr₇C₃, Cr₃C₂ and CrC. Monocarbide CrC is stable in the temperature range 1500–2100 K. Carbide formation enthalpy $\Delta H_{298}^\circ = -10.9$ kJ/mol

For reactions of the formation of chromium carbides, the Gibbs energy change in the temperature range 1500–2000 K is described by the equations:



Carbon is dissolved in solid chromium in small quantities. The temperature dependence of the solubility of carbon in chromium is described by the equation

$$\lg[\%C]_{\text{Cr}} = -9887/T + 4.3 \quad (973 - 1673 \text{ K}).$$

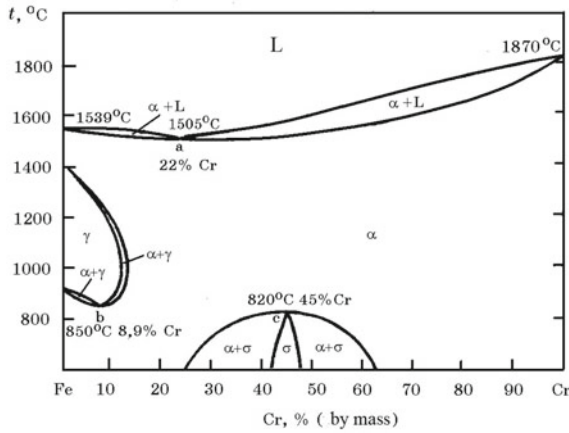


Fig. 7.1 Equilibrium state diagram of the Fe–Cr system

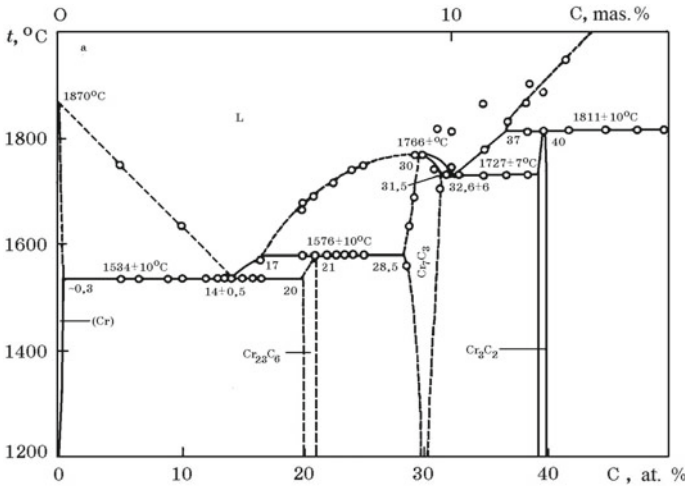


Fig. 7.2 Diagram of the equilibrium state of the Cr–C system

Cr–Fe–C system (Fig. 7.4). In this system, there are phases: α -solid solution of carbon in chromium, carbides $(Cr, Fe)_{23}C_6$; $(Cr, Fe)_7C_3$; $(Cr, Fe)_3C_2$ and intermetallic FeCr (σ -phase).

With an increase in the carbon concentration in the 70% Cr–Fe–C system, the liquidus temperature decreases from 1640 °C at 0% C to 1400 °C at 3–3.2% C, and then, it rises and reaches 1700 °C at 8%.

Cr–Si system. In the Cr–Si system, thermodynamically strong silicides Cr_3Si , Cr_5Si_3 , $CrSi$ and $CrSi_2$ are formed (Table 7.1; Fig. 7.5). Silicides Cr_3Si and Cr_5Si_3

Fig. 7.3 Diagram of the equilibrium state of the Cr–C system with presence of carbide CrC

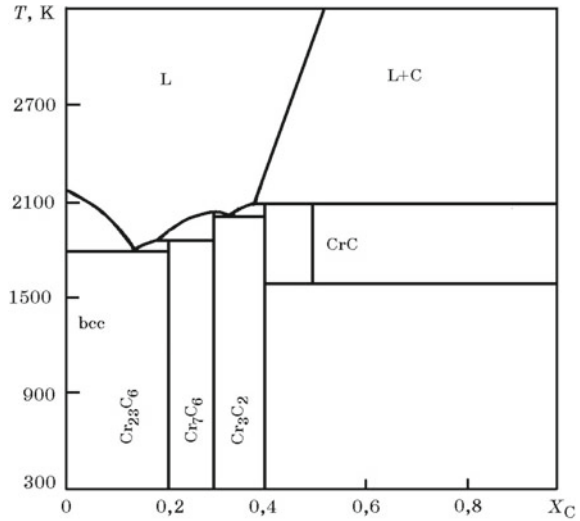


Fig. 7.4 Isoconcentration sections of the diagram Cr–Fe–C at 70% Cr (without specifying the σ -phase; S-melt; K_1 - $Me_{23}C_8$; K_2 - Me_7C_3 ; MK-solid solution of C in Cr)

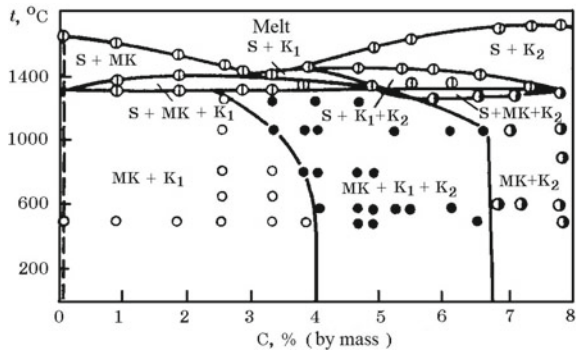


Table 7.1 Some properties of silicides of iron and chromium

Type of silicide	Silicide	Si, %	$-\Delta H_{298}^\circ$, kJ/mol	ρ , g/cm ³	T_m , K
Me ₃ Si	Fe ₃ Si	14.36	93.85	7.18	1261
	Cr ₃ Si	15.26	138.27	6.43	2043
Me ₅ Si ₃	Fe ₅ Si ₃	23.18	244.70	6.47	1261
	Cr ₅ Si ₃	24.45	326.8	5.86	1993
MeSi	FeSi	33.46	73.70	6.16	1683
	CrSi	36.05	79.61	5.36	1748
MeSi ₂	FeSi ₂	50.15	81.28	4.99	1493
	CrSi ₂	51.93	123.18	4.69	1748

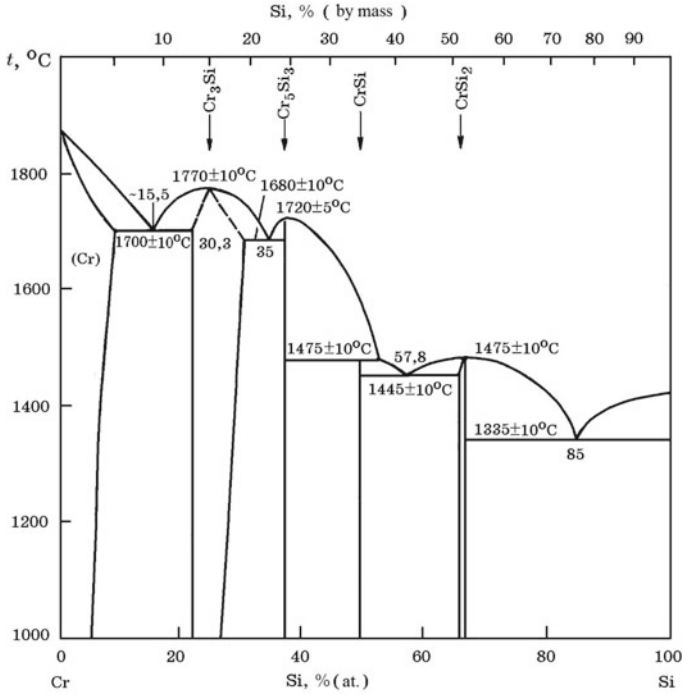


Fig. 7.5 Equilibrium state diagram of the Cr–Si system

melt congruently at 1770°C and 1720°C , respectively, and CrSi —incongruently at 1475°C . At the same temperature, CrSi_2 silicide melts congruently.

The first partial enthalpies of mixing chromium with liquid silicon $\Delta H_{\text{Cr}}^\infty = -82.0$ and silicon with liquid chromium $\Delta H_{\text{Si}}^\infty = -135.0$ kJ/mol.

In the ternary Cr–Fe–Si system, iron–chromium silicides are formed $(\text{Cr, Fe})_3\text{Si}$; $(\text{Cr, Fe})_5\text{Si}_3$; $(\text{Cr, Fe})\text{Si}_2$.

Cr–Si–C system (Fig. 7.6). The structural components in this system are a solid solution of silicon and carbon in chromium; carbides Cr_{23}C_6 , Cr_7C_3 and Cr_3C_2 ; silicides Cr_3Si , Cr_5Si_3 , CrSi , CrSi_2 ; α - and β -modifications of SiC ; silicocarbide compound $\text{Cr}_5\text{Si}_3\text{C}_x$ (Novotny phase). Complex silicocarbides are formed in the Cr–Fe–Si–C system: $(\text{Cr, Fe})_3\text{C}_2$, $(\text{Cr, Fe})_7\text{C}_3$, $(\text{Cr, Fe})_{14}\text{Si}_4\text{C}_3$, $(\text{Cr, Fe})_5\text{Si}_3\text{C}_6$, $(\text{Cr, Fe})\text{Si}$ (Table 7.2).

Cr–P system (Fig. 7.7). Phosphides Cr_3P , Cr_2P , CrP , CrP_2 , etc. are formed in this system. In solid chromium, phosphorus is dissolved in small quantities and is released in the form of phosphides during crystallization of alloys.

The Gibbs energy change equations for the reactions of Cr_3P and Cr_2P formation in the temperature range 1350–1680 K are:

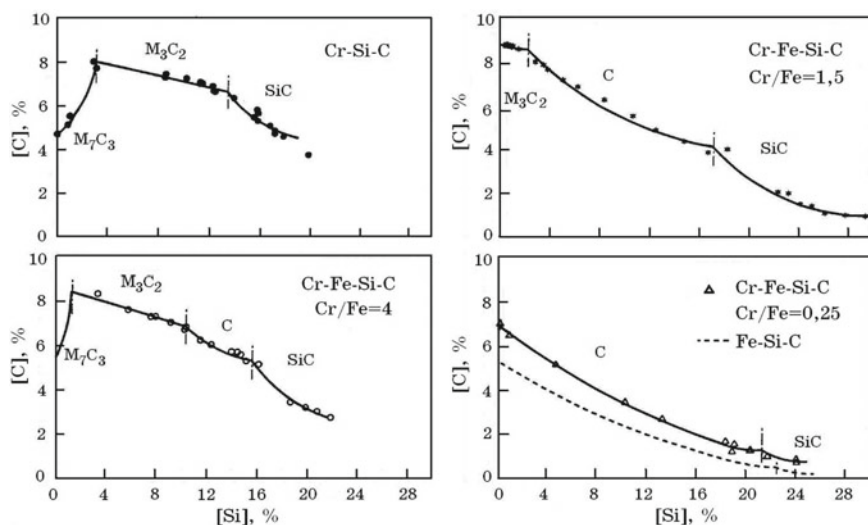
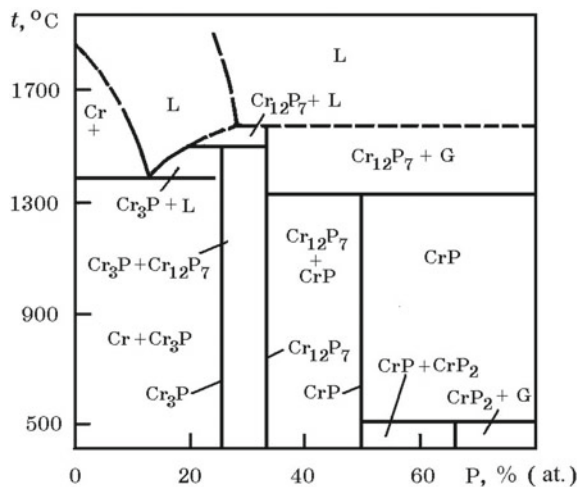


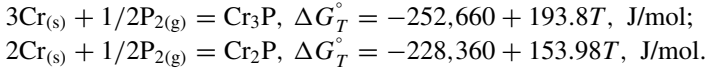
Fig. 7.6 Silicon-carbon ratios in the Cr-Fe-Si-C system at a temperature of 1600 °C

Table 7.2 Chemical composition, %, compounds in the Cr-Fe-Si-C system

Stoichiometric compound formula	Cr	Fe	Si	C
(Cr, Fe) ₃ C ₂	83–85	2.5–4.0	–	13
(Cr, Fe) ₇ C ₃	75–76	15–16	–	9
(Cr, Fe) ₁₄ Si ₄ C ₃	68–70	15–18	11.5–16	4–5
(Cr, Fe) ₅ Si ₃ C ₆	45–48	23–30	22–25	2
(Cr, Fe)Si	33–35	28–30	32–34	–

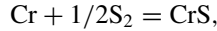
Fig. 7.7 Isobaric sections of the Cr-P phase diagram at a pressure of 1 kPa





Chromium with phosphorus forms stronger phosphides than iron. Therefore, the dephosphorization of chromium alloys by the oxidative method is ineffective.

Cr–S system. There are stable sulfides CrS, Cr₃S₄ and Cr₂S₃, as well as metastable Cr₇S₈ and Cr₃S₆. The Gibbs energy change of the reaction of the formation of monosulfide from elements in the temperature range 1375–1507 K is described by the equation



$$\Delta G_T^\circ = -202,312 + 56.0T, \text{ J/mol}.$$

Cr–O system. Oxides CrO₃, Cr₂O₃, Cr₃O₄, CrO are known. In the region indicated in Fig. 7.8 temperatures and partial pressures of oxygen, Cr₂O₃ and Cr₃O₄ can exist, with Cr₃O₄ in a very narrow temperature range of 1650–1705 °C.

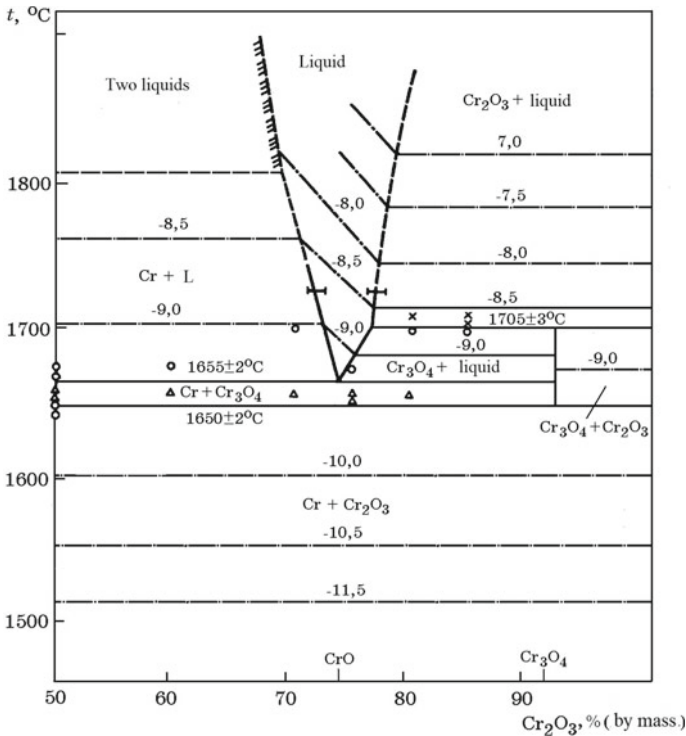


Fig. 7.8 Equilibrium state diagram of the Cr–Cr₂O₃ system (p_{O_2} , kPa) Dash-dotted lines—logarithm of oxides dissociation pressure

The temperature dependences of the Gibbs energy of the reactions of formation of Cr_2O_3 and CrO have the form:

$$2\text{Cr} + 3/2\text{O}_2 = \text{Cr}_2\text{O}_3, \Delta G_T^\circ = -1,153,703 + 275.2T, \text{ J/mol};$$

$$2\text{Cr} + \text{O}_2 = 2\text{CrO}, \Delta G_T^\circ = -516,552 + 384.9T, \text{ J/mol}.$$

Cr–N system. Nitrogen with chromium form a solid solution and nitrides Cr_2N (11.87% N) and CrN (21.22% N):

$$4\text{Cr} + \text{N}_2 = 2\text{Cr}_2\text{N}; \Delta G_T^\circ = -216,942 - 48.07T \lg T + 275.8T, \text{ J/mol};$$

$$2\text{Cr}_2\text{N} + \text{N}_2 = 4\text{CrN}; \Delta G_T^\circ = -267,520 - 48.07T \lg T + 347.7T, \text{ J/mol}.$$

CaO– Cr_2O_3 system (Fig. 7.9). Calcium chromite-chromate $9\text{CaO} \cdot 4\text{CrO}_3 \cdot \text{Cr}_2\text{O}_3$ with melting point 1774°C and CaCrO_4 chromate, which decomposes according to the peritectic reaction, are formed in the system. A particularly strong compound in the system is calcium chromate $\text{CaO} \cdot \text{Cr}_2\text{O}_3$. Under oxidizing conditions, a number

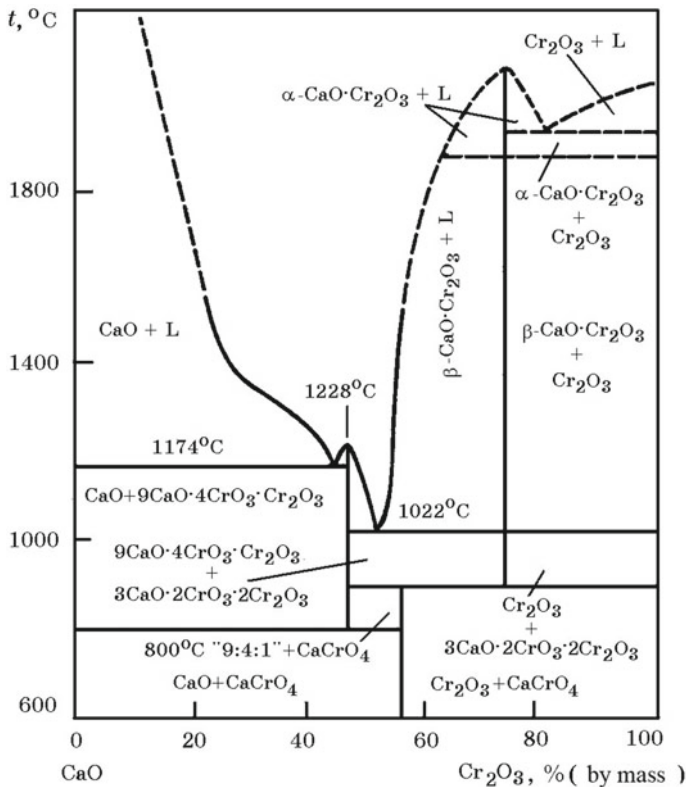
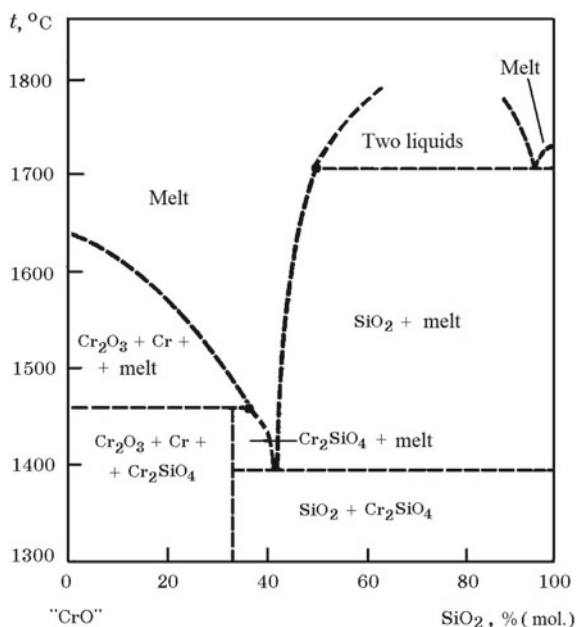


Fig. 7.9 Equilibrium state diagram of the CaO–Cr₂O₃ pseudo-binary system

Fig. 7.10 Diagram of the equilibrium state of the CrO–SiO₂ system



of low-melting compositions are formed in the CaO–Cr₂O₃ system. This feature of the system is used to obtain a chromium oxide melt Cr₂O₃ with lime during the smelting of silicothermic ferrochromium by mixing ore–lime melt with ferrosilicochromium outside the furnace, lime-chromium melt during the aluminothermic method of ferrochromium production, etc. At a content of 30–60% Cr₂O₃, the liquidus temperature in the CaO–Cr₂O₃ system does not exceed 1773 °C.

CrO–SiO₂ system (Fig. 7.10). In this system, one compound is formed, chromium orthosilicate 2CrO·SiO₂(Cr₂SiO₄), which decomposes according to the peritectic reaction. Chromium oxide (“CrO”) in its pure form at low temperatures is thermodynamically unstable and disproportionate in air according to the scheme: 3«CrO» → Cr₂O₃ + Cr. Silica stabilizes CrO, forming chromium orthosilicate. The heat and change in the entropy of the formation of CrO from elements are $\Delta H_{298}^{\circ} = -399.9 \text{ J/mol}$ and $S_{298}^{\circ} = 58.28 \text{ J/(mol K)}$.

7.2 Chromium Minerals and Ores

The main minerals of chromium-containing ores are mineral formations of the chromite-type FeO·Cr₂O₃ (68% Cr₂O₃ and 32% FeO), although pure chromite is not found in the earth’s crust, but was found in meteorites. The chromite mineral belongs to the isomorphous minerals of the cubic system, the so-called spinels, with the general formula MeO·Me₂O₃, where Me—bivalent-(Mg²⁺, Fe²⁺ etc.), Me^l—are

trivalent metals (Cr^{3+} , Al^{3+} , Fe^{3+}). In natural minerals, chromium is replaced by aluminum, and Fe^{2+} iron is replaced by magnesium. Chromites are minerals from the group of spinels of the composition $(\text{Mg}^{2+}, \text{Fe}^{2+})(\text{Cr}^{3+}, \text{Al}^{3+}, \text{Fe}^{3+})_3\text{O}_4$.

The ores contain the following main mineral varieties of chromium-spinelides: magnesiochromite $(\text{Mg}, \text{Fe})\text{O}\cdot\text{Cr}_2\text{O}_3$; chrompicotite $(\text{Mg}, \text{Fe})\text{O}(\text{Cr}, \text{Al})_2\text{O}_3$ and alumochromite $\text{FeO}\cdot(\text{Cr}, \text{Al})_2\text{O}_3$. Grains of chromium spinels are cemented with serpentine of composition $3(\text{Mg}, \text{Fe})\text{O}\cdot 2\text{SiO}_2\cdot x\text{H}_2\text{O}$ or ferruginous cement. The components of gangue in ores are serpentine, talc $\text{Mg}_6(\text{Si}_8\text{O}_{20})\text{OH}$, chlorite, magnesite, quartz, iron hydroxides, etc.

In the CIS countries (Kazakhstan, Russia), there are quite large explored and developed deposits of chromium (chromite) ores. The most explored and studied are the deposits of the Kempirsai chromite-bearing massif (Kazakhstan). High chromium ores (45–65% Cr_2O_3) are characteristic of this massif. Such high chromium concentrations are relatively rare for deposits in other regions, where the amount of Cr_2O_3 is 25–35%.

Along with the deposits of the Kempirsai massif, extended deposits of the Saranovsky massif in the Middle Urals, containing ores with 33–39% Cr_2O_3 , and the Pobuzhsky deposit in Ukraine are of industrial importance. In recent years, a large chromium ore deposit has been discovered on the Yamal Peninsula (Russia). Currently, mining of chromium ore for the smelting of ferrochromium is carried out at the South Kempirsai deposit, the Donskoy Mining and Processing Plant (DonGOK), and at the Saranovsky deposit.

One of the most important indicators of the metallurgical value of chromite ores of the DonGOK is the ratio $\text{MgO}/\text{Al}_2\text{O}_3$, which, during the development of the upper ore horizons, gradually increases and reaches ≥ 2.0 . For this reason, the slag of smelting ferrochromium becomes highly magnesian, which complicates the process. Taking into account the large potential reserves of low-grade chromite ores and the possibility of successful use of ferrochromium with a low chromium content, the chromium content in high-carbon ferrochromium is set from 45 to 95%, which allows the use of chromite ores and concentrates with a lower chromium content. This provides an increase in the extraction of chromium from ore to 90% and the expansion of the raw material base of chromium. The following are requirements for the chemical composition of chromite ores in Kazakhstan:

Grade of ore	Ore-1	Ore-2
Cr_2O_3 , % (no less)	50	47
SiO_2 , % (no more)	7.0	10.0
$\text{Cr}_2\text{O}_3/\text{FeO}$	3.5	3.0
P, % (no more)	0.008	0.008

As mentioned above, chromium in ores is in chromium spinels, the compositions of which are given below, %:

Field	Cr ₂ O ₃	Fe ₂ O ₃	FeO	Al ₂ O ₃	MgO
“Zhemchuzhina”	62.9	10.4	2.1	9.6	14.2
“40 years of Kazakhstan”	61.9	0.5	14.2	8.6	14.7

In spinels of the Saranovsky chromite deposit, the ratio is lower than in spinels of the Kempirsai massif. The use of a mixture of chromite ores from the DonGOK and the Saranovsky deposit lowers this ratio in slag, which improves the process of slag formation during smelting of ferrochromium.

The largest deposits of chromium ores are in Africa (South Africa, Zimbabwe), India and Turkey. In the USA and Canada, low-grade chromium ores are mined in small quantities. The consumption of chromium ore is constantly growing, which is associated with an increase in the proportion of metal alloyed with chromium.

7.3 The Technology of Obtaining High-Carbon Ferrochromium

Ferrochromium is divided into three groups: high, medium and low carbon. The chemical composition of commodity high-carbon ferrochromium is given in Table 7.3, and *founding* ferrochromium in Table 7.4. In this context, *founding* means

Table 7.3 Chemical composition of high-carbon ferrochromium, %

Grade	Cr, no less	C	Si	P	S
			No more		
FeCr650A	65	6.5	2.0	0.03	0.06
FeCr 650B	65	6.5	2.1	0.05	0.08
FeCr 800A	65	8.0	2.0	0.03	0.06
FeCr 800B	65	8.0	2.0	0.05	0.08
FeCr 800CA	60	8.0	5.0–10.0	0.03	0.03
FeCr 800CB	60	8.0	5.0–10.0	0.05	0.05

Table 7.4 Chemical composition of the foundry ferrochromium^a, %

Grade	Cr, no less	C	S	Si	P
		No more			
FeCrF ^a	65	–	–	–	0.04
FeCrF 850	65	8.5	0.07	2.0	0.04
FeCrF 850A	65	8.5	0.06	2.0	0.04
FeCrF 900	65	9.0	0.06	2.0	0.04

^aF—foundry

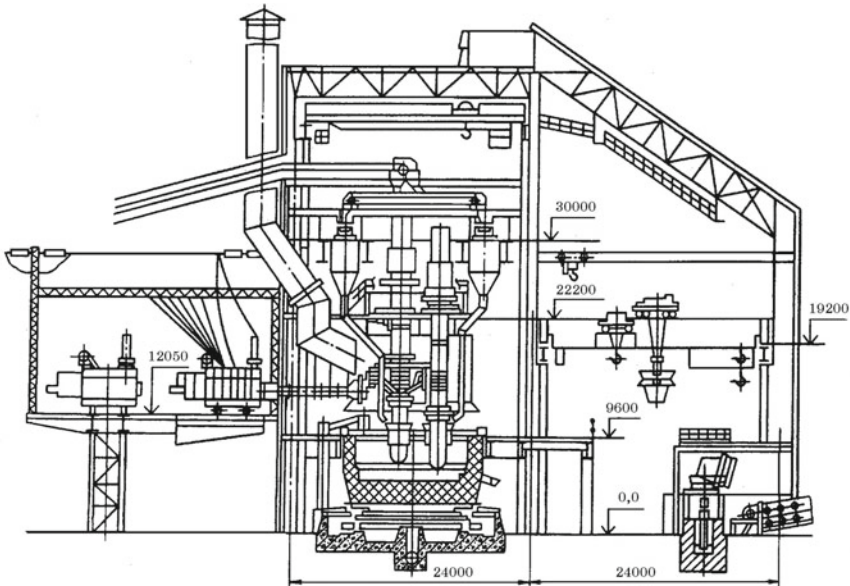
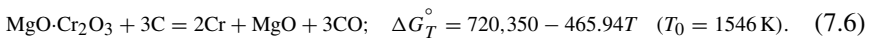
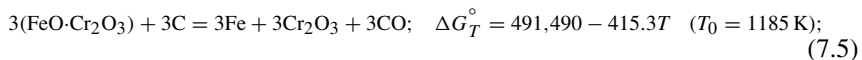
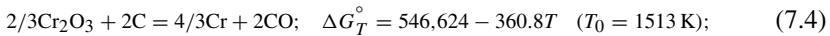
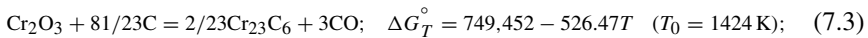
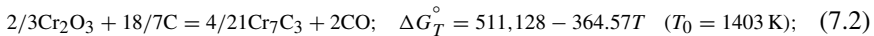
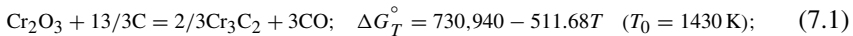


Fig. 7.11 Cross section of a melting unit with closed electric furnaces 33 MV A for the smelting of high-carbon ferrochromium

purposed for further processing. Calculation of the charge for smelting high-carbon ferrochromium is given in Appendix C.

The production of high-carbon ferrochromium is based on the reduction of chromium and iron from chromite ores by carbon in a continuous way in ore-smelting circular closed electric furnaces with a capacity of 16.5–33 MV A with magnesite lining (Fig. 7.11). The characteristics of these furnaces are given in Table 7.5.

Below are the main reactions for the reduction of chromium from carbon oxides:



The first three reactions (7.1)–(7.3) describe the reduction of chromium from Cr_2O_3 by carbon to form carbides Cr_3C_2 , Cr_7C_3 and Cr_{23}C_6 . The theoretical temperatures at which these reactions begin are slightly different. The reduction of chromium

Table 7.5 Characterization of ore-smelting electric furnaces for smelting high-carbon ferrochromium

Parameter	RK-16,5	RKZ-33M1
Voltage on the high side, kV	110	110
Transformer power, MV A	16.5	40
Power of capacitor banks, MV A	–	36
Secondary voltage when the control device is switched on under load, V	130–210	261–95
Working voltage steps, V	–	231
Maximum current on the electrode, kA	52.5–65.0	93
Power factor (cos φ) at the working stage	–	0,92
Active power of electric furnace, MW	–	31,7
Diameter of a bath, mm	9500	9500
Bath depth, mm	2975	3850
Number of electrodes	3	3
Diameter of electrodes, mm	1200	1500
Diameter of electrode cycle, mm	3300	4250

from Cr_2O_3 to pure chromium is thermodynamically less likely than to carbides. Therefore, using carbon as a reducing agent, high-carbon ferrochromium is always obtained. An analysis of the data presented allows us to conclude that iron must first be reduced from chromite, then chromium from Cr_2O_3 oxide to carbides, and only then chromium from the chemical compound $\text{MgO}\cdot\text{Cr}_2\text{O}_3$.

For the smelting of high-carbon ferrochromium, chromite ore and carbonaceous reducing agents—coke, semi-coke and gas coal—are used. Alloy's recycled waste is also introduced into charge. Ferrochromium can also be smelted using sinter and/or pellets from chromite ores. When calculating the charge, it is assumed that the extraction of chromium is 92%, iron 95%, and the excess reducing agent for melting in closed furnaces is 2%, open—10%. The mixture contains: chromite ore, slag from the production of ferrosilicochromium, quartzite, coke, own metal wastes.

The technological scheme for the production of high-carbon ferrochromium is shown in Fig. 7.12. Metal and slag are discharged from the furnace together 3–4 times per shift. Slag dump contains %: 4–6 Cr_2O_3 ; 30 SiO_2 ; 45 MgO ; 15 Al_2O_3 ; 1 FeO ; 1 CaO . The high MgO content in the slag is associated with its high content in ore. Slag ratio 1. Specific consumption of charge materials in the smelting of high-carbon ferrochromium, kg/t: 2000–2200 chromite ore; 30–100 quartzite; 200–400 coke. Electricity consumption 3400–3600 kWh/t.

High-carbon ferrochromium is also smelted in a plasma furnace, which makes it possible to efficiently solve a number of problems: use pulverized and low-grade chromite ores, as well as cheap coal. Among the other positive features of the use of plasma melting are the independence of the input power from the resistance of the charge, lower losses of chromium with slag, as well as a high concentration of

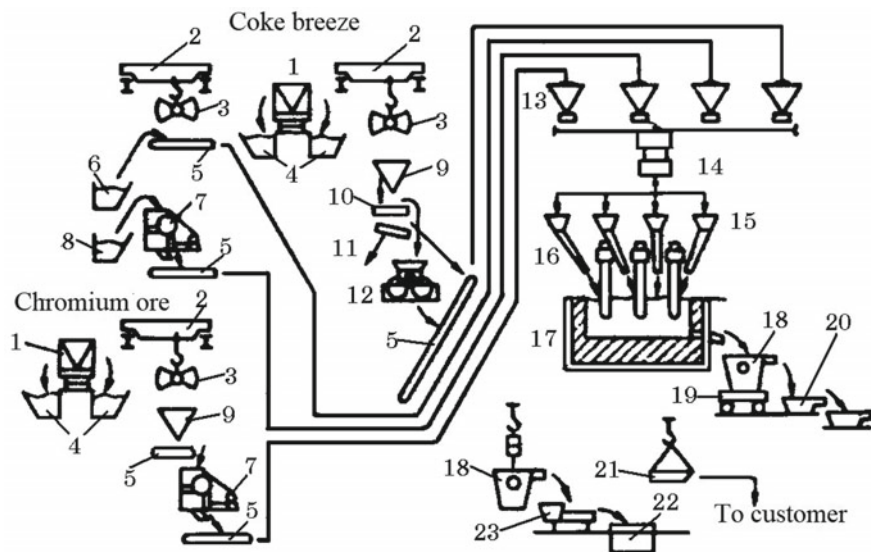


Fig. 7.12 Technological scheme for the production of high-carbon ferrochromium. 1—railway carriage; 2—overhead crane; 3—grab; 4—bins; 5—plate feeder; 6—screenings of quartzite; 7—jaw crusher; 8—own returns; 9—hopper; 10—double screening screen; 11—screenings; 12—two-roll crusher; 13—dosing hopper with feeder; 14—dosage trolley; 15—furnace bunkers; 16—pipe-chute; 17—ore-smelting furnace; 18—ladle for receiving alloy; 19—trolley; 20—slag; 21—box; 22—tank for granulation of the alloy; 23—trough

power, which provides higher performance at the same power of the power source. Ferrochromium was melted in an experimental plasma furnace with a power of 3 MV A with a water-cooled arch and a wall to the slag line. A plasma arc formed in argon was created between the cooled cathode and the melt. Chromite ore was loaded into a plasma furnace along with coal and flux. Using low-grade chromite concentrate (38.2% Cr_2O_3 ; 24.2% Fe_2O_3), ferrochromium with 54% Cr and 8% C was obtained. The extraction of chromium was 92%, and the specific electric energy consumption was 6500 kWh/t alloy.

7.4 The Technology of Obtaining Ferrosilicochromium

Commodity and foundry (for further processing) grades of ferrosilicochromium are produced (Table 7.6). Commodity ferrosilicochromium is used mainly for deoxidation and alloying of steel. Foundry ferrosilicochromium FeSiCr48V ($\geq 45\%$ Si, $\geq 24\%$ Cr, $\leq 0,04\%$ P and $\leq 0,02\%$ C) is used as a reducing agent in the production of low-carbon ferrochromium by the silicothermic method.

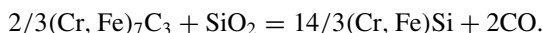
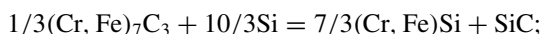
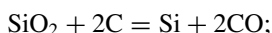
There are two methods for producing ferrosilicochromium: single- (slag) and two-stage (slag-free). In Russia and Kazakhstan, a two-stage method is used, which is

Table 7.6 Chemical composition of ferrosilicochromium, % (GOST 11861-77)

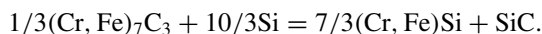
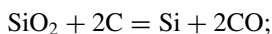
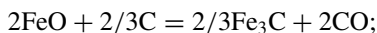
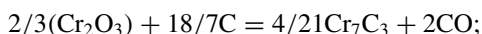
Grade	Si	Cr, no less	C	P	S
			No more		
FeSiCr 13	10–16	55	6.0	0.04	0.03
FeSiCr 20	16–23	48	4.5	0.04	0.02
FeSiCr 26	23–30	45	3.0	0.03	0.02
FeSiCr 33	30–37	40	0.9	0.03	0.02
FeSiCr 40	37–45	35	0.2	0.03	0.02
FeSiCr 48	Over 45	28	0.1	0.03	0.02

based on the reduction of silicon from silica (quartzite) by carbon in the presence of carbon ferrochromium. In the one-stage (slag) method, chromite ore, quartzite and coke are used in the charge.

The two-stage method for producing ferrosilicochromium is based on reactions:



Ferrosilicochromium is smelted in a two-stage process by a continuous process in ore-smelting furnaces with carbon lining with a capacity of 16.5–33 MV A (Fig. 7.13). The one-step method for smelting ferrosilicochromium is, as noted above, not used at ferroalloy plants in Russia and Kazakhstan. Conducted pilot industrial melting in a powerful furnace did not give positive results. For smelting, Kazakhstani chromium ore, quartzite and coke were used. In the smelting process, iron and chromium oxides are reduced from chromite ore and silicon from quartzite by a carbonaceous reducing agent by the reactions:



Comparative data on the specific consumption of charge materials and electricity during the smelting of ferrosilicochromium with different silicon contents

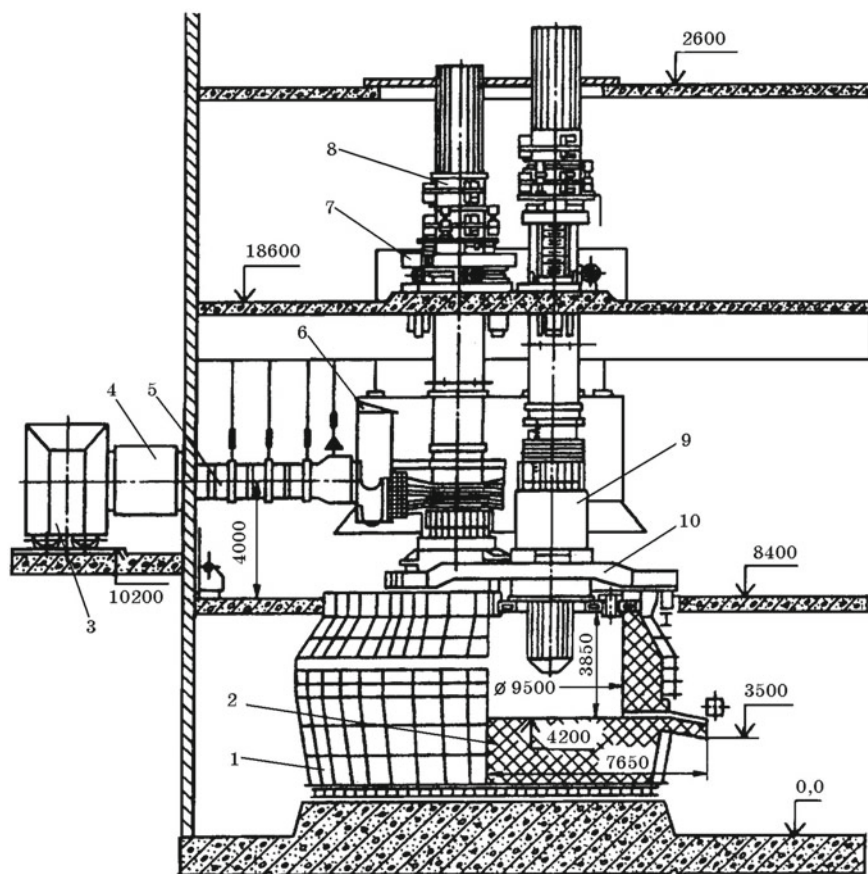


Fig. 7.13 Ore-smelting electric furnace RKZ-33M01. 1—casing; 2—lining; 3—transformer; 4—fence compensator short network; 5—short network; 6—installation of screens; 7—hydraulic lift; 8—device bypass electrodes; 9—electrode holder; 10—arch

by two-stage and one-stage methods are given in Table 7.7. The energy consumption during the smelting of ferrosilicochromium by the two-stage method is given without taking into account its specific consumption during the smelting of the high-carbon ferrochromium.

7.5 The Technology of Obtaining Low-Carbon Ferrochromium

Low-carbon ferrochromium (Table 7.8) is obtained by the silicothermic method, reducing chromium and iron-chromite ore with silicon ferrosilicochromium in the

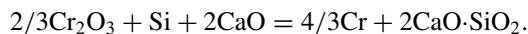
Table 7.7 Specific consumption of materials and electricity in the smelting of ferrosilicochromium by two-stage (numerator) and one-stage (denominator) methods

Parameter	Content of Si, %				
	13	23	33	43	50
<i>Consumption of material, kg/t</i>					
Quartzite	298/634	520/881	742/1134	965/1323	1121/1464
Chromium ore	– /1908	– /1600	– /1420	– /1145	– /923
Coke breeze	117/543	220/575	312/625	424/678	308/712
Charge ferrochromium	1089/–	911/–	803/–	648/–	525/–
Steel shavings	8/30	41/82	62/84	93/105	115/116
Electric power consumption, kWh/t	1500/4770	2450/5660	3390/7040	4350/7770	5110/8870

Table 7.8 Chemical composition of low-carbon ferrochromium, %

Grade	Cr, no less	C	Si	P	S	Al
		No more				
FeCr001A	68	0.01	0.8	0.02	0.02	0.7
FeCr 001B	68	0.01	0.8	0.03	0.02	0.7
FeCr 002A	68	0.02	1.5	0.02	0.03	–
FeCr 002B	68	0.02	1.5	0.03	0.03	–
FeCr 003A	68	0.03	1.5	0.02	0.03	0.7
FeCr 003B	68	0.03	1.5	0.03	0.03	0.7
FeCr 004A	68	0.04	1.5	0.02	0.03	0.3
FeCr 004B	68	0.04	1.5	0.03	0.03	0.3
FeCr 005A	65	0.05	1.5	0.03	0.03	–
FeCr 005B	65	0.05	1.5	0.05	0.03	–
FeCr 006A	65	0.06	1.5	0.03	0.03	0.3
FeCr 006B	65	0.06	1.5	0.05	0.03	0.3
FeCr 010A	65	0.10	1.5	0.03	0.03	0.3
FeCr 010B	65	0.10	1.5	0.05	0.03	0.3
FeCr 015A	65	0.15	1.5	0.03	0.03	0.3
FeCr 015B	65	0.15	1.5	0.05	0.03	0.3
FeCr 025A	65	0.25	2.0	0.03	0.03	–
FeCr 025B	65	0.25	2.0	0.05	0.03	–
FeCr 050A	65	0.50	2.0	0.03	0.03	–
FeCr 050B	65	0.50	2.0	0.05	0.03	–

presence of calcium oxide (lime) to reduce the activity of SiO_2 in the slag and increase the activity of Cr_2O_3 . The process in general can be represented as the total reaction



Optimum conditions for the process are ensured when the basicity of slag = 1.7–1.9. With a higher basicity, calcium chromite $\text{CaO}\cdot\text{Cr}_2\text{O}_3$ may be formed in the slag, which worsens the conditions for the reduction of chromium and increases the loss of chromium with slag. There are two methods for smelting ferrochromium.

The essence of the *first* method (*one-stage furnace*) is that melting is carried out in an arc electric furnace with graphite electrodes. The mixture, consisting of chromite ore, ferrosilicon chromium and lime, is melted in a furnace. The melt is maintained until a state close to equilibrium between the resulting ferrochromium and slag is reached. In this case, the carbon content in ferrochromium increases due to its receipt from graphitized electrodes.

The essence of the *second* method (*mixing*) is that the chromite ore and lime are melted in an arc furnace with graphite electrodes, and then, the ore–lime melt and liquid ferrosilicon chromium are mixed in a ladle reactor. At the same time, carbon penetration from electrodes into ferrochrome is reduced, which makes it possible to obtain ferrochrome with a carbon content of 0.02–0.03%. In both methods of smelting ferrochromium, chromite ore, ferrosilicochromium and lime should have a low content of carbon and phosphorus.

Furnace method. In the single-stage furnace method for producing low-carbon ferrochromium, melting is carried out by a batch process in an electric arc furnace with a capacity of 5 MV A with an inclined bath lined with magnesite brick (Chap. 6, Fig. 6.19). Smelting technology consists of the following operations: (1) bath filling, (2) loading of the entire sample of ferrosilicochrome of the first filling on the bottom, loading set and feeding of the ore–lime part of the charge; (3) the melting of the first filling of the mixture; (4) loading of ferrosilicochromium and ore–lime part of the charge of the second filling; (5) the melting of the second filling of the mixture; (6) the release of metal and slag.

Below are the main provisions of the technology for smelting low-carbon ferrochromium according to the current technology at JSC “Chelyabinsk Electrometallurgical Integrated Plant” (ChEMK). The chromium ore arriving at the plant (0.003% P) is sieved on a screen with a fraction of less than 30 mm being allocated for melting. Lime is obtained by calcining limestone in rotary drum kilns. When smelting class “A” ferrochromium, the phosphorus content in lime should not exceed 0.006%. Ferrosilicochromium (0.030% P) use fractions of 20–40 mm. The fines formed during crushing of ferrosilicochromium chromium ingots containing an increased amount of carbon (in the form of SiC) is not used in smelting.

Ferrochromium is smelted in electric arc furnaces with a tilting bath equipped with furnace transformers (Table 7.9).

The electric mode is supported by regulators operating on the principle of comparing the electrode current with phase voltage. Melting takes place on the third stage.

Table 7.9 Electrical parameters of furnace transformers

Stage	Furnaces 31-32			Furnaces 33-34			Furnaces 35-38		
	Capacity, kV A	Voltage, V	Amperage, A	Capacity, kV A	Voltage, V	Amperage, A	Capacity, kV A	Voltage, V	Amperage, A
1	7600	365	12,000	8000	384	12,000	5000	369	7825
2	6900	331	12,000	7600	365	12,000	5000	343	8400
3	6580	317	12,000	7230	347	12,000	5000	321	8975
4	6310	304	12,000	6080	292	12,000	4550	293	8975
5	5810	280	12,000	5625	270	12,000	4150	269	8975

Smelting of low-carbon ferrochromium includes two periods: After the first period, slag is discharged from the furnace, and after the second, metal and slag are discharged. The consumption of materials of one filling period is as follows, kg: chromium ore—5200–5800; lime—4200–4700; ferrosilicochromium—1700–1900.

The technology for smelting ferrochromium with a content of 0.50–0.25% of grade FeCr050–FeCr025 consists of the following operations for the melting periods. In the first period of smelting after the release of the metal, 700–1000 kg of ferrosilicochromium is given to the bottom for gaining a load, the electrodes are lowered and after the current load is set, the rest of the ferrosilicochromium is given along with the ore–lime part of the charge, which is melted and discharged into slag. In the second period, 700–1000 kg of ferrosilicochromium is given to increase the load on the hearth, electrodes are lowered onto it, and after the current load is set, the rest of the ferrosilicochromium is given along with the ore–lime part of the charge, after melting of which metal and slag are released. When smelting ferrochromium grades FeCr015, 025, 050, ferrosilicochromium is loaded into the furnace with the charge.

At the end of each period, 25–50 kg of crushed ferrosilicon is loaded into the melt for a more complete reduction of chromium.

The basicity of the slag in the smelting of low-carbon ferrochromium is supported by 1.70–1.89. The resulting slag contains %: 48.0–51.0 CaO; 27.0–30.0 SiO₂; 4.5–5.0 Cr₂O₃; 0.8–1.0 FeO.

On average, for smelting in terms of 100 kg of chromium ore, the energy consumption is 150–160 kWh. The total energy consumption in the first period, as a rule, exceeds the consumption in the second period by 1200–2000 kWh.

When melting ferrochromium of grades FeCr005 and FeCr006, the amount of ferrosilicochromium in the first period exceeds its amount in the second period of melting by 700–1000 kg, which contributes to a more complete recovery of chromium from slag. The amount of lime for melting is calculated based on the need to obtain slag with a basicity of 1.71 and a CaO content of 45–46 wt%. This is due to the fact that when the CaO content is less than 46%, the amount of formed calcium carbides is small and the carburization of the alloy due to the electrodes is reduced. A sample of lime per 100 kg of chromium ore to produce slag with a CaO content of 45–46% is 70–75 kg.

The charge consumptions for the smelting periods of low-carbon ferrochromium grades FeCr005 and FeCr006 are given below, kg:

	Chromium ore	Lime	Ferrosilicochromium
1st period	5600–5800	3600–4000	2000–2400
2nd period	5600–5800	3600–4400	1200–1400

A feature of technological operations in the smelting of ferrochromium grades FeCr005–FeCr006 is as follows.

In the first period, approximately one-fifth of a portion of ferrosilicochromium is loaded onto the bottom of the furnace bath; after a steady current load has been set, the ore–lime part of the charge is loaded into the furnace; after the formation of a liquid

melt, under the electrodes, the remaining part of ferrosilicochromium is given in small portions of 200–250 kg; slag is produced. In the second period, approximately one-third of a portion of ferrosilicochromium is loaded onto the bottom of the furnace; after a set of current load, the ore–lime part of the charge is loaded into the furnace; during the formation of a liquid melt, the rest of the ferrosilicochromium is specified in the furnace; smelting ends with the release of the melt into the ladle with slag of the 1st period.

The basicity of the slag for smelting ferrochromium with a low carbon content is $\text{CaO/SiO}_2 = 1.7$, while the slag corresponds to the composition, %: 45–46 CaO; 26–27 SiO₂; 5.0–6.0 Cr₂O₃; 1.0–1.3 FeO.

Mixing method. The obtaining of ferrochromium by a method of mixing ore–lime melt with ferrosilicochromium is characterized by a number of features. On the stage of fusion of chromite ore and lime due to the lack of a metal phase and high oxidation potential of the oxide melt–furnace atmosphere system, the carbon content in the ore–flux melt is usually low. In the process of mixing the reacting media, there are no graphite electrodes—one of the sources of carbon in ferrochromium in the furnace version of the silicothermic method for its production. During the mixing of melts, a large amount of heat is released due to the exothermicity of the reduction reactions of chromium and iron oxides with silicon of ferrosilicochromium, as well as the interaction of CaO with SiO₂. Excess of this heat makes it possible to use, along with liquid also partially solid ferrosilicochromium, which improves the economy of production of low-carbon ferrochromium. The method of melting mixing is characterized by high kinetic parameters of the interaction of components in the ore–flux melt - ferrosilicochromium system, due to which the rate of reduction of chromium and iron oxides with silicochromium (at the beginning of the mixing stage), and then the refining of the formed low-carbon ferrochromium from silicon is incomparably higher than with the furnace version. In practice, accelerating the refining of ferrochromium from silicon, which corresponds to a decrease in the Cr₂O₃ content in the slag, is also achieved by multiple overflows (up to 4–6 times) of the reacting ferrochromium—slag system from the ladle to the ladle. These and other factors are important in producing very low-carbon ferrochromium.

Charge materials. When producing ore–lime melt, charge components are used: chromite ore and ferroalloy lime ($\text{CaO} \geq 89\%$, $\text{CO}_2 \leq 2\text{--}4\%$ with a particle size of 5–50 mm). Along with chromite ore, chromite ore concentrates can be used ($\text{Cr}_2\text{O}_3 \geq 48\%$; $\text{Cr}_2\text{O}_3:\text{FeO} = 3.5$; $\text{SiO}_2 \leq 8,0\%$, $\text{CaO} \leq 0,8\%$; $\text{P} \leq 0.05\%$). After controlling the chemical composition, especially the phosphorus content, the initial charge materials are grouped depending on the level of phosphorus concentration, since ferrochromium can be obtained by carefully selecting relatively pure phosphorus charge materials to produce ore–lime melt and silicochromium. Liquid or solid (granular) ferrosilicochromium is used, containing, depending on the grade of smelted ferrochromium, 48–51% Si and 28.5–29% Cr. Both liquid and granular ferrosilicochromium should contain $\leq 0.020\%$ P.

Characteristics of electric furnaces. Under the conditions of ChEMK, the electric furnace complex for the production of low-carbon ferrochromium by mixing chromium–lime melt with ferrosilicochromium includes ore-smelting furnaces for the

smelting of high-carbon ferrochromium, ferrosilicon chromium and an arc furnace for fusion of chromite ore with lime.

A workshop was built at ChEMK for the production of low-carbon ferrochromium by mixing as a part of one closed electric furnace of the RKZ-33M type to produce ferrochromium, three closed electric furnaces of the RKZ-33M2 type for smelting ferrosilicon chromium and three electric furnaces with an arch of the type RKZ-10.5RN for the production of ore–flux melt.

To intensify the process of fusion of chromite ore with lime in electric furnaces RKZ-10.5PPH1, preliminary joint firing of ore and limestone at temperatures up to 1100 °C in rotary drum furnaces with a length of 75 and a diameter of 3.6 m installed at 23.6 m is provided. This allows hot feed the mixture by gravity through the tubes directly into the electric furnace RKZ-10.5PPH1 for smelting ore–lime melt (Fig. 7.14).

The furnace bath is lined with magnesite brick, the electrodes are graphite, with a diameter of 400 mm. The process is conducted periodically. The charge for each smelting is calculated on the basis of: 73–82 kg of lime is set per 100 kg of chromite ore, which should ensure the production of ore–lime melt of 27–29% Cr_2O_3 and 40–43% CaO. In order to accelerate the formation of the melt, a small amount of silicochromium is introduced into the furnace with the initial charge. The interaction of the latter with the melt is accompanied by the formation of silica, which reduces the melting temperature, and the heat generated by the reaction intensifies the process of accumulation of the melt.

The mixing of melts. The ore–lime melt is poured from the furnace into a ladle with magnesite lining. Before receiving the melt, the ladle is weighed on a balance

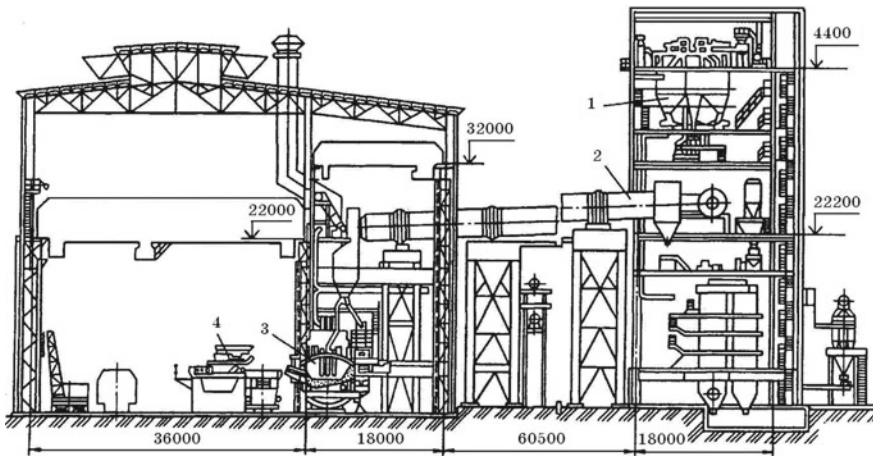


Fig. 7.14 Cross section of the workshop with an electric furnace of the type RKZ-10.5RRN1 for smelting chromium–lime melt from a preheated charge: 1—dosing unit; 2—tubular rotary kiln; 3—electric furnace; 4—installation for mixing melts for the production of carbon-free ferrochromium outside the furnace

(measurement limits from 0.5 to 25 tons). To reduce heat loss, the melt in the ladle is covered with scattered slag from previous heats. The melt ladle is mounted on the balance, and the mass of the melt and the amount of solid additives are determined. By the content of Cr_2O_3 in the melt and the mass of solid additives, the required amount of ferrosilicochromium is found. Ferrosilicochromium is poured into the ladle located on the balance. The calculated amount of ferrosilicochromium added by overhead crane is indicated by an audible alarm mounted on the balance. Ferrosilicochromium is filled at a speed corresponding to the speed of the recovery processes in the ladle (~200 kg of ferrosilicochromium/min.). At the end of the pouring of ferrosilicochromium, the contents of the reactor ladle are poured into another ladle and back into the reactor ladle. The number of overflows is determined by the rate of refining of ferrochromium from silicon and can reach six.

It is known that in order to reduce Cr_2O_3 in dump slag, mixing can be carried out in stages. Initially, an excess amount of ferrosilicochromium is filled into the ore–flux melt, and ferrochromium with a high silicon content is obtained. In the second stage, this alloy is refined from silicon to obtain ferrochromium with a low silicon content and slag with a high concentration of Cr_2O_3 . The latter restores ferrosilicochromium in a new mixing cycle.

In practice, the option of “doubling” the heats is implemented. Initially, ferrosilicochrome with an excess of 100–150 kg from the calculated value is poured into the ore–lime melt when solid additives are fed. After two and four reladlings, the melt in the ladle is covered with highly basic scattered slag. Then, ferrosilicochromium with a deficit (~100 kg) is poured into the ore–lime melt of the next release when applying the usual solid filling. The slag of the first heat is drained, and the ferrochromium is poured into the second ladle, where the metal of the first heat and the metal and slag of the second heat are mixed. Mixed melts are poured from ladle to ladle, brought to the required content of silicon in ferrochromium and poured.

Ferrochromium casting. Low-carbon ferrochromium is poured into cast iron molds with crumbs of the corresponding brands of ferrochromium. The thickness of the ingots does not exceed 80 mm. To obtain ferrochromium ingots with a columnar structure, it is cast under slag or with preliminary evacuation of liquid ferrochromium in a ladle in a vacuum chamber.

The specific consumption of charge materials for the obtaining of ferrochromium by the mixing method, kg/t: chromite ore (50% Cr_2O_3) 1750; ferrosilicochromium (48% Si) 570; lime 1370; electrodes 18. The energy consumption is 2750 kWh/t, and the useful extraction of chromium is ~80%. The heat balance of the mixing process is characterized by the following data. Input heat: ore–lime melt 65.8%, liquid ferrosilicon chromium 11.2%, exothermic reactions 23%. Heat consumption: heating the alloy 14.4%, heating the slag 55.4%, heating the ladle and other types of heat transfer 6.7%, excess heat to increase the process temperature and melting the solid charge 23.5%.

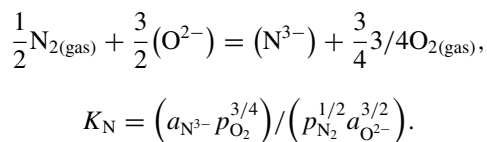
Ferrochromium, obtained by mixing (as well by furnace) from chromites of Kazakhstan, contains impurities of non-ferrous metals, %: 0.01–0.04 Co; 0.0005 Sn; 0.004 As; 0.004–0.01 Sb; 0.004 Ti; 0.07 Al; 0.015–0.030 P; 0.02 S.

In a number of cases, for example, in the smelting of corrosion-resistant chromium–nickel steels for nuclear energy, the reduced content of cobalt and other impurities in ferrochromium is relatively high. A decrease in cobalt concentration can be achieved by selective reduction. For this, a small amount of ferrosilicochromium is poured into the ore–lime melt. Due to the significantly lower chemical affinity of cobalt to oxygen, compared with chromium, cobalt passes into the metal phase enriched with this and other easily reducible metals. The ore–lime melt with 20–25% Cr₂O₃, which is purified from cobalt and partially from iron and phosphorus, is poured into another ladle, and the calculated amount of ferrosilicochromium is poured into it. The resulting low-carbon ferrochromium has the composition: 81–88% Cr; 0.07–0.014% P; 0.003–0.008% Co. The mixing method allows one to obtain a number of ligatures, containing, as a rule, easily recoverable elements: Mo, W, Mn, etc.

Along with the positive aspects, the mixing method has some drawbacks, including the difficulty of obtaining ferrochromium with a low nitrogen content, as well as the need to comply with the conditions for a safe concentration of hexavalent chromium in dust and gas emissions, etc.

During the mixing of melts, especially at the stage from ladle to ladle, due to the contact of liquid ferrochromium (probably the slag phase) with air, the nitrogen content in the melts increases, which reduces the metallurgical properties of ferrochromium. The interaction of liquid ferrochromium with nitrogen-containing gas phases has been fully studied.

Significantly less attention is paid to studying the solubility of nitrogen in slag oxide melts, although interest in these issues has increased in recent years. Molecular nitrogen can interact with oxide melts by reaction:



Since the issue of the solubility of nitrogen in an ore–flux melt with regard to specific technological parameters for its preparation still requires further study, it can be assumed that in order to achieve low nitrogen contents in low-carbon ferrochromium, it is necessary, first of all, to reduce the contact and time of interaction of the ferrochromium melt with air during chromium ore alloying with lime, as well as when reladling.

The requirement of a low nitrogen content in ferrochromium for the smelting of particularly low-carbon chromium–nickel steels and chromium superferrites is justified by the need to increase the corrosion resistance of a metal intended for use in aggressive environments. In the ferrochromium of silicothermic and aluminothermic production, the nitrogen content reaches 0.06–0.10%. To obtain corrosion-resistant stainless low-carbon steels without titanium, the concentration of nitrogen in ferrochromium should not exceed 0.02%.

The difficult task of producing low-nitrogen ferrochromium in a silicothermic way can be solved by the method of vacuum-thermal solid-phase processing of ferrochromium in vacuum resistance furnaces or its degassing in induction vacuum furnaces.

Technical and economic indicators for the smelting of low-carbon ferrochromium significantly depend on the quality of chromium (chromite) ore. With a decrease in its Cr_2O_3 content, the specific consumption of ore, ferrosilicochromium, lime and electricity increases. This fundamentally important point is confirmed by the following calculation data. The calculations were performed for the conditions of changing the Cr_2O_3 content from 42 to 50% in 2% increments (Table 7.10).

The waste of silicon of ferrosilicochromium is accepted according to practice data equal to 17.5%, and the consumption of lime—to obtain furnace slag with a basicity of $\% \text{CaO}/\% \text{SiO}_2 = 1.87$. A decrease in the Cr_2O_3 content in the slag with a decrease in chromium oxide in the ore from 6.18% for 50% Cr_2O_3 to 5.18% for ore with 42% Cr_2O_3 (Table 7.11) is due to the dilution of the slag mainly by MgO .

With a decrease in Cr_2O_3 in chromium ore, the calculated production indicators of low-carbon ferrochromium (in terms of a charge of 100 kg of chromium ore) change (Table 7.12), the portion of ferrosilicochromium decreases (from 33 to 28.2 kg) and, therefore, the amount of reduced chromium entering the bath of the furnace with ferrosilicochromium, and the mass of ferrochromium obtained (from 53.16 to 45.7 kg) and the amount of chromium in it (from 35.29 to 29.8 kg) are also reduced. It is important to note that, ultimately, the amount of commercial ferrochromium is reduced from 48.0 kg (50% Cr_2O_3) to 40.6 kg (42% Cr_2O_3).

Thus, with a deterioration in the quality of chromium ore by the content of the leading oxide Cr_2O_3 in it, the most important indicators of the production efficiency of low-carbon ferrochromium are significantly reduced, which is illustrated by the data given in Table 7.13.

An increase in the MgO concentration in the slag when using less quality chromium ore has a negative effect on the physicochemical properties of the slag, transferring it to the region with an increased melting temperature.

Table 7.10 Model chemical compositions of chromium ore used as initial data for calculating the parameters of the technology for producing ferrochromium by the mixing method

Oxide	The content of oxides in the ore, %				
	42.0	44	46	48	50
Cr_2O_3	42.0	44	46	48	50
FeO	11.2	11.4	11.6	11.8	12.0
SiO_2	12.0	10.9	9.74	8.58	7.4
MgO	23.5	22.5	21.5	20.5	19.5
Al_2O_3	6.6	6.81	6.96	7.12	7.4
LOI	4.3	3.99	3.72	3.44	3.2
$\% \text{Cr}/\% \text{Fe}$ in the ore	3.3	3.39	3.49	3.58	3.87

Table 7.11 Slag composition of the production of low-carbon ferrochromium when using chromium ore with different contents of Cr_2O_3

Parameter	The content of Cr_2O_3 in ore, %				
	42	44	46	48	50
Content of Cr in FeSiCr, %	24	24	24	24	24
<i>Estimated values</i>					
• Cr content in metal, %	65.1	65.41	65.79	66.07	66.39
• The degree of reduction, Cr, %	80	80	80	80	80
• Transition of Cr to metal, %	83.80	83.81	83.77	83.78	83.76
<i>Slag composition, %</i>					
Cr_2O_3	5.18	5.422	5.695	5.924	6.188
FeO	0.35	0.355	0.363	0.368	0.375
SiO_2	26.2	26.28	26.34	26.46	26.53
MgO	15	14.39	13.84	13.18	12.6
CaO	49	49.15	49.25	49.47	49.61
Al_2O_3	4.31	4.398	4.513	4.595	4.703
In slag CaO/ SiO_2	1.87	1.87	1.87	1.87	1.87

Table 7.12 Estimated production indicators of low-carbon ferrochromium

Parameter	The content of Cr_2O_3 in ore, %				
	42	44	46	48	50
Chromium ore, kg	100	100	100	100	100
FeSiCr, kg	28.2	29.5	30.5	31.9	33
Lime, kg	81.8	82.23	82.03	82.65	82.65
Chromium set, kg	35.5	37.19	38.79	40.5	42.13
Received ferrochromium, kg	45.7	47.64	49.4	51.35	53.16
Chromium content, kg	29.8	31.16	32.5	33.93	35.29
Extraction of Cr in the metal, %	83.8	83.81	83.77	83.78	83.76

Table 7.13 Estimated indicators of 1 base tons of commodity low-carbon ferrochromium (60% Cr)

Parameter	The content of Cr_2O_3 in ore, %				
	42	44	46	48	50
Chromium ore, physical, kg	2274	2160	2061	1966	1883
Chromium ore 50% Cr_2O_3 , kg	1910	1901	1897	1888	1883
FeSiCr, kg	641	637	629	627	621
Lime, kg	1860	1776	1691	1625	1556
The proportion of Cr FeSiCr in the mixture, %	117.83	112.63	107.89	103.90	100
Electricity, %	117.83	112.63	107.80	103.90	100

7.6 Vacuum Processes of Decarburization and Degassing of Ferrochromium

Until the beginning of the 60s, low-carbon ferrochromium was produced mainly by a *furnace silicothermic method* and in small quantities by an expensive *aluminothermic* process. However, due to the relatively high content of carbon and nitrogen in silicothermic ($>0.06\%$ C; 0.04% N) and aluminothermic ($>0.03\%$ C; 0.1% N) ferrochromium, these alloys did not satisfy the requirements, presented by steel-making. At the first stage of the search for technologies for deep decarburization of ferrochromium, efforts were focused on studying the process of carbon oxidation of liquid ferrochromium in a vacuum. However, chromium in the solid and liquid state has a relatively high vapor pressure; therefore, decarburization of liquid chromium (ferrochromium) in a vacuum is accompanied by a loss of chromium due to its evaporation. This process has proved difficult to implement.

To solve the problem of producing ferrochromium with very low contents of carbon and nitrogen, a method for refining ferrochromium in a solid state was developed and introduced. The essence of this technology is as follows. Ingots of silicothermic ferrochromium with $0.10\text{--}0.15\%$ C are subjected to solid vacuum-heat treatment in resistance electric furnaces at $1450\text{--}1500\text{ }^{\circ}\text{C}$ and a pressure of $1\text{--}0.1\text{ Pa}$ for $20\text{--}24\text{ h}$. Under vacuum and high temperature, conditions are created for the development of the decarburization process of the metal due to the oxygen contained in it.

The technology was implemented in a three-chamber continuous resistance furnace (Fig. 7.15).

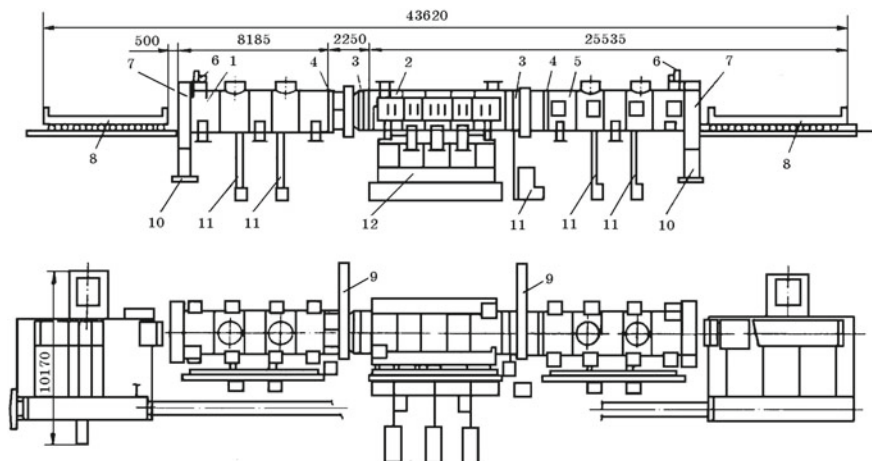


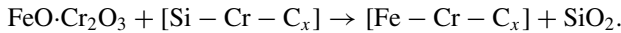
Fig. 7.15 Vacuum resistance electric furnace to obtain vacuum-thermic ferrochromium. 1—cooling chamber of ferrochromium; 2—isothermal treatment chambers; 3—vacuum locks; 4—compensators; 5—preheating chamber; 6—cover lifting mechanism; 7—a cover; 8—trolley; 9—vacuum locks; 10—frame; 11—fore-vacuum pumps; 12—booster pumps

The total installed capacity of the furnace is 1.5 MV A. The furnace has three chambers. The temperature in the preheating chamber is 1000 °C, in the isothermal holding chamber 1450–1500 °C. The third chamber is designed to cool ferrochromium and is not lined. Ferrochromium, which has undergone vacuum heat treatment, contains a small amount of C, N, H and oxide inclusions. There is also a method for decarburization in vacuum of crushed high-carbon ferrochromium, previously oxidized in the solid state.

7.7 Oxygen-Converter and Silicothermic Methods of Obtaining Medium-Carbon Ferrochromium

Medium-carbon ferrochromium (Table 7.14) can be obtained by silicothermic and oxygen-converter methods.

Silicothermic method. An earlier method is a flux-free silicothermic method involving the reduction of chromium and iron of chromite ore by silicon of ferrosilicochromium



With the flux-free method chromium extraction is low, therefore, the flux method is currently used. Melting is carried out in arc furnaces of refining type with a capacity of 5 MV A. The extraction of chromium is 76–80%. 1413 kg of chromium ore (50% Cr₂O₃) are consumed per 1 ton of medium-carbon ferrochromium; 519 kg of ferrosilicochromium (48% Si); 100 kg of metal from slag separation; 1241 kg of lime; 14 kg of electrode mass at a power consumption of 2129 kWh/t.

Oxygen-converter method. This method is based on the process of carbon oxidation of high-carbon ferrochromium with gaseous oxygen. The chemistry of the process can be described by the reactions:

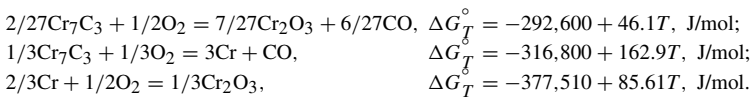


Table 7.14 Chemical composition of medium-carbon ferrochromium, %^a

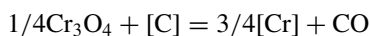
Grade	C	P	Grade	C	P
	Less than			Less than	
FeCr100A	1	0.03	FeCr 200B	2	0.05
FeCr 100B	1	0.05	FeCr 400A	4	0.03
FeCr 200A	2	0.03	FeCr 400B	4	0.05

^aFor all grades 65% Cr, 2% Si, 0.04% S

An analysis of the above dependences shows that in the initial period of purging of ferrochromium at relatively low temperatures, the oxidation of chromium and chromium carbide Cr_7C_3 to Cr_2O_3 develops. With a decrease in carbon concentration from 7–8 to 6–5% and lower, the bond strength of carbon atoms with chromium increases, since new groups are formed corresponding to Cr_{23}C_6 carbide (5.8% C). The decarburization reaction of a ferrochromium melt of such a composition in general form can be described by the equation



The theoretical temperature for the onset of carbon oxidation of Cr_{23}C_6 carbide by oxygen of Cr_2O_3 oxide is higher than that of carbon carbide Cr_7C_3 , which also requires a higher process temperature. To calculate the equilibrium concentrations of carbon and chromium when refining ferrochromium from carbon with the participation of slag saturated with chromium oxides, by the reaction



recommended equation (for $p_{\text{CO}} = 0.1$ MPa at 1873–2073 K) is:

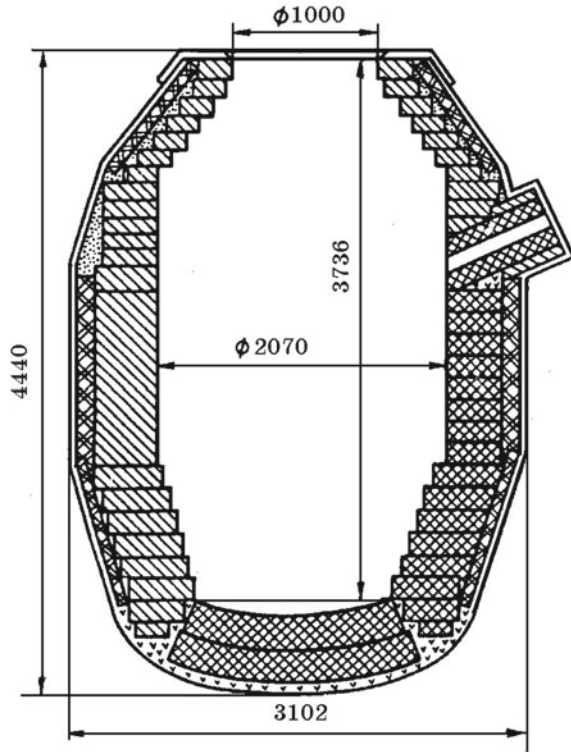
$$\lg[\% \text{Cr}]/[\% \text{C}] = -10850/T + 7.12.$$

Calculations using the above equation show that at 1873, 1973 and 2073 K, the equilibrium carbon content is, respectively, 3.1, 1.7 and 0.92%.

The technology for the production of ferrochromium in a 15-ton converter with the top oxygen supply through a water-cooled lance has been mastered (Fig. 7.16).

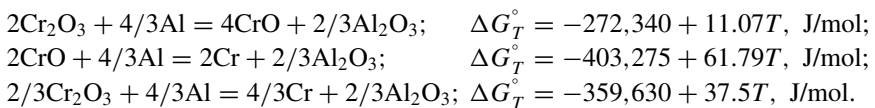
From 7 to 11 tons of high-carbon foundry ferrochromium, obtained in the same workshop in an ore-smelting electric furnace, is poured into the converter through the neck. Converted liquid alloy for purging in the converter contains, %: ≥ 60 Cr; ≤ 1.0 Si; ≤ 0.05 P; ≤ 0.06 S, carbon content is not limited. 80–100 m³ of oxygen is consumed per 1 ton of filled metal. After melting, 600–800 kg of scrap of medium-carbon ferrochromium are set into the metal, and before the metal is drained, 15–20 kg of granular ferrosilicochromium grade FeSiCr48 is used to partially recover and liquefy the slag. The release of metal and slag is carried out in a metal receiver, followed by casting into the mold. Total amount of 1230–1260 kg of carbon ferrochromium, 5–8 kg of aluminum and ~ 100 m³ of oxygen is consumed per 1 ton of finished alloy with 80–81% chromium extraction.

Fig. 7.16 Converter for decarburization of ferrochromium



7.8 Aluminothermic Method for Producing Metallic Chromium and Ferrochromium

Metallic chromium (Table 7.15) is produced by aluminothermic method. The reduction of chromium by aluminum occurs with the formation of an intermediate oxide CrO. The process is characterized by the following reactions:



For the smelting of metallic chromium, chromium oxides with a total chromium content in terms of $\text{Cr}_2\text{O}_3 > 99\%$ and 98% are used. Primary aluminum powder is used as a reducing agent. In out-of-furnace smelting, sodium nitrate containing $>99\%$ NaNO_3 is introduced into the charge to obtain the missing amount of heat. Lime is used as a flux. Calcium oxide forms compounds with a low melting point with Al_2O_3 (Fig. 7.17). The introduction of CaO in the mixture reduces the melting point of the slag. Under oxidizing conditions, it is possible to form calcium chromite-chromate

Table 7.15 Chemical composition of metallic chromium, % (GOST 5905-80)^a

Element	Cr99A	Cr99B	Cr98,5	Cr98	Cr97
Cr	99.0	99.0	98.5	98.0	97.0
Si	0.3	0.3	0.4	0.5	0.5
Al	0.2	0.5	0.5	0.7	1.5
Fe	0.6	0.6	0.6	0.8	1.2
C	0.03	0.03	0.03	0.04	0.05
S	0.02	0.02	0.03	0.03	0.04
P	0.02	0.02	0.02	0.03	0.03
Cu	0.01	0.01	0.02	0.04	0.05
As	0.01	0.01	0.01	–	–
Bi	0.0005	0.0005	0.0005	–	–
Sb	0.008	0.008	0.008	–	–
Zn	0.006	0.006	0.01	–	–
Pb	0.0008	0.0008	0.001	–	–
Sn	0.004	0.004	0.004	–	–
Co	0.005	–	–	–	–
N	0.04	0.05	–	–	–

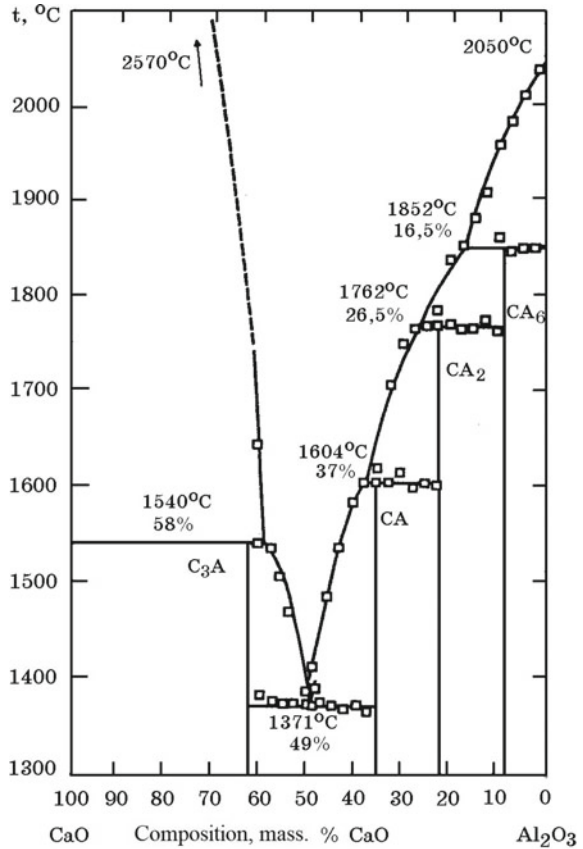
^aCr content—no less, for the rest—no more

9CaO·4CrO₃·Cr₂O₃ ($t_m = 1218$ °C). This facilitates the production of chromium-lime melts before the reduction of chromium from its oxide with aluminum during the preliminary melting of part of the oxides in an electric furnace during the smelting of metallic chromium and low-carbon ferrochromium.

Possible options for producing metallic chromium: melting in a stationary furnace for a block, melting in a leaning hearth with the release of metal and slag, electric furnace melting with preliminary melting of some oxides without aluminum in an electric arc furnace.

Melting of metallic chromium on the block is carried out in a detachable cast iron hearth with a lining in the lower part of the walls with magnesite brick and a bottom made of magnesite powder. The horn is installed in a special chamber. Melting is carried out using a mixture consisting of chromium oxide, aluminum powder and sodium nitrate. Smelting is carried out with a lower ignition, initially setting 10–15% of the total charge into the furnace. They ignite the ignition mixture, consisting of magnesium powder or shavings of magnesium and nitrate, and then, after the start of recovery, load the rest of the charge, evenly distributing it over the surface of the melt, and close the furnace to reduce heat loss. The resulting ingot is cooled in water and then crushed. The specific consumption of materials for producing metallic chromium with 97% Cr is, kg/t: 1650 Cr₂O₃; 620 aluminum powder; 110 lime; 140 sodium nitrates. Chromium recovery is 88%. The metal usually contains, %: 98–99.3 Cr; 1.1–0.1 Al; 0.3–0.1 Si; 0.3–0.6 Fe; 0.01–0.02 C; 0.04–0.006 P; <0.02 S; 0.03–0.2 N.

Fig. 7.17 Equilibrium state diagram of the CaO–Al₂O₃ system



The technological scheme for the production of metallic chromium, which also includes the reduction of slag, the preparation of CrAl ligature and high-carbon ferrochromium, the processing of final slag into a semi-product for synthetic slag or high-alumina cement clinker (HACC), is shown in Fig. 7.18.

In the production of high purity aluminothermic chromium, out-of-furnace smelting and casting of chromium are carried out in sealed chambers with the creation of reduced pressure in them (Fig. 7.19).

The mixture, consisting of chromium oxide of high purity, calcium chromate, chromic anhydride and aluminum powder (grade A99), is pelletized. Then, the pellets are fired at 400–500 °C to remove moisture and oxidize impurity carbon. The charge is melted in the reaction hearth. Metal and slag are discharged from the furnace into molds installed in the casting chamber. The resulting chromium contains from 0.001 to 0.01% of nitrogen and carbon of each and hydrogen of 1–2 cm³/100 g. Using the above components, the content of impurities is significantly reduced: iron (0.08–0.3%), silicon (0.03–0.16%) and non-ferrous metals. The extraction of chromium is

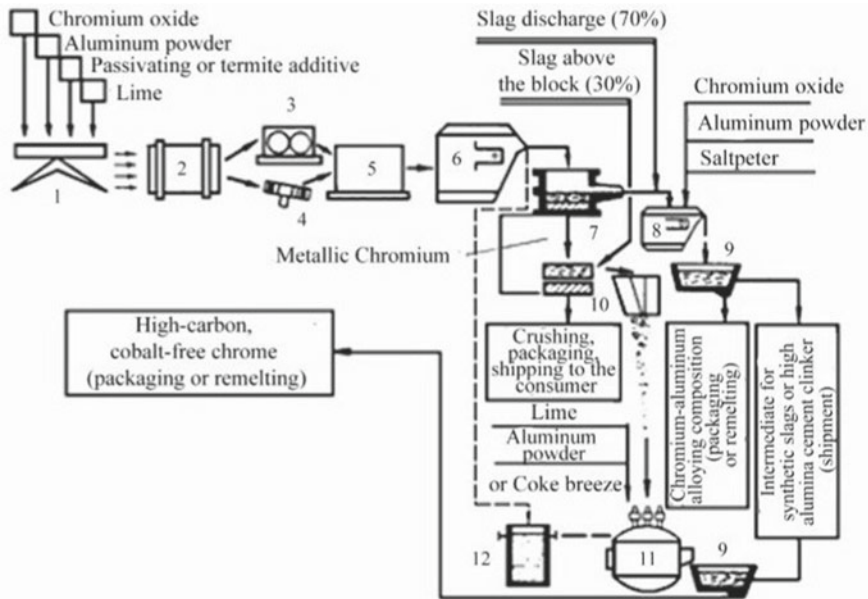


Fig. 7.18 Technological scheme for the production of metallic chromium with the additional slag recovery and obtaining an intermediate product or clinker of high-alumina cement: 1—scales; 2—mixer; 3—briquetting press; 4—plate granulator; 5—drying oven; 6—smelter for smelting metallic chromium; 7—mold for metal and slag; 8—hearth for additional slag recovery; 9—slag; 10—crusher for slag; 11—electric furnace for additional recovery of slag; 12—casting ladle

93%, the use of aluminum is 97.5%. Specific consumption of materials, kg/t: 1550 Cr_2O_3 ; 595 aluminum powder; 100 lime; 130 sodium nitrates.

The aluminothermic low-carbon ferrochromium has the following chemical composition, %:

Grade	Cr	C	Si	S	P	Al
FeCr003A	75	0.03	0.5	0.015	0.010	0.4
FeCr004A	70	0.04	0.7	0.020	0.018	0.5

Chromite concentrate (58.5% Cr_2O_3 ; 1.6% SiO_2 ; 10% Al_2O_3 ; 14% MgO), primary aluminum powder, lime and a small amount of nitrate are used as starting charge materials. Melting is carried out in the leaning melting hearth. The specific heat of the process is 3100–3180 kJ/kg, which ensures a process temperature of 2360 °C. The extraction of chromium during smelting is 89%, and the through extraction of chromium, taking into account losses during enrichment, is ~58%. Technical and economic indicators of obtaining aluminothermic low-carbon ferrochromium are given in Table 7.16. Slag contains, %: 60 Al_2O_3 ; 2–4 Cr_2O_3 ; 10–13 CaO ; 20–24 MgO ; 0.8–1 FeO ; 0.8–1.5 SiO_2 ; it is sent for processing to obtain a high-alumina semi-product or a high-alumina cement clinker according to the above scheme (Fig. 7.18).

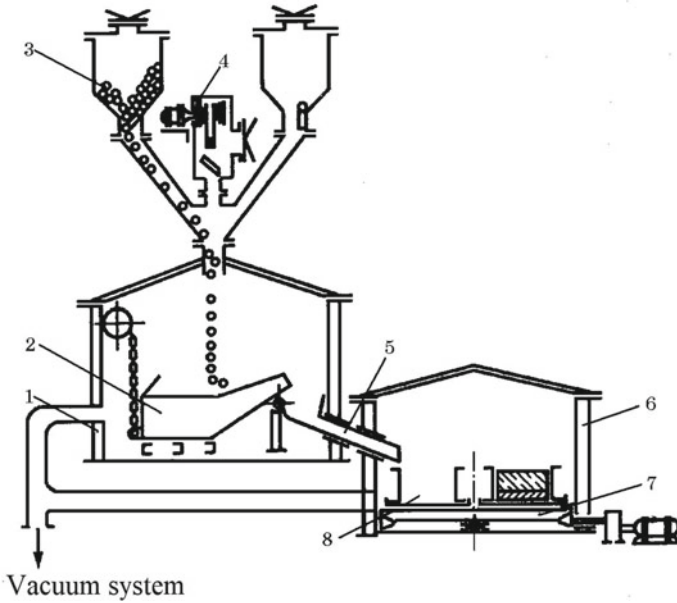


Fig. 7.19 Two-chamber installation for out-of-furnace smelting of alloys under vacuum and in a neutral atmosphere: 1—a melting chamber; 2—tilting hearth; 3—hoppers for pellets; 4—device for ignition of the mixture; 5—trough for the release of melting products; 6—casting chamber; 7—rotary table; 8—molds

Table 7.16 Technical and economic indicators of the smelting process low-carbon ferrochromium aluminothermic method

Parameter	Smelting option		
	Out-of-furnace on the block	Electric furnace on the block	Electric furnace with the release of the melt
<i>Consumption of materials, t</i>			
Concentrate	2.215	1.756	1.640
Aluminum	0.710	0.466	0.445
Saltpeter	0.411	0.032	0.030
Lime	—	0.466	0.335
Electrodes	—	0.016	0.014
Power consumption, kWh/t	—	1240	1140
Unit productivity, %	—	100	125

Table 7.17 Chemical composition of nitrided ferrochromium, % (GOST 4757-91)

Ferrochromium	Cr	C, ≤	Si	P, ≤	S, ≤	N
Fused FeCr...CIN3	45–75	0.10	≤1.5	0.03	0.025	2.0–4.0
Sintered FeCr...CIN7	45–75	0.10	≤1.5	0.03	0.025	2.0–4.0
		0.10	≥1.5	0.03	0.025	4.0–10.0

7.9 The Technology of Producing Nitrided Ferrochromium

Nitrided ferrochromium is used for the smelting of chromium–nickel–manganese and chromium manganese austenitic and other steels in order to partially replace scarce nickel and increase the physical–mechanical properties of metal products. In the CIS countries, nitrided ferrochromium is produced with a nitrogen content of up to 10% (Table 7.17).

Two types of nitrided ferrochromium are distinguished: *fused* and *sintered*. Fused ferrochromium with a content of 2.0–4.0% N is obtained by nitrogen saturation of a liquid low-carbon ferrochromium in induction furnaces, as well as in plasma-arc melting. The dissolution of molecular nitrogen in liquid ferrochromium is accompanied by heat; therefore, the content of nitrogen dissolved in liquid ferrochromium decreases with increasing temperature.

Low-carbon ferrochromium with a low silicon content, deoxidized by aluminum, is nitrided, providing conditions that exclude the formation of an oxide film (slag) on the surface of the melt. Gaseous nitrogen must be thoroughly cleaned of oxygen and H₂O. These conditions are most fully satisfied when nitriding ferrochromium in vacuum induction furnaces. Nitriding of liquid medium-carbon ferrochromium can also be performed in an oxygen converter. In this case, a converter with a lateral supply of nitrogen to liquid ferrochromium is used. The possibility of obtaining nitrided ferrochromium using plasma technology is shown. In all cases, ferrochromium is obtained with 1–2% dissolved nitrogen, evenly distributed over the height of the ingot.

Nitrided sintered ferrochromium (Table 7.18) is a nitrogen-saturated powder (4–10% N) of high-carbon ferrochromium decarburized in vacuum. Sintered nitrided ferrochromium can also be obtained by nitriding a powder of low-carbon silicothermic ferrochromium. The essence of the method consists in heating small fractions of ferrochromium in an atmosphere of molecular nitrogen at temperatures that ensure the thermodynamic stability of (Cr, Fe)₂N and (Cr, Fe) N nitrides and a high rate of the nitriding process.

An industrially developed method is the nitriding of briquettes of low-carbon ferrochromium, obtained by the vacuum method of decarburization of high-carbon ferrochromium. After the end of the decarburization process in vacuum resistance furnaces at 1100 °C, nitrogen (99.5% N₂) is introduced into the furnace at a pressure of 100 kPa. The resulting briquettes of nitrided ferrochromium are cooled to 600–800 °C in a nitrogen atmosphere at a pressure of 3–4 kPa. Then, air is let into the

Table 7.18 Chemical composition of nitrated low-carbon ferrochromium, % (GOST 4757-79)^a

Grade	Cr, no less	C	Si	P	S	Al	N, no less
		No more					
FeCrL100A	65	0.06	1.0	0.02	0.02	0.2	1.0
FeCrL100B				0.03			
FeCrL200A	65	0.06	1.0	0.03	0.02	0.2	2.0
FeCrL200B				0.04			
FeCrL400A	65	0.06	1.0	0.03	0.04	0.2	4.0
FeCrL400B				0.04			
FeCrL600A	60	0.03	1.0	0.03	0.04	0.2	6.0
FeCrL600B				0.04			

^aNitrided low-carbon ferrochromium is produced with a mass fraction of C \leq 0.02% in all grades; \leq 0.03% in brands FeCrL100A, FeCrL200B, FeCrL200A, FeCrL400A, FeCrL400B; with a mass fraction of Al \leq 0.1% in all brands

furnace and subsequently cooled in air. For 1 ton of nitrided ferrochromium with 6–8% N, 60% Cr and 0.01% C, 1100 kg of high-carbon foundry ferrochromium are consumed; 150 m³ of nitrogen at an electric energy consumption of 9500 kWh.

Chapter 8

Metallurgy of Ferrotungsten



Tungsten was discovered and isolated in the form of tungsten anhydride WO_3 in 1781 by the Swedish chemist C. Scheele from the tungsten mineral, later called scheelite. The tungsten content in the earth's crust is 10^{-4} %. Ferrotungsten was first obtained in 1893 by the aluminothermic method.

Tungsten is widely used in modern technology in the form of pure metal and in a number of alloys. It is used for alloying tool, structural, high speed and other steels; it is part of cermet alloys with high hardness and wear resistance, tungsten carbide-based hard alloys, heat-resistant and some special alloys. The refractoriness and low vapor pressure at high temperatures make tungsten indispensable for parts of electric vacuum devices in radio and X-ray technology, as well as for producing filaments and spirals in incandescent lamps. In various areas of technology, some chemical compounds of tungsten are used, for example, Na_2WO_4 , WS_2 , etc.

8.1 Properties of Tungsten and Its Compounds

Tungsten—an element of the VIb group of the Periodic system of elements. The atomic number of tungsten is 74, the atomic mass is 183.85, the configuration of the electron shell is $4f^{14}5d^46s^2$, the valency is from 2 to 6 (the most stable compounds of higher valency), the density is $19.3\text{--}19.9 \text{ g/cm}^3$, the melting point of tungsten is $3410 \text{ }^\circ\text{C}$, the boiling point $5930 \text{ }^\circ\text{C}$.

W–Fe system. Tungsten narrows the γ -Fe region (Fig. 8.1). With a standard tungsten content in industrial ferrotungsten $>60\%$, the melt temperature is about $2580 \text{ }^\circ\text{C}$. Solutions of tungsten in iron-based melts are close to ideal, at $1600 \text{ }^\circ\text{C}$ $\gamma_{\text{W(Fe)}}^{\circ} = 1$.

W–O system. Tungsten forms a series of oxides WO_2 , W_4O_{11} and WO_3 with oxygen (Fig. 8.2). Some properties of oxygen compounds of tungsten are given below:

Fig. 8.1 Equilibrium state diagram of the W-Fe system

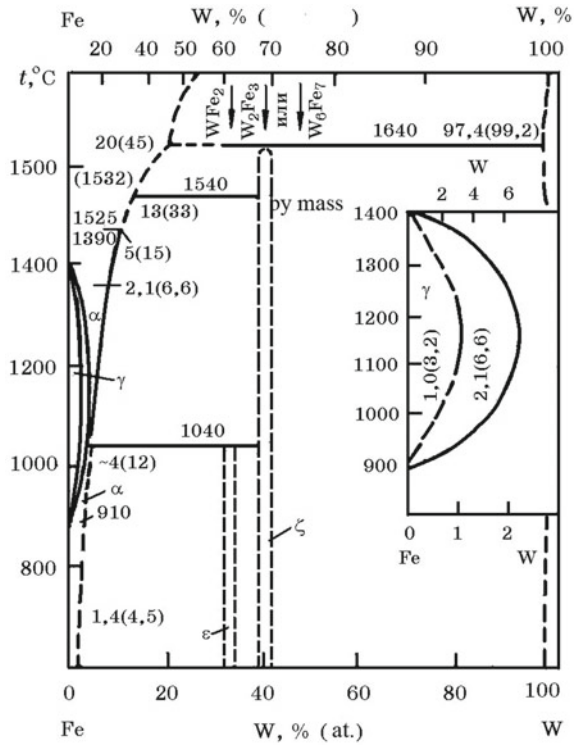
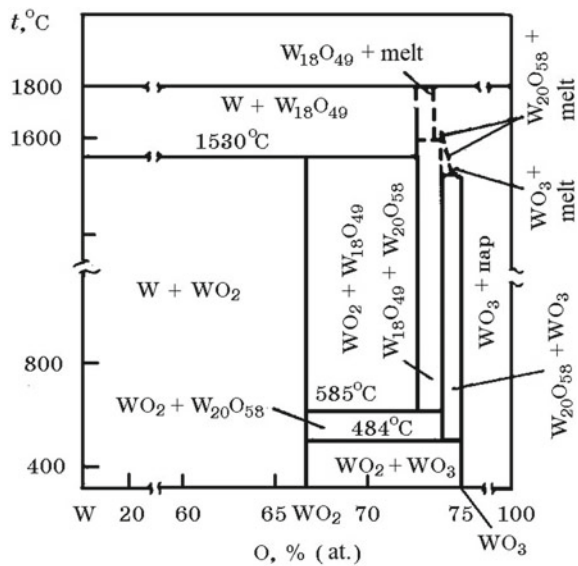


Fig. 8.2 Equilibrium state diagram of the W-O system



Oxide	WO ₃	WO ₂
Color	Lemon yellow	Dark brown
Crystal cell	Monoclinic	Monoclinic
Density, g/cm ³	7.2–7.4	10.9–11.1
ΔC_p° , J/(mol K)	79.7	55.8
$\Delta H_{\text{for}}^\circ$, kJ/mol	–841.3	–588.1
S_{298}° , J/(mol K)	81.6	50.6

The temperature dependences of the Gibbs energy change of oxide formation reactions have the form:

$$W_{(s)} + 3/2O_2 = WO_{3(s)}; \quad \Delta G_{298}^\circ = -134,333 + 42.63T \lg T + 383.3T, \quad \text{J/mol};$$

$$W_{(s)} + O_2 = WO_{2(s)}; \quad \Delta G_{298}^\circ = -578,930 + 152.98T, \quad \text{J/mol}.$$

W–C system. In the W–C system (Fig. 8.3), carbides W₂C (3.07% C) and WC (6.12% C) are formed. Gibbs energy of the formation of tungsten carbides W₂C and WC from

Fig. 8.3 Equilibrium state diagram of the W–C system

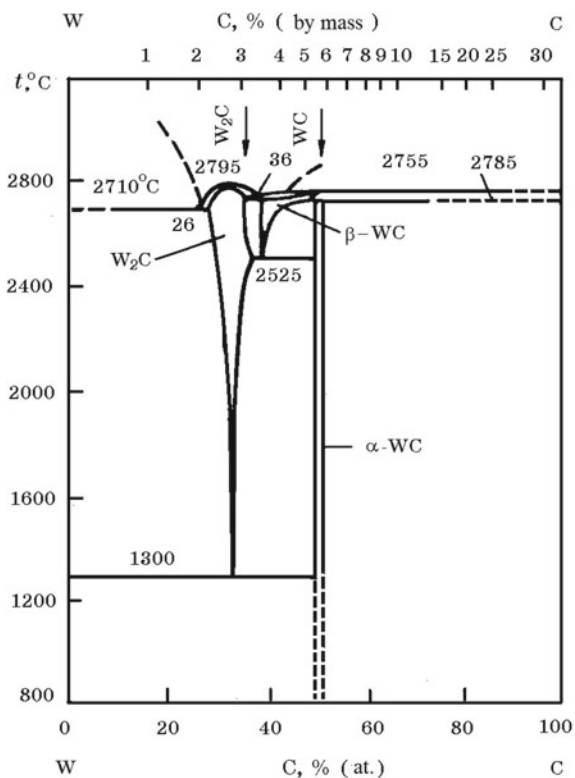
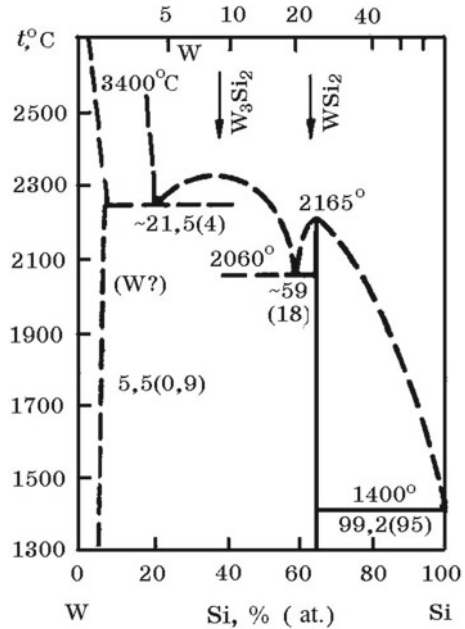
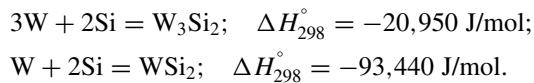


Fig. 8.4 Equilibrium state diagram of the W–Si system



elements, respectively, is equal to: $\Delta G_{298}^{\circ}(\text{W}_2\text{C}) = -49,100 \text{ J/mol}$, $\Delta G_{298}^{\circ}(\text{WC}) = -37,620 \text{ J/mol}$. The density of W_2C is 17.5 g/cm^3 , WC is 15.5 g/cm^3 , and the melting point is, respectively, 2795 and $2785 \text{ }^{\circ}\text{C}$.

W–Si system. In the W–Si system (Fig. 8.4), silicides W_3Si_2 (9.21% Si) and WSi_2 (23.3% Si) are formed by the reactions:



Melting temperature W_3Si_2 — $2310 \text{ }^{\circ}\text{C}$, WSi_2 — $2065 \text{ }^{\circ}\text{C}$.

8.2 Tungsten Minerals, Ores and Concentrates

Tungsten minerals. The following minerals are mainly of industrial importance: Ferberite FeWO_4 , Hubnerite MnWO_4 , Wolframite $(\text{Fe}, \text{Mn})\text{WO}_4$ and Scheelite CaWO_4 (Table 8.1). Hubnerite and ferberite alone rarely occur; usually, they form an isomorphous mixture—wolframite, in which manganese and iron can replace each other in the mineral lattice. Tungsten ores contain an average of 0.2–0.5% WO_3 , rarely exceeding 1%. Often, they include molybdenum, tin, copper, arsenic and other minerals. The main deposits of tungsten ores in the CIS countries are located in Russia

Table 8.1 Some properties of tungsten minerals

Mineral	Chemical formula	WO ₃ , %	W, %	ρ , g/cm ³	Mohs hardness
Ferberite	FeWO ₄	76.3	60.5	7.5	4.5
Hubnerite	MnWO ₄	76.6	60.7	7.1	4.0
Wolframite	(Fe,Mn)WO ₄	76.5	60.6	7.1–7.5	4.0–4.5
Scheelite	CaWO ₄	80.6	63.9	5.8–6.2	4.5–5.0

and Kazakhstan. Rich tungsten ores are mined in China, Korea, Burma, USA, Spain, Portugal, Bolivia and Australia.

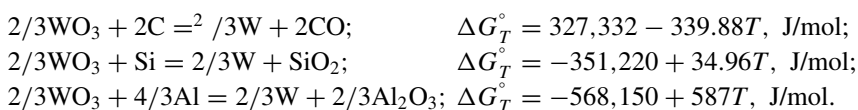
Tungsten concentrates. Ores are subjected to enrichment in various complex ways to obtain concentrates (Table 8.2). To obtain pure WO₃ oxide, necessary for the production of tungsten metal, complex chemical and hydrometallurgical schemes for processing scheelite and tungsten concentrates are used.

Scheelite concentrates contain 45–65% WO₃. The gangue is represented by quartz, calcite and fluorite. Associated minerals are often molybdenite and powellite. In the concentrates of the Tyrny-Auz deposit (North Caucasus, Russia), the content of oxidized molybdenum, part of which is isomorphically associated with scheelite, reaches 2.5–3%. Processing such concentrates allows one to obtain pure WO₃ oxide. Tungsten concentrates with a high sulfur content (1–7%) are subjected to oxidative roasting in a single-hearth furnace (hearth area 18 m²), and a concentrate containing 0.12–0.56% S is obtained.

8.3 The Technology of Obtaining of Ferrotungsten by Carbon-Silicothermic Method

The requirements of the standard for the composition of ferrotungsten are given in Table 8.3.

Tungsten has a small chemical affinity for oxygen and can be reduced from its oxides by carbon, silicon and aluminum:



Ferrotungsten of grades FeW72, FeW70 and FeW65 are obtained by reduction of carbon and silicon concentrates in an ore-smelting furnace; grades FeW70 (a), FeW75 (a) and FeW80 (a) are smelted by the aluminothermic method.

To obtain ferrotungsten by the carbon-silicothermic method, a smelting method is used with scooping the alloy out of the furnace. Melting is carried out in a furnace with a capacity of 5 MV A. The furnace bath is lined with magnesite brick. During the melting process, the magnesite lining from the surface is partially replaced by

Table 8.2 Chemical composition of tungsten concentrates, % (GOST 213-83)

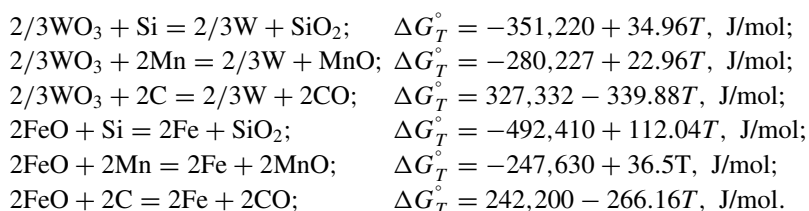
Grade	WO ₃ , no less	MnO ₂	SiO ₂	P	S	As	Sn	Cu	Mo	CaO	Pb	Sb	Bi	Moisture
		No more												
KVG-1	65	17.5	5	0.05	0.7	0.08	0.15	0.10	0.1	–	0.2	0.2	0.20	2
KVG-2	60	15	5	0.05	0.8	0.05	0.2	0.15	0.2	–	0.4	0.3	0.30	1.5
KSh-1	60	2.0	6.5	0.04	0.6	0.05	0.08	0.10	1.0	–	–	–	–	6
KMSh-1	65	0.1	1.2	0.03	0.3	0.02	0.01	0.10	3.0	–	0.01	0.01	0.01	4
KMSh-2	60	0.1	4	0.04	0.3	0.04	0.02	0.08	3.0	–	0.1	0.01	0.01	6

Table 8.3 Chemical composition of ferrotungsten, %

Grade	W, no less	Mo	Mn	Si	C	P	S
		No more					
FeW80(a)	80	6.0	0.2	0.8	0.10	0.03	0.02
FeW75(a)	75	7.0	0.2	1.1	0.15	0.04	0.04
FeW70(a)	70	7.0	0.3	2.0	0.2	0.06	0.06
FeW72	72	1.0	0.4	0.5	0.3	0.04	0.08
FeW70	70	2.0	0.5	0.8	0.5	0.06	0.10
FeW65	65	6.0	0.6	1.2	0.7	0.10	0.15
Grade	Cu	As	An	Al	Pb	Bi	Sb
	No more						
FeW80(a)	0.10	0.04	0.04	3.0	0.01	0.01	0.01
FeW75(a)	0.20	0.05	0.05	5.0	–	–	–
FeW70(a)	0.30	0.06	0.08	6.0	–	–	–
FeW72	0.15	0.04	0.08	–	0.02	0.02	0.02
FeW70	0.20	0.05	0.10	–	–	–	–
FeW65	0.30	0.08	0.20	–	–	–	–

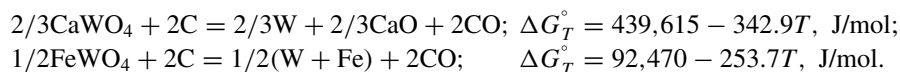
ferrotungsten, and the working lining is a refractory metal skull. For melting, tungsten concentrate, petroleum and pitch coke, granular ferrosilicon (FS65 or FS75), steel shavings and tungsten-containing slag obtained from remelting dust and waste are used. The composition of the charge is calculated taking into account the transition of impurities into the alloy in the following amounts, %: Mo—100; Cu—100; As—15; S—15; Sn—30.

By the nature of the ongoing physicochemical processes and the operations used, melting is divided into three periods. After the third, last period, ferrotungsten is in the furnace bath, containing, %: 3–8 Si; 1.7–4.5 Mn; 0.2–2 C; 50–55 W. In the first period, the alloy is refined from Si, Mn and C, which passed into it when finishing the slag (previous melting) with oxides of tungsten concentrate loaded into the furnace according to the reactions:

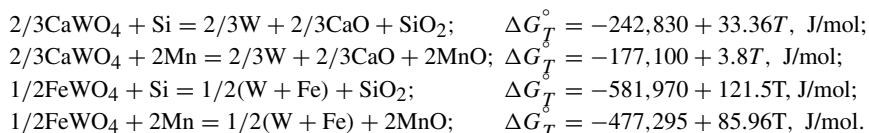


At the beginning of the first period, slag with a high tungsten content obtained by remelting dust from electrostatic precipitators and dust from battery cyclones is loaded into the furnace. To reduce the tungsten viscosity, steel chips are introduced

into the furnace, lowering the melting point of the tungsten-containing alloy, and then, the concentrate is filled. An oxidizing slag is formed in the furnace, containing, %: 16–23 WO₃; 15–20 FeO; 28–32 SiO₂; 10–15 MnO; 8–10 CaO; 1–3 MgO; 2–4 Al₂O₃. To increase the refining rate, the temperature of the slag and metal is increased, running the furnace at maximum power. At the end of the first period, they start filling tungsten concentrate with coke, seeking to obtain working slag of the second period with a content of 10–12% WO₃. The reduction of tungsten and iron contained in the concentrate in the first and second periods of melting occurs mainly with coke carbon by the reactions:



In the reduction of tungsten and iron, silicon and manganese remaining in the metal after the third period of the previous melting (period of the repeated reduction of slag) take part



By the end of the first period, the metal has a standard content of tungsten and impurities. In the second period, the duration of which is 1–1.5 h, the working voltage is reduced from 178–187 to 149 V, trying to warm the metal as best as possible and ensure its solid–liquid state. Scooping of the alloy in the second period is carried out by a special machine installed on the working platform (Fig. 8.5). The alloy from the furnace is scooped up with a removable carbon steel spoon containing 50 kg of metal. A spoon with metal is immersed in a tank of water and cooled, and an ingot is knocked out on a special device. To evenly scoop out the alloy, the furnace bath is rotated.

The goal of the third period is to reduce WO₃ from slag with silicon of ferrosilicon to ≤0.25% WO₃. The metal is enriched with silicon and manganese. The tungsten concentration in the alloy gradually decreases from 65–72 to 52–54%. After receiving the analysis of another slag sample with a content of ≤0.25% WO₃ (usually 0.05–0.15%), it is kept in the furnace for 10–15 min, and then, slag is discharged. The final slag contains, %: 0.05–0.2 WO₃; 0.3–2 FeO; 45–50 SiO₂; 15–20 MnO; 25–30 CaO. After the slag is released from the furnace, the metal of the following composition remains, %: 66–70 W; 5–7 Si; 0.7–2.5 Mn; 0.03–0.14 S; 0.1–0.2 C.

Per one ton of ferrotungsten is consumed, kg: 1530 tungsten concentrate (60% WO₃); 108 ferrosilicon FS75; 87 pitch coke; 40 electrode mass at a power consumption of 3550 kWh. Tungsten recovery is usually 99%. The main share in the cost of ferrotungsten is concentrate (96–98% of the total cost); therefore, in the process of producing the alloy, measures are taken to reduce losses of tungsten with slag, exhaust gases and dust. In order to capture the dust formed during filling concentrate,

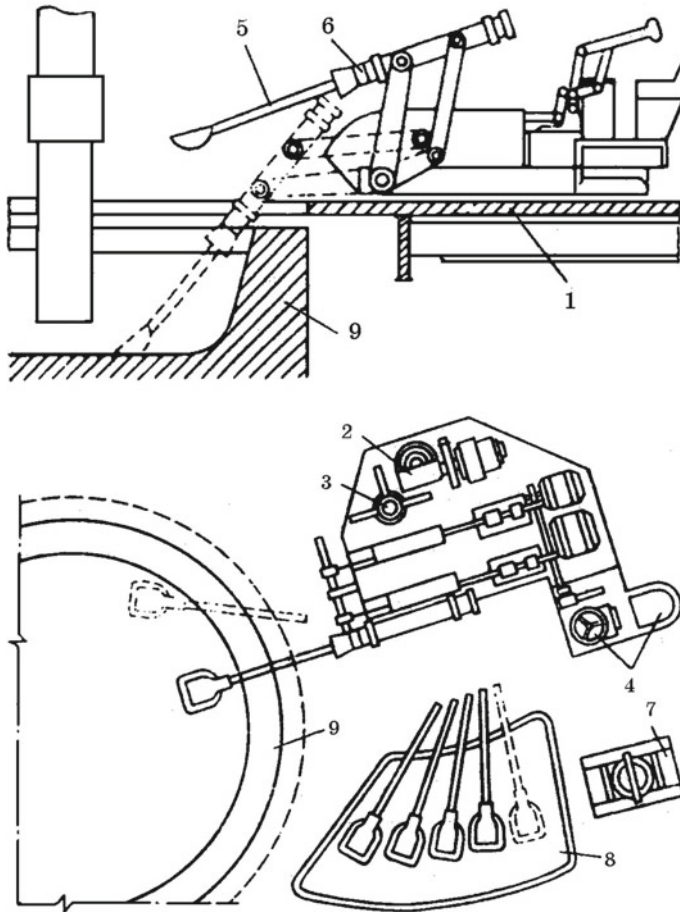
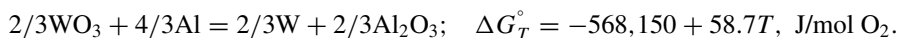


Fig. 8.5 Ferrotungsten scoop machine. 1—Work site; 2—rotation mechanism; 3—axis of rotation; 4—control panel; 5—a spoon; 6—capture; 7—device for knocking out an ingot; 8—stand; 9—electric furnace

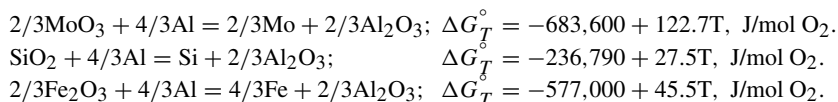
containing evaporating tungsten oxides (WO_3 and WO_2), furnaces are equipped with battery cyclones and electrostatic precipitators. Sublimates are condensed during cooling and collected in electrostatic precipitators. The dust is melted in a separate electric furnace, and an alloy with 40–50% Pb; 45–50% Bi and 5–8% Sn is obtained, which is sent to non-ferrous metallurgy plants for processing, and slag with 35–40% WO_3 is returned to the furnace melting ferrotungsten. The dust trapped in battery cyclones is similar in chemical composition to the charge loaded into the furnace. After briquetting, it is also used in smelting. The average actual composition of the obtained ferrotungsten is as follows, %: 74.31 W; 0.22 Si; 0.16 Mn; 0.14 C; 0.07 S; 0.028 P; 0.11 Cu; 0.1 Sn; 0.001 Pb; 1.45 Mo; 0.01 Bi and 0.01 Sb.

8.4 The Technology of Ferrotungsten Production by Aluminothermic Method

Ferrotungsten of the grades FeW80 (a), FeW75 (a) and FeW70 (a) with a high content of tungsten is obtained by the aluminothermic method (Table 8.3). The process is based on the reduction of tungsten trioxide with aluminum:



The concentrate used to produce ferrotungsten contains impurity oxides of Mo, Si and Fe; therefore, the main reaction is accompanied by the following processes:



For melting, mainly scheelite concentrate is used (Table 8.2). The amount of heat generated by these reactions does not ensure the normal course of melting (due to the high melting point of the alloy) and good separation of metal from slag. Therefore, melting is carried out in a three-phase electric furnace with a transformer 1000 kV A with magnesite lining. The diameter of the furnace bath is 800–1000 mm, and the height is 1200 mm. The bath (crucible) of the furnace is removable and has an outlet for slag; graphite electrodes with a diameter of 200 mm. The mixture of the following composition is used, kg: 100 scheelite concentrate; 23 powder of primary aluminum; 3 iron cutting; 4–5 iron oxide; 1 lime. To increase the extraction of tungsten, slag crusts, metal wastes of the previous melts and trapped dust are introduced into the charge. Depending on the crucible volume of the furnace, 2500–5000 kg of concentrate is consumed for smelting. Per 1 t of ferrotungsten is consumed, kg: 1555 scheelite concentrate; 345 primary aluminum powder; 20 lime; 80 iron oxide; 45 iron die cutting at an electric power consumption of 424 kWh. The tungsten attraction is 99%. Commodity alloy contains, %: 83–83.5 W; 4–4.75 Mo; 1.25–1.28 Si; 6.9–7.5 Fe; 0.026–0.047 Cu.

Chapter 9

Metallurgy of Ferromolybdenum



Molybdenum belongs to the group of rare metals. It was discovered in 1782 by the Swedish chemist P. Gjelm, who isolated molybdenum acid. Its content in the earth's crust is $1.1 \times 10^{-4}\%$.

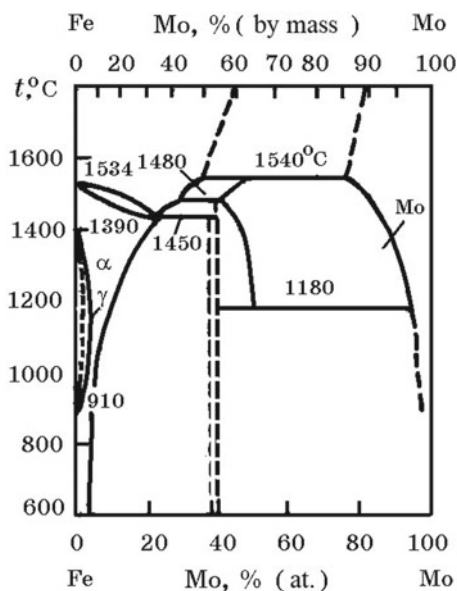
Molybdenum and its alloys are widely used in various branches of technology and industry, but the main consumer is ferrous metallurgy—70–80% of the obtained molybdenum is used for the production of alloy steels. The rest is used in the form of pure metallic molybdenum and alloys based on it, alloys with non-ferrous and rare metals, as well as in the form of chemical compounds. Molybdenum metal is the most important structural material in the production of electric lighting lamps and electric vacuum devices. Molybdenum wire and tape are widely used as heaters for high-temperature furnaces. An important role is played by molybdenum as an alloying element in heat-resistant and acid-resistant alloys based on nickel, cobalt and chromium. Some chemical compounds of molybdenum are used, so MoS_2 molybdenum sulfide is used as a lubricant in friction pairs, MoSi_2 molybdenum disilicide is used for heaters, etc.

9.1 Properties of Molybdenum and Its Compounds

Molybdenum—an element of the VIb group of the Periodic system of elements. The atomic number of molybdenum is 42, the atomic mass is 95.94; configuration of the outer electron shell of an atom $4d^55s^1$, melting temperature 2622 °C, boiling 4840 °C, density 10.23 g/cm³.

Mo-Fe system. Iron and molybdenum form FeMo , Fe_7Mo_6 intermetallic compounds and solid solutions (Fig. 9.1). The melting point of the alloys decreases slightly with an increase in the molybdenum content to 37.5%, and a further increase in the molybdenum content leads to its significant increase. A binary alloy with 55–58% Mo melts at a temperature exceeding 1650 °C. The maximum solubility

Fig. 9.1 Equilibrium state diagram of the Mo–Fe system



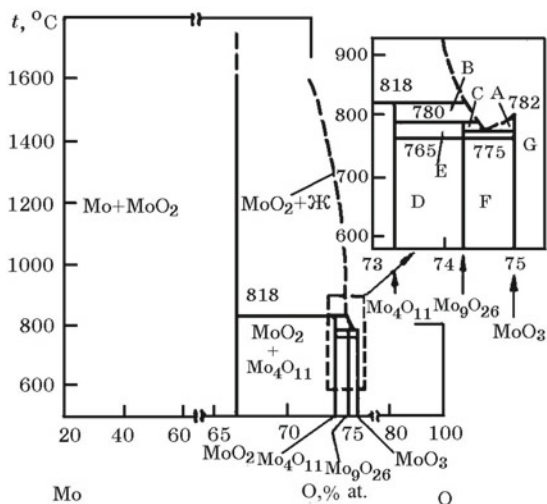
of iron in solid molybdenum at 1610 °C is 25% (at.). Solutions of molybdenum in iron-based melts are close to ideal, at 1600 °C $\gamma_{\text{Mo(Fe)}}^{\circ} = 1$.

Mo–O system. Oxygen in solid molybdenum dissolves in small quantities. With oxygen, molybdenum forms the oxides: MoO_3 ; MoO_2 ; Mo_3O ; $\text{Mo}_{17}\text{O}_{47}$; $\text{MoO}_{2.80}$; Mo_8O_{23} (Fig. 9.2).

The thermodynamic constants of molybdenum oxides are as follows:

Fig. 9.2 Equilibrium state diagram of the Mo–O system

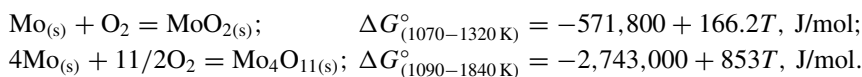
A— $\text{MoO}_3 + \text{L}$; B— $\text{Mo}_4\text{O}_{11} + \text{L}$; C— $\text{Mo}_9\text{O}_{26} + \text{L}$;
 D— $\text{Mo}_4\text{O}_{11} + \text{Mo}_9\text{O}_{26}$;
 E— $\text{Mo}_4\text{O}_{11}(\beta) + \text{Mo}_9\text{O}_{26}$;
 F— $\text{Mo}_9\text{O}_{26}(\gamma) + \text{MoO}_3$;
 G— $\text{Mo}_9\text{O}_{26}(\beta) + \text{MoO}_3$



$$\Delta H_{298}^{\circ}(\text{MoO}_3) = -754.9 \text{ kJ/mol}; \quad \Delta S_{298}^{\circ}(\text{MoO}_3) = -78.2 \text{ J/(mol K)};$$

$$\Delta H_{298}^{\circ}(\text{MoO}_2) = -586 \text{ kJ/mol}; \quad \Delta S_{298}^{\circ}(\text{MoO}_2) = 48.44 \text{ J/(mol K)}.$$

The temperature dependence of the Gibbs energy for the reactions of the formation of molybdenum oxides is described by the equations:



Gaseous MoO_3 formed at 520–720 °C consists of a vapor mixture of molecules of various compositions over MoO_3 , the pressure of which at different temperatures is as follows:

Temperature, °C	700	785	850	955	1150
p_{MoO_3} , kPa	0.29	2.66	26.6	133.0	980.7

Evaporation of MoO_3 increases in the presence of water vapor. At 690 °C and a water vapor pressure of 798 kPa, the vapor pressure of MoO_3 increases by about 4 times, since complex $\text{MoO}_3 \cdot \text{H}_2\text{O}$ molecules are formed. These properties of MoO_3 are associated with increased evaporation and possible losses of molybdenum oxides during roasting of molybdenum nitrate (MoS_2) concentrate.

MoO_3 oxide features are a low melting point (1068 K) and a high vapor pressure above it. The relative composition of the $\text{MoO}_{3(s)}$ vapor for various temperatures is characterized by the following data, %:

T , K	800	900	1000
Mo_3O_9	75.5	54.5	36.0
Mo_4O_{12}	23.2	37.6	44.5
Mo_5O_{15}	1.3	7.9	19.5

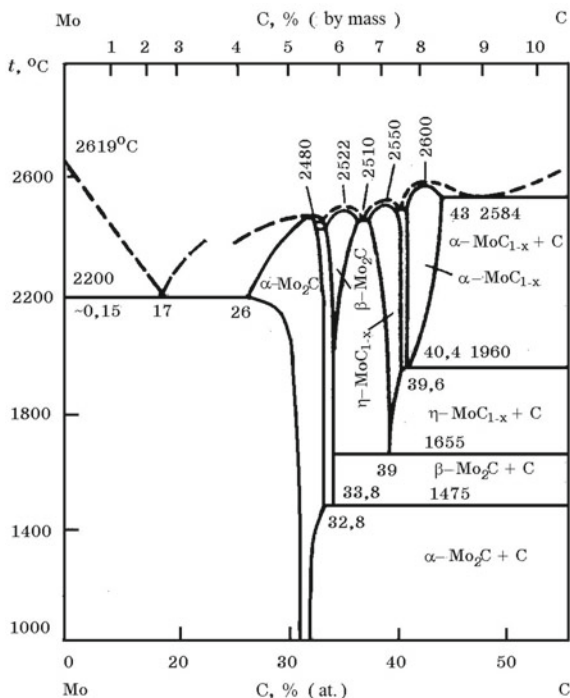
The temperature dependence of the total vapor pressure (MPa) over $\text{MoO}_{3(s)}$ has the form

$$\lg P_{\text{tot}} = -1545/T + 0.526.$$

Mo–C system. Molybdenum with carbon form carbides Mo_2C (5.88% C) and MoC_{1-x} (Fig. 9.3). Mo_2C carbide melts without decomposition at 2480 °C. The thermodynamic characteristics of Mo_2C are as follows: $\Delta H_{298}^{\circ} = -10,660 \text{ J/mol}$; $\Delta S_{298}^{\circ} = 65.90 \text{ J/(mol K)}$. The dependence of the Gibbs energy on the reaction temperature of the formation of Mo_2C is described by the expression:

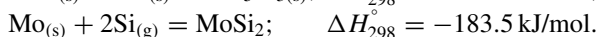
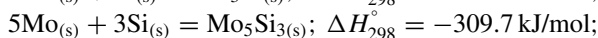
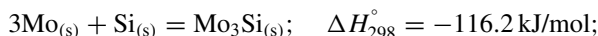


Fig. 9.3 Equilibrium state diagram of the Mo–C system



Small amounts of carbon dissolve in solid molybdenum to form a solid carbon solution of molybdenum. The formation of carbides $(\text{Fe}, \text{Mo})_3\text{C}$ and $(\text{Fe}, \text{Mo})_{23}\text{C}_6$ was established in the ternary system Mo–Fe–C; $(\text{Fe}, \text{Mo})_6\text{C}$; $(\text{Mo}, \text{Fe})_2\text{C}$.

Mo–Si system. The silicides Mo_3Si (8.86% Si), Mo_5Si_3 (14.89% Si) and MoSi_2 (36.84% Si) are known in this system (Fig. 9.4). The enthalpy of reactions of the formation of silicides from elements is characterized by the following data:



The silicide MoSi_2 exists in the α - and β -modifications, and the transformation temperature of $\alpha\text{-MoSi}_2 \leftrightarrow \beta\text{-MoSi}_2$ is equal to 1900 °C. The maximum solubility of silicon in Mo reaches 3.52% (at.) at 2053 °C.

Mo–Al system. Aluminides are known in this system. MoAl_{12} , MoAl_6 , MoAl_5 , MoAl_4 , Mo_3Al_8 , Mo_3Al .

Mo–P system. Phosphides are formed in the system Mo_3P (9.72% P), MoP_2 (39.23% P). Phosphide MoP forms a eutectic with molybdenum at 12% P ($t_{\text{eu}} = 1650$ °C).

Mo–S system. Molybdenum sulfides Mo_2S_3 , MoS_2 and MoS_3 are known (Fig. 9.5). Mo_2S_3 sulfide is not stable below 665 °C, and when heated (at normal pres-

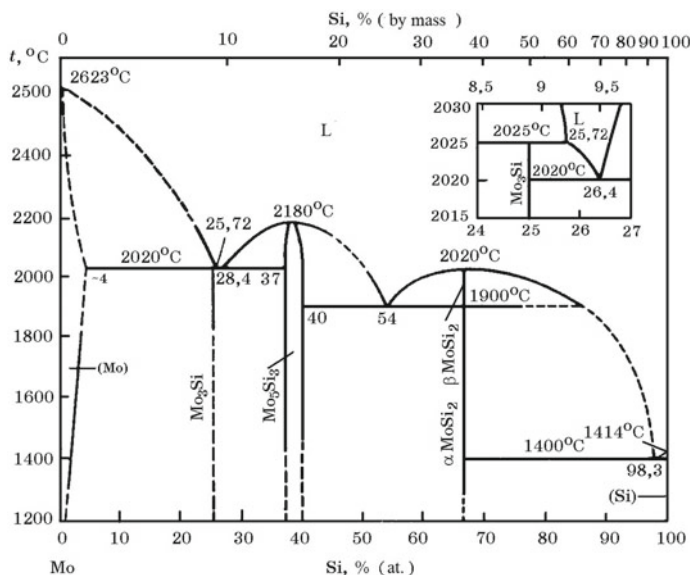
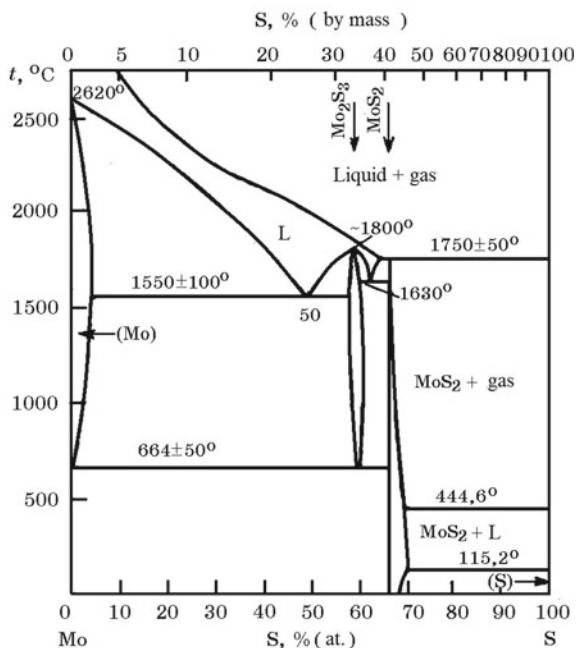
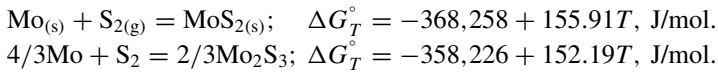


Fig. 9.4 Equilibrium state diagram of the Mo-Si system

Fig. 9.5 Equilibrium state diagram of the Mo-S system



sure), it dissociates. For sulfide formation reactions, the equations of the temperature dependence of the Gibbs energy are



9.2 Molybdenum Minerals, Ores and Concentrates

The following molybdenum minerals are known: molybdenite MoS_2 , powellite CaMoO_4 , sulfite PbMoO_4 , molybdite (ferrimolybdite) $\text{Fe}_2(\text{MoO}_4)_3 \cdot n\text{H}_2\text{O}$ ($n = 7-8$), molybdenum scheelite $\text{Ca}(\text{W}, \text{Mo})\text{O}_4$. The most common mineral is molybdenite, and the main molybdenum-containing mineral in concentrates used to produce ferromolybdenum. Molybdenite lies in quartz veins, often together with scheelite (CaWO_4), tungsten ($\text{Fe}, \text{Mn})\text{WO}_4$, cassiterite SnO_2 , chalcopyrite CuFeS_2 and other minerals, such as arsenic and bismuth. Ores are divided into simple quartz–molybdenum, copper–molybdenum and molybdenum–tungsten. Simple quartz–molybdenum ores contain from a few tenths to 1% Mo.

Skarn (polycrystalline, formed as a result of the replacement of some minerals by others) molybdenum–tungsten ores contain molybdenite together with scheelite (CaWO_4), pyrite (FeS_2) and chalcopyrite, the content of which is usually insignificant. This type of ores includes ores of the Tyrny-Auz deposit of molybdenum–tungsten ores in the North Caucasus. Molybdenum ores are concentrated mainly by flotation. When molybdenum–tungsten ores are enriched in the Tyrny-Auz deposit, molybdenite is initially isolated by flotation. A certain part of vanillite (CaMoO_4) is isomorphically associated with scheelite (CaWO_4), and molybdenum concentrates contain a certain amount of tungsten.

For the production of ferromolybdenum, molybdenite concentrates are used (Table 9.1), which are obtained after preliminary oxidative firing in order to remove sulfur.

9.3 Oxidative Firing of Molybdenum Concentrate

Unlike the ores and concentrates used in the production of most ferroalloys, molybdenite concentrates contain up to 35% S, represented mainly by molybdenum MoS_2 , sulfides of copper, iron and other elements. Therefore, the concentrate is subjected to oxidative calcination to convert molybdenum sulfide into oxygen compounds MoO_2 and MoO_3 . The sulfur oxidation of sulfide minerals occurs with atmospheric oxygen with the formation of MoO_2 by reaction

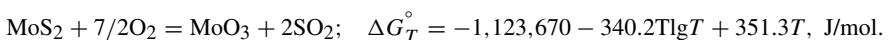
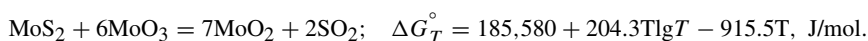


Table 9.1 Chemical composition of molybdenite concentrates, %

Grade	Mo, no less	SiO ₂	As	Sn	P	Cu	Na ₂ O	WO ₃	Sb
		No more							
KMG-B	58.0	0.3	0.04	0.01	0.01	0.01	0.8	2.0	0.01
KMG-1	56.0	0.4	0.04	0.01	0.01	0.01	0.8	4.5	0.01
KMG-2	54.0	0.7	0.07	0.01	0.02	0.02	1.0	5.0	0.01
KMF-0	52.0	4.0	0.03	0.02	0.02	0.4	–	–	–
KMF-1	51.0	5.0	0.04	0.03	0.03	0.4	–	–	–
KMF-2	48.0	7.0	0.06	0.05	0.04	0.8	–	–	–
KMF-3	47.0	9.0	0.07	0.07	0.05	1.5	–	–	–
KMF-4	45.0	12.0	0.07	0.07	0.05	2.5	–	–	–

followed by the interaction of MoO₃ with molybdenum sulfides



The oxidation of MoS₂ to MoO₃ is exothermic and is accompanied by the release of a large amount of heat; therefore, external heating is necessary only at the end of the firing process, when the amount of molybdenum sulfide in the firing product becomes small. Along with this, oxidation processes of sulfides of other metals (FeS₂, Cu₂S, ZnS, NiS, etc.), which are present as impurities in commercial molybdenum concentrates, also occur.

Firing is carried out in an oxidizing atmosphere in vertical eight-hearth furnaces (Fig. 9.6) with a diameter of 6.8 m at a maximum temperature of 680–750 °C. Higher temperatures can lead to large losses of molybdenum due to the evaporation of MoO₃. The residual sulfur content in the concentrate should not exceed 0.05–0.15%. The capacity of one kiln is 950 kg/h of calcined concentrate.

The calcined molybdenum concentrate (CMC) must have the chemical composition shown in Table 9.2. In addition to those indicated in Table 9.2 elements, the concentrate contains, %: 14–16 CaO; 0.5–3.2 FeO; 1.2–1.4 MgO; 0.6–0.8 Al₂O₃; 0.10–0.25 P; 0.5–0.15 W, as well as a small (≤0.005% of each) amount of non-ferrous metals (Sb, Bi, Zn, Cd). Part of the molybdenum (<10%) in the calcined concentrate is MoO₂, and the rest is MoO₃.

9.4 The Technology of Producing Ferromolybdenum by an Out-of-Furnace Silicoaluminothermic Method

The requirements of the standard for the composition of ferromolybdenum are given in Table 9.3.

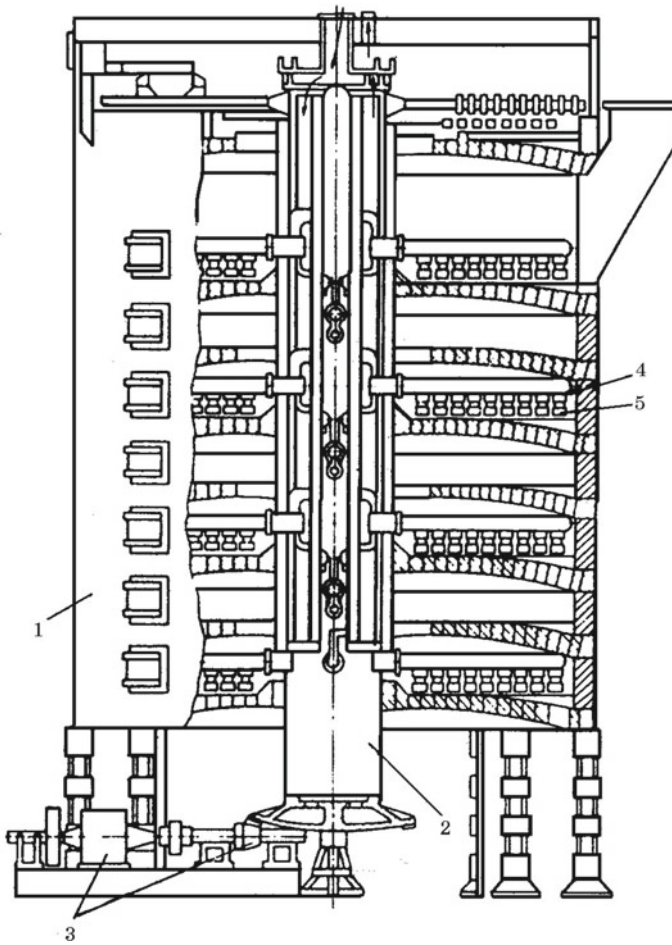


Fig. 9.6 Vertical multihearth molybdenite firing kiln. 1—Casing of the furnace; 2—vertical rotating shaft; 3—conical pair; 4—ridges; 5—blades

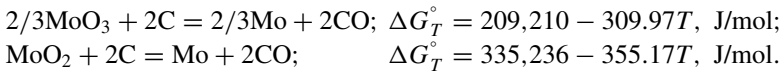
Table 9.2 Chemical composition of the calcined molybdenum concentrate (CMC), %

Grade	Mo, % no less	P	S	As	Cu	SiO ₂	Sn	C
		No more						
CMC-1	55	0.03	0.15	0.05	0.60	5.00	0.03	0.20
CMC-2	53	0.05	0.18	0.06	1.00	7.00	0.05	0.50
CMC-3	50	0.08	0.20	0.07	1.50	9.00	0.07	1.00

Table 9.3 Chemical composition of ferromolybdenum, %

Grade	Mo, no less	W	Si	C	P	S	Cu
		No more					
FeMo60(nk)	60	0.3	0.5	0.05	0.05	0.10	0.5
FeMo60	60	0.3	0.8	0.05	0.05	0.10	0.5
FeMo58(nk)	58	0.5	0.5	0.08	0.05	0.10	0.8
FeMo58	58	0.5	1.0	0.08	0.05	0.12	0.8
FeMo55	55	0.8	1.5	0.10	0.10	0.15	1.0
FeMo50	50	–	3.0	0.50	0.10	0.50	2.0
FeMo60(nk)	0.02	0.01	0.01	0.01		0.01	0.01
FeMo60	0.02	0.01	0.01	0.01		0.01	0.01
FeMo58(nk)	0.03	0.02	0.02	0.01		0.01	0.01
FeMo58	0.03	0.02	0.02	0.01		0.01	0.01
FeMo55	–	0.05	0.05	–		–	–
FeMo50	–	0.10	0.10	–		–	–

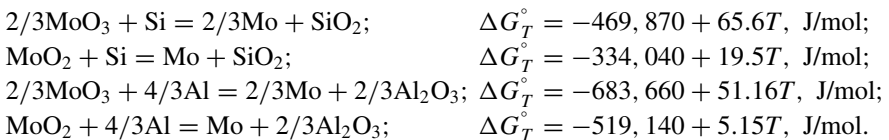
Molybdenum has a relatively small chemical affinity for oxygen. Therefore, it can be reduced with carbon at low energy costs for the reactions:



However, the reduction of molybdenum oxides by carbon is accompanied by the formation of carbides Mo_2C and MoC_{1-x}

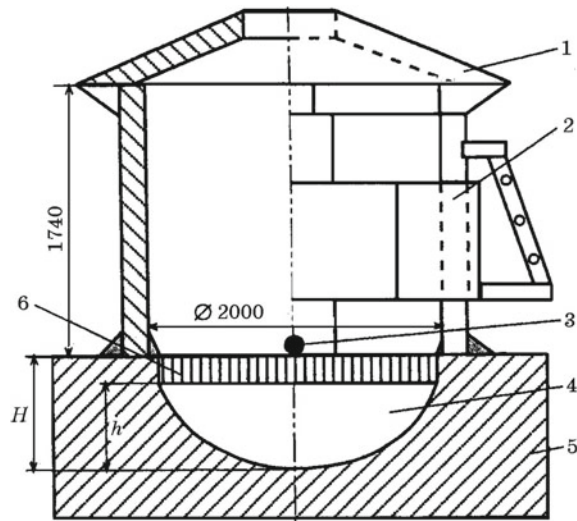


Consequently, the carbothermic reduction of molybdenum oxides will result in the production of carbon ferromolybdenum. The carbon content in ferromolybdenum is limited ($\leq 0.05\text{--}0.5\%$ C); therefore, it is obtained by the metallothermic (sili-coaluminothermic) method. The interaction of MoO_3 and MoO_2 with silicon and aluminum proceeds according to the reactions:



Ferromolybdenum is smelted by the out-of-furnace silicoaluminothermic method with an upper ignition from calcined molybdenum concentrate (50–55% Mo) with the use of ferrosilicon–aluminum (60–65% Si; 10–12% Al), aluminum grains, iron

Fig. 9.7 A melting hearth for smelting of ferromolybdenum. 1—Arch; 2—melting shaft; 3—notch hole; 4—metal ingot (block); 5—sandy bottom; 6—super block slag, H —the height of the metal receiver; h is the height of the metal layer

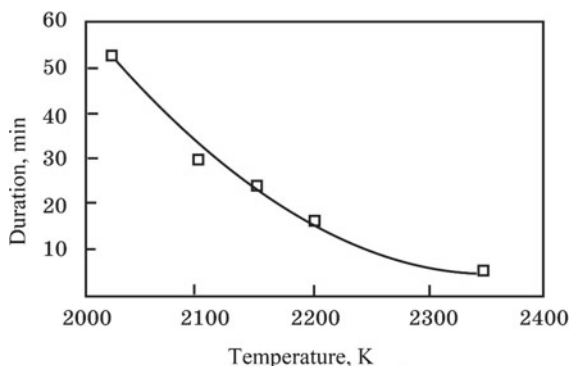


ore, steel shavings and lime. The mixture is poured into a lined shaft located on a sandy bottom with a recess for liquid metal (Fig. 9.7).

The process proceeds only due to the heat released as a result of the reduction reactions of oxides of molybdenum, iron and other elements with silicon and aluminum. After completion of the reduction reactions and holding the melt to precipitate droplets of ferromolybdenum, the slag is discharged from the shaft into the slag pot. To prevent the exit of contact slag with a high content of metallic inclusions located above the metal, a slag layer about 200 mm high remains above the ingot. After complete solidification, the ingot is removed from the sandy bottom along with super block slag, cooled with water and purified. The resulting ferromolybdenum waste is remelted together with a metallothermic mixture or in an electric arc furnace. The amount of waste increases if metallothermic smelting is carried out at a low temperature.

Out-of-furnace smelting of ferromolybdenum consists of two periods: I—self-propagating reaction, gas and flame evolution (10–20 min); II—separation of reaction products into a metal ingot and slag (30–40 min). The duration of period I is regulated by a change in the specific heat release rate of the charge (kJ/kg of charge), based on the results of previously conducted industrial melts. The heat released in the charge volume is mainly used for heating the molten metal and slag melts, which initiates the process and the propagation rate of the reaction of the interaction of the charge components. The melt temperature of the I period determines the indicators of the II period and the final result of melting, since in the II period the heat of the I period is used to compensate for the concomitant heat consumption and heat loss to the environment due to the enthalpy of the superheated melt in the I period. According to measurements made on industrial melts, the duration of the I period is determined by the temperature of the formed melt (Fig. 9.8).

Fig. 9.8 Dependence of the duration of the I period of smelting ferromolybdenum from the maximum process temperature



In some cases, low-grade molybdenum concentrates and intermediate products containing 27–40% Mo and an increased amount of impurities are used to obtain ferromolybdenum, %: 3–30 SiO₂; 1.1–1.7 Cu; 3–15 Fe₂O₃. Ferromolybdenum melts carried out using such a concentrate on a batch calculated according to the current method are characterized by a protracted interaction of the batch components, a low process temperature, a high content of molybdenum in the slag (0.8–1.5%) and a large amount of waste. In this case, slag and waste are remelted in an electric furnace. Due to the low temperature of metallothermic smelting, the absorption of carbon charge materials by ferromolybdenum increases. To increase the specific heat of the charge, part of the ferrosilicon–aluminum is replaced with aluminum grains based on the calculation: 1 kg of silicon is stoichiometrically equivalent to 1.286 kg of aluminum (when interacting with MoO₃, 1 kg of silicon releases 14,780 kJ, and 1 kg of aluminum—17,271 kJ or 17% more). Since the processing of low-grade raw materials requires a high consumption of aluminum grains, it is possible to use electric furnace melting of ferromolybdenum.

Chapter 10

Metallurgy of Ferrovandium



Vanadium was discovered in 1801 by the Mexican mineralogist A. M. del Rio. The content of vanadium in the earth's crust is 0.015%; it is a fairly common, but dispersed element in rocks and minerals.

The main consumer of vanadium is ferrous metallurgy (up to 95% of all metal produced). Vanadium is used as one of the main alloying elements in the smelting of high-speed, alloyed instrumental, cold-resistant structural, rail and other steels. When vanadium alloys up to 0.15–0.25%, the strength, toughness, fatigue resistance and wear resistance of steel sharply increase. Vanadium is both a deoxidizing and carbonitride forming element. Forming carbides, vanadium changes the structure of steel; in austenitic steels, stabilizes ferrite at high temperatures and low carbon content. Vanadium is also used for alloying cast iron. It prevents graphitization, stabilizes cementite and significantly increases the bleaching depth of cast iron, while increasing its toughness. Vanadium is used for alloying titanium, niobium and chromium alloys, which are widely used in aviation, rocket, space and other fields of technology. Heat-resistant and corrosion-resistant vanadium-based alloys are used in aerospace engineering.

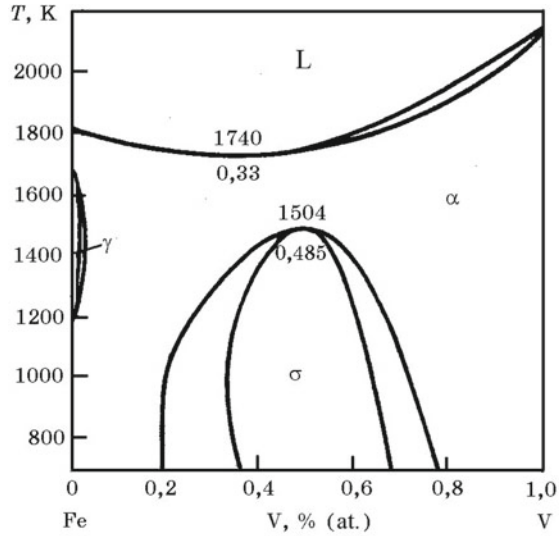
Vanadium reduces the activity of oxygen in iron, at 1600 °C the interaction parameter $e_{O(Fe)}^V = -0.14$. The minimum concentration of oxygen in iron during deoxidation with vanadium at 1600 °C is 0.0153% at 2.32% V.

Pure metallic vanadium is used in nuclear energy and in the manufacture of electronic devices.

10.1 Properties of Vanadium and Its Compounds

Vanadium—an element of the Vb group of the Periodic system of elements. Atomic number 23, atomic mass 50.941, configuration of the electron shell $3d^33p^4$, valencies 2, 3, 4 and 5, melting point 1920 °C, boiling point 3400 °C, density 6.11 g/cm³.

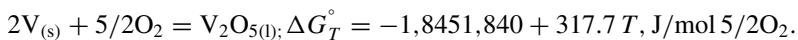
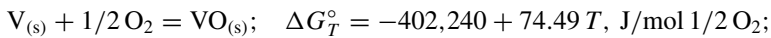
Fig. 10.1 Equilibrium state diagram of the V-Fe system



V-Fe system. Vanadium forms with iron a continuous series of solid solutions with a minimum melting point of 1740 K (Fig. 10.1). Below 1504 K, the σ -phase exists in a wide temperature range. Solutions of vanadium in iron-based melts are characterized by negative deviations from ideal behavior at 1600 °C $\gamma_{V(Fe)}^{\circ} = 0.08$.

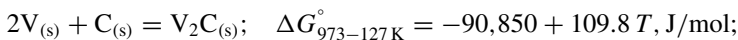
V-O system. Vanadium forms with oxygen a number of oxides, including: VO; V_2O_3 ; V_2O_5 (Fig. 10.2), the melting points of which are, respectively, equal: 1790; 1957; 680 °C. Density of oxides, g/cm³: VO—5.76; $V_2O_{3.4}$.87; V_2O_5 —3.36.

With an increase in the oxidation state of vanadium, the acidic properties of oxides and their chemical resistance are enhanced. Many vanadium oxides are characterized by rather wide areas of homogeneity (Fig. 10.2). The temperature dependence of the Gibbs energy of the reactions of the formation of VO and V_2O_5 is described by the equations:



In the V-Fe-O system, a FeV_2O_4 compound is formed with a spinel-type crystal structure, as well as a series of solid solutions with wide ranges of homogeneity.

V-C system. Vanadium with carbon forms carbides (Fig. 10.3) by reactions



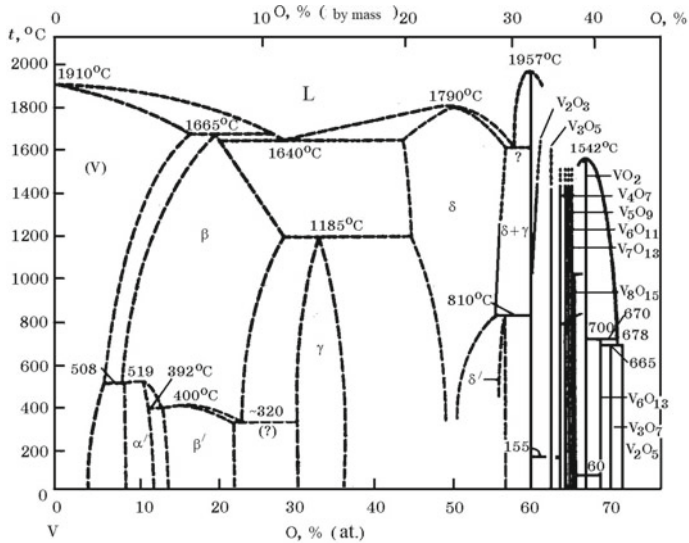


Fig. 10.2 Equilibrium state diagram of the V–O system α - V_2O_3 ; β - V_4O_7 ; γ - V_2O_3 ; δ - VO

Fig. 10.3 Equilibrium state diagram of the V–C system

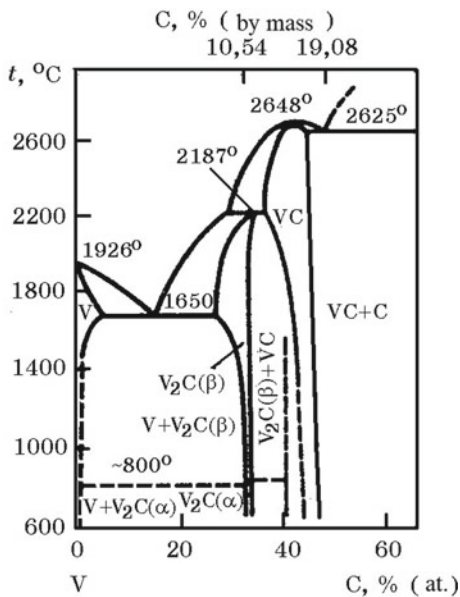
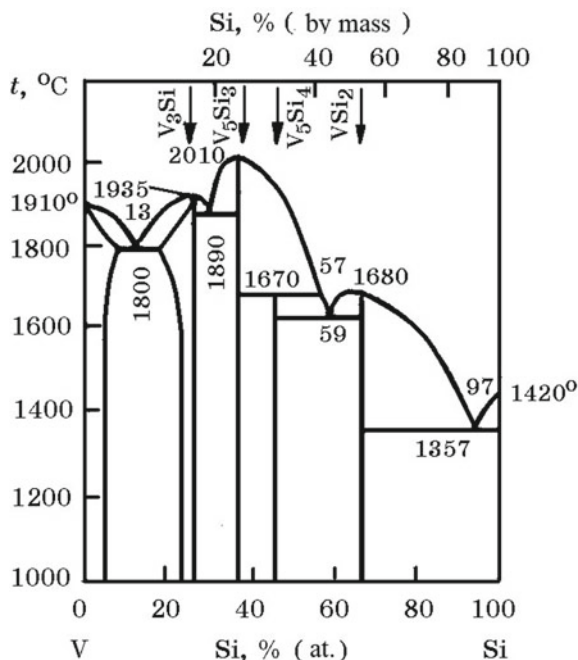


Fig. 10.4 Equilibrium state diagram of the V–Si system



V–Si system. Vanadium silicides V_3Si , V_5Si_3 , V_5Si_4 and VSi_2 are known (Fig. 10.4). The homogeneity region of VSi_2 is insignificant; the boundaries of the homogeneity region of V_3Si are in the range of 21.4 and 25% (at.) Si. The silicide formation enthalpy: (V_5Si_3) = -402 kJ/mol; (VSi_2) = -113 kJ/mol.

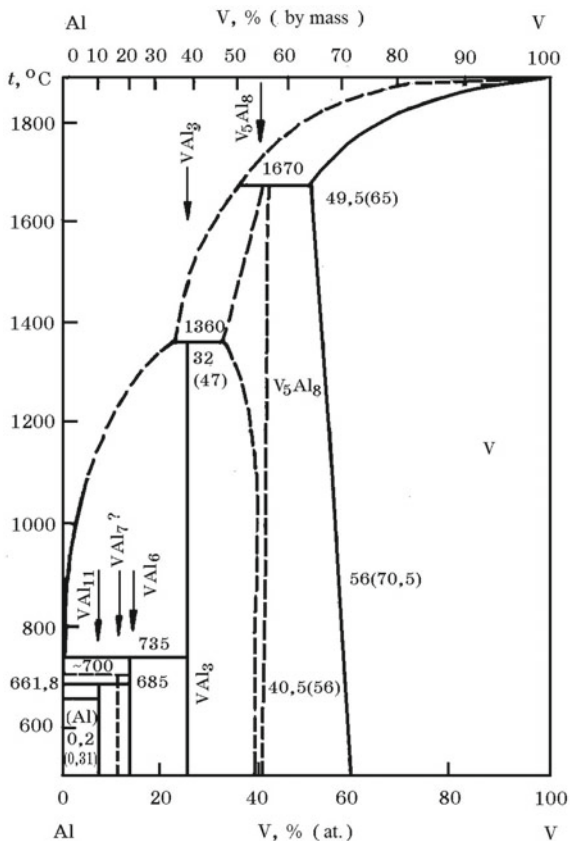
V–Al system. A series of chemical compounds of vanadium with aluminum is formed in the system (Fig. 10.5). Aluminides VAI_3 and V_5Al_8 melt incongruently at 1360 and 1670 °C, respectively.

V_2O_5 –CaO system. The system was studied in the range of 10–73% CaO (Fig. 10.6). Five invariant equilibria were established at temperatures of 615, 755, 995, 1340 and 1365 °C. The existence of three calcium vanadates was confirmed: $CaO \cdot V_2O_5$ (23.55% CaO), $2CaO \cdot V_2O_5$ (38.15% CaO) and $3CaO \cdot V_2O_5$ (48.05% CaO), melting congruently at temperatures of 715, 1015 and 1405 °C, respectively. There are three eutectic compositions in the system: E1 (25% CaO), $t_{E1} = 775$ °C; E2 (39% CaO), $t_{E2} = 995$ °C; E3 (50.5% CaO), $t_{E2} = 1340$ °C. Compound $4CaO \cdot V_2O_5$ (52.22% CaO) melts incongruently and forms peritectic at 1365 °C. The structure of $4CaO \cdot V_2O_5$ is similar to $4CaO \cdot P_2O_5$. No other compounds were detected in the V_2O_5 –CaO system up to 73% CaO.

V_2O_5 – Al_2O_3 system. In the system, the $Al_2O_3 \cdot V_2O_5$ compound is formed, which melts incongruently at 695 °C (Fig. 10.7).

V_2O_5 –FeO system. With FeO, vanadium oxide V_2O_5 forms spinels $FeO \cdot V_2O_3$ and $2FeO \cdot V_2O_3$. These compounds are refractory and play a significant role in the

Fig. 10.5 Equilibrium state diagram of the V–Al system



preparation of V₂O₅. Vanadium is present in the form of these compounds in ores and slags, although it is customary to recalculate its amount on the V₂O₅ content.

10.2 Vanadium Minerals, Ores and Concentrates

Minerals containing vanadium are of industrial importance: titanomagnetite (Fe, V, Ti)₃O₄, culsonite (Fe, V)₃O₄, roscoelite K(V, Al, Mg)₃(AlSi₃)O₁₀ · (OH)₂, carnotite K₂(UO₂)₂(VO₄) · 3H₂O. Industrial ores are classified into the following groups (subgroups in brackets): (1) vanadium ores, >3% V₂O₅ (roscoelite ores); 2) complex vanadium ores of non-ferrous and rare metals, ≥1% V₂O₅ (carnotite, vanadium bauxite); (3) ferrous metal ores, ≤1% V₂O₅ (magnetite, titanomagnetites, oolitic brown iron ore); (4) fuels and other minerals, ≤1% V₂O₅ (asphalts, bitumen, shales, coals, phosphorites).

Fig. 10.6 Equilibrium state diagram of the V_2O_5 -CaO system

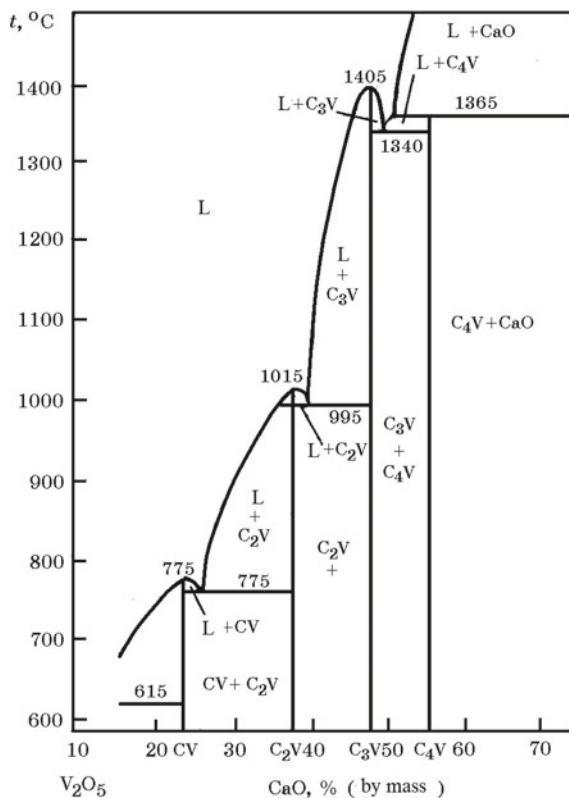
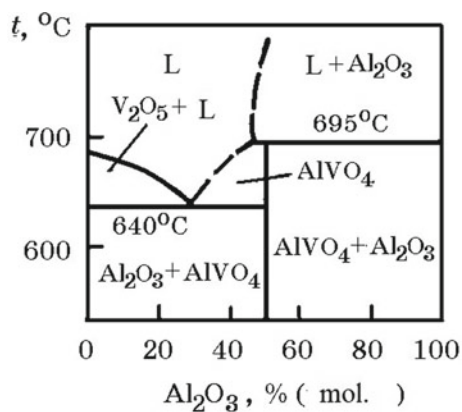


Fig. 10.7 Equilibrium state diagram of the V_2O_5 - Al_2O_3 system



In Russia, the main raw material base is the Kachkanar iron ore deposit with vanadium. Titanomagnetite ores from the Kusinsky, Pervouralskoye and other deposits are also used. Among the promising titanomagnetite deposits that are being prepared for operation, the Chineisky ore complex located in Transbaikalia in the north of the Chita Region in the Baikal-Amur Mainstream. According to explored reserves of vanadium (more than 50 million tons), this deposit is unique and has no equal in the world. Ordinary ore contains, %: 25–35 Fe; 4–7 TiO₂; 0.35–0.55 V₂O₅. Copper (0.01–0.4%), cobalt, platinum and palladium are contained in these ores as associated elements.

In Ukraine, there is a Kerch iron ore deposit containing 0.13–0.15% V₂O₅, but these ores are highly phosphorous (1.0% P) and sour (0.2% S).

10.3 Technology of Metallurgical Processing of Vanadium-Containing Concentrates

The main source of vanadium is titanomagnetite ores, the concentrates of which are obtained by enrichment (Table 10.1; Fig. 10.8) for the metallurgical processing in order to obtain V₂O₅ and ferrovanadium. The industrial technology for extracting vanadium from titanomagnetite is based on a multistage metallurgical and chemical process with the production of commercial vanadium pentoxide (V₂O₅).

Metallurgical processing. The main stages of the processing of the iron–vanadium concentrate to produce rich vanadium oxide slag and intermediate for the smelting of vanadium-containing steels are shown in Fig. 10.9. The technological scheme includes the main stages: (1) preparation of vanadium-containing ores for smelting by sintering or pelletizing; (2) blast furnace smelting; (3) cast iron devanadation; (4) chemical extraction of vanadium from slag, etc.

Blast furnace smelting of iron–vanadium concentrate has some features compared to conventional smelting of cast iron. For a more complete transition of vanadium to cast iron, the process is conducted at 1300–1350 °C and a slag basicity of 0.8–0.9. The result is cast iron containing, %: 0.45 V, 0.1–0.35 Si, 0.25 Ti. Cast iron, into which 81–83% of vanadium passes, is sent for devanadation to an oxygen converter. The resulting converter slag containing 12–24% V₂O₅ is used for chemical processing for the production of V₂O₅ oxide or directly for the smelting of vanadium alloys.

Slags contain V³⁺ in the vanadium spinel (Fe, Mn, Mg) O · (V, Fe, Al, Cr)₂O₃. Below is the chemical composition of the slag during the devanadation of molten iron in the converter by purging with oxygen from above and air with bottom purging, %:

Compound	V ₂ O ₅	SiO ₂	FeO	MnO	CaO	MgO	TiO ₂	Cr ₂ O ₃
Oxygen purge from above	14.02	22.5	44.5	5.6	1.2	–	7.0	2.0
Bottom air purge	13.51	20.4	34.3	5.5	0.7	1.1	6.4	1.6

Table 10.1 Chemical composition of vanadium-containing ores and concentrates, %

Field	Fe ₂ O ₃	FeO	V ₂ O ₅	TiO ₂	SiO ₂	Cr ₂ O ₃	Al ₂ O ₃	MnO	CaO	MgO	P	S
<i>Ores</i>												
Kusinsky	34-38	28-31	0.63-0.68	13-14	4-10	0.5-0.7	4-8	0.2-0.3	2-3	4-5	0.01-0.02	0.01
Pervouralskoye	32-36	21-23	0.50-0.60	4.0	12-16	0.1-0.2	10-12	0.2-0.3	5-7	6-8	0.01-0.02	0.06
Kerch	54.3	-	0.13-0.15	-	19.4	-	8	5	1.9	0.4	1.0	0.2
<i>Concentrates</i>												
Lisakovskoe	60.5	-	0.12	-	7.5	-	6.94	0.39	1.36	0.90	0.83	-
Ayatskoe	55.0	-	8.14	-	11.0	-	7.11	0.2	1.69	1.78	0.4	-
Pudozhgorskoe	52.0	-	1.03	15.0	6.5	-	-	0.4	-	-	0.010	-
Kachkanar	53.3	26.7	0.55	2.7	6.6	0.1	2.66	0.37	3.1	3.0	0.01	0.04

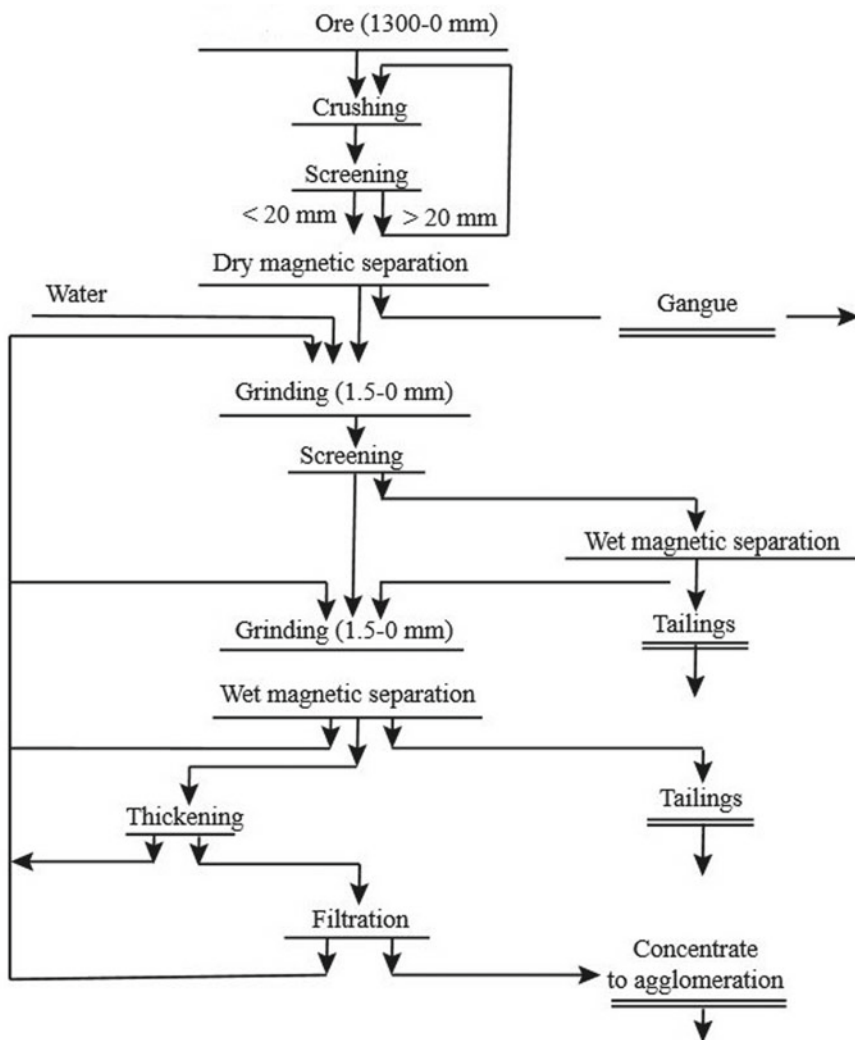


Fig. 10.8 Schematic diagram of the enrichment of Kachkanar ores

10.4 The Technology of Chemical Processing of Vanadium-Containing Slag

The slag entering the chemical processing to obtain technical vanadium pentoxide is subjected to crushing, then sent to a joint grinding with soda (NaCO_3) and subsequent firing ($1000\text{--}1100\text{ }^\circ\text{C}$) for 3 h (Fig. 10.10). The purpose of oxidative firing of the charge is the conversion of iron, vanadium and manganese oxides to higher ones and the formation of water-soluble vanadium compounds.

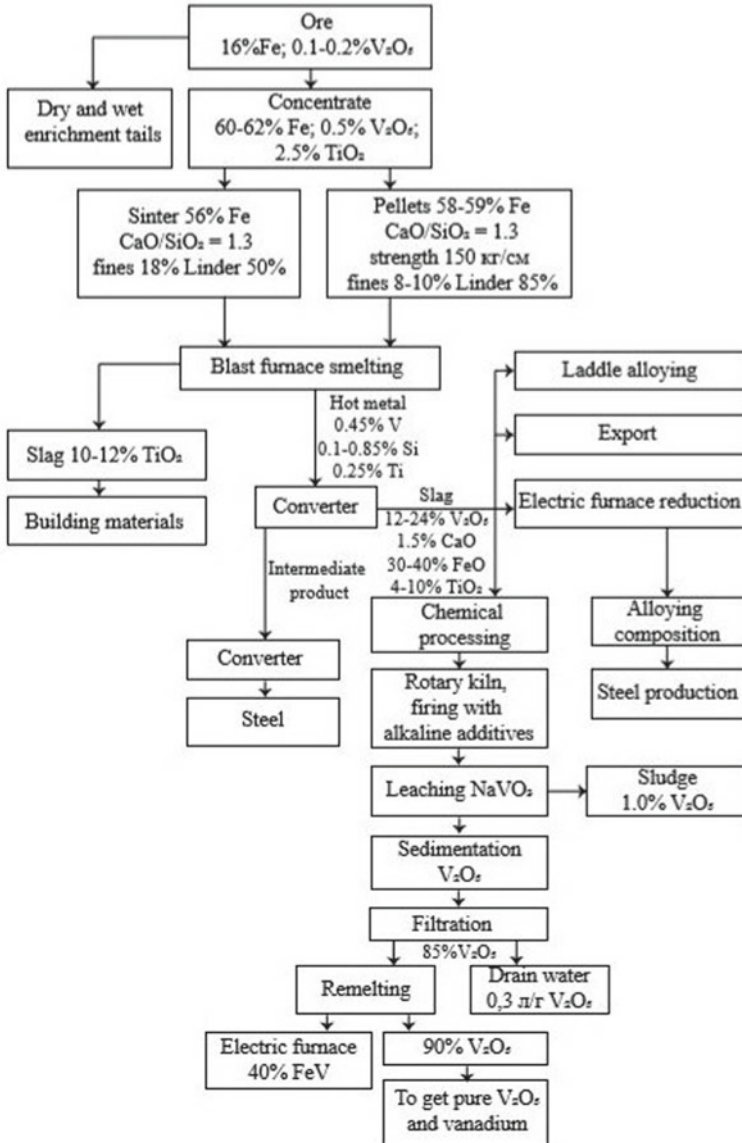


Fig. 10.9 Technological scheme of the metallurgical processing vanadium-containing titanomagnetites of the Kachkanar deposit

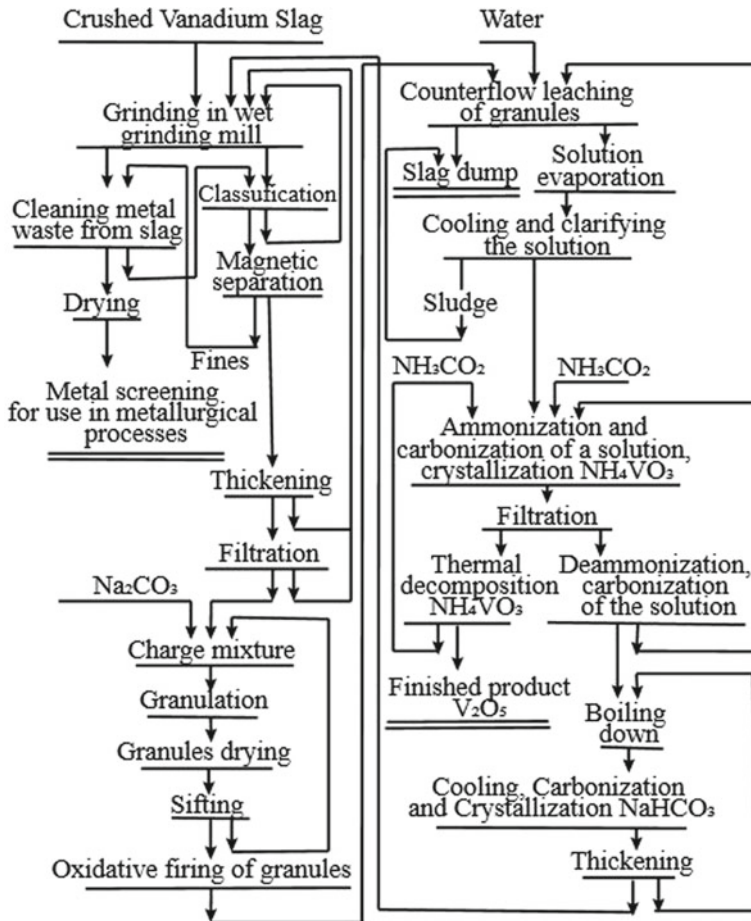
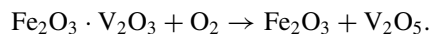
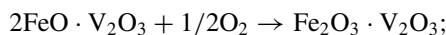


Fig. 10.10 Vanadium leaching from converter slag

The process of oxidation of slag can be represented by the reactions:

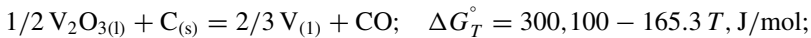
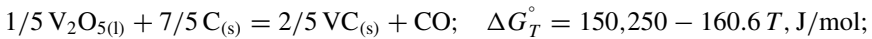
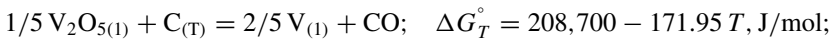


The content of sodium salts in the mixture provides vanadates that are readily soluble in water and in dilute solutions of acids and carbonates. In this case, the amount of water-soluble compounds of pentavalent vanadium increases. Leaching of vanadium compounds from the calcined charge is carried out in two stages with the deposition of V_2O_5 . Apply weakly acid leaching, acid extraction of vanadium in the layer under pressure, the process of continuous deposition of vanadium compounds.

At the stages of pulp filtration, automatic filters are installed. The technology allows the production of vanadium pentoxide with a content of 90% V_2O_5 or more and 0.010–0.015% P. Hydrated vanadium pentoxide is obtained with a particle size of 200–500 nm and is melted in a hearth furnace at 1000–1100 °C.

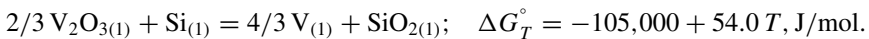
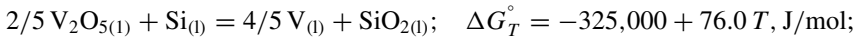
10.5 Thermodynamics of Vanadium Reduction from Oxides

The reduction of vanadium by carbon proceeds according to the reactions:

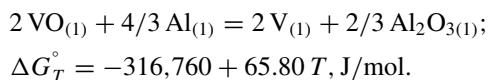
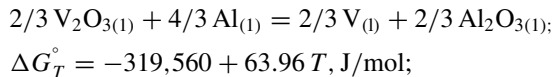
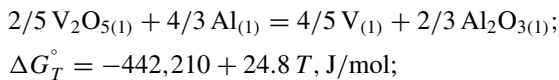


The use of carbon as a reducing agent results in a metal with a high carbon content due to the formation of VC carbide.

Reduction of vanadium by silicon occurs according to the reactions:



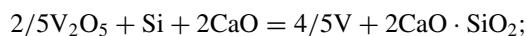
Aluminum reduces vanadium more completely than silicon, due to the high strength of Al_2O_3 :



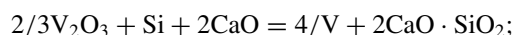
When producing ferrovanadium, it is necessary to take into account that the specific heat of V_2O_5 reduction by aluminum, equal to 119.3 kJ/mol, exceeds the necessary 87.9 kJ/mol; therefore, during aluminothermic smelting, the introduction of ballast additives is required to reduce the specific heat of the process.

10.6 The Technology of Producing Ferrovanadium by Silicoaluminothermic Method

The chemical composition of ferrovanadium is given in Table 10.2. The main amount of ferrovanadium is obtained by reduction of V_2O_5 with silicon ferrosilicon and aluminum in the presence of lime. The reduction reactions of V_2O_5 with silicon in the presence of CaO have the form:



$$\Delta G_T^\circ = -470,000 + 75.0T, \text{ J/mol};$$



$$\Delta G_T^\circ = -250,000 + 54.0T, \text{ J/mol}.$$

The technological process of smelting ferrovanadium in the electric arc furnace of the steelmaking type with a capacity of 3 MV A includes three periods. The purpose of the first period is the reduction of vanadium from the circulating (return) smelting products of the third period of the previous smelting. A furnace charge is loaded into the furnace, consisting of recycled slag, lime, ferrosilicon, aluminum, vanadium pentoxide, metal screenings and steel crops. As a result of the reduction processes, the V_2O_5 content in the slag decreases to 0.25–0.35%, the metal at the

Table 10.2 Composition of ferrovanadium, % (GOST 27130-94)

Grade	V	Si	Al	C	S	P	As	Cu	Mn	Ni
		No more								
FeV50U0.4	48–60	1.8	0.2	0.40	0.02	0.07	0.01	0.2	2.7	–
FeV50U0.5	48–60	2.0	0.3	0.50	0.02	0.07	0.01	0.2	4.0	–
FeV50U0.6	48–60	2.0	0.3	0.60	0.03	0.07	0.02	0.2	5.0	–
FeV50U0.3	>50	2.0	2.5	0.30	0.10	0.10	0.05	0.2	0.2	–
FeV50U0.75	>50	2.0	2.5	0.75	0.10	0.10	0.05	0.2	0.2	–
FeV40U0.5	35–48	2.0	0.5	0.50	0.05	0.08	0.03	0.4	2.0	–
FeV40U0.75	35–48	2.0	0.5	0.75	0.05	0.08	0.03	0.4	4.0	–
FeV40U1	35–48	2.0	0.5	1.00	0.05	0.10	0.03	0.4	6.0	–

end of the period contains 25–30% V, 20–24% Si and 0.3–0.5% C. Low vanadium slag is discharged from the furnace.

In the second period, the main operations are reduction of V_2O_5 with silicon and aluminum, production of a metal with a content of $\geq 35\%$ V and 10–12% Si, finishing and production of dump slag. Vanadium pentoxide and lime are charged into the furnace. After melting the mixture, the metal and slag are mixed to accelerate the recovery of vanadium. At this time, the metal contains 6–8% Si, and the slag contains 8–10% V_2O_5 . Ferrosilicon and aluminum are then charged, reducing vanadium from the slag. Fifteen–twenty min before the end of the second period, a metal sample is taken, which should contain 35–40% V, 9–12% Si and 0.4–0.6% C, and slag—not more than 0.35% V_2O_5 . Slag with such V_2O_5 content is discharged from the furnace.

In the third period (refining), silicon dissolved in the metal is oxidized with vanadium pentoxide and ferrovanadium of a given composition is obtained. High vanadium slag is used in the first period of the next heat. At the beginning of the third period, vanadium pentoxide and lime are loaded into the furnace. At the end of the period, the metal and slag are mixed. When ferrovanadium contains $\leq 2\%$ Si, it is discharged into a ladle lined with magnesite-coated chamotte. Slag of the third period contains 12–16% V_2O_5 ; it is released into slag pot. Ferrovanadium is poured into vertical cast iron molds. For one smelting of ferrovanadium in an electric arc furnace, 7865 kg of charge materials are consumed, including 2150 kg of vanadium pentoxide, 1010 kg of FS75 grade ferrosilicon, 105 kg of aluminum and 4100 kg of lime (Table 10.3).

A feature of the three-period technology for the production of ferrovanadium by the silicoaluminothermic method in an electric arc furnace is that the smelting is carried out according to the “ring” mode (Fig. 10.11). Fine dust formed during the smelting of ferrovanadium is captured using bag filters. Disposal of captured dust improves the performance of ferrovanadium.

Table 10.3 Consumption of charge materials, recycled slag and silicon metal by periods of smelting during the smelting of ferrovanadium, kg

Material	Melting period			Total
	1st	2nd	3rd	
Technical pentoxide	250	1000	900	2150
Lime	1100	2000	1000	4100
Steel crops	100	–	–	100
Metal screening	400	–	–	400
Recycling slag of the third period	1931,91	–	–	–
Ferrosilicon FS75	800	210	–	1010
Aluminum	50	55	–	105
Siliceous metal (recycled)	–	1417.22	1865.94	–
Total	4631.91	4682.22	3765.94	7865

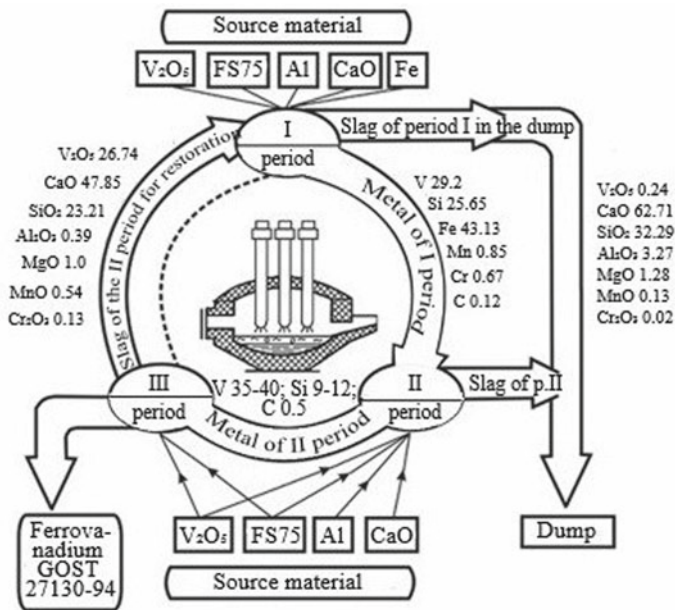


Fig. 10.11 Three-period technological scheme for obtaining a standard ferrovanadium in an electric arc furnace by silicoaluminothermic method

10.7 The Technology for Production of Ferrovanadium by the Aluminothermic Method

Aluminothermic smelting method allows to obtain ferrovanadium with a low carbon content (Table 10.4).

The mixture consists of vanadium pentoxide, aluminum powder, steel chips and lime with a reduced content of impurities. The maximum metal yield is achieved at 30–40% lime by weight of vanadium pentoxide. Results are improved with small additions of magnesium oxide. The metal contains, %: 82–84 V; 1–2 Si; ≤0.05 P; 0.1 Ti; 1.5 Mn; ≤4.5 V₂O₅. Extraction of vanadium in the alloy is 90–94%.

The vanadium content in the waste slag can be reduced by melting with preheating in an electric arc furnace. Initially, the process is conducted with an excess of aluminum in the charge in an electric arc furnace with a capacity of 350 kV A

Table 10.4 Chemical composition of ferrovanadium, % (GOST 27130-86)

Grade	V	Mn	Si	C	Cu	As	Al	P	S	Cr
		No more								
FeV75U0.1	78–80	0.4	0.8	0.10	0.1	0.05	2.0	0.05	0.05	0.5
FeV75U0.15	78–80	0.6	1.0	0.15	0.1	0.05	2.5	0.10	0.10	0.5

without power supply. After the end of the aluminothermic process, the furnace is turned on. By heating the slag, they improve the conditions for the reduction of vanadium and the deposition of metal skulls. Slag containing vanadium <1% is drained, the metal is refined from aluminum using V_2O_5 or FeO. Slag with a high V_2O_5 content is used in the mixture of the next heat. The extraction of vanadium with this method increases to 95–97% with an electric energy consumption of 4100–4500 kWh/t, aluminum consumption 1–1.2 t/t of vanadium. The metal contains >80% V and <0.15% C.

10.8 Ferrosilicovanadium Production Technology

Ferrosilicovanadium (Table 10.5) is obtained directly from converter slag in an electric furnace by a periodic process by reducing vanadium with silicon of ferrosilicon using lime and fluorspar as fluxes.

For alloying structural steels, alloys of the V–Mn–Fe system are smelted (Table 10.6). Alloys with $\leq 2.5\%$ C are obtained by the silicothermic batch method, and carbon alloys are obtained by the carbothermic method. It is advisable to use such alloys for alloying structural steels with vanadium and deoxidizing them with manganese, since the cost of 1 ton of vanadium in them is 35–40% lower than its cost in ferrovandium.

Table 10.5 Chemical composition of ferrosilicon vanadium, %

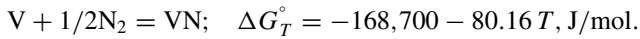
Grade	V, no less	Si	Ti	Mn	Cr	C	P	S
			No more					
FeSiV-K1	10	14	3.0	10	2.5	1.5	0.10	0.03
FeSiV-K1A	10	10–20	3.0	10	4.0	1.5	0.15	0.03
FeSiV-K2	8	20	5.0	15	4.0	3.0	0.20	0.08

Table 10.6 The chemical composition of the alloys of the V–Mn–Fe system, %

Grade	Mn	V	C	Si	P	S
			No more			
FeMnV-1	40–50	7–10	2.5	3	0.1	0.005
FeMnV-2	45–55	4.5–6.0	2.5	3	0.1	0.005
FeMnV-3	60–65	3.0–4.5	2.5	3	0.1	0.005
FeMnV-4	45–55	4.5–6.0	6.5	5	0.1	0.005
FeMnV-5	60–65	3.0–4.5	6.5	5	0.1	0.005
FeMnV-6	75–78	1.5–2.5	7.5	5	0.1	0.005

10.9 The Technology of Production of Nitrided Ferrovanadium

Vanadium at temperatures above 700 °C actively interacts with molecular nitrogen (other nitrogen-containing substances) to form VN nitride (78.5 V, 21.5% N) by reaction



The melting point VN is 2360 °C. Vanadium ferroalloys with nitrogen are used for the production of steels with nitride hardening. Vanadium-based nitrided ferroalloys can be obtained in various ways: (1) by solid-phase (900 °C) saturation of the alloy powder with nitrogen (6–8% N); (2) by purging the melt with nitrogen (3.0–4.0% N); (3) plasma nitriding (0.3–0.5% N). Ferrosilicon vanadium can also be nitrated. The addition of nitrided vanadium to a steel bath is accompanied by dissolution of nitrogen, and during crystallization of ingots and heat treatment of rolled metal, vanadium nitride is released as an independent phase VN or carbonitride V (C, N).

Chapter 11

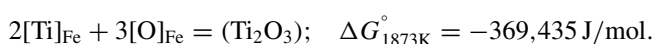
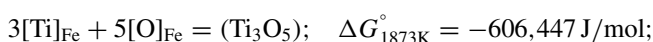
Metallurgy of Ferrotitanium



Metallic titanium was obtained only in 1910 by the American scientist M.A. Hunter. According to the content in the earth's crust, titanium takes the tenth place (0.57%); it is more than manganese, chromium, vanadium copper and some other metals.

Compared to other construction materials, titanium is characterized by high specific strength and corrosion resistance. The titanium is mainly spent on the needs of aerospace and rocket technology and marine shipbuilding. In metallurgy of high-quality steels and alloys, titanium is used for alloying, deoxidation and degassing, mainly in the form of ferrotitanium.

Titanium dissolved in iron is characterized by a high affinity for oxygen:



Titanium lowers the activity of oxygen in iron; at 1600 °C, the interaction parameter $e_{\text{O}(\text{Fe})}^{\text{Ti}} = -0.541$. The minimum concentration of oxygen in iron during deoxidation with titanium at 1600 °C is $1.065 \times 10^{-3} \%$ at 0.564% Ti.

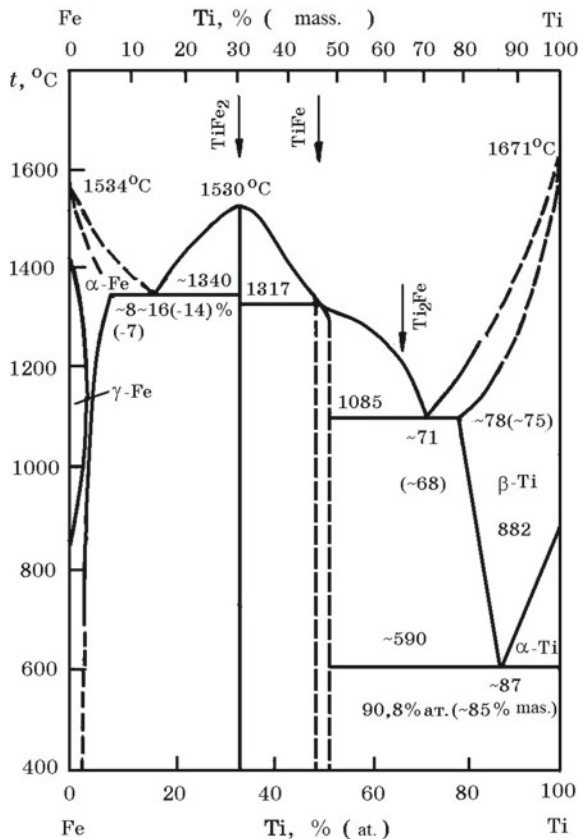
In the smelting of corrosion-resistant and heat-resistant steel, titanium is used as a stabilizer that binds carbon to strong carbides and prevents the formation of chromium carbides. Titanium reduces intergranular corrosion and improves the weldability of corrosion-resistant chromium–nickel steels. Technically, pure titanium is used for the manufacture of chemical reactors, tanks, pipelines, fittings, pumps and other products operating in aggressive environments. Titanium is used to make equipment for the food industry and reconstructive surgery due to its biological harmlessness.

11.1 Properties of Titanium and Its Compounds

Titanium—an element of the IVb group of the Periodic system of elements. The atomic number of titanium is 22, the atomic mass is 47.88, the configuration of the electron shell $3d^24s^2$, exhibits a valence of 2, 3 and 4, a density of 4.5 g/cm^3 , a melting point of titanium of $1671 \text{ }^\circ\text{C}$, and a boiling point of $3260 \text{ }^\circ\text{C}$. Titanium exists in two allotropic modifications: α -Ti with a hexagonal close-packed lattice ($a = 0.2951 \text{ nm}$, $c = 0.4697 \text{ nm}$) and β -Ti with a cubic body-centered lattice ($a = 0.3269 \text{ nm}$). The transformation temperature of α -Ti \leftrightarrow β -Ti is $883 \text{ }^\circ\text{C}$.

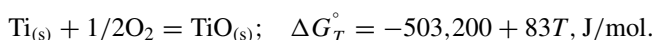
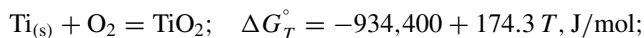
Ti-Fe system. In the liquid state, titanium and iron form a solution with unlimited solubility, while in the solid state, they form intermetallic compounds TiFe_2 and TiFe (Fig. 11.1). The TiFe_2 compound melts congruently at $1530 \text{ }^\circ\text{C}$, and TiFe melts congruently at $1317 \text{ }^\circ\text{C}$. Titanium belongs to the group of ferrite-forming elements and therefore significantly narrows the γ -region (region of the austenitic structure). Solutions of titanium in iron-based melts are characterized by significant negative deviations from ideal behavior, at $1600 \text{ }^\circ\text{C}$ $\gamma_{\text{Ti(Fe)}}^\circ = 0.00726$.

Fig. 11.1 The equilibrium state diagram of the Ti-Fe system



Ti–O system. Oxides are formed in the system: TiO_2 ; Ti_3O_5 ; Ti_2O_3 ; TiO (Fig. 11.2).

In the Ti_2O_3 – TiO_2 composition range, a number of intermediate oxides Ti_2O_5 , Ti_4O_7 , etc. are known. The formation of titanium oxides in the temperature range 1500–1940 K occurs according to the reactions:



Ti–C system. With carbon (Fig. 11.3), titanium forms a thermodynamically strong TiC carbide (density 4.4 g/cm^3) by reaction

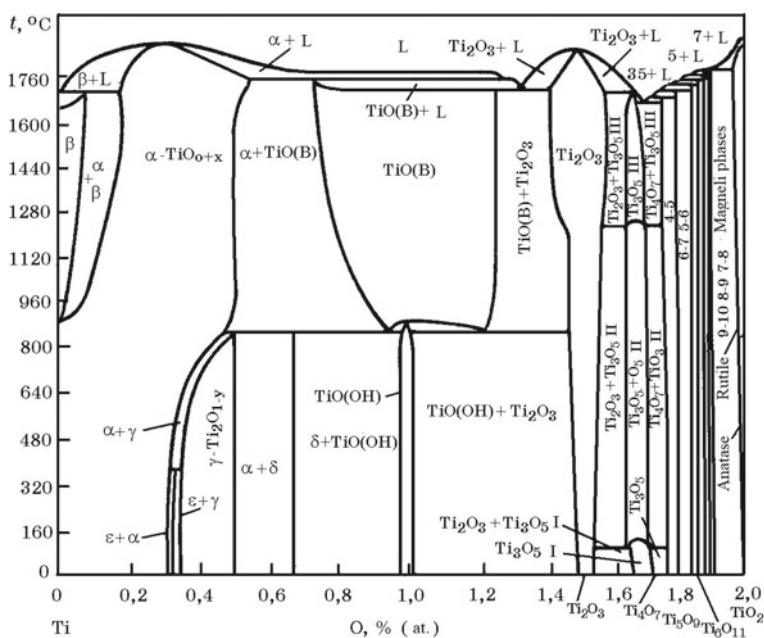
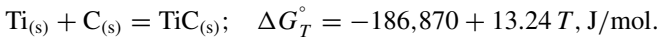
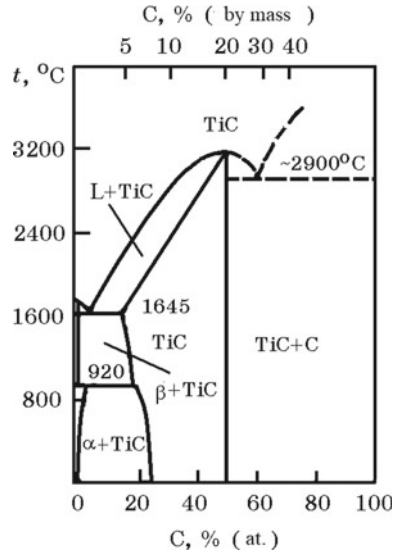


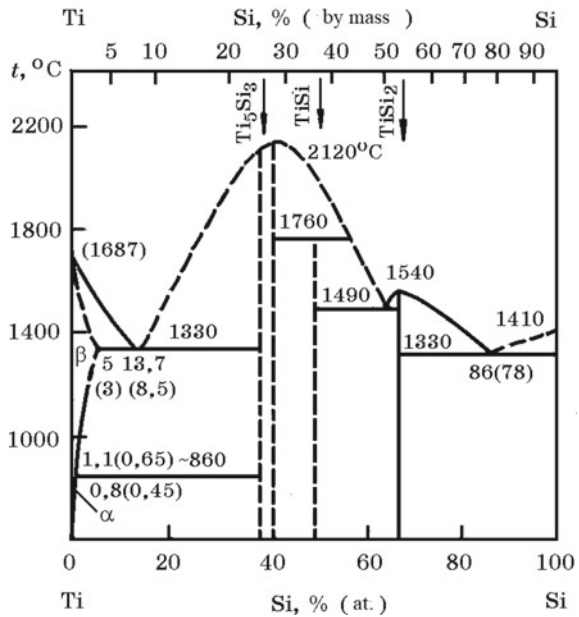
Fig. 11.2 The equilibrium state diagram of the Ti–O system. (α -TiO_x—solid solution of oxygen in titanium; ϵ —solid solution of oxygen in titanium); H , L —high- and low-temperature modifications of titanium monoxide TiO; I, II, III—phases of the magnesi; 4—Ti₄O₇; 5—Ti₅O₉; 6—Ti₆O₁₁; 7—Ti₇O₁₃; 8—Ti₈O₁₅

Fig. 11.3 The equilibrium state diagram of the Ti–C system

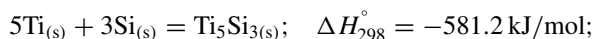


Ti–Si system. The silicides Ti_5Si_3 , TiSi , TiSi_2 are known in the system (Fig. 11.4). Silicides Ti_5Si_3 and TiSi_2 melt congruently at 2120 and 1540 °C, respectively, and

Fig. 11.4 The equilibrium state diagram of the Ti–Si system



TiSi monosilicide incongruently at 1760 °C. All silicides have high thermodynamic strength. Titanium silicides are formed by reactions:



Ti–Al system. Titanium with aluminum forms solid solutions and a number of compounds—aluminides: Ti_3Al , TiAl , TiAl_2 and TiAl_3 (Fig. 11.5). Aluminides Ti_3Al , TiAl have a wide region of homogeneity.

FeO–TiO₂ system. To optimize the technological parameters of producing ferro-titanium, data on the state diagrams of binary and complex oxide systems are important. In the FeO–TiO₂ system (Fig. 11.6), there are $2\text{FeO} \cdot \text{TiO}_2$ compounds; $\text{FeO} \cdot \text{TiO}_2$; $\text{FeO} \cdot 2\text{TiO}_2$ and four eutectics.

CaO–TiO₂ system. TiO₂ oxide has acidic properties; therefore, with the basic oxide CaO, it easily forms the corresponding compounds, the compositions of which are still being specified (Fig. 11.7). The temperature dependence of the Gibbs energy of the reaction for the formation of $\text{CaO} \cdot \text{TiO}_2$ compound has the form

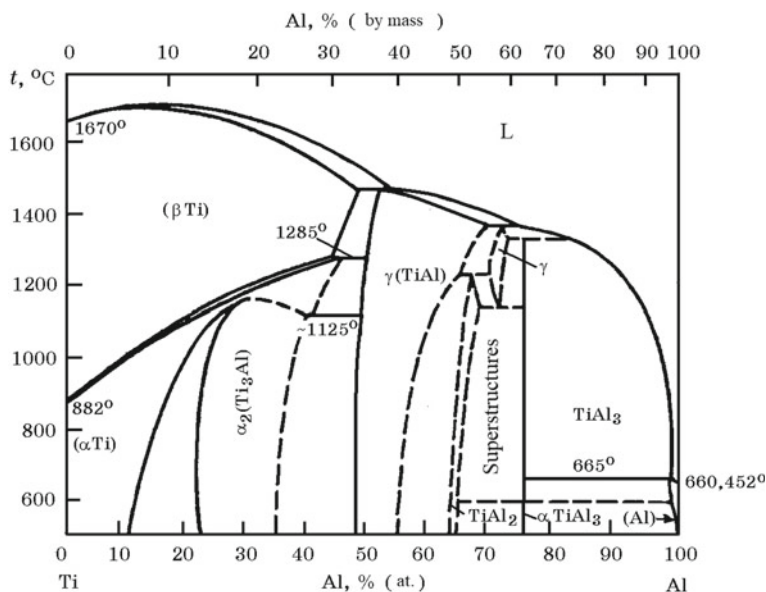


Fig. 11.5 The equilibrium state diagram of the Ti–Al system

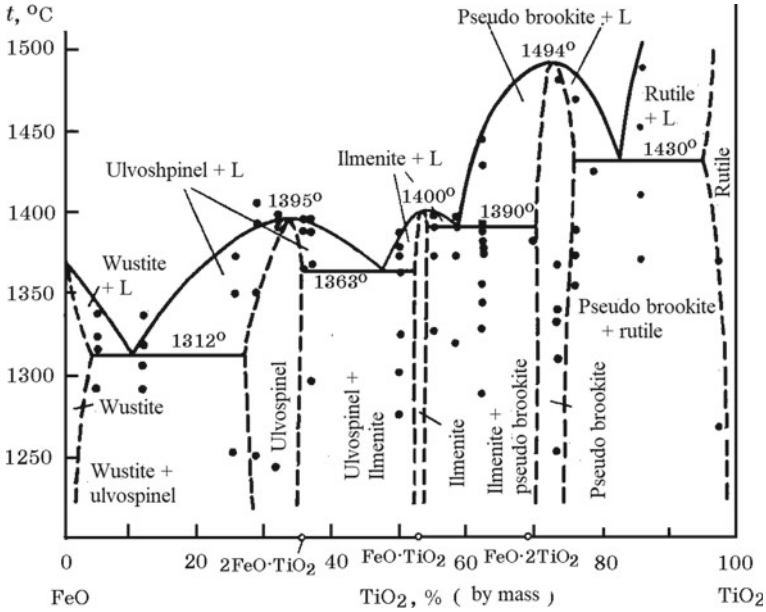


Fig. 11.6 The equilibrium state diagram of the FeO–TiO₂ system

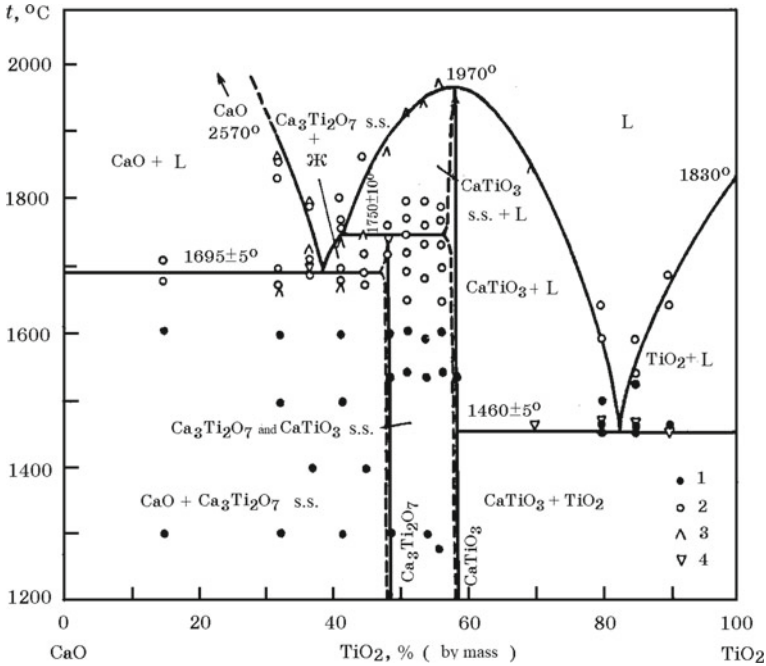


Fig. 11.7 The equilibrium state diagram of the CaO–TiO₂ system. Results obtained: 1—hardening method; 2—in a cascade furnace; 3—on fired samples; 4—thermal analysis

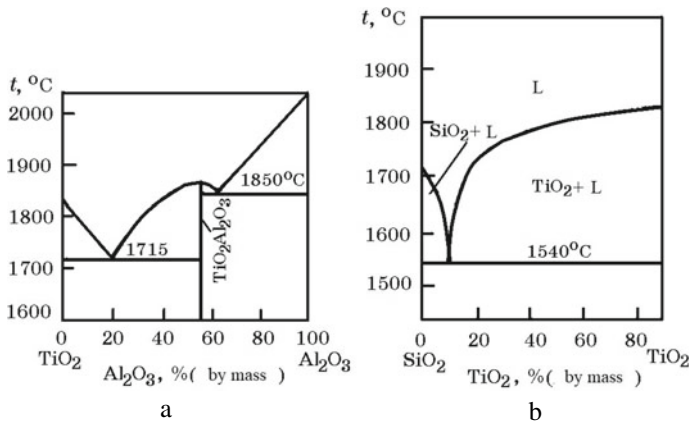


Fig. 11.8 The equilibrium state diagram of the Al₂O₃-TiO₂ (a) and SiO₂-TiO₂ (b) system

$$\Delta G_{\text{T}}^{\circ} = -71360 - 11.14T, \text{ J/mol} \quad (1527-1728 \text{ K}).$$

TiO₂-Al₂O₃ and TiO₂-SiO₂ systems. In the TiO₂-Al₂O₃ system, the only TiO₂ · Al₂O₃ compound was found (Fig. 11.8a). Two acid oxides TiO₂ and SiO₂ do not form compounds; there is a eutectic at 10% TiO₂ (Fig. 11.8b).

CaO-SiO₂-TiO₂ system. The system has compounds and eutectics (Fig. 11.9). The stability fields of individual mineral phases are outlined in bold lines; the concentration fields of sphene, perovskite, rutile and silica are highlighted.

11.2 Titanium Minerals, Ores and Concentrates

Many titanium minerals are known, which are combined into five groups: rutile (TiO₂), ilmenite (FeO · TiO₂), perovskite (CaO · TiO₂), niobotantalotitanates (pyrochlore) [(Na, Ca ...) (Nb, Ti)₂O₆(F, OH)] and sphene [CaTi(SiO₄) · (O, OH, F)]. The variety of minerals in the rutile group (anatase TiO₂, brookite TiO₂, leucoxene TiO₂ · nH₂O, nigrin (Ti, Fe)O₉, etc.) is explained by the proximity of the sizes of ionic radii $\gamma_{\text{Ti}^{4+}} = 0.064 \text{ nm}$, $\gamma_{\text{Nb}^{5+}} = 0.069 \text{ nm}$, $\gamma_{\text{Fe}^{2+}} = 0.083 \text{ nm}$, which makes possible the isomorphic substitution of titanium by other metals. The most important and most common mineral is ilmenite. It forms continuous solid solutions with geikilite MgO · TiO₂ and hematite Fe₂O₃. The main importance for metallurgy of ferrotitanium are ilmenite, titanomagnetite, and titanocirconium ores. They are subjected to enrichment by gravitational, magnetic and flotation methods. For the smelting of ferrotitanium, titanium concentrates are used (Table 11.1).

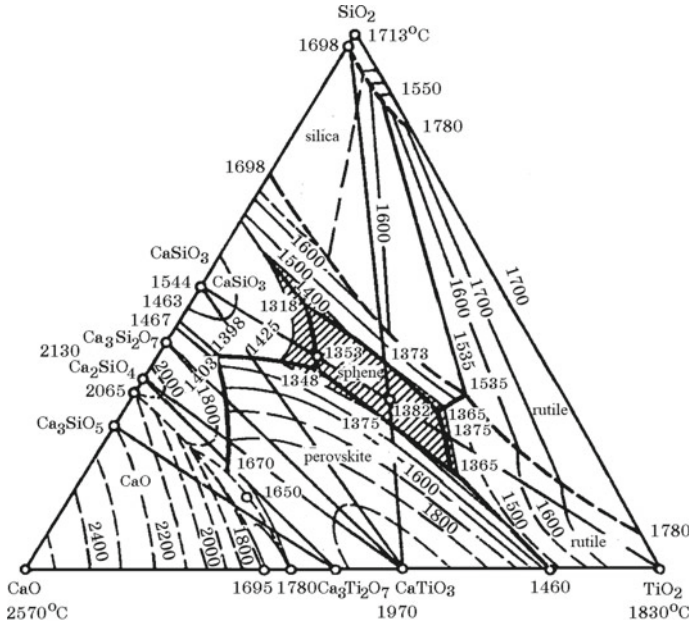


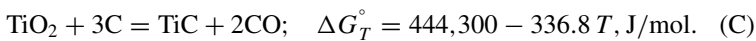
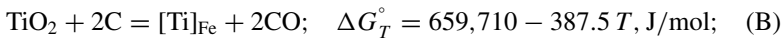
Fig. 11.9 The equilibrium state diagram of the CaO–TiO₂–SiO₂ system

Table 11.1 The chemical composition of titanium concentrates, %

Concentrate	TiO ₂	Fe ₂ O ₃	Fe	SiO ₂	Al ₂ O ₃	MgO	MnO	V ₂ O ₅	S
Ilmenite from a placer deposit	63.1	26.5	–	2.7	3.4	1.6	1.0	0.12	0.04
	52.8	–	33.5	1.33	1.50	0.61	0.54	0.24	0.05
Ilmenite from titanomagnetite	44.3	–	36.5	2.16	2.55	2.52	0.68	0.22	0.4
Iron and titanium from placers	59.8	–	20.4	2.6	6.12	0.60	0.77	0.20	–

11.3 Thermodynamics of Titanium Oxides Reduction

The reduction of titanium with carbon from ilmenite and rutile occurs with the formation of an alloy with iron with a high-carbon content by the reactions:



Total reaction (A) + (B):



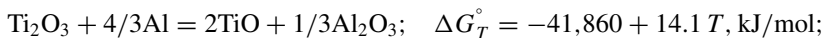
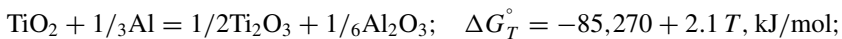
The theoretical temperatures of the onset of reactions (C) and (D) are 1320 and 1470 K, respectively. Thus, the reduction of titanium from TiO_2 is most likely to occur to titanium carbide. This is confirmed by practice, when the melting of ilmenite produces ferrocotitan with a high-carbon content: 35–40% Ti; 5–8% C; 1–3% Si (Fe and other impurities—the rest). High-carbon alloys can be used in the deoxidation and alloying of carbon steels.

Silicon has a lower chemical affinity for oxygen than titanium; therefore, TiO_2 reduction by silicon is possible only at a high content of silicon and iron in the ferroalloy. Silicon titanium reduction reaction

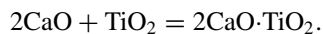
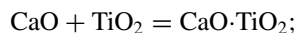


can occur when the content of iron in the charge, which dissolves titanium, and with a high concentration of silicon in the metal. Thus, the reduction of titanium from TiO_2 by silicon leads to the production of ferrosilicotitanium containing 20–25% Ti; 20–25% Si; ~1% C. Such a ferroalloy in steelmaking has limited application.

The reduction of titanium from ilmenite with aluminum occurs according to the reactions:



TiO oxide has the basic properties and is able to enter into compounds with alumina, forming $\text{TiO} \cdot \text{Al}_2\text{O}_3$, which leads to a decrease in TiO activity and complicates the reduction of titanium. To slow down the process of binding TiO with alumina, freshly calcined lime is introduced into the mixture. Calcium oxide, as a strong base, replaces TiO, forming $\text{CaO} \cdot \text{Al}_2\text{O}_3$. An excess of CaO in the mixture leads to an undesirable decrease in the activity of titanium dioxide by the reactions:



Lime has a great influence on the viscosity and fluidity of slag. Its optimal amount in the charge is ~20% of the mass of aluminum. The aluminothermic method for producing ferrotitanium is the most common. Over the past years, it has been significantly improved and is used in several versions: both in the usual secondary furnace, and with the use of electric furnaces with preheating of the charge and the use of an

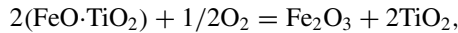
iron-thermal precipitator. Ferrotitanium slags are re-reduced in the steelmaking-type furnace to obtain a high-alumina (68–78% Al_2O_3) intermediate with 14–17% CaO , which is used as a clinker to produce high-alumina cement.

11.4 Oxidative Firing of Titanium Concentrates

Ferrotitanium is obtained from ilmenite concentrates, the chemical composition of which is given below:

Grade of concentrate	CII-1	CII	CIL-1	CIL-2	CIM
Ilmenite, no less	97	96.5	97	96.5	96.5
Titanium dioxide	50–54	60–64	57–60	57–60	52–60
Sulfur, no more	0.08	0.10	0.13	0.16	0.20
Chromium oxide, no more	0.05	0.05	0.05	0.05	0.10
Moisture, no more	1.5	1.5	1.5	1.5	6.5

For the smelting of standard ferrotitanium, sulfur in the concentrate should be $\leq 0.03\text{--}0.04\%$. The sulfur content is reduced by oxidative firing of the concentrate in rotary kilns at $600\text{--}800^\circ\text{C}$. During firing, in addition to sulfur oxidation, FeO is oxidized to Fe_2O_3 by reaction



which helps to increase the thermality of the mixture during melting and a higher recovery of titanium. Below are the compositions of the concentrate before and after firing, %:

Components	TiO_2	SiO_2	MnO	Fe_{tot}	FeO	Fe_2O_3
Before firing	49.16	0.49	2.7	36.19	40	10.7
After firing	48.55	0.48	2.65	35.95	20	28.2

11.5 The Technology of Ferrotitanium Production by Aluminothermic Method

The technology of producing ferrotitanium provides for the reduction of titanium from its oxides with aluminum. The grades of ferrotitanium are shown in Table 11.2.

The main energy parameter of the melting is the specific heat of the process—the amount of heat released, referred to 1 kg (δH) or 1 mol ($\delta H'$) of melting products

Table 11.2 The chemical composition of ferrotitanium, % (GOST 4760-91)

Grade	Ti	Al	Si	C	P	S	Cu	V	Mo	Zr	Sn
		No more									
FeTi70C05	68–75	5	0.5	0.2	0.05	0.05	0.2	0.6	0.6	0.6	0.10
FeTi70C08 ^a	68–75	4	0.8	0.3	0.03	0.03	0.3	1.8	2.0	1.5	0.15
FeTi 70C05C _n 03	65–75	5	0.5	0.3	0.03	0.03	0.3	2.5	2.5	1.0	0.30
FeTi 70C1	68–75	5	1	0.4	0.05	0.05	0.4	3.0	2.5	2.0	0.15
FeTi 35C5	28–40	8	5	0.2	0.04	0.04	2	0.4	0.2	0.2	0.04
FeTi 35C7	28–40	9	7	0.2	0.07	0.05	2	0.8	0.5	0.2	0.05
FeTi 35C8	28–40	14	8	0.2	0.07	0.07	3	1.0	1.0	0.7	0.08
FeTi 30	28–37	8	4	0.12	0.04	0.03	0.4	0.8	0.4	0.2	0.01
FeTi 20	20–30	5–25	5–30	1.0	0.08	0.03	–	–	–	–	–

^aNot more than 0.8% Mn and 0.8% Cr

(metal and slag), which provides the necessary melt temperature after the end of the process Tr. The relationship between T_m and $\delta H'$ can be described by the equation

$$\delta H'_{\text{req}} = (T_m + C)/[K(1 - q_m)],$$

where the coefficients K and C obtained by calculations for the process of smelting ferrotitanium are 32.6 and 170, respectively, and q_m —heat loss during smelting can be taken to be 0.11. The temperature T_m should be 2260 K. Then for this process

$$\delta H' = (2260 + 170)/[32.6(1 - 0.11)] = 83.6 \text{ kJ/mol.}$$

In the reduction of titanium from titanium dioxide by aluminum, the necessary heat is released as a result of the reduction of iron and titanium from their oxides present in ilmenite concentrates. It is believed that for a successful out-of-furnace process to occur, it is necessary to have the ratio $\text{Fe}_2\text{O}_3 : \text{TiO}_2 = 1$. In the Ural ilmenites, this ratio is even somewhat larger. Part of the additional heat is introduced as a result of heating the mixture to 560–720 K.

The technological scheme of the most common variant of melting ferrotitanium is shown in Fig. 11.10. Ferrotitanium is smelted in a collapsible cast iron hearth, consisting of split halves or several sections. The hearth is mounted on a trolley whose platform is lined with refractory bricks. The heated walls of the hearth are lined by spraying with an aqueous solution a mixture of ground magnesite (95%), water glass (0.7%) and refractory clay (4.3%). Lining thickness 10–15 mm. The prepared furnace on a trolley is fed into a melting chamber equipped with bunkers for a charge, screws for feeding it into a furnace, and a dust collection and ventilation unit. The process is conducted with a lower ignition, for which, before the start of smelting, ~200 kg of charge is poured onto the hearth, and an ignition mixture (nitrate and magnesium chips) is placed on top of it. The ignition mixture is ignited with a

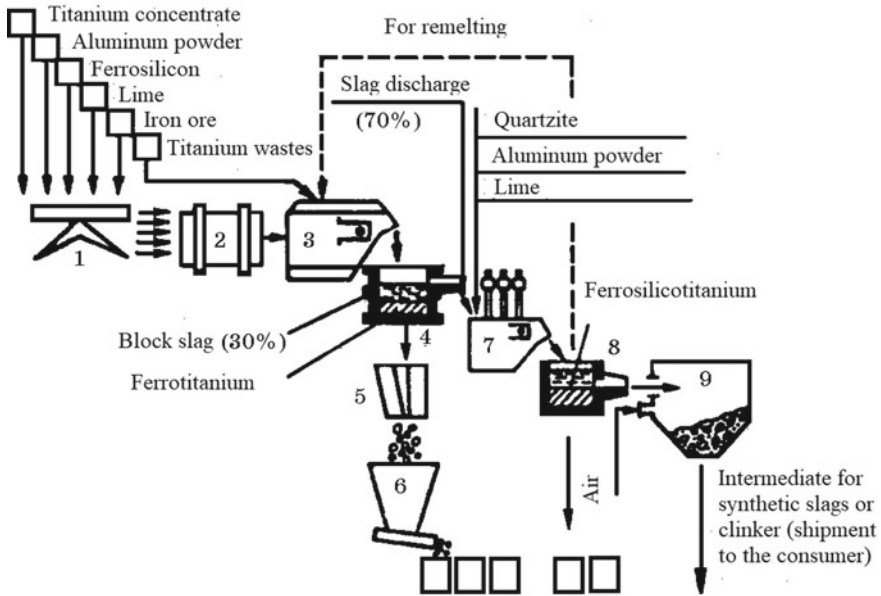


Fig. 11.10 Technological scheme for the production of ferrotitanium with the reduction of slag and the production of intermediate or clinker of high-alumina cement. 1—scales; 2—mixer; 3—melting furnace for smelting ferrotitanium; 4—mold for metal and slag; 5—crusher; 6—packaging machine; 7—electric furnace for recovery; 8—storage; 9—installation for dry granulation

special electric igniter or magnesium shavings. As soon as the exothermic processes become intense, the prepared mixture from the bunkers is fed into the furnace using a screw in small portions.

Melting is usually carried out with a charge of the charge, designed to receive an ingot with a mass of 3–4.5 tons. The melting time at 4.2 tons of concentrate is 15–18 min. The charge of charge materials per 1 ton of ferrotitanium is, kg: 940 ilmenite concentrate; 400 aluminum powder; 100 lime; 24 ferrosilicon FS75; 130 iron ore; 9 titanium waste (Table 11.3).

The phase composition of ferrotitanium depends on the content of titanium and impurities. The microstructure of a 70% alloy is represented by eutectic, and other

Table 11.3 The approximate composition of the mixture for smelting ferrotitanium, kg

Charge components	Ilmenite concentrate	Iron ore	Aluminum powder	Ferrosilicon	Lime	Salt
Ignition mixture	–	100	30–38	12–20	15–25	–
The main part of the charge	100	15–30	46–60	0–6	8–12	0–2
Iron-termite reducing agent	–	100	35–40	–	10–25	–

alloy grades are represented by iron titanides TiFe_2 , TiFe (Fig. 11.1). The excess phases in ferrotitanium are TiN nitride, AlTi aluminide, TiS sulfide. Oxide inclusions are mainly represented by corundum ($\alpha\text{-Al}_2\text{O}_3$), β -alumina mixed with TiO_2 and Cr_2O_3 , mullite $3\text{Al}_2\text{O}_3 \cdot 2\text{SiO}_2$, gehlenite $2\text{CaO} \cdot \text{Al}_2\text{O}_3 \cdot \text{SiO}_2$, and sphene $[\text{CaTi}(\text{SiO}_4)(\text{O}, \text{OH}, \text{F})]$ and ilmenite $\text{FeO} \cdot \text{TiO}_2$.

In the case of smelting with an upper ignition, the entire prepared, dosed and mixed batch is loaded into the melting furnace and, using the ignition mixture, is ignited from above; the melting process goes from top to bottom. After melting, the volume of liquid products in the hearth takes about 1/3 of the hearth. The used volume of the hearth is three times less than in the case with the lower igniter, when the charge gradually melts and the melting products can fill the entire volume of the hearth. Insufficient use of the volume of the hearth reduces labor productivity, a larger workshop is required, metal losses increase when it is cleaned of slag and lining. At the same time, smelting with an upper ignition is simpler, since it is enough to fill the hearth by charge using a bucket and the process can already be carried out. When working with the upper ignition, a high melting speed is achieved, which is due to the heating of the lower layers of the mixture with the dropping liquid melting products. The removal of the charge from the hearth during the smelting process is less than with the lower ignition. The disadvantage of working with the upper ignition is the impossibility of regulating the rate of penetration of the charge, which sometimes leads to a very rapid process, accompanied by emissions. The lower ignition method is more efficient; therefore, it is used in most out-of-furnace processes. Higher technical and economic indicators for the smelting of ferrotitanium are possible as a result of electric heating of the slag. A significant effect is achieved during out-of-furnace melting with the release of metal and slag. This makes it possible to conduct smelting in a heated furnace with its repeated use.

A valuable raw material for producing ferrotitanium is a concentrate containing perovskite ($\text{CaO} \cdot \text{TiO}_2$). In this case, ~25% of ilmenite concentrate is replaced with perovskite concentrate, iron ore is introduced into the charge and lime is excluded. Since the heat of exothermic reactions of aluminum oxide reduction is insufficient, the perovskite concentrate is heated to 600–700 °C before melting so that the temperature of the charge reaches ~300 °C. Extraction of titanium in this process is 75–80%.

The smelting of ferrotitanium by an out-of-furnace aluminothermic method is possible due to the heat released during the reduction of titanium oxides, which is supplemented by the heat of chemical reactions of reduction of iron from Fe_2O_3 and FeO , which is sufficient for the process to proceed. However, the consumption of aluminum for the reduction of thermodynamically unstable iron oxides is not justified due to its high cost; therefore, one of the effective methods for producing alloys with titanium is electric furnace with preliminary melting of the oxide part of the charge under the influence of heat generated by electric energy. The technological scheme of smelting ferrotitanium with its reduction from liquid slag is shown in Fig. 11.11.

High-alumina cement of the following composition is obtained from pre-reduced slag, %: 68–71 Al_2O_3 ; 14–17 CaO ; 1–2 ($\text{SiO}_2 + \text{FeO}$), refractoriness 1670–1710

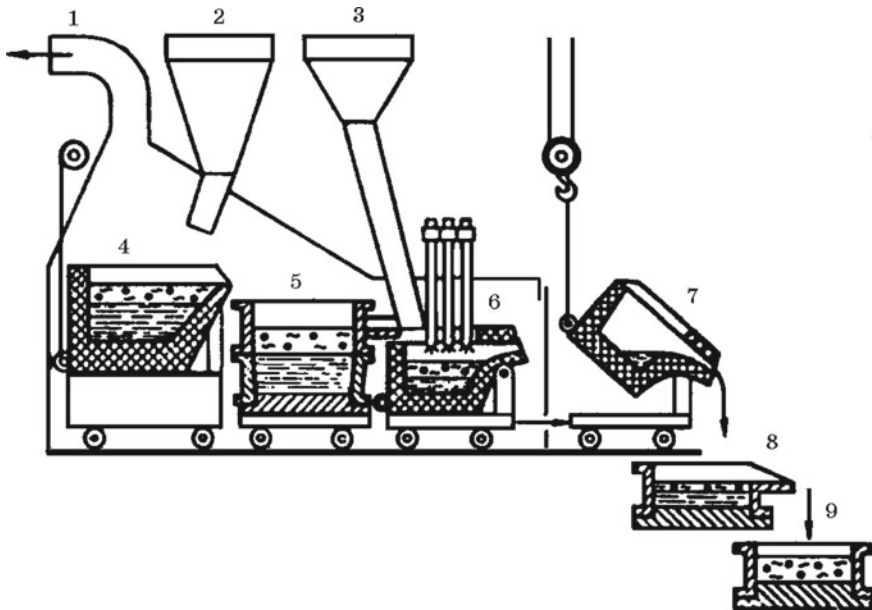


Fig. 11.11 Technological scheme for the re-reduction of liquid slag of ferrotitanium. 1—gas cleaning pipe; 2—charge hopper for smelting ferrotitanium; 3—charge hopper for slag recovery; 4—hearth for smelting ferrotitanium; 5—mold for metal and slag; 6—electric furnace for slag recovery; 7—roll-out bathtub of an electric furnace; 8—storage; 9—slag

°C. Cement corresponds to grades 400–700. The solid slag of ferrotitanium can be reduced in a small-capacity steelmaking electric furnace with a bath lined with carbon material.

11.6 The Technology of Producing Metallic Titanium with Magnesium-Thermic Reduction

High-purity titanium, used as a structural material, is obtained according to a complex multistage scheme for processing titanium concentrates. Initially, the concentrate is subjected to electric melting in ore-smelting furnaces with a unit capacity of 10–15 MV A (Fig. 11.12) to obtain fine high-titanium slag. A small amount of coke breeze set with the charge ensures the reduction of iron oxides from ilmenite melt; therefore, the content of titanium oxides in the slag in terms of TiO_2 reaches 82–84%, and the FeO content decreases to 3–4%. The slag at the outlet has a temperature of 1700 °C. In the second stage, the titanium slag is chlorinated with gaseous chlorine in the presence of carbon to obtain titanium tetrachloride $TiCl_4$. Titanium tetrachloride

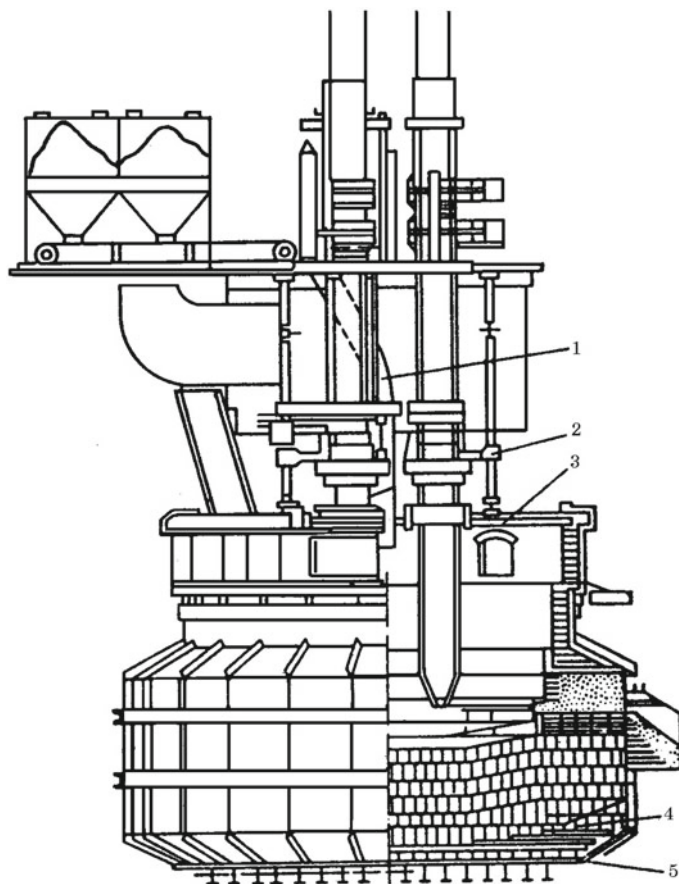
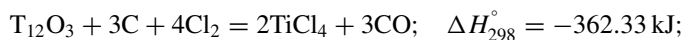
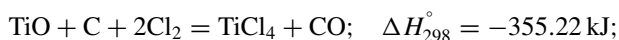
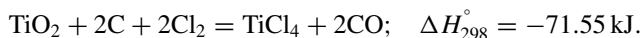


Fig. 11.12 The design of the furnace for smelting titanium slag. 1—tube for feeding the mixture; 2—electric supply system; 3—water-cooled arch; 4—magnesite lining; 5—furnace casing

TiCl_4 is a colorless, transparent liquid that fumes in air. Melting point of TiCl_4 minus $24.1\text{ }^\circ\text{C}$, boiling point $136.3\text{ }^\circ\text{C}$, density 1.73 g/cm^3 , heat of formation $\Delta H_{\text{form}}^\circ = -804\text{ kJ/mol}$.

The slag powder is briquetted with a carbon reducing agent before chlorination. Chlorination of briquettes is carried out in special reactors—chlorinators, which are a shaft resistance electric furnace. Carbon in the composition of briquettes reduces titanium and ensures the occurrence of chlorination reactions at lower temperatures, which makes these reactions thermodynamically irreversible:





Along with the reduction and chlorination of titanium, chlorine reacts with other oxides, which leads to the formation of chlorides SiCl_4 , FeCl_2 , AlCl_3 , etc. According to the Gibbs energy of the chlorination reactions, the slag-forming oxides are arranged in the series: FeO , K_2O , Na_2O , Y_2O_3 , CaO , MnO , MgO , TiO_2 , Fe_2O_3 , SiO_2 , Cr_2O_3 and Al_2O_3 . The oxides up to TiO_2 are completely chlorinated, Al_2O_3 , SiO_2 , Cr_2O_3 to a lesser extent.

A distinctive feature of chlorides is their lower melting and boiling points than oxides. A sharp difference in the physical properties of chlorides allows us to separate them by conventional thermal distillation followed by fractional condensation.

Metallic titanium (sponge) is produced by a metallothermic process, reducing titanium from TiCl_4 with magnesium by an exothermic reaction



For standard conditions $\Delta H_{298}^\circ = -446.1 \text{ kJ}$ and $\Delta G_{298}^\circ = -478 \text{ kJ/mol}$. The process is carried out in an inert gas atmosphere. The technological scheme of the process of obtaining a titanium sponge is shown in Fig. 11.13.

The reaction mass obtained at the stage of TiCl_4 reduction with magnesium in an electric furnace (Fig. 11.14) at 930–950 °C, after cooling, is sponge titanium, the pores of which are filled with magnesium and MgCl_2 . Its composition is 60% Ti, 20–30% Mg and 10–20% MgCl_2 .

Sponge titanium can be purified from Mg and MgCl_2 by vacuum-thermal and hydrometallurgical methods. The appropriateness of applying the first or second method is determined by several factors. Vacuum-thermal cleaning of sponge titanium from impurities is based on a significant difference in the volatility of magnesium, magnesium chloride and metallic titanium. Refining processes are accompanied by energy consumption and require constant heat supply. The titanium sponge is processed into compact titanium by smelting ingots in vacuum arc furnaces.

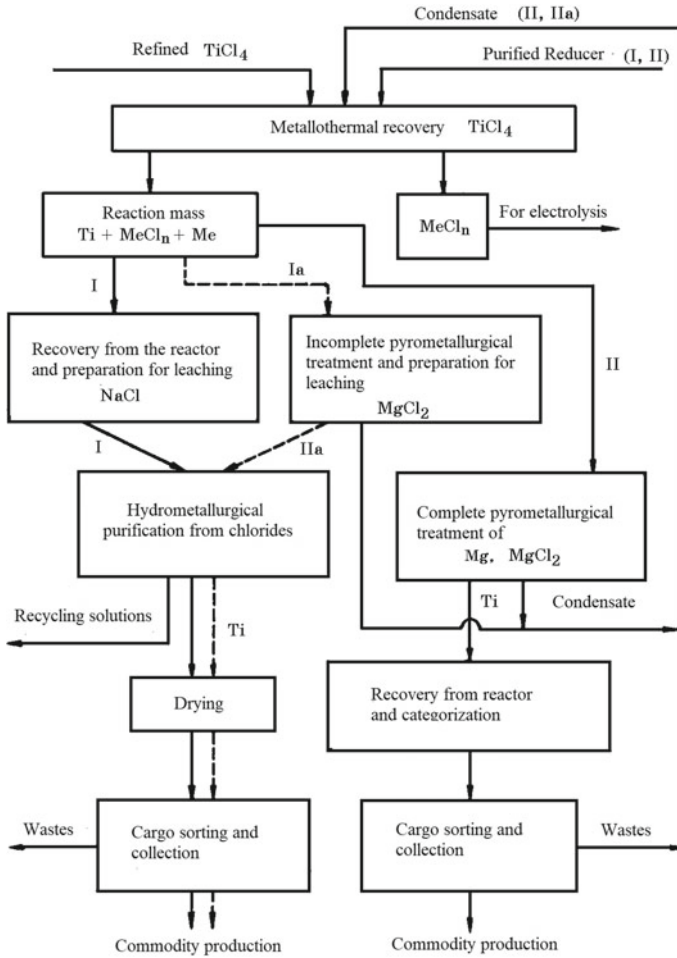


Fig. 11.13 Schematic diagram of metallothermic titanium production based on titanium tetrachloride

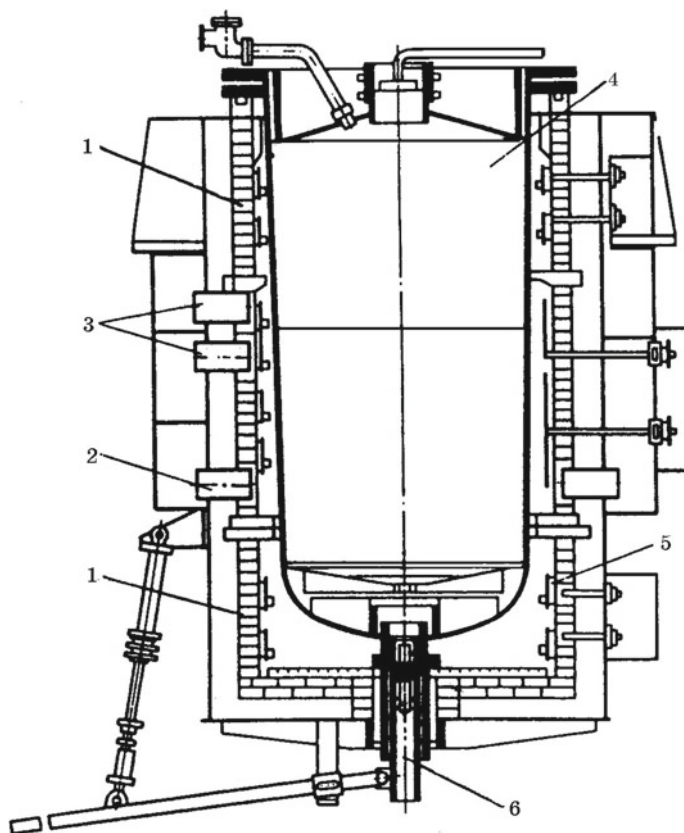


Fig. 11.14 Titanium tetrachloride reduction scheme. 1—electric furnace; 2—channel for the removal of hot air; 3—tuyere for supplying cold air; 4—recovery apparatus; 5—heaters; 6—drain pipe

Chapter 12

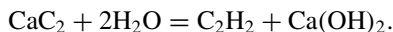
Alkaline Earth Metal Ferroalloys



Alkaline earth metals (AEM): beryllium, magnesium, calcium, strontium and barium belong to the IIA group of the Periodic system of elements. The peculiarity of the configuration of the outer electron shell of Be ($2s^2$), Mg ($3s^2$), Ca ($4s^2$), Sr ($5s^2$) and Ba ($6s^2$) atoms determines their high chemical affinity for oxygen and very low solubility in iron. At 1600 °C, it dissolves in liquid iron, at. %: 2.2 Mg; 0.078 Ca; 0.018 Sr and 0.00012 Ba. Due to the high vapor pressure, the use of these metals in pure form in steelmaking and foundry is difficult. In addition, pure AEM have a high cost and are scarce. At the same time, the growing demand for metallurgy in the AEM necessitates their production in the form of alloys. Since AEM practically do not interact with iron, but form thermodynamically strong silicides, this problem is solved by smelting siliceous ferroalloys with AEM. The largest in volume is the production of silicocalcium; silicon ferroalloys containing other alkali metal alloys are smelted in a smaller volume.

12.1 Calcium Carbide and Silicocalcium

Metallic calcium was obtained in 1808 by the English chemist G. Davy. The calcium content in the earth's crust is 2.96%. The use of calcium, first of all, is based on its high activity to oxygen and halogens; it is used as a reducing agent for the production of chromium, uranium, thorium from their oxides, for the deoxidation and degassing of steels, cast irons, bronzes, etc. Calcium is widely used in alloys with lead for cable sheaths. An alloy of calcium with silicon (silicocalcium) is used as a deoxidizer and desulfurizer in the production of steel. The alloy of calcium with carbon–calcium carbide (CaC_2) is widely used in the chemical industry and in organic synthesis in the production of synthetic rubber and calcium cyanamide (CaCN_2). Processing calcium carbide with water, acetylene (C_2H_2) is obtained by the reaction



12.1.1 Properties of Calcium and Its Compounds

The atomic number of calcium is 20, the atomic mass is 40.08, the density is 1.54 g/cm³, the melting point is 839 °C and the boiling point is 1495 °C. In compounds, calcium is divalent and chemically very active. Calcium is allotropic metal: up to 443 °C, α -Ca modification with a face-centered cubic lattice ($a = 0.558$ nm) is stable; in the range of 443–842 °C, β -Ca with a volume-centered cubic lattice ($a = 0.448$ nm) is stable.

Ca–O system. The oxides CaO, CaO₂ (peroxide), CaO₄ (hyperoxide), CaO₆ (ozonide) are known in the system (Fig. 12.1). The most stable is CaO, melting point 2613 °C, boiling point above 3000 °C, density 3.37 g/cm³. Types of phase transformations, temperatures and compositions are given in Table 12.1.

The temperature dependences of the Gibbs energy of the reactions of CaO formation considering the aggregate state of calcium have the form:

$$2\text{Ca}_s + \text{O}_2 = 2\text{CaO}_s; \quad \Delta G_{298-1124\text{K}}^\circ = -126,8600 + 198T, \text{ J/mol}; \quad (\text{A})$$

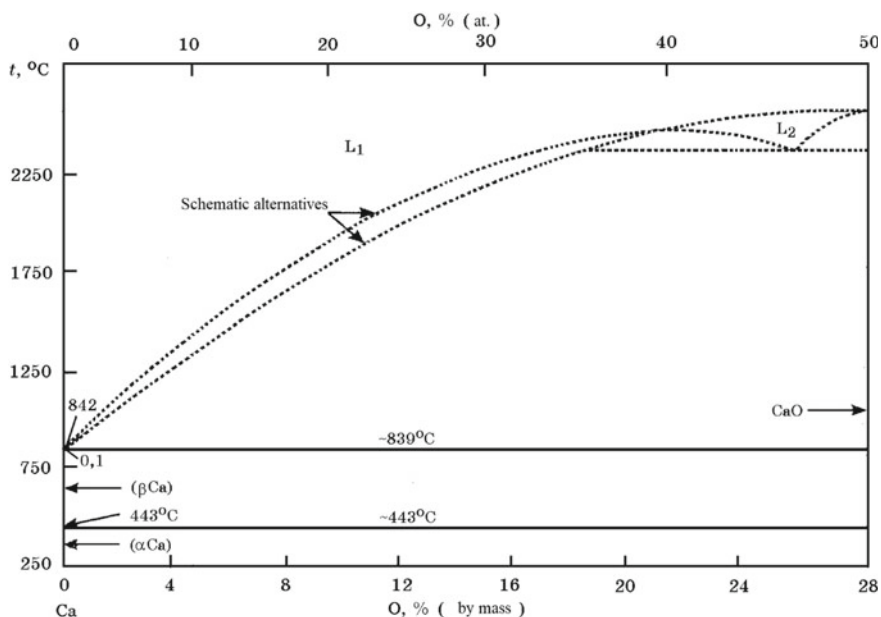
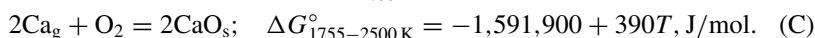
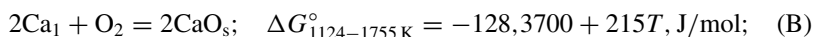


Fig. 12.1 Diagram of the equilibrium state of the Ca–O system (assumed position of the liquidus line at $P = 0.1$ MPa)

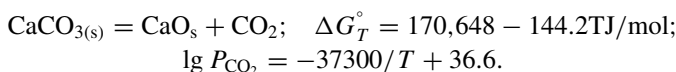
Table 12.1 Phase transformations in the Ca–O system (condensed state)

Transformation	Temperature, °C	Type of transformation
$L \rightarrow (\beta\text{-Ca}) + \text{CaO}$	~839	Eutectic
$(\beta\text{-Ca}) \rightarrow (\alpha\text{-Ca})$	~443	Eutectoid
$(\beta\text{-Ca}) \rightarrow (\alpha\text{-Ca})$	443±3	Allotropic
$L \rightarrow (\beta\text{-Ca})$	842±3	Melting
$L \rightarrow \text{CaO}$	2613±25	Melting



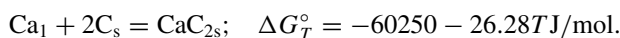
The temperature of the onset of thermal dissociation of CaO (condition $\Delta G_T^\circ = 0$, $P_{\text{O}_2} = 101 \text{ kPa}$) by reaction (A) is 6400 K, by reaction (B) 5970 K.

CaO oxide is the main component of lime, which is obtained at the plants by calcining limestone (CaCO_3). The chemistry of the thermal dissociation of CaCO_3 is described by the reaction



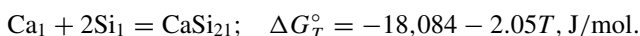
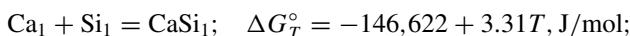
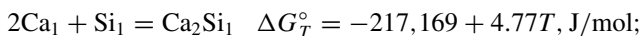
Pressure $P_{\text{CO}_2} = 101.3 \text{ kPa}$ is reached at 1183 K.

Ca–C system. When Ca interacts with carbon, calcium carbide CaC_2 is formed (62.54% Ca; 37.46% C)



The melting point of CaC_2 is 2430 K; the density is 2.204 g/cm^3 . Thermodynamic constants of calcium carbide: $\Delta H_{\text{orp}}^\circ = -58.49 \text{ kJ/mol}$, $S_{298}^\circ = 69.8 \text{ J/(mol K)}$, $C_p^\circ = 62.6 \text{ kJ/(mol K)}$, $\Delta G_{298}^\circ = -64.8 \text{ kJ/mol}$.

Ca–Si system. Calcium with silicon forms silicides: Ca_2Si ; Ca_5Si_3 ; CaSi ; Ca_3Si_4 ; CaSi_2 (Fig. 12.2). Temperature dependences of Gibbs energy of calcium silicide formation reactions are described by the following equations:



CaO–SiO₂ system. As follows from the state diagram (Fig. 12.3), during the interaction of CaO with SiO_2 , a series of silicates $3\text{CaO} \cdot \text{SiO}_2$, $2\text{CaO} \cdot \text{SiO}_2$, $3\text{CaO} \cdot 2\text{SiO}_2$ and $\text{CaO} \cdot \text{SiO}_2$ are formed, which are characterized by relatively high thermodynamic strength (Table 12.2).

Temperature dependences of Gibbs energy for the formation of calcium silicates are given below:

Fig. 12.3 The equilibrium state diagram of the CaO-SiO₂ system

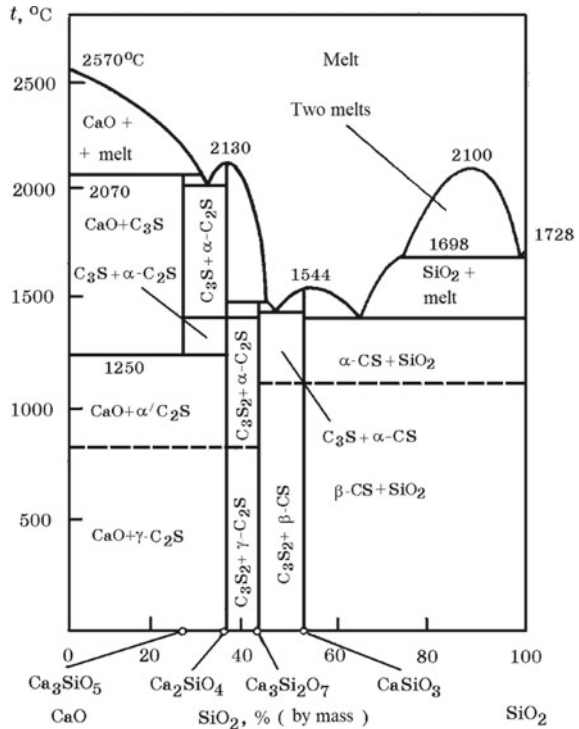


Table 12.2 Thermodynamic properties of calcium silicates

Calcium silicate	ΔH_{298}° , kJ/mol	ΔG_{298}° , kJ/mol	S_{298}° , kJ/(mol · K)	$C_{P, 298}^{\circ}$, kJ/(mol · K)	T_m , °C
CaO-SiO ₂	- 1633	- 1548	80.67	85.18	1544
2CaO-SiO ₂	- 2312	- 2198	120.67	126.7	2130
3CaO-SiO ₂	- 2198	- 2189	127.5	128.5	2050

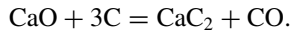
12.1.2 Calcium Carbide Smelting Technology

Calcium exists in the form of various minerals: limestone, chalk and other carbonate rocks. Limestone is widely used in ferrous and non-ferrous metallurgy as a fluxing material (in the production of fluxed agglomerate, in the smelting of cast iron and high-carbon ferromanganese). Limestone (CaCO₃), a natural material for the production of lime, used in the metallurgical, construction industry and for the production of soda (CaO).

The physicochemical nature of the process of smelting calcium carbide, as well as the type of ore-smelting electric furnaces used to produce it, are in many respects like the carbon reducing production of ferroalloys. The interest in this process is also

since CaC_2 is formed as an intermediate product in the smelting of silicocalcium. The melting diagram of the $\text{CaO}-\text{CaC}_2$ system is shown in Fig. 12.4.

Technical calcium carbide is a crystallized melt containing $\geq 80\%$ CaC_2 and 10–15% CaO . Modern technology for the production of calcium carbide is based on the reduction of calcium from calcium oxide (freshly calcined lime, less often limestone) to CaC_2 by carbonaceous reducing agents according to the total reaction



The temperature dependence of the Gibbs energy of the total reaction can be obtained by summing the partial reactions:

$$\text{Ca}_s + 2\text{C}_s = \text{CaC}_2; \quad \Delta G_T^\circ = -57360 - 28.5T, \text{ J/mol};$$

$$\text{CaO}_s = \text{Ca}_1 + 1/2\text{O}_2; \quad \Delta G_T^\circ = 644,850 - 107.5T, \text{ J/mol};$$

$$\text{C}_r + 1/2\text{O}_2 = \text{CO}; \quad \Delta G_T^\circ = -118,000 - 84.5T, \text{ J/mol};$$

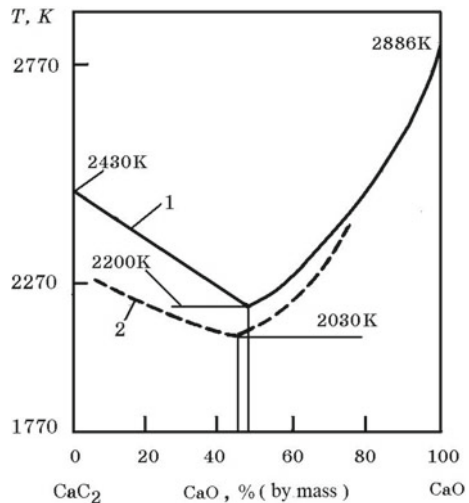
$$\text{CaO}_s + 3\text{C}_s = \text{CaC}_2 + \text{CO}; \quad \Delta G_T^\circ = 466,550 - 229.6T, \text{ J/mol}.$$

The theoretical temperature of the beginning of the total reaction for CaC_2 production ($\Delta G_T^\circ = 0$, $P_{\text{CO}} = 101 \text{ kPa}$) is 2030 K. The sulfur and phosphorus contained in the charge components (lime and carbon reducing agents) are dissolved in the melt of calcium carbide during melting. Calcium forms a fairly strong compound with sulfur CaS according to the reactions:

$$2\text{Ca}_1 + \text{S}_2 = 2\text{CaS}_s; \quad \Delta G_{1124-1760\text{K}}^\circ = -1,104,900 + 208.8T, \text{ J/mol};$$

$$2\text{Ca}_g + \text{S}_2 = 2\text{CaS}_s; \quad \Delta G_{1760-2000\text{K}}^\circ = -1,410,770 + 381.3T, \text{ J/mol}.$$

Fig. 12.4 The melting diagram of the $\text{CaO}-\text{CaC}_2$ system 1—pure component; 2—components of technical purity



When interacting with moisture, calcium phosphide forms phosphorous hydrogen (phosphine, PH_3)—a poisonous gas; therefore, its content in acetylene is limited to $\leq 0.08\%$ (volume). Impurities contained in lime and coke ash are a source of unwanted oxides ($\leq 2\% \text{Al}_2\text{O}_3$, $\leq 2\% \text{SiO}_2$) in carbide. In preparing the mixture for melting, lime should contain 92–95% CaO and 1–2% CO_2 . The solid carbon content in coke is 85–89%; coke should be dried to a moisture content of $\leq 1\%$. Lime is used with a particle size of 8–10 mm, coke 8–25 mm. The quality of technical calcium carbide is subject to specific requirements (Table 12.3).

Electric furnaces for smelting calcium carbide. In modern plants, calcium carbide is smelted in ore-smelting furnaces with circular or rectangular baths with a unit capacity of 60 MV A. As a result of the reconstruction, the unit capacity of the furnace reaches 80 MV A (Fig. 12.5). Furnaces with a capacity of 60(80) MV A with a rectangular bathtub of $10.9 \times 8.9 \times 5.6$ m in size and 3200×850 mm rectangular electrodes can be used. The furnace bath is covered with water-cooled elements. Around each electrode in the shelter of the bath, there are slots (funnels) 300 mm wide for feeding the charge. The interelectrode space is blocked by gas trapping funnels that capture up to 80% of top gas. With a furnace power of 60(80) MV A, the maximum voltage is 167(202) V, the average is 142(177) V and the current is 110 kA. Per 1 ton of calcium carbide (%), 72 CO ; 4.9 CO_2 ; 7.8 H_2 ; 0.1 CH_4 ; the rest is N_2) 250–330 m^3 of gas is released. The dust content of the gas is 100–150 mg/m^3 . The gas is purified. For the purification of 1000 m^3 of gas, 2.7–3.5 m^3 of water is consumed. Calcium carbide melt is discharged through a taphole into water-cooled drums.

Along with the described furnace, medium-power furnaces are also in operation, the characteristics of which are given below:

Table 12.3 Quality requirements for calcium carbide

Parameter	Norm for grades		
	Top grade	1	2
Volume C_2H_2 , l/kg, (no less) for pieces in sizes, mm:			
50–80	295	285	275
25–80	–	285	265
25–50	–	280	260
2–25	–	260	240
Volume fraction of PH_3 in acetylene, % (no more)	0.07	0.08	0.08
Mass fraction, % (no more): sulfide phase	0.5	1.2	1.2
Free carbon calcium oxide	1.0 1.7	Not standardized	

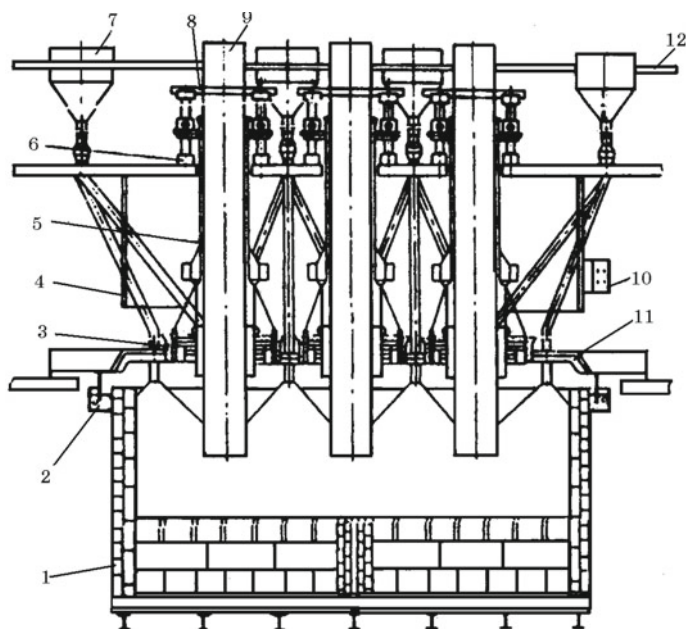


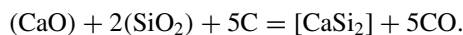
Fig. 12.5 Closed carbide furnace with rectangular bathtub 1—bath; 2—sand shutter; 3—dry seal; 4—an umbrella; 5—electrode holder; 6—mechanism electrode movements; 7—charge supply path; 8—mechanism for moving (bypassing) the electrodes; 9—electrodes; 10—short network; 11—shelter; 12—electrode extension pad

Conventional number of the furnace	1	2	3	4	5	6
Active power of the furnace, MW	26.5	29.5	34.8	36.5	39.5	40.5
The apparent resistance of the furnace, $\mu\Omega$	1.489	1.310	1.251	1.218	1.201	1.096
$\cos \varphi$	0.92	0.84	0.89	0.88	0.87	0.87
Average secondary voltage, V	119.6	113.8	128.0	131.1	129.1	129.5
Secondary stage current strength, kA	80.3	86.8	102.1	101.6	107.6	118.2

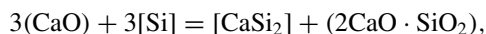
Ore-smelting electric furnaces are equipped with devices for automatic control of the furnace power, feed rate of the bath with the charge, the position of the electrodes in the furnace. Programs, algorithms and control schemes for the process of smelting calcium carbide have been developed. The computer circuit calculates and maintains the optimum temperature of the process by adjusting the position of the electrodes, supplied power, as well as controlling the flow of lime and coke and their ratio.

12.1.3 Silicocalcium Smelting Technology

In industrial practice, there are three methods for smelting silicocalcium. The carbothermic method is the most common. Its essence consists in the joint reduction of calcium and silicon from their oxides with carbon by the reaction



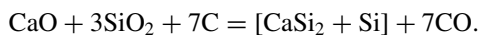
The silicothermic method is based on the reaction of reduction of calcium from calcium oxide by silicon ferrosilicon



and calcium carbide on the reduction of silicon quartzite by carbon carbide CaC_2 .

Carbothermic method. The charge consists of metallurgical lime ($\geq 87\%$ CaO; $\leq 0.010\%$ P) with a grain size of 40–100 mm, quartzite (95% SiO_2) with a grain size of 25–200 mm, coke-nut (ash content 11–13%) with a grain size of 5–20 mm and coal. The charge components are subject to stringent sulfur requirements, since calcium and sulfur form a thermodynamically strong CaS sulfide (55.54% Ca; 44.46% S). The sulfur content in silicocalcium can reach 0.2%. The main sources of sulfur are quartzite (50–55%), coke (20–30%) and coal (10–15%).

High calcium silicocalcium grades (SiCa20, SiCa30) (Table 12.4) are obtained in open electric furnaces with a capacity of 16.5 MV A. The process in general can be described by the reaction:



The formation of thermodynamically strong atomic groups close to CaSi_2 reduces the activity of calcium and silicon and facilitates the conditions for the reduction of these elements from their oxides ($\text{PCO} = 0.1$ MPa is achieved at 1600 °C).

Intermediate reactions proceed with the formation of SiC and CaC_2 . However, excess carbon in the charge must be avoided to prevent carbide from overheating the bathtub of the furnace. The dosage of the charge components is carried out

Table 12.4 Requirements for the chemical composition of silicocalcium, %

Grade	Ca, no less	Fe	Al	C	P
			No more		
SiCa10	10	25	1.0	0.2	0.02
SiCa15	15	20	1.0	0.2	0.02
SiCa20	20	15	2.0	1.0	0.04
SiCa25	25	10	2.0	0.5	0.04
SiCa30	30	6	2.0	0.5	0.04

from the required ratio in the charge. The approximate composition of the charge is the following, kg: 85 lime; 200 quartzite; 30 coal; 50 charcoal; 85–95 coke. When smelting alloys of grades SiCa10, SiCa15, ~40 kg of iron shavings are added to the charge. The charge is calculated taking into account the practical use of each element. Therefore, when calculating the composition of the charge for the alloy grade SiCa30 take calcium extraction of 67%, and silicon—75%. When smelting silicocalcium, special attention is paid to controlling the processes of slag formation, since slag, having a higher density, is deposited on the hearth, which leads to its overgrowing and disruption of the furnace. Below is the composition of silicocalcium slag smelted by the carbon thermal method, %:

Component	CaO	SiO ₂	Al ₂ O ₃	SiC	CaC ₂
SiCa30	15–20	45–55	2–3	10	10–15
SiCa15	63–68	30–33	0.3–0.7	–	$C = 0.5–0.7$

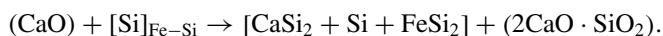
Slag with a high content of calcium carbide exhibits greater fluidity and reduces the concentration of sulfur in silicocalcium. However, they make it difficult to cast due to poor separation of slag from the metal.

The electric mode of operation of furnaces with a capacity of 16.5 MV A: current 54.4 kA, voltage 134 V. Despite the observance of the optimal parameters of the technology for producing silicocalcium, over time, the furnace bath overgrows with a skull consisting of a half-reduced mixture. Stops and bathtub refining are required. To avoid outage in practice, this problem is partially solved by periodically transferring the furnace to smelting 45% ferrosilicon. The alloy and slag are released during a normal melting course every 2 h into a ladle with carbon lining of the walls and chamotte bottom. The alloy is poured into lined molds. Below is the chemical composition of silicocalcium obtained by the carbon thermal method, %:

Component	Si	Ca	Fe	Al	S	P	C
SiCa30	64.12	30.52	3.77	1.59	0.09	0.02	1.29
SiCa25	67.60	28.24	3.19	1.57	0.05	0.02	0.97

The use of carbonaceous reducing agents with a high content of sulfur and ash (Al₂O₃) is accompanied by an increase in the concentration of sulfur and aluminum in the alloy. Under high-temperature conditions, aluminum is reduced by carbon to Al₄C₃ carbide and dissolved in the alloy. Therefore, the use of charge components with a high Al₂O₃ impurity content makes it difficult to obtain silicocalcium with an acceptable aluminum concentration ($\leq 2\%$).

The *silicothermic method* for producing silicocalcium is based on the reaction of reduction of calcium oxide with silicon ferrosilicon by the total reaction



Since the chemical affinity of silicon to oxygen is lower than that of calcium, the reaction can proceed toward silicocalcium due to a significant decrease in calcium activity, which is achieved by a high silicon content in the alloy. Equilibrium of the reaction is achieved at relatively low concentrations of calcium in the alloy; therefore, silicocalcium (ferrosilicocalcium) with a calcium content of $\leq 20\%$ can be obtained by the silicothermic method.

Silicocalcium in a silicothermic way is smelted in open furnaces by a batch process. The composition of the charge, kg: 200 lime; 196 ferrosilicon FS75; 30 fluorspar (CaF_2). The use of scarce fluorspar is because highly basic slags are viscous and non-technological. Addition of fluorspar dilutes the slag and improves the conditions for the separation of smelting products during casting. The extraction of calcium is 20–30%, and the use of silicon ferrosilicon is 75–85%. 25–35% of aluminum, 15–30% of sulfur, 15–35% of phosphorus, 25–30% of magnesium goes into the alloy from the charge; part of the calcium goes into the gas phase. The actual chemical composition of the silicocalcium grade SiCa15 of two industrial testing is given below, %:

Component	Si	Ca	Fe	Al	S	P	C
Melt 1	59.0	17.64	19.43	0.71	0.01	0.016	0.05
Melt 2	61.79	16.43	21.21	0.49	0.01	0.010	0.06

The quality of silicothermic silicocalcium in terms of sulfur and carbon is higher than that of carbothermic. Comparative technical and economic indicators of the smelting of silicocalcium by carbothermic and silicothermic methods are given in Table 12.5.

Silicocalcium of various particle sizes (2–0; 2–5; 5–20 and 20–200 mm) is supplied to steel mills. The use of silicocalcium in steelmaking for its deoxidation

Table 12.5 Consumption of charge materials and electricity when smelting silicocalcium

Name	SiCa15	SiCa30	SiCa15	SiCa10
	Carbothermic method		Silicothermic method	
Material consumption, kg:				
Quartzite	1436	1875	–	–
Lime	456	748	960	940
Coal	281	265	–	–
Charcoal	244	370	–	–
Dry coke	388	600	–	–
Ferrosilicon FS65	–	–	917	805
Steel shavings	318	–	–	–
Electrode mass	107	134	–	–
Electrodes	–	–	12.5	10.5
Power, kWh/t	8893	11,800	1670	1415

in pieces or in the form of fine fractions is accompanied by large losses of calcium due to its low density and its high activity with respect to atmospheric oxygen and ladle slag oxides. The best use of silicocalcium is achieved by using it in the form of a flux-cored wire, manufactured according to the technology of production of a powder welding shell.

Calcium carbide method. The carbothermic method described above for smelting silicocalcium by co-reducing Si and Ca from quartzite and lime (limestone) with carbon, despite its apparent simplicity, has a number of significant drawbacks. First, this method makes it difficult to melt silicocalcium with a content of 32–35% Ca due to the accumulation in the bath of the furnace of a complex composition of the skull on the bottom and walls of the bath, consisting of melted interaction products of SiO_2 and CaC_2 . Since silicocalcium has a density lower than the skull of a complex heterogeneous composition, the alloy under the electrodes is located above the hearth overgrown with the skull. This violates the electric melting mode and the course of the furnace as a whole. As noted above, for these reasons, the furnace is forced to periodically be transferred to the smelting of ferrosilicon FS45 to bring the bath to the desired state, for the subsequent smelting of silicocalcium or to repair the furnace. These disadvantages are largely eliminated by obtaining silicocalcium by the carbide calcium two-stage method. In the first stage, technical calcium carbide is smelted from lime (limestone) and coke, and in the second stage, silicocalcium is smelted from calcium carbide and quartzite. The technology of the two-stage method for smelting silicocalcium has been known for a relatively long time, but has not found wide application.

In recent years, a technology and ore-smelting electric furnaces of a ferroalloy type have been developed for the production of silicocalcium by a calcium carbide two-stage method. Experiments on the smelting of silicocalcium using calcium carbide, quartzite, coke and charcoal in a three-phase furnace were carried out. In the calculations, it was assumed that 60% of the time the furnace works with silicocalcium (3245–3445 t/year) and 40% of the time ferrosilicon (5000–5250 t/year). To ensure this amount of silicocalcium, calcium carbide in an amount of 1950–3450 t/year is required. The production of silicocalcium in an amount of 3000–4000 t/year allows smelting about 1 million tons of high-quality steel using the most active deoxidizer—silicocalcium, containing 32–35% Ca. The specific consumption of charge materials and electricity during the smelting of silicocalcium grade SiCa30 using calcium carbide, quartzite and carbonaceous reducing agents is given below, kg/t:

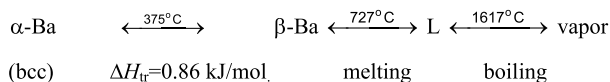
Material	Quartzite	Calcium carbide	Coke breeze	Charcoal	Electrodes	Power, kWh/t
Option 1	1650	600	580	170–200	115	1250
Option 2	1700–2000	600–1000	560–580	170	–	12,000–15,000

12.2 Ferrosilicobarium and Aluminobarium

The metal barium in the form of an amalgam was obtained in 1808 by the English chemist H. Davy by electrolysis of $\text{Ba}(\text{OH})_2$. The barium content in the earth's crust is 0.05%; it does not occur in the free state in nature. The practical use of barium metal is small. Usually, barium is fused with some metal that imparts resistance to barium. In small amounts, barium is used in metallurgy for the deoxidation and modification of steel, deoxidation and purification of sulfur and gases of copper, lead, etc. Barium is also added in small amounts to some antifriction materials, for example, to lead used for printing fonts. Barium alloys with nickel are used in electrodes of engine spark plugs and in radio tubes. Barium compounds are most widely used in various industries: BaO_2 , BaS , BaCrO_4 , BaMnO_4 , etc.

12.2.1 Properties of Barium and Its Compounds

Barium properties. Barium atomic number 56, atomic mass 137.33, density 3.78 g/cm^3 , melting point $710 \text{ }^\circ\text{C}$, boiling point $1640 \text{ }^\circ\text{C}$, oxidation state 2, rarely 1. Barium exists in two allotropic modifications. Below are the barium-phase transition temperatures:

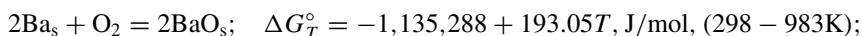


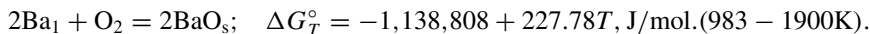
The equilibrium point of three phases: solid, liquid and vaporous—at a temperature of $710 \text{ }^\circ\text{C}$ and a pressure of 1.185 Pa . The equation of temperature dependence of vapor pressure over liquid barium for the temperature range $983\text{--}1959 \text{ K}$ has the form:

$$\lg P = 20.408 - 8304/T - 4.036 \lg T.$$

Ba–O system. BaO oxide (10.43% O) is formed in the system, which is colorless crystals with a cubic lattice, density 5.7 g/cm^3 . When BaO is heated in O_2 medium at a temperature of $\sim 500 \text{ }^\circ\text{C}$, BaO_2 peroxide is obtained—also colorless crystals, but with a hexagonal lattice, density 4.96 g/cm^3 . Above $500 \text{ }^\circ\text{C}$, BaO_2 thermally dissociates to form BaO and O_2 . BaO_2 is a charge component for obtaining Al–Ba alloys.

The melting point of BaO $2017 \text{ }^\circ\text{C}$, when heated, sublimates. BaO is obtained by thermal decomposition of BaCO_3 carbonate at $700\text{--}900 \text{ }^\circ\text{C}$. Temperature dependences of the Gibbs energy of BaO formation reactions are described by the equations:

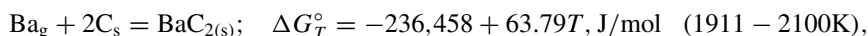
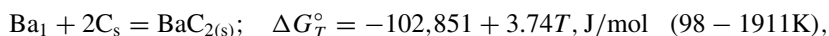
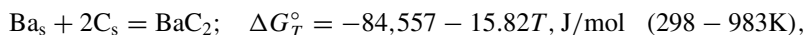




The equation of the temperature dependence of vapor pressure over solid BaO has the form

$$\lg P(\text{Pa}) = 10.99 - 19,700/T \quad (1200 - 1700\text{K}).$$

Ba–C system. The system has one BaC₂ compound (14.88% C). Temperature dependences of the Gibbs energy of the reactions of formation of BaC₂ carbide have the form:

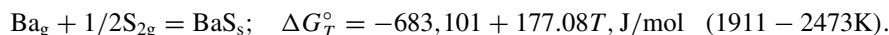
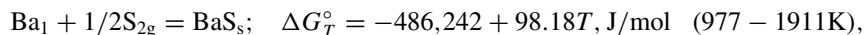


BaC₂ as well as carbides of other metals of group IIA of the Periodic system has an ionic type of chemical bond. BaC₂ carbide crystallizes in a face-centered tetragonal lattice of CaC₂ type, decomposes at temperatures above 2000 °C and has a density of 3.895 g/cm³.

Ba–Si system. Barium silicides BaSi (16.93% Si) and BaSi₂ (28.97% Si) are known (Fig. 12.6). The solubility of silicon in solid barium is very small; at a eutectic temperature of 630 °C, it does not exceed 0.14% (at.).

Ba–Al system. The BaAl₄ compound is formed in the system (Fig. 12.7). The thermodynamic constants of barium-containing ferroalloys important for electrometallurgy are summarized in Table 12.6.

Ba–S system. Barium with sulfur forms several sulfides (Fig. 12.8), of which the BaS compound (18.93% S) melting at 2200 °C is well studied (the position of BaS in the diagram is not shown). The fusion of barium and sulfur yielded compounds Ba₂S (10.45% S), BaS₂ (31.83% S), BaS₃ (41.19% S). The transformation temperatures of these sulfides are shown in Fig. 12.8. BaS sulfide crystallizes into a cubic lattice of the NaCl type ($a = 0.6381 \text{ nm}$), density 4.252 g/cm³. When stored in air, BaS absorbs CO₂, forming BaCO₃ and H₂S. When calcined in air, BaS is oxidized to BaSO₄. The temperature dependences of the Gibbs energy of the reactions of BaS formation from elements are described by the equations



The high thermodynamic strength of barium sulfide allows the use of barium as a desulphurizer of cast iron and steel.

Ba–P system. In the Ba–P system, following compounds are known BaP₃; BaP₂; BaP_{1.82}; Ba₄P₅; Ba_{1.1}P; Ba₄P₃; Ba₃P²; Ba₂P₂. The most refractory Ba₃P₂ phosphide melts congruently at a temperature of 1340 °C.

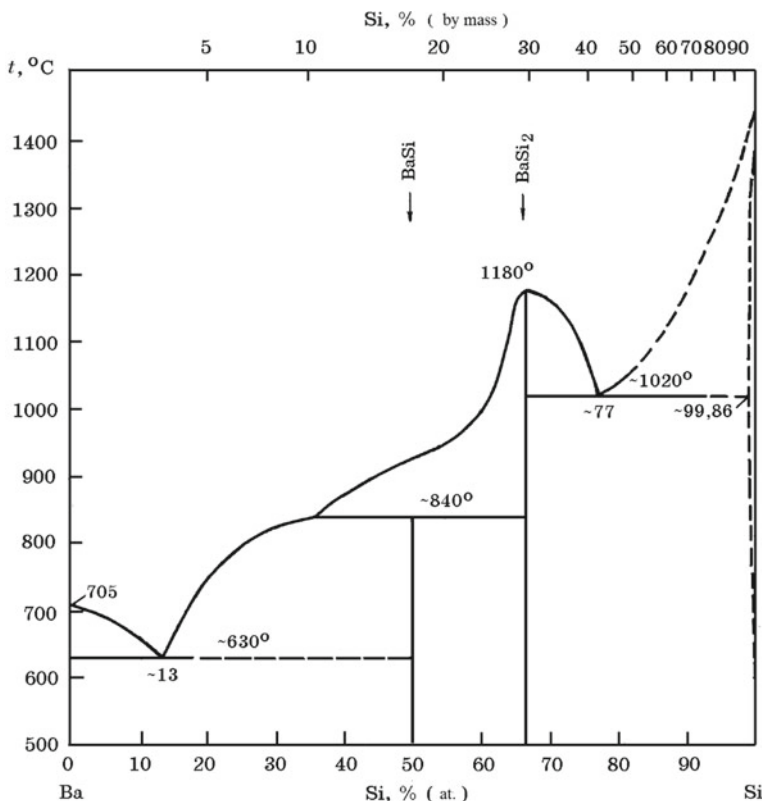


Fig. 12.6 Equilibrium diagram of Ba-Si system

BaO-CO₂ system. Barium carbonate BaCO₃ (77.69% BaO; 0.22% CO₂) exists in several modifications: up to a temperature of 840 °C the modification of α -BaCO₃ with a rhombic lattice is stable; in the range of 840–960 °C, β -BaCO₃ with a hexagonal lattice; at 982 °C— γ -BaCO₃ with a cubic lattice. α -BaCO₃ \rightarrow β -BaCO₃ transition enthalpy $\Delta H^\circ = 16.3$ kJ/mol. When heated above 964 K, BaCO₃ dissociates with the formation of BaO and CO₂. The equation for the temperature dependence of CO₂ pressure over BaCO₃ has the form

$$\lg P_{\text{CO}_2} = -11.30 + 13,670/T.$$

BaCO₃ forms solid solutions with SrCO₃, CaCO₃ and BaO. Barium carbonate is toxic, MPC = 0.5 g/cm³.

Barium hydroxide Ba(OH)₂. It exists in two versions: the low-temperature modification of α -Ba(OH)₂ at 246 °C changes to β -Ba(OH)₂; $\Delta H_{\text{tr}} = 3.6$ kJ/mol. The melting point of Ba(OH)₂ is 408 °C. Ba(OH)₂ is toxic, MPC = 0.5 mg/m³; when heated, decomposes into BaO and H₂O, about 800 °C decomposes completely to

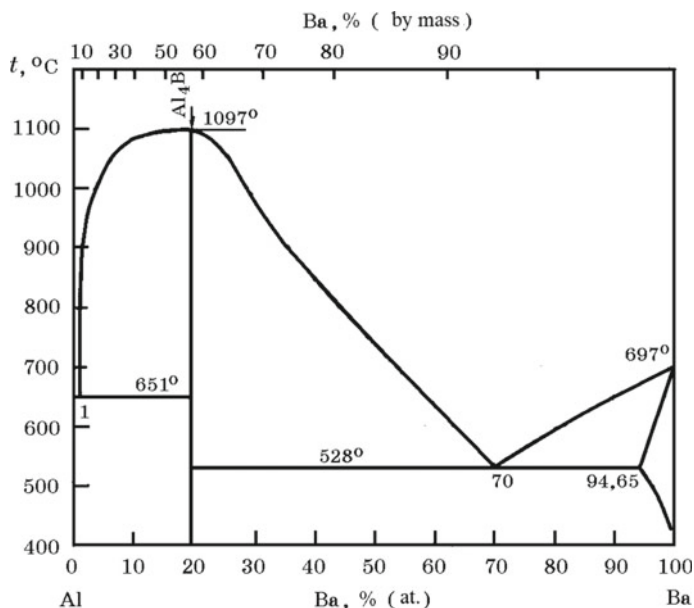


Fig. 12.7 Equilibrium diagram of Ba–Al system

Table 12.6 Thermodynamic constants of some barium compounds

Compound	$-\Delta G_{298}^{\circ}$, kJ/mol	$-\Delta H_{298}^{\circ}$, kJ/mol	S_{298}° , J/(mol K)	T_m , °C
BaO	520.5	553.02	70.34	2017
BaS	455.62	450.8	78.3	2473
BaSO ₄	1348.0	1459.0	132.1	1580
BaCO ₃	1208.1	1201.1	112.0	T_{decomp} 691
BaC ₂	81.5	75.42	87.78	2600
BaSiO ₃	1615.4	1532.2	109.5	1877
Ba ₂ SiO ₄	2273.5	2160.9	175.8	2423
BaAl ₄	62.7	66.9	198.1	1097

BaO. The equations of the temperature dependence of vapor pressure over solid and liquid B (OH)₂, respectively, have the form:

$$\lg P(\text{Pa}) = 14.892 - 184,964/09.155T,$$

$$\lg P(\text{Pa}) = 9.847 - 118,767/19.155T.$$

Barium sulfate. In nature, barium is represented by the ore mineral *barite* BaSO₄, which is used for the smelting of barium-containing ferroalloys. When heated, BaSO₄ dissociates by reaction

Thermodynamic property	$-\Delta H_{298}^{\circ}$, kJ/mol	S_{298}° , J/(mol K)
BaO · 2SiO ₂ (BS ₂)	2554.7	154.1
2BaO · 3SiO ₂ (B ₂ S ₃)	4190.3	265.8
BaO · SiO ₂ (BS)	1598.1	112.2
2BaO · SiO ₂ (B ₂ S)	2294.9	182.1
3BaO · SiO ₂ (B ₃ S)	2936.1	252.9

Barium disilicate 2BaO · SiO₂ has two modifications: at a temperature of 1350 °C α-2BaO · SiO₂ turns into disilicate β-2BaO · SiO₂ which melts at 1760 °C. The density of the disilicate is 3.73 g/cm³. The temperature dependence of the Gibbs energy of the disilicate formation reaction is



Data on the thermodynamic properties of compounds in the BaO–SiO₂ system are of great importance in the analysis of the process of producing ferrosilicobarium.

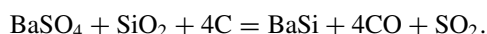
BaO–Al₂O₃ system. A number of aluminates are formed in the system (Fig. 12.10). The compositions and melting points of barium aluminates formed in the system are given below:

Composition	BaO, %	Al ₂ O ₃ , %	T_m , °C
BaO · 6Al ₂ O ₃	20.0	80.0	1925
BaO · Al ₂ O ₃	60.1	39.9	1830
3BaO · Al ₂ O ₃	80.7	19.9	1750

12.2.2 Ferrosilicobarium Smelting Technology

The main raw material for the production of barium and its compounds is barite, which is reduced with coal in flame furnaces by reaction $\text{BaSO}_4 + 4\text{C} = \text{BaS} + 4\text{CO}$; the resulting soluble BaS is processed into other barium salts.

Barium ferroalloys can be obtained using carbon, silicon and aluminum as reducing agents. The most economical is the *carbothermic* method of smelting a barium-containing ferroalloy—ferrosilicobarium using barite concentrate (65.7% BaO; 34.3% SO₃), quartzite and coke. The joint reduction of Ba and Si from this charge can be described by the reaction



Melting is carried out in an electric arc furnace by a continuous process. Ferrosilicobarium obtained by the carbothermic process contains, %: 27–35 Ba; 46–52 Si;

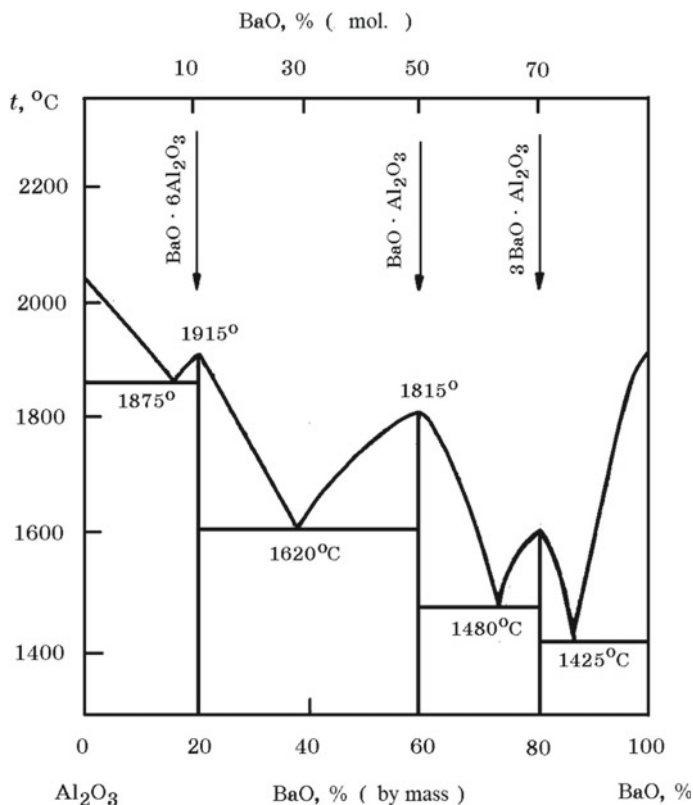


Fig. 12.10 Equilibrium diagram of BaO–Al₂O₃ system

8–25 Fe; 0.15–0.3 C; 0.02–0.10 S; composition of furnace slag, %: 19–26 Ba_{tot}; 25–37 SiO₂; 3–7 C; 3–5 S.

The *silicothermic* process is based on the reduction of barium from BaO with silicon ferrosilicon (FS75)



In this way, ferrosilicobarium with a barium content of up to 25% or a complex alloy containing Ba and Ca is obtained. Melting is carried out in an electric arc furnace by a periodic process. The composition of the charge, kg: 100–120 BaO; 190 FS75; 200 lime; 50 fluorspar. The resulting complex ferroalloy contains, %: 5 VA; 15 Ca; 27 Fe; 1.5 Al, the rest is Si.

12.2.3 Aluminobarium Smelting Technology

Alloys of the Al–Ba system are characterized by high deoxidizing ability, since each component individually has a high affinity for oxygen. These ligatures can also be used as modifiers of the structure of structural steels and various alloys based on iron.

The basis of the technological process for the smelting of barium aluminum ligatures is the reduction reaction of barium oxides with aluminum. The mixture is made so that in the alloy 40–45% Ba is obtained with a regulated Si and Fe content (Table 12.7).

Charge composition: per 100 kg of Barium oxide (IV) ($\geq 93\%$ BaO₂), 55.8 kg of aluminum grit (0–0.1 mm $\leq 20\%$, 0.1–1.0 mm $\geq 70\%$ and 1.0–3.0 mm $\leq 15\%$); 11.0 kg of fluorite concentrate ($\geq 95\%$ CaF₂).

The aluminum barium ligature is obtained by the out-of-furnace aluminothermic method in a cast iron mold with a diameter of 1 m and a height of 0.6 m with an extension—a shell of sheet-iron iron with a thickness of 5–10 mm. The dosage of the mixture is carried out at the rate of 200–250 kg of Barium oxide (IV). The charge is mixed in a drum-type mixer made of corrosion-resistant steel with a capacity of 0.5 m³ (12 revolutions/min). Melting is carried out with the upper fuse. Due to the low density of the ligature, the block of the resulting alloy is located above the slag. The block is cooled and then crushed.

Barium oxide (IV) belongs to the group of toxic substances with strong oxidizing properties. The mixture may ignite outside the melting chamber. In the air of the working zone of the smelting site, the maximum permissible concentration of BaO₂ is set at ≤ 0.05 mg/m³.

12.3 Ferrosilicostrontium

Strontium was discovered in 1790 by the English chemist A. Crawford; metallic strontium was first isolated in 1808 by the English scientist G. Davy. The strontium content in the earth's crust is $4 \times 10^{-3}\%$; it does not occur in nature in a free state. Strontium is used for the deoxidation of copper and bronze, deep desulfurization and dephosphorization of special steels and alloys. An alloy of strontium with lead and tin is used for the manufacture of battery anodes. In electronics, radio and lighting engineering, strontium compounds are used as active materials for solid-state lasers, in the manufacture of electrodes, thermistors, phosphors photocells. Strontium compounds

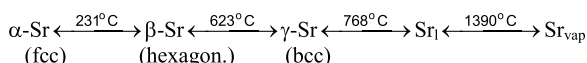
Table 12.7 The chemical composition of Al–Ba ligatures, %

Grade	\geq Ba	\leq Si	\leq Fe	Al
ABA-45	45	0.9	0.7	Remain
ABA-40	40	1.0	0.8	Remain

are used in the manufacture of certain varieties of optical glasses, highly refractory ceramics and other products.

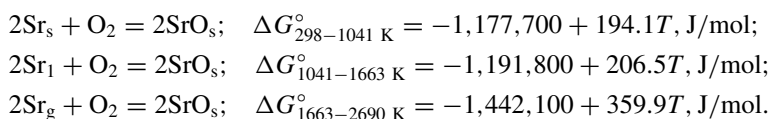
12.3.1 Properties of Strontium and Its Compounds

Strontium properties. Strontium atomic number 38, atomic mass 87.62, density 2.63 g/cm^3 , melting point $770 \text{ }^\circ\text{C}$, boiling point $1380 \text{ }^\circ\text{C}$, oxidation state 2, rarely 1. Natural strontium consists of four stable isotopes: $^{88}_{38}\text{Sr}$ (82.56%), $^{86}_{38}\text{Sr}$ (9.86%), $^{87}_{38}\text{Sr}$ (7.02%) and $^{84}_{38}\text{Sr}$ (0.56%). The metal exists in three allotropic modifications, the transformation of which takes place at the following temperatures:



where fcc means face-centered cubic lattice.

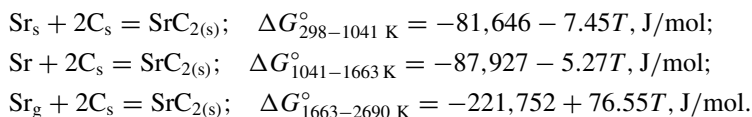
Sr–O system. SrO oxide is formed in the system, which is colorless crystals with a density of 4.7 g/cm^3 , melting point SrO $2660 \text{ }^\circ\text{C}$. Upon calcination of SrO in O_2 medium at high pressure, SrO_2 peroxide is formed. During the interaction of SrO with H_2O , $\text{Sr}(\text{OH})_2$ hydroxide is formed—colorless hygroscopic crystals, melting point $535 \text{ }^\circ\text{C}$, density 3.632 g/cm^3 . The temperature dependences of the Gibbs energy of the reactions of the formation of SrO oxide upon the interaction of strontium (solid, liquid, gas) with molecular oxygen are as follows:



The dependence of vapor pressure over SrO under the assumption that SrO dissociation does not take place is described by the equation

$$\lg P_{\text{tot}} (\text{atm.}) = 1.44 + 1.908 \lg T - 25,950/T (700 - 1600\text{K}).$$

Sr–C system. A thermodynamically strong carbide SrC_2 is formed in the system. The temperature dependences of the Gibbs energy of reactions of the formation of carbide with the participation of strontium in a different state of aggregation are described by the equations:



The vapor pressure of strontium over SrC_2 carbide can be described by the equation

$$\lg P_{\text{Sr}}(\text{atm.}) = 3.74 - 11,846/T(1200 - 1500\text{K}).$$

Sr–Si system. The silicides SrSi (24.23% Si) and SrSi_2 (38.99% Si) are formed in the system (Fig. 12.11). The silicides SrSi and SrSi_2 melt congruently. There are three eutectics in the system; the existence of the Sr_2Si compound is also reported.

SrO–CO₂ system. Strontium carbonate SrCO_3 (colorless crystals) exists in several polymorphic modifications:

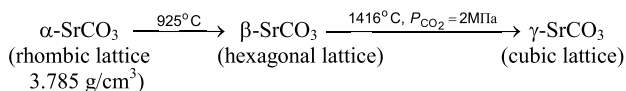
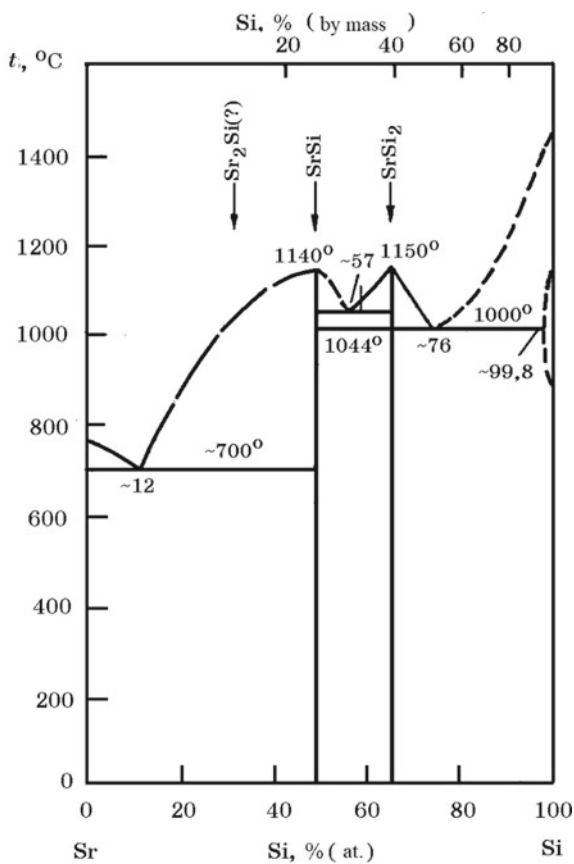


Fig. 12.11 Equilibrium diagram of Sr–Si system



The melting point of SrCO_3 is 1494 °C. Upon heating, SrCO_3 dissociates by reaction



The equations of the temperature dependence of the thermal dissociation pressure SrCO_3 have the form

$$\lg P_{\text{CO}_2}(\text{Pa}) = 12.767 - 11,549/T(1093 - 1193\text{K});$$

$$\lg P_{\text{CO}_2}(\text{Pa}) = 11.942 - 10,579/T(1203 - 1323\text{K}).$$

SrO–SiO₂ system. In the system, there are crystalline phases (silicates) $2\text{SrO} \cdot \text{SiO}_2$, $\text{SrO} \cdot \text{SiO}_2$ (Fig. 12.12). The melting point of $2\text{SrO} \cdot \text{SiO}_2$ has not been precisely determined, but it is above 1700 °C. The $\text{SrO} \cdot \text{SiO}_2$ compound melts congruently. Strontium silicates are characterized by a relatively high thermodynamic strength, which is confirmed by the Gibbs energy given below for the reactions of their formation from components:



SrO–Al₂O₃ system. In this system, the existence of $4\text{SrO} \cdot \text{Al}_2\text{O}_3$, $3\text{SrO} \cdot \text{Al}_2\text{O}_3$, $\text{SrO} \cdot \text{Al}_2\text{O}_3$, $\text{SrO} \cdot 2\text{Al}_2\text{O}_3$ and $\text{SrO} \cdot 6\text{Al}_2\text{O}_3$ compounds was established (Fig. 12.13). The $4\text{SrO} \cdot \text{Al}_2\text{O}_3$ compound has two modifications: high-temperature (α - $4\text{SrO} \cdot \text{Al}_2\text{O}_3$) and low-temperature (β - $4\text{SrO} \cdot \text{Al}_2\text{O}_3$). The properties of a number of strontium compounds are given in Table 12.8.

Fig. 12.12 Equilibrium diagram of SrO – SiO_2 system

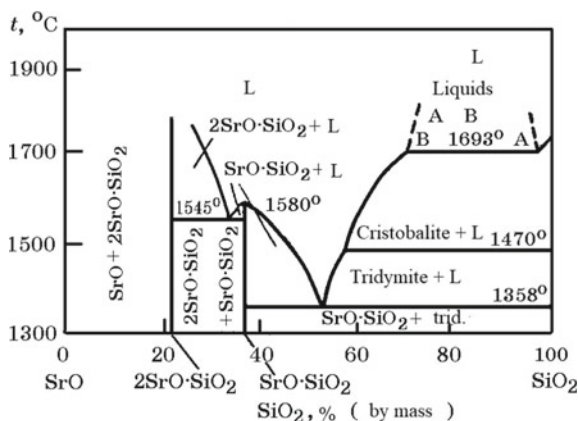


Fig. 12.13 Equilibrium diagram of SrO–Al₂O₃ system

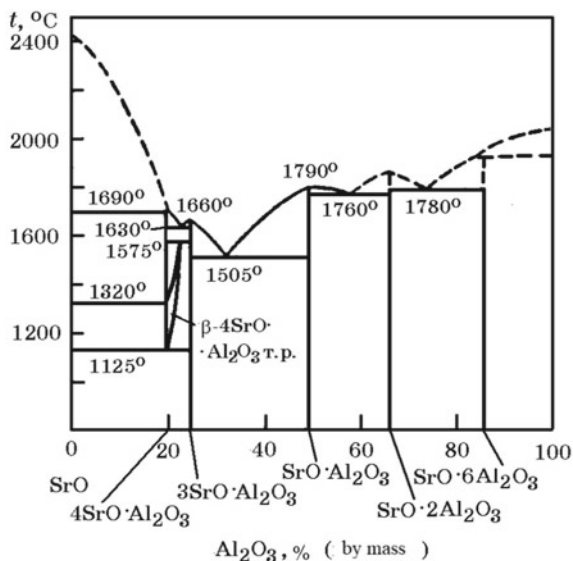


Table 12.8 Physicochemical properties of strontium compounds

Compound	$-\Delta H_{298}^{\circ}$, kJ/mol	$-\Delta G_{298}^{\circ}$, kJ/mol	S_{298}° , J/(mol K)	$C_{P, 298}^{\circ}$, J/(mol K)	T_m , K
SrO	590.5	559.3	55.44	45.0	2660
SrSO ₄	1443.5	1345.5	117.8	101.6	2000
Sr ₃ P ₂	693.9	–	–	–	–
SrCO ₃	1224.3	1143.2	99.48	81.5	–
SrSi	188.1	–	–	–	1140
SrSi ₂	188.1	–	–	–	1150
Sr ₂ Si	380.8	–	–	–	–
SrSiO ₃	1629.4	1544.1	96.3	88.4	–
Sr ₂ SiO ₄	2297.7	2182.4	153.4	134.2	–

12.3.2 Minerals and Ores of Strontium

Strontium forms about 40 minerals, of which celestine SrSO₄ and strontianite SrCO₃ are of industrial importance. Strontium is present as an isomorphous impurity in various magnesium, calcium (Sr, Ca)₂ · B₁₄O₂₃ · 8H₂O and barium minerals and is also found in natural mineralized waters (about 24% of the total strontium reserves). Part of strontium in the ocean is concentrated in ferromanganese nodules.

12.3.3 Ferrosilicostrontium Smelting Technology

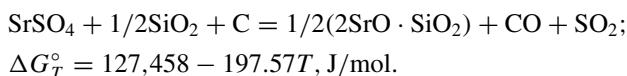
Strontium is present in natural mineral formations mainly in the form of celestine SrSO_4 . Celestine concentrate contains about 86% SrSO_4 . During the high-temperature interaction of SrSO_4 sulfate with carbon, SrS sulfide is formed



In the presence of SiO_2 , the reduction of strontium to silicide proceeds according to the reaction



Along with the silicide phase, with a lack of carbon in the system, reactions occur with the formation of strontium silicates



Ferrosilicostrontium is obtained in an electric arc furnace with a capacity of 160 kV A at a voltage of 30 V and a current of 1500 A. The mixture consists of celestine concentrate, quartzite, coke and iron chips. The obtained ferrosilicostrontium contains, %: 8–10 Sr; 48–59 Si; Fe is the rest. The slag ratio is 1.5. In pilot campaigns for smelting ferrosilicostrontium in a large laboratory furnace, the specific energy consumption was high, and the useful use of strontium was low. Improving the technology for smelting ferrosilicon strontium will reduce energy consumption.

To obtain a complex alloy of strontium with barium, as well as direct alloying of steel and Sr and Ba alloys, it is rational to use concentrates containing carbonates SrCO_3 and BaCO_3 . The concentrate with a particle size of up to 10 mm has the following chemical composition, %:

SrO	BaO	CaO	SiO ₂	MgO	K ₂ O	Na ₂ O	FeO	CO ₂
5.5	16.0	21.5	24.8	0.9	3.0	1.5	4.0	18.0

12.4 Ferrosilicon Magnesium

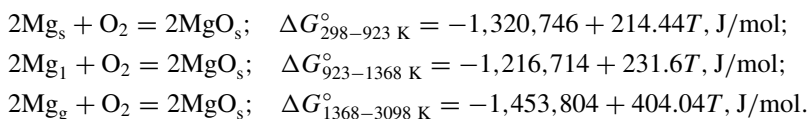
Magnesium was discovered in 1808 by the English chemist G. Davy, and the metallic magnesium was obtained in 1828 by the French chemist A. Bussy. The magnesium content in the earth's crust is relatively high—2.35%.

12.4.1 Properties of Magnesium and Its Compounds

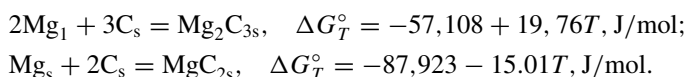
Magnesium properties. The atomic number of magnesium is 12, the atomic mass is 24.305, the density is 1.74 g/cm³, the melting point is 650 °C, the oxidation state is 2, rarely 1. Natural magnesium consists of three stable isotopes $^{24}_{12}\text{Mg}$ (78.60%), $^{25}_{12}\text{Mg}$ (10.11%) and $^{26}_{12}\text{Mg}$ (11.29%). Magnesium has a hexagonal crystal lattice. The temperature dependence of vapor pressure over liquid magnesium has the form

$$\lg P = 16,7974 - 7844.2/T + 2.548 \cdot 10^{-4}T - 2.7280 \lg T \quad (407 - 1390\text{K}).$$

Mg–O system. MgO oxide is formed in the system, melting point 2827 °C, boiling point 3600 °C, density 3.58 g/cm³. Temperature dependences of the Gibbs energy of MgO formation reactions are characterized by the following equations:



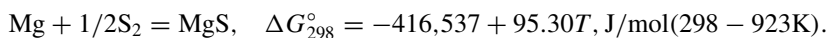
Mg–C system. Magnesium with carbon forms carbides MgC₂ and Mg₂C₃. The density of MgC₂ is 2.204 g/cm³. The temperature dependences of the Gibbs energy of the reactions of the formation of magnesium carbides have the form:



During the interaction of magnesium carbide with H₂O, C₂H₂ and a mixture of hydrocarbons are formed.

Mg–Si system. With silicon, Mg forms silicide Mg₂Si (36.56% Si) (Fig. 12.14).

Mg–S system. When heated, magnesium and sulfur form MgS sulfide—crystals with a cubic lattice, the melting point is about 2200 °C, with a density of 2.86 g/cm³. The equation for the temperature dependence of the Gibbs energy of the MgS formation reaction has the form



MgO–CO₂ system. Magnesium carbonate MgCO₃ dissociates upon heating by reaction



MgO–SiO₂ system. Compounds 2MgO · SiO₂ and MgO · SiO₂ are formed in the system (Fig. 12.15). Temperature dependences of Gibbs energy of reactions of formation of silicates from oxides are described by the equations:

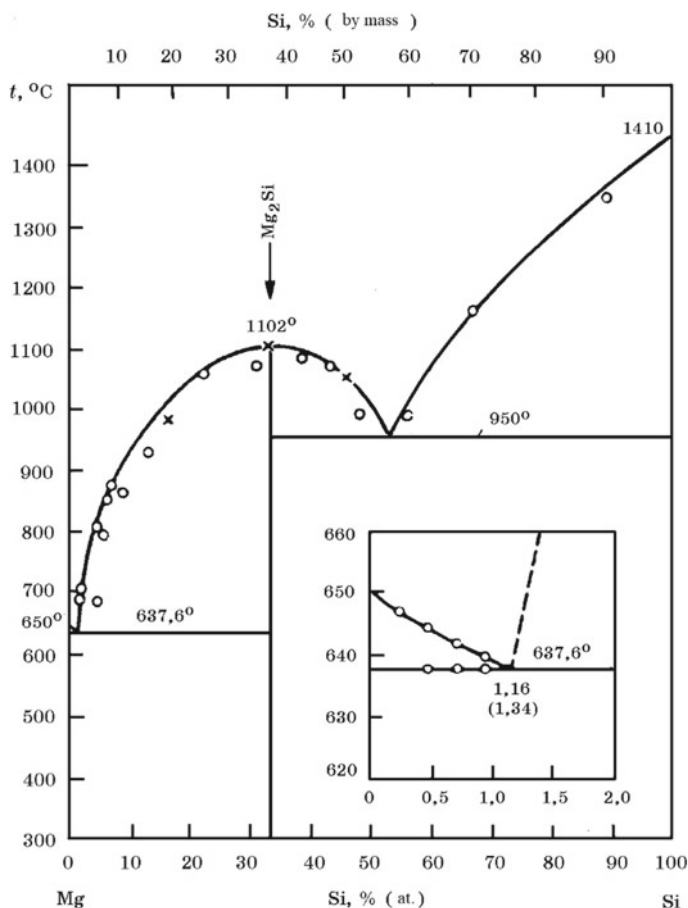
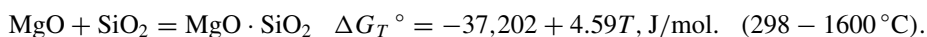
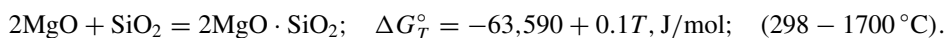


Fig. 12.14 Equilibrium diagram of Mg-Si system



The thermodynamic properties of the compounds most important for electrometallurgy of magnesium-containing ferroalloys are given in Table 12.9.

12.4.2 Minerals and Ores of Magnesium

Magnesium in nature exists in the form of various minerals: carbonates [MgCO_3 , (Ca, Mg) CO_3], chlorides ($\text{MgCl}_2 \cdot 6\text{H}_2\text{O}$, etc.), sulfates ($\text{MgSO}_4 \cdot \text{H}_2\text{O}$, etc.), silicates ($3\text{MgO} \cdot 2\text{SiO}_2 \cdot 2\text{H}_2\text{O}$, etc.), magnesium oxide hydrate $\text{Mg}(\text{OH})_2$, periclase MgO ,

Fig. 12.15 Equilibrium diagram of MgO–SiO₂ system

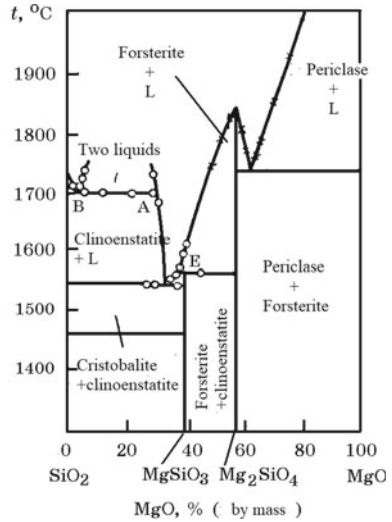


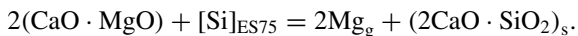
Table 12.9 Physicochemical properties of some magnesium compounds

Compound	$-\Delta H_{298}^{\circ}$, kJ/mol	$-\Delta G_{298}^{\circ}$, kJ/mol	S_{298}° , J/(mol K)	$C_{P, 298}^{\circ}$, J/(mol K)
MgO	601.5	568.7	26.95	37.24
Mg(OH) ₂	923.8	832.6	63.1	76.9
MgS	351.12	338.6	50.28	45.5
MgCO ₃	1110.06	1011.1	65.32	76.0
Mg ₂ Si	79.2	76.7	67.8	68.4
MgSiO ₃	1547.4	1458.8	67.8	81.8
Mg ₂ SiO ₄	2169.8	2048.2	95.1	118.6

etc. The world production of MgO is based on calcining MgCO₃, extraction from sea water or from brines; the roasting product contains 75–96% MgO, and more than 97% from seawater and brines.

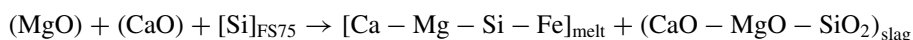
12.4.3 Technology for Producing Magnesium and Magnesium Ferroalloys

The main amount of pure magnesium is obtained by electrolysis of chloride compounds. Known methods for producing magnesium by reducing magnesium from MgO or calcined dolomite CaO · MgO in vacuum using silicon (ferrosilicon). The vacuum-thermal process is described by the total reaction

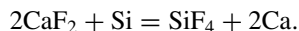


In the reaction zone, Mg evaporates, and in the cooled zone of the metal retort (Fig. 12.16) condenses. After cooling the retort, magnesium is extracted as druse. Along with silicon, aluminum can be used as a reducing agent.

A silicothermic method for the production of magnesium in the form of ferrosilicon-magnesium by reducing magnesium with silicon ferrosilicon under normal pressure in ferroalloy arc furnaces has been developed and mastered. The mixture consists of magnesite, lime, dolomite, ferrosilicon and fluorspar (CaF_2). The process in general can be represented by the scheme:



The maximum Mg content in the alloy (2.3–2.6%) is obtained when the ratio in the mixture is $\text{MgO}:\text{CaO} = 0.3$ and $\text{CaF}_2 : (\text{CaO} + \text{MgO}) = 0.1\text{--}0.15$. Excess fluorspar in the mixture leads to a loss of silicon due to the reaction



Despite the mastery of the above methods for producing pure Mg and a complex alloy of the Ca–Mg–Si–Fe system, in practice ferrosilicon magnesium is obtained by dissolving ingot magnesium obtained by the electrolytic method in liquid ferrosilicon. A combined technology has been developed for the production of magnesium-containing ferrosilicon. At the first stage, the alloy with 2.2–2.4% Mg is melted in the

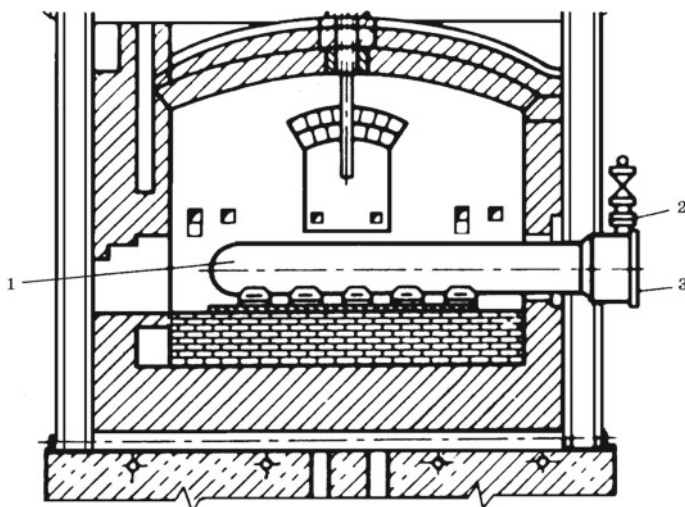


Fig. 12.16 Scheme of the installation for producing magnesium silicothermic process in vacuum retort. 1—retort; 2—crane; 3—cover

arc furnace using a mixture (FS65, FS75, CaO, magnesite grains), and at the second stage, the Mg content is increased to 6–7% by dissolution of pigment magnesium in this alloy. The alloy contains, %: 5–7 Mg; 53–65 Si; Fe is the rest. The disadvantage of this method is the large waste (loss) of magnesium, the light effect and intense smoke formation.

12.5 Beryllium

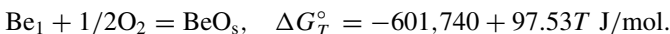
Metal beryllium was first obtained in 1828 by the German chemist F. Wöhler and the French chemist A. Bussy independently. Beryllium is a rare element; its average content in the earth's crust is 6×10^{-4} %. Beryllium is widely used in various branches of technology and industry. In metallurgy, it is used in the smelting of copper-beryllium bronzes, alloys with aluminum, magnesium and other non-ferrous metals, for deoxidation and alloying of steel and cast iron. Due to the coarse-crystalline structure, pure iron-beryllium structural alloys have not been used. However, in combination with nickel and chromium, it is possible to obtain chromium-gel steels (12% Cr, 11% Ni, 1% Be), which have high strength and hardness at elevated temperatures. Beryllium is one of the best materials for neutron reflectors in nuclear reactors. Beryllium oxide is used for the manufacture of particularly high refractory products (the melting point of BeO is 2810 K).

12.5.1 Properties of Beryllium and Its Compounds

Atomic number of beryllium 4, atomic mass 9.01, density 1.85 g/cm³, melting point 1284 °C, boiling point 2450 °C. In the compounds, beryllium is divalent and chemically very active. Beryllium is a polymorphic metal; it exists as α -Be with an hcp lattice in the range of 273–1523 K and β -Be with a bcc lattice in excess of 1523 K.

In the **Be-Fe binary system**, Be₇Fe, Be₅Fe, Be₂Fe, BeFe₃ compounds, and iron-based phases have a rather wide homogeneity region. The most refractory is iron beryllide Be₂Fe ($t_m = 1490$ °C). A number of intermetallic phases are also formed in the **Be-Ni system**, including BeNi ($t_m = 1600$ °C).

In the **Be-O system**, BeO oxide is formed by the reaction



BeO is stable in vacuum, a reducing atmosphere, and rapidly evaporates in the presence of H₂O. The temperature dependence of BeO vapor pressure is described by the equation

$$\lg P_{\text{tot}} \text{ (MPa)} = 10.156 - 33,240/T.$$

In the **Be–C system**, Be_2C carbide is formed, which, when heated in an argon atmosphere (0.1 MPa), dissociates at a temperature of 2473 K.

Unlike other alkaline earth metals, beryllium with silicon does not form silicides, and the **Be–Si system** has the form of a simple eutectic diagram. The eutectic contains 60.5% Si, and $t_{\text{ev}} = 1490$ °C. There are no intermetallic compounds in the **Be–Al system**, which also has the form of a simple eutectic diagram. The eutectic contains 99.15% Al, and $t_{\text{eu}} = 646$ °C.

12.5.2 Beryllium Minerals and Ores

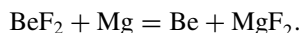
Of the known beryllium minerals, $3\text{BeO} \cdot \text{Al}_2\text{O}_3 \cdot 6\text{SiO}_2$ beryl, $\text{Be}_4\text{Si}_2\text{O}_7(\text{OH})_2$ bertrandite, and Al_2BeO_4 chrysoberyl are of industrial importance. Other minerals rich in beryllium: BeSiO_4 phenakite, helvite $(\text{Mn, Fe, Zn})_4\text{Be}_3\text{Si}_3\text{O}_{12}\text{S}$, and beryllite $(\text{Ba, Be})_2\text{Si}_2\text{O}_7$ are of low abundance.

World reserves of beryllium ores are estimated at 380 thousand tons by the content of beryllium.

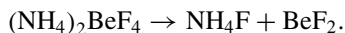
There are a number of methods for extracting beryllium from industrial beryllium ores containing 10–13% BeO , 16–19% Al_2O_3 , 64–70% SiO_2 , 1–2% alkali metal oxides, 1–2% iron and other metal oxides. The essence of the fluoride method consists in roasting beryl with Na_3FeF_6 at 750 °C in order to convert beryllium into a water-soluble Na_2BeF_6 compound. In the subsequent stages, technical grade beryllium hydroxide is isolated, which is then dissolved in sulfuric acid. By treatment with aluminum, high-purity beryllium hydroxide $\text{Be}(\text{OH})_2$ is precipitated from the solution. In the sulfate method, beryllium ore is melted at 1625 °C and tempered in water to obtain amorphous glass, which is heated in rotary kilns to 900–1000 °C, and then ground to a fraction <127 μm , mixed with concentrated sulfuric acid and leached at 200–300 °C. As a result of further multistage processing of the solution, $\text{Be}(\text{OH})_2$ is isolated.

12.5.3 Beryllium Production Technology

Metallic beryllium is obtained by reducing beryllium fluoride BeF_2 with magnesium by reaction



Beryllium fluoride is obtained from $\text{Be}(\text{OH})_2$ after transferring it to a solution with the release of $(\text{NH}_4)_2\text{BeF}_4$ and subsequent decomposition of this salt in an induction furnace with a graphite crucible by the reaction



The technology for producing beryllium is as follows. A mixture of BeF_2 and magnesium is loaded into a graphite crucible and heated to $1300\text{ }^\circ\text{C}$. After melting, beryllium and slag containing BeF_2 and MgF_2 are poured into a graphite mold in which the metal solidifies in the form of skulls of various sizes containing up to 97% Be. The extracted beryllium skulls are subjected to further multistage metallurgical and chemical processing in order to obtain structural beryllium.

Beryllium metal can also be obtained by electrolysis of BeCl_2 . Beryllium chloride is obtained by chlorination of BeO in the presence of carbon at $1000\text{ }^\circ\text{C}$. The electrolyte consists of BeCl_2 , alkali metal chlorides and has a melting point of $330\text{--}350\text{ }^\circ\text{C}$. Beryllium in the form of flakes is deposited on a nickel cathode (the anode is graphite). Ingots and castings are obtained from flakes by the method of vacuum arc or electron beam melting. Beryllium is also obtained from powder metallurgy technology.

Beryllium and its compounds are highly toxic substances; therefore, its production and use is associated with strict adherence to safety rules for working with toxic materials.

Chapter 13

Metallurgy of Ferroniobium



Niobium was discovered in 1801 by the English scientist C. Hatchet in a mineral found in Colombia and named by him Columbia. In 1844, the German chemist G. Rose discovered a new element and called it niobium. It was later established that niobium is the same element as Colombia. The niobium content of the earth's crust is $2 \times 10^{-3}\%$.

The main areas of application of niobium and its alloys are rocket science, aviation and space technology, radio engineering, and nuclear energy. Niobium is used for alloying non-ferrous metals. In ferrous metallurgy, niobium is widely used in the form of ferroniobium for microalloying structural steels, low-alloy pipe steels for main oil pipelines, and chromium–nickel stainless steels to prevent intercrystalline corrosion. Niobium lowers the activity of oxygen in iron, at 1600 °C the interaction parameter $e_{O(Fe)}^{Nb} = -0.12$. The minimum oxygen concentration in iron during deoxidation with niobium at 1600 °C is 0.0192% at 1.96% Nb.

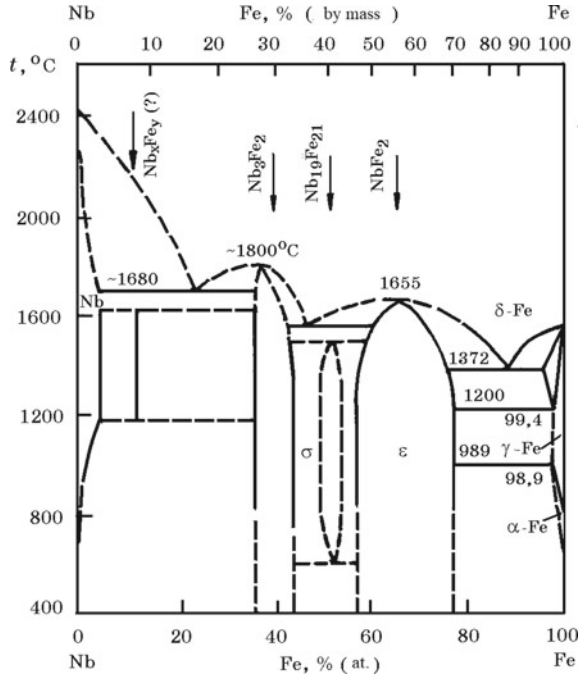
Niobium compounds are also used: Nb₂O₅ oxide (a catalyst in the chemical industry, in the production of refractories and special glasses), nitrides, carbides, and niobates.

13.1 Properties of Niobium and Its Compounds

Niobium is an element of the Vb group of the Periodic system of elements. Atomic number 41, atomic mass 92.90, electron shell configuration 4d⁴5s¹, melting point 2470 °C, boiling point 4927 °C, density 8.57 g/cm³. Pentavalent niobium compounds are most stable, but compounds with oxidation states of 4, 3, 2 and 1 are known.

Nb–Fe system. Niobium and iron in a liquid state form a continuous series of solutions, in the solid state, compounds Nb₃Fe₂, Nb₁₉Fe₂₁, NbFe₂ (Fig. 13.1). Alloys of the ferroniobium type with 50–70% (Nb + Ta) have a melting point of 1620–1580 °C. The heat of formation of NbFe₂ $\Delta H_{298}^{\circ} = 61.45$ J/mol. Solutions of

Fig. 13.1 Equilibrium diagram of Nb–Fe system

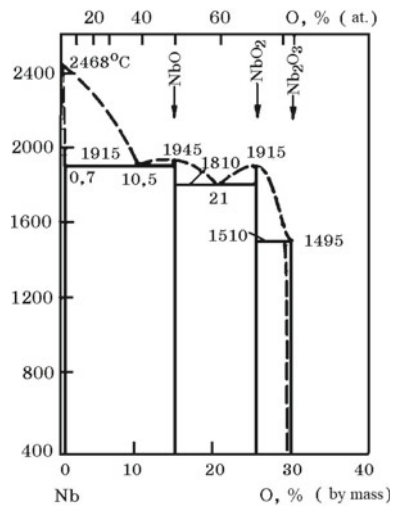


niobium in iron-based melts are characterized by negative deviations from ideal behavior, at 1600 °C $\gamma_{\text{Nb(Fe)}}^{\circ} = 0.2$.

Nb–O system. In this system, stable oxides are formed (Fig. 13.2).

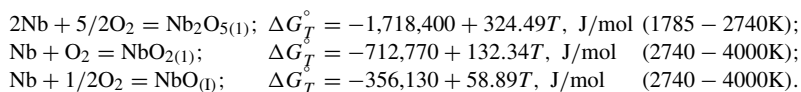
Below are the thermodynamic properties of niobium oxides:

Fig. 13.2 Equilibrium diagram of Nb–O system



Oxide	NbO	NbO ₂	Nb ₂ O ₅
$-\Delta H_{298}^{\circ}$, kJ/mol	419.25	794.2	1897.7
S_{298}° , kJ/(mol K)	45.98	54.34	137.18

The temperature dependence of the Gibbs energy of the reactions of the formation of oxides is described by the equations:



Nb–C system. Thermodynamically strong carbides are formed in the system (Fig. 13.3).

Carbides Nb₂C (5.43–5.83% C) and NbC (11.45% C, density 7.82 g/cm³) are formed by peritectic reactions. The temperature dependences of the Gibbs energy of carbide formation reactions are described by the equations:

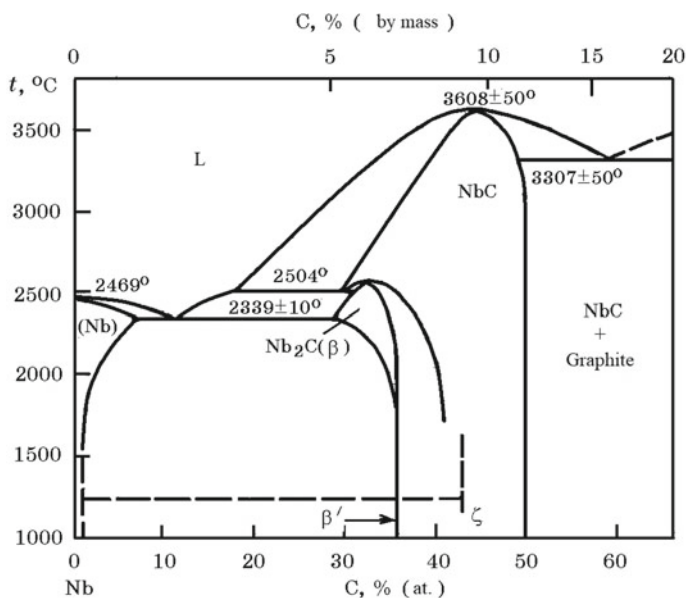
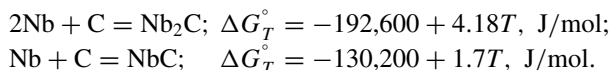
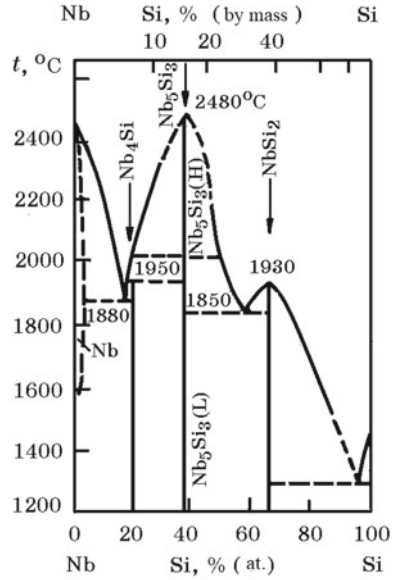


Fig. 13.3 Equilibrium diagram of Nb–C system

Fig. 13.4 Equilibrium diagram of Nb–Si system



The standard carbide enthalpy is NbC $\Delta H_{298}^\circ = -137.94$ kJ/mol, entropy $S_{298}^\circ = 35.03$ J/(mol K), and the carbide Nb₂C $\Delta H_{298}^\circ = -186.01$ kJ/mol, $S_{298}^\circ = 63.95$ J/(mol K).

Nb–Si system. Niobium with silicon forms the silicides Nb₄Si, Nb₅Si₃, NbSi₂ (Fig. 13.4), the thermodynamic properties of which are given below:

Silicides	Nb ₄ Si	Nb ₅ Si ₃	NbSi ₂
$-\Delta H_{298}^\circ$, kJ/mol	87.78	652.1	125.4
Melting temperature, °C	2580	2440	2150

Nb–Al system. Several niobium aluminides are formed in the Nb–Al system: NbAl_3 , Nb_2Al and Nb_3Al (Fig. 13.5).

Nb–P system. Niobium actively interacts with phosphorus, forming thermodynamically strong phosphides NbP (25% P) and NbP_2 (40% P). NbP has a wide region of homogeneity ($\text{NbP}_{0.8-1.2}$).

Nb_2O_5 –CaO system. Several calcium niobates are known: $\text{CaO}\cdot\text{Nb}_2\text{O}_5$, $2\text{CaO}\cdot\text{Nb}_2\text{O}_5$ and $3\text{CaO}\cdot\text{Nb}_2\text{O}_5$ (Fig. 13.6).

Fig. 13.5 Equilibrium diagram of Nb–Al system

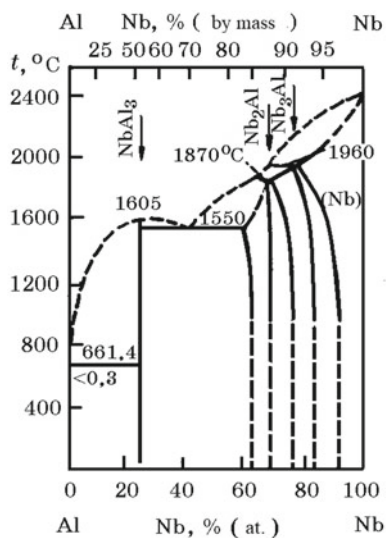


Fig. 13.6 Equilibrium diagram of Nb_2O_5 –CaO system

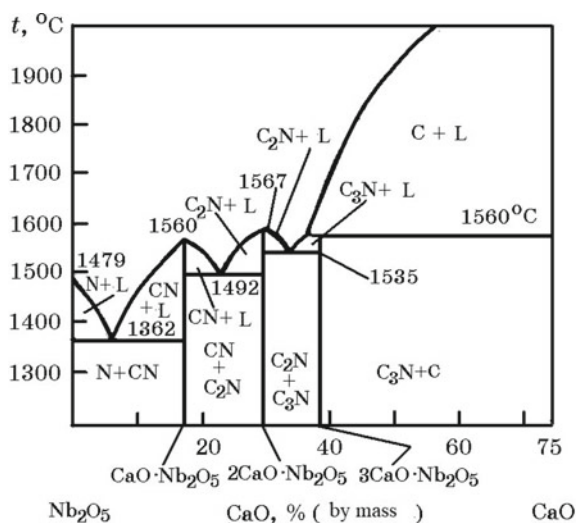


Fig. 13.7 Equilibrium diagram of Nb_2O_5 – SiO_2 system

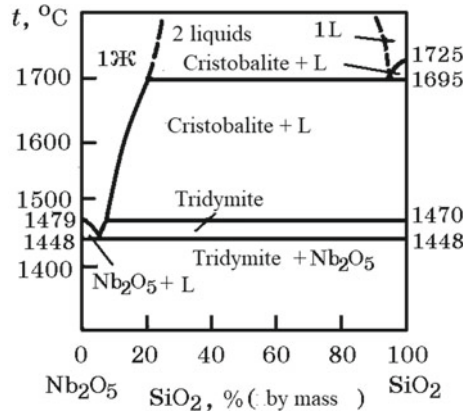
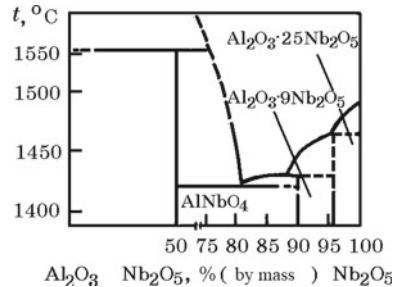


Fig. 13.8 Equilibrium diagram of Nb_2O_5 – Al_2O_3 system



Nb_2O_5 – SiO_2 system. Oxides of Nb_2O_5 and SiO_2 , which are acidic in nature, do not form chemical compounds (Fig. 13.7). Above 1695 °C, there is a large region of two immiscible liquids.

Nb_2O_5 – Al_2O_3 system. The oxides Nb_2O_5 and Al_2O_3 interact with the formation of compounds $\text{Al}_2\text{O}_3 \cdot \text{NbO}$, $\text{Al}_2\text{O}_3 \cdot 9\text{Nb}_2\text{O}_5$ and $\text{Al}_2\text{O}_3 \cdot 25\text{Nb}_2\text{O}_5$ (Fig. 13.8).

13.2 Niobium Minerals and Ores

There is a large group of tantalum niobates minerals, which are natural complex compounds in which niobium and tantalum are complexing agents. The generalized formula of these minerals is $A_n B_m X_p$, where A is the large cations (Ca^{2+} , REM^{3+} , U^{4+} , Th^{4+} , Na^+ , less often Pb^{2+} , Sb^{2+} , Bi^{3+}) and medium (Fe^{2+} , Mn^{2+} , Mg^{2+}) sizes; B is Nb^{5+} , Ta^{5+} , substituted by Ti^{4+} , Sn^{4+} , Fe^{3+} ; X – O^{2-} , OH^- , F^- . Of the more than 130 known minerals of niobium (tantalum), about six are considered industrial. The most important minerals for producing niobium are the minerals that make up niobium ores: columbite (Fe , Mn) $(\text{Nb}$, $\text{Ta})_2\text{O}_6$ (50–67% Nb_2O_5) and pyrochlore (Ca , Na) $_2(\text{Nb}$, Ta , $\text{Ti})_2\text{O}_6(\text{OH}$, $\text{F})$ (40–70% Nb_2O_5). Loparite (Ca , Na , Ce) $(\text{Ti}$, Nb ,

Ta)O₃ (7–20% Nb₂O₅) is of less importance. Loparite is a perovskite (CaTiO₃) rich in niobium and rare-earth metals, in which calcium is replaced by rare-earth metals, and titanium is replaced by niobium and tantalum with the formation of the following minerals: knopite (CeTiO₃), disanalite (Ca, Na, Ce) (Ti, Nb, Fe)O₃ and loparite.

Industrial suitable niobium ores, from which it is economically feasible to obtain niobium concentrates, contain ≥ 0.15 –0.20% Nb₂O₅. In the known richest niobium ores, up to 1–4% Nb₂O₅ is contained. Brazil (84.2% of reserves), Canada (9.8%) and Zaire (4.2%) occupy a leading place in the mineral resource base of niobium.

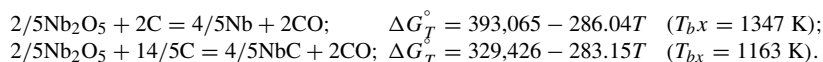
A promising deposit of niobium ore in Russia is Belozimskoye. However, the difficulty in obtaining conditioned concentrates from the ore of this deposit is due to the high phosphorus content and high natural radioactivity.

Using X-ray spectral microanalysis and petrographic studies, the nature of phosphorus in crude concentrates of pyrochlore was studied [1]. It has been established that phosphorus does not form chemically bonded compounds with niobium, but is mainly represented by apatite, which is present in the form of individualized excreta and fine impregnations in niobium minerals—pyrochlore and columbite of varying degrees of ironization. The presence of thin impregnations of apatite in the iron minerals of niobium prevents a sufficiently complete separation of phosphorus and niobium. The unequal magnetic susceptibility of the mineral differences of phosphorus and niobium makes it possible to use the magnetic separation method to isolate enriched niobium concentrate suitable for smelting niobium-based alloys. Non-magnetic tails containing 4% (Nb₂O₃ + Ta₂O₃) and 30–32% P₂O₅, after separation of pyrochlore by other enrichment methods (flotation, triboseparation, etc.) can be used as phosphorus-containing raw materials.

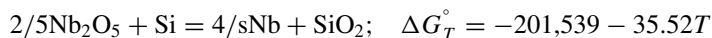
The technology of metallothermic production of niobium alloys from high phosphorus concentrates of the Belozimskoye deposit was developed by converting phosphorus to ferrophosphorus in a special electrometallurgical processing.

13.3 Thermodynamics of Niobium Reduction Reactions

The process of reduction of niobium from Nb₂O₅ with carbon can be represented by the reactions ($T_{b,r}$ —temperature of the beginning of reduction, $\Delta G_T^\circ = 0$):

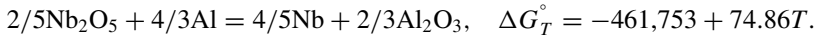


In the reduction of niobium by silicon by reaction

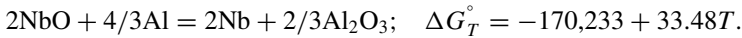


extraction of niobium in the silicothermic process is small, and an alloy containing 50–60% Nb is obtained with a high silicon content (5–8%).

An analysis of the reduction reactions of niobium from aluminum oxides is very important for the development and improvement of aluminothermic processes for producing ferroniobium. The total reaction of the interaction of Nb_2O_5 with aluminum is described by the equation



The thermodynamically most complex stage is the reduction of NbO



In the temperature range 2000–2300 K, aluminothermic reduction of Nb_2O_5 proceeds quite fully, and the extraction of niobium into the alloy reaches 99.8%.

13.4 The Technology for Producing Ferroniobium by Aluminothermic Method

The niobium content in ferroniobium can be from 40 to 65% (Table 13.1). As niobium-containing types of raw materials use technical niobium pentoxide (Table 13.2), as well as niobium concentrates, the actual content of controlled components in technical niobium pentoxide intended for the production of alloying alloys is as follows, %: 81.2–99.5 Nb_2O_5 ; 0.1–1.2 Ta_2O_5 ; 0.02–1.8 SiO_2 ; 0.06–0.9 TiO_2 ;

Table 13.1 Chemical composition of ferroniobium, % (GOST 16773-85)

Grade	Σ (Nb + Ta), no less	Ta	Si	Al	Ti	C	S	P	Quality grade
		No more							
FeNb60	55–65	1.0	1.5	3.0	1.0	0.1	0.03	0.10	Higher
FeNb58	50–65	1.0	2.0	6.0	1.0	0.2	0.03	0.15	Higher
FeNb58 (F)	50–65	–	2.0	6.0	2.0	0.3	0.05	0.40	First
FeNb55C	50–65	–	15.0	4.0	8.0	0.2	0.03	0.30	First
FeNb50C	40–65	–	20.0	6.0	–	0.5	0.05	0.50	First

Table 13.2 Chemical composition of technical niobium pentoxide, %

Grade	$\text{Nb}_2\text{O}_5 + \text{Ta}_2\text{O}_5$, no less	P	S	C	TiO_2	Fe_2O_3	SiO_2	LOI at 600 °C
		No more						
0	95	0.15	0.1	0.10	0.8	2	0.3	1
1	90	0.25	0.1	0.15	1.0	3	0.3	2
2	85	0.40	0.2	0.15	1.0	Not limited	3.0	3

0.09–3.9 Fe₂O₃; 0.05–0.4 P; 0.03–0.1 C; 0.01–0.2 S; ≤0.02 As; ≤0.0006 Pb; ≤0.03 Sn; 0.3–2.5 LOI at 600 °C.

The aluminothermic method for producing ferroniobium has several options: (1) out-of-furnace smelting per block; (2) out-of-furnace smelting with the release of metal and slag; (3) melting in an arc furnace.

Out-of-furnace aluminothermic smelting per block. This method is not widespread, as it has drawbacks, the main of which are the combination of the reduction process and crystallization of metal and slag in one unit, the increased consumption of charge and refractory materials, the high labor costs of lining, dismantling melting furnaces and cleaning metal from refractories and slag. The one-time use of the smelting furnace during smelting to the unit is associated with the movement of each furnace with liquid smelting products from the smelting chamber to the cooling section of the workshop or the movement of the exhaust hood and bunkers for loading the charge to the stationary smelting units.

Out-of-furnace smelting with the release of metal and slag. Out-of-furnace smelting with the release of metal and slag significantly expanded the capabilities of the metallothermic method for producing alloys with a high melting point, in particular, ferroniobium. The smelting of ferroniobium grades FeNb60, FeNb58, etc. by out-of-furnace method from technical niobium pentoxide is carried out in an inclined smelter lined with magnesite brick. The heat of the exothermic reaction is enough to carry out the process. The mixed charge from the hopper enters the trough into the melting unit mounted on the trolley. The mixture consists of 100 kg of niobium pentoxide, 52–60 kg of aluminum, 38–40 kg of iron pellets, 20 kg of iron oxide, 30 kg of lime and 0.1 kg of nitrate (NaNO₃). Melting is carried out with a lower ignition at a charge penetration rate of 160–180 kg/(m² min). The mass of industrial smelting is calculated on 1000–1200 kg of Nb₂O₅. The discharge of metal and slag is carried out by tilting the smelter into a cast iron not lined mold, at the bottom of which an ingot of metallic chromium 200–220 mm thick is laid. The melt is cooled in the mold for 2.5 h; then, it is disassembled and after an additional exposure for 2 h, the metal and slag are sent for cutting. For 1 base t of alloy (50% Nb) is consumed, kg: 758 niobium pentoxides (100% Nb₂O₅); 385 aluminum powder; 275 iron ore; 86 lime; 31 magnesite powder. The dump slag of ferroniobium contains, %: 70–75 Al₂O₃; 9–12 CaO; 3–6 MgO; 0.3–0.5 Nb₂O₅, they are a valuable raw material for the production of alumina, refractories, cement, etc. During crystallization of slag, the mineral phases MgO·Al₂O₃ are successively formed (10–15%); CaO·₂Al₂O₃ (75–85%); (Ca, K,Na)·Nb₂O₅(O, F) (0.5–3%). The properties of this slag after grinding correspond to the properties of high-alumina refractory cements.

Arc furnace melting. When processing low-grade niobium concentrates, electric furnace smelting is economically justified, which can be carried out according to the following options: (1) melting aluminum in an electric furnace with subsequent loading of the ore–flux part of the charge; (2) the melting of the ore–flux part of the charge with subsequent loading of aluminum powder, including with a drawback (for the selective reduction of part of the oxides); (3) the melting of part of the ore–flux components of the charge, followed by the melting of the remaining ore part in a mixture with aluminum powder when the furnace is turned off; (4) a single-stage

joint melting of the mixed charge in an electric furnace to make up for the heat that is missing for the normal course of the process, including the subsequent casting of the resulting alloy. The first method is characterized by low productivity of the furnace. In this process, especially in the initial period, the interaction of oxides with aluminum is not regulated. The degree of extraction of niobium does not exceed 70–80%, aluminum loss as a result of burning reaches 30–40%.

The second method has found industrial application for the selective reduction of niobium ores containing high concentrations of tin (2% SnO_2) and phosphorus (0.15% P_2O_5). As a result of smelting, a slag containing 47% ($\text{Nb}_2\text{O}_5 + \text{Ta}_2\text{O}_5$) is obtained; 0.03% Sn and 0.04% P_2O_5 and a metal containing 2.3% Sn; 0.06% P; 3.3% (Nb + Ta + Zr + Ti). This option of smelting most fully combines the advantages of aluminothermic reduction with the possibility of using electricity to intensify the process and smelting a mixture containing the necessary amount of flux (lime) to increase the extraction of niobium. Then the rich niobium slag in a mixture with lime is melted in an arc furnace, which contains molten iron scrap. Commodity alloy contains, %: 66.2 Nb; 4.9 Ta; 0.02 Sn; 0.03 P; 0.2 Al; 1.0 Si; 2.3 Mn; 0.004 S, final slag—4.6% (Nb + Ta). The extraction of niobium in the alloy in the second stage is 95.2%; end-to-end recovery in two stages 85%.

Industrial single-stage smelting of ferroniobium from pyrochlore concentrates is carried out in an arc steel-smelting furnace, lined with magnetite brick. After heating the bath, an iron-thermal mixture consisting of 1000 kg of non-enriched iron ore, 350 kg of secondary aluminum and 200 kg of lime is melted under arcs. The charge of industrial smelting per 100 kg of pyrochlore concentrate includes 28–33 kg of secondary aluminum powder, 3–10 kg of iron ore and 5–12 kg of iron die cutting. The first melting after heating and washing the furnace is carried out at a voltage of 140 V, the duration of melting with 1200 kg of concentrate is 50 min, the second melting with 1500 kg of concentrate—70 min, the subsequent melting with 1700 kg of concentrate—90 min. A detachable cast iron mold for receiving metal and slag is prepared in the process of the previous melting: A part of the slag is poured onto the bottom of the mold lined with magnesite brick, which, cooling down during the next melting, forms a skull on the walls necessary to increase the durability of the mold and obtaining a clean surface of the ingot. Dismantling of the mold is carried out after 2.5 h after discharge, after another 2 h, the metal and slag are discharged onto a cooling stand for cutting.

Ferroniobium has the following chemical composition, %: 56–62 (Nb + Ta); 10.7–12.5 Si; 2–6 Al; 3–8 Ti; 0.10–0.25 P; 0.05–0.15 C; 0.004–0.5 S. To reduce the silicon content of ferroniobium after discharge of the waste slag and formation of oxidative slag (from niobium concentrate and lime), oxygen can be purged, but this reduces the extraction of niobium.

Reference

1. Lyakishev NP, Gasik MI, Anelok LI, Gladkikh VA (1995) Study of the nature of phosphorus in niobium-containing concentrates. *Metally* 2:3–6 (in Russian)

Chapter 14

Ferrosilicozirconium and Ferro-Alumino-Zirconium



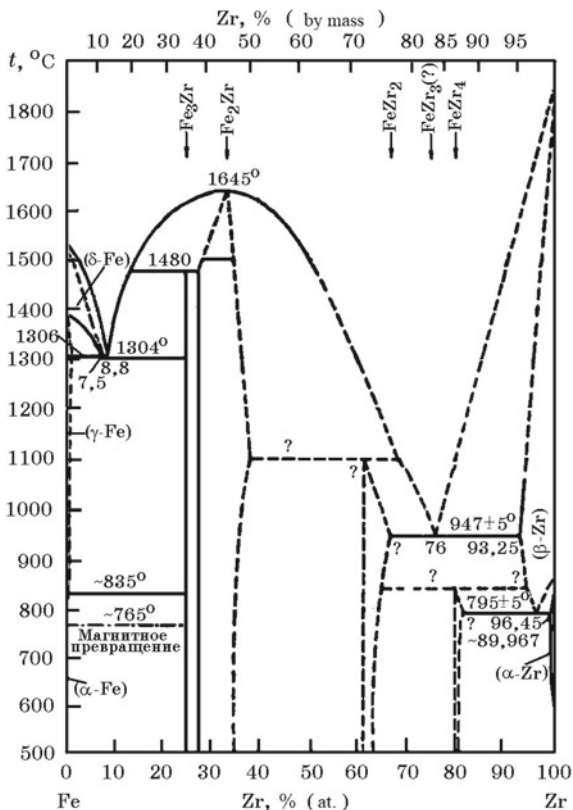
Powdered zirconium was obtained in 1824 by J. Berzelius and plastic zirconium in 1925 by A. van Arkel and I. de Boer. The zirconium content in the earth's crust is 1.7×10^{-2} %. Zirconium-based alloys purified from hafnium are used as structural materials in nuclear reactors. Zirconium is used for alloying a number of alloys based on magnesium, titanium, nickel, molybdenum, niobium and other metals, which are used as structural materials, for example, for aircraft. Windings of superconducting magnets are made from alloys with niobium. In cermet materials, the metal base is zirconium, and the ceramic base is ZrO_2 oxide. In ferrous metallurgy, zirconium is used as a deoxidizer and a microalloying additive in steelmaking. The minimum concentration of oxygen in iron during deoxidation with zirconium at 1600 °C is 2.48×10^{-4} % at 0.104% Zr. Zirconium significantly reduces the activity of oxygen in iron; at 1600 °C, the interaction parameter = 2.1. In steelmaking and foundry, zirconium refractoriness is used.

14.1 Properties of Zirconium and Its Compounds

Zirconium—an element of the IVb group of the Periodic system of elements. Atomic number 40; atomic mass 91.22, electron shell configuration $4d^25s^2$, density 6.49 g/cm³, melting point 1855 °C and boiling point 4350 °C. Zirconium is characterized by oxidation state 4; lower oxidation states 2 and 3 are known for its compounds with halogens. Zirconium exists in two modifications: α -Zr with a hexagonal lattice (density 6.5107 g/cm³) and β -Zr with a cubic lattice; α -Zr \leftrightarrow β -Zr phase transition temperature is 863 °C.

Zr–Fe system. In the Zr–Fe system, there are chemical compounds Zr_4Fe , Zr_3Fe , Zr_2Fe , $ZrFe_2$ and $ZrFe_3$ (Fig. 14.1). The most refractory is the $ZrFe_2$ compound. The value of the minimum integral enthalpy of formation of binary alloys of the Zr–Fe system at 47% (at.) Zr is $-(15 \pm 0,4)$ kJ/mol. Zirconium solutions in iron-based melts

Fig. 14.1 Equilibrium diagram of Zr-Fe system



are characterized by significant negative deviations from ideal behavior at 1600 °C $\gamma_{Zr(Fe)}^{\circ} = 0.037$.

Zr-O system. Oxides ZrO_2 and ZrO are known (Fig. 14.2). For the reaction $Zr + O_2 = ZrO_2$

$$\Delta G_T^{\circ} = -1099758 + 177.9T, \text{ J/mol} \quad (1773 - 2273 \text{ K}).$$

Zirconium dioxide is a polymorphic oxide. The monoclinic form of α - ZrO_2 is stable at room temperature; above 1205 °C, α - ZrO_2 turns into the tetragonal form of β - ZrO_2 , which is stable up to 2330 °C. At temperatures above 2330 °C, β - ZrO_2 passes into the cubic modification of γ - ZrO_2 . For α - $ZrO_2 \leftrightarrow \beta$ - ZrO_2 transformations, the presence of hysteresis is characteristic, i.e., mismatch in the temperature ranges of the direct and reverse transition. For crystals of the same purity, the temperature of the $\rightarrow \beta$ transition varies from 1160 to 1190 °C, and for the $\beta \rightarrow \alpha$ transition for the same crystals, it ranges from 1070 to 1100 °C. The enantiotropic (i.e., reversible) transformation of $\gamma \leftrightarrow \beta$ occurs at 2330 °C with a minimum hysteresis of 30°.

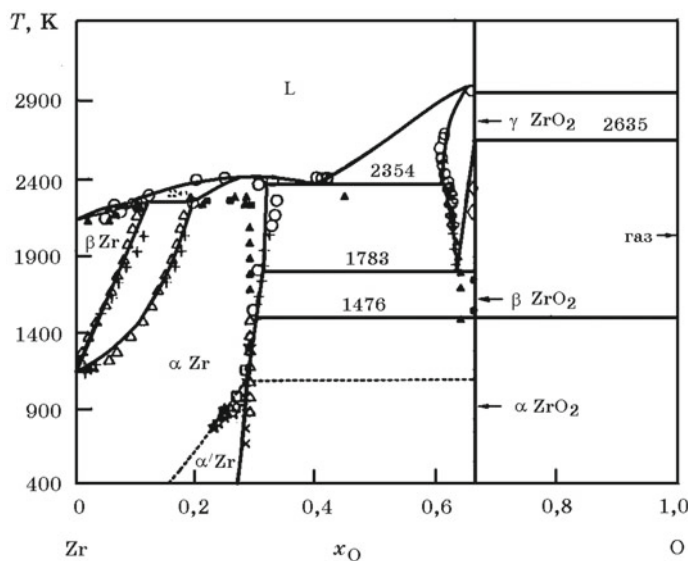


Fig. 14.2 Equilibrium diagram of Zr–O system

Zr–C system. Zirconium forms ZrC carbide with carbon (Fig. 14.3) with a melting point of 3530 °C and a density of 6.66 g/cm³

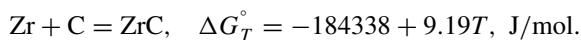


Fig. 14.3 Equilibrium diagram of Zr–C system

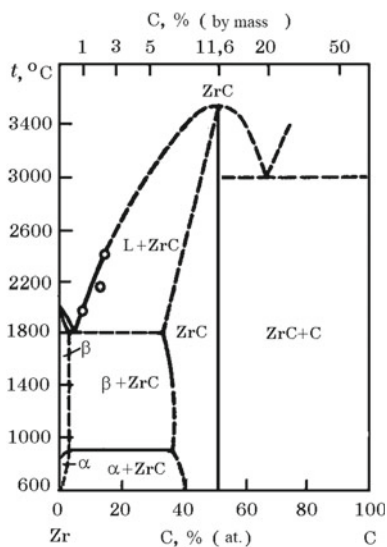
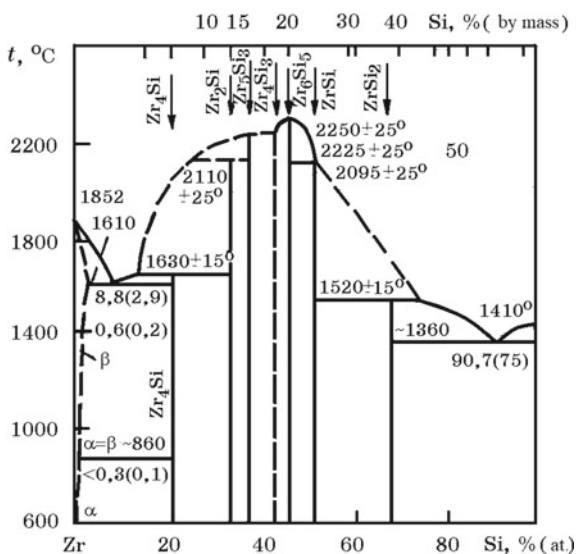


Fig. 14.4 Equilibrium diagram of Zr–Si system



The enthalpy of ZrC formation $\Delta H_{298}^{\circ} = -199.86$ kJ/mol, entropy $S_{298}^{\circ} = 33.14$ J/(mol K).

Zr–Si system. There are a number of zirconium silicides (Fig. 14.4). The most thermodynamically strong is Zr_6Si_5 ($\Delta H_{298}^{\circ} = -841.55$ kJ/mol), the melting point is 2250 °C. Less than 0.2% Si dissolves in zirconium; no zirconium is found in the solution in silicon.

Zr–Al system. Zirconium aluminides are numerous (Fig. 14.5). The most strong compounds in this system are $ZrAl_3$, $ZrAl_2$ and Zr_3Al_2 with a melting point of 1580, 1645 and 1595 °C, respectively. The solubility of aluminum in α -Zr is 3.5%, aluminum in β -Zr is dissolved in an amount of 0.14%.

ZrO₂–SiO₂ system. In the ZrO₂–SiO₂ system, one ZrO₂·SiO₂ compound is formed (Fig. 14.6). The zircon mineral ZrO₂·SiO₂ is widespread in nature, in which a certain amount of zirconium can be replaced by hafnium and thorium. Zircon usually refers to alluvial deposits, where it is associated with other stable minerals.

ZrO₂–Al₂O₃ system. The equilibrium diagram of the ZrO₂–Al₂O₃ system has a simple eutectic form (Fig. 14.7).

ZrO₂–CaO system. In the ZrO₂–CaO system, CaZrO₃ and CaZr₄O₉ compounds are formed, as well as a series of CaO solid solutions in ZrO₂ of monoclinic, tetragonal and cubic crystal structures (Fig. 14.8).

14.2 Zirconium Minerals, Ores and Concentrates

Zirconium is a rare element. It is part of many rocks, but its concentration is low. The most common minerals are zircon (ZrO₂·SiO₂), baddeleyite (ZrO₂) and eudialyte [Na₄(Ca,Ce,Fe²⁺)₂ZrSi₆O₁₇](OH,Cl₂). Two minerals—zircon and baddeleyite—are

Fig. 14.5 Equilibrium diagram of Zr–Al system

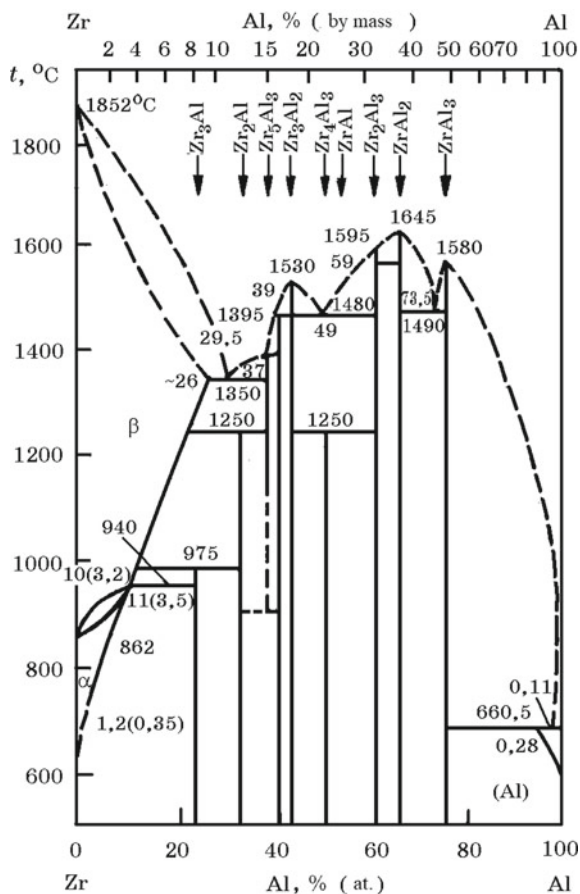
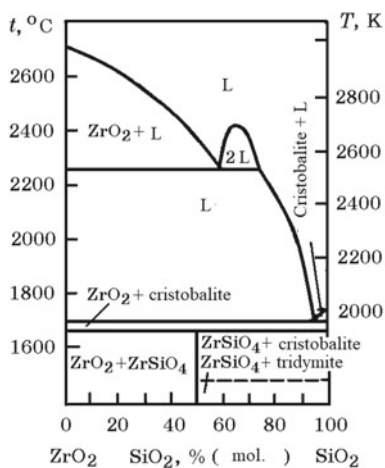


Fig. 14.6 Equilibrium diagram of ZrO₂–SiO₂ system



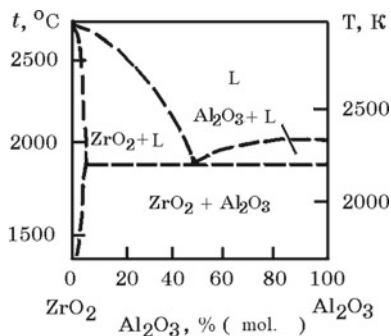


Fig. 14.7 Equilibrium diagram of ZrO_2 - Al_2O_3 system

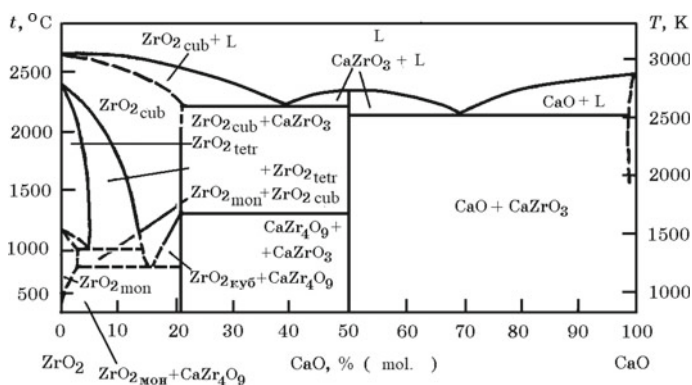


Fig. 14.8 Equilibrium diagram of ZrO_2 - CaO system

of industrial importance. The vast majority of zircon is mined from placer deposits. The composition of the obtained zirconium concentrates is given in Table 14.1.

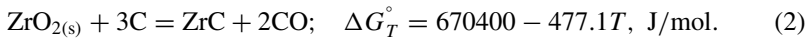
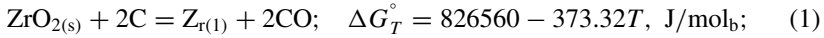
Table 14.1 Chemical composition of zircon concentrates, % (GOST 4882-74)

Grade	ZrO ₂	Fe ₂ O ₃	TiO ₂	Al ₂ O ₃	SiO ₂
CZP ^a	65	0.09	0.03	1.8	Remain
CZZ-1 ^a	65	0.1	0.4	2.0	Remain
CZZ-2 ^a	60	—	—	—	Remain

^aThe content of other oxides for the grades of KCP and KTsZ-1: 0.1% CaO; 0.1% MgO; 0.15% P₂O₅

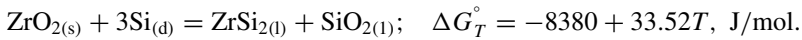
14.3 Thermodynamics of Zirconium Reduction Reactions

The process of carbon reduction to obtain pure zirconium and its carbide is described by the reactions



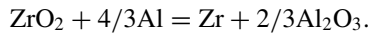
The theoretical temperature of the onset of reactions (1) and (2) is 1940 and 1405 °C, respectively; therefore, the reduction of zirconium from oxides with carbon always occurs to ZrC carbide, and not to pure zirconium.

The reaction of reduction of zirconium from ZrO₂ with silicon has the form



Due to the lower chemical affinity of silicon to oxygen compared with zirconium, not pure zirconium is produced, but melts of zirconium silicides.

The reaction of ZrO₂ with aluminum takes the form



This reaction is basic in the production of ferro-alumino-zirconium.

14.4 The Technology for Producing Ferrosilicozirconium by Aluminothermic Method

Produced ferrosilicozirconium must satisfy the chemical composition requirements listed in Table 14.2.

Table 14.2 Chemical composition of ferrosilicozirconium, %

Grade	Zr	Al	C	P	S	Cu	Si:Zr
	Not less	No more					
FeSiZr50	45	9.0	0.2	0.14	0.02	3.0	0.55
FeSiZr40	38	7.5	0.2	0.15	0.02	3.0	1.1
FeSiZr35	35	6.0	0.2	0.15	0.02	3.0	1.3
FeSiZr30	28	6.0	0.4	0.20	0.04	3.0	1.5
FeSiZr25	20	5.0	0.5	0.25	0.04	3.5	1.7

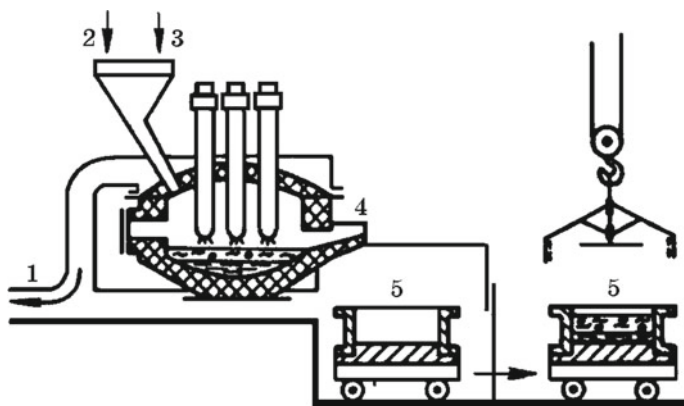


Fig. 14.9 Technological scheme of units for producing ferrosilicocirconium, 1—gas exhaust path; 2, 3—supply of material; 4—arc furnace; 5—mold

Ferrosilicocirconium is smelted by the aluminothermic method using fluxes (lime and fluorspar) or non-flux melting (flux-free process) with the simultaneous production of two products—ferrosilicocirconium and zircon electrocorundum. To ensure the *thermality* of process and the introduction of iron into the alloy, magnetite, low-phosphorous iron ore (>60% Fe) is used. Rich ore with silica content <7% is more preferred. The ore has a particle size of up to 3 mm. To reduce zirconium, a powder of primary or secondary aluminum is used (depending on the requirements for impurities in the alloy). The technology involving the production of zircon electrocorundum is more effective.

Ferrosilicocirconium is smelted in an electric furnace on a block or with the release of metal. The technological scheme of units in the production of ferrosilicon zirconium in an electric furnace with the separation of melting into two periods and the release of the melt is shown in Fig. 14.9.

The steelmaking type furnace with a 1 MV·A transformer has a carbon lining of the hearth of blocks or hearth mass, which is coked for 8–10 h under current with periodic shutdown of the furnace. The mixture is calculated for obtaining an alloy with a zirconium concentration of 50–54%. The melting indices of ferrosilicocirconium with the release of the melt and the use of secondary aluminum per 1 ton of alloy are as follows. Consumption of materials, kg: 1094 zircon concentrate (60% ZrO₂); 542.2 secondary aluminum powder; 423.2 lime; 65.0 ferrosilicon FS75; 114.0 iron ore; 24.0 nitrate. Electricity consumption is 1506 kWh/t. Extraction of zirconium is 82.3%. The average mass of smelting is 1283 kg. The resulting ferrosilicocirconium has a chemical composition, %: 50–51 Zr; 26–27 Si; 5–8 Al; 0.1–0.13 C. Slag composition, %: 7–9 ZrO₂; 54–56 Al₂O₃; 28–30 CaO; 0.5–2.5 SiO₂; 1.3–1.6 MgO and 0.2–0.5 FeO. Slags have the following mineral composition 10–15% MgO·Al₂O₃; 60–70% CaO·2Al₂O₃; 10–15% ZrO₂; 4–5% CaO·Al₂O₃ + 2CaO·Al₂O₃·SiO₂.

The melting of ferrosilicocirconium with the simultaneous production of zirconium electrocorundum (Table 14.3) is a one-step process.

Table 14.3 Chemical composition of zircon electrocorundum, %

Grade ^a	ZrO ₂	SiO ₂	CaO	MgO	Fe _{tot}
	No less	No more			
ZrC-35	35	2.5	2	2	2
ZrC-30	30	3.0	2	2	2
ZrC-25	25	3.5	2	2	2
ZrC-20-1	20	1.5	1	1	1
ZrC-20-2	20	3.5	3	3	2

^aAl₂O₃—basis

The charge weighing 2100–2400 kg includes zircon concentrate, aluminum powder from secondary aluminum, ferrosilicon and iron ore. Lime is not introduced into the mixture. Burden materials should contain a minimum amount of calcium and magnesium oxides, passing into electrocorundum and reducing the hardness of abrasive products obtained from zirconium electrocorundum. The composition of the charge is determined by the brand of electrocorundum: With a decrease in the amount of aluminum powder, the degree of reduction of zirconium decreases, the ZrO₂ content in electrocorundum increases, and the concentration of zirconium in the alloy decreases (Table 14.4). Melting is carried out in steelmaking electric furnace with carbon lining. After the melting of 2/3 of the mixture, the resulting

Table 14.4 Composition of the charge and the chemical composition of the metal and zircon electrocorundum

Parameter	Brand of corundum		
	ZrC-20	ZrC-30	ZrCK-15
<i>Charge composition, kg</i>			
Concentrate	100	100	100
Iron ore	20	20	20
Secondary aluminum	48.0–52.5	40.0–43.3	38.0
Ferrosilicon FeSi75ferrosilicon FeSi75	0–8.0	0–12.0	–
Estimated mass of metal, kg	49–54	48–57	40
<i>Metal content, %</i>			
Zr	42.8–47.2	34.9–40.7	40.6
Si	25.5–31.0	29.5–36.7	30.2
Al	3.1–6.2	1.2–2.5	1.8
Estimated weight of electrocorundum, kg	117–119	110	110–112
<i>The chemical composition of electrocorundum, %</i>			
ZrO ₂	25.4–26.4	33.2–34.1	38.8
Al ₂ O ₃	68.5–70.5	60.4–68.5	36.4
SiO ₂	1.2–1.6	1.7–3.1	1.8

electrocorundum is poured into a metal mold. At the end of the smelting, part of the slag (electrocorundum) is discharged to the bottom of another mold and, after cooling (after 3 min), metal and slag are discharged.

14.5 The Technology for Producing Ferro-Alumino-Zirconium by Aluminothermic Method

The composition of ferro-alumino-zirconium is given in Table 14.5. The initial components used are materials: zirconium dioxide (technical), zircon concentrate, iron oxides (in the form of iron ore pellets and scale), aluminum, sodium nitrate and lime (Table 14.6).

The aluminothermic process is characterized by a complex set of physicochemical interactions. The thermal impulse to the beginning of the aluminothermic process gives the reaction



Table 14.5 Chemical composition of ferro-alumino-zirconium, % (TU 14-5-40-84)

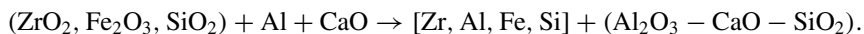
Grade	Zr	Al	Si	C	H	S	Ni
	No less		No more				
FeAlZr18	18	18	3.5	0.08	0.08	0.008	0.4
FeAlZr15	15	18	3.0	0.20	0.15	0.01	0.4

Note Fe—the rest

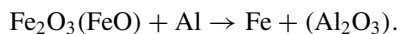
Table 14.6 Composition of the mixture for the smelting of ferro-alumino-zirconium (composition, %: 22 Zr; 18 Al; 4.3 Si)

Component	The mass of the components of the charge, kg			
	Ignition	Ore recovery	Ore smelting	Total
Zirconium dioxide	–	480	–	480
Zirconium concentrate	150	–	–	150
Mill scale	20	400	180	600
Iron ore pellets	–	200	–	200
Sodium nitrate	35	–	–	35
lime	40	350	100	490
Aluminum powder	90	590	80	760
Total	335	2050	360	2715

and the formation of the metal phase is due to the development of a number of reactions, which in general are represented by the scheme:



At the final stage of smelting, a mixture consisting of iron oxide, lime and aluminum powder is fed to the melt in the bathtub of the furnace. The chemistry of this process in general can be described by the reaction



In parallel with the accumulation of the metal phase, the processes of formation of the slag phase are going on, these processes are very dynamic. The slag phase at the end of the smelting is a multicomponent oxide melt.

Chapter 15

Ferroaluminum and Silicoaluminum



Aluminum was first obtained in 1854 by the French chemist A. E. Saint-Clair DeWillemin reduction of Na_3AlCl_6 double chloride with sodium metal. In terms of prevalence in nature, aluminum occupies the third place after oxygen and silicon and the first among metals. Its content in the earth's crust is 8.8%. Aluminum combines a very valuable range of properties: low density, high thermal and electrical conductivity, high ductility and good corrosion resistance. The combination of physical, mechanical and chemical properties of aluminum determines its widespread use in all areas of technology, especially in the form of alloys. In electrical engineering, aluminum successfully replaces copper. Ultra-pure aluminum is used in the manufacture of electric capacitors and rectifiers. Aluminum is used to protect metal surfaces from atmospheric corrosion. Aluminum is one of the most common alloying additives in alloys based on copper, magnesium, titanium, nickel, zinc and one of the main deoxidizing agents for steel and alloys based on iron. Aluminum significantly reduces the activity of oxygen in liquid iron, at 1600 °C the interaction parameter $e_{O(\text{Fe})}^{\text{Al}} = -1.17$. The minimum concentration of oxygen in iron during deoxidation with aluminum at 1600 °C is $1.35 \times 10^{-4} \%$ at 0.254% Al.

15.1 Properties of Aluminum and Its Compounds

Aluminum is an element of the IIIa group of the Periodic Table. Atomic number 13, atomic mass 26.98, configuration of the outer electron shell $3s^2 3p^1$, density 2.69 g/cm^3 , melting point 660 °C, boiling point 2452 °C. The most stable compounds are trivalent aluminum, but compounds with oxidation states of 2 and 1 are known.

Al-Fe system. The state diagram of the Al-Si system is shown in Fig. 15.1. With solid iron, aluminum forms the aluminides FeAl_6 , FeAl_3 , Fe_2Al_6 , FeAl_2 and Fe_3Al . Aluminum solutions in iron-based melts are characterized by significant negative deviations from ideal behavior, at 1600 °C $\gamma_{\text{Al}(\text{Fe})}^\circ = 0.049$.

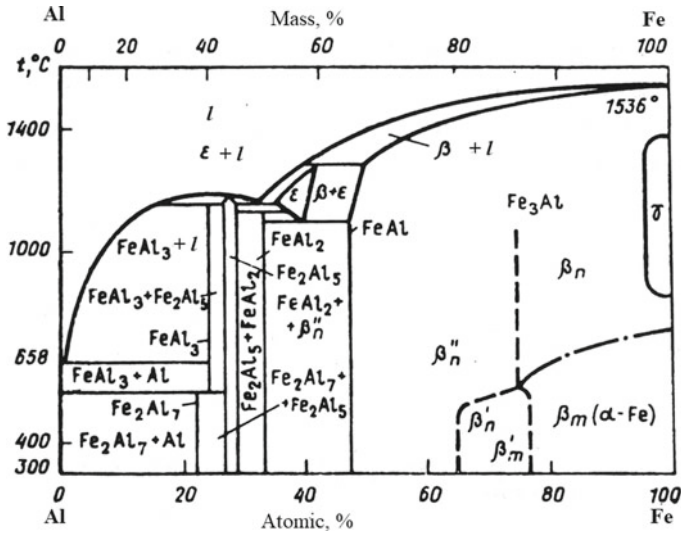


Fig. 15.1 Equilibrium diagram of Al-Fe system

Al-Si system. The state diagram of the Al-Si system of the eutectic type is shown in Fig. 15.2. The solubility of silicon in solid aluminum at a eutectic temperature is ~1.5%. Aluminum does not dissolve in solid silicon.

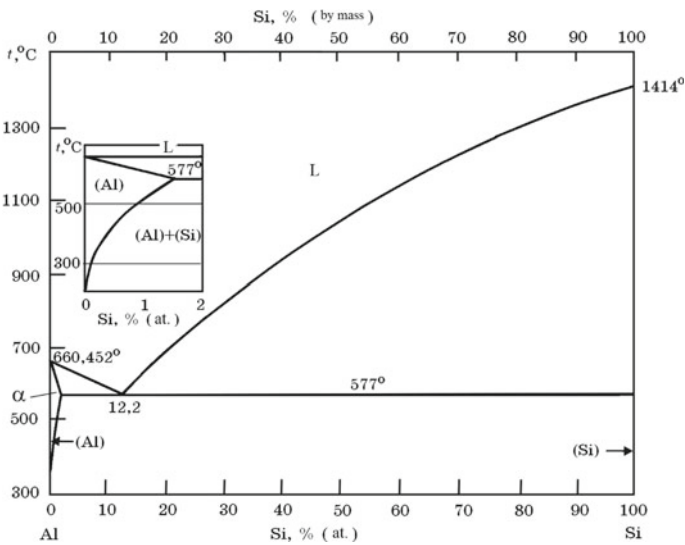


Fig. 15.2 Equilibrium diagram of Al- Si system

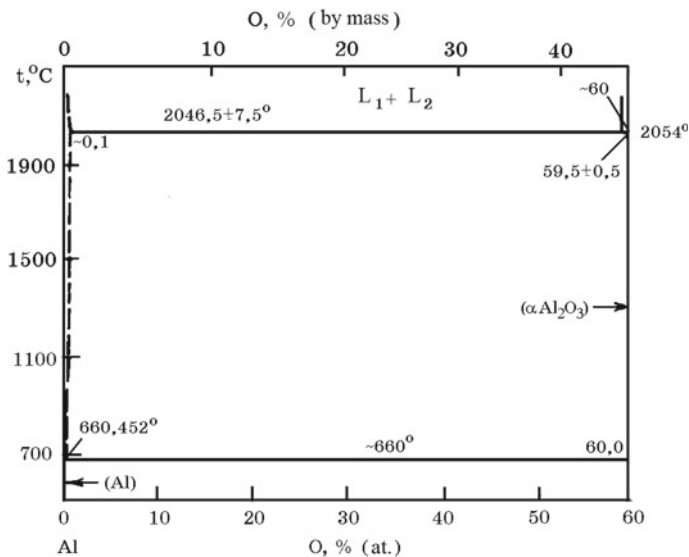


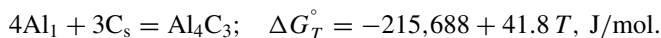
Fig. 15.3 Equilibrium diagram of Al–O system

Al–O system. The higher oxide Al_2O_3 melts at 2054°C and boils at 2452°C (Fig. 15.3). The temperature dependence of the Gibbs energy of the reaction of formation of Al_2O_3 is described by the equation

$$4/3\text{Al}_l + \text{O}_2 = 2/3\text{Al}_2\text{O}_3; \quad \Delta G_{1500-2000\text{K}} = -636,210 - 10,47T \lg T + 223 T, \text{ J/mol.}$$

At high temperatures, depending on the redox potential of the gas phase, suboxides AlO , Al_2O and Al_2O_2 can be in the vapor state.

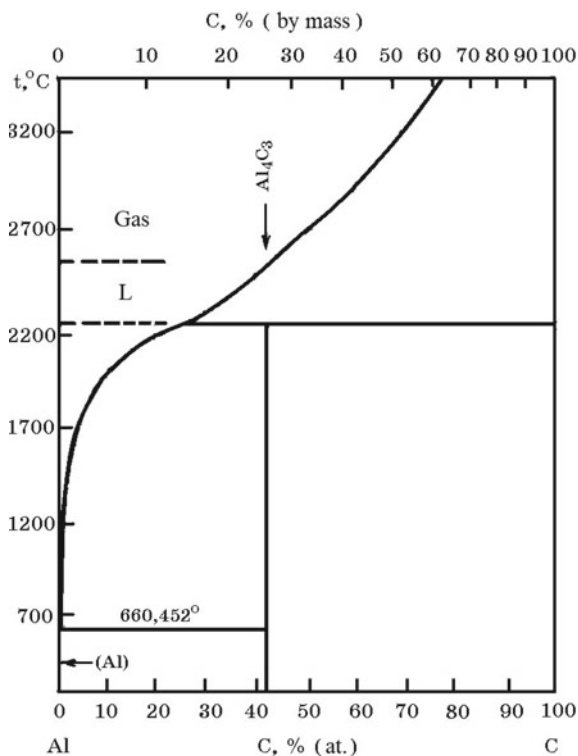
Al–C system. The interaction of aluminum with carbon is accompanied by the formation of Al_4C_3 carbide (Fig. 15.4) by the reaction



The solubility of C in liquid Al is negligible, which follows from the following data:

Temperature, °C	1200	1100	1000	800
% (at.)	0.71	0.35	0.31	0.22
% (by mass)	0.32	0.16	0.14	0.1

Fig. 15.4 Equilibrium diagram of Al–C system



Al–Si–C (Al_4C_3 –SiC) system. In this system (Fig. 15.5), two ternary compounds are formed: Al_4SiC_4 (15.46% Al; 15.35% Si; 26.22% C) and Al_8SiC_7 (68.5% Al; 8.54% Si; 25.61% C), which incongruently melt at 2350 and 2360 K, respectively.

Al–O–C (Al_2O_3 – Al_4C_3) system. When aluminum is reduced from Al_2O_3 by carbon, thermodynamic conditions are created for the formation of refractory oxycarbides $\text{Al}_4\text{O}_4\text{C}$ (58.6% Al; 34.7% O; 6.52% C) and Al_2OC (65.8% Al; 19.51% O; 14.69% C) (Fig. 15.6). Tetracarbide $\text{Al}_4\text{O}_4\text{C}$ is stable up to 1890 °C. At this temperature, it peritectically transforms into Al_2OC and liquid. At ~2000 °C, monooxycarbide Al_2OC also peritectically transforms into Al_4C_3 carbide and liquid. The eutectic composition $\text{Al}_2\text{O}_3 + \text{Al}_4\text{O}_4\text{C}$ melts at ~1835 °C.

Al–Ca system. In the smelting of silicoaluminum for the subsequent metallurgical processing in order to obtain casting alloys, calcium is considered as an impurity element. In this regard, it is of interest to know the phase equilibrium in the Al–Ca system (Fig. 15.7). A number of calcium aluminides are formed in the system, among which Al_2Ca (57.44% Al; 42.56% Ca) is the most refractory. The temperature dependences of the Gibbs energy of the formation of calcium aluminides are described by the equations:

$$\Delta G_T^\circ(\text{Al}_4\text{Ca}) = -28,968 + 15.296 T, \text{ J/mol};$$

Fig. 15.5 Equilibrium diagram of Al_4C_3 -SiC system

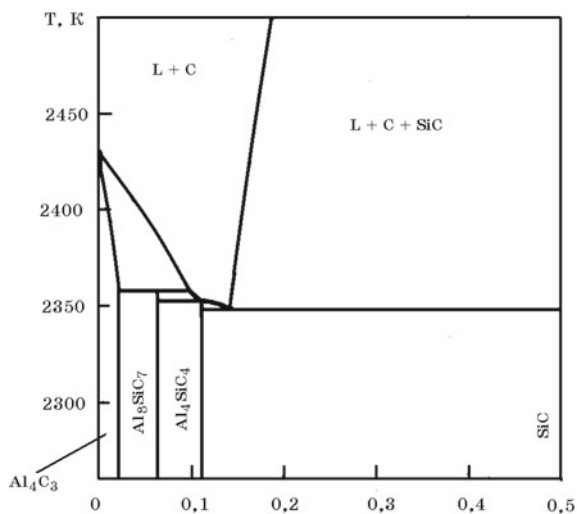
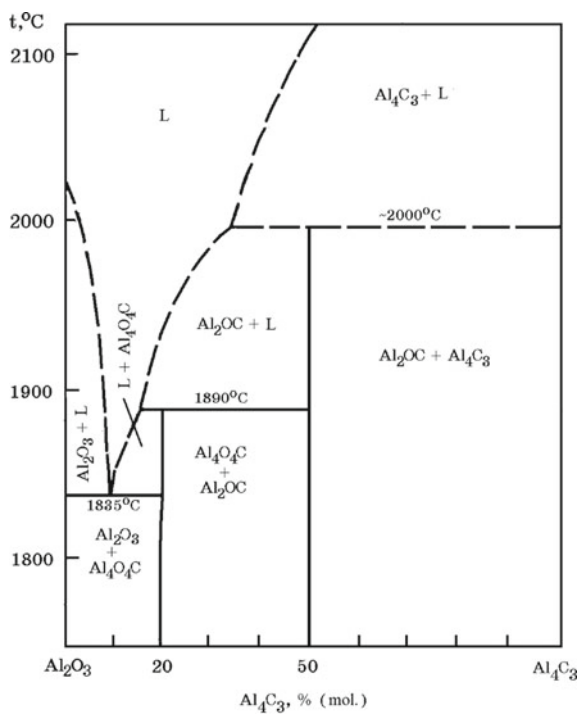


Fig. 15.6 Equilibrium diagram of Al_2O_3 - Al_4C_3 system



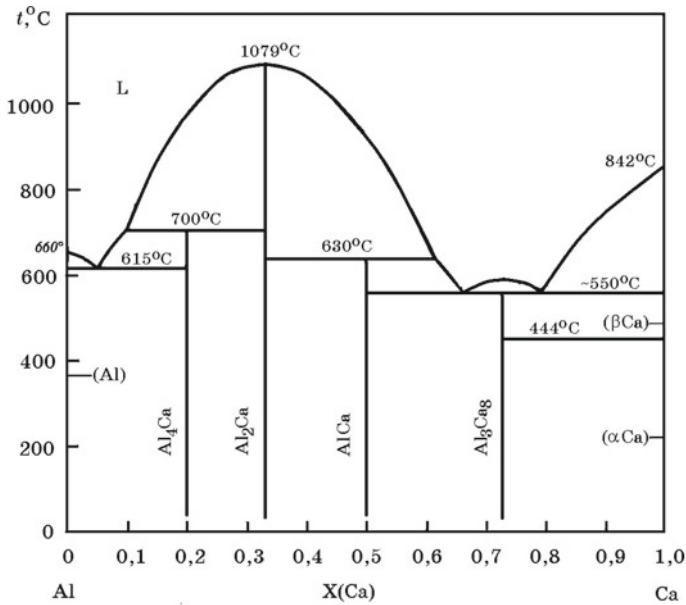


Fig. 15.7 Equilibrium diagram of Al–Ca system

$$\Delta G_T^\circ(\text{Al}_2\text{Ca}) = -41,732 + 19.156 T, \text{ J/mol.}$$

15.2 Aluminum Minerals and Ores

In its free form, alumina (Al_2O_3) is found in nature in the form of the α - Al_2O_3 corundum mineral. Minerals containing alumina are known and widely used: kaolin $\text{Al}_2\text{O}_3 \cdot 2\text{SiO}_2 \cdot 2\text{H}_2\text{O}$, disthene–sillimanite $\text{Al}_2\text{O}_3 \cdot \text{SiO}_2$, mullite $3\text{Al}_2\text{O}_3 \cdot 2\text{SiO}_2$, etc. The main ore for producing aluminum is bauxite, the alumina in which is represented by self-dependent minerals: gibbsite $\text{Al}(\text{OH})_3$ (65,4% Al_2O_3), boehmite γ - $\text{AlO}(\text{OH})$ (85% Al_2O_3) and the diaspore α - $\text{AlO}(\text{OH})$ (85% Al_2O_3). Impurity minerals accompanying bauxite are represented by SiO_2 , TiO_2 , CaO , MgO , MnO , P_2O_5 , V_2O_5 , etc.

15.3 Ferroaluminum Production Technology

The chemical composition of electrothermic ferroaluminum should be as follows: for grades FeAl10–8–11.9% Al; FeAl15—12–16.9% Al; FeAl20–17–21.9% Al;

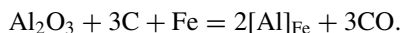
Table 15.1 Consumption of the components of the mixture in the smelting of ferroaluminum, kg

Component	FeAl10	FeAl15	FeAl20	FeAl23
Electrocorundum	245	370	440	560
Steel shavings	900	845	790	755
Coke breeze (13% ash)	125	190	290	290

FeAl23—22–24% Al. Impurity content for all grades (no more): 4% Si, 4% C, 0.06% S, 0.06% P. Ferroaluminum is smelted in closed ore-smelting furnaces of high power. The alloy smelting technology consists in the reduction of aluminum from electrocorundum, obtained from bauxite sinter of any composition, staurolite concentrate (48–50% Al₂O₃, 34–36% SiO₂ and ~15% Fe₂O₃) or other aluminosilicate raw materials. Electrocorundum obtained from low-grade bauxite by reduction of silica and iron by carbon contains, %: 91–96 Al₂O₃, 1–3 SiO₂, 1–2 TiO₂, ~0.5 MgO, 0.8–3 CaO. At the same time, ferrosilicon grades FS20 and FS25 are also obtained.

At the first stage, for 1 ton of electrocorundum and 500–800 kg of ferrosilicon, 1600–1700 kg of low-grade bauxite, 250–300 kg of coke, 600–850 kg of steel shavings are consumed at an electric power consumption of ~5000 kWh. The second stage is a continuous process with the periodic release of metal and a very small amount of smelting (2–3%). As the mixture is used electrocorundum, coke and steel chips are used as charge components (Table 15.1).

The formation of compounds Al₄C₃, Al₂OC and Al₄O₄C does not develop, they are well destroyed by iron, and reduced aluminum dissolves in it, ensuring a successful reaction



During production of aluminum ferroalloys, aluminum is reduced from raw materials at high temperature with the appearance of a liquid phase, as well as by dissolution of reduced aluminum in the metal component. The technology for the production of other alloys with aluminum is based on this principle.

15.4 Silicoaluminum Production Technology

Alloys of aluminum with silicon (the general name silumins) are widely used to produce castings for various functional purposes. In world practice, these alloys are obtained by fusion of electrolytic aluminum with pure silicon. To obtain aluminum from industrial alumina, it is necessary, first of all, to have high-quality bauxite (with a SiO₂ content of not more than 2–3%), a large specific consumption of chemical

reagents (NaOH) and electric energy (~16,000 kWh/t of aluminum). At the same time, rocks containing Al_2O_3 and SiO_2 in chemically bound form are widespread in nature.

In the 60 s, an electrometallurgical technology for the smelting of aluminum–silicon alloy (60% Al—40% Si) was developed and implemented under industrial conditions (Fig. 15.8).

The essence of the technology consists in the joint reduction of aluminum and silicon from Al_2O_3 and SiO_2 oxides by carbon. The mixture consists of disthene–sillimanite concentrate ($\text{Al}_2\text{O}_3 \cdot \text{SiO}_2$), industrial alumina (Al_2O_3), kaolin ($\text{Al}_2\text{O}_3 \cdot 2\text{SiO}_2 \cdot 2\text{H}_2\text{O}$) and a carbonaceous reducing agent. Kaolin is represented mainly by the mineral kaolinite, which consists of aluminum oxide, silica and water; the mineral contains, %: 39.5 Al_2O_3 ; 46.6 SiO_2 ; 13.9 H_2O . For the production of silumin, dry enrichment kaolin of the KZS-37, KZZ-36, KZZ-35 grades are used (Table 15.2).

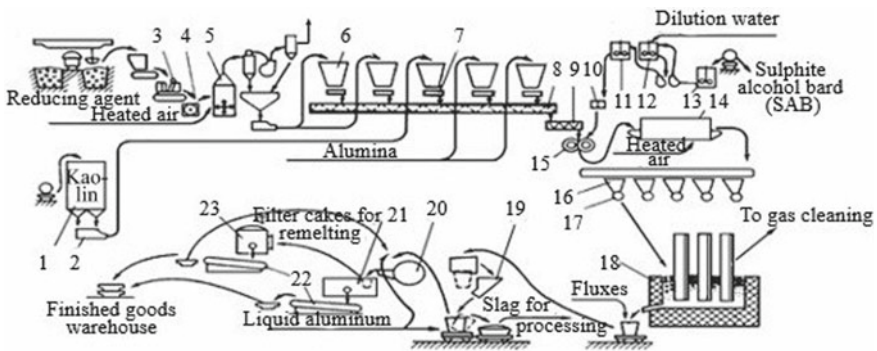


Fig. 15.8 Technological scheme for producing an aluminum alloy with silicon by the electrothermic method: 1—pneumatic screw pump; 2—silo warehouse of kaolin, disthene–sillimanite; 3—jaw crusher; 4—hammer crusher; 5—air-loaded shaft mill; 6—hopper; 7—dispenser; 8—auger; 9—mixer; 10—slotted dispenser; 11–13—mixers; 14—dried; 15—press; 16—hopper; 17—spool feeder; 18—ore-smelting furnace; 19—refining of the primary alloy; 20—mixer; 21—vacuum filter furnace; 22—foundry conveyor; 23—gas furnace

Table 15.2 Chemical composition of kaolin, % (GOST 20080-74)

Component	Norm on grades			Actually
	KZS-37	KZS-36	KZS-35	
Al_2O_3 , no less	37	36	35	35.0–37.0
Fe_2O_3 , no more	0.4	0.5	0.8	0.4–0.8
CaO, no more	0.6	0.7	0.8	0.41–0.8
TiO_2 , no less	0.4	0.6	0.8	0.41–0.6
Moisture, no more	1.0	1.0	1.0	0.5

Table 15.3 Chemical composition of metallurgical alumina, %

Grade	Impurities, no more						LOI at 300–1100 °C, no more
	SiO ₂	Fe ₂ O ₃	TiO ₂ + K ₂ O ₅ + Cr ₂ O ₃ + MnO	ZnO	P ₂ O ₅	Amount of Na ₂ O + K ₂ O in terms of Na ₂ O	
G0	0.03	0.05	0.02	0.02	0.002	0.5	1.2
G00	0.02	0.03	0.01	0.01	0.02	0.4	1.2
G000	0.02	0.01	0.01	0.01	0.001	0.3	0.6

Table 15.4 Chemical composition of disthene–sillimanite concentrate, %

Parameter	Norm	Actually
Al ₂ O ₃ , no less	54	55.0–59.0
Fe ₂ O ₃ , no more	0.8	0.5–0.8
CaO, no more	0.2	–
MgO, no more	0.4	–
TiO ₂ , no more	2.5	0.4–1.3
Moisture, no more	0.5	0.3–0.5
particles with sizes no more 0.315 mm	0.5	–
Bulk density, kg/cm ³	–	1.94

Technical alumina consists of a polymineral mixture of various modifications of Al₂O₃, of which the highest-temperature modification is α -Al₂O₃. Metallurgical alumina of grades G0, G00, G000 is used. The mass fraction of alumina is determined by the difference of 100% and the sum of the mass fractions of impurities (Table 15.3) and mass loss during calcination.

The concentrate is represented by two main minerals—disthene (65%) and sillimanite (30%), which differ in crystal structure and have one chemical formula Al₂O₃·SiO₂ (62.96% Al₂O₃; 37.04% SiO₂). Disthene-sillimanite concentrate (granular) (Table 15.4) is obtained as a side product in the processing of titanium–zircon sands.

To adjust the charge during the melting of briquettes, quartzite (98% SiO₂) is used in the ore-smelting arc electric furnace. A gas-coal concentrate mixed with petroleum coke is used as a reducing agent. The concentrate is obtained by mechanical enrichment of gas coals with a high content of volatile substances (32–38%). This concentrate is characterized by a low ash and Fe₂O₃ content in the ash composition (Table 15.5).

Petroleum coke is a product of slow coking at a temperature of 580–700 °C of residual products obtained during oil refining. These components are briquetted using sulfite-alcohol bards, a side product of sulfite pulping of wood. After drying, the briquettes are subjected to reduction smelting in open ore-smelting three-electrode

Table 15.5 Chemical composition of the gas-coal concentrate, %

Parameter	Norm	Actually
Ash, no more	3.75	2.5–5.0
Moisture, no more	3.0	2.2–5.0
Volatiles	35.5	33.0–38.0
Iron oxides, no more	0.8	0.8–1.1
Solid carbon	56.5	62.0–51.0
Coal ash:		
Fe ₂ O ₃	–	13–25.0
SiO ₂	–	42–50.5
MgO	–	1.5–5.0
TiO ₂	–	0.4–1.5
The bulk density of the fraction 13–60 mm, t/m ³	–	0.8

furnaces. The process is carried out continuously with the working ends of self-baking electrodes with a diameter of 1200 mm immersed in the charge. The rated power of the furnace transformer group is 16.5 MV A (5.5×3).

In general, the chemistry of the process can be represented as a balance reaction



Actually, the process takes place with the formation of intermediate compounds SiO_g, SiC, Al₄O₄C, Al₂OC and Al₄C₃, which greatly complicates the choice of rational electrical and technological parameters of the furnace.

Silicoaluminum is released into the ladle while refining it from the slag using fusible fluxes. The primary refined aluminum–silicon alloy released from the furnace has the following chemical composition, %:

Al	Si	Fe	Ti	Zr	Cr
55–62	38–42	1.3–2.0	0.5–1.0	0.2–0.6	0.50–1.5

Slag has a heterogeneous composition and includes skulls of the alloy, oxide and carbide parts. This slag is used in steelmaking as a deoxidizer. The silicoaluminum refined in the ladle is subsequently subjected to metallurgical processing in order to obtain castings of a wide range. For this purpose, the alloy is diluted with liquid electrolytic aluminum. In this case, the melting point of the alloy decreases, and the solubility of impurity metals (Fe, Ti, Zr, Ca) decreases with the formation of solid intermetallic compounds. By filtration, the liquid alloy is purified from intermetallic compounds and then poured into ingots. A number of casting alloys have been mastered, which are used for casting parts of motor vehicles and the automotive industry.

Chapter 16

Ferroboron and Boron Carbide



For the first time, free boron was obtained in 1808 by Louis Joseph Gay-Lussac and Louis Jacques Tenard by heating B_2O_3 boron oxide with metallic potassium. The boron content in the earth's crust is $3 \times 10^{-4} \%$. Boron is used for microalloying steels and some cast alloys to improve their hardenability and mechanical properties. Surface saturation of steel parts with boron (to a depth of 0.1–0.5 mm) improves not only wear resistance, but also corrosion resistance. Boron and its compounds (BN, B_4C , BP, etc.) are used as dielectrics and semiconductor materials. Boric acid and its salts (primarily borax), borides, etc., are widely used.

16.1 Properties of Boron and Its Compounds

Boron is an element of the IIIa group of elements of the Periodic table of D. I. Mendeleev. The atomic number of boron is 5, the atomic mass is 10.811, the configuration of the outer electron shell is $2s^2 2p$, the oxidation state is 3, the melting point is $2074^\circ C$ and the boiling point is $3658^\circ C$. More than 10 allotropic modifications of boron are known. Natural boron consists of two stable isotopes $^{10}_5B$ (19.57%) and $^{11}_5B$ (80.43%).

B–Fe system. Boron forms compounds with iron—borides: Fe_2B , FeB , FeB_2 (Fig. 16.1). Some properties of iron borides are given in Table 16.1.

Iron borides are thermodynamically strong chemical compounds. The dissolution of boron in liquid iron is accompanied by the release of a large amount of heat. The partial and integral enthalpies of the formation of liquid boron-iron alloys are given below (at $1680^\circ C$, in kJ/mol):

Fig. 16.1 Equilibrium diagram of Fe–B system

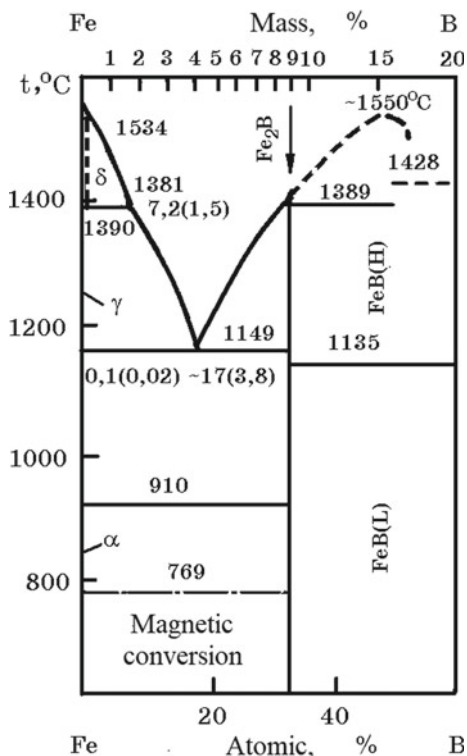


Table 16.1 Some properties of iron borides

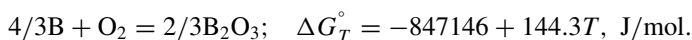
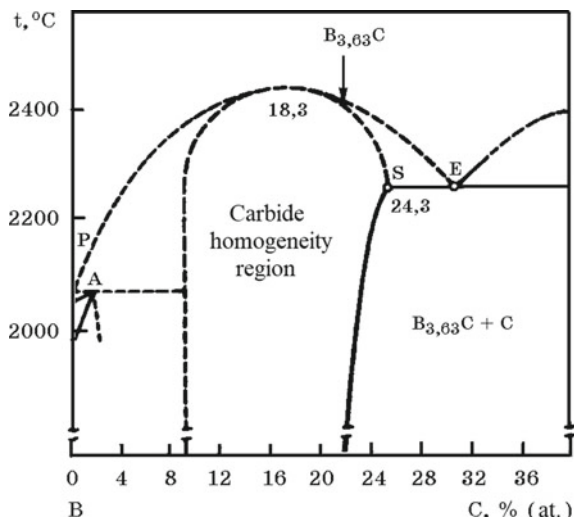
Boride	B, %	T_m , K	ρ , g/cm ³	$-\Delta H_{298}^\circ$, J/mol
Fe ₂ B	8.79	1653	6.98	54,470
FeB	16.17	1830	6.47	71,230
FeB ₂	27.83	2348	5.00	–

X_B	0	0.1	0.3	0.5
$-\Delta \bar{H}_B$	73.23	74.12	58.03	7.93
$-\Delta \bar{H}_{Fe}$	0	0.01	4.99	39.29
$-\Delta H$	0	7.42	20.90	23.60

Boron solutions in iron-based melts are characterized by significant negative deviations from ideal behavior, at 1600 °C $\gamma_{B(Fe)}^\circ = 0.022$.

B–O system. A number of oxides with different B:O ratios from 7:1 to 4:5 are known in the system. Thermally most stable is B₂O₃. The melting point of B₂O₃ is 450 °C. The interaction of boron with molecular oxygen is described by the reaction

Fig. 16.2 Equilibrium diagram of B–C system



The temperature dependence of the vapor pressure B_2O_3 is described by the equation

$$\lg P_{\text{tot}} (\text{Pa}) = -19,000/T + 12.771.$$

Heat of sublimation of B_2O_3 $\Delta H_{\text{csub}}^\circ = 375.14 \text{ kJ/mol}$.

B–C system. In this system, B_4C carbide is formed, which has a wide concentration region of homogeneity (Fig. 16.2).

The heat of formation of B_4C carbide from elements $\Delta H_{298}^\circ = -71.48 \text{ kJ/mol}$, standard entropy $S_{298}^\circ = 27.08 \text{ J/(mol K)}$, which indicates its thermodynamic strength. The melting point of boron carbide is $\sim 2450^\circ \text{C}$.

B–Si system. Boron with silicon forms thermodynamically strong compounds—boron silicides SiB_3 , SiB_6 and SiB_n (Fig. 16.3).

B–Al system. Boron aluminides are known— AlB_2 , AlB_{10} and AlB_{12} (Fig. 16.4).

16.2 Boron Minerals and Ores

The main minerals of boron: boracite— $(\text{Mg,Fe,Mn})_3[\text{ClB}_2\text{O}_3]$, szaibelyite (ascharite)— $\text{Mg}_2[\text{B}_2\text{O}_5] \cdot \text{H}_2\text{O}$, colemanite— $\text{Ca}[\text{B}_3\text{O}_4(\text{OH})_3]$, kernite— $\text{Na}_2[\text{B}_4\text{O}_6(\text{OH})_2] \cdot 3\text{H}_2\text{O}$, borax— $\text{Na}_2[\text{B}_4\text{O}_7(\text{OH})_4] \cdot 8\text{H}_2\text{O}$.

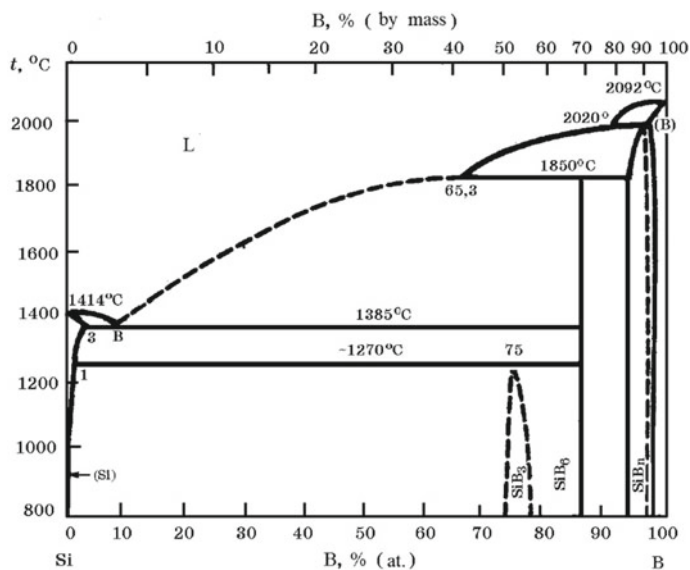


Fig. 16.3 Equilibrium diagram of B-Si system

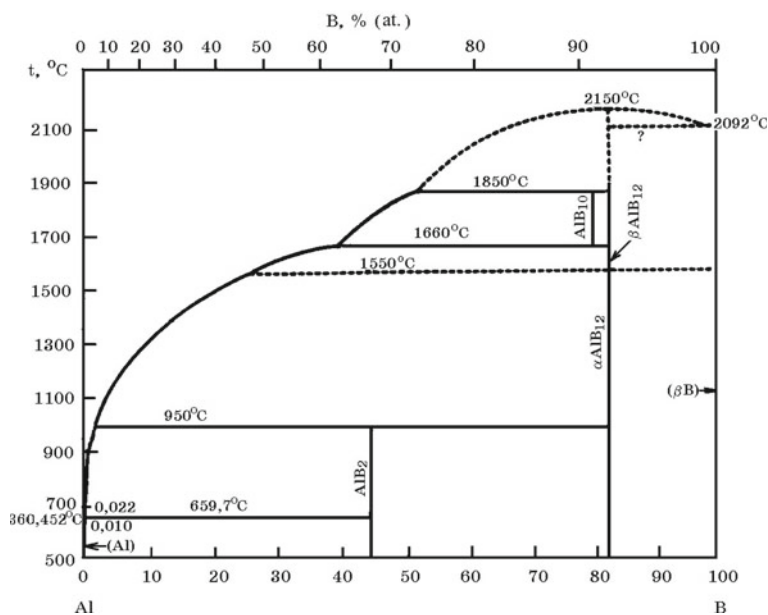


Fig. 16.4 Equilibrium diagram of B-Al system

Table 16.2 Chemical composition of concentrates of boron-containing materials, %

Name	B ₂ O ₃ , no less	CaO	MgO	SiO ₂	Fe ₂ O ₃	Na ₂ O	H ₂ O
		No more					
Boric anhydride	95.0	–	–	–	0.0065	–	3–5
Calcium diborate (CaO·B ₂ O ₃ ·2H ₂ O)	38.0	35.6	1	2.0	0.04	0.1	22
Boric acid (H ₃ BO ₃)	99.5	–	–	0.8	0.0065	–	–
Sodium octaborate (Na ₂ B ₈ O ₁₃)	74.0	–	–	1.0	–	23.0	–

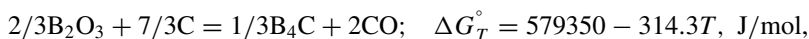
The largest borate ore deposit in the former USSR is the Inder deposit, located in northwestern Kazakhstan. The ores of the Inder deposit have the following composition, %: 8–30 B₂O₃; 1,5–13 SiO₂; 15–25 CaO; 10–30 MgO; 2–5 FeO; 2–6 Na₂O; 2–3 C; 5–10 S; ≤ 0,01 P. Concentrates, boric acid (H₃BO₃), boric anhydrite (B₂O₃), calcium diborate (CaO·B₂O₃·2H₂O) and sodium octaborate (Na₂B₈O₁₃) are obtained from this ore, and ferroboral and ferrosilicoboral are melted. Table 16.2 shows the chemical composition of ore concentrates used for smelting boron alloys. When producing rich ligatures, pure (>98% B₂O₃) and commercial anhydride are used.

16.3 Thermodynamics of Boron Reduction Reactions

B₂O₃ reacts with carbon to produce pure boron in the form:



The theoretical temperature of the onset of the reaction ($\Delta G_T^\circ = 0$; $P_{\text{CO}} = 101 \text{ kPa}$) is 1926 K. The reaction of B₂O₃ with carbon to form B₄C carbide is thermodynamically preferable



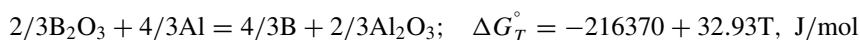
theoretical reaction starts temperature 1843 K.

The reaction of reduction of boron from B₂O₃ by silicon



is incomplete, the metal contains a large amount of silicon and only 2–4% V.

Boron reduction reaction by aluminum



is thermodynamically the most preferred of the considered reactions.

16.4 The Technology of Ferroboron Production

The ferroboron produced by the *aluminothermic method*, according to the chemical composition, must satisfy the requirements given in Table 16.3.

To obtain ferroboron and its alloys, electric furnace melting per block is most widely used. The bulk of the charge in the smelting of ferroboron grades FeB17 and FeB10 includes borate ore and secondary aluminum shavings (0.1% C, 5% Si, 0.01% S; 7% Cu; P—traces). The iron thermite precipitator consists of iron oxide (0.2% C; 1.2% Si; 0.02% S; 0.03% P and 0.12% Cu) and secondary aluminum shavings. The share of iron precipitator is 20–23% of the total mass of the charge. The ignition mixture includes calcined borate ore, iron oxide and secondary aluminum. Exemplary charge compositions for smelting ferroboron are given in Table 16.4.

Ferroboron is smelted in an electric furnace with a capacity of 100 kV A. The metal receiver is lined with magnesite brick. The furnace bath mounted on a trolley is rolled under the electrodes. Melting can be divided into three periods: The formation of a

Table 16.3 Chemical composition of ferroboron, %

Grade	B, no less	Si	Al	C	S	P	Cu
FeB20	20	≤2	≤3	≤0.05	≤0.01	≤0.015	≤0.05
FeB17	17	≤3	≤5	≤0.20	≤0.02	≤0.03	≤0.10
FeB17A	17	≤4	≤0.5	4	–	–	–
FeB10	10	7–15	8–12	–	–	–	–
FeB10A	10	≤5	8–12	–	–	–	–
FeB6	6	≤12	6–12	–	–	–	–
FeB6A	6	≤5	6–12	–	–	–	–

Table 16.4 Composition of the mixture to obtain aluminothermic ferroboron (numerator—t, denominator—%)

Component	Ignition mixture	Main mix	Precipitator
Borate ore	1.25/11.62	92.5/81.86	6.25/13.34
Mill scale	6.25/58.14	– /–	30.0/64.03
Aluminum powder	2.00/18.62	20.5/18.14	10.6/22.63
Iron shavings	1.25/11.62	– /–	– /–
Total	10.75/100	113.0/100	46.85/100

melt, the reduction of oxides and the processing of slag by precipitant. The resulting ferroboron contains, %: 10–11 V; 7–12 Si; 0.03–0.2 Al. Per 1 ton of alloy (base boron content 5%) is consumed, kg: 1200 calcined ore; 500 secondary aluminum in the form of chips; 60–70 aluminum in the form of ingots; 130 steel shavings; 380 mill scale; 20 lime at a power consumption of 500 kWh. Boron extraction is 60–65%. Slag has the following composition, %: 6–10 B₂O₃; 0.6–1.2 SiO₂; 10–14 CaO; 3–7 MgO; 2–4 FeO; 65–73 Al₂O₃. The mineralogical composition of slag was as follows: corundum (α -Al₂O₃); calcium hexa-aluminate (CaO·6Al₂O₃); spinel (MgO·Al₂O₃); calcium aluminates (CaO·Al₂O₃ and CaO·Al₂O₃); calcium borates (2CaO·B₂O₃; CaO·B₂O₃). Slag density is 3.58–3.94 g/cm³. The material balance of smelting ferroboron by the aluminothermic method is given in Table 16.5. Ferroboron smelting is also possible in a tilting furnace with the release of alloy and slag. This makes it possible to use a heated furnace bath for the next melting, which helps to reduce the consumption of refractories and the melting cycle.

Traditionally, ferroboron is produced by an expensive aluminothermic method, reducing B₂O₃ with aluminum powder. At the same time, it is advisable to use high-percentage ferroboron (20–28% B) obtained by *carbothermic technology* when smelting steel of a large tonnage range with a content of 0.2–0.5% C.

Boron, as a microalloying element, even with small additives in steel, has a great influence on the complex of mechanical properties and contributes to the saving of expensive and scarce alloying elements, mineral raw materials and energy resources. Boron affects the hardenability of steel, and this manifests itself most significantly when its concentration in the solid solution is in the range of 0.001–0.004%, therefore, ferroboron with 20% V and carbon content up to 6% can be used (Table 16.6).

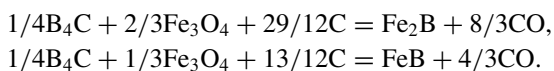
The carbothermic technology for producing ferroboron is based on the use of associated materials for the production of boron carbide (B₄C). The mixture for melting ferroboron consists of boron-containing materials, in which boron is contained in the form of B₄C, as well as Fe₃O₄ scale and petroleum coke. The chemistry of the process can be described by the reactions:

Table 16.5 Material balance of ferroboron smelting in electric furnaces per unit using boric anhydride

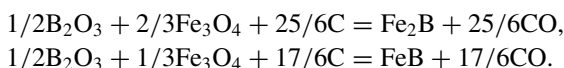
Set	Amount (kg)	Obtained	Amount (kg)
Boric anhydride (93% B ₂ O ₃)	1200	Ferroboron (21.77% B)	1095
Iron ore (90% Fe ₂ O ₃)	1400	Drain slag (9.43% B ₂ O ₃)	1200
Aluminum (99,2% Al)	1167	Block slag (10.6% B ₂ O ₃)	1858
Lime (88% CaO)	340	Hearth (12.7% B ₂ O ₃)	167
Periclase brick	265	Flue dust (28.1% B ₂ O ₃)	30
Total	4372	Total	4350

Table 16.6 Chemical composition of carbothermic ferroboron, %

Grade	B, no less	Si	Al	C	S	P	Cu
		No more					
FeB10	10	2	3	6	0.02	0.03	0.1
FeB20	20	2	3	6	0.02	0.03	0.1



When using associated material— B_2O_3 dust trapped in bag filters without the use of components containing B_4C , the process can be represented by the reactions:



The relatively low temperatures of the onset of reactions are explained by the formation of thermodynamically strong chemical compounds in the reaction products Fe_2B (8.79% B; 91.2% Fe) and FeB (16.17% B; 83.8% Fe).

Along with the mill scale, it is recommended to use iron shavings to reduce the specific energy consumption in charge mixtures. The charges of charge components and electricity per 1 ton when receiving a ferroboron with 20% of B are given below:

Associated B_4C -containing material ($-63 \mu m$), kg	239
Slurry of boron carbide, kg	34.5
Return waste of ferroboron of previous heats, kg	302
Mill scale, kg	531
Iron shavings, kg	362
Electricity, kW h	3916

The resulting ferroboron contains, %: 21.6–24.9 B; 0.3–0.8 C; 0.1–0.2 Si; 0.3–0.7 Al; 0.003–0.004 S; 0.012–0.018 P.

Ferroboron additive in steel, previously deoxidized with a strong deoxidizer (aluminum), provides high absorption of boron (up to 70%) with its stable content (0.0020–0.0025% B).

16.5 The Technology of Boron Carbide Production

Boron carbide— B_4C (Tetrabor trademark) and products based on it are widely used in various branches of technology and industry, in powder metallurgy, for the manufacture of structural ceramics (armor plates, facing armor of aircraft and

Table 16.7 Chemical composition of boron carbide, % (GOST 5744-74)

Grit number	B ₄ C	B _{tot}	B ₂ O ₃	C _{tot}	Grit number	B ₄ C	B _{обм}	B ₂ O ₃	C _{tot}
	No less		No more			No less		No more	
	16	91.6	72	0.5		5	M40. M14	92.0	72
12–16	93.0	73	0.45	4	M10. M7	84.0	65	0.25	10
5–3	90.0	71	0.40	6	M5	84.0	65	0.25	10

helicopter cockpits), shockproof clothing (bulletproof vests), as well as in nuclear energy as absorbers of thermal neutrons in adjustable rods of nuclear reactors. In the metalworking industry, B₄C is used in grinding and polishing operations.

The melting point of B₄C carbide is 2450 °C. The temperature dependence of the Gibbs energy of the reaction for the formation of B₄C from elements is described by the equation

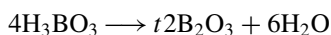
$$4B + C = B_4C, \quad \Delta G_T^\circ = 544368 + 2.763 \cdot 10^{-3}T^2 - 138.84T, \text{ J/mol.}$$

Boron carbide is supplied in the form of a grinder (number 16), grinding powder (numbers 12, 10, 8, 6, 5, 3) and micropowder (M40, M28, M20, M14, M10, M7, M5). According to the chemical composition, boron carbide must satisfy the requirements given in Table 16.7.

The chemistry of the process in general can be represented by the reaction



which is the sum of the low-temperature conversion of orthoboric acid



and the main high-temperature reaction



Based on the data of thermodynamics, kinetics and the mechanism of this complex process, a process has been developed for the production of boron carbide using orthoboric acid and a carbonaceous reducing agent in a specially designed arc furnace (Fig. 16.5). An electric arc furnace with an installed transformer power of 2 MV A has two metal non-lined casings. The outer casing is stationary, the inner one is movable. The outer casing has a diameter of 2 m and a height of 2 m, and the inner one has a diameter of 1.6 m and a height of 1.2. The outer casing is mounted on a trolley—hearth, and the inner casing is suspended on rods and can move vertically along the course of the melting of boron carbide, for which there is a mechanism for moving this casing. The outer casing along the upper edge passes into the so-called false casing, which is a sectional bell 0.5 m high with an upper diameter of 3.1 m.

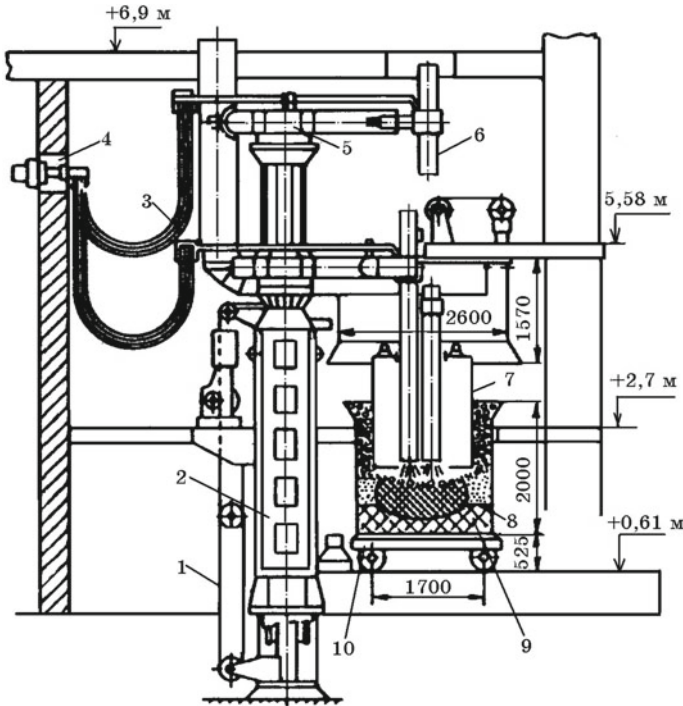


Fig. 16.5 General view of the arc furnace for smelting boron carbide by a block process 1—cable; 2—rack mechanism for moving the electrode; 3—flexible cable; 4—aperture; 5—sleeve of the electrode holder; 6—electrode; 7—movable casing; 8—outer casing; 9—hearth; 10—roll-out trolley

The bottom of the trolley is laid out of graphite blocks with a section of 0.4×0.4 m. The furnace is powered emitted from a three-phase transformer with a capacity of 2 MV A, having 12 voltage levels on the low side from 69.6 to 145 V at a current of 7–10 kA. The graphitized electrodes with a diameter of 300 mm are used.

The prepared mixture for smelting boron carbide is poured into the socket and enters the annular gap between the outer and inner shells. During the melting process, the inner casing is heated from electric arcs to 600–700 °C, as a result of which the boric acid melts, and the charge mixture ($\text{H}_3\text{BO}_3 + \text{carbon}$) acquires mobility. At these temperatures, H_3BO_3 dehydration occurs with the formation of boric anhydride B_2O_3 and H_2O . The mixture consists of orthoboric acid H_3BO_3 and a carbonaceous reducing agent with a very low ash content ($\leq 0.5\%$). Boric acid contains H_3BO_3 , %: ≥ 99.9 —grade A; ≥ 99.6 —grade B; ≥ 98.6 —grade B. The components of the charge are metered carefully and fed in powder form for melting.

A heterogeneous oxide-carbon melt, as the inner casing rises, flows by gravity under the electrodes into the combustion zones of the electric arcs, which are practically covered by this melt. The arrival of the molten charge under the electrodes is controlled by the rate of rise of the inner casing, which is consistent with the rate

of reduction reactions and, ultimately, with the rate of formation of a boron carbide block of a homogeneous structure from the liquid carbide phase that corresponds to the composition of formula B_4C . At the end of melting, the electrodes, the inner and false casings are lifted, the trolley—hearth with the deposited block of boron carbide (weighing 250–300 kg) is rolled out into the main span of the workshop. After cooling the block, it is transferred to the overpass for subsequent crushing. The trolley with the installed outer casing is rolled up to the workplace for new smelting.

The developed technology for the electric melting of boron carbide in an electric furnace, of the described design, allows to obtain a block of boron carbide of the following composition, %: 75–77 B_{tot} ; 1–2 B_2O_3 ; 22–24 C_{tot} 1–3 C_{free} ; 95–98 B_4C . Five tons of boric acid, 1.6 tons of petroleum coke (or shavings from mechanical turning of graphite electrodes at electrode plants) are consumed per 1 ton of crushed block of boron carbide; 0.15 tons of graphitized electrodes, 18,000 kWh of electricity.

Chapter 17

Ferrous Alloys with Rare-Earth Metals



According to the classification, rare-earth metals (REM) include lanthanum ($z = 57$), lanthanides (elements from cerium to lutetium, $z = 58/71$), as well as scandium ($z = 21$) and yttrium ($z = 39$). REM—elements of the third group of the Periodic system of elements. Of the 17 elements of the REM family belonging to the group of rare-earth metals, mainly three are used in ferrous metallurgy: yttrium, lanthanum and cerium, although other rare-earth metals can be present in various amounts in ferrous alloys of this type. Ferrous alloys with rare-earth metals are used in the production of steel for deoxidation, modification of the steel structure and changes in the composition of non-metallic inclusions, since MnO, SiO₂ and Al₂O₃ contained in the oxide phases can be reduced by rare-earth metals introduced into liquid steel.

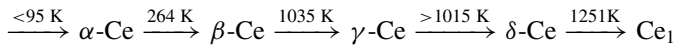
17.1 Properties of Rare-Earth Metals and Their Compounds

Yttrium was discovered in 1794 by the Finnish chemist I. Godolin. The yttrium content in the earth's crust is $2.8 \cdot 10^{-3}\%$. The atomic number of yttrium is 39, the atomic mass is 88.90. Natural yttrium consists of one stable isotope $^{89}_{39}\text{Y}$. The configuration of the outer electron shells is $4d^1 5s^2$, and the oxidation state is 3. Yttrium is an allotropic metal, up to 1482 °C, the α -Y modification with a hexagonal lattice with a density of 4.45 g/cm³ is stable. Above 1482 °C, the β -Y modification with a cubic lattice of the α -Fe type is stable. The melting point of yttrium is 1528 °C, and the boiling point is about 3320 °C. The vapor pressure at 1450 °C is 6.15×10^{-2} Pa.

Lanthanum was discovered in 1939 by the Swedish chemist C. Mozander. The lanthanum content in the earth's crust is $1.8 \times 10^{-3}\%$. The atomic number of lanthanum is 57, and the atomic mass is 138.90. Natural lanthanum consists of

two stable isotopes of ${}^{139}_{57}\text{La}$ (99.911%) and radioactive ${}^{138}_{57}\text{La}$ (0.089%) with a half-life of 2×10^{11} years. The configuration of the electron shell is $5d^1 6s^2$, and the oxidation state is 3. Up to a temperature of 277°C , the hexagonal modification of α -La is stable; in the range 277 – 861°C , a cubic lattice with a density of 6.19 g/cm^3 is stable; in the range 861 – 920°C , the γ -modification with a cubic lattice of the α -Fe type, with a density of 5.97 g/cm^3 . The melting point of lanthanum is 920°C ; the boiling point is 3454°C .

Cerium was discovered in 1803 independently by the German scientist M.G. Klaprot and Swedish I.Ya. Berzelius. The cerium content in the earth's crust is $4.5 \times 10^{-3}\%$. Atomic number of cerium 58, atomic mass of 140.12. There are four stable isotopes in natural cerium: ${}^{136}_{58}\text{Ce}$ (0.19%), ${}^{138}_{58}\text{Ce}$ (0.25%), ${}^{140}_{58}\text{Ce}$ (88.48%) and ${}^{142}_{58}\text{Ce}$ (11.08%). The configuration of the outer electron shells of the cerium atom is $4f^2 6s^2$, the oxidation state is 3, less often 4, and the cerium has a melting point of 798°C . 4 crystalline modifications of cerium are known



Yttrium oxide Y_2O_3 melts at 2430°C , boils at 4300°C (Fig. 17.1). It exists in two modifications: up to 2277°C , a cubic crystal lattice is preserved, and at a higher temperature, it is hexagonal.

Lanthanum oxide La_2O_3 melts at 2313°C . The temperature dependence of the Gibbs energy of the reaction of the formation of La_2O_3 from elements is described by the equation

$$2\text{La} + 3/2\text{O}_2 = \text{La}_2\text{O}_3, \quad \Delta G_{298-1000\text{K}}^\circ = -1,869,290 + 38.45T \lg T - 405.04T, \text{ J/mol.}$$

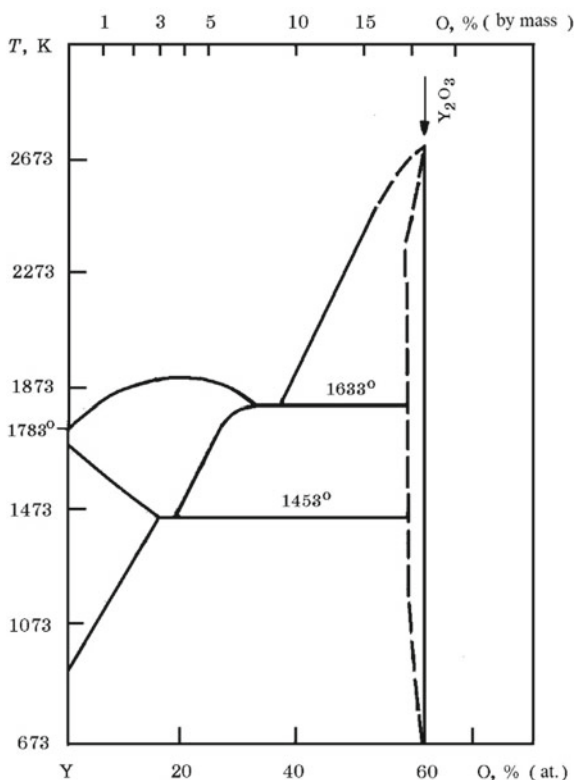
Cerium oxide CeO_2 melts at 2400°C (Fig. 17.2). Gibbs energy of CeO_2 formation = -1024.5 kJ/mol . Ce_2O_3 oxide is not stable, in the presence of O_2 , it is rapidly oxidized with the release of a large amount of heat.

Y-Fe system. Yttrium with iron forms four chemical compounds: YFe_9 ; YFe_4 ; YFe_3 ; YFe_2 (Fig. 17.3). In the liquid state, yttrium and iron form continuous solutions.

La-Fe system. Lanthanum with iron does not form chemical compounds. In the liquid state, they have unlimited solubility. The boundary solubility of lanthanum in solid iron does not exceed 0.1% (at.). At a content of 91.5% (at.) La, a eutectic is formed ($t_{\text{eut}} = 785^\circ\text{C}$). Solutions of lanthanum in iron-based melts are characterized by significant positive deviations from ideal behavior, at 1600°C $\gamma_{\text{La(Fe)}}^\circ = 9.3$.

Ce-Fe system. Two chemical compounds CeFe_2 and CeFe_5 were established in the system (Fig. 17.4). Cerium solutions in iron-based melts are characterized by negative deviations from ideal behavior, at 1600°C $\gamma_{\text{Ce(Fe)}}^\circ = 0.322$.

Fig. 17.1 Equilibrium diagram of Y–O system



Y–C system. The existence of carbides YC , Y_2C_3 and YC_2 was established in the system (Fig. 17.5).

La–C system. The existence of two carbides La_2C_3 and LaC_2 was established in the system (Fig. 17.6). LaC_2 carbide has a tetragonal crystal lattice, density 5.35 g/cm^3 , melts at 2360°C .

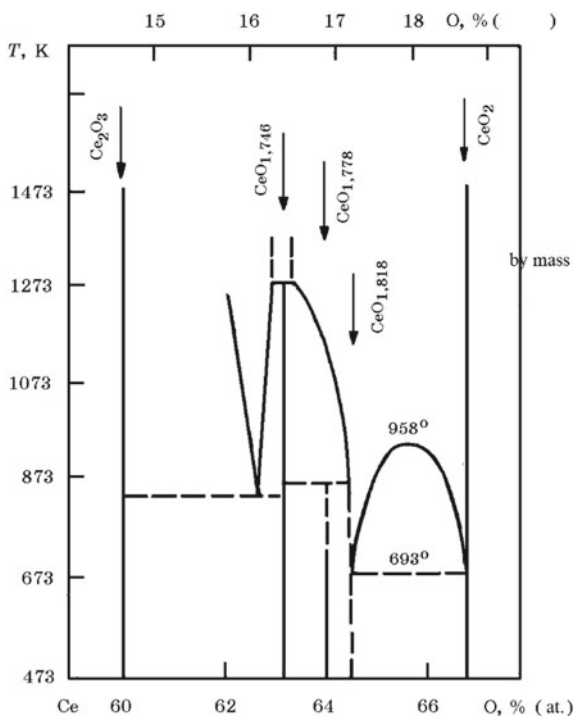
Ce–C system. The system contains carbides Ce_2C_3 and CeC_2 . Ce_2C_3 carbide has a cubic lattice, and CeC_2 carbide has a tetragonal lattice, a density of 5.6 g/cm^3 and a melting point of 2290°C .

Y–Si system. There are four yttrium silicides in the system: Y_5Si_3 ; Y_5Si_4 ; YSi ; Y_3Si_5 (Fig. 17.7). The solubility of yttrium in solid silicon is negligible. The most important properties of the YSi compound: rhombic crystal system, melting point 1835°C and density 4.33 g/cm^3 .

La–Si system. Compounds $LaSi$, La_3Si_2 and $LaSi_2$ are known. The melting temperature of $LaSi_2$ is taken equal to 1520°C . This silicide crystallizes in tetragonal crystal system and has a density of 5.05 g/cm^3 .

Ce–Si system. Known silicides— $CeSi$, Ce_5Si_3 and $CeSi_2$. $CeSi_2$ silicide crystallizes in tetragonal crystal system and has a density of 5.31 g/cm^3 .

Fig. 17.2 Equilibrium diagram of Ce–O system



17.2 Minerals, Ores and Concentrates of Rare-Earth Metals

Rare-earth metals are relatively widespread in nature. If the aluminum content in the earth's crust is taken as 100 units, then the amount of rare-earth metals will be 0.18, which is much more than copper and cobalt (0.12), uranium (0.10), tungsten (0.060) and molybdenum (0.001). In nature, rare-earth metals are found in the form of oxides, phosphates, carbonates, fluorocarbonates and other compounds. The main minerals containing rare-earth metals are: bastnesite (Ce, La) \cdot (FCO₃) with a density of 4.2–5.2 g/cm³; xenotime YPO₄ with a density of 4.45–4.59 g/cm³ containing 63.1% YPO₄ and up to 5% UO₂, 3% ZrO₂, sometimes ThO₂; monazite (Ce, La, Nd, Th) \cdot (PO₄), includes ThO₂ impurities (up to 10%), UO₂ (6.6%), ZrO₂, etc. Monazite is most often found in pegmatite rocks and is used as raw material for cerium production and thorium. Loparite—a mineral of the REM fluorocarbonate group with the formula Ca(Ce, La)₂[CO₃]F₂ contains 30.5% Ce₂O₃; 10.44% CaO and 24.58% CO₂. The minerals of the pyrochlore group have the general formula (Ca, Na, U, Ce, Y)_{2-m} \cdot (Nb, Ta, Ti)₂O₆(OF)_{1-m} \cdot H₂O and are divided into minerals rich in rare-earth metals, tantalum, uranium, titanium and other elements.

The main industrial sources of rare-earth metals are bastnesite, monazite and xenotime. The first of them forms its own deposits, the other two—secondary ones:

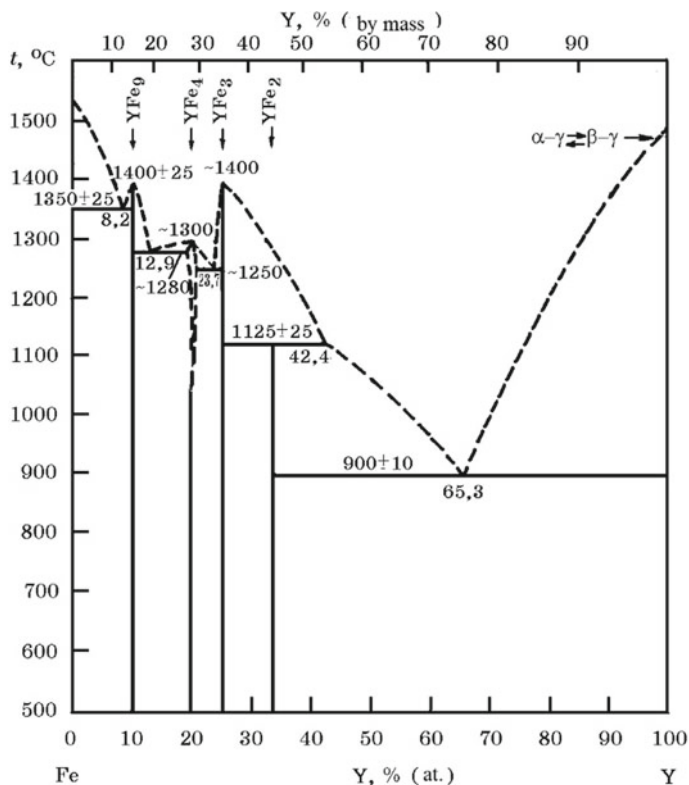


Fig. 17.3 Equilibrium diagram of Y-Fe system

ilmenite–rutile–zircon, tin and other placers. About 16% of yttrium comes from uranium waste. Ores containing REM minerals are usually subjected to gravitational enrichment to isolate heavy minerals—monazite, xenotime, etc. Monazite from a mixture with other minerals is isolated by a combination of gravitational, electromagnetic and electrostatic methods. Chemical methods for the processing of concentrates include leaching, separation of radioactive impurities, separation of chemical concentrates, separation of the rare-earth metals themselves and the preparation of metals. Bastnesite concentrates are leached with hydrochloric acid, and cerium concentrate is isolated from the undissolved precipitate. Loparite and bastnesite concentrates are also processed by chlorination. The monazite and bastnesite concentrates currently used contain 60 and 70% of rare-earth metals, respectively. The mass fraction of each element of rare-earth metals in these concentrates is characterized by the following data, %:

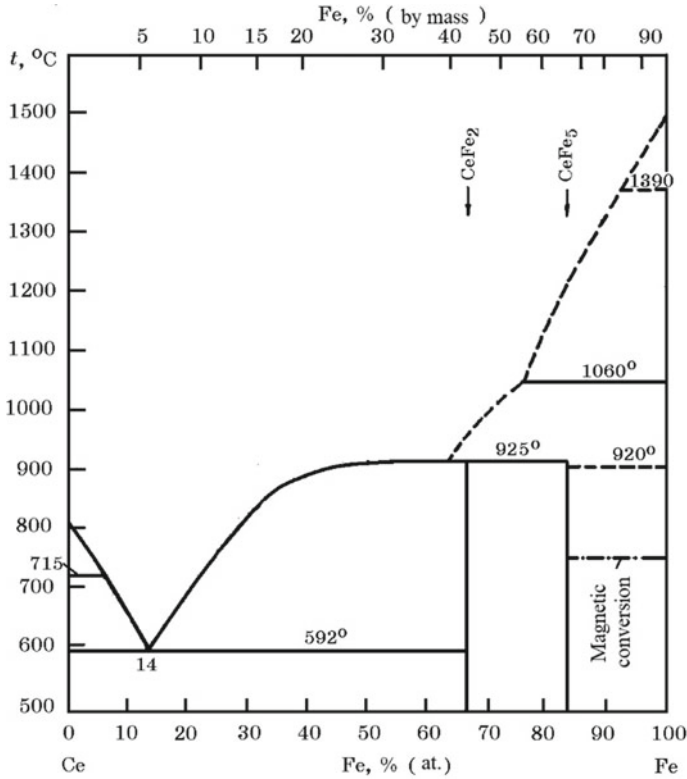
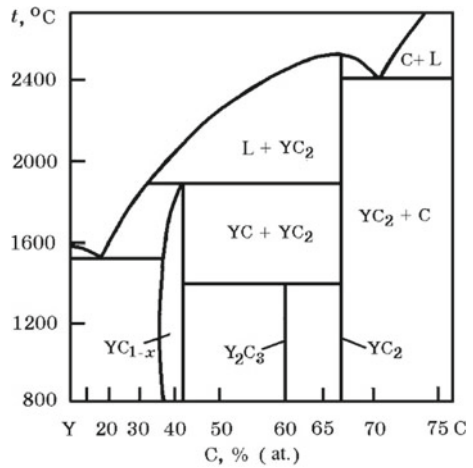


Fig. 17.4 Equilibrium diagram of Ce-Fe system

Fig. 17.5 Equilibrium diagram of Y-C system



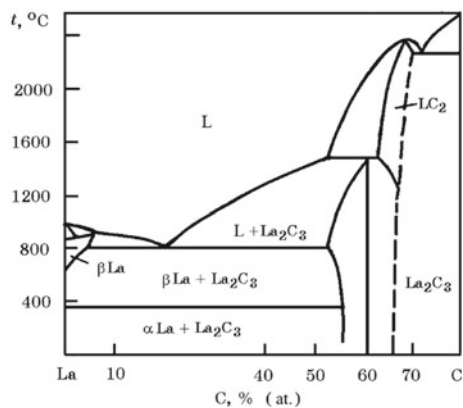


Fig. 17.6 Equilibrium diagram of La-C system

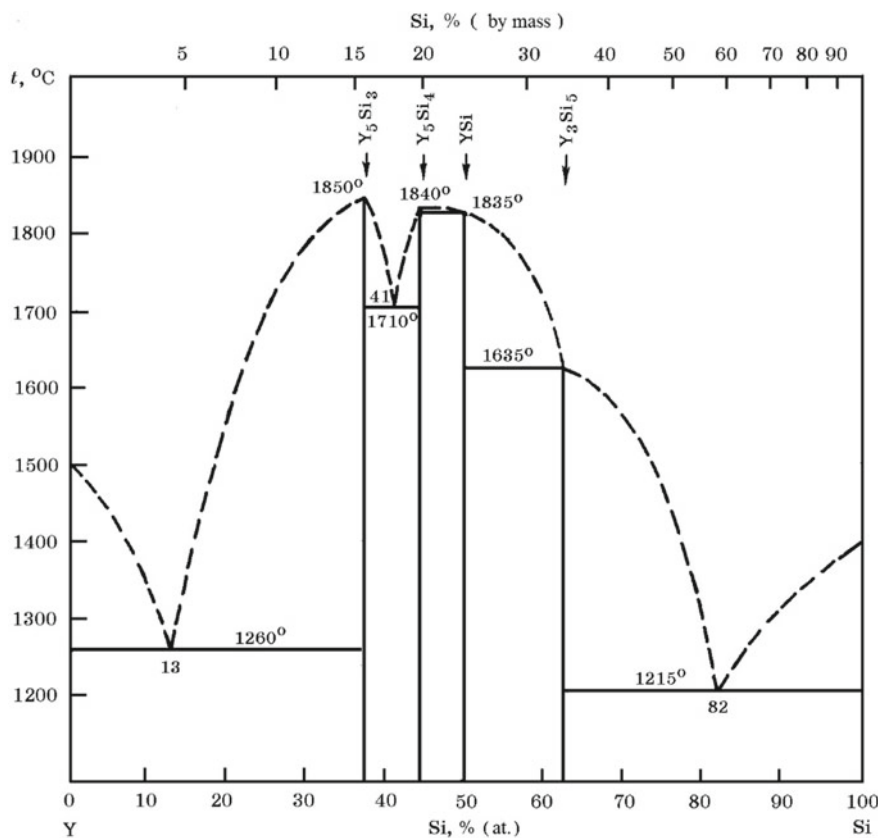


Fig. 17.7 Equilibrium diagram of Si-Y system

Table 17.1 Chemical composition of ferroalloys with rare-earth metals, %

Grade	ΣREM	Si	Al
FS30REM30	30–40	30–50	(2–4)/(4–8) ^a
FS30REM20	20–30	30–55	(2–3)/(3–6)
FS30REM15	15–20	30–60	(2–6)/6–10)
FS30REM10	10–15	30–60	(2–3)/3–6)
FS30REM5	5–10	30–60	(2–8)/(6–15)

^aAluminothermic

Metal	La	Ce	Pr	Nd	Sm	Eu
<i>Concentrate</i>						
Monazite	22	44.9	5.6	17.8	3.2	0.1
Bastnesite	34	50	4.0	11.0	0.5	0.1

17.3 The Technology for Producing Ferroalloys with Rare-Earth Metals

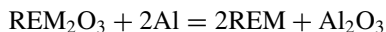
Ferroalloys with rare-earth metals and silicon (Table 17.1) are smelted by the *carbothermic* method in ore-smelting furnaces by the continuous method. The mixture contains a concentrate of rare-earth metals, quartzite, a carbon reducing agent and steel chips. Accurate carbon dosing is of particular importance for the reduction of REM and silicon oxides, since when the amount of carbon deviates from the charge, a carbide deposit is formed on the hearth of the furnace (SiC, REMC, REMC₂, REM oxides and SiO₂) and a sufficiently good extraction of REM is not achieved. REM production occurs by reaction



The reaction is significantly developed at $T > 2000$ K. The reduction of rare-earth metals is thermodynamically facilitated due to a decrease in their activity upon dissolution in silicon and iron. In a ferroalloy with 30–40% rare-earth metals, the elements of rare-earth metals are part of silicides. Recovery processes are accompanied by the formation of oxycarbides and carbides.

An increase in the content of rare-earth metals in the alloy leads to a decrease in metal recovery due to the formation of gaseous oxides (rare-earth metals) and an increase in the amount of slag. Slag density with increasing silicon content in the alloy approaches the density of the metal melt. It is advisable to melt alloys containing not higher than 35–45% REM, which leads to a more complete use of REM in the smelting of steel and pig iron.

A significant number of ligatures containing REMs are produced by the *aluminothermic method*. Gibbs energy of the reaction of reduction of rare-earth metals by aluminum



is positive, therefore, to achieve a sufficient degree of REM extraction into the metal, there must be an increased amount of aluminum in the charge and, consequently, in the alloys, and the process must be carried out with the supply of a large amount of heat. Aluminum is introduced into the charge >100% of theoretically necessary (obtaining a ligature containing 3–7% Al) and a significant amount of silicon, which creates additional favorable conditions for reducing the activity of rare-earth metals when they are dissolved in silicon.

Ligature is smelted in an arc furnace with a lining of the hearth and walls of the carbon mass. The power of the transformer of the steelmaking tupe furnace is 1.8 MV·A. The mixture includes a concentrate of rare-earth metals yttrium or cerium subgroup, a concentrate of lanthanum oxide containing 40–47% CeO₂ and 41–48% (La₂O₃ + Nd₂O₃ + Pr₂O₃). The reducing agent is a powder of primary or secondary aluminum (depending on the chemical composition of the resulting ligature). Ferrosilicon FS75, low-phosphorus iron concentrate (>63% Fe) are introduced into the charge, and freshly calcined lime and fluorspar are used as fluxes. Per 100 kg of concentrate is consumed, kg: 32–41 aluminum powder; 110–125 ferrosilicon; 30–37 lime; 0–5 iron concentrate and fluorspar. The mixture is introduced up after a set of electrical load. The mixture is divided into two parts: the first part, %: 55–75 concentrate, 60–65 lime, 60 ferrosilicon, 42 aluminum powder. First, the first part of the charge is melted with its gradual and uniform loading, and after holding the melt under current for 5–7 min, the remaining ferrosilicon, aluminum powder, lime and rare-earth metals are introduced. At the end of the melting of the second part of the charge and holding the melt under current, the slag and metal are discharged into a lined crucible mounted on a pallet in the melting chamber. Then, the crucible is cooled and rolled out of the chamber, the notch is cut, and the metal is released into the cast iron mold.

The density of the metal containing, %: 11–40 rare-earth metals; 33–52 Si; 7–9 Al; 5–6.3 Ca; 0.01–0.03 C; 12–20 Fe, fluctuates between 3.3 and 3.9 g/cm³, and the slag density is 3.0–3.6 g/cm³, which can cause loss of rare-earth metals with slag. When fluorspar and sodium chloride are introduced into the slag, the slag density decreases, which helps to improve the separation of metal from slag. The consumption of materials per 1 ton of master alloys with rare-earth metals is as follows, kg: 565/520 concentrate of oxides of rare-earth metals; 210/203 aluminum powder; 225/225 lime; 695/630 ferrosilicon FS75; 35/33 iron ore; power consumption 2149/2184 kWh/t (the numerator is for the ligature of the yttrium subgroup, and the denominator is for the ligature of the cerium subgroup).

According to this technology of smelting ligatures with rare-earth metals, the reduction of oxides of rare-earth elements in the first stage of melting is carried out by silicothermic process, and in the second, by aluminothermic. Studies have shown

a high degree of extraction of rare-earth elements into metal (92–97%) and the production of lime-alumina slag with a low content of rare-earth metals (1.6–4.8%). Further, the development of this technology for smelting ligatures with rare-earth metals allowed to increase the extraction of rare-earth metals in metal to 92–95% and to reduce the cost of 1 ton of ligature (30% rare-earth metals). The lime-alumina slag obtained in the production process with a content of 50–60% Al_2O_3 , 35–40% CaO and up to 5% REM oxides is effectively used in out-of-furnace steel processing.

Electrolytic method. REM in its pure form and as a *mischmetal* (>98% REM, including >45% Ce and 25% La) is obtained by electrolysis of anhydrous rare-earth metals in the presence of alkali metal chlorides at 800–900 °C in steel devices, walls secondly serve as the cathode and graphite rods as the anode. Individual REMs are obtained by metallothermic reduction of their fluorides. As reducing agents, Ca, less often Mg and also Na are used. The resulting individual REMs are refined in a vacuum. Obtaining REM by electrolysis requires a large specific consumption of electric energy (~15 to 16 kWh/kg).

Chapter 18

Iron–Carbon Alloys



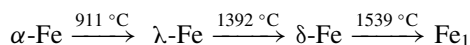
Iron was known in prehistoric times. A method for producing iron from ores was invented in the western part of Asia in the second millennium BC; after that, the use of iron spread to Babylon, Egypt, Greece—the Iron Age replaced the Bronze Age.

According to the content in the earth's crust, iron is in fourth place (4.65 wt%) and second among metals (after aluminum). Iron forms about 300 minerals—oxides, sulfides, silicates, carbonates, etc. Iron is the most important metal of modern technology. In its pure form, due to its low strength, it is practically not used. The bulk of the iron is used in the form of alloys that are very different in composition and properties. Iron alloys account for ~95% of all metal products.

18.1 Properties of Iron and Its Compounds

Iron is an element of group VIIIb of the Periodic system of elements, refers to the transition elements of the iron triad. Atomic number 26, atomic mass 55.847, electron shell configuration $3d^64s^2$, valencies 2 and 3, melting point 1539 °C, boiling point ~3200 °C, density 7.874 g/cm³ at 20 °C, and at the melting point, the density of solid iron is 7.265 g/cm³.

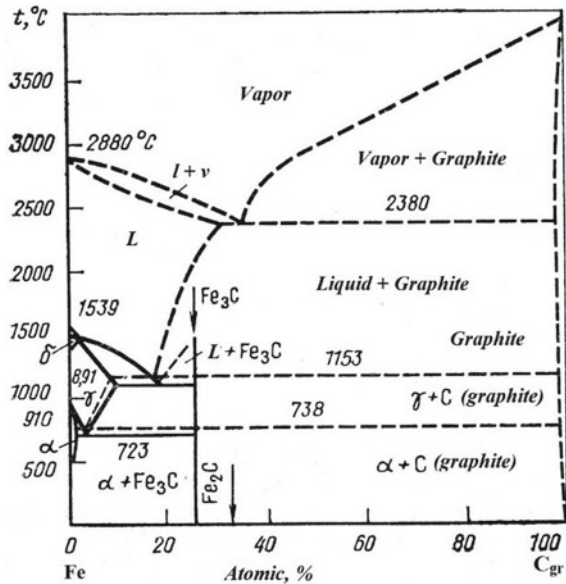
Iron—polymorphic metal: when heated, the body-centered α -Fe lattice transforms into a face-centered γ -Fe, which transforms into a body-centered δ -Fe



Iron is ferrimagnetic—Curie point is 769 °C.

Fe–C system. The state diagram of the Fe–C system is shown in Fig. 18.1. Iron carbides Fe₃C (cementite), Fe₂C (chalipite) and others are known. In the system, the main phases are ferrite (solid solution of carbon in α -Fe), austenite (solid solution

Fig. 18.1 Equilibrium diagram of Fe–C system



of carbon in γ -C) cementite (Fe_3C) and graphite. Alloys with 0.8% C undergo a eutectoid transformation, and with 4.3% C, they undergo a eutectic transformation. With increasing carbon content, the melting point of iron decreases, and the eutectic temperature is 1153 °C. With increasing temperature, the solubility of carbon in iron increases.

$$[\%C]_{\text{Fe}} = 1.30 + 2.5 \cdot 10^{-3} t(^{\circ}\text{C}).$$

Carbon solutions in liquid iron are characterized by negative deviations from ideal behavior, at 1600 °C $\gamma_{\text{C}(\text{Fe})}^{\circ} = 0.538$. Introduction of Cr, Mn, Ti into the melt increases the solubility of carbon, and Si, P, S decrease, Ni and Co do not significantly affect the solubility of carbon in iron.

Fe–O system. The state diagram of the Fe–O system is shown in Fig. 18.2. In the system, FeO , Fe_3O_4 and Fe_2O_3 compounds are formed (Table 18.1), as well as several phases of variable composition (solid solutions). When heated, thermal dissociation of oxides occurs in the series $\text{Fe}_2\text{O}_3 \rightarrow \text{Fe}_3\text{O}_4 \rightarrow \text{FeO} \rightarrow \text{Fe}$. Hematite Fe_2O_3 dissociates by reaction



The reaction in the temperature range 900–990 K proceeds in a homogeneous region, and in the range of 1030–1200 K, the oxygen pressure corresponds to the

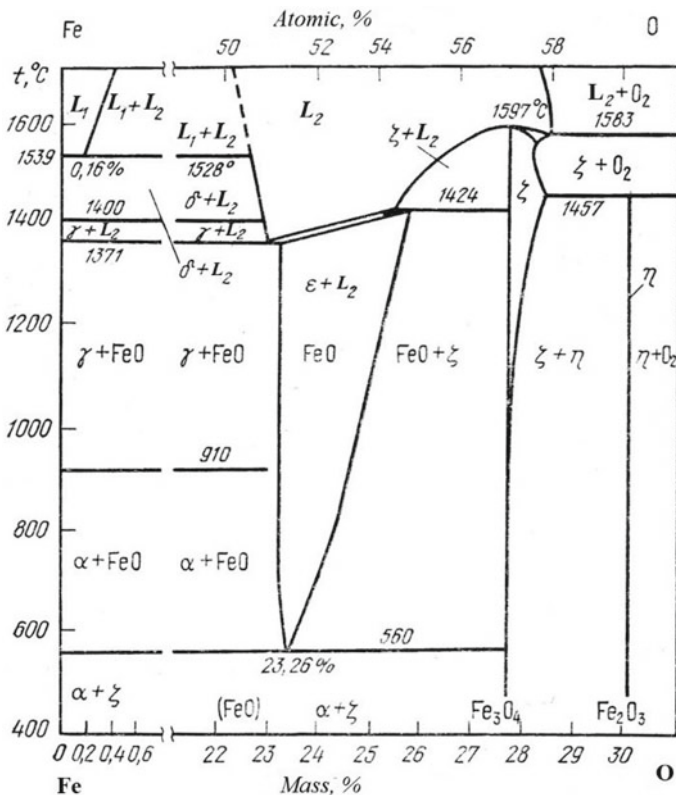
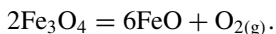


Fig. 18.2 Equilibrium diagram of Fe–O system

Table 18.1 Thermodynamic constants of oxygen compounds of iron

Compound	$-\Delta H_{298}^{\circ}$, kJ/mol	$-\Delta G_{298}^{\circ}$, kJ/mol	S_{298}° , J/(mol K)	$C_{p, 298}^{\circ}$, J/(mol K)	T_m , K
FeO	264.60	244.06	57.51	48.07	1693
Fe ₃ O ₄	1116.06	1013.19	146.04	146.05	Decays
Fe ₂ O ₃	821.37	739.60	87.36	103.66	1838
Fe(OH) ₃	576.61	486.97	60.31	74.70	–
Fe(OH) ₂	561.14	479.27	88.16	96.97	–

pressure above the mechanical mixture of Fe₂O₃ and Fe₃O₄. The dissociation pressure of stoichiometric Fe₂O₃ is 250 times greater than the dissociation pressure of magnetite Fe₃O₄, which proceeds by reaction



The solubility of oxygen in liquid iron increases with temperature: in the temperature range 1539–1850 °C, it is described by the equation

$$\lg[\%O] = (-6629/T) + 2.939,$$

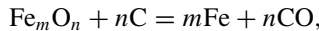
and in the temperature range 1850–2046 °C

$$\lg[\%O] = (-9830/T) + 4.496,$$

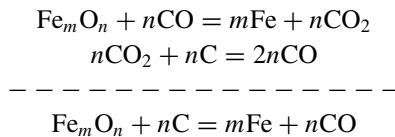
at 1600 °C, the solubility of oxygen in liquid iron is 0.235%. Oxygen solutions in iron are characterized by significant negative deviations from ideal behavior, at 1600 °C $\gamma_{O(\text{Fe})}^\circ = 0.0105$, and the interaction parameter $e_{O(\text{Fe})}^O = -0.17$. Carbon reduces the activity of oxygen in liquid iron, at 1600 °C the interaction parameter $e_{O(\text{Fe})}^C = -0.421$. The minimum concentration of oxygen in iron during carbon deoxidation at 1600 °C and $p_{\text{CO}} = 1 \text{ atm}$ is $2.453 \times 10^{-3\%}$ at 2.443% C.

18.2 Reduction of Iron by Carbon and Gases

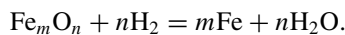
Iron oxides can be reduced with solid carbon and gases: carbon monoxide (CO), hydrogens (H₂), methane (CH₄) and mixtures thereof. The reduction of oxides with solid carbon proceeds according to the reaction



which should not be equated with the processes of direct production of iron by reduction of oxides, bypassing the blast furnace. Since the contact of interacting solid phases is constantly broken, above 900 °C, the process occurs with the participation of the gas phase



The reduction of iron oxides with hydrogen proceeds according to the reaction



The equilibrium equations in the Fe–O–C and Fe–O–H systems are found by combining the known equilibrium reactions in the Fe–FeO, FeO–Fe₃O₄, Fe₃O₄–Fe₂O₃ systems with the reactions

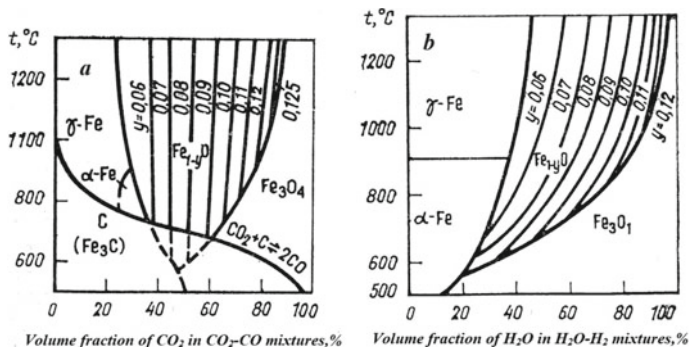
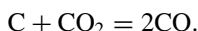
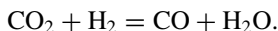


Fig. 18.3 Balance between iron, wustite, magnetite and mixtures of CO_2 - CO -C (a) and hydrogen-water vapor (b)



C-O and H-O systems are connected by equilibrium



The calculation results in the Fe-O-C and Fe-O-H systems are shown in Fig. 18.3. As can be seen from the above data, iron oxides can be reduced by carbon to iron ($p_{\text{tot}} = 0.1 \text{ MPa}$) at temperatures above 710°C . At lower temperatures, recovery proceeds to wustite. Below the equilibrium curve of the reaction of interaction of carbon dioxide with carbon, the gas mixture is supersaturated with carbon, and therefore, it falls out into an independent phase.

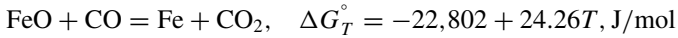
In accordance with the principle of A. A. Baikov, during the reduction of iron oxides, the transformation process below 570°C proceeds according to the scheme $\text{Fe}_2\text{O}_3 \rightarrow \text{Fe}_3\text{O}_4 \rightarrow \text{Fe}$, and above 570°C , with the formation of wustite as an intermediate phase: $\text{Fe}_2\text{O}_3 \rightarrow \text{Fe}_3\text{O}_4 \rightarrow \text{FeO} \rightarrow \text{Fe}$. Gibbs energy value for exothermic reaction



and for the endothermic reaction



Exothermic reduction of wustite to iron by carbon monoxide



18.3 Cast Iron Electrothermics

The first electric ore-smelting furnaces for the smelting of cast iron (electric blast furnaces) appeared in 1908. The upper part of the furnace was made in the form of a shaft copying the profile of the blast furnace, and in the lower part of the large-diameter furnace, electrodes were placed at an angle to the vertical (Fig. 18.4).

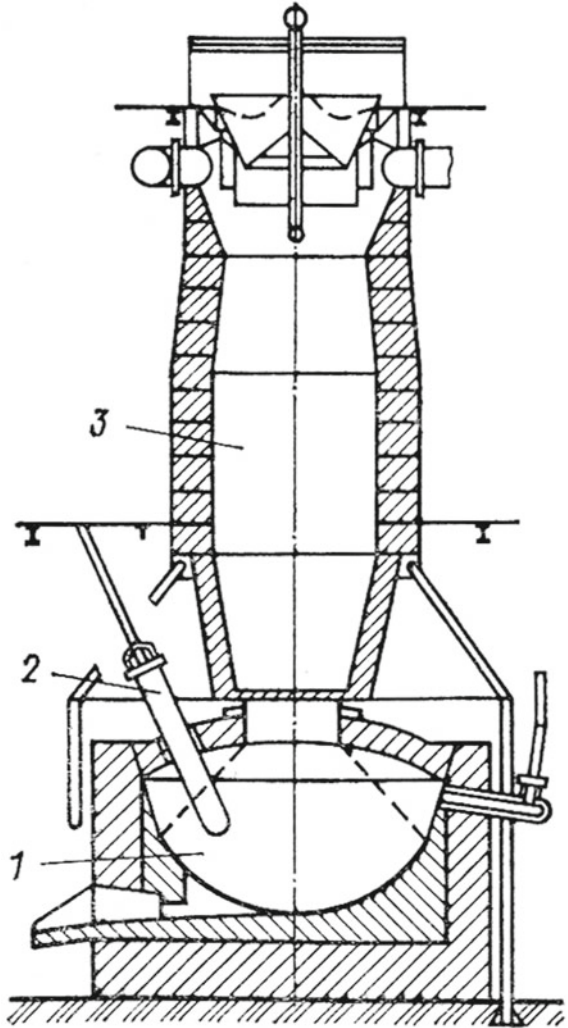
Due to the fact that the consumption of the carbon reducing agent when using the electrothermic method decreases due to heat generation during passage of the current through the charge and burning of high power electric arcs, the amount of released gases is small, their temperature is lowered, and the reduction of iron oxides by carbon monoxide in the upper part of the shaft furnace practically does not receive development. This explains that all electric furnaces for the smelting of cast iron in terms of basic structural parameters are similar to ore-smelting electric furnaces used for smelting ferroalloys by a continuous method.

Such furnaces are called low-shaft furnaces. In 1965–1966, furnaces with an installed transformer capacity of 60 MV·A were put into operation (Fig. 18.5), in which 123 tons of pig iron (4% C, 1% Si, 0.07% S) consumed 1523 kg of pellets (950 kg of iron), 400 kg of coke, 234 kg of limestone, 122 kg of dolomite. Melting is carried out on slag basicity $(\text{CaO} + \text{MgO})/\text{SiO}_2 = 1.36$; the specific energy consumption is 2464 kWh/t of pig iron or 69.8% of the total heat supply balance, 28.3% of the heat comes from the oxidation of carbon and 1.9% from the processes of slag formation. 57.4% of heat is consumed for the reduction of oxides, limestone and dolomite decomposition is 4.4%, moisture evaporation is 0.8%, pig iron heat is 9.4%, slag heat is 7.3%, and blast furnace gas is 17.5%.

Iron smelting with the use of fluxed sinter reduces the specific energy consumption up to 2000 kWh/t. The use of partially metallized and heated charge is promising. Heating and preliminary reduction of the charge in tube furnaces heated with the top gas increase the productivity of electric furnaces, and the energy consumption decreases to 1000–1800 kWh/t at a coke consumption of ~300 kg. The basicity of slag in an electric furnace is usually maintained at the level of $(\text{CaO} + \text{MgO})/\text{SiO}_2 = 1.4\text{--}1.8$. To reduce the viscosity of the slag, it is advisable to have 8–12% MgO in it. Top gas contains %: 60–75 CO; 25–30 CO₂; 8–10 N₂; 2–3 H₂; ~1% CH₄; 0.3–0.4 O₂, while blast furnace gas contains %: 24–30 CO; 9–18 CO₂; 55–59 N₂; 0.2–0.5 H₂; 1–2 CH₄.

A feature of the bath structure is the formation of a “pillow” consisting of coke mixed with lime. In this zone, there are also drops of cast iron, falling to the bottom, where they create a metal bath. Slag fills mainly the free spaces in the lower part of the coke layer. There is no metal or slag directly under the electrodes, and there is “dry” coke heated in a working furnace to 2000–3000 °C. The mechanism of the passage of electric current in the furnace is not completely clear, but, apparently,

Fig. 18.4 Scheme of an electric blast furnace,
1—bath; 2—electrodes;
3—shaft



between the pieces of coke “pillow” in the places of contact, small electric arcs are formed. Most of the power is released in areas around the bottom of the electrodes. The electrical conductivity of the charge located in the upper part of the furnace is small, and the main part of the charge conductivity currents passes through the coke layer. Large coke accumulates in it, while small coke is spent on the reduction and heating of the charge in the zone of preliminary preparation of the charge. To control the electrical resistance of the furnace bath, two coke fractions are used: 0–20 and 30–60 mm; the power of the high-temperature electric arc discharge depends on the ratio of their quantities.

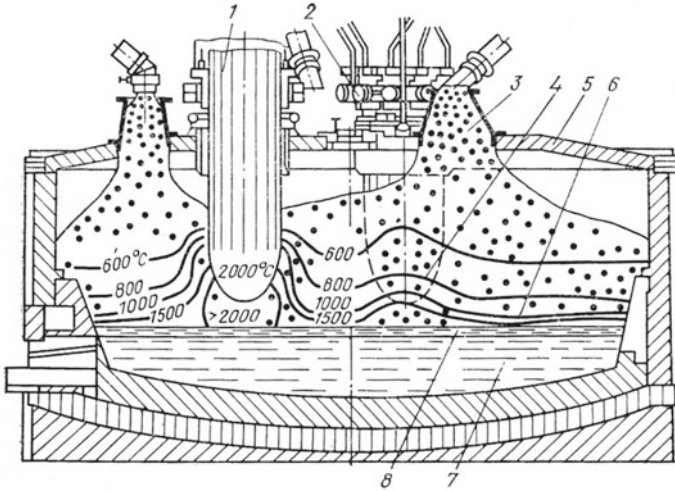


Fig. 18.5 Diagram of the structure of the bath of an ore-smelting furnace for smelting cast iron, 1—electrode; 2—contact node; 3—charge; 4—coke layer; 5—arch; 6—fine coke mixed with lime; 7—metal; 8—slag

At the end of the twentieth century, processes were developed for the production of iron and cast iron with the use of low-temperature plasma. As an example, in Fig. 18.6, the scheme of cast iron production, developed by the Swedish company SKF Steel,

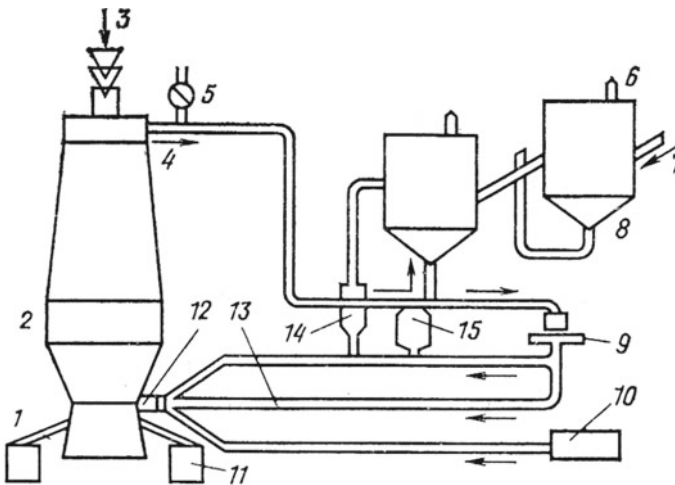


Fig. 18.6 Scheme for producing cast iron using low-temperature plasma, 1—slag; 2—recovery and melting zones; 3—coke; 4—gas; 5—pressure control; 6—ore feeder; 7—dry concentrate; 8—preliminary recovery; 9—compressor; 10—coal dust; 11—cast iron; 12—plasma generator; 13—regenerated gas; 14—prerestored concentrate; 15—slag-forming additives

is given. In the process, a plasma generator, iron ore concentrate, previously partially reduced by exhaust gases, and coal dust are used. The process eliminates the use of sintering machines and the production of coke. The specific investment in this process is 1/3, and operating costs—80% of the costs in the normal production of cast iron. The conclusion about the effectiveness of such processes can be made after a long and comprehensive study of the operation of industrial furnaces.

Chapter 19

Metallurgy of Ferronickel



Nickel metal was first obtained in 1751 by the Swedish chemist A. Kronstedt, who proposed the name of the element. A much cleaner metal was obtained in 1804 by the German chemist I. Richter. The nickel content in the earth's crust is $5.8 \times 10^{-3}\%$. The overwhelming majority of nickel is used to produce alloys with other metals (Fe, Cr, Cu, etc.) that are distinguished by high mechanical, heat-resistant, anti-corrosion, electrical and thermoelectric properties. A significant amount of nickel is consumed for the production of alkaline batteries and anti-corrosion coatings. Malleable nickel in its pure form is used for the manufacture of sheets, tubes, etc. Nickel is also used in the chemical industry for the production of special chemical equipment and as a catalyst for many chemical processes.

19.1 Properties of Nickel and Its Compounds

Nickel—an element of the VIIIb group of the Periodic system of elements refers to the transition elements of the iron triad. Atomic number 28, atomic mass 58.71, configuration of the electron shell $3d^8 4s^2$, density 8.92 g/cm^3 , melting point 1451°C and boiling point 2960°C , exhibits a variable valence from 1 to 4, most often 2. Under normal conditions, nickel exists in the form β -modifications with face-centered cubic lattice («fcc»), but being subjected to cathodic atomization in hydrogen, forms a α -modification having a hexagonal lattice. Nickel is ferrimagnetic—Curie point 358°C .

Ni–Fe system. Solid alloys of the Ni–Fe system are a continuous series of solutions based on γ -Fe; in the liquid state, both elements also have unlimited solubility (Fig. 19.1). Solutions of nickel in liquid iron are characterized by negative deviations from ideal behavior at 1600°C $\gamma_{\text{Ni(Fe)}}^\circ = 0.617$, and solutions of iron in liquid nickel are also characterized by negative deviations from ideal behavior at 1600°C $\gamma_{\text{Fe(Ni)}}^\circ = 0.355$.

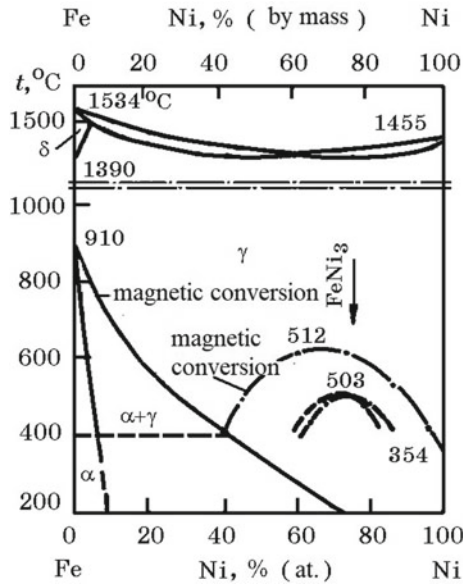
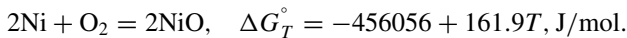


Fig. 19.1 Equilibrium diagram of Ni-Fe system

Ni-O system. Oxygen in nickel dissolves in noticeable amounts (Fig. 19.2), at 1873 K the solubility is 0.6%.

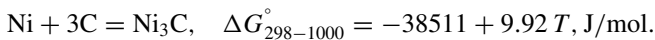
Nickel forms oxides NiO and Ni₂O₃ with oxygen. The standard heat of formation is NiO $\Delta H_{298}^\circ = -239.74$ kJ/mol. The temperature dependence of the Gibbs energy of the reaction for the formation of NiO from elements is described by the equation



Summary data on the thermodynamic constants of nickel compounds are given in Table 19.1.

Ni-C system. The state diagram of the Ni-C system has a simple eutectic form (Fig. 19.3).

In the Ni-C system, metastable carbide Ni₃C exists (prototype Fe₃C)



The solubility of carbon in liquid nickel in the temperature range of 1400–1700 °C is described by the equation

$$\lg X_C = 1.55 - 896/T,$$

where X_C is the carbon content, % (at.). Carbon solutions in liquid nickel are characterized by negative deviations from ideal behavior at 1600 °C $\gamma_{C(\text{Ni})}^\circ = 0.82$.

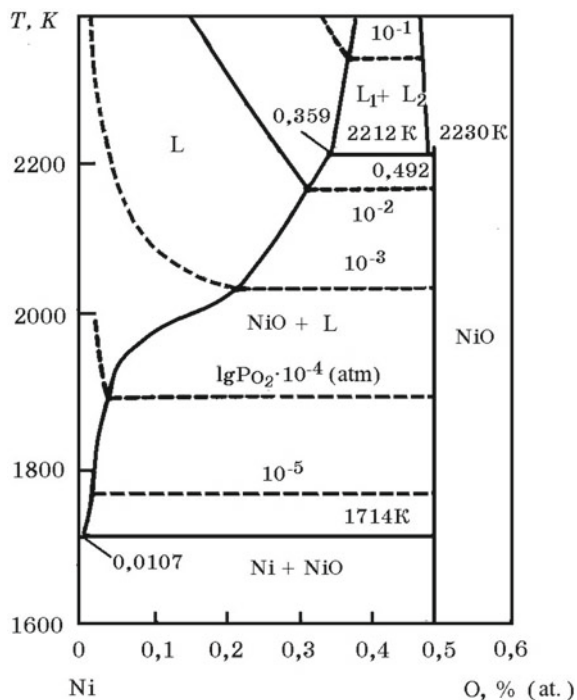


Fig. 19.2 Equilibrium diagram of Ni–O system

Table 19.1 Thermodynamic constants of nickel compounds

Compound	ΔH_{298}° , kJ/mol	ΔG_{298}° , kJ/mol	S_{298}° , J/(mol K)	$C_{p, 298}^{\circ}$, J/(mol K)
NiO	–239.74	–221.59	37.99	44.33
NiS	–80.33	–76.81	52.96	47.11
Ni ₃ S ₂	–192.46	–186.61	133.88	117.65
NiSi	–86.35	–84.76	46.80	44.76
NiSi ₂	–87.02	–86.23	64.85	65.27
Ni ₃ C	–75.31	–25.10	–	–
Ni ₂ P	–184.09	–	–	–

Ni–Si system. Nickel with silicon forms a series of thermodynamically strong silicides Ni₃Si (13.76% Si), Ni₃Si₂ (16.07% Si), Ni₂Si (19.31% Si), Ni₅Si₃ (24.19% Si), NiSi (32.37% Si) and NiSi₂ (48.90% Si) (Fig. 19.4). Silicon in significant quantities dissolves in solid nickel, and an increase in the concentration of silicon in nickel reduces the melting point of alloys.

Ni–Al system. In this system, there are a number of aluminum nickelides NiAl₃ (42.03% Ni), Ni₂Al₃ (59.19% Ni), NiAl (68.51% Ni), Ni₅Al₃ (78.3% Ni) and Ni₃Al

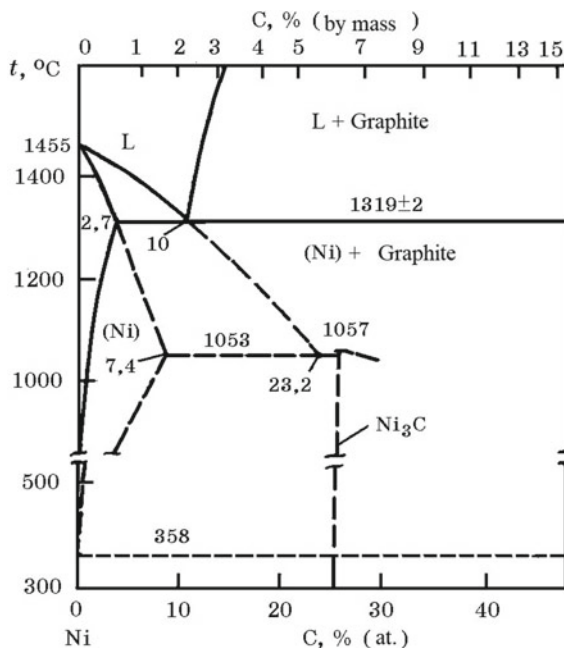


Fig. 19.3 Equilibrium diagram of Ni–C system

(86.71% Ni) (Fig. 19.5). The solubility of aluminum in solid nickel is quite large, although nickel in solid aluminum has an extremely low solubility.

Ni–S system. In this system, sulfides Ni_3S_2 (26.7% S), NiS (35.33% S), Ni_3S_4 (42.14% S) and Ni_2S (52.22% S) are formed (Fig. 19.6). In solid nickel, the solubility of sulfur in equilibrium with Ni_3S_2 sulfide does not exceed 0.005%.

Ni–P system. Of the many phosphides in the Ni–P system, Ni_5P_2 and Ni_2P are the most stable (Fig. 19.7). Phosphide Ni_3P is isomorphic to Fe_3P and Mn_3P . An increase in phosphorus in nickel decreases the liquidus temperature from 1452 °C for pure nickel to a eutectic temperature of 880 °C at 11% P. The partial heat of dissolution of phosphorus in nickel is $\Delta \bar{H}_T^\circ = -251 \text{ kJ/mol P}$ (in iron— $\Delta \bar{H}_T^\circ = 140 \text{ kJ/mol P}$).

Nickel silicate systems. In the NiO– SiO_2 system, the Ni_2SiO_4 compound is known. The Gibbs energy of the reaction for the formation of nickel orthosilicate from oxides is described by the equation



Continuous solid solutions are formed in the ternary MgO–NiO– SiO_2 system. Within 50% (mol.) Ni_2SiO_4 + 50% (mol.) Mg_2SiO_4 —the system is truly binary. The CaO–NiO– SiO_2 system contains the ternary compound $\text{CaNiSi}_2\text{O}_6$, which coexists with SiO_2 , CaSiO_3 , NiSiO_4 and NiO.

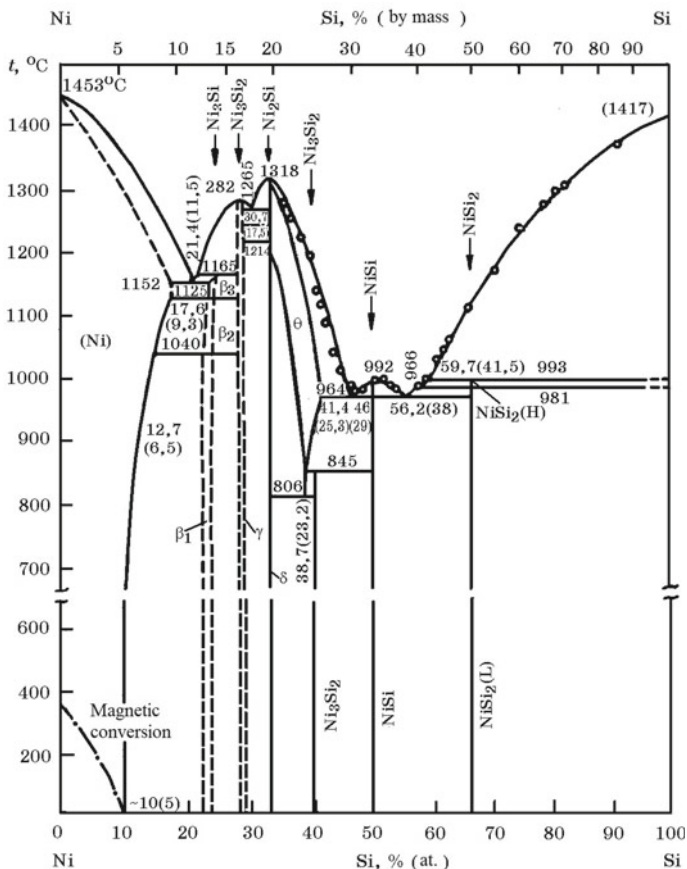


Fig. 19.4 Equilibrium diagram of Ni-Si system

19.2 Nickel Minerals and Ores

More than 100 minerals containing nickel are known, the most important of which are millerite NiS , pentlandite $(\text{Fe, Ni})_9\text{S}_8$, nickaline NiAs , violarite Ni_2FeS_4 , zigenite $(\text{Co, Ni})_3\text{S}_4$, polydimitite Ni_3S_4 , fletcherite $\text{Cu}(\text{Ni, Co})_2\text{S}_4$ and native nickel (as part of meteorites). From ores containing various amounts of these minerals, 80% of all nickel was obtained in the world in the early 90s of the twentieth century. However, their reserves are limited (14% of the global nickel reserves), therefore, low-grade silicate ores, the nickel content of which barely reaches 1–2%, are becoming increasingly involved in production. These are the so-called laterite ores. Silicate ores are divided into magnesia, siliceous and aluminous varieties, depending on the composition of the gangue. Large reserves of iron ores containing nickel (50–60% Fe and 1–1.5% Ni) are known, among which limonite and saprolite nickel-containing ores are distinguished.

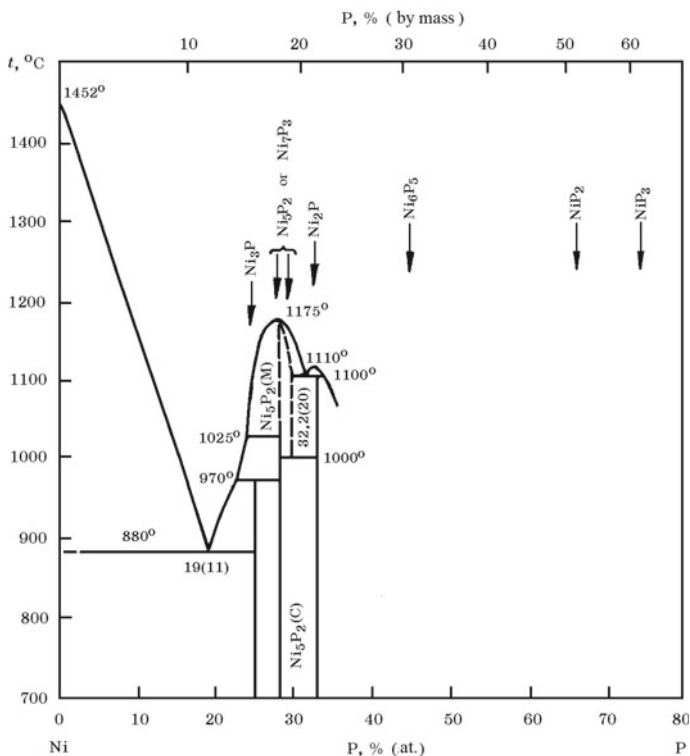


Fig. 19.7 Equilibrium diagram of Ni-P system

Below is the chemical composition of lateritic ores, %:

Component	Ni	Co	Fe	MgO
<i>Ore</i>				
Limonite	1.26	0.10	46.5	0.1
Saprolite	2.20	0.01-0.05	15-20	15-20

Oxidized nickel ores are complex minerals. Among the main nontronites is $\{Fe^{3+} [(OH)_2Al_{0.33}Si_{3.67}O_{10}]Na \cdot (H_2O)_4\}$, which belongs to the group of smectites—hydroxylaluminosilicates. The group of smectites also includes minerals: montmorillonite, beidellite, hectorite and saponite. Their general formula is represented as: $X_{0.33}Y_2Si_4O_{10}(OH)_2 \cdot 4H_2O$, where X is Ca or Na; Y— Fe^{3+} , Al, Cr, Mg, Ni, Zn, Li.

These mineral formations may include $\leq 14\%$ Al_2O_3 , $\leq 8\%$ MgO and in small amounts of CaO ($\leq 2\%$), K_2O and Na_2O , in some cases also NiO and Cr_2O_3 .

Along with nontronite, ores also contain montmorillonite, a clay mineral with a variable chemical composition: $M^+ [(Al_{2-y}Mg)Si_4O_{10}(OH)_2]^{-y} n \cdot H_2O$, where M^+ is Na^+ , Li^+ , K^+ and, in some cases, $0.5 M^{2+}$ (Ca^{2+} , Mg^{2+} , etc.). Iron hydroxide, which

is a mineral component of ore, contains up to 80% Fe₂O₃, 4–8% SiO₂, 1.2% Al₂O₃, 1% MgO and 13% H₂O. Among the minerals composing this clay ore, serpentine (Mg, Fe, Ni_{8-x}, Al_x)·Si_{4-x}·Al_xO₁₀(OH)₈ is also included.

One of the potential nickel- and cobalt-containing types of mineral raw materials is ferromanganese nodules of the world's oceans. The chemical composition of nodules varies widely, %: 0.75–50.4 Mn; 0.83–32.4 Fe; 0.037–2.46 Ni; 0.1–2.57 Co; 0.014–1.9 Cu. Reserves of oceanic nodules of the Pacific Ocean are about 10¹² tons. However, all these deposits are confined to the deep-water central regions of the World Ocean. The possible production of nickel from them is ~15 billion tons, taking into account the average nickel content in nodules of 1.24%.

19.3 The Technology of Production and Refining Ferronickel

Ferronickel is produced at the Pobuzhsky ferronickel plant (Ukraine) using oxidized nickel-containing ores from the Pobuzhsky deposit (0.9–1.0% Ni) and imported—relatively rich in nickel content (2.0–2.7%). Open-pit mined nickel ore from Pobuzhsky deposit has the following chemical composition, %: 0.9–1.0 Ni; 0.05–0.09 Co; 20 Fe; 32–44 SiO₂; 5–7 Al₂O₃; 4–6 MgO; 1.2–2.0 CaO; 1–2 Cr₂O₃. When using Pobuzhsky ore, low-grade ferronickel (4–6% Ni) is obtained at a high specific energy consumption, imported nickel ore from New Caledonia allows smelting ferronickel with a content of 15–25% Ni (Table 19.2).

The technological scheme for producing ferronickel in electric furnaces includes the following main stages (Fig. 19.8):

- preparation and averaging of nickel-containing ore in an open warehouse;
- preparation, dosing of charge materials and firing of a mixture consisting of ore, limestone, anthracite and recycled dust in rotary kilns;
- smelting of ferronickel in ore-smelting electric furnaces using a hot charge (cinder) from rotary tube furnaces;

Table 19.2 Chemical composition of ferronickel production Pobuzhsky plant

Grade	Ni	Co	Si	C	Cr	S	P	Fe
FeNi-5M	5–25	0.3–0.6	<0.3	<0.1	<0.3	<0.08	<0.03	Basis
FeNi-6	12–18	0.5–0.8	<0.4	1.0–2.5	<2.0	<0.1	<0.03	Basis
FeNi20*	15–25	**	<0.4	1.0–2.5	<2.0	<0.4	<0.03	Basis

* According to ISO 6501:1998 (E)

** Ratio Co/Ni = 1/20 ÷ 1/40, only for information

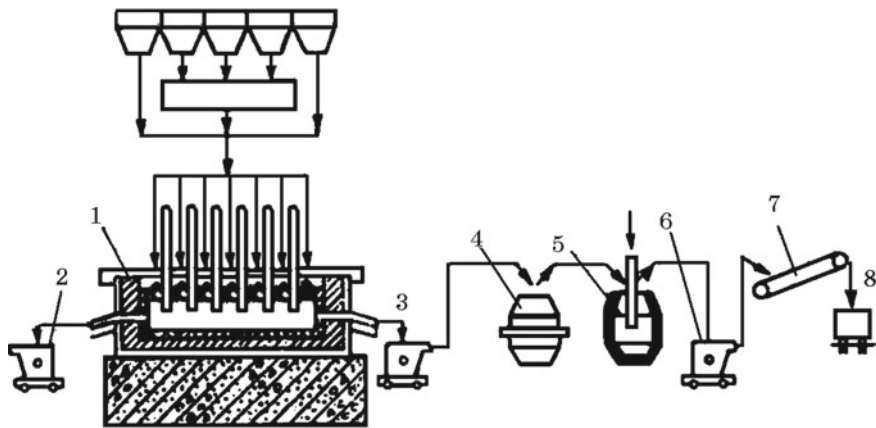


Fig. 19.8 Technological scheme for the production of ferronickel, 1—electric furnace; 2—slag bucket; 3—nickel refining bucket; 4—converter with acid lining to remove Si and Cr; 5—a converter with a basic (periclase) lining for dephosphorization; 6—bucket; 7—filling machine; 8—railway car

- refinement of ferronickel by methods of out-of-furnace desulfurization of the melt in the ladle, followed by purging of the ferronickel with oxygen, first in the converter with acid and then with the basic lining;
- casting of refined ferronickel on conveyor-type filling machines.

When smelting ferronickel using low-grade Pobuzhsky nickel ore, the mixture for firing in tubular rotary kilns consists of the following components: 1 ton of dry ore, 352 kg of limestone, 106 kg of anthracite bar and 5 kg of recycled dust. The furnaces have a diameter of 3 m and a length of 75 m. The firing zone in the furnace is 9–12 m. Fuel oil is used, the consumption of which is 85.5 kg per 1 ton of dry ore. The torch temperature reaches 1200 °C, and the charge temperature does not exceed 850 °C in order to avoid overheating and the formation of ring crusts. Ovens operate on a counter-current principle. The temperature of the exhaust gases is 220–300 °C, and the charge (cinder) is 840 °C.

The hot cinder comes from a tube furnace into an ore-smelting electric furnace with a unit capacity of $3 \times 16.7 = 50.1$ MV A (Fig. 19.9). The furnace bath has dimensions of $25.75 \times 9.54 \times 4.76$ m. The lining of the bath: The hearth and walls in the area of ferronickel are fire-resistant brick, and in the slag zone are carbon blocks. The furnace is equipped with six self-baking electrodes with a diameter of 1200 mm. The maximum current in the electrode is 41.4 kA. The process is conducted at voltage levels corresponding to 500, 403 and 297 V. Melting products are produced separately through notches for ferronickel and for slag. With the melting of 1 ton of cinder, 120–140 kg of rough ferronickel and 650–700 kg of slag are obtained. The composition of the furnace slag is given below, %:

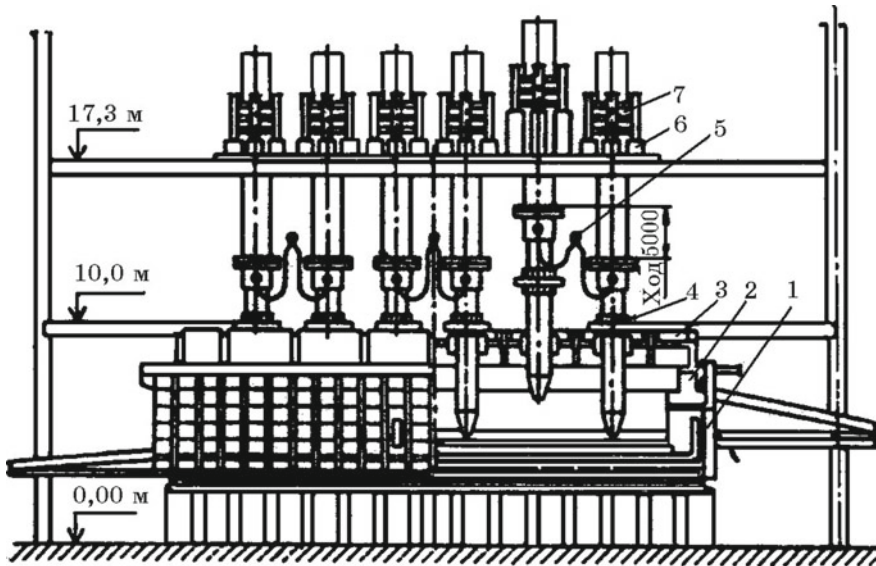


Fig. 19.9 Diagram of a furnace for smelting ferronickel, 1—casing of the furnace; 2—lining; 3—arch; 4—sealant; 5—current lead; 6—mechanism for moving the electrode; 7—electrode bypass mechanism

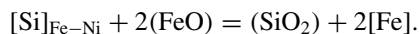
Component	Ni	Co	Fe	SiO ₂	CaO	MgO
Slag 1	0.02	0.023	10.5	51.7	21	4.5
Slag 2	0.06	0.006	8.4	50.0	25	6.0

Slag is used as a building material. When using imported ore, waste slag has a higher content of MgO and Al₂O₃.

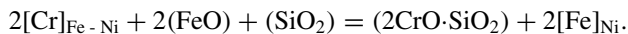
Ferronickel refining. Since ferronickel has a high sulfur content coming from a carbonaceous reducing agent and from ore, it is subjected to preliminary out-of-furnace desulfurization in a ladle with sodium carbonate (soda). The process of sulfur removal can be generally represented by the reaction



When desulfurizing ferronickel in a ladle (soda consumption 4–5% of the metal weight) (Fig. 19.8), the degree of desulfurization is 50–60%. Partially purified from sulfur, ferronickel is poured into the converter with an acid lining and is purged with oxygen to remove chromium and silicon. Silicon oxidation proceeds by the reaction:



Acidic slag promotes the transition of chromium from ferronickel to slag by reaction



The dump slag of refining ferronickel in an acidic converter has the following composition, %: 52–55 SiO₂; 15–25 Fe; 1.7 CaO; 2–6 MgO; 1–8 Cr₂O₃; 3 Al₂O₃; 0.09 Ni. After refining in the converter with the acid lining, the ferronickel is poured into the converter with the basic lining (Fig. 19.8) and converted to remove phosphorus. The process of phosphorus oxidation in the main converter in the presence of highly basic slags occurs according to the reaction



When the melt is purged with oxygen in a converter, carbon oxidation occurs along with dephosphorization when a higher temperature is reached.

Ferronickel is poured on conveyor machines. The weight of the ingot is 25–35 kg. The basic conversion slag has the following composition, %: 15–20 CaO; 5–10 SiO₂; 35–50 FeO; 0.05 Ni; 0.005 Co; 1–10 Cr₂O₃. Slag of acidic and basic conversion undergoes magnetic separation to extract particles of ferronickel. The specific energy consumption for metallurgical processing of 1 ton of Pobuzhsky dry nickel-containing ore with 1% Ni is 810 kWh/t or 78,200 kWh per 1 ton of nickel. When using the ore with 2.5–3.0% Ni, specific energy consumption is two times lower. Nickel extraction in rough ferronickel is 96.76%, nickel loss with dust is about 0.25%, 0.34% goes into sludge; 2.65% Ni in waste slag. Due to the relatively large amount of recycled ore dust containing 2.41% Ni, it is necessary to agglomerate it, since its use without agglomeration is accompanied by increased dust entrainment from rotary tube furnaces.

Sources of sulfur in the charge are carbonaceous reducing agent and fuel oil (1.8% S), and phosphorus—carbonaceous reducing agent and nickel ore. When fired in a tubular rotary kiln, 32.13% of the sulfur goes into the cinder, and the rest goes into gases and dust. From the reducing agent, sulfur almost completely passes into the cinder, and from fuel oil to cinder—16.48%. Phosphorus enters with nickel ore, a reducing agent and almost completely enters the cinder.

A technology is being developed for producing ferronickel by purging a melt of iron-nickel ore with a reducing gas. The nickel content in the resulting product increases tenfold compared with the original ore and is about 70%. The reduced metal with stirring coagulates and precipitates, forming a bottom metal phase—ferronickel. With the addition of 20% limestone and with a total nickel content of 0.10% in the slag, the nickel concentration in ferronickel reaches 70% with the recovery of 93.1%. The extraction of iron in ferronickel is 4.2%.

Chapter 20

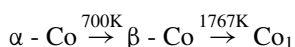
Metallurgy of Cobalt



Metal cobalt was first obtained in 1735 by the Swedish chemist G. Brandt. The cobalt content in the earth's crust is $4 \cdot 10^{-3}$. Natural cobalt contains two stable isotopes: ^{59}Co (99.83%) and ^{57}Co (0.17%); of the obtained artificial radioactive isotopes, the most important is ^{60}Co . Cobalt is mainly used to produce heat-resistant, corrosion-resistant, magnetic and other special alloys and steels. In powder metallurgy, cobalt is part of various superhard compositions (WC-Co, ZrC-Co, etc.). Powdered cobalt, as well as Co_3O_4 , serves as catalysts. Fluoride CoF_3 is used as a strong fluorinating agent, Tenar's blue, and especially cobalt and potassium silicate—as paints in the ceramic and glass industries. Radioactive cobalt ^{60}Co is used as a radiation source (cobalt gun).

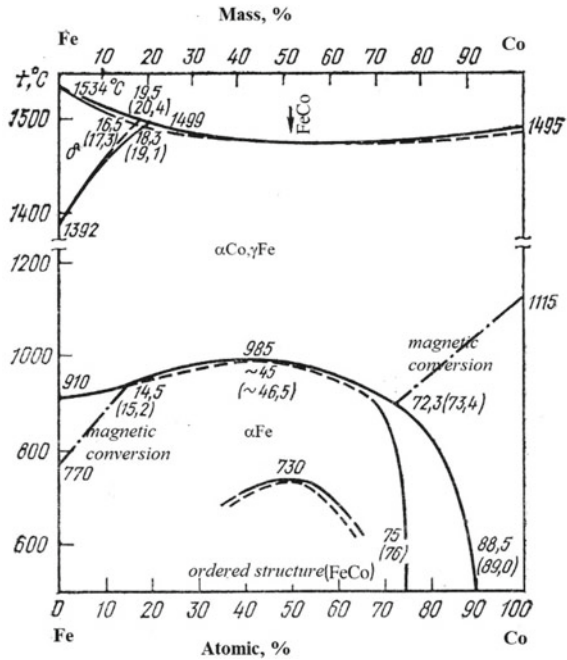
20.1 Properties of Cobalt and Its Compounds

Cobalt is an element of group VIIIb of the Periodic system of elements, refers to the transition elements of the iron triad. Atomic number 27, atomic mass 58.9332, configuration of the electron shell $3d^74s^2$, valencies 2 and 3, melting point 1494 °C, boiling point 2960 °C, density 8.8 g/cm³ at 20 °C. Cobalt is ferromagnetic—Curie point 1121 °C. Cobalt has two modifications: α -Co with an hcp lattice and β -Co with an fcc lattice.



Co-Fe system. Cobalt dissolves unlimitedly in iron (Fig. 20.1), stabilizing the austenitic structure (γ -Fe). Superstructures of Fe_3Co , FeCo and FeCo_3 were detected. Melts of the Co-Fe system are close to ideal solutions, at 1600 °C $\gamma_{\text{Co(Fe)}}^\circ = 1.051$, $\gamma_{\text{Fe(Co)}}^\circ = 1.590$.

Fig. 20.1 Equilibrium diagram of Fe-Co system



Co-O system. Cobalt with oxygen forms two stable compounds, Co_3O_4 ($\text{CoO} \cdot \text{Co}_2\text{O}_3$) and CoO , whose melting points are 1240 and 2978 K, respectively. Co_2O_3 oxide is stable only in the form of $\text{Co}_2\text{O}_3 \cdot \text{H}_2\text{O}$ hydrate, CoO_2 oxide is unstable, decomposes at temperatures above 100 °C. In liquid cobalt, oxygen dissolves by reaction

$$1/2\text{O}_2 = [\text{O}]_{\text{Co}}, \quad \Delta G_T^\circ = -84,935 - 7.61 T, \text{ J/mol.}$$

Co-C system. Carbon dissolves in solid and liquid cobalt. A solid solution of carbon in cobalt (carbon in an α -solid solution) forms a eutectic with graphite ($T_{\text{eut}} = 1582 \text{ K}$) at 2.9% C (Fig. 20.2).

The dependence of the solubility of carbon in liquid cobalt (molar fractions) is described by the equation

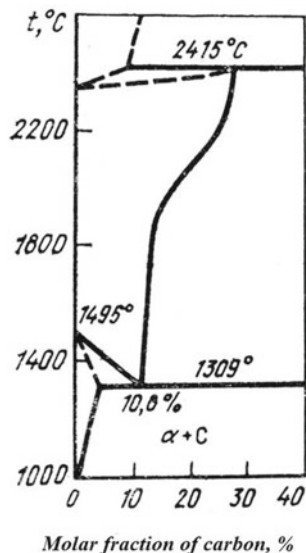
$$\lg X_C = -1050/T - 0.265.$$

There is evidence of metastable carbides CoC_2 and CoC_3 existing at temperatures above 450 and 500 °C, respectively. The temperature dependence of the Gibbs energy of the reaction for the formation of CoC_2 carbide is described by the equations:

$$2\text{Co}_{(s)} + \text{C}_{(g)} = \text{Co}_2\text{C}_{(s)}, \quad \Delta G_{1500-1767\text{K}}^\circ = 16,535 - 8.75 T, \text{ J/mol,}$$

$$2\text{Co}_{(l)} + \text{C}_{(g)} = \text{Co}_2\text{C}_{(s)}, \quad \Delta G_{1767-2000\text{K}}^\circ = 13,814 - 8.37 T, \text{ J/mol.}$$

Fig. 20.2 Equilibrium diagram of Co-C system

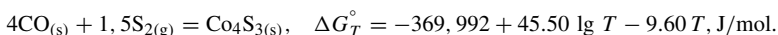
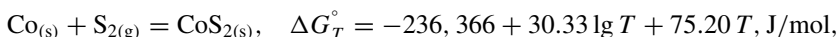
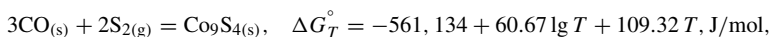
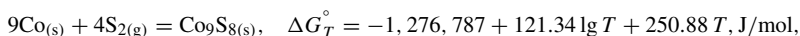


The solubility of carbon in Fe-Co-C melts depends on the temperature and cobalt content—with an increase in the cobalt content, the carbon concentration in them decreases.

Co-Si system. A series of silicides Co_2Si , Co_3Si_2 , CoSi , CoSi_2 , CoSi_3 is formed in the system (Fig. 20.3).

Co-Al system. A number of aluminides Co_2Al_9 , CoAl_{13} , Co_2Al_5 , CoAl are formed in the system. The most thermodynamically stable is CoAl , which melts at a temperature of 1645 °C.

Co-S system. This system is important for cobalt metallurgy, since the main minerals containing cobalt are represented by its sulfides. Sulfides are formed in the system: Co_4S_3 , Co_9S_8 , CoS , Co_3S_4 , CoS_2 (Fig. 20.4). The temperature dependence of the Gibbs energy of sulfide formation reactions is described by the equations:



Co-P system. Cobalt with phosphorus forms phosphides CoP_2 , CoP and CoP_3 .

Co-N system. Cobalt forms nitrides with nitrogen Co_3N and Co_2N .

CoO-SiO₂ system. Calcium orthosilicate Co_2SiO_4 is formed in the system (Fig. 20.5).

Fig. 20.3 Equilibrium diagram of Co-Si system

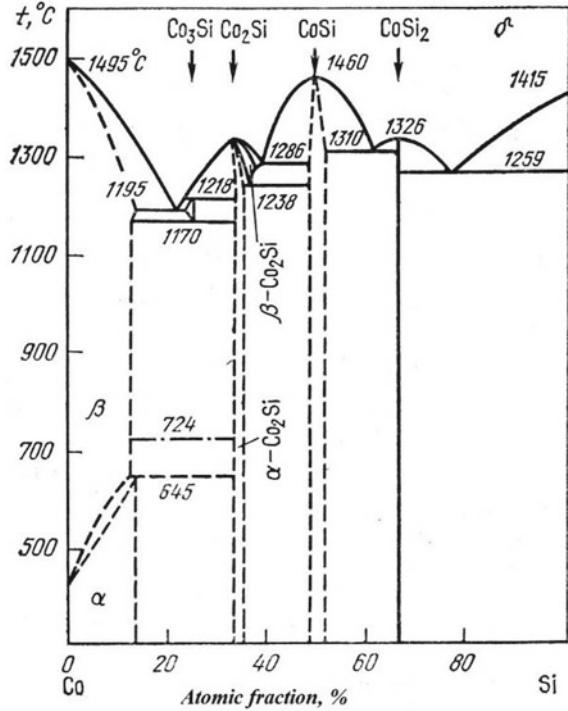


Fig. 20.4 Equilibrium diagram of Co-S system

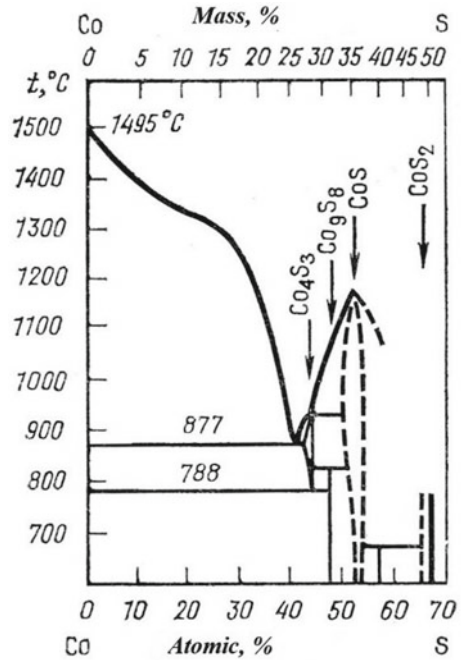


Fig. 20.5 Equilibrium diagram of CoO-SiO₂ system

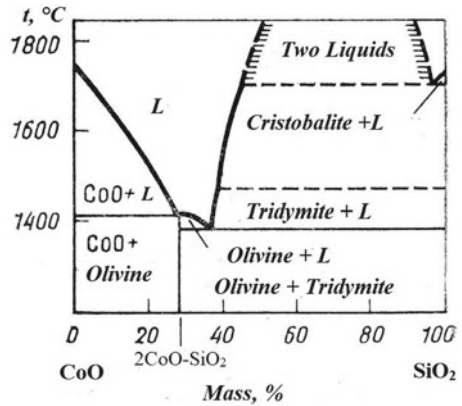
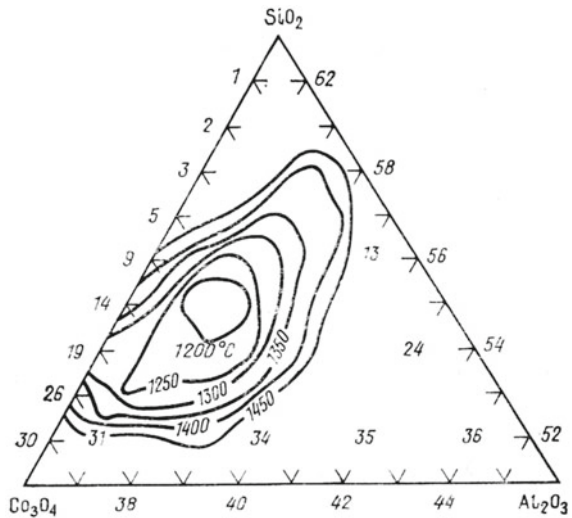


Fig. 20.6 Melting isotherms in the system Co₃O₄-Al₂O₃-SiO₂



Co₃O₄-Al₂O₃-SiO₂ system. Melting isotherms in the ternary system are shown in Fig. 20.6. There is a range of compositions with a melting point of 1200 °C.

20.2 Cobalt Minerals and Ores

The cobalt content in the ores is usually low, so it is mined as an accompanying metal in the processing of polymetallic ores. The largest producers of cobalt are Zaire, where about half of the world’s reserves are concentrated, Zambia, Japan, France and the USA.

Cobalt minerals and industrial ores containing cobalt are divided into three groups: arsenic, sulfur and oxidized. The cobalt content in these ores can vary from hundredths to 4%.

Arsenic cobalt ores. In these ores, cobalt is contained in the form of compounds with arsenic (arsenides) and/or sulfur (sulfoarsenides). Among the most important minerals in these ores, CoAsS cobaltin (35.41% Co; 45.26% As; 19.33% S) is noted, in which up to 5% cobalt can be replaced by iron. In Russia, arsenic cobalt ores are located in Tuva (Aksinskoe deposit). A large deposit of such ores is located in Morocco.

Sulur ores. In these ores, cobalt can be contained in the form of sulfide minerals: cobalt-pentlandite (Co, Fe, Ni)₉S₈, linneite (Co, Ni)₃S₄, carrolite Cu(Co, Ni)₂S₄, etc. Such polymetal ores contain up to 2.5–3% Co. In Russia, sulfur ores are located in the Krasnoyarsk Territory and on the Kola Peninsula. This type of ore is mined in Canada.

Oxidized ores. These ores are also polymetallic. In oxidized ores, silicate-nickel and sulfur ores are isolated containing up to 1–4% Co. Ores of this type are represented by the Pobuzhsky group of nickel ores (Ukraine). They contain %: 0.8–1.0 Ni; ≤0.08 Co; 1.7–2.5 Cr; 0.05–1.12 Cu; 0.1–0.3 Mn. The gangue is represented by silica (SiO₂) and iron oxides (Fe₂O₃). These ores are the feedstock for producing ferronickel, into which cobalt passes.

20.3 The Technology of Cobalt Production

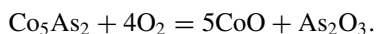
Metallic cobalt must meet the requirements given in Table 20.1.

Table 20.1 Chemical composition of metallic cobalt, %

Grade	Co, no less	Al	B	Fe	Si	Cd	Mn	Cu	As
	No more								
CO0	99.98	0.01	0.0003	0.003	0.001	0.003	0.0005	0.001	0.0005
CO1Au	99.35	–	0.0004	0.200	–	0.001	0.03	0.02	0.001
CO1A	99.30	–	0.0005	0.200	–	0.001	0.07	0.03	0.002
CO1	99.25	–	–	0.200	–	–	0.07	0.03	0.002
CO2	99.30	–	–	0.500	–	–	0.10	0.08	0.005
Grade	Mg	Ni	Sn	Sb	S	Pb	C	P	Zn
	No more								
CO0	0.001	0.005	0.0003	0.001	0.0003	0.0003	0.005	0.0005	0.001
CO1Au	–	0.30	0.0004	0.004	0.0006	0.0006	0.02	0.002	0.002
CO1A	–	0.30	0.001	0.004	0.0010	0.0010	0.02	0.003	0.003
CO1	–	0.30	–	0.004	–	–	0.03	–	–
CO2	–	0.50	–	0.010	–	–	0.10	–	–

In world practice, several technological schemes are used for processing cobalt-containing ores. The choice of a particular cobalt extraction method is determined by the mineralogical features of the ore.

Cobalt–arsenic ores are processed according to the pyro-hydrometallurgical scheme. At the first stage, the concentrate is subjected to firing, resulting in thermal dissociation of arsenides and then to sulfatized firing. The oxidation process of cobalt arsenide in general can be described by the reaction



The cinder after calcination is leached out with hydrochloric acid and treated with chlorine, and the cake is cyanidated in order to extract noble metals. After cleaning the solution from impurities and extracting noble metals, a pure solution of cobalt chloride is subjected to electrolysis.

Cobalt-containing sulfide ores are processed in various ways. In Russia, the leading method for the processing of nickel–cobalt-containing raw materials is the electromelting of sulfide ores. The purpose of sulfide ore smelting is to convert nickel, cobalt and copper to the sulfide phase, called *matte*. The second melting product is slag, which is a melt of oxides. The matte and slag in the bath of the electric furnace are separated by density. The sulfide melt, which has a high density, accumulates on the bottom of the furnace, and the slag is located above the matte layer. Sulfide melt is released from the furnace, its approximate composition, %: 7.12 Ni; 6.01 Cu; 0.37 Co; 61.0 Fe; 27.8 S; 5.8 FeO; 5.9 Fe₃O₃. The matte is poured into the converter and purged with an oxygen. The purpose of the conversion is the oxidation of iron sulfide and its conversion into converter slag. As a result of conversion, a sulfide melt is obtained, enriched with sulfides of nickel, cobalt and copper, called *nismatte*, the composition of which, %: 20.2 Ni; 30.3 Cu; 1.97 Co; 3.6 Fe; 23.6 S. Converter slag has the composition, %: 0.38 Ni; 0.19 Co; 46.5 Fe; 6.7 Fe₃O₄; 26.4 SiO₂.

Electric smelting slag containing nickel, cobalt and copper is not sent to the dump but is subjected to the so-called depletion operation. The essence of this operation is as follows. Electric furnace slag is poured into an ore-smelting furnace (Fig. 20.7) together with the part of nickel–cobalt concentrate and melted. Get the matte of depletion of slag containing, %: 8.4 Ni; 6.1 Cu; 1.0 Co; 60.3 Fe; 23.1 S.

An example is the material balance of the conversion of copper–nickel matte at the Severonickel plant (Norilsk). 25.8% Co and 50.9% Ni are supplied to the converter processing with matte of reduction melting, and 27.0% Co and 21.0% Ni with matte of depletion melting. In addition, an anode slurry is introduced into the converter, with which 12.5% Co and 6.8% Ni are added. With recycled products, 2.1% Co and 3.7% Ni are supplied. Metal wastes are also used in melting, with which 25.3% Co and 15.5% Ni are supplied. Cobalt and nickel are distributed between the smelting products as follows: 34.4% Co and 72.3% Ni go to nismatte, and 63.9% Co and 17.6% Ni go to converter slag. Thus, most of the cobalt is concentrated in the slag. An increase in cobalt extraction is achieved by subsequent cycles of depletion melting—slag conversion. The task of pyrometallurgical redistribution of ores is the maximum conversion of cobalt to converter slag. Cobalt-rich converter slag is melted

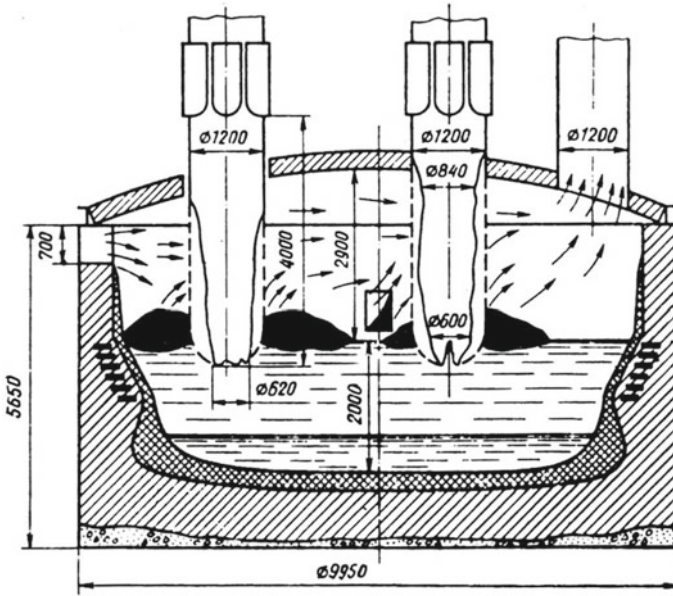
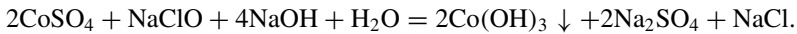
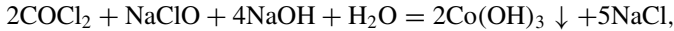


Fig. 20.7 Ore-smelting furnace for slag depletion

on cobalt matte, which is leached with hydrochloric or sulfuric acids. Ultimately, a solution of cobalt and nickel chlorides or sulfates is obtained. Cobalt is separated from nickel by sodium hypochlorite according to the reactions:



Almost all nickel remains in solution. The black precipitate of $\text{Co}(\text{OH})_3$ is calcined to remove moisture; the resulting Co_3O_4 oxide is reduced with hydrogen or carbon. Cobalt metal containing 2–3% of impurities (Ni, Fe, Cu, etc.) can be purified by electrolysis.

Multistage end-to-end technology for the extraction of cobalt and nickel is very energy consuming. Almost 6.2 tons of standard fuel are consumed per 1 ton of electrolytic nickel, and 45 tons of standard fuel per 1 ton of nickel in ferronickel.

Depending on the mineral composition of the ores and the content of cobalt in them, various hydrometallurgical schemes for the extraction of nickel and cobalt are also used. The scheme of the main stages of obtaining cobalt and nickel from Cuban lateritic (oxidized) ores is shown in Fig. 20.8.

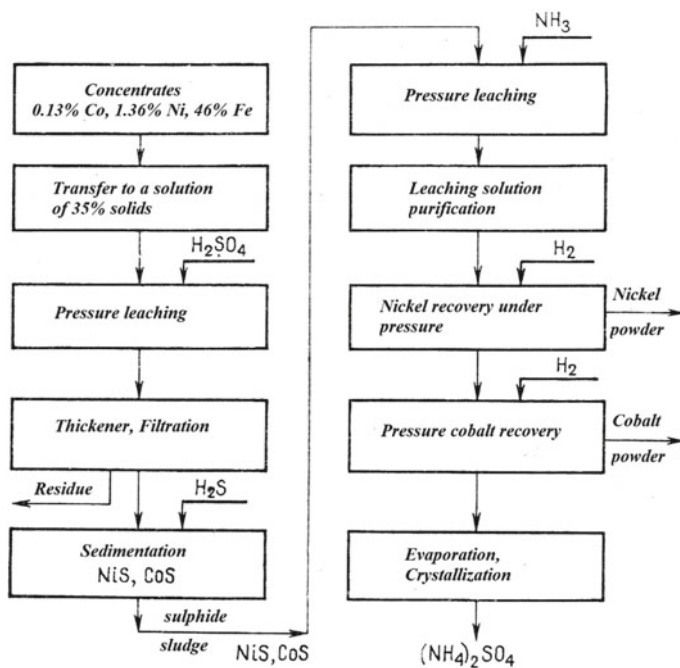


Fig. 20.8 Scheme for obtaining cobalt from laterite ores

Chapter 21

Metallurgy of Ferrophosphorus



Phosphorus was discovered in 1669 by the German chemist H. Brand, who received a substance glowing in the dark when urine was evaporated. The phosphorus content in the earth's crust is $9.3 \cdot 10^{-2} \%$. Natural phosphorus consists of one stable isotope ^{31}P . Six isotopes were obtained, of which ^{32}P was the most important (half-life of 14.22 days). The ^{32}P isotope is used as a labeled atom. In metallurgy, phosphorus is used as alloying and deoxidizing additives in the production of non-ferrous alloys (bronze, fechral, chromium, etc.), steels with high resistance to atmospheric corrosion.

21.1 Properties of Phosphorus and Its Compounds

Phosphorus—an element of the Vb group of the Periodic system of elements. Atomic number 15, atomic mass 30.97, electron shell configuration $3s^2 3p^3$, density 2.4 g/cm^3 , melting point of white phosphorus $44 \text{ }^\circ\text{C}$, boiling point $257 \text{ }^\circ\text{C}$. In compounds, phosphorus exhibits an oxidation state of +5, +3 and -3.

Elemental phosphorus exists in the form of several allotropic modifications, the main of which are white, red and black. White phosphorus is obtained in the solid state upon rapid cooling of phosphorus vapors, which occurs during the condensation of phosphorus vapors under conditions of electrothermal production. Heating of white phosphorus without air access to $250\text{--}300 \text{ }^\circ\text{C}$ is accompanied by its conversion to red phosphorus. Black phosphorus is formed from white when it is heated to $200\text{--}220 \text{ }^\circ\text{C}$ at a pressure of $12\text{--}17 \text{ GPa}$.

Fe-P system. The state diagram of the Fe-P system is shown in Fig. 21.1. The solubility of phosphorus in $\alpha\text{-Fe}$ at room temperature does not exceed 0.015% , and the maximum solubility in $\alpha\text{-Fe}$ at eutectic temperature is 2.55% . Phosphorus closes the γ region. Phosphorus forms phosphides with iron Fe_3P , Fe_2P , FeP and FeP_2 by reactions

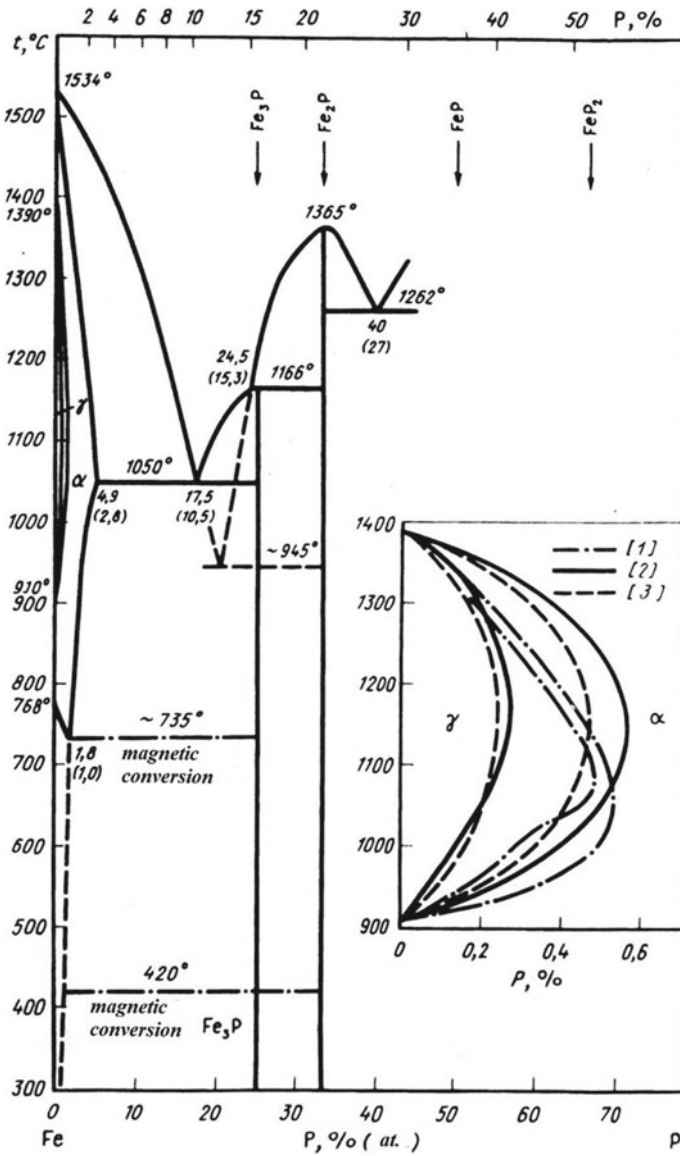
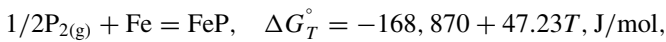
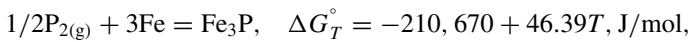
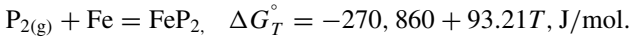
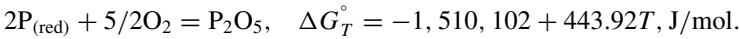
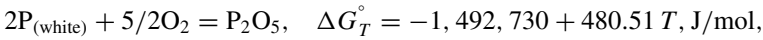


Fig. 21.1 Equilibrium diagram of Fe-P system





P-O system. Phosphorus forms oxides with oxygen: P_4O , P_4O_2 (P_2O), P_2O_6 (PO_3), P_4O_6 (P_2O_3), P_4O_{10} (P_2O_5) and $(PO_2)_n$. In phosphorus electrothermy, the oxides P_2O_5 and P_2O_3 are of the greatest importance. The melting point of P_2O_5 is 563 °C, a density of 2.39 g/cm³; the melting point of P_2O_3 is 23.8 °C, and the density is 2.135 g/cm³. The temperature dependence of the Gibbs energy of the reactions of the formation of P_2O_5 is described by the equations



Solid P_2O_5 peroxide can exist in tetragonal, rhombic and hexagonal modifications. When heated, P_2O_5 evaporates.

CaO- P_2O_5 system. A number of calcium phosphates are formed in the system (Fig. 21.2), the most durable of which is calcium triphosphate $3CaO \cdot P_2O_5$ or $Ca_3(PO_4)_2$; it melts without decomposition at 1810 °C.

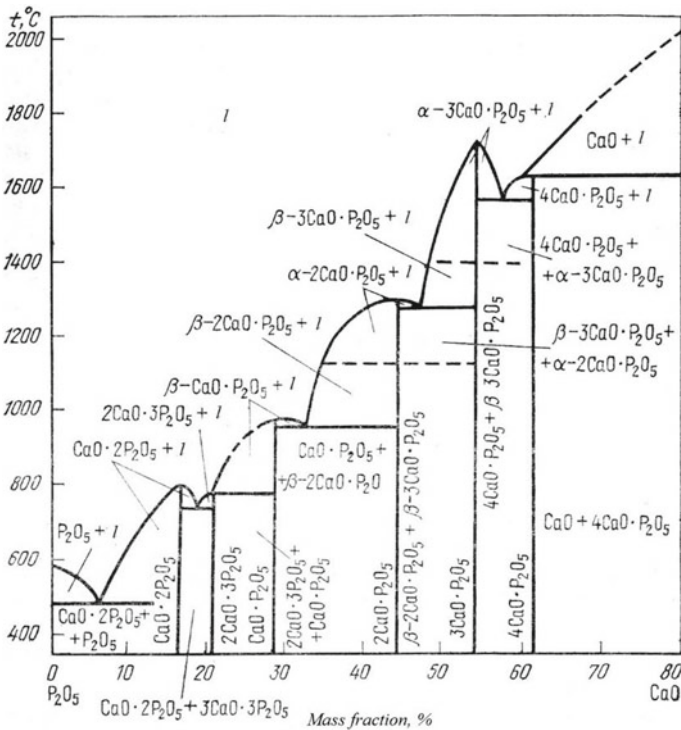
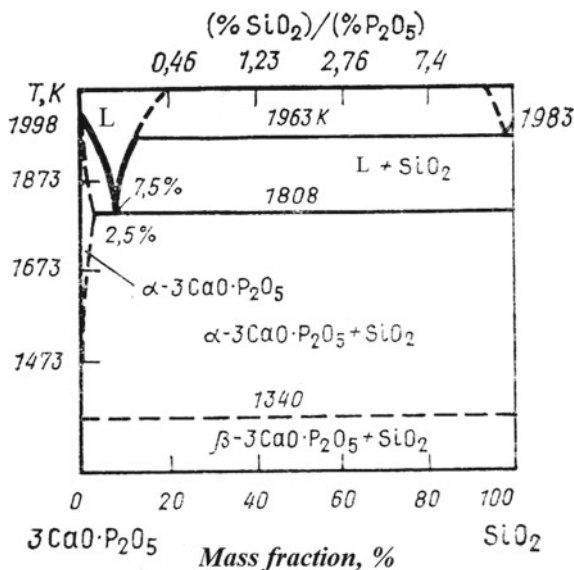


Fig. 21.2 Equilibrium diagram of CaO- P_2O_5 system

Fig. 21.3 Equilibrium diagram of $\text{CaO-P}_2\text{O}_5\text{-SiO}_2$ system



$\text{CaO-P}_2\text{O}_5\text{-SiO}_2$ system. In the system (Fig. 21.3), there are compounds $5\text{CaO}\cdot\text{P}_2\text{O}_5\cdot\text{SiO}_2$ —silicocarnotite and $7\text{CaO}\cdot\text{P}_2\text{O}_5\cdot 2\text{SiO}_2$ —nagelschmidite as well as several solid solutions: 1) based on calcium orthosilicate ($2\text{CaO}\cdot\text{SiO}_2$) containing up to 2% P_2O_5 ; 2) isotypic K_2SO_4 and containing 3.5–6% P_2O_5 ; 3) with a variable content of P_2O_5 —12.5–36%; 4) based on $\alpha\text{-}3\text{CaO}\cdot\text{P}_2\text{O}_5$ with SiO_2 content from 0 to 5%.

The slags of the electrothermal production of phosphorus are close in composition to this system.

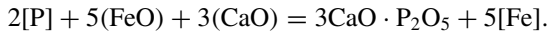
21.2 Minerals and Ores of Phosphorus

About 180 minerals containing phosphorus are known, mainly phosphates, of which apatite and phosphorite are the most common.

Apatite $3(\text{Ca}_3(\text{PO}_4)_2)\cdot\text{Ca}(\text{F}, \text{Cl})_2$ is a mineral from the group of calcium phosphate salts containing a variable amount of fluorine and chlorine. It may contain as impurities up to 10% oxides of manganese, strontium, rare-earth metals, as well as <1% Na, K, etc. Along with F^- and Cl^- , $(\text{OH})^-$, O^{2-} , CO_3^{2-} are present in apatite, and therefore, fluorine and chlorohydroxides are isolated, carbonate hydroxyapatites, as well as manganapatite and others. Fluorapatite contains 42.3% P_2O_5 , and chlorapatite 41.1% P_2O_5 . The melting point of fluorapatite is 1660 °C, chlorapatite 1530 °C. Deposits of apatite are classified as endogenous, having magmatic origin.

Phosphorite–calcium phosphate $\text{Ca}_3(\text{PO}_4)_2$ is a mineral that is part of natural mineral formations called phosphorites. Deposits of phosphorites are exogenous (sedimentary) in nature.

When smelting phosphorus-containing iron ores in a blast furnace, phosphorus goes into cast iron. When converting such cast iron, phosphorus is oxidized and passes into slag



Below is the composition of the converter slag of the Karaganda Metallurgical Plant, %:

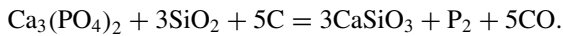
Component	P_2O_5	CaO	SiO_2	Al_2O_3	MgO	MnO	Fe_{tot}
Intermediate slag	9.15	45.00	18.80	2.72	4.32	5.10	18.70
Final slag	4.48	51.50	12.96	1.57	2.73	3.78	25.20

After preparation, intermediate slag can be used as fertilizer, and final slag can be used in the construction industry.

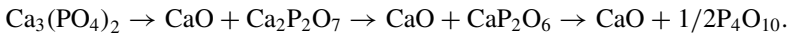
The content of P_2O_5 in phosphate ores varies widely—25–34%. Gangue is represented by dolomite, quartz, clay minerals, hydroxides, etc.

21.3 Thermodynamics of Phosphorus Reduction Reactions

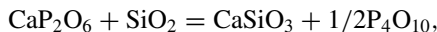
The process of reduction phosphorus from calcium triphosphate can be represented by the reaction



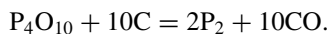
The endothermic effect of the reaction at 1600 K is 1455.47 kJ/mol. According to a number of authors, the dominant role in this process is played by P_4O_{10} oxide, which is formed upon dissociation according to the scheme



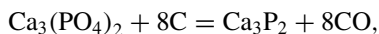
Silica in the composition of the mixture promotes the formation of P_4O_{10} by reaction



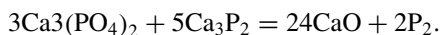
and phosphorus appears due to the solid-phase reduction of P_4O_{10} with carbon



According to other authors, during the reduction of $\text{Ca}_3(\text{PO}_4)_2$ by carbon, it is possible to form calcium phosphide as an intermediate product

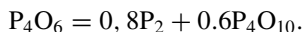
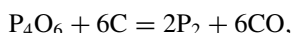


which then interacts with calcium triphosphate by reaction

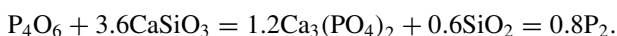
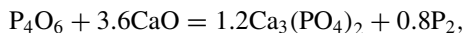


However, this process is not thermodynamically feasible. There are other hypotheses of the mechanism of phosphorus production during the reduction of calcium triphosphate by carbon, which have not received practical confirmation.

The most likely mechanism at the first stage of the interaction of $\text{Ca}_3(\text{PO}_4)_2$ with carbon is the formation of $\text{Ca}_3(\text{PO}_3)_2$. In the subsequent stages, the formation and participation of P_4O_6 in the reactions, which, unlike P_4O_{10} , can appear in the process due to its displacement from $\text{Ca}_3(\text{PO}_3)_2$ with silica, play a significant role. At the final stage, the appearance of elemental phosphorus may be the result of reduction and disproportionation reactions.



If CaO , CaSiO_3 and SiO_2 are present in the system during solid-phase reduction, then reactions are possible



21.4 Preparation of Phosphorites for Electrofusion

In relation to phosphorite ores of Russian deposits, technological enrichment schemes have been developed and tested that allow obtaining concentrates suitable for further processing (Table 21.1).

Phosphorite concentrates have a relatively fine particle size distribution and high moisture content. The melting of such concentrates will be accompanied by increased dust formation, a high concentration of hydrogen in the exhaust gases, as well as a loss of phosphorus in the form of $\text{PH}_{3(g)}$, therefore, phosphorite ore should be subjected to heat treatment, and the concentrates should be agglomerated before electric melting.

Table 21.1 Chemical composition of phosphorite concentrates, %

Mineral Deposit	P ₂ O ₅	CaO	F	R ₂ O ₃	Fe ₂ O ₃	Al ₂ O ₃	MgO	LOI	CO ₂
Oshurkovskoe	37.67	50.20	2.80	1.80	–	–	0.50	–	2.95
Beloziminskoe	36.35	47.90	2.83	–	3.26	1.10	2.11	0.70	–
Seligdar	34.10	49.40	1.90	–	0.70	0.50	2.70	8.30	–

In the practice of phosphorus production, decarbonizing ore roasting is used, and the concentrates are sintered, pelletized or briquetted.

Sintering of phosphorite concentrates. The essence of the process, the hardware and technological design and the sequence of operations for the preparation and sintering of charge are similar to the process of sintering of manganese concentrates (Sect. 25.2.1). Fine fractions of coke are used as fuel. To increase the yield and reduce small fractions of the sinter, additives of lignin, acids, ferrophosphorus, etc., are used, which ensures the required quality of the sinter.

Pelletizing phosphorite concentrates. Pelletizing is carried out on disk granulators with subsequent firing of pellets on a conveyor machine. The concentrate is preliminarily moistened for 1–6 h for complete capillary saturation of the finest dispersed fractions, and pellets are fired at a temperature of 1150–1200 °C to harden them with the participation of the liquid phase.

Briquetting of phosphorite concentrates. When briquetting, magnesium ligno-sulfonate (a type of sulfide-alcohol bards) is used as a binder. The consumption of magnesium lignosulfonate is 4–6%, the moisture content of the mixture is 10%, the specific pressing pressure is 300 MPa, and the mechanical compressive strength of the briquettes exceeds 100 MPa. Drying at 150 °C increases the mechanical strength of the briquettes.

21.5 Electric Furnaces for Phosphorus Reduction

Initially, the unit capacity of phosphorus furnaces in the USSR did not exceed 4.2 MV · A, in 1968, furnaces with a capacity of 24 and 50 MV · A were introduced, and in 1974, furnaces with a capacity of 72 MV · A. A typical RKZ-80F phosphor furnace is shown in Fig. 21.4. The main parameters of phosphor furnaces of various capacities are given below:

Power, MV · A				
Nominal	10	30	50	72
actual	8	25	45	–
Bath size, mm				
diameter	6450	8000	8280	
height	3350	4000	4200	

(continued)

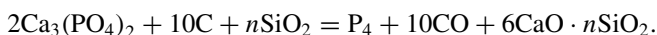
(continued)

Power, MV · A				
Nominal	10	30	50	72
Diameter of electrode, mm	1400	1400	1400	1700
Distance between electrodes/diameter of the electrode	1,96	2.1	2.4	
Average gas temperature leaving the furnace, °C	175	310	520	

Phosphorus furnaces work only in a hermetic mode, since the product of reduction—phosphorus is in a vapor state. The electrodes are continuous, self-baking. A constant distance must be maintained between the end of the electrode and the bottom (melt).

21.6 Phosphorus Electrothermics

The process of producing phosphorus can be represented by the reaction



At the same time, the oxides of iron, manganese, vanadium, niobium and other elements contained in phosphorites, fluxes and coke ash are reduced, forming a metal phase on the bottom of the furnace. A part of the reduced phosphorus is dissolved in the metal, as a result of which a by-product is formed—ferrophosphorus. The binding of iron, manganese, vanadium, niobium and other elements to phosphides facilitates the thermodynamic conditions for the reduction of these metals.

Phosphorus reduction occurs from phosphate-silica melts having a high viscosity, which sharply decreases in the temperature range of 1400–1450 °C, and with further heating to 1500 °C and higher, the viscosity decreases slightly. The final slag has a low P₂O₅ content. With the natural modulus of acidity (SiO₂/CaO) of phosphorites, the slag viscosity should significantly increase after P₂O₅ reduction; therefore, acid flux (SiO₂) introduced into the charge, binding CaO to CaO·SiO₂ silicate, increases the acidity and reduces the viscosity of the final slags.

The gases discharged from the pressurized furnace contain CO, vapor phosphorus, F₄, PH₃, H₂, H₂O (steam), as well as pyrolysis products of organic impurities and solid particles of the charge. The volumetric amount of phosphorus vapor in the exhaust gases is ~10%, PH₃ ~0.2%. The temperature of the exhaust gases from the furnace should be 250–300 °C in order to eliminate the condensation of phosphorus. Dust removal of gases is performed in two-section electrostatic precipitators. Dust content of gases is 40–80 g/m³. The steam-gas mixture purified from dust enters the condensation unit, in which liquid white phosphorus of technical purity condenses under water at a temperature of at least 50 °C. Ferrophosphorus, as it accumulates, is periodically released from the furnace, poured and delivered to consumers in pieces.

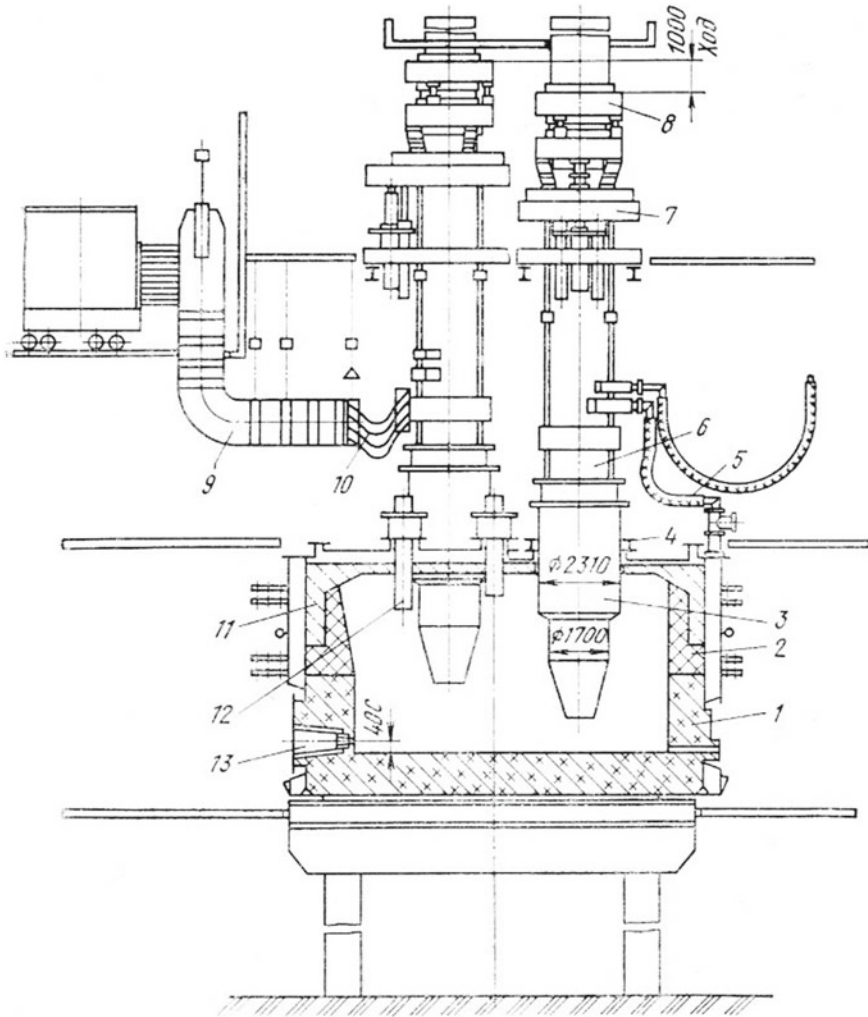


Fig. 21.4 Electric furnace for volatilization of phosphorus, 1—casing; 2—lining; 3—cylinder; 4—stuffing box; 5—water cooling system; 6—electrode holder; 7—hydraulic lift; 8—device for bypassing the electrodes; 9—short network; 10—flexible conductor; 11—arch; 12—loading tubes; 13—slag notch

When receiving phosphorus in an electric furnace RKZ-80F from 1 ton of phosphorite, 96 kg of phosphorus can be obtained as part of top gas. The beneficial use of phosphorus is 85%, and its conversion to ferrophosphorus is 4–5%. The specific energy consumption with an active furnace power of 55–59 MW is 13,300 kWh/t. The chemical composition of the associated alloy—ferrophosphorus, %: 15–30 P; 8–12 Si; 2–4 Mn; 55–70 Fe.

Chapter 22

Ferroselenium and Ferrotellurium



Selenium was discovered by the Swedish chemist J. Berzelius in 1817. Selenium is a rare dispersed element, and its content in the earth's crust is $6 \times 10^{-5} \%$. Selenium and selenides are typical semiconductors. Selenium is used in electronics and electrical engineering in semiconductor devices, photocells, thermoalloys, and it is used for whitening and dyeing glass, to obtain wear-resistant rubber, to improve the workability of high alloy steels and alloys, as a catalyst and oxidizing agent in organic synthesis, as well as for the production of pigments and drugs. Selenium is obtained from sludges from electrolytic refining of copper, sulfuric acid and pulp and paper production.

Tellurium was discovered by the Hungarian engineer F. Müller in 1782. The first systematic studies of the chemistry of tellurium were made by J. Berzelius in 1830. Tellurium is one of the rarest elements, and its content in the earth's crust is $1 \times 10^{-7} \%$. Tellurium is used as a semiconductor in devices, thermocouples, and it is used in the vulcanization of rubber, for bleaching cast iron, as a component of lead and lead–antimony alloys, in microbiology and medicine—for the diagnosis of diphtheria.

22.1 Properties of Selenium, Tellurium and Their Compounds

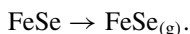
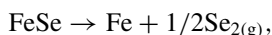
Selenium and tellurium—elements of the VIa group of the Periodic system of elements. Atomic numbers 34 and 52, respectively, have atomic masses 78.96 and 127.60, configuration of electron shells $3d^{10}4s^24p^4$ and $4d^{10}5s^25p^4$, densities 4.79 and 6.25 g/cm^3 , melting points 215 and $450 \text{ }^\circ\text{C}$ and boiling points 685 and $990 \text{ }^\circ\text{C}$. In compounds, selenium and tellurium exhibit an oxidation state of +4, +6 and -2 .

Selenium is polymorphic; gray hexagonal selenium is resistant; amorphous red is released during the reduction of selenic acid from solutions; when heated, it passes

into hexagonal. Two monoclinic and two cubic modifications are known. When the melt cools, glassy selenium forms.

Tellurium is a chemical analogue of sulfur and selenium with more pronounced metallic properties. Tellurium is silver-white with a metallic luster, brittle, when heated becomes plastic. It crystallizes in the hexagonal system.

Fe-Se, Mn-Se, Nb-Se systems. The state diagram of the Fe-Se system is shown in Fig. 22.1. The system contains selenides FeSe and FeSe₂. Selenides at 750–800 °C can sublime and dissociate with the transition of selenium to the vapor phase according to the reactions:



Selenium has a significant effect on the surface properties of iron. At 1500 °C, every 0.01% Se (when the selenium content in iron is up to 0.05%) reduces the surface tension by 150–200 MJ/m².

Fig. 22.1 Equilibrium diagram of Fe-Se system

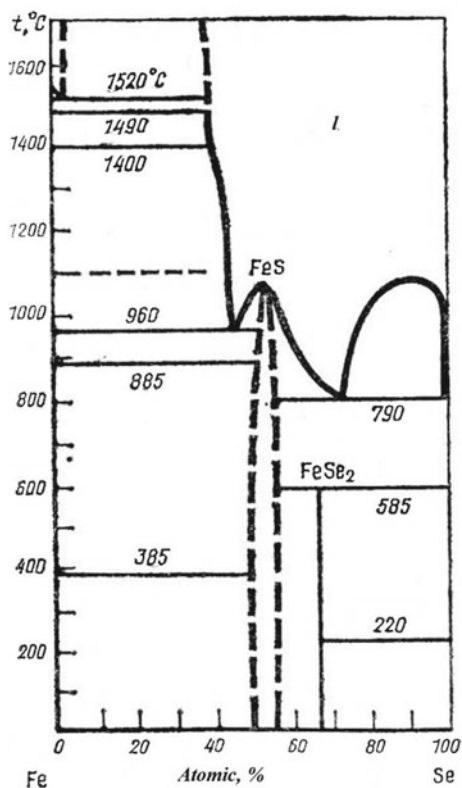
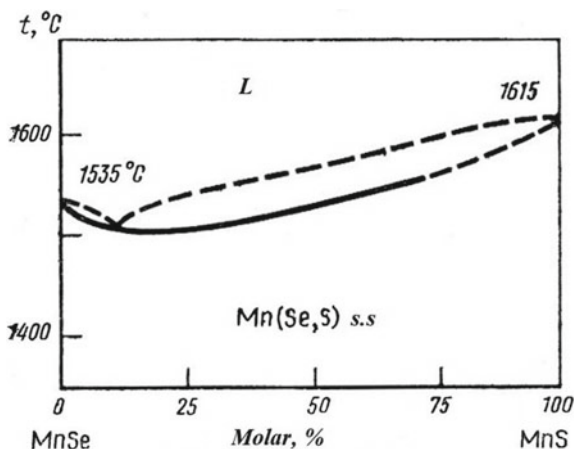


Fig. 22.2 Equilibrium diagram of MnSe-MnS system



Manganese with selenium forms MnSe and MnSe₂ compounds; MnSe selenide forms a continuous series of solid solutions with MnS sulfide (Fig. 22.2). Selenides are known in the Nb-Se system Nb₂Se₉, NbSe₃, NbSe₂.

Fe-Te, Mn-Te, Cr-Te systems. Tellurium, like selenium, actively interacts with metals. In the Fe-Te system, there are tellurides FeTe and FeTe₂. The solubility of tellurium in solid iron is very small. At a temperature of 1000 °C, tellurium does not diffuse into iron. Tellurides of manganese (Fig. 22.3) and chromium (Fig. 22.4) have a relatively high melting point.

22.2 Selenium and Tellurium Ores

The main source for selenium production is lead-zinc and copper-nickel ores. The richest in selenium is ore of copper-pyritic deposits—up to 0.07% Se. In 1991, confirmed reserves of selenium were, thousand tons: Chile 33; USA 19; Canada 15; Zambia 7; Peru 7; Mexico 5; Australia 2; India 1; other countries 40. Minerals of selenium (selenides of noble and heavy metals, native selenium) do not have industrial significance. During the processing of copper concentrates, 60–80% of selenium is concentrated in electrolyte sludge, 1–5% is lost with waste slag and 20–40% is sublimated in the form of SeO₂ ($t_{\text{sub}} = 317\text{ °C}$). Around 80% of selenium is produced from copper-electrolyte sludge, 15%—from sulfuric acid sludge and 5%—from intermediates of lead-zinc and other plants.

Hydrothermal deposits of gold and non-ferrous metals enriched in tellurium are known; about 40 minerals of tellurium are associated with them, the most important are altaite, tellurobismuthite and other tellurides. Tellurium impurities in pyrite and other sulfides are characteristic. Tellurium is recovered in the processing sulfide ores

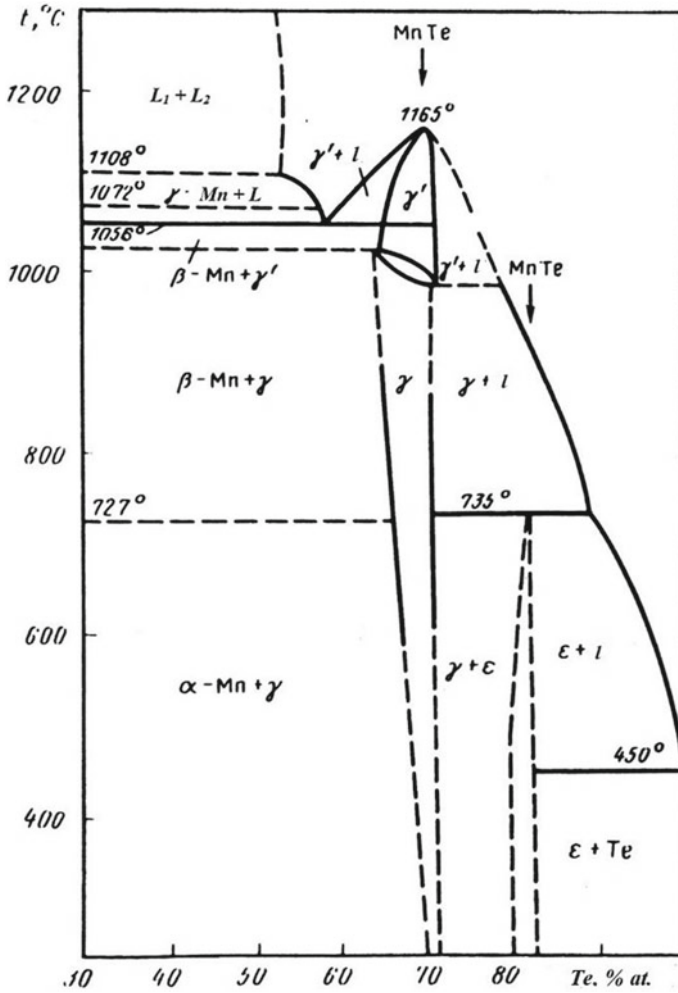


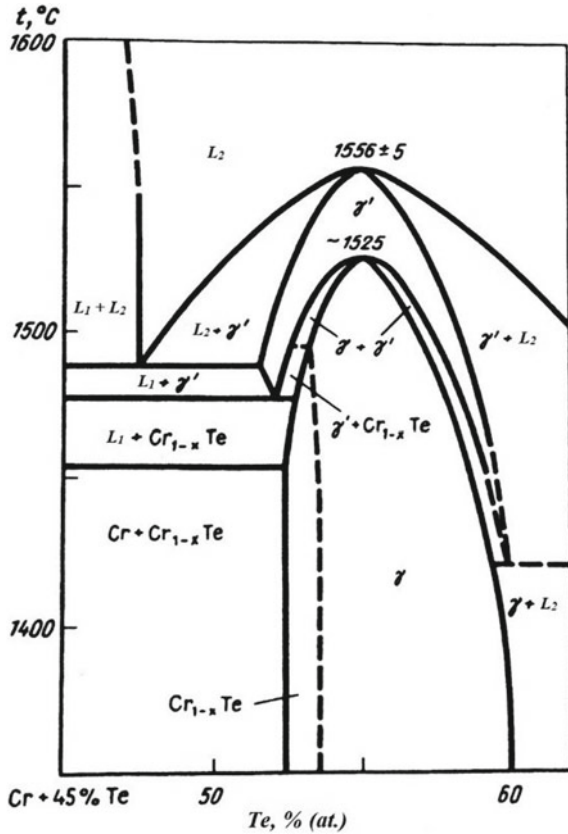
Fig. 22.3 Equilibrium diagram of Mn-Te system

from intermediates of copper and lead–zinc production, as well as from some gold-bearing ores. The main raw materials for tellurium production are copper electrolysis sludges containing 0.5–2% Te.

22.3 Alloying Steel with Selenium and Tellurium

In the steel industry, selenium is used in the form of ferroselenium. With a relatively small production of selenium, in recent years, there has been an increasing

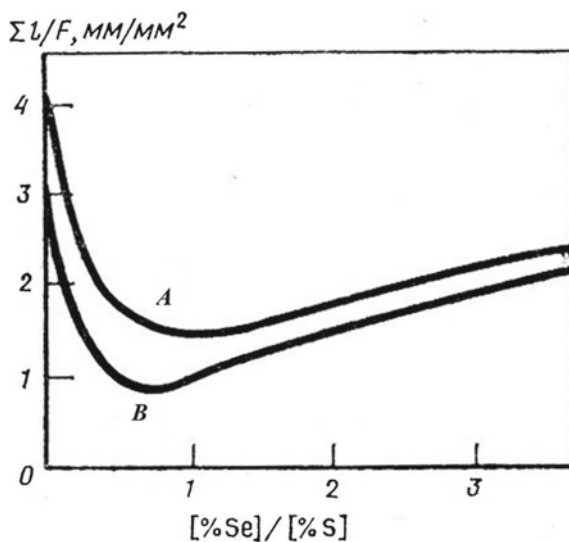
Fig. 22.4 Equilibrium diagram of Cr-Te system



volume and range of smelted steels containing selenium. It is established that when alloying with selenium (0.14%) steel containing 0.37% C, the mechanical properties of cast and deformed metal, as well as the machinability of products by cutting, are improved. Improving the properties of steel is achieved due to the influence of selenium on the shape and distribution of sulfides in the metal. Alloying steel with selenium leads to the formation of sulfonium selenides $Mn(S, Se)$ in the metal. In the absence of selenium, sulfur is bound into manganese sulfide MnS , which during hot rolling is rolled into elongated long inclusions, which reduces the resistance of pipes to hydrogen sulfide corrosion. In a metal containing selenium, sulfo-selenides are deformed much more difficult. As follows from Fig. 22.5, at $\alpha = 0.8$, the relative length of sulfide inclusions in steel containing 0.2% C decreases by 2–3 times; therefore, steel with small globular sulfide-selenide inclusions is obtained. A thin sulfide layer $(Mn, Me)(S, Se)$ is formed on the cutting edge of a tool made of steel containing selenium, which ensures high tool life even at a cutting speed of 200 m/min.

Tellurium, like selenium, has limited solubility in solid iron. When introduced into steel, tellurium interacts with manganese to form the $MnTe$ compound. The fusibility of this compound (1165 °C) can be the cause of grain-boundary destruction of steel

Fig. 22.5 Influence of the ratio on the relative extent ($\Sigma l/F$), inclusions in carbon steel (A—steel 20; B—steel 20YU4, Russian grade)



during rolling. When selenium and tellurium are introduced into steel, the rate of interaction of nitrogen with the molten metal decreases. It is believed that with the introduction of selenium (tellurium), it becomes possible to obtain converter steel and electric steel by the nitrogen content at the open-hearth steel level.

When alloying stainless steel with selenium, the resistance of the cutting tool is lower, and the quality of the machined parts is worse; therefore, the widespread use of selenium should be preceded by a detailed study of its effect on each steel grade.

The technology of alloying steel and cast iron with pure selenium and tellurium has difficulties mainly due to the low melting (boiling) temperatures of these metalloids. Therefore, methods have been developed for producing ferroselen by sintering iron powder with selenium in closed metal reactors at 620–830 °C. Iron selenides even at 750–800 °C can sublime and dissociate with the transition of elemental selenium to the gas phase. Sintered ferroselen briquettes have a density of 4.6 g/cm^3 . Ferroselenium is added to steel and cast iron in the form of such briquettes.

The use of tellurium for alloying metals and alloys due to large losses by evaporation is not rational. It is advisable to develop complex ferroalloys containing tellurium for industrial use.

Chapter 23

Metallurgy of Electrocorundum



Corundum ($\alpha\text{-Al}_2\text{O}_3$) is found in nature as a rock-forming material. Its deposits are known in the Urals, in Yakutia and other regions of Russia. Pure varieties of natural corundum contain 95–98% Al_2O_3 , but they are rare. As a rule, natural corundum contains impurities that reduce its quality. Therefore, the need for mechanical engineering, metallurgy and other industries in corundum as an abrasive and alumina-containing material is met by an artificial corundum called electrocorundum.

23.1 Corundum Properties

Electrocorundum is a crystallized melt based on alumina (96–98% Al_2O_3), and the main mineral phase of which is its trigonal modification of $\alpha\text{-Al}_2\text{O}_3$. The unit cell of corundum has the shape of an acute-angled rhombohedron with an edge length of 0.513 nm and a flat angle of $55^\circ 6'$. The molecular weight of the corundum is 101.96, the true density is 3.99 g/cm^3 , the melting point is 2043–2109 °C, and the heat of fusion is 109.2 kJ/mol. Melting is accompanied by a 23.5% increase in volume.

The nature of the Al–O chemical bond determines the structural features of liquid corundum. Its melt is represented by complex ions formed as a result of thermal dissociation of aluminum oxide according to the scheme



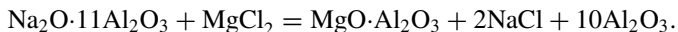
The existence of these complex ions is confirmed by the experimentally determined particle radii. Above 2250 °C, AlO_2^- and AlO^+ ions can dissociate into aluminum and oxygen. The alumina melt obtained by plasma crystallizes in the form of $\gamma\text{-Al}_2\text{O}_3$. This suggests that the structure of the high-temperature melt is similar to the structure of cubic $\gamma\text{-Al}_2\text{O}_3$.

An important characteristic of corundum melt is its electrical conductivity and viscosity: with increasing temperature, the electrical conductivity of the corundum melt increases, and the viscosity decreases. The boiling point of corundum melt is 2980 °C. This temperature is conditional, since in the gas phase there are not Al_2O_3 molecules, but mainly monatomic aluminum and oxygen and lower amounts of lower aluminum oxides Al_2O , AlO and Al_2O_2 .

23.2 Electrocorundum Technology

Depending on the alumina-containing raw material, the composition of the mixture and the technology of smelting, the electrocorundum is divided into *normal*, *monocorundum* and *white electrocorundum*. The most common is normal electrocorundum, which is obtained by reducing smelting of bauxite. To obtain monocorundum, bauxite is also used as an alumina-containing material, however, the physicochemical nature of the processes occurring during electrofusion and crystallization of the melt has a fundamental difference from the processes of obtaining normal electrocorundum. In the production of monocorundum, the mixture consists of bauxite, a carbonaceous reducing agent and a material containing sulfur in the form of pyrite. During electric melting, iron oxides and silica are reduced, and sulfur, interacting with Al_2O_3 , forms an oxysulfide melt, during the crystallization of which large $\alpha\text{-Al}_2\text{O}_3$ crystals are formed. Processing the crushed product with water promotes the decomposition of aluminum sulfide (Al_2S_3) and the release of corundum grains.

The starting material for producing white electrocorundum is technical alumina, containing, %: $>70\%$ $\alpha\text{-Al}_2\text{O}_3$; $<0.08\%$ SiO_2 ; 0.02% Fe_2O_3 ; $<0.4\%$ ($\text{Na}_2\text{O} + \text{K}_2\text{O}$), the moisture content should be less than 0.5%. Electric melting is carried out in order to obtain an alumina melt, the subsequent crystallization of which gives $\alpha\text{-Al}_2\text{O}_3$. The impurity content is limited, %: $<0.02\text{--}0.10$ Fe_2O_3 ; $<0.1\text{--}0.3$ SiO_2 ; $<0.2\text{--}0.6$ Na_2O ; $<0.1\text{--}0.25$ C. The main harmful impurity oxide in the white oxide metal melt is Na_2O , supplied with industrial alumina in the form of sodium aluminate $\text{Na}_2\text{O}\cdot 11\text{Al}_2\text{O}_3$. There are a number of ways to reduce it in industrial alumina. One of the methods involves treating alumina with boric acid H_3BO_3 , and then firing the mixture at 1350–1550 °C. The sodium borates formed in this process are sublimated. Among others, the method of heat treatment of alumina moistened with a solution of MgCl_2 should be noted. In the process of heating, a reaction occurs.



Sodium chloride is sublimated already at 1400 °C. Thus, sodium is removed as volatile compounds. There is also known a method of reducing the harmful effects of sodium oxide by the addition of aluminum metal to the alumina melt, which reduces sodium oxide.

Varieties of white electrocorundum are the so-called *titanium* (0.7–1.5% TiO₂), *chromium* (0.8–2.0% Cr₂O₃) and *zirconium* electrocorundum, which are obtained by alloying the melt with oxides TiO₂, Cr₂O₃ and ZrO₂, respectively.

23.3 Normal Corundum Technology

For the smelting of normal electrocorundum and monocorundum, bauxite is used. The main chemical component of bauxite is alumina, and a number of oxides are present as impurities: Fe₂O₃, SiO₂, TiO₂, CaO, MgO, MnO, P₂O₅, V₂O₅, etc. The most undesirable impurity is calcium oxide, the permissible content of which should not exceed 0.1%. During smelting, calcium oxide is not reduced, and upon crystallization forms calcium hexaaluminate CaO·6Al₂O₃, the abrasive ability of which is much lower than that of α-Al₂O₃. Bauxite for the production of abrasive electrocorundum must meet the requirements below:

Grade	EB-1	EB-2
Complex quality indicator B, no less than	41	31
Al ₂ O ₃ content, % (not less)	50	43
Content, % (no more):		
S	0.3	0.3
P ₂ O ₅	0.5	0.5
CaO	0.1	0.25

The complex quality indicator B of bauxite is calculated by the formula

$$B = (\%Al_2O_3) - 2(\%SiO_2).$$

To obtain normal electrocorundum, only those bauxites are suitable for which the ratio, called the calcium module of M_{CaO}, is not lower than 250. Of these bauxites, normal electrocorundum can be melted with an acceptable amount of calcium hexaaluminate. Silica content is also strictly regulated in bauxite: the lower the SiO₂ content, the higher the technical and economic indicators of the production of abrasive aluminum oxide. The ratio, called the silica modulus, should be greater than 10–12. If the increased silica content in bauxite worsens the production economy, then an increase in the content of calcium oxide even by a hundredth of a percent sharply reduces the abrasive properties of normal electrocorundum. High-quality normal electrocorundum is obtained from low-calcium and low-silicon bauxites (Table 23.1).

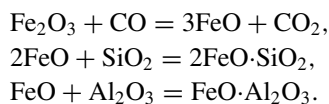
Carbonaceous reducing agents. The traditional reducing agent for bauxite electrofusion is anthracite concentrate. In recent years, anthracite has been replaced by petroleum coke fines, since it contains almost ten times less calcium oxide than anthracite. The composition of carbonaceous reducing agents is given below, %:

Table 23.1 Chemical composition of bauxite, %

Country	Mineral deposit	Al ₂ O ₃	SiO ₂	Fe ₂ O ₃	TiO ₂	CaO	LOI	M _{SiO₂}	M _{CaO}
Greece	Parnassus	57.8	2.7	24.9	2.7	0.30	11.6	21.4	193
	Helikon	56.2	3.0	26.3	2.7	0.20	11.6	18.7	251
North Macedonia	Krushevo	46.7	4.9	22.4	3.0	0.30	22.7	9.5	156
Serbia	Vlasenitsa	53.5	4.4	27.8	2.7	0.09	11.5	12.1	595
Guinea	Debele	47.7	2.85	22.45	2.85	0.05	24.1	16.1	954

Component	Al ₂ O ₃	SiO ₂	Fe ₂ O ₃	TiO ₂	CaO	MgO	C	Volatiles
Anthracite	1.95	2.1	2.2	0.15	0.60	0.20	89.0	3.8
Petroleum coke fines	0.19	0.20	0.28	0.05	0.05	0.03	89.0	10.2

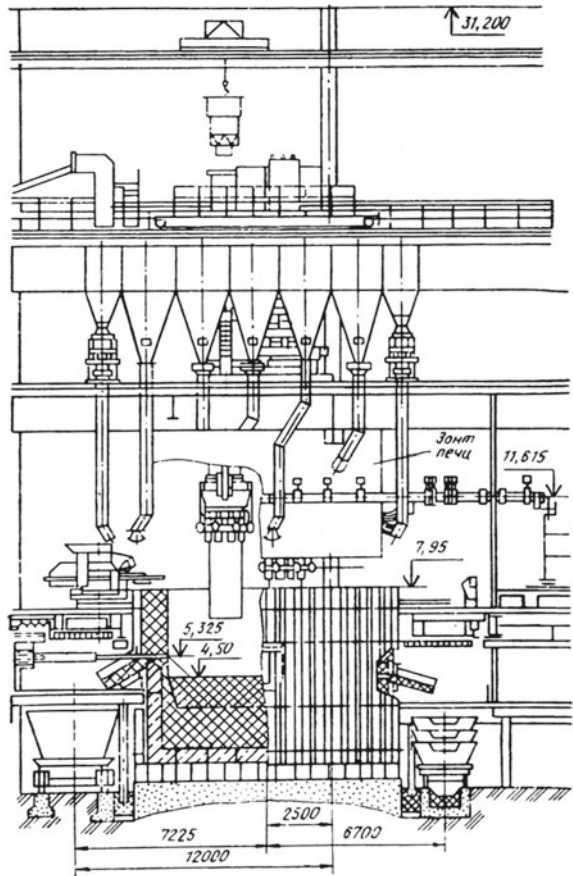
Sintering of bauxite. The melting of raw bauxite is accompanied by the formation of dust and gases, increased specific energy consumption and is unsafe, since the process is accompanied by emissions of the charge. Therefore, bauxite is subjected to sintering. A mixture of anthracite and petroleum coke fines in a ratio of 60:40 is used as fuel. When sintering, redox reactions occur. The combustion of a mixture of anthracite and petroleum coke leads to an increase in temperature, which ensures the course of bauxite dehydration, reduction of iron oxides to FeO monoxide, followed by its interaction with silica and alumina according to the reactions:



Guinean bauxite sinter has a chemical composition, %: 61.1 Al₂O₃; 4.5 SiO₂; 18.7 Fe₂O₃; 8.9 FeO; 3.0 TiO₂; 0.17 CaO; 1.8 Ca; 2.0 LOI. Modules: M_{CaO} = 360; M_{SiO₂} = 13.6.

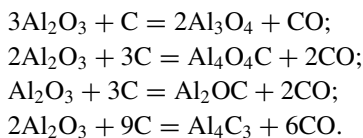
Electrofusion of bauxite sinter. Normal electrocorundum is smelted in ore-smelting electric furnaces of unit power 10.5 (Fig. 23.1) and 16.5 MV A. Two methods are used: melting per block and melting with release. Melting on the block is carried out by a batch process with simultaneous crystallization of the melt in non-lined steel casings cooled externally by water, which are mounted on a trolley. After melting, the tub is rolled out, and a new one is rolled in its place. This is an old inefficient method, which is characterized by the formation of a large number of return charge, difficult conditions for disassembling and sorting the corundum block. More progressive is the electric melting with the release, which is carried out in a stationary bath with a lining from a magnesite brick bath. Although in this case, the process is periodic, however, charge return is excluded, further, reprocessing of electrocorundum is simplified. After melting is completed, the corundum melt is released through a notch into a lined mold, and the crystallized corundum is crushed into a piece and grain.

Fig. 23.1 Ore-smelting furnace for smelting electrocorundum with the release of melt and associated ferrosilicon



The composition of the charge and the electric melting mode are the same for both methods. The mixture is composed of bauxite sinter and a reducing agent—anthracite or petroleum coke fines. Due to the increased content of calcium oxide in the anthracite ash, it is now completely replaced by the fines of petroleum coke. During smelting, the reduction of iron and silicon oxides with carbon leads to the enrichment of the oxide melt with alumina (up to 96–98%). A by-product of the process is low-grade ferrosilicon (8–12% Si). The higher silicon content in ferrosilicon makes it weakly magnetic, which makes it difficult to remove metal skulls at the stage of magnetic enrichment of normal corundum grain. With increasing silicon content in ferrosilicon, its density decreases, which worsens the conditions for the separation of liquid metal particles and corundum melt in density. The precipitation of metal drops is also affected by the viscosity of the corundum melt, which increases with increasing silica content in the oxide melt.

With an excess of carbon reducing agent compared with stoichiometrically necessary for the reduction of impurity oxides, Al_2O_3 may interact with carbon to form various suboxides and oxycarbides:



The formation of these compounds upon receipt of normal electrocorundum is unacceptable, since they reduce its abrasive properties.

With the aim of heating the lower layers of the molten electrocorundum and more complete deposition of the skulls of the associated ferrosilicon, they increase the voltage at the electrodes 1.5–2 h before the release. For the same purpose, steel shavings are added on the melt mirror 30–40 min before release. The control of the melting process is carried out according to the chemical analysis of electrocorundum samples, which are taken by freezing the melt on an immersed steel rod. A melt containing 96.5–97.5% Al_2O_3 is considered ready for release. 1590 kg of bauxite sinter, 164 kg of petroleum coke fines, 70 kg of steel shavings, 70 kg of slag from smelting per block and 2720 kWh of electricity are consumed for 1 ton of normal electrocorundum.

The properties of a grinding grain and abrasive products from normal and white electrocorundum are influenced by the sizes of corundum crystals and other mineral phases. In this regard, an important link in the technology of electrocorundum is crystallization of the melt and cooling of the ingot. Melts of pure substances crystallize at a constant temperature. For a corundum melt, this temperature is 2324 K. The impurities contained in electrocorundum determine its crystallization in a certain temperature range of tens of degrees. Since the thermal conductivity of the corundum melt is relatively high, the viscosity is relatively low, and the melt is characterized by high crystallization ability. Without the adoption of appropriate measures, ingots of small mass have a fine crystalline structure. In the case of melting on a block, the mass of crystallizable melt reaches 30 tons; therefore, $\alpha\text{-Al}_2\text{O}_3$ crystals are larger than in ingots obtained by melting with release. Fine-grained electrocorundum can be obtained by casting it on water-cooled rolls.

An important indicator of the quality of grain of normal electrocorundum is the content of the so-called magnetic material in it. In addition to ferrosilicon, a number of titanium oxides and some of its more complex compounds exhibit magnetic properties. In this regard, in the process of magnetic enrichment, along with the skulls of ferrosilicon, other compounds are also removed. The smaller the amount of magnetic material in the source and magnetized grain, the higher the quality of the grain. The quality of grain of normal electrocorundum can be improved by treating it in chlorine vapor at a temperature of 150–350°C, which results in the chlorination of metal impurities of the grain and their sublimation in the form of volatile chlorides. However, the amount of calcium hexaaluminate during these and other methods of

removing ferrous and other magnetic fractions does not decrease, as a result of which melting of normal electrocorundum should be carried out so that a certain amount of SiO_2 remains in the melt. This allows avoiding the binding of calcium oxide only in $\text{CaO}\cdot 6\text{Al}_2\text{O}_3$ during the crystallization process and ensures the formation of anorthite $\text{CaO}\cdot\text{Al}_2\text{O}_3\cdot 2\text{SiO}_2$, which increases the yield of corundum. The higher residual content of titanium oxides in the corundum melt also reduces the formation of calcium hexaaluminate due to the binding of part of calcium oxide.

Along with the abrasive industry, the consumer of electrocorundum is also ferrous metallurgy. Extensive experience has been gained in producing electrocorundum for synthetic aluminum-lime slag (42–45% Al_2O_3 ; 48–50% CaO), which are used for out-of-furnace steel processing. Based on electrocorundum, compositions of high-quality refractories have been developed.

Chapter 24

Electrofused Fluxes



Electrofused fluxes obtained in specialized workshops of ferroalloy and metallurgical plants are widely used for electroslag remelting of steel and alloys, as well as in welding production. The method of electroslag remelting (ESR), the compositions of the fluxes and the technology for their preparation were developed by the Institute of Electric Welding named after E.O. Paton (National Academy of Sciences of Ukraine). Steel and alloys of various chemical composition and purpose are subjected to refining by the ESR method; therefore, fluxes with certain physicochemical properties are required for ESR.

24.1 Requirements for Fluxes and Methods for Their Preparation

The most widespread fluxes based on calcium fluoride (CaF_2) are used for the ESR of high alloy steels and alloys containing active elements (Al, Ti, etc.). According to the CaF_2 content, fluorine-containing fluxes can conditionally be divided into several groups (Table 24.1). In the fluxes of the first group, the amount of CaF_2 is 85–90% or more (ANF-1, used for ESR of high alloy steels and alloys, including carbon, aluminum, titanium, bromine, etc.). The fluxes of the second group cover the compositions of the CaF_2 - Al_2O_3 system (ANF-6, used for ESR of bearing, tool and other special steels and alloys). The third group includes fluxes based on the CaF_2 - Al_2O_3 - CaO - MgO system with a limited SiO_2 content (ANF-25, used in ESR of structural steels not alloyed with aluminum and titanium). The fourth group includes fluxes with a high SiO_2 content (ANF-28, used for ESR of structural steels not alloyed with aluminum and titanium).

For the production of fluorine-containing fluxes, fluorite concentrates are used, which are obtained by enrichment of fluorspar ores (Table 24.2). Ores mined from the bowels contain only 30–60% CaF_2 and a relatively large amount of harmful and

Table 24.1 Chemical composition of fluxes, %

Grade	CaF ₂	SiO ₂	Al ₂ O ₃	CaO	MgO	FeO	S	P	C
ANF-1	90	2.5	3.0	5.0	–	0.5	<0.05	<0.02	<0.1
ANF -6	Basis	2.5	25–31	8.0	–	0.5	<0.05	<0.02	<0.1
ANF -25	50–60	2–7	12–20	10–15	10–15	0.5	<0.07	<0.03	<0.1
ANF -28	41–49	20–24	5.0	26–32	6.0	0.5	<0.06	<0.03	<0.1
ANF -29	37–45	11–15	13–17	24–30	2–6	0.5	<0.06	<0.03	<0.1
ANF -32	34–42	5–9	24–30	20–27	2–6	0.5	<0.06	<0.03	<0.1
AN -291	10–20	2.5	35–45	20–28	17–27	0.5	<0.05	<0.02	<0.1
AN -295	11–17	2.5	49–56	26–31	6.0	0.5	<0.05	<0.02	<0.1

Table 24.2 Chemical composition of fluorite ores, %

Mineral deposit	CaF ₂	SiO ₂	CaCO ₃	Al ₂ O ₃	P ₂ O ₅	S	Other components
Kalanguyskoe	49.8	45.5	0.60	–	–	3.5	0.6
Harankhoy	43.4	25.6	0.88	1.3	0.45	0.17	28.05
Yaroslavl	40.2	10.2	12.5	0.97	–	–	–
Tashkent	56.1	31.3	2.1	1.2	0.33	0.51	8.45

difficult to remove from the ores silica, sulfur and phosphorus. Fluorite concentrates used for smelting ESR fluxes should contain no more than 1–2% SiO₂ and possibly less sulfur and phosphorus (not more than 0.02% each). However, fluorite concentrates supplied to ferroalloy plants contain up to 3% SiO₂, 0.08–0.4% P₂O₅ and 0.03–0.2% S (Table 24.3). Among other charge materials, when smelting fluxes, the following are used: alumina (<0.05% SiO₂; <0.001% P); caustic magnesite (88–89% MgO; <1.3% SiO₂; <2% Al₂O₃; <1.8% CaO; <0.01% P; <0.5% S); quartz sand.

Table 24.3 Chemical composition of fluorite concentrates, %

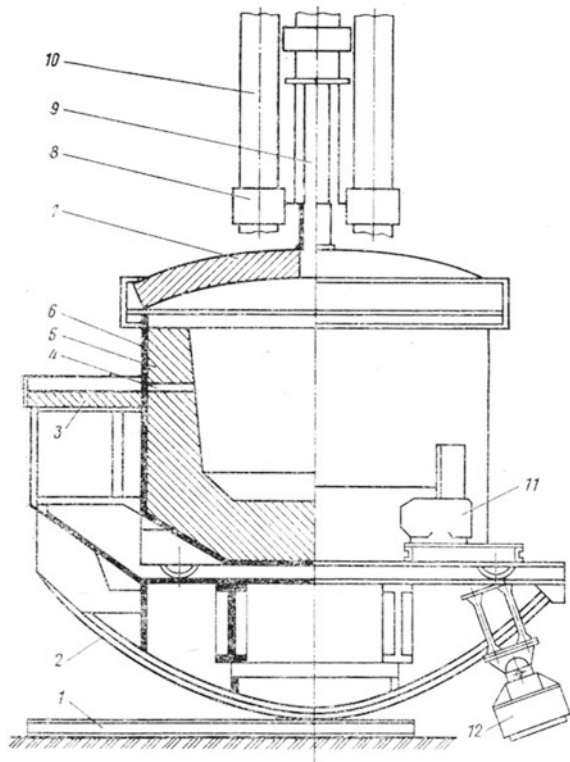
Concentrate	CaF ₂	SiO ₂	CaO	P	S
Yaroslavl	92.0	2.4	1.3	0.046	0.042
Tashkent	95.0	1.7	0.8	0.070	0.310
Harankhoy	95.2	3.0	0.9	0.080	0.050
Thailand	98.0	1.1	0.4	0.185	0.030
Korean	93.5	1.9	0.7	0.040	1.25

24.2 Flux Electrofusion

The essence of flux smelting technology is the fusion of metered charge components in arc furnaces. For smelting, three-phase arc furnaces of the DF-400 type (with a flux capacity of 0.4 t) and OKB-6063 (flux capacity of up to 3 t) are used (Fig. 24.1). The furnace bath is lined with carbon blocks and sintering carbon mass, and the furnace arch is drawn from magnesite brick. Graphite electrodes are with a diameter of 350 mm.

Melting is carried out by gradually loading the charge mixture at a stable current load. The charge loading speed should correspond to the power consumption. When melting multicomponent blends, fluorite concentrate is set at the end of melting to reduce dust and gas emissions and fluorine losses. When electrofusing fluxes, their release and granulation are combined. Flux granulation can be done wet or dry. During wet granulation, the liquid flux is drained from the furnace through an intermediate chute into a receiving tank with water, in which a basket for receiving flux granules is installed. The flux stream is broken by a stream of water under pressure. During dry granulation, the flux is sprayed with a stream of dried compressed air.

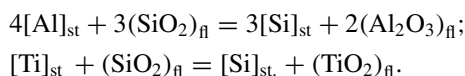
Fig. 24.1 Flux smelting arc furnace: 1—main beam; 2—cradle; 3—drain trough; 4—notch; 5—lining; 6—a casing of the furnace; 7—arch; 8—electrode holder; 9—rack electrode holder; 10—electrode; 11—bath movement mechanism; 12—hydraulic bath furnace



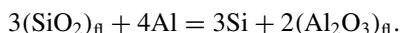
It is also possible to release the melt into a mold with subsequent grinding. Wet granulation is accompanied by absorption of moisture by the flux, which makes it necessary to dry. The increased moisture content of the flux can lead to an increase in hydrogen in metal ingots during ESR or welds. Fluxes are dried in rotary drum furnaces at a temperature of 400–500 °C. When controlling the quality of fluxes, the chemical composition, moisture content, bulk density, uniformity and color of the grain are determined.

24.3 Impurities Behavior in Flux Electrofusion

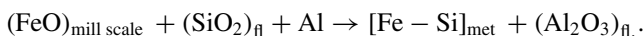
Silica. In fluoride fluxes, the silica content should not exceed 1%, since in ESR of steel and alloys containing aluminum, titanium and other highly active elements, they are oxidized by the reactions:



To reduce SiO_2 in the flux during alloy fusion, the metal phase (200–400 kg) is induced on the hearth and aluminum is added to the molten flux to reduce SiO_2 by reaction



Silicon formed by this reaction dissolves in iron, which reduces the activity of silicon. As an iron-containing additive, mill scale can be used as part of the charge, which is reduced together with silica by the reaction



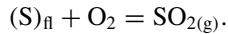
The formation of an iron–silicon melt not only reduces the activity of silicon, but also increases the density of the metal melt, which improves the deposition of metal skulls on the bottom. When processing molten flux with aluminum, phosphorus and manganese are reduced, the associated iron–silicon metal after 20–25 flux smelting should be drained from the furnace, since the concentration of silicon and phosphorus in it increases from smelting to smelting, which makes it difficult to melt fluxes of high quality in terms of SiO_2 and P content.

Phosphorus. As noted above, in the treatment of molten flux with aluminum, dephosphorization of the flux occurs. In fluorite concentrate, phosphorus is in the form of calcium phosphate. The dephosphorization process can be described by the reaction $(\text{Ca}_3(\text{PO}_4)_2)_{\text{fl}} + \text{Al} \rightarrow \text{P}_2 + (\text{Al}_2\text{O}_3 \cdot \text{CaO})_{\text{fl}}$.

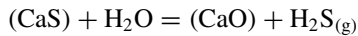
Reduced phosphorus dissolves in the metal phase. Phosphorus reduction can also occur during the interaction of the silicon of the metal phase with $\text{Ca}_3(\text{PO}_4)_2$ melt by the reaction $(\text{Ca}_3(\text{PO}_4)_2)_{\text{fl}} + [\text{Si}]_{\text{Fe-Si}} \rightarrow \text{P}_2 + (\text{CaO}\cdot\text{SiO}_2)_{\text{fl}}$.

As a result of these reactions, the phosphorus content in the metal phase increases from smelting to smelting. The discharge of the associated metal through 20–25 heats makes it possible to obtain a flux with an acceptable phosphorus content.

Sulfur. When the charge is melted, sulfur contained in various materials, and then in the flux melt, can be oxidized by the oxygen in the furnace atmosphere.

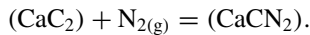
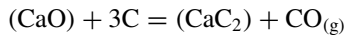


During granulation of the flux, the sulfur content decreases by 20–30% as a result of its interaction with water.



To obtain a flux with a consistently low sulfur content, it is necessary to use high-quality charge components for sulfur.

Nitrogen. In ESR of steels and alloys, as well as in welding, in some cases it is necessary to avoid the influx of nitrogen from the flux. However, in electrofused fluxes, the nitrogen content is usually increased. A directly proportional relationship was established between the content of nitrogen and carbon in the flux. Apparently, the nitrogen in the flux is contained in the form of calcium cyanamide CaCN_2 , which is obtained as a result of reactions:

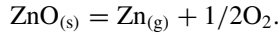


The nitrogen content in the flux can be reduced by adding sodium oxide and other compounds capable of oxidizing cyanamide to the melt.

Impurities of non-ferrous metals. Feldspar ores and fluorite concentrates obtained from them may contain non-ferrous metal impurities (Pb, Zn, Sn, Bi, etc.). The content of these elements in steels and alloys smelted by the ESR method is strictly regulated, therefore stringent requirements are also imposed on fluxes for the concentration of non-ferrous metals. When the charge materials are melted and the molten flux is aged, the content of lead and zinc can be halved, while tin and bismuth are not noticeably removed. Lead and tin are removed mainly in the form of gaseous oxides. The evaporation of PbO_2 and SnO_2 is characterized by a reaction



The resulting zinc oxide $\text{ZnO}_{(\text{t})}$ dissociates upon heating by reaction



A slight decrease in bismuth upon receipt of electrofused flux is apparently due to its low content.

To obtain fluxes, it is effective to use waste slag of ferroalloy production. So, for example, during the flux smelting of AN-42 (30–34% SiO₂; 9–14% MnO; 13–18% Al₂O₃; 12–18% CaO; 14–20% CaF₂; < 1.0% Fe₂O₃; <0, 03% S; <0.03% P), they usually use commercial manganese oxide concentrate, which in addition to high cost is characterized by an increased concentration of phosphorus (0.2–0.3%). Therefore, instead of manganese concentrate, it is proposed to use dump slag of metal manganese (25–27% SiO₂; 16–19% MnO; 43–46% CaO; <0,01% P).

Chapter 25

Preparation of Charge Materials for Ferroalloys Smelting



25.1 Drying Manganese Concentrates

The use of fine and wet concentrates reduces the productivity of electric furnaces, worsens their technical and economic parameters and is unsafe for maintenance personnel, since high moisture content contributes to an increase in hydrogen concentration in top gas. In winter conditions, wet concentrates can freeze, which complicates unloading; therefore, when preparing for electric melting, they are dried in fluidized bed furnaces, while humidity decreases from 15 to 9% (Fig. 25.1). The following indicators, e.g., manganese concentrates, [1] characterize fluidized bed furnaces and drying modes:

Dry concentrate furnace productivity (t/h)	61.5
Moisture content of the initial concentrate (%)	15.4
Gas flow velocity (m/s)	7.6
The height of the layer of material on the grate (cm)	8.0
Temperature of combustion products under the grate (°C)	600
Drying time (s)	70
Differential pressure in the layer (Pa)	800
Natural gas consumption per 1 ton of wet concentrate (m ³)	7.66
Heat consumption per 1 kg of evaporated moisture (J)	3500
Specific moisture removal (kg/(m ² h))	580
Temperature (°C)	
Exhaust gas	100
Discharge concentrate	1000

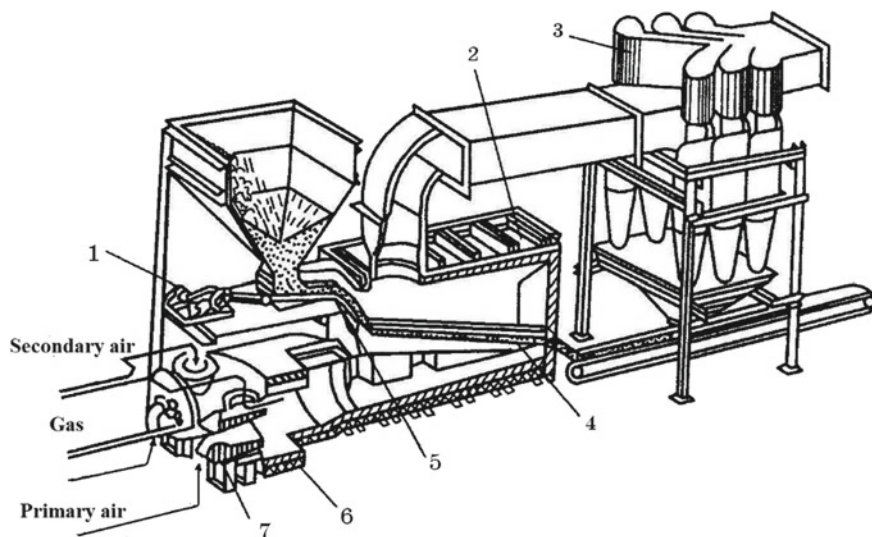


Fig. 25.1 Installation for drying manganese concentrates. 1—carriage feeder; 2—chamber; 3—cyclone; 4—gas distribution grill; 5—a directing tray; 6—a chamber for mixing combustion products with air; 7—burners

25.2 Sinter Production

25.2.1 Manganese Ore Sintering

The principles underlying the sintering of iron-containing materials are also applicable for sintering in the ferroalloy industry. Sintering of manganese ore is based on high-temperature sintering of fine-grained material due to the heat generated during fuel combustion. The heating temperature is determined by the formation in a sufficient amount of the liquid phase during the melting of the fusible components of the charge. The disadvantage of sintering is the high fuel consumption and the production of sinter with a low melting point, which reduces the temperature in the ore-smelting furnace and worsens the course of the carbothermic process. Sinter plant is also the source of the lion's share of harmful emissions.

The theoretical foundations of the theory of sintering of manganese ores were laid by the work of Hooper and Dancoisne [2–4]. The evolution of sintering methods from traditional traveling grate sintering for larger capacities to steel belt sintering for smaller capacities is reflected in sufficient detail in the world metallurgical literature [5]. Next, we briefly review the results of laboratory studies, full-scale tests and the experience of the practical use of sintering in the ferroalloy industry, filling in, among other things, the lack of information on the results obtained in the USSR and in Russia.

Table 25.1 Chemical composition of sinter, mass%

Concentrate grade	Mn	SiO ₂	CaO	MgO	Al ₂ O ₃	Fe	P
II	40.2	23.4	3.5	1.41	5.98	4.62	0.226
III	31.8	36.8	4.0	1.49	3.66	4.74	.216

Until 1973, ferroalloy plants of the USSR did not have sinter plants. The results of one of the first experiments on the sintering of manganese concentrate held in 1957 are described in [6]. More than 120 tons of manganese concentrate were sintered. In the early 1960s, the sinter was periodically produced on sinter machines at the Zaporizhzhya Abrasive Plant or the Bogdanovsky sinter factory (Ukraine). The obtained manganese ore non-fluxed sinter was used for smelting silicomanganese at the Zaporizhzhya Ferroalloy Plant (ZFP). In 1963, the Mekhanobrchermet Institute carried out sintering of manganese ores and concentrates from the Nikopol deposit, as well as fine flotation concentrates [7]. Manganese concentrates of II-III grades and washed carbonate ore were used. The content of the fraction of 40–12 mm in the sinter was 52–65%. The yield of a fraction of less than 5 mm was 9–10% (Table 25.1).

The sinter plant at the Nikopol Ferroalloy Plant (NFP) was commissioned in 1973 [8] and in 1979 sinter plant was also commissioned at the ZFP. The sintering plant of NZF is designed to provide the ferroalloys smelting unit with sinter and prepared charge materials, and it is equipped with AKM-3-100 sintering machines. The flowchart of sinter plant flows and equipment is shown in Fig. 25.2.

Two types of manganese sinters are produced: non-fluxed and fluxed. Non-fluxed sinters are divided into four grades (Table 25.2). Sinter AMNV-1 is produced from a mixture of grade I oxide concentrate and mixed grade I manganese concentrates. Sinter of other grades is obtained from oxide and oxide-carbonate concentrates taken in various ratios [9]. The sinter production technology has been mastered with the introduction of up to 20% carbonate low-silica concentrate into the sinter charge.

The specific productivity of the sintering machine is 1.2 t/(m² h). The consumption of materials per 1 ton of sinter was 1200 kg of manganese ore, 120 kg of coke, 5.6 m³ of natural gas and power consumption 90 kWh.

More than 100 different types of sinter were produced at the sinter plant of the Mekhanobrchermet Institute [10] (Fig. 25.3). The main parameters of sintering and physicochemical properties of the sinter obtained in semi-industrial and industrial conditions are given in Table 25.3.

In the first series of experiments, the non-fluxed and fluxed sinters were produced from manganese concentrate, represented by fractions of 0–10 mm, with a basicity modulus of 0.25–3.0. In the second series, sinter was obtained from a carbonate concentrate with a reduced silica concentration in fractions of 3–10 mm, with a natural basicity and fluxed to a basicity modulus of 1.2–3.0. In the third series, the sinter was obtained from a mixture of manganese oxide concentrate and carbonate concentrate with a reduced silica content in various ratios. In the fourth series, sinter was produced using sludge and slags of the ferroalloy production, as well oxide and carbonate manganese concentrates with a low concentration of silica. In the fifth series, under

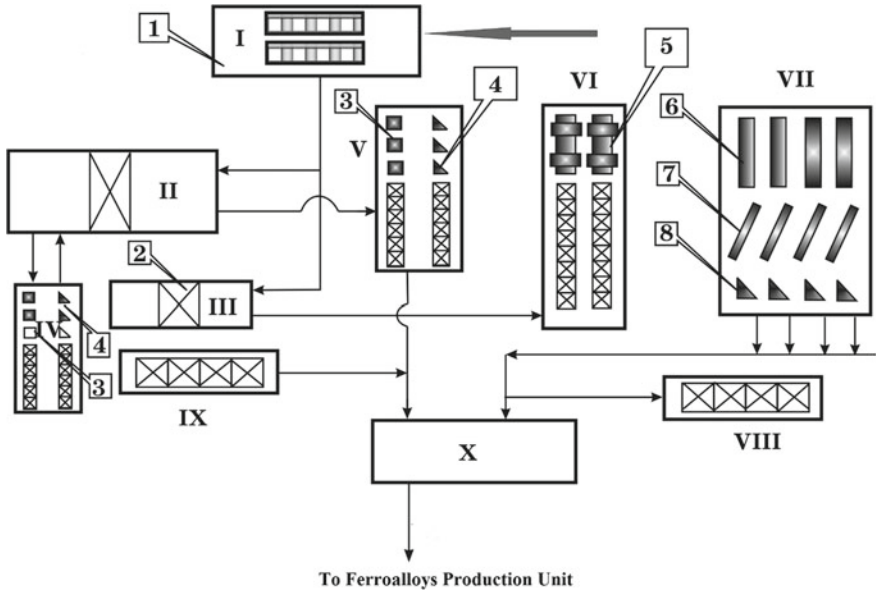


Fig. 25.2 Scheme of technological flows and equipment of sintering plant NZF: I—car dumpers body; II, III—raw materials warehouse No. 1 and No. 2, respectively; IV, V—building for the preparation of materials No. 2 and No. 1, respectively; VI—housing of charge bins; VII—sintering building; VIII—a site for the shipment of sinter; IX—hopper shipment unit; X central distribution point; 1—rotary car dumper, 2—clamshell cranes, 3—four-roll coke crushers, 4—coke screens, 5—mixing drums, 6—inter machines, 7—linear sinter coolers, 8—sinter screens

Table 25.2 Quality requirements for non-fluxed and fluxed manganese sinter

Parameter	Sinter grade				
	FMNV-1	FMNV -2	SMNSH	SMNZH	SMF
Content, %					
Mn (no less)	45.0	36.0	41.0	44.0	36.0
Fe (no more)	—		—	5.0	—
Ratio Mn:Fe (no less)				8.0	
Basicity				1.5 ± 0.3	
Coarseness, mm	5–200	5–200	5–200	5–200	5–200
Fraction content, %					
5 mm (no more)	5.0	8.0	5.0	5.0	8.0
20–200 mm (no more)	75.0	63.5	69.0	75.0	70.0
Strength of fraction 5 mm (no less)	76.0	72.0	4.0	5.0	70.0

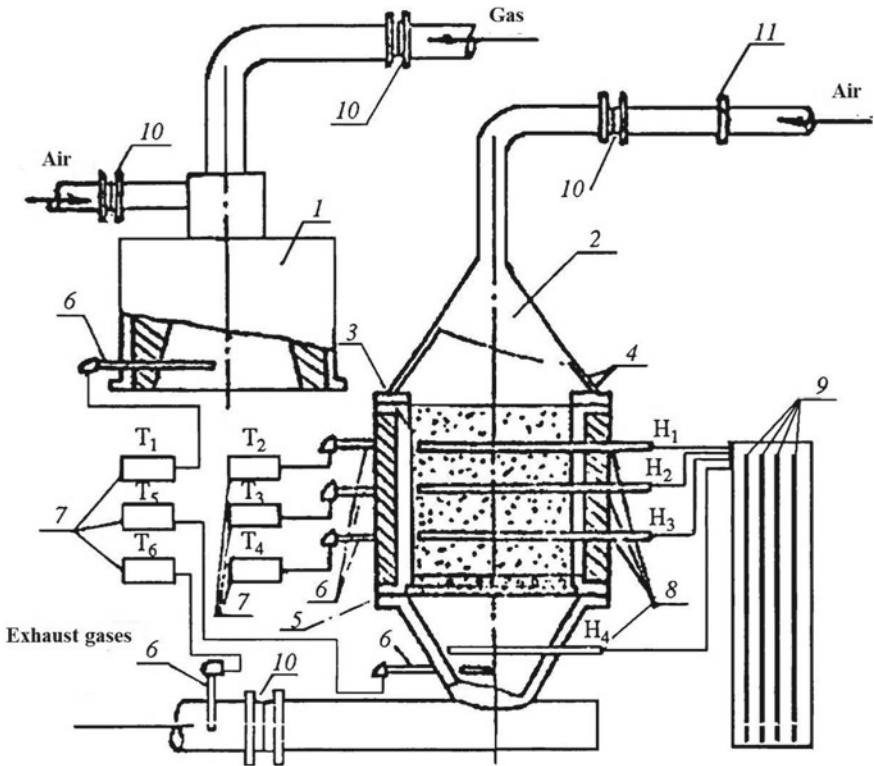


Fig. 25.3 Scheme of the sinter plant: 1—movable lined hearth, 2—removable cap, 3—sintering bowl with heat insulation, 4—sintering charge, 5—bed, 6—thermocouple, 7—potentiometers, 8—impulse tubes, 9—pressure gauges with water filling, 10—diaphragms for measuring the amount of gas, air, exhaust gases, 11—valve

Table 25.3 Sintering parameters and sinter quality

Test #	The height of the sintered layer, mm	Vacuum, Pa	Solid fuel consumption, kg/t	Return share, %	Sinter yield, %	Mechanical strength, %		Basicity, (CaO + MgO)/SiO ₂
						Shock	Abrasion	
1	380	10,000	95–135	20–50	58–63	76–79	7–9	0.25–3.0
2	380	10,000	110–145	20–50	48–62	75–78	8–10	1.2–3.0
3	380	10,000	95–130	20–50	59–64	76–78	8–9	0.25–1.2
4	380	10,000	95–100	20–30	62–64	74–77	8–11	0.25–0.70
5	380–480	8000	98–145	20–25	59–72	74–79	7–9	0.25–2.5

industrial conditions, at the sinter plant of NFP, the non-fluxed manganese sinter FMNV-1, FMNV-2 and the sinter intended for slag remelting—SMNSHA, as well as the fluxed sinter SMO, the basicity module of which ranged from 0.7 to 2, were obtained. The sixth series of experiments (for comparison) is represented by a sinter of various basicity, obtained from oxide and carbonate manganese concentrate under the conditions of the Bogdanovsky sinter factory in a layer 600–760 mm high. It was found that the sinter fractions of 5–25 mm are most resistant to mechanical stress.

The Mekhanobrchermet Institute together with the Ordzhonikidze Mining and Processing Plant introduced a technology for sintering manganese concentrates—oxide (gravity and flotation concentration) and carbonate in a high layer (600 mm) [11]. The consumption of coke breeze decreased by 3.0–3.5%, the strength of the sinter increased by 4.0–4.5% and the specific productivity of the sinter machine increased by 2.8% compared with sintering of sinter in a layer with a height of 350–400 mm. In the enrichment of waste manganese-containing slag by hydraulic precipitation, a metal concentrate is obtained containing 80–90% of the metal phase of a fraction of 0–3 mm.

In [12], the preparation of manganese sinter on the sintering plant with a volume of 0.02 m³ from a mixture consisting of grade II manganese concentrate (38.2% Mn), metal concentrate (56.1% Mn), fuel and return was described. Before sintering, the mixture was averaged, pelletized on a granulator and then mixed with fuel and sinter fines. The optimal amount of metal concentrate in the sinter charge is 10%, and a further increase reduces the sintering speed of the charge and the strength of the sinter.

Production of manganese sinter using anthropogenic materials (sludge from sinter plant, dust from ventilation systems, granulated slag, screenings of slag processing, sludge from flux-smelting production, etc.) is described in [13]. Different amounts of a mixture of secondary materials (10, 15, 20%, options 2–4) were introduced into the basic charge, consisting of grade II concentrate, carbonate concentrate, sinter fines and fuel (option 1). The ratio of the components of the secondary materials in all cases is as follows, %: sludge 60; granulated slag 25, dust of ventilation systems 7 and screenings of slag processing 8. In options 5, 6, in order to compensate for the decrease in the manganese content in the sinter, metal concentrate (option 5) and screenings of slag processing were introduced (option 6). The introduction into the sinter charge of secondary materials is accompanied by a decrease in the concentration of manganese in the sinter by 0.4–1.5% compared with the base case. The addition of 2–3% of ferroalloys crushing fines and metal concentrate to the charge increases the manganese content in the finished sinter to a basic level.

It is noted that the maximum strength is achieved with fuel consumption in the amount of 7–7.5%; however, the performance of sinter machines is reduced by 15–20%. Alloy smelting performance improves with increasing carbon content in the sinter [14].

The non-fluxed sinter obtained from oxide concentrates consists of tephroite 2MnO·SiO₂, Hausmannite Mn₃O₄, Jacobsite MnFe₂O₄ and the vitreous phase; sinter fluxed with limestone and dolomite consists of Hausmannite, CaO·Mn₂O₃ solid

solution, dicalcium silicate $2\text{CaO}\cdot\text{SiO}_2$, tephroite, $\text{CaO}\cdot\text{MnO}\cdot\text{MgO}$ solid solution, tricalcium silicate $3\text{CaO}\cdot\text{SiO}_2$, merwinite $3\text{CaO}\cdot\text{MgO}\cdot 2\text{SiO}_2$ and $\text{CaO}\cdot\text{MnO}$ solid solution.

Fluxed manganese sinter with a basicity of 1.0–1.6 is destroyed due to hydration of lime particles, structural heterogeneity and an increased number of vitreous phases, decomposition of $\text{CaO}\cdot\text{MnO}$ solid solutions, polymorphism of mineral phases, mainly calcium orthosilicate, and hydration of solid solutions supersaturated with calcium oxide. During storage and use, the sinter fluxed by screenings of burnt dolomite does not lose its technological strength.

At the sinter plant of the Zlatoust mining department, sintering of finely ground (3–0 mm) manganese concentrate from ore of the Dzhezdinsky deposit of Kazakhstan was carried out [15].

Manganese ores of Central Kazakhstan in comparison with ores of the Chiatour and Nikopol deposits contain significantly less phosphorus and therefore are of particular value in the production of ferroalloys.

The main ore-forming mineral in the concentrate is braunite (Mn_2O_3); psilomelane ($\text{MnO}\cdot\text{MnO}_2\cdot\text{H}_2\text{O}$) is present in a smaller amount. Of non-metallic minerals, quartz (10–15%) and sand-alumina matter are contained. Braunite is represented by dense aggregates, psilomelane forms small irregularly shaped areas composed of fine-grained, weakly crystallized aggregates. Quartz is present in the form of separate clusters, as well as individual grains among the ore mass. The true density of the concentrate is 3.67 g/cm^3 , the temperature of the onset of softening is $1070\text{ }^\circ\text{C}$, and the softening interval is 70° . A specific feature of the granulometric composition of the concentrate is a small amount (13.47%) of particles with a particle size of less than 0.16 mm.

Coarseness, mm	Yield, %	Coarseness, mm	Yield, %
3.0–2.5	0.77	0.315–0.2	14.66
2.5–1.6	4.66	0.2–0.16	9.11
1.6–1.0	15.95	0.16–0.063	10.11
1.0–0.63	18.07	0.063–0.05	2.45
0.63–0.4	11.07	0.05–0	0.91
0.4–0.315	2.08		

The chemical composition of the concentrate, %: 33.6 Mn; 27.98 SiO_2 ; 5.41 Al_2O_3 ; 2.91 Fe; 1.37 CaO; 0.46 MgO; 0.28 $2\text{Na}_2\text{O} + \text{K}_2\text{O}$; 0.74 LOI and P 0.044.

Sintering of the concentrate with determination of the optimal process parameters (fuel consumption, bed height, charge moisture, amount of return, etc.) was carried out in sinter cups with a diameter of 115 and 300 mm. Coke breeze 3–0 mm in size was used. The mixture was ignited with the combustion products of natural gas for 1 min at a vacuum of 5884 Pa (600 mm of H_2O). During the sintering process, a constant vacuum was maintained at 7845 Pa (800 mm of H_2O). An increase in coke consumption from 5 to 10% with a charge layer height of 215 mm increased the sintering speed (from 10.2 to 23.5 mm/min) and yield by more than 2 times with a

simultaneous increase in the strength of the sinter. The yield (fraction of more than 10 mm) increased from 28.8 to 80.4%, and the degradability of the sinter decreased from 50.7 to 15.4%. A further increase in coke consumption (up to 12%) reduced the sintering rate, the softening temperature of the sinter decreased from 1070 to 1000 °C, and the softening interval increases from 50 to 120°. With the addition of bentonite in the amount of 0.5% to the mixture as a result of improving the lumpiness of the mixture and increasing its gas permeability, the sintering rate increased by 11% and the sinter plant productivity—by 15%.

Sintering of blends with a low (5%) consumption of coke breeze resulted in a porous sinter of fine-grained structure. The sinter consisted of pyrolusite (MnO_2), braunite (Mn_2O_3), Hausmannite (Mn_3O_4), glass and cristobalitized grains of quartz. The role of the binder was performed by glass, in which thin crystals of tephroite ($2\text{MnO}\cdot\text{SiO}_2$) and cristobalite were present. The sinter obtained at a coke consumption of 7–8% had a dense and less porous structure with a fine-grained structure of ore grains compared to the sinter with a coke consumption of 5%. In such sinter, braunite prevailed in the form of single-crystal aggregates.

In 2001, the technology of sintering the concentrate of the Dzhezdinsky mining and processing plant from low-grade oxidized ores was also mastered there [16]. In this case, the concentrate of carbonate ore of the Polunochnoe deposit and slag from smelting of silicomanganese were used (Tables 25.4 and 25.5).

The temperature of the beginning of softening of the mixture was determined by the initial shrinkage of briquettes with a height and diameter of 20 mm prepared from the raw materials preliminarily crushed to a class <0.1 mm. The temperature at the end of softening was taken to be such that the shrinkage of the samples was 40%. The temperature of the onset of softening of the charge was 1160–1180 °C, which corresponds to the melting temperature of the eutectoid compounds of the $\text{CaO}\text{-MnO}\text{-SiO}_2$ system.

For the Dzhezdinsky concentrate in the sinter bowl with a diameter of 350 mm, the consumption of coke breeze was set at 9% for a charge with a temperature of 20 °C. In industrial conditions, when there is a hot return in the charge, the consumption of solid fuel is reduced by 0.5–1.0%. The introduction of slag and Polunochnoe concentrate into the charge improves the mechanical strength of the sinters. Their destructibility both upon storage in air and upon exposure to water after 20 days is insignificant (3.7–5.1%). The greatest destruction occurs during the first day due to relaxation of thermal stresses arising in the cake (Fig. 25.4).

The mastering of the sintering was carried out in two stages: in the first—the agglomeration of the Dzhezdinsky concentrate with manganese slag, and in the second—the Polunochnoe concentrate was additionally introduced into the charge. For the charge, the ore part of which consisted of 92% of Dzhezdinsky concentrate and 8% of slag, the following indicators characterized the process:

- the temperature of the mixture is 40 °C, its moisture content is 8.0–8.5%;
- consumption of coke breeze 8.1–8.3%; return amount 25–30%; charge layer height 180–190 mm; ignition temperature 1100–1150 °C; vacuum 650–700 mm H_2O ;

Table 25.4 Chemical composition of the raw materials for the production of sinter, %

Material	MnO _{tot}	SiO ₂	Al ₂ O ₃	P	S	TiO ₂	Fe _{tot}	Na ₂ O	K ₂ O	CaO + MgO	LOI
Dzhezdzinsky concentrate	30.67	29.5	8.86	0.03	0.32	0.32	2.73	0.65	2.76	2.44	3.13
Polynochnoe concentrate	29.52	14.53	0.21	2.80	0.48	0.22	4.15	0.17	0.50	6.40	2.80
Silicomanganese slag	10.40	39.83	11.81	0.04	0.60	–	2.20	–	–	20.29	–

Table 25.5 Granulometric composition of raw materials for sinter production, %

Material	Fraction, mm						
	5–20	2–5	1–2	0.5–1	0.1–0.5	0.074–0.1	<0.074
Dzhezdzinsky concentrate	–	4.5	18.5	20.5	48.9	0.8	6.8
Polunochnoe concentrate	–	6.3	16.7	18.0	47.0	0.6	11.4
Silicomanganese slag	100						

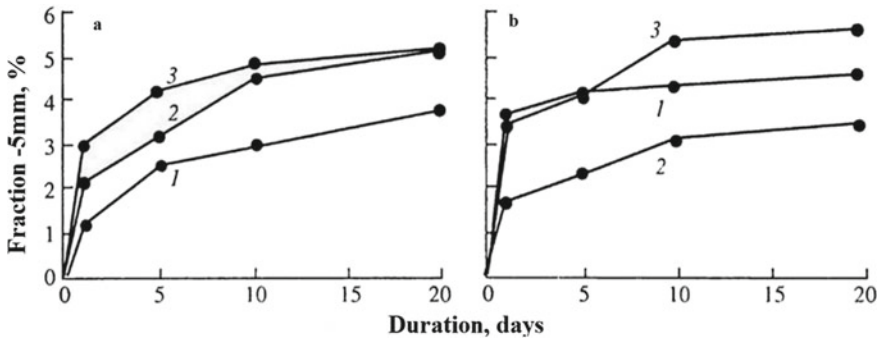


Fig. 25.4 Index of sinter degradability during storage in air (a) and aging in water (b): 1—Dzhezdzinsky, 3—Polunochnoe and 2—mixtures of Dzhezdzinsky concentrate with 6% of slag of smelting of silicomanganese

- collector temperature 120 °C; the temperature in the last vacuum chamber 140 °C; sinter machine productivity 0.84 t/(m² h); fraction content <5 mm in the sinter 18%; sinter strength according to GOST 15137-77: fraction content >5 mm—62.0%, fraction content <0.5 mm—11.8%.

The use of a mixture consisting of 78.7% Dzhezdzinsky concentrate, 8.0% slag and 6.2% Polunochnoe concentrate eliminates breakthroughs and increases the stability of the sinter machine. The layer height was increased to 220 mm, and the vacuum was increased to 800 mm H₂O and reduced the consumption of solid fuel by 1.0–1.3% without deteriorating the strength of the cake (Table 25.6).

An experimental batch of sinter (%: Mn 32.37; Fe 3.86; SiO₂ 28.30; CaO 2.37; Al₂O₃ 5.44; MgO 0.82; P 0.051) was used at “Chelyabinsk Electrometallurgical Integrated Plant (ChEMK)” for smelting ferrosilicomanganese. An experimental campaign showed the possibility of obtaining a standard alloy SiMn17 with a content of 0.08% P. At the same time, a decrease in the consumption of lump ore, coke and shavings was noted.

Studies with manganese ores of the Polunochnoe deposit [17] showed that in the process of producing fluxed sinter, lime is combined not only with gangue silica, but also with manganese silica—manganese monticellite to form calcium silicate. In the fluxed sinter, in comparison with the non-fluxed, in monticellite, the content of manganese silicates decreases from 70 to 45 mol% and the amount of calcium

Table 25.6 Indicators of experimental sintering and the strength of the sinter

Charge#	Ore part of charge, %			Sintering speed, mm/min	Exhaust gas temperature, °C	Specific capacity, t/(m ² h)	Strength, %	
	D	P	S				>5 mm	<0.8 mm
1	100	–	–	10.0	290	0.73	62.6	14.3
2	90	–	10	10.1	310	0.735	63.7	13.3
3	90	10	–	11.5	300	0.78	65.7	14.0

Note 1. Additional sintering indicators: consumption of coke breeze ~9%; charge moisture 6.7–7.1%; return amount 30%; layer height 200 mm; initial depression of 650 mm H₂O; 2. D—Dzhezdinsky concentrate; P—Polunochnoe concentrate; S—silicomanganese slag

silicate increases from 30 to 55 mol%. As a result of this, during the sintering, the amount of free oxides of manganese—Hausmannite and braunite—increases from 25–30 to 40–50%. When smelting carbon ferromanganese in an industrial electric furnace using the raw materials under consideration on an fluxed sinter, the furnace productivity increased by 8.5% compared to unfluxed sinter, electric power consumption decreased by 7.5%, and manganese extraction increased. However, its use in smelting is complicated due to its low strength, dispersion due to hydration of non-assimilated lime particles, structural heterogeneity and an increased number of vitreous phases, decomposition of CaO-MnO_x solid solutions, mineral phase polymorphism and hydration of solid solutions and calcium orthosilicate saturated with calcium oxides. During heating and reduction of the sinter, its strength decreases due to the formation of cracks caused by the thermal expansion of the structural components and the solid-phase reduction of Mn₃O₄ to MnO, accompanied by a change in volume.

Non-fluxed sinter of oxide concentrates consist of tephroite (2MnO·SiO₂), Hausmannite (Mn₃O₄), small amounts of Jacobsite (MnFe₂O₄) and the vitreous phase. The quantitative ratio of these phases varies depending on the chemical composition of the initial manganese concentrates

In the production of fluxed sinter, the introduction of fluxes (limestone, dolomite) into the charge changes the mineral composition of the sinter. The main phase components of the sinter with a basicity of 1.0 are %: manganosite (MnO) + Hausmannite (Mn₃O₄) 30–40, glaucochroite (CaMnSiO₄) 45–50, rankinite (3CaO·2SiO₂) and glass. Up to 3–5% of structurally free CaO is also present. Sinters with a basicity of 1.5 are distinguished by a smaller amount of glaucochroite and a large (up to 10%) CaO. Accordingly, the amount of Ca₂SiO₄ increases. The presence of free CaO and an increase in the amount of dicalcium silicate capable of inversion with an increase in volume up to 12% are apparently the main reason for the sharp decrease in the strength of the sinter with an increase in its basicity to 1.5. A further increase in basicity to 2.0–3.5 changes the phase composition. Glaucochroite, which is found in the most low-basicity microvolumes, almost completely disappears. The predominant manganese oxide is manganosite. In addition to it, another non-silicate component of the solid solutions (Mn, Ca)-O and (Ca, Mn)-O, as well as calcium-manganese oxide

of the oxidation zones (CaMn_4O_8) is observed. Tricalcium silicate ($3\text{CaO}\cdot\text{SiO}_2$) appears in the sinter structure, and the amount of rankinite decreases. Dicalcium silicate in an amount of 20–40% is present in the form of α' - and β -modifications stabilized by manganese oxides. It was found that α' - Ca_2SiO_4 within the flux shell is observed in sinters starting from a basicity of 1.5. As the equilibrium phase in the sintering melt, α' - Ca_2SiO_4 appears with a basicity >2.0 , while it is the most high-temperature first phase crystallizing in the sinter. X-ray spectral analysis showed that the α' -modification is stabilized by manganese oxides in an amount of 1.8–5.8% in terms of MnO. With a mass fraction of 0.3–1.6% MnO, it undergoes a polymorphic conversion to β - Ca_2SiO_4 .

High temperature does not always solve the problem of obtaining a durable moisture-resistant sinter, since the resulting calcium oxide CaO is not completely assimilated by the oxides of manganese and silica contained in manganese ore. One of the reasons for this is the formation of continuous layers of calcium oxide particles, consisting of $2\text{CaO}\cdot\text{SiO}_2$ and $3\text{CaO}\cdot\text{SiO}_2$, which inhibit mass transfer. During sintering of iron ore fluxed sinter, these layers are broken by iron oxides, while manganese oxides exhibit weak disruption properties of calcium ortho- and trisilicate at agglomeration temperatures. Therefore, one of the main areas, according to [6], is the development of the compositions of the blends and the parameters of the process of sintering of manganese raw materials, which would ensure a high rate of mass transfer in the sintering mixture under the condition of complete assimilation of lime. The increased amount of iron oxides in the sinter charge facilitates the penetration of manganese deep into the particles of lime with the formation of phase $4(\text{Mn, Fe})\cdot\text{O}\cdot 4\text{CaO}\cdot\text{SiO}_2$.

The phase composition of sinters obtained from ores of the Polunochnoe deposit was studied in [18]. Non-fluxed sinter is represented by a large pore black cake. Sinter is characterized by a large heterogeneity in structure, composition and porosity. The silicate bond is 25–30 vol%. The ore part of the sinter is represented by solid solutions based on the lattices of α - and γ -Hausmannite and, to a lesser extent, by solid solutions based on the Jacobsite $(\text{Mn, Fe})_3\text{O}_4$ lattice and a small amount of manganosite MnO. The silicate binder of complex composition includes numerous quartz grains of sand. They are fused, practically have no reaction zone from the surface and are cracked inside.

The fluxed sinter of oxidized manganese ore is represented by a black porous cake with numerous “whites” of quartz sand grains and unburnt limestone. When stored for 12 days, 50% of the sinter is crumbled into fines. The sinter is also characterized by heterogeneity in structure and phase composition. The fluxed sinter has a larger amount of silicate binder, more diverse. Some quartz grains are assimilated by the melt. The amount of silicate binder is 30–40 vol%, unevenly distributed in the mass of the sinter. In some areas, the binder reaches about 40 vol%.

The ore part of the sinter is represented by solid solutions based on the lattices of Hausmannite, Jacobsite and manganosite. An increase in the content of the latter is characteristic. Its distribution in the sinter is uneven and is local in nature. The forms of extraction of ore minerals are the same as in the non-fluxed sinter.

The silicate binder is crystalline, but there is also colorless and yellowish-brown glass. The main crystalline phase is manganese monticellite. Dendritic pyroxene is contained in a small amount. In the areas of limestone inclusions, calcium ferrites are formed in the form of a melt together with rounded grains of β -dicalcium silicate $2\text{CaO}\cdot\text{SiO}_2$. Here also, the tricalcium silicate $3\text{CaO}\cdot\text{SiO}_2$ -rankinite is formed. Dicalcium silicate is also present in other parts of the silicate bond of the sinter in a finely dendritic form. Free coke grains are contained.

Non-fluxed sinter from carbonate manganese ore is similar in composition and structure to sinter obtained from oxidized manganese ore. The difference is in the amount of silicate binder, which is 40–45 vol%. The ore part of the sinter includes solid solutions based on a lattice of Hausmannite, Jacobsite and manganosite. The silicate bond is mainly represented by manganese monticellite and coarse-grained glass, in which inclusions of manganese sulfides in the form of small skulls are observed.

The fluxed sinter from manganese carbonate concentrate is represented by black cake, large pore with a mass of “whites” of quartz and unreacted lime. When stored after two weeks, it crumbled, forming more than 50% of the fines. The sinter is heterogeneous in structure and composition: The amount of silicate binder increases, and locally its content exceeds 50 vol%. The distribution of ore phases of the sinter is very uneven, and eutectics appear. The content of solid solutions based on manganosite increases. Areas of solid solutions based on wustite are present. Jacobsite is sometimes deposited on the surface of manganosite grains. The number of other ore phases decreases. Around the lime inclusions, phases are formed: calcium ferrites, β - $2\text{CaO}\cdot\text{SiO}_2$, $3\text{CaO}\cdot\text{SiO}_2$ and silicate binder are coarse crystalline. The main phase is manganese monticellite. The eutectic of monticellite-manganosite appears. Colorless and yellow-brown glass with inclusions of manganese is present.

Thus, sinters obtained from oxidized and carbonate manganese ores have a similar phase composition. The main manganese-containing minerals are solid solutions based on Hausmannite and Jacobsite. The silicate bond is well developed with a predominance of tephroite and manganese monticellite. With fluxing, manganosite appears in large quantities, with Hausmannite and Jacobsite. The content of the silicate binder, which is mainly represented by manganese monticellite, increases, β -dicalcium silicate appears in noticeable amounts, and the eutectic manganosite monticellite appears.

The industrial development of the end-to-end technological scheme and processes for the production of manganese magnesium sinter and smelting with its use of ferrosilicomanganese SiMn17 (Russian grade) was carried out in 2012 [16]. In the production of manganese magnesium sinter in the pilot campaign, 9 thousand tons of magnesium silicate waste slag from smelting rich ferronickel (15–20% Ni) were used. Sinter was produced in the sintering plant of NFP on sinter machines AKM-105 and was used in the charge of ore-smelting arc furnaces. When smelting in the base period, the sinter of the current production was used (chemical composition, %: 47.4 Mn, 28.5 SiO_2 , 8.5 Cao, 2.2 MgO, 2.3 Fe, 0.17 P) and in the experimental period—manganese magnesium sinter. The chemical composition of the sinters is shown in Table 25.7.

Table 25.7 Chemical composition of the manganese magnesia sinter

Components, %	Sinter production periods, 2012				
	26.03–04.04	05.04–17.04	18.04–30.04	01.05–17.05	18.05–31.05
Mn	36.4	38.4	38.1	39.1	38.9
SiO ₂	28.9	27.4	27.3	26.2	26.2
CaO	5.2	4.9	4.8	–	5.1
MgO	7.0	5.9	5.8	5.9	5.5
Fe	3.2	3.1	3.1	3.2	2.9
P	0.16	0.16	0.16	0.16	0.7

The specific consumption of charge materials and the chemical compositions of the sinters are shown in Table 25.8.

The total amount of ferrosiliconmanganese smelted during the experimental period amounted to 24,879 tons. For all periods of SiMn17 smelting using manganese magnesia sinter, the useful extraction of manganese from charge manganese-containing components in the alloy increased from 87.6% (in the base period) to 88.7–92.7% (in experimental periods). The relationship between the extraction coefficients of manganese and silicon for the base and experimental periods is well illustrated by Fig. 25.5.

The smelting of SiMn17 using manganese magnesia sinter is accompanied by a decrease in the specific consumption of quartzite (74.2–114.9 kg/t). During the pilot campaign, it was confirmed that the specific energy consumption primarily depends on the manganese content in the sinter and charge. In the first period of the campaign, with a decrease in the manganese content in the sinter to 36.4% and in the specified charge to 35.2% (against 38.2% in the base period), the specific energy consumption increased by 111.5 kWh/t; with an increase in the manganese set with

Table 25.8 Specific consumptions of charge components and power for ferrosiliconmanganese smelting with manganese magnesia sinter

Charge components, %	Ferrosiliconmanganese production periods, 2012					
	01.03–20.03	26.03–04.04	05.04–17.04	18.04–30.04	01.05–17.05	18.05–31.05
Mg Sinter	–	1354.1	1405.9	1362.6	1349.5	1441.2
Sinters 1, 2	1397.0	–	–	–	–	–
Mn ore	170.1	178.9	49.5	–	–	–
Mn concentrate	–	–	52.8	121.4	118.0	95.6
Coke	390.2	399.1	367.8	394.0	357.5	369.8
Quartzite	332.0	217.1	243.3	257.8	244.2	245.2
Iron ore	67.5	41.8	39.1	113.3	90.0	53.7
Power, kWh/b-t	3949.6	4061.1	39.0	3931.0	3872.0	3902.0

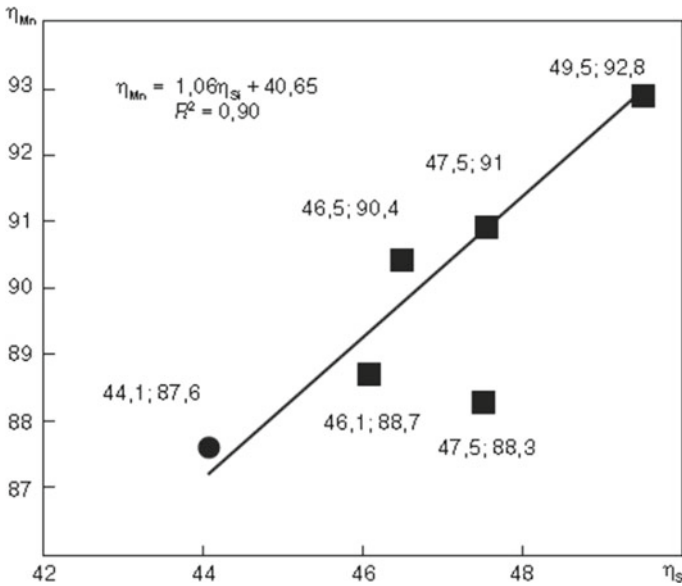


Fig. 25.5 Correlation between the extraction coefficients of manganese (η_{Mn}) and silicon (η_{Si}) during the smelting of ferrosiliconmanganese using manganese magnesia sinter

the charge to 36.8–37.7%, the specific electric energy consumption decreased by 18.6–107.6 kWh/t. With a decrease in the specific consumption of magnesia-silicate slag in the sinter charge to 121 kg/t and, consequently, the MgO content in the dump slag SiMn17 to 8.8%, the efficiency of manganese recovery decreased to 88.3%. The reduction in coke consumption reached 8.8% in the experimental period.

25.2.2 Chromium Ore Sintering

According to its mineralogy, chromium ores are represented by chromium spinels (or chromites) of the composition $(Fe,Mg)O \cdot (Cr,Al)_2O_3$. The industrial value of the raw material is determined by its Cr_2O_3 content (more than 50%) with a fairly high Cr_2O_3/FeO ratio (not less than 2.5), SiO_2 content not more than 10% and P (not more than 0.015%). The chemical composition of chromium ore (the content of the leading element, harmful impurities and the ratio of chromium to iron) determines the possibility or impossibility of producing ferrochromium with a chromium content of more than 65%. Along with the chemical composition of chromium ore raw materials, for the use of chromium ore in the smelting of high-carbon ferrochromium in ore-smelting electric furnaces operating on alternating current, there are size requirements (10–100 mm), where the –10 mm fraction should not enter the composition of the charge in the furnace due to its removal from the working space with exhaust

gases. Fine fractions formed in the process of mining and beneficiation of chromite ores are of limited use in ferroalloy production, especially in the preparation of ferroalloys by the silicothermic method [6, 19].

The advantage of sintering is the absence of the need for regrinding of chromite ore fraction $-10 + 0$ mm, and the main problem is the high-melting temperature of chromium ore raw materials, reaching 1700–1800 °C, adversely affecting the stability of the sintering equipment. To reduce sintering temperatures, various fluxing materials are used: quartzite, sand, microsilica and some others, differing in their chemical, mineralogical, fractional compositions and price.

The problem of sintering of chromium ores is the high-melting temperature of both the grains of the ore material and the host rock containing chromium spinel, while the formation of a sufficient amount of liquid phase (melt) is necessary for the conditions for obtaining a strong sinter. In the production of chromium sinter, the ratios of magnesium and aluminum silicates forming the liquid phase during the interaction of the components of fluxing materials and the host rock of chromites begin to play an important role [20].

Under industrial conditions, chromium ore sintering is carried out in Japan [19]: a mixture consisting of chromium ore, coke, magnesite and silica is sintered at 1550 °C. Sinter has high strength and yield of 85%.

In [21], the technology of preliminary preparation of chromium ore by sintering was developed, where sodium silicate was used as a binder. However, these developments were not mastered due to the aggressiveness of sodium vapor released during the subsequent melting of such agglomerated raw materials in an electric furnace. Studies of the sintering of a mixture consisting of 70% chromite ore (53% Cr_2O_3) and 30% return with a grain size of 0–6 mm [22] showed that even with an increase in coke consumption up to 10%, the sinter has low strength. Due to the weakly fused structure of the sinter, the yield of fines less than 5 mm was more than 35%. To improve the strength of the sinter, up to 7–45% of iron ore concentrate and 12–20% of limestone were introduced into the charge in order to form fusible compounds. Such a technique inevitably led to a decrease in the ratio of the concentrations of chromium and iron.

In [23], the results of studying the sintering of chromium ore fines without the use of fluxes with a change in the height of the layer of sintered mixture from 200 to 240 mm are presented. It was shown that sintering of chromium ore is possible without fluxes with a high coke consumption (18–20%). However, this increases the temperature of the exhaust gases (from 600 to 860 °C), which can adversely affect the stability of the process equipment. Successful sintering can be carried out with the addition of fluxes, which significantly reduce the temperature of formation and melting of the components of the mixture.

The undoubted advantage of sinter production is its high productivity. At the same time, large capital investments are needed to organize the production of sinter, while the construction time of the sinter plant and the return on investment can be very long. Sintering machines are complex and bulky units that require significant capital and operating costs. At the same time, sintering does not always ensure a high-quality cake; in some cases, the sinter with a low-melting point is obtained, which reduces the

temperature in the ore-smelting furnace and worsens the course of the carbothermic process. It is also known that this process leads to serious environmental pollution. The sinter plant as part of a ferroalloy plant is the dominant source of harmful emissions into the atmosphere.

25.3 Pelletizing

Pelletizing is the process of sintering moistened finely ground materials, based on their ability to form spherical granules when rolling without applying direct pressure. Hardened pellets obtained from finely ground concentrates have good reducibility, sufficient strength during overloading and recovery and uniformity in size and chemical composition. In addition, when firing pellets, fuel consumption is approximately half as much as during sintering, and the emission of carbon and nitrogen oxides, the main harmful components in sinter wastes, is significantly reduced or even absent.

For the smelting of manganese ferroalloys in ore-smelting furnaces, fired pellets obtained from fine fractions of manganese concentrate, flotation concentrates and sludge, trapped dust, etc., are used (Fig. 25.6, [23]). In the production of pellets in disk and drum granulators, material is with a mass fraction of -0.074 mm of not less than 90–95%. Industrial manganese concentrates of a fraction larger than 0.1 mm are crushed. Pellets are strengthened by low-temperature drying or firing at 1150–1220 °C. During firing, a liquid phase forms, cementing the components of the pellet.

In the USSR, the first major work on the technology for producing pellets from manganese concentrates was carried out back in the 1970s. Studies have been performed on the pelletizing of oxide and carbonate flotation concentrates obtained from Chiatura manganese ore with the addition of sulfite-alcohol bards (SAB). At a rate of 6–8% SAB, pellets with a compressive strength of 40–60 kg/pellet were obtained that satisfy the requirements for charge materials for smelting manganese alloys in an ore-smelting furnace [24]. At the Kashima plant (Japan), for the smelting of high-carbon ferromanganese in the furnace with a capacity of 40 MV A, manganese concentrates are pelletized on a pelletizer with a capacity of 110 t/h, and then pellets are fired at a temperature of 1150–1220 °C on a rotary kiln with a diameter of 3.5 and a length of 75 m.

When smelting ferromanganese, the specific energy consumption was reduced, and the furnace productivity increased [6].

Manganese oxide ore pellets are also produced in Brazil. A concentrate of class 0–6.4 mm, containing 41% manganese, 7.5% iron and 6.4% silicon oxide, is subjected to reductive magnetizing firing at 820–850 °C, after regrinding to a particle size (-0.147) mm and magnetic separation pelletized in a bowl granulator with bentonite added as a binder. Then the pellets are dried, fired at a temperature of 1300 °C and cooled. After sifting out the fines, pellets of 6.4–19 mm class are sent to the smelting. Pellets in terms of physical properties satisfy the requirements of ferroalloy production.

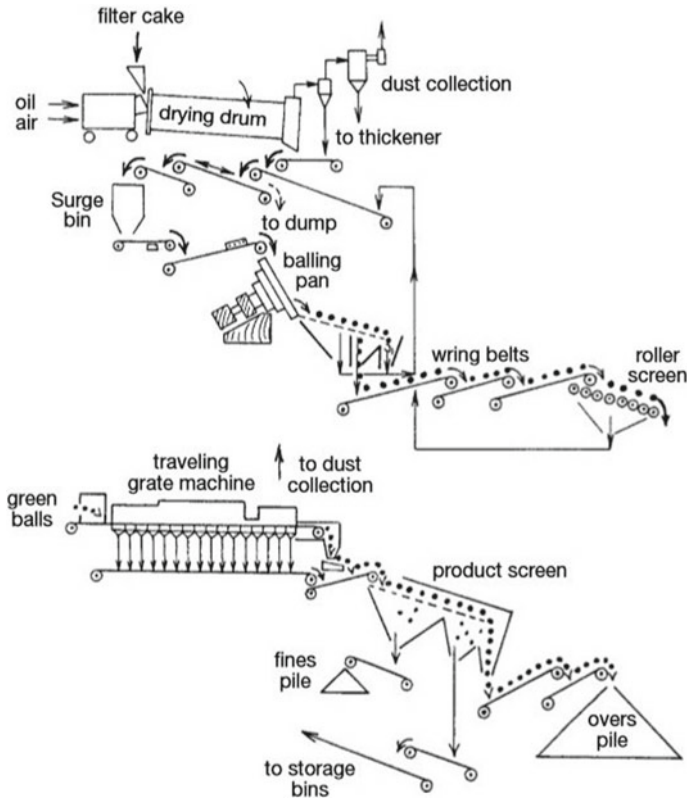


Fig. 25.6 Simplified flow diagram of a two-stage manganese ore agglomeration plant; (above) concentrate drying and balling stage; (below) pellet strengthening stage [23]

To obtain raw pellets in [25], following components were used: the concentrate of the Grushevsky processing plant (C1 and C2), ground limestone with a grain size of up to 0.2 mm (L) and bentonite (B). In Table 25.9, which shows the properties of the starting materials and firing products, the following designations are indicated: P1, P2—calcined, non-fluxed and fluxed pellets of laboratory experiments and P3—calcined semi-industrial pellets.

The content of fractions finer than 50 μm in a C1 concentrate is 30–40%. The moisture content in the concentrates filtered on a disk vacuum filter is 27–30%. Raw pellets were obtained on a pelletizer with a diameter of 1000 mm and a side height of 180 mm during periodic operation with a charge of 12–15 kg (the speed of the bowl was 50–60 rpm, and the angle of inclination was 43–48°). Within 3–5 min, the loaded material at a moisture content of 20–27% is rolled into pellets with a grain size of 10–20 mm. Pelletizing with the addition of 0.5% bentonite does not increase the strength of the pellets in a wet and dried state. Pellets without additives have a

Table 25.9 Chemical composition of charge materials and products of firing

Material	Mn	MnO ₂	MnO	Fe ₂ O ₃	SiO ₂	Al ₂ O ₃
C1	36.2	41.0	13.2	3.0	15.0	1.65
C2	35.8	40.5	–	–	16.4	1.73
L	–	–	–	–	1.0	–
B	–	–	–	–	58.9	17.8
P1	43.0	18.1	40.7	5.3	17.7	2.0
P2	39.6	21.6	33.6	3.4	15.9	1.9
P3	37.4	15.1	36.2	8.61	22.4	2.1
Material	CaO	MgO	LOI	P	Na ₂ O	K ₂ O
C1	5.97	2.63	13.5	0.41	0.8	1.98
C2	4.48	2.32	16.2	0.40	–	–
L	54.0	1.15	43.2	0.005	–	–
B	3.0	1.73	7.5	0.001	0.43	0.43
P1	7.0	3.29	–	0.47	0.84	1.68
P2	15.3	3.44	–	0.43	0.84	1.56
P3	5.78	2.42	3.0	0.40	0.8	1.20

crushing strength in the raw form of 0.8–0.9 kg per pellet and 3.8–4.0 kg per pellet in a dried state. Removal of volatiles during heating lasts 30–35 min.

Fired pellets are mainly represented by Hausmannite. The heat for decomposing MnO₂ to Mn₃O₄ is 258 kcal/kg manganese, which corresponds to a heat consumption of 86 thousand kcal per ton of dry charge, taking into account 10% of fired return. To compensate for heat consumption, an addition to the charge during pelletizing of 1.4% of solid fuel is required. The firing temperature of unfluxed and fluxed pellets is 1160 and 1190 °C, respectively. Slow heating of the pellets (not more than 70–80 degrees per minute) and slow cooling (at a speed of up to 150 degrees per minute) are required.

Manganese pellets were fired in a bowl with a diameter of 210 mm. A layer of fired granules 20–30 mm high was placed under a layer of crude pellets to protect the bowl lattice from overheating. Pellets were loaded into the bowl with a layer 400 mm high. Firing unfluxed pellets and cooling take 57–60 min (Table 25.10). When firing with combined fuel (0.57% of coke was rolled into the pellet and 2% rolled onto the surface), the specific productivity of the installation was up to 0.45–0.5 kg/m² h.

For production of raw pellets (P3) with a size of 10–20 mm, a pelletizer with a diameter of 5.5 m and a side height of 0.8 m was used with a rotation speed of 7–9 rpm at an angle of inclination of the bottom of the bowl to the horizon of 52°, the bowl rotation speed of 8–8.5 rpm, moisture content of the pellets 17–22% and the capacity of a pelletizer—12–15 tph. The average height of the pellet layer on the machine was 260 mm. Pellets withstood 25–30 drops from a height of 300 mm, the bulk density was 1.45 t/m³, and the apparent specific gravity was 1.95–2.0 g/cm³. Pellets were fired on a conveyor machine with an absorption area of 18 m².

Table 25.10 Pellet firing indices in the bowl (P1, P2) and on the firing machine (P3)

Parameter	P1	P2	P3
Bulk density			
Raw pellets	1.24	1.22	1.45
Fired pellets	1.65–1.75	1.5	1.45
Specific capacity, t/m ² h	0.25	0.22	0.36–0.40
Maximum vacuum, mm H ₂ O	210	160	290
Heat consumption, kcal/t, thousands	–	–	1020
Compressive strength, kgF/pellet	200	205	60–70
Tumble test, %	14.0	25.8	16–25
Return yield, %	10–11	12–13	8–15

The manganese flotation concentrate (C2) contained 35–50% of the fraction finer than 50 μ and 21–24% of moisture. Up to 10% non-ground return of 5–0 mm particle size was added to this concentrate.

The firing machine had six vacuum chambers, and the cooling of the pellets to 100–150 °C ended on the vacuum chamber (zones V and VI). Useful suction area of the machine is 15 m² (Fig. 25.7). In the drying zone (I), a temperature of 350–400 °C was maintained, in the heating zone II—800 °C and in the firing zone (III and IV) above the layer of pellets—within 1100–1150 °C. Granulometric composition of P3 pellets is as follows:

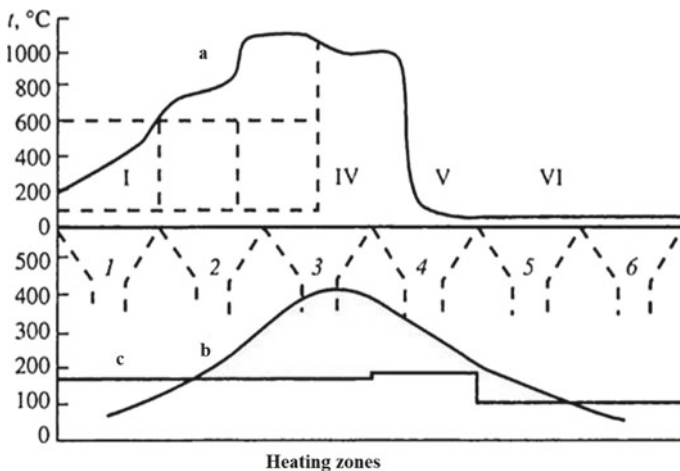


Fig. 25.7 Distribution of gas temperature and technological zones along the length of a firing semi-industrial machine; and at the temperature above the layer, in the vacuum chambers (1–6) and at the fans; I—drying, II—heating, III, IV—the first and second firing, V—recuperation, VI—cooling

Fraction (mm)	+15	15–10	10–5	5–3	3–0
Content (%)	5.5	58.5	26.9	4.4	4.7

The productivity of the firing machine for the finished product varied within 4.5–6.2 t/h.

Fired pellets were used at the Nikopol Ferroalloy Plant in a 1200 kV A furnace. Due to the high phosphorus content in the pellets, ferromanganese was obtained in two stages—first low-phosphorous slag was melted (phosphorus content up to 0.03%) and then carbon ferromanganese.

In [26], the properties of pellets from flotation concentrates of I and II classes and hydrometallurgical concentrates (soda enrichment method), as well as from a mixture of concentrates: flotation concentrate 40% and hydrometallurgical 60% (charge No. 1), flotation 50% and dithionate 50% (charge No. 2) were studied. Pellets were fired using natural gas and combined fuel—solid and natural gas. Fine coal with a fineness of -0.16 mm was either rolled onto the surface or rolled into pellets. The duration of firing pellets with combined fuel with coal rolled onto the surface is less than firing with one gas. When firing with gas pellets containing 1–1.2% of solid fuel rolled inside, the process time decreases and the quality of the pellets improves. When firing with gas, the duration of the pellets in the zone of maximum temperature is the longest, when firing with combined fuel, the shortest. In concentrates, manganese is present in the form of MnO_2 , which is reduced to Mn_3O_4 ; therefore, the firing method affects the physicochemical and thermophysical properties of the pellets.

Pellets from dust of metallic manganese, sludge and slag of metallic manganese were studied in [27]. The pellets were dried in air for 3–4 days. Smelting in a furnace with a capacity of 1600 kV A was carried out on a conventional charge (option 1) with sinter (2) and pellets (3), in which dust, sludge and slag were used (Table 25.11). Sinter and pellets from manganese-containing waste were not destroyed. When using pellets, the best indicators of smelting of silicomanganese are obtained.

At the Zestafoni Ferroalloy Plant on a granulator with a diameter of 3000 mm, pellets were obtained from manganese dust of gas cleaning, which is captured during the smelting of ferro- and silicomanganese [28]. The size of the pellets is 10–30 mm; composition, %: Mn 33.6; SiO_2 12.6; CaO 1.5; P 0.18. Together with the concentrate (47.3% Mn), pellets together with concentrate (1:1) produced standard carbon ferromanganese in an industrial furnace.

Reductive firing of manganese ore-carbon pellets has been tested, which excludes the formation of skulls in a rotary kiln [29]. Fine materials were used (flotation concentrate, 8–10% of fine reducing agent, 1% of bentonite). The mixed batch was pelletized in a 2-m diameter pellet mill. Raw pellets were fed to the grate of the roasting machine, where they were gradually dried at a temperature of 400–450 °C and then heated at 800–900 °C with hot gas leaving the rotary kiln. Heated pellets entered a rotary kiln, where further heating and reduction took place at 1070–1100 °C in the atmosphere created by a low coefficient of excess air (0.7–0.9) during

Table 25.11 Comparison of the indicators for the preparation of silicomanganese on a different charge

Parameter	Smelting Options		
	1	2	3
Furnace capacity, b.t/day	3.12	3.57	3.97
Chemical composition of alloy, %			
Mn	71.1	71.2	17.5
Si	17.7	18.5	72.1
P	0.50	0.50	0.47
Slag ratio	1.8	1.68	1.64
Slag basicity (CaO + MgO/SiO ₂)	0.24	0.26	0.33
Extraction, %			
Mn	64.5	66.9	70.15
Si	36.7	37.8	39.9
Power consumption, kWh/b.t	5140	5096	4909

the combustion of natural gas and the quantity of coal fed into the furnace 15–20%. The pellets contained MnO had high strength—compressive strength of 120–180 kg/pellet, and the destruction index in a standard tumble testing was 90–93%. The cold pellets were melted in an ore-smelting electric furnace (1200 kV A) for ferromanganese using the flux method. Its productivity increased by 22%, and the specific consumption of coke and electricity decreased by 52 and 29%, respectively.

The results of a series of experimental melts of 75% ferrosilicon using pelletized charge consisting of quartzite, brown coal semi-coke and iron ore concentrate were presented in [30]. The initial ore materials and return were ground in a dry grinding ball mill to a particle size of 85–90% of class 0.074–0 mm and fed into a twin-shaft mixer, where they were mixed with wet semi-coke. Brown coal semi-coke had the following composition, (%): C_{tot}—65, 8; V^r—11, 9; A^c—18, 8; W—4, 7.

The moisture content of the charge varied from 4 to 8% (before the granulator 5–7%). The content of the fraction class 0.074–0 mm was in the range of 65–75%. A binder (sulfite liquor solution) was prepared in autoclaves and adjusted to a density of 1.14–1.15 kg/l in mixer tanks. The mixture contained 53.0% quartzite, 41.5% semi-coke, 5.5% iron ore concentrate and 15–20% return (in excess of 100%). Finished pellets obtained with a binder consumption of 5.0–5.5% (in terms of solid sulfite liquor) had the following technical characteristics: compressive strength 40–90 kgF/pellet, impact strength 65–88.5%, abrasion strength 10–25%; yield of fraction 15–0 mm 20–40%; bulk density 0.821 t/m³; true density 2.5 g/cm³; apparent density 1.61 g/cm³; porosity 35.4%.

The pelletized charge contained an average of 27.5% carbon. Initially, experimental melting of 75% ferrosilicon was carried out in a 1200 kV A furnace at a rated voltage on the low side of the transformer of 81.9 V and a current of up to 6.8 kA. Taking into account the obtained melting results in a 1200 kV A furnace, industrial

melting of 75% ferrosilicon was carried out in an open three-phase furnace with a capacity of 14 MV A, equipped with an automatic charge metering system and having the following basic geometric parameters, mm: bath diameter 5400; bath depth 2200; electrode diameter 1100; the diameter of the electrodes cycle 2600–2700. Comparative experimental melts of 75% ferrosilicon on conventional and pelletized charges were carried out at a linear voltage of 173 V and a current of 49.2 kA. Five experimental blends were studied using pellets from 698 to 3292 kg per 1 ton of FeSi75 and coke consumption from 329 kg/t to 80 kg/t, respectively. The best results were obtained when 25% pellets with brown coal semi-coke were added to a conventional charge. According to this option of melts, an increase in furnace productivity and a decrease in the specific consumption of coke were achieved.

Two lines for the production of chromium ore pellets on steel tape using Outotec technology in 2009 were commissioned at DonGOK (Kazakhstan Republic). The technology, successfully used in a number of countries (South Africa, Brazil, Greece, India, Turkey, etc.) since 1989, provides for the possibility of producing both oxidized and ore-carbon pellets [20]. The cost of pellets is increased using expensive binders (liquid glass, lignosulfonate and bentonite). This technology uses chromium concentrate of a fraction of 0–3 mm from an enrichment plant and raw chromium ore of a fraction of 0–10 mm. Coke and ore fines are subjected to additional grinding, and bentonite is used as a binder. One of the serious problems of this technology is the resistance of the steel belt of the conveyor machine, on which the pellets are fired. In order to prevent failure of the tape due to sticking of the material, as well as oxidation of the tape itself due to heat changes associated with periodic downtime of the equipment, it is necessary to strictly monitor the loading mode, the state of the tape itself, and prevent interruptions in the technological and thermal conditions.

Despite the successful testing of pelletizing technology in the production of ferrochromium, there are a number of disadvantages of this technology: the need for additional grinding of fines of chromium ore; the use of expensive, harmful binders (liquid glass, lignosulfonate); high wear of steel tape due to high process temperatures; small pellets in diameter of 8–15 mm.

The production technology of boron-containing chromium ore pellets was developed in Kazakhstan [20]. Borate ores of the Inder deposit are used as a component that reduces the melting temperature. The pellets obtained using this technology are characterized by high strength, but also require preliminary grinding of chromium ore, which leads to additional costs.

Thus, the brief analysis of the known methods of agglomeration by pelletizing small fractions showed their high efficiency, which reduces the specific energy consumption, increases the productivity of the furnace and manganese extraction. The disadvantages of the pelletizing process include the need for regrinding of the material and firing of pellets, which increases their cost.

25.3.1 Cold Bonded Pellets (CBP)

The first projects for the production of cold bonded pellets (CBP) with Portland cement as a binder began relatively recently. Since 1970, an industrial factory with a design capacity of 1.6 million tons of pellets per year has been operating in Sweden using the *Grangcold* method. The CBP technology is quite widespread for the recycling of metallurgical production wastes: In 1978, a plant for pelletizing the blast furnace dust with a capacity of 550 thousand tons of pellets per year was commissioned in Nagoya (Japan); since 1979, a plant with a capacity of 120 thousand tons of steel making dust pellets per year has been operating at a plant in Oita (Japan) [31]. An example of CBP technology for the pelletizing of fine chromite ore is the cold bond process (COBO, Sweden), which is patented in a number of countries [32] and was mastered on an industrial scale [33]. At present, there are at least 20 large industrial factories and cold agglomeration plants with a total capacity of about 4 million tons of pellets and briquettes per year.

The principal feature of the CBP methods is the use of binders, usually of cement type. Binding agents are compositions based on heterogeneous disperse systems of the solid-liquid type, the components of which enter into physical and chemical interaction with each other, forming a plastic, easily workable mass that turns into a strong stone-like body under certain conditions [34].

Cold agglomeration is characterized by a variety of methods used. The classification of binders and cold agglomeration methods is presented in Fig. 25.8.

Various methods of carbonization are based on the use of binder's compositions such as S-G. The formation of stone-like body occurs as a result of the interaction of the binder (usually lime) with carbon dioxide (flue gases) at a partial pressure less or

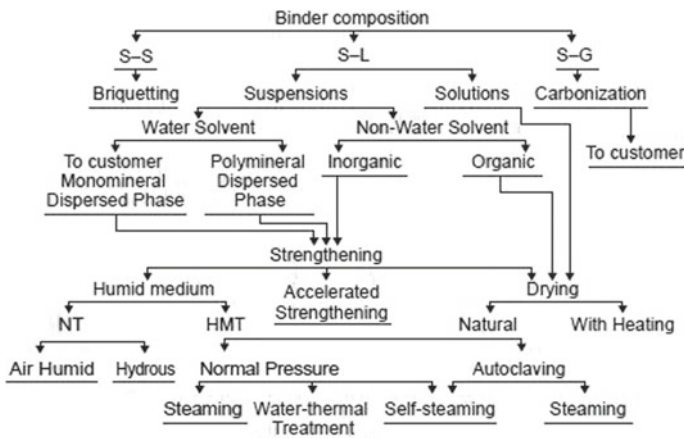


Fig. 25.8 Classification of binders and cold agglomeration methods [9] (S-S—solid-solid; S-L—solid-liquid; S-G—solid gas; NT—normal temperatures; HMT—heat and moisture treatment)

more than atmospheric, at normal and elevated temperatures, with and without the use of catalysts.

CBP methods based on the use of S-L binding compositions include various types of heat treatment: drying (at normal temperatures and with heating), strengthening in a humid environment (at normal temperatures and heat and moisture treatment at atmospheric and elevated pressures) and combined methods (accelerated strengthening).

25.3.1.1 Cold Strengthening Under Normal Conditions

Strengthening in an air-humid environment at ordinary temperatures in the technology of binders is called normal strengthening. In the methods of normal strengthening, hydraulic bonding of Portland cement type (Portland cement with additives, slag Portland cement and magnesia, alumina Portland cement) is most common.

The above-mentioned Grangcold method works using slag or Portland cement [35]. The technological scheme of the production of cold bonded pellets according to the Grangcold method is presented in Fig. 25.9.

The binder, containing about 50% of cement clinker and 50% of granulated blast furnace slag and special additives, is crushed first in a rod mill and then in a two-chamber ball mill with pebble load. Iron ore concentrate pulp with 40% of the solid

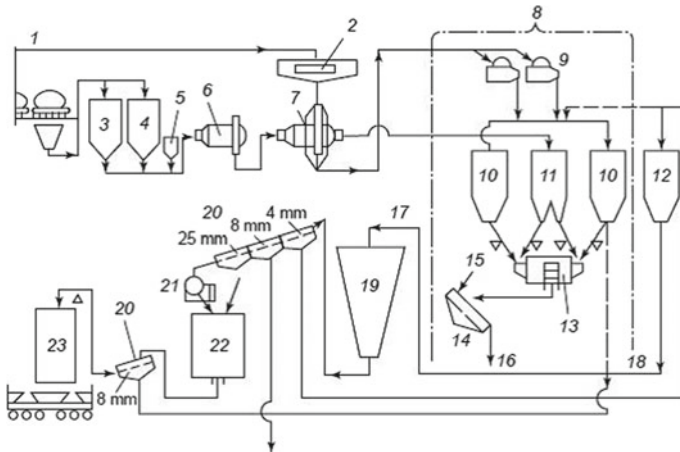


Fig. 25.9 Technological scheme of the production of pellets by the method of Grangcold [35] (1—pipeline supply of concentrate from the processing plant; 2—thickener; 3—clinker; 4—slag; 5—additives; 6—rod mill; 7—ball mill; 8—lines for obtaining pellets; 9—filter; 10—concentrate hopper; 11—cement hopper; 12—underlying material with a particle size of 4 mm; 13—rod mill mixer; 14—dish granulator; 15—water; 16—raw pellets; 17—raw pellets + bedding concentrate; 18—bedding concentrate; 19—bunker for strengthening; 20—crash; 21—crusher; 22—the second bunker for strengthening; 23—bunker for loading pellets into railway wagons)

is fed first into the thickener, from which it is fed with a 75% solid into a ball mill. Filter cake, containing 8–9% moisture, enters the concentrate bunker.

Mixing the concentrate and the binder before pelletizing is carried out in a rod mill mixer with two-sided loading and central unloading. To obtain uniformly sized raw pellets with proper strength, 8–9% of water is fed into a pan granulator with a diameter of 6 m. Raw pellets arrive at the conveyor, where they preliminarily load concentrate from a separate bunker. Then the raw pellets are poured with concentrate (the operation prevents the pellets from sticking together when kept in the bunker at the first stage of strengthening). A mixture consisting of 2/3 of the pellets and 1/3 of the concentrate enters the bunker (60 m high), where the pellets pass through the first strengthening stage. After 30–40 h of movement through the bunker, the pellets arrive at the conveyor at the screen to separate the concentrate and fines less than 4 mm (sent to the bunker to pour the raw pellets); destroyed pellets fraction 4–8 mm (used as raw material in agglomeration); pellets with a particle size of more than 25 mm (are fed for crushing and then returned to the mixture).

Pellets with a size of 8–25 mm are sent to the second bunker, where, when stored for 5 days, they acquire up to 70–80% of final strength. Next, the pellets are delivered to the open warehouse for final strengthening within 2–3 weeks. Grangcold cold bonded pellets have strength after drying of 200 kg/pellet (for a particle size of 15 mm), a tumble test—92% (yield of +6.3 mm class), moisture content of 6.5%, Fe content of 59.7%, with basicity about one.

Mechanical strength of CBPs from manganese sinter fines using different percentages Portland cement as a binder was studied [36]. While the addition of Portland cement enhances the green pellet compressive strength, it retards the green drop strength. This is due to the difference in the mechanism of pellet rupture that took place in each test. Increasing amount of water added improves to a large extent the mechanical properties of green pellets as a result of increasing the number of liquid bridges inside the pellets. The amount of cement, amount of water added, as well as the curing time of pellets at room temperatures play very important roles in the mechanical properties of the produced pellets. Pellets produced with 9% cement and 13% water and cured at room temperature for 28 days show reasonable properties. The ferromanganese alloy produced from the smelting of these pellets has a chemical composition within the range of the standard alloy.

In recent years, attempts have been made to use alternative binders for the production of CBP. In particular, a technology was developed and pilot tested for the production of non-fired manganese pellets from high-silicon manganese ore of a fraction of 0–5 mm without regrinding using a reducing agent and as a clay binder [37]. Pilot tests have shown that it is possible to obtain CBPs dried at 100 °C from fines of ore fractions of 0–5 mm, using a reducing agent and clay as a binder, with an average strength of 15.5–20.0 kg/pellet, which satisfy the strength characteristics of the requirements for charge materials for smelting in low-shaft ore-smelting furnaces, which was also confirmed in the pilot industrial tests for smelting ferrosiliconmanganese. The removal of fractions of 0–8 mm from the batch of fines and their feeding into the batch in the form of agglomerated material (pellets) increased the technical and economic indicators of the smelting process of ferrosiliconmanganese.

Application of the composite binder based on dextrin and bentonite for the pelletizing of Indian chromite ores is described in [38]. High Cr/Fe ratio and high MgO content in these ores demand high firing temperatures and longer firing cycles but often result in low strength fired pellets. High-temperature reduction studies revealed that pellets were resistant to disintegration up to 1200 °C. Pilot scale arc furnace trials were also carried out to compare the performance of CBPs with sintered chromite pellets and found that for a constant power input, smelting rate was faster for CBPs than sintered pellets. Loss of Cr to slag was reduced in case of cold bonded pellets usage.

The pelletizing of manganese dust of aspiration systems (30% Mn) with a particle size <0.05 mm (80%), coke breeze (5–0 mm) in a 1:1 ratio with sulfite-alcohol bards (SAB) as a binder was described in [39]. Pellets had high strength. During smelting of silicomanganese in a furnace with a capacity of 1600 kV A, the specific consumption of electric energy and materials was reduced by 8%, and the productivity of the furnace and the extraction of manganese were increased by 3–8% compared to working on a conventional charge with sinter.

25.3.1.2 Cold Agglomeration at Moderate Temperatures

Cold agglomeration of ore materials at moderate temperatures is carried out with binders combined with autoclaving (i.e., processing at temperatures of 100–400 °C and pressure of 10–15 atm.).

An example of such method is given by the mentioned previously COBO process. A schematic diagram of the cold bond (COBO) process for iron ore materials is presented in Fig. 25.10.

Raw pellets are obtained on a disk granulator from a mixture prehomogenized in a rod mill. As a rule, the mixture consists of 2/3 of the coarse-grinding concentrate (–0.250–0.400 mm) and 1/3 of the finely dispersed concentrate (–0.005–0.008 mm) and a binder, which can be used up to 10% of slaked lime or quicklime, up to 10% cement, calcined dolomite or 2–20% finely ground steelmaking slag. Raw pellets, if necessary, are dried with hot air, loaded into cylindrical trolleys and, after some exposure, are fed to an autoclave, which is kept at a temperature of 160–230 °C for 6–24 h.

The finished pellets with a diameter of 12 mm, containing 7–10% of the binder, have a compressive strength of 100–200 kg/pellet. The strength of cold bonded pellets can be enhanced by the addition of highly dispersed silica: pellets from 90% concentrate and 10% slaked lime had strength of 103 kg/pellet; the introduction of 3% of powdered silica into the charge increased the compressive strength of the pellets to 183 kg/pellet.

Hydroxides or alkali metal carbonates (0.25–1.0%) can be used as additives to lime (University of Michigan method [39]).

In laboratory conditions, autoclaved pellets with increased basicity (1.2–2.5) were obtained from manganese concentrate (87% fraction of 0.074 mm) and lime [37].

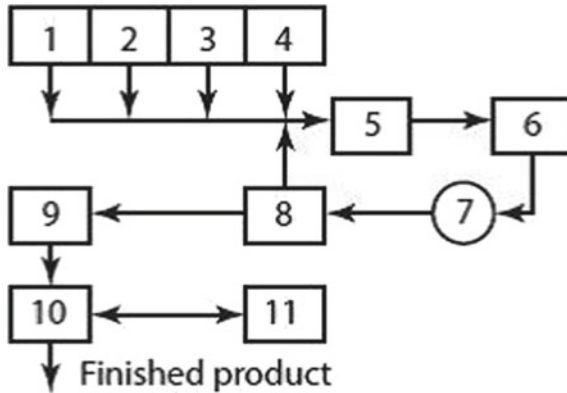


Fig. 25.10 Technological flow diagrams of the cold bond (COBO) process [32] (1—bin of iron-containing material with a particle size of at least 80% of the class—0.250 mm; 2—bunker of iron-containing material with a particle size of 80% of the class—0.050 mm; 3—binder bin with a particle size of 80% class—0.025 mm; 4—bunker of additives of 80% class size—0.005 mm; 5—rod mill; 6—scales; 7—roll mixer; 8—disk pelletizer; 9—roll screen; 10—dryer; 11—trolley; 12—discontinuous autoclave)

Raw pellets had a strength of 3.6 kg/pellet at a moisture content of 6%. After autoclaving, the strength reached 40–60 kg/pellet, and the abrasion in the tumble testing was 6%. Pellets did not collapse upon sharp heating to 1000 °C; they are suitable for smelting carbon ferromanganese.

In [40], it was found that after exposure to autoclaved pellets for 2 h under the steam, the pellets were not destroyed. The heat resistance of autoclaved pellets was determined by introducing into a furnace heated to 400, 600, 800 and 1000 °C. At all temperatures, the pellets did not break. The temperature of the onset of melting increases with increasing basicity of the pellet 0.5, 0.8, 1.3 and 1.8 and is, respectively, 1215, 1285, 1350 and 1400 °C. For pellets with a quantity of lime 5, 10 and 20%, the initial strength is, respectively, 52, 69 and 80 kg/pellet, after firing at 900 °C—45, 35 and 25 kg/pellet.

Pellets were prepared from manganese concentrate, crushed to 0.074 mm, lime to 0.08 mm on a pelletizer with a diameter of 5 m with a plate rotation speed of 9–10 rpm at a productivity of 15 t/h, and the charge moisture was 12%. Hardening in the autoclave occurred at a vapor pressure of 1.3 MPa and a temperature of 182–190 °C. Pellets had a strength of 70 kg/pellet, abrasion resistance of 10%, and the content of the 5% grade is 5 mm. The pellets contained, %: Mn 33.6; CaO 15.0; MgO 1.9; SiO₂ 13.9; P 0.19. High-carbon ferromanganese with the use of pellets was smelted in an NFP electric furnace (transformer capacity 1600 kV A). Pellets stabilized the operation of the furnace and the current load. Extraction of manganese into metal increased by 2.5%.

The implementation of non-firing pelletizing methods reduces the capital costs for the construction of factories by 2–3 times in comparison with the high-temperature firing technology and ensures lower energy consumption. At the same time, the

construction of factories of small capacity is cost-effective [41, 42]. It is also important that the non-fired agglomeration of the material remains almost unchanged in the composition and properties of the feedstock, as a result of which the reduction processes in them begin earlier and proceed more intensively [31]. With a rational selection of a binder, which will ensure the production of non-fired pellets without regrinding, pelletizing, both at cost and quality indicators of pelletized material, can quite compete with other methods of pelletizing.

One of the most important advantages of cold agglomeration methods are environmental indicators of technology. In the absence of high-temperature treatment in the production of cold bonded pellets, compared with firing methods, emissions of carbon oxides, nitrogen, sulfur compounds and volatile organic compounds, including polyaromatic compounds such as dioxins and furans, are not formed.

25.4 Briquetting

Significant volumes of finely dispersed, effectively recyclable materials are created in the process of extraction and beneficiation of raw materials for ferroalloy production during their transportation to ferroalloy plants and ferroalloy smelting. In particular, the mining and processing plants have accumulated large reserves of manganese ore fines with manganese content below the marketable value.

The use of finely dispersed raw materials without their agglomeration in ore-smelting furnaces disrupts the normal course of the process, leading to an increase in dust generation, a decrease in productivity and metal extraction rate, increased risks of accidents and number of hot downtime, and as a result, deteriorates technical and economic indicators of the furnace generally.

25.4.1 *Basic Industrial Technologies of Briquetting in Ferrous Metallurgy*

The most widely used technologies are briquetting using roll presses, vibropressing and stiff vacuum extrusion (SVE).

25.4.1.1 **Briquetting Using Roller Presses**

The principle of operation of such presses is that the briquetted mixture is fed into the gap between two rolls rotating toward each other, on the surface of which symmetrically located cells in the form of semi-briquettes are arranged in a checkerboard pattern. During the rotation of the rolls, there is a convergence of cells, the capture of the material and its sealing compression. The briquetted material is subjected to

bilateral compression, which contributes to a more uniform distribution of its density by volume. Then, as the rolls rotate, the cells diverge, and the briquette drops out of the cell under its own gravity. In some cases, in the designs of roller presses, precompressing dispensers are used for preliminary agglomeration of the briquetting charge in order to increase its bulk weight, which allows for an increase in the compressive load and the overall performance of the press.

The processes occurring in the briquetted mass in a roller press can, to a certain degree, be described by methods of the general pressing theory. The compaction process can be divided into three stages. The first stage is the reorientation of particles without changing their shape and size. In the second stage, the deformation of the soft and the destruction of brittle particles of material take place. At the last stage, plastic changes in the structure of the material occur, and its compaction occurs.

The strength of briquettes produced in this way depends on a number of factors: the particle size and component composition of the briquetted material, the magnitude of the applied pressing force, the moisture of the charge, the duration of the pressing process, the shape and size of the cells of the sleeves and friction coefficients.

The factor limiting the effectiveness of compaction of the material to be pressed is the presence of air, which is “trapped” inside the material during compression and is released after the external pressure ceases, thus leading to a softening of the briquette. The amount of pressed air can be 30–70% of the initial volume of air in the material. It is this factor that causes the frequent reduction in the strength of raw roll briquettes. Air displacement can also be difficult due to the presence of a binder that occupies a significant proportion of the pores. To avoid this phenomenon, it is necessary to ensure maximum removal of air from the briquetted mixture. Air removal can be facilitated by a reduction in the rate of material compression itself, facilitating the release of air from a decreasing pore space. Note that during vibropressing and in stiff vacuum extrusion, as we will see in the following sections, the removal of air from the briquetted mass is an important component of the technology and is achieved by displacing the air as a result of high-frequency vibrations in the vibropress and the complete removal of air from the stiff extruder’s working chamber.

The maximum particle size for roller briquetting usually does not exceed 5–6 mm. At the same time, multifractionality is a factor favoring briquetting efficiency, since in this case the space between large particles is filled with smaller particles, which contributes to the displacement of air from the material.

When briquetting multicomponent mixtures, one should also take into account the difference in the manifestation of the elastic–plastic properties of the individual components, leading to a significant difference in the degrees of compaction. Figure 25.11 illustrates the degree of compaction of roll briquettes based on manganese ore fines with the addition of various carbon-containing materials (coal or peat). It is seen how significantly the degree of compaction of the mixture varies depending on the physicomaterial properties of the components of the mixture.

The growth of the applied pressure, which means an increase in the energy consumption for briquetting, leads to a decrease in the porosity of the briquette, which may reduce its metallurgical value in the reduction processes. Moreover, such a measure makes sense only for briquetting without a binder, since the application of

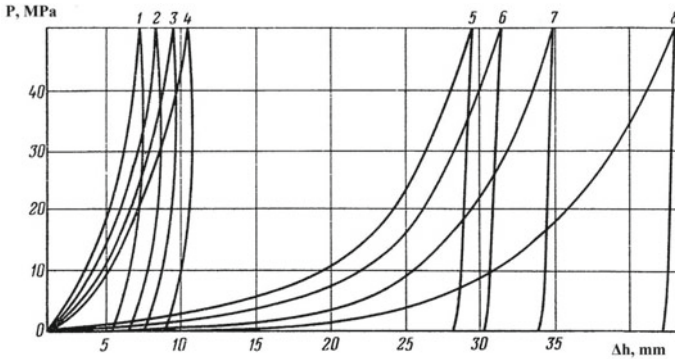


Fig. 25.11 Degree of compaction of the mixture with coal and peat components depending on the compression load (1-4—manganese ore fines and coal in proportions of 70:30, 60:40, 50:50 and 40:40, respectively; 5-8—manganese ore fines and peat in proportions of 70:30, 60:40, 50:50 and 40:40, respectively)

high pressure can lead, for example, in the case of using organic binders, to squeezing the binder onto the surface of briquettes and sticking them together.

The structure of the material pressed in the rollers undergoes changes due to elastic and irreversible deformation, destruction of the particles of the pressed material and the formation of cracks in it (at pressures above 10 MPa). Figure 25.12 shows the structure of a roller pressed briquette (manganese ore fines—47.6%, dust of the gas cleaning system—38.1%, coal—9.5% and lignosulfonate as a binder—4.8%) in comparison with the structure of extrusion briquette (manganese ore fines—66%, gas cleaning dust—28%, cement—5% and bentonite—1%).

It can be seen that as a result of high pressure (up to 100 MPa), the briquette structure is characterized by the presence of many large cracks and low porosity. The occurrence of such cracks may be due to elastic expansion after the finished briquette leaves the cells, which leads to a decrease in its strength.

A feature of roller briquetting is the limitation on the moisture content of the charge material (not higher than 5–10%). The required low moisture content of the charge limits the use of a binder that hardens by hydration, for example, cement, or

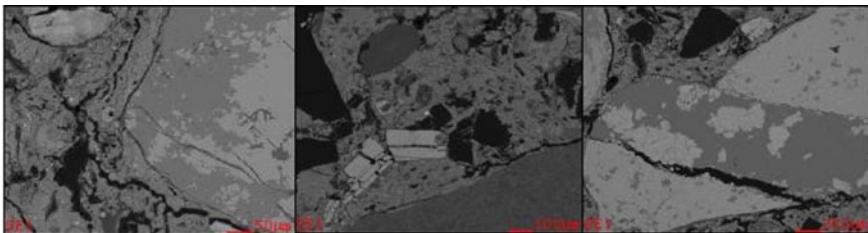


Fig. 25.12 Structure of the roller pressed briquette

requires the creation of combined binders with an increased content of cement in their composition.

The strength of the briquettes is significantly affected by the duration of the pressing process. For example, the duration of pressing for rolls with a diameter of 1.1 m at a frequency of rotation of 8–11 revolutions per minute is only 0.29–0.38 s. Exposure of the briquette under pressure allows not only more fully to force out the air from the narrowing pore space without the formation of pressed “air pockets,” but also to reduce the amount of elastic deformations that can lead to its softening. The increase in pressing time is achieved by restrictions on the speed of rotation of the rolls.

Operating experience of roller presses with traditional cell shapes showed that the displacement of the contacting cells resulted in the asymmetry of the briquettes formed, and the strength of the contact area of the halves of such a briquette is only 10–20% of the strength of the rest of the briquette mass. Due to the incomplete closure of cells of this type, a significant amount of return (up to 30%) may be formed when the roller press operates with the traditional form of cells.

This form of cells does not require combining half-molds, allows doubling the volume of the charge captured by the cells in the compaction zone and refuse from pressing and allows achieving high workability in the manufacture of interchangeable sleeves in the conditions of briquetting factories in the metallurgical enterprises.

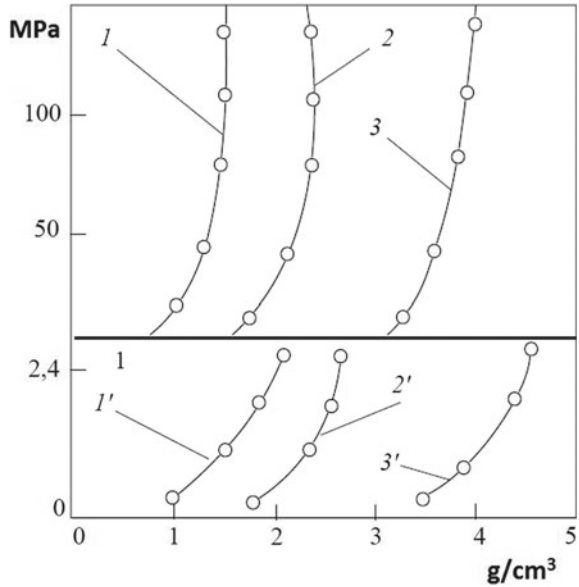
The sizes of the briquettes manufactured by roller presses depend on the type of the metallurgical unit in which they are used as a charge component. One of the largest roller presses producers, Köppern, uses the following briquette sizes: $33 \times 30 \times 20$ mm for blast furnace briquettes and briquettes for direct iron production reactors, $46 \times 34 \times 20$ mm for electric arc furnaces, ore-smelting furnaces and basic oxygen converters and $62.5 \times 53 \times 34$ mm for cupola furnaces.

In roller briquetting, energy is expended on overcoming the friction forces between the particles of the material and the walls of the cells of the bandage and on the friction between the particles of the material themselves. The frictional forces in briquetting without a binder are important. If the magnitude of the adhesion force of the briquette with the surface of the cell exceeds the value of its tensile strength, the briquette is broken into two halves that remain in the cells.

25.4.1.2 Vibropressing for Briquetting

The possibility of applying vibration for the agglomeration of natural and anthropogenic raw materials in metallurgy is due to a number of reasons. The very first experience of vibratory molding in powder metallurgy in the late 40 s of the last century showed that the use of vibration when filling powder into a mold or in the process of compaction allows significantly reducing the required compressive load and homogenizing the distribution of its density over the volume. It was found that at vibrations with a frequency exceeding 50 Hz, the bonds between the particles in the compacted dry powder are destroyed and the internal friction in the compressible mass sharply decreases, which facilitates the convergence of particles and compaction

Fig. 25.13 Comparison of the degree of compaction of the material during static pressing (1-3) and vibropressing (1'-3'). 1, 1'—boron carbide; 2, 2'—silicon carbide; 3, 3'—titanium carbide



of the mixture. In this case, a higher degree of compaction is achieved lower than during compression, the values of the applied pressing pressures, which is well illustrated in Fig. 25.13.

Another important physical process that occurs when vibration is applied to a formable mass containing gel phases is the so-called thixotropy (the word comes from ancient Greek *thixis* “touch” and *tropous* “to turn”)—a decrease in viscosity (liquefaction) under mechanical action and thickening in state of rest. Manifestations of thixotropy underlie the process of vibration compaction of concrete. Under the influence of vibration, the cement gel transforms into a sol, simplifying the movement (convergence) of solid aggregate particles under the action of its own gravity, which leads to compaction of concrete. Similar processes take place during briquetting with the use of cement binder, when, due to the reversible transformation of a cement gel into sol when exposed to vibration, at the stages of its liquefaction, particles of the briquetted charge approach each other under the action of their own gravity, which contributes to compaction of the briquette, and the air displaced by the approaching particles is released on the surface of the compressible mass in the form of bubbles. The thixotropy of the gel and the reduction of internal friction due to the oscillatory movements of the particles caused by vibration lead to the fact that the briquetted mass acquires some properties of the liquid, which simplifies the molding.

It is clear that thixotropy plays a key role in vibropress briquetting. It is no coincidence that almost all known vibropress briquette factories use cement as a binder. That is why the moisture content of the charge components plays an important role in briquetting with vibropressing. Its quantity should be sufficient to preserve the properties of the cement gel and for further hydration hardening of the cement. Usually,

its content in the briquetted mixture is limited to 5–8% by weight of the briquette. The cycle of vibratory compaction lasts less than 30–40 s, which is obviously not enough for the cement to “set”. As a result, newly formed vibropress briquettes have a very low mechanical strength, which does not allow them to be transported and stacked like roll briquettes. Therefore, the equipment of the vibropress briquetting factories includes special mechanisms to transport and accumulate finished products on pallets. In addition, to speed up the curing of briquettes, their “steaming” is used—heat and humidity treatment at a temperature of 70–95 °C in an atmosphere of saturated steam. Movement of moisture and steam in a briquette that has not yet become strong may lead to its softening.

The requirements for the granulometric composition of the briquetted charge during vibropressing are not as rigid as for roller briquetting (less than 5–6 mm). An important advantage of this method of briquetting is the possibility of agglomeration of materials with a particle size of up to 10 mm. Figure 25.14 gives appearance of the manganese ore fines briquette obtained by the method of vibropressing, showing the presence of large particles of material in the structure of the briquette.

The properties of briquettes produced by the method of vibropressing are significantly influenced by the vibration parameters (duration, amplitude and frequency). Insufficient intensity of vibration may not lead to the manifestation of thixotropy, which will not allow achieving the required values of the density of the briquetted mass. Too intense vibration can lead to stratification of the briquetted mass and also degrade the density characteristics of the briquette. There is no theoretical basis for choosing a vibration mode. In each case, we are talking about the experimental

Fig. 25.14 Vibropressed manganese ore fines briquette



testing of such modes on the bench models. To some extent, recommendations on the vibration modes developed in the technology of concrete vibration compaction may be useful. The whole process of vibrocompaction can be formally divided into two stages. The first is the rearrangement of large particles of a formable mixture and the formation of a macrostructure, and the second is a manifestation of the thixotropy of the cement gel and the formation of a microstructure. For the first stage, it is recommended to apply vibration, which causes low-frequency oscillations with large displacement amplitude to overcome the friction forces of the non-compacted particles. At the second stage, higher frequencies of vibration are advisable.

The methods of the theory of similarity and dimension allow determining which factors influence the process of compaction of the vibrating mass. The main parameters that determine the process of vibrocompaction are ten values: N is the power of vibration exposure, $[Fl/t]$; A is the amplitude of oscillation, $[l]$; ω is the angular frequency of oscillations, $[1/t]$; t is the duration of the vibration; ρ is the density during vibroforming, $[Ft^2/l^4]$; τ_0 —shear resistance of the briquetted mixture, $[F/t^2]$; ν —mixture viscosity, $[Ft/l^2]$; l —the specific size of the forming zone, $[l]$; β is the linear damping coefficient of oscillations; g —gravitational acceleration. Here, F is force, t is time, and l is length. In accordance with the well-known π -theorem, the number of dimensionless combinations of defining parameters in the case of vibropressing is equal to 7. These combinations can be represented as follows:

$$\rho l^3 A^2 \omega^3 l^3 / N^2; \rho A^2 \omega^2 / \tau_0; \rho A \omega l / \beta \nu; \rho A \omega l / \nu; N t / \tau_0 l^3; N t^2 / \nu l^3; A \omega^2 / g$$

The dependence of the density of the mixture during vibropressing can be obtained from the equation in general:

$$\rho (A^2 \omega^3 l^3 / N^2; A^2 \omega^2 / \tau_0; A \omega l / \beta \nu) = f(N t / \tau_0 l^3; N t^2 / \nu l^3; A \omega^2 / g; A \beta)$$

The qualitative conclusions from the dependencies obtained in this way are reduced to the fact that the process of compaction of the mass during vibropressing is influenced by the acceleration of oscillations ($A\omega^2$), and the duration of the process is associated with the specific power of the vibration effect and with the properties of the briquetted mixture. The higher the vibration amplitude, the more effective the compaction is.

The process of vibropressing consists of several stages. The pallet is mounted on the vibrating table. The briquetted mixture prepared in the mixer with the addition of a binder is poured into a replaceable mold tooling—a matrix. Next, the mixture is compressed by the punch, a kind of “mirror” reflection of the matrix, ideally entering it exactly like a piston in a cylinder, and the vibration of the whole unit is turned on. The duration of the vibration cycle is 15–40 s. At the end of the molding cycle, the vibration is automatically turned off, the pressure in the hydraulic system decreases, the matrix rises, and the formed briquettes remain on the process pallet. The low strength of freshly formed briquettes does not allow them to be delivered to the zone of curing by the conveyor. Preserving the integrity of freshly formed briquettes requires special measures. Briquettes are transported, remaining on technological

pallets. Pallets with freshly formed briquettes along the conveyor are fed to a special hoist drive, from where a stack of pallets is delivered to the heat treatment zone. After accumulating the required number of pallets on the pallet stacker, they are removed and further transportation to the heat treatment chamber is carried out by an automatic stacked cart moving along the rails. It is possible to transport a stack of pallets to the heat treatment zone and with the help of a transborder consisting of transfer and dispensing carts, which ensures the accuracy of the installation of pallets in the heating chambers. The duration of heat treatment can reach 24 h or more. The temperature in the chamber is 70–95 °C. The cost of heat treatment chambers can exceed 20% of the cost of equipment and engineering costs. After heat treatment, the briquettes on the pallets are moved to the stacker and further using a hydraulic pusher to the finished product conveyor for further unloading to the warehouse or loading onto a vehicle. The pallets freed from briquettes are returned to the vibropress. With a briquette line capacity of up to 130 thousand tons of briquettes per year, the number of formable pallets can exceed one million pieces. The cost of technological pallets may exceed the cost of the vibropress itself. In general, the cost of special mechanisms and devices for automatic lines of vibropressing allowing ensuring the preservation of raw briquettes intact until delivery to the heat treatment chambers and the return of pallets can double the cost of vibropress. It is clear that in the absence of automation of these procedures, the capacity of the briquetting plant will be significantly lower. The cost of automation can be up to 50% of the cost of the vibropress.

In connection with the specifics of vibropressing, the productivity of a vibropress is usually understood as the number of units of products produced during an hour or eight-hour shift. First of all, productivity depends on the degree of automation, which affects the rate of removal of pallets with raw briquettes from the working area. Equipment productivity essentially depends on the sizes and volume of briquettes. Therefore, the performance is sometimes offered to compare the number of pallets filled in a certain period of time. According to the results of operation of the known automated vibropress briquette factories, their productivity does not exceed 20–30 tons of briquettes per hour.

The size of briquettes is 60–100 mm; the most widely used form is a hexagonal prism. Such a size of vibropressed briquettes can lead to their “bridging” when unloaded into the bunker (Fig. 25.15). The smaller the size of the briquette produced, the lower the performance of the vibropress.

25.4.1.3 Stiff Vacuum Extrusion Briquetting Technology

Extrusion is a process used to create objects with a fixed cross-section profile. The material is pushed through the die of the desired cross section. This method has found a great distribution in the industry of the production of ceramic bricks. Vacuum is maintained in the working chambers of modern brick-making extruders, which contributes to achieving greater uniformity and density of the product. Stiff vacuum extrusion (SVE) technology is applied in the production of ceramic bricks in 64 countries around the world, including the USA, Britain, Germany, South Korea and

Fig. 25.15 Unloading of vibropressed briquettes from the car



South Africa. The world’s largest brick factory in Saudi Arabia produces a million bricks per day using SVE technology.

In accordance with brick industry terminology, the word “stiff” is used to describe the process of extrusion, which is carried out at pressures ranging from 2.5 to 4.5 MPa and moisture contents ranging from 12 to 18% (Table 25.12).

One of the basic criteria determining the suitability of extrusion material is its plasticity—a trait that assures that it can be effectively pushed through the holes in die. A necessary condition for the status of plasticity is complying with the granulometric composition and moisture content requirements for SVE. In some cases, additional pulverization may be required in order to achieve the desired plasticity of material.

Unlike a roller press and vibropress briquetting, shear stress plays an important role in SVE agglomeration. Shear stress occurs when the mixture is processed in the screw feeder, in pug mills, and then in the extruder. Based on a comparison of coal briquette porosity values in various pressing options (compression and its combination with torsion), it was found that more dense briquettes (less porous) are formed in the combined pressing option (under identical values of applied pressure). With full compression, a significant proportion of energy is expended on the elastic

Table 25.12 Types of extrusion

Type of extrusion	Low-pressure extrusion	Medium-pressure extrusion	High-pressure extrusion	
Designation used in structural ceramic industry	Soft extrusion	Semi-stiff extrusion	Stiff extrusion	
Extrusion moisture, % on dry	10–27	15–22	12–18	10–15
Extrusion pressure, MPa,	0.4–1.2	1.5–2.2	2.5–4.5	Up to 30

deformation of the particles themselves, while, in the presence of shear stress, the convergence of particles on the surface forces activation distance is more effective. In full compression of close-packed particles, each particle only comes into contact with its immediate neighbors and is subjected to compression load. Under shear stress, the particles of the adjacent layers are subjected to abrasion due to contact with irregular surfaces, which can lead to crushing, the opening up of new surfaces and, hence, to an increase in the number of contacts between particles of the mixture.

The effect of shear stress can also be used to homogenize the mixture prior to its agglomeration by the SVE method.

Homogenization consists of souring of the mixture with the addition of a plasticizer and subsequent storing of such a mixture for some time before further processing. This method allows achieving a high degree of homogeneity of the mixture for subsequent agglomeration. The plasticizer consumption during the agglomeration of the homogenized charge, in comparison with the charge without prior homogenization, is markedly reduced. Study of the brex structure with and without homogenization by means of scanning electronic microscopy revealed differences in the structure and distribution of pores (Fig. 25.16).

One can see that pore size is significantly smaller in the brex made from a sheared and soured mix. The results suggest the use of a shearing extruder to prepare a briquetting mass for homogenization and have been used in the implementation of a number of briquette factory projects.

Typical layouts of the SVE briquetting line are shown in Fig. 25.17.

The mixture of raw materials is fed by a front loader feeder, equipped with wear-resistant spiral cast iron auger elements made of a chromium alloy. Next, the prepared mixture with added binder and plasticizer is fed for mixing in the pug sealer. The line can also contain primary open pug mill. The pug sealer consists of a large open part and the sealing node. The open part consists of a trough and blades for mixing. The blades are fastened to the steel rod shaft by bolted clamps, making it possible to rotate the blades to adjust the angle at which the processing takes place and, thereby,

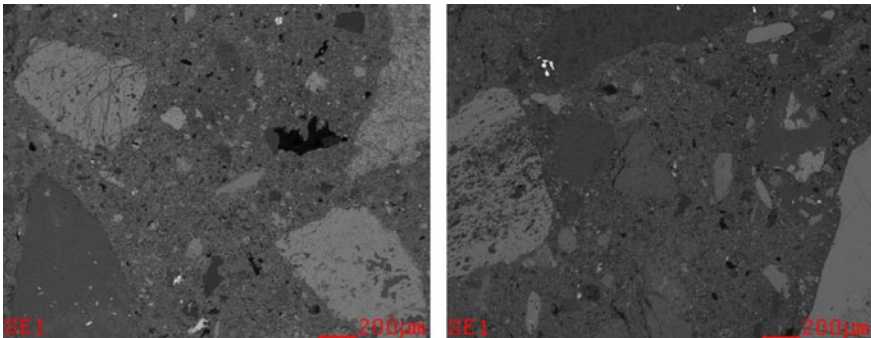


Fig. 25.16 Structure of the brex structure. Left—without souring; right—with souring during 4 h after shearing

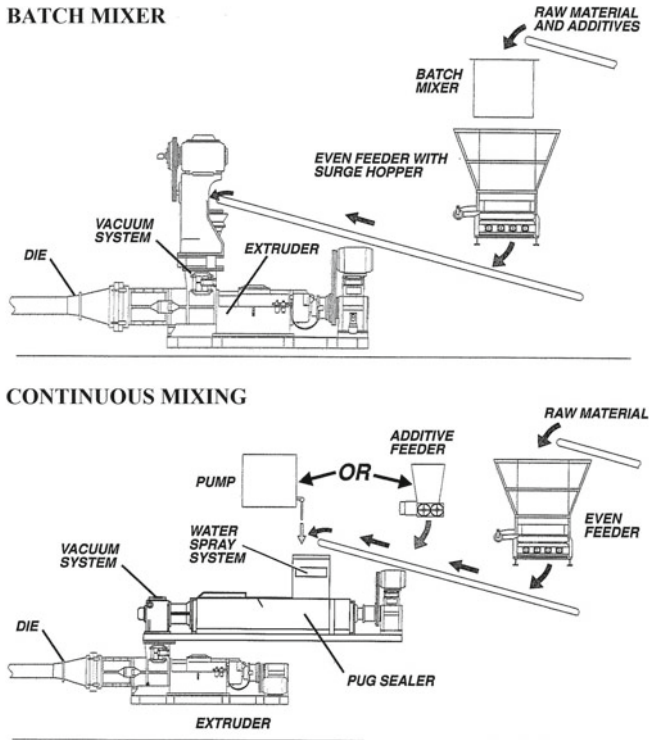


Fig. 25.17 Typical layouts of SVE briquetting line

change the machine’s performance. The pug sealer is combined in a single unit with the extruder and is positioned above it.

The mixture enters the vacuum chamber partially agglomerated (Fig. 25.18), and due to the high vacuum inside the chamber the pieces of the mixture immediately crumble into isolated particles, which fall down on the blades of the auger. It is known that air adsorbed by the surface of particles of plastic material in the form of polymolecular layers held by Van der Waals forces slows down their wetting with water, prevents the mass from being evenly compacted and contributes to an increase in elastic deformations during plastic molding, forming delamination as well as microcracks. Filling the pores, the air also prevents the penetration of moisture into them, separates the particles of the mass, acting as a leaner. Evacuation leads to the removal of air from the pores and promotes closer contact of the particles.

The vacuum is maintained throughout the working volume of the extruder up to the die. The pressure of the vacuum is at least 100 mm Hg (in absolute value). The area of the vacuum in the working chamber of the extruder and pug sealer is shown in Fig. 25.19. The combination of mechanical pressure and vacuum in the working extruder chamber helps to remove almost all compressible air from the material before densifying, which allows them to be immediately transported by



Fig. 25.18 Partial agglomeration of the mix in pug sealer

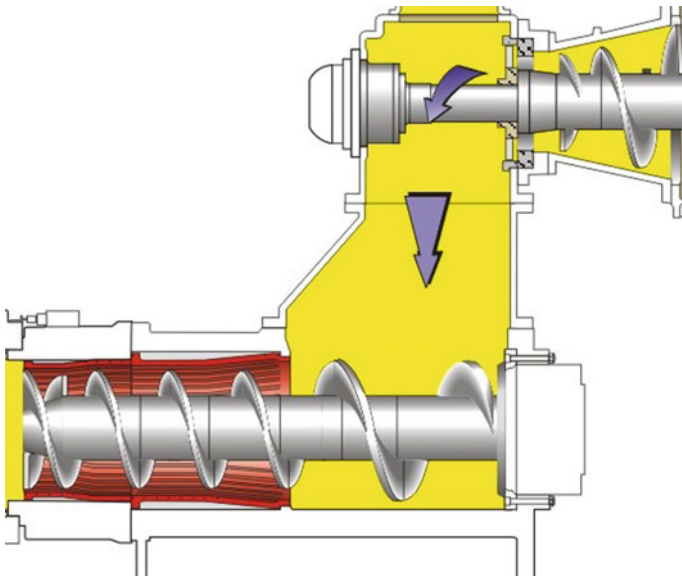


Fig. 25.19 Vacuum areas in extruder and pug sealer

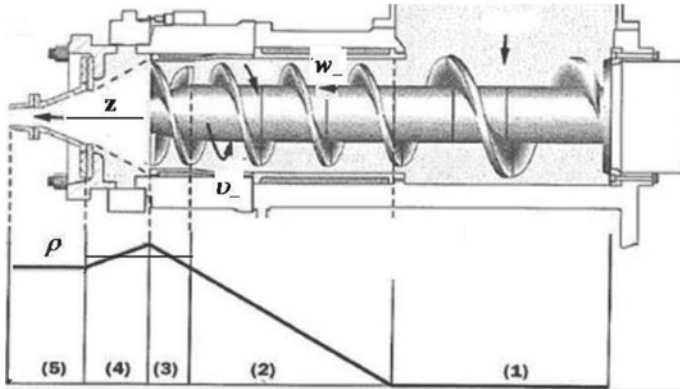


Fig. 25.20 Stages of densifying in the working zone of the extruder. 1—conveying, 2—densifying, 3—metering, 4—pressure distributing, 5—die

conveyors and stacked almost without the formation of a fine fraction. In addition, as is well known, the vacuum slightly decreases the viscosity of the cement paste, which facilitates its uniform distribution in the briquetting mass and improves its interaction with water. This circumstance in combination with a higher density of the briquetting mass, due to the removal of air from it, leads to a decrease in the consumption of cement binder.

Due to rotation of the auger blades in the working chamber of the extruder, formable mass performs translational and rotational motion, which is slowed by the walls (Fig. 25.20).

In the conveying zone, material is loose and moves along the barrel without densification. Bulk density remains unchanged. Zone 2 is the densifying region where the loose material is compacted. In zone 3, metering is achieved by way of the special geometry of the wings of the point auger. Zone 4 serves the purpose of distributing the pressure generated by the metering zone more evenly over the die, thus tending to yield a more even flow through it. In zone 5, the brex are squeezed out of the holes in the die which completes the process of their formation.

Table 25.13 gives a comparison of roller pressing briquetting and vibropressing briquetting with briquetting using a stiff extrusion method.

The high performance of stiff extruders, the possibility of agglomeration without predrying the charge and the lower consumption of binder caused a growing interest in extrusion briquetting technology.

The first experience of the operation of SVE lines in comparison with the experience of roller press and vibropress briquetting factories made it possible to designate some specialization of the known methods of briquetting. Namely for the briquetting of dry materials with organic binders, when the achievement of high hot strength of briquettes is not required, roller press briquetting allows to obtain mechanically strong briquettes due to the application of high pressure (up to 150 MPa). Vibropressing allows agglomeration of a mixture containing a substantial part of large

Table 25.13 Comparison of briquetting technology

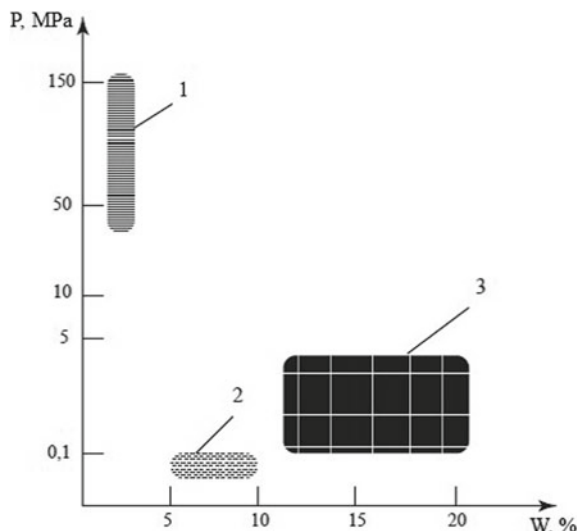
Process characteristics and properties of briquettes	Briquetting units and their characteristics		
	Vibropress	Roller press	Stiff Extrusion
Maximum performance	20 t/h	50 t/h	100 t/h
Compaction pressure	0.02–0.10 MPa	40–150 MPa	3.5–4.5 MPa
Binder content (Cement) in briquette, %	8–10	15–16	4–6
Heat treatment of raw briquettes	80 °C (10–12 h)	Drying of charge	Not required
Returns	Absent	30% of production	Absent
Briquettes shape	Prism, cylinder	Pillow	Any shape
Briquette size, mm	80 × 80,	30 × 40 × 50	5–50
Charge moisture content, %	Less than 5%	Less than 10%	12–18%
The ability to store raw briquettes in a pile	Absent	Possible	Possible
<i>Utilities:</i>			
Electricity	42.6 kWh/t	45.0 kWh/t	33 kWh/t 0
Natural gas	47 m ³ /t	0	0
Heat	0.3 GCal/t	0	0
Compressed air	90 m ³ /t	0	

fractions (up to 10 mm and more), but requires special measures to preserve the strength of raw briquettes (moving on pallets, heat and moisture treatment) and does not allow moisture of the briquetted mixture to exceed 12–15%. Stiff extrusion is irreplaceable when agglomerating thin materials and is able to agglomerate mixtures with a moisture content of up to 20% at compacting pressures an order of magnitude lower than in a roller press (3.5 MPa). In particular, this technology allowed the agglomeration of EAF dust and gas cleaning dust of ferroalloy production, which practically could not be briquetted with either roller presses or vibropresses. The possibility of agglomeration of wet materials allows either to completely abandon the drying of raw materials or to significantly reduce the cost of such drying. A comparison of these technologies in parameters such as the applied pressure and moisture contents of the agglomerated mixture is given in Fig. 25.21.

One of the most common anthropogenic raw materials is dust and sludge from gas cleaning of ferroalloy furnaces. The specific dust emissions of ferroalloy furnaces are 8–30 kg/ton of ferroalloys. The content of manganese oxides in dust in the production of silicomanganese is 21–34.3%, in the production of ferromanganese—30–35%; chromium oxides in dust in the production of ferrochromium—22–30% [43].

The experience of using briquettes in the charge of ferroalloy furnaces has confirmed the effectiveness of this kind of agglomeration technology. The first industrial experience of using briquettes based on manganese ore concentrates in the charge of the ore-smelting furnace was obtained in 1961, when 160 t of roll briquettes made of manganese ore concentrate (30.9% Mn; 4% Fe; 0.0577% P; 26.95% SiO₂; P/Mn

Fig. 25.21 Comparison of technologies of briquetting according to the parameters of briquetting (applied pressure and moisture content of the charge). 1—roller pressing, 2—vibropressing, 3—stiff vacuum extrusion



= 0.0018; 0.33% S; 1.9% CaO; 4.05% BaO) were used in a 2500 kV A furnace of the Zestafoni Ferroalloy Plant (Georgia) [44]. The results of the heats showed that this type of charge component is quite effective.

In 1966, full-scale industrial testing was carried out at the same plant for the smelting of ferrosilicomanganese in industrial ore-smelting furnaces using ore briquettes of manganese concentrate from the Chiatura deposit in the charge [45]. For industrial experiments, briquettes were made on a roller press with a capacity of 5 tons per hour from ore with a particle size of 5–0 mm on a binder of sulfite-alcohol bard (SAB) with a density of 1.2 g/cm³. With an ore moisture content of 4% and an addition of 8% binder, the mixture was stirred for 15 min. Next, the mixture was subjected to heat treatment. The fact is that the binding properties of the SAB are due to the occurrence of polymerization processes in it, leading to the formation of long chains of molecules in the body of the briquette. The polymerization reaction in the presence of manganese is most fully realized at temperatures of 160–180 °C. For iron ore briquettes, the polymerization temperature reaches 200 °C. Thus, the achievement of the required values of the strength of the briquettes required their drying at temperatures of 50–300 °C. Silicomanganese was smelted on a charge with ore briquettes in a three-phase open ferroalloy furnace with a capacity of 16.5 MV A. The furnace worked normally and stably, the gas permeability of the charge was good, and the flame was distributed evenly throughout the furnace. After 112 h of experimental melting, it was concluded that sufficiently strong briquettes can be obtained from manganese ore of this size suitable for use in the charge of ferroalloy furnaces. When working on ore briquettes, the furnace productivity increases, and the power consumption and the consumption of reducing agent are reduced.

In 1970, the Dnepropetrovsk Metallurgical Institute studied the indicators of smelting of commercial silicomanganese on a briquetted mixture of concentrates

of manganese oxides I and II of the Nikopol deposit in a ratio of 1: 1 and on sinter made from the same mixture [46]. Before briquetting, the mixture of concentrates of a fraction of 10–0 mm was ground to a size of 3–0 mm. Briquettes were made on a semi-industrial roller press at a pressure of 500 kg/cm², and the binder was a mixture of bitumen, fuel oil and SAB in an amount of 10% by weight of the charge. The charge was mixed in tanks with steam heated (to activate the polymerization of the SAB). Briquettes of two compositions were prepared and melted: with an excess of reducing agent (coal) in the amount of 50%, introduced to create a skeleton in the briquette and to increase its strength (mixture of concentrates—54.5%, river sand—9.1%, coal—27.3%, a mixture of bitumen and fuel oil—3.6%, SAB—5.5%), with a stoichiometric amount of reducing agent required for the reduction of silicon and manganese (a mixture of concentrates—60.6%, river sand—10.1%, coal—20.2%, a mixture of bitumen and fuel oil—3.6%, SAB—5.5%). Laboratory tests showed that the physical properties of raw briquettes were superior to those for fired briquettes, so they refused to fire the briquettes. The values of mechanical strength and heat resistance were higher for raw briquettes. Commodity silicomanganese was smelted on raw briquettes in the charge. Semi-industrial smelting on briquettes of the above composition and on sinter was carried out in a three-phase open ore-smelting furnace with a capacity of 1.2 MV A at a voltage of 81.60–85.89 V and a current of 6000–6500 A with a continuous process with a closed top chamber.

Briquettes with an excess of reducing agent had a high electrical conductivity that, when melted, led to a significant increase in the load current and as a result to the rise of the electrodes and the opening of the top. To eliminate this phenomenon, 10% manganese concentrate was added to the briquette charge. Thus, 14 tons of briquettes with an excess of reducing agent, 1.2 tons of concentrate and 200 kg of dolomite were melted. Melting silicomanganese on briquettes containing a stoichiometric amount of reducing agent passed without any complications. The load was steady; except for briquettes, nothing was added to the furnace. Comparative data of heats at different loads (briquettes, sinter) showed that the melting of silicomanganese on briquettes should be more preferable than melting on the sinter.

The results of pilot heats formed the basis for the construction and commissioning in 1976 of a briquette factory at the site of the Zestafoni Ferroalloy Plant. Manganese ore briquettes (with the addition of gas cleaning dust and without it) were produced by roller presses of Sahut Conreur Company (France).

Briquetted charge was also used for smelting ferrosilicon. At the Zaporizhia plant of ferroalloys (Ukraine), briquettes were produced of sand, coking coal and iron ore concentrate. The mixture was heated and stirred in a steam mixer and then pressed with a roller press. Raw briquettes were subjected to roasting at a temperature of 600–800 °C for 10–13 h to achieve a reduction degree of 70–80%. Smelting of ferrosilicon on the briquetted charge was carried out in a 3.5 MV A furnace. When working on briquettes, the furnace productivity increased, the power consumption and reducing agents rates decreased [47]. The smelting of ferroalloys from briquetted charge became widespread in the USA, France, Japan and Germany [48].

Melting technology of low-phosphorus carbon ferromanganese with 100% briquetted charge was described in [49]. In 1987, experimental tests of this technology were carried out by Victor Dashevskii under the conditions of the Nikopol Ferroalloy Plant in comparison with the traditional technology. A three-phase ore-smelting furnace with a capacity of 3600 kV A with coal lining was used as a melting unit. The essence of the technology was the smelting of carbon ferromanganese with the required low-phosphorus content using the non-flux method on the charge, the ore part of which, in addition to graphite concentrate, contains a concentrate obtained by chemical enrichment of sludge. Low-phosphorus manganese slag obtained in the smelting of carbon ferromanganese by the fluxless method is used as a raw material in the smelting of low-phosphorus silicomanganese, refined ferromanganese and metallic manganese. The results of the experimental heats with 100% briquettes showed that the briquetted charge provided an economically acceptable solution to the problem of smelting high-quality ferromanganese from highly phosphorous manganese ores.

In 1988, the first vibropressing briquetting factory with a capacity of 110 thousand tons of briquettes for ferrochromium smelting was built at Vargön Alloys in Sweden [50]. Since 1991, this method of briquetting has been used in France by Eurometa SA for the agglomeration of the fines of the crushing of ferroalloys [51]. Ferroalloy fines briquettes were used in the foundry business. Since 2001, Aaltvedt Betong AS's vibropress factory has been operating in Norway, producing briquettes for Eramet. Manganese ore fines and gas cleaning dust are briquetted. Binder—Portland cement (10–12% of the mass of the briquette). An example of the successful application of vibropress briquetting technology for the agglomeration of manganese-containing anthropogenic materials, including ferroalloy fines, is the experience of the South African company Assmang at the plant in Cato Ridge. Vibropress briquettes made of silicomanganese on a “toll” basis were also produced in the USA for the Felman Company.

The technology of smelting manganese ferroalloys using ore-dust briquettes was developed at the Zestafoni Ferroalloy Plant [52]. The need for disposal of dust and sludge from furnace gas cleaning was due to the large volume of its formation (50 thousand tons annually). Taking into account the metallurgical evaluation of waste, their dispersed state and physicochemical properties, it was proposed to mix dry dust with previously dehydrated sludge and make briquettes from such a mixture with the addition of manganese ore concentrate. It has been established that to obtain mechanically strong briquettes (specific crushing force of 8–12 MPa), the optimum parameters of briquetting are moisture content of the charge 4–6%, binder content (SAB) 6–8%, amount of fine component (dust, sludge) 30% and minimum pressure of roller press 19.6 MPa. The comparative kinetics of the reduction of dust sludge and ore briquettes and of manganese sinter was investigated. It was found that briquettes gave the greatest degrees of reduction at different temperatures. The utilization of manganese and silicon from wastes increased due to the presence of closely bound carbon and the inhibition of the formation of silicates, in contrast to the sinter. The results of high-carbon ferromanganese heats showed that the furnace productivity in the case of using briquettes increased from 73.33 to 75.67 tons/day,

and the specific power consumption decreased by 90 kWh/ton. Coke consumption decreased by 34 kg/ton.

The first successfully implemented project with the use of stiff vacuum extrusion (SVE) technology in the ferroalloy industry was the production of extruded briquettes (BREX, [53]) and their use in the charge for ferronickel smelting at BHP Billiton in Cerro Matoso (Montelibano, Colombia) [54] in the framework of the RKEF (rotary kiln–electric furnace) process. The nickel content in this ore is usually small and ranges from 0.8 to 3.0%. During the RKEF process, laterite ores are sieved, ground and added into a charge with a certain iron, nickel, SiO₂ and MgO content. After that, the charge material is roasted and partially metallized with coal or coke fines. These semi-product and residual coke are then delivered to the electric furnace where ferronickel is smelted. In Cerro-Matoso, the RKEF process entails the use of briquetted fines of nickel laterite ore.

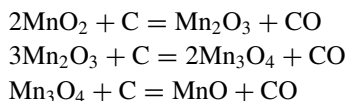
SVE technology has not previously been used for the agglomeration of manganese and chromium ores. The first attempt to use it for such purposes took place in 2010. A full-scale pilot testing of this technology was conducted using brex as a charge component of industrial submerged EAF. The possibility of obtaining metallurgically valuable brex based on various combinations of manganese ore fines and dry gas cleaning dust formed during the production of silicomanganese was studied in [55].

As in the case of blast furnace briquettes, the metallurgical properties of ferroalloy briquettes must ensure their integrity before entering the workspace of the reduction unit (cold strength) and in complex physical and chemical processes that occur at high temperatures under the reducing conditions of ore-smelting furnaces (hot strength).

The metallurgical properties of ferroalloy briquette must ensure that the “melting rate” and “reduction rate” are equal. If the melting rate of ore materials is greater than the rate of formation of the metal and the final slag, then partially reduced slags are formed. Such slags penetrate into the lower horizons of the furnace, the reduction process turns into an unfavorable slag regime, the slag boils, and, in general, the normal operation of the furnace is disturbed. Otherwise, there is a need to intensify melting by increasing the input of electric power into the unit. The equality of the rates of melting and metallization ensures the entry of metal and non-aggressive slag from the layer of charge materials into the furnace hearth.

The peculiarity of the processes of reducing oxides of iron and manganese in the ore-smelting electric furnace is associated with the passage of a portion of the electric current through charge materials. When using briquettes with a substantial content of carbonaceous reducing agent in its composition, the current begins to flow through the body of the briquettes, heating them, which significantly speeds up the reduction processes inside the briquette, and the direct passage of current through the briquette can lead to its destruction. The choice of the optimal content of reducing agent in the briquette should also take into account the possibility of reducing the cold strength of the briquette by adding a carbonaceous reducing agent. At the same time, the presence of a carbonaceous reducing agent sharply raises the temperature at which softening of briquettes begins and leads to an increase in the permissible critical current density [6]. In case of close contact of particles of manganese ore with

carbon in briquettes, the reduction of higher oxides can occur with the participation of carbon:



25.4.2 Metallurgical Properties of Brex on the Basis of Manganese Ore Concentrate

Brex from primary oxidized manganese ore concentrate were manufactured on the industrial SVE line in India. They were manufactured on the industrial SVE line in India. Portland cement (5% mass) was used as a binder; bentonite (1% mass) was used as a plasticizer. Table 25.14 shows the chemical composition of the primary oxidized manganese concentrate.

The share of particles larger than 0.071 mm is 22%; the manganese content of these particles is 35.4%. The share of particles smaller than 0.071 mm is 78%; the manganese content of these particles is 38.77%. Iron particles distributed in the samples of the concentrate in both size range evenly—3.81–3.86%. The surface area of cement particles exceeds 4000 cm²/g. The chemical composition of cement is (%): CaO—62–64; MgO—2.5 (max.); SiO₂ 22–24; Al₂O_{3-4.5}; Fe₂O_{3-4.5}; SO₃—1.8; alkali—0.6. The chemical composition of bentonite (%) is SiO₂₋₅—8.4; Al₂O₃—12.6; CaO = 0.8; Fe₂O₃—10.6; alkali—4.4.

Physical and mechanical properties of the brex were measured after three-day strengthening in an open warehouse. The compressive strength was equal to 30 kgF/cm² and was measured on the Tonipact 3000 equipment (Germany) in accordance with the DIN 51067 standard. The open porosity was determined in accordance with DIN 51056 and amounted to 14.39%. Brex density averaged 2.59 g/cm³.

A specially designed unit (Figs. 25.22 and 25.23) was used to study the behavior of industrial brex samples from primary oxidized manganese concentrate during heating in a reducing atmosphere.

The physical and mechanical properties of brex after heating at different temperatures are given in Table 25.15.

The results of the phase analysis of the samples of initial brex and brex after heating for 2 h in a reducing atmosphere are presented in Table 25.16.

Table 25.14 Chemical composition of primary oxidized manganese concentrate

Elements	Mn	Fe	SiO ₂	Al ₂ O ₃	CaO	MgO	P	S	Zn
Content, %	38	3.84	10	1.36	17	0.76	0.07	0.10	0.084

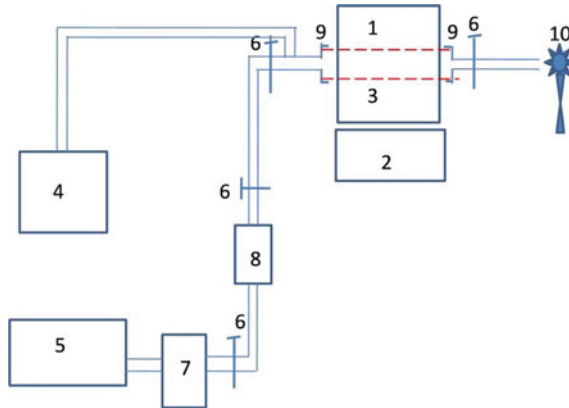


Fig. 25.22 Installation diagram to study brex behavior when heated in reducing atmosphere. 1—oven, 2—controller, 3—hollow corundum tube with samples, 4—vacuum pump, 5—compressor, 6— isolation valve, 7—drying device, 8—flow meter, 9—gate valve, 10—burner

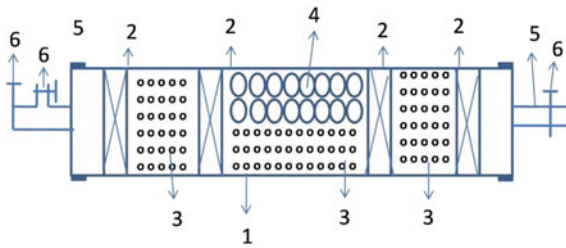


Fig. 25.23 Method of sample positioning in an experimental unit for studying brex behavior when heated in a reducing atmosphere. 1—hollow corundum tube, 2—perforated unit, 3—coke breeze, 4—samples (ore or brex), 5—gate valve, 6— isolation valve

Table 25.15 Physical and mechanical properties of brex after heating at different temperatures

Properties /Temperature, °C	1000	1100	1200	1300
Porosity, %	43.48	39.10	32.22	15.02
Density, (kg/cm ³)	2.31	2.49	2.82	3.28
Compressive strength (kgF/cm ²)	34	43	47	61

It is seen that in the presence of iron oxides an iron-manganese melt was formed, from which manganese was subsequently recovered.

Table 25.16 Main phases of brex from primary oxidized concentrate

Temperature, °C	Phases
20	Hausmannite (Mn ₃ O ₄); Bixbyite ((Mn,Fe) ₂ O ₃); Rhodonite (MnSiO ₃); Bixbyite C (FeMnO ₃)
1000	Jacobsite (MnFe ₂ O ₄); Fe _{0.798} Mn _{0.202} O.
1100	Fe _{0.798} Mn _{0.202} O.
1200	Fe _{0.798} Mn _{0.202} O.; Fe _{0.664} Mn _{0.336} O.
1300	Fe _{2.08} Mn _{0.92} O ₄ ; Fe _{0.798} Mn _{0.202} O.
1400	Manganese

25.4.3 Metallurgical Properties of Brex Based on Manganese Ore Concentrate and Baghouse Dusts of Silicomanganese Production

Chiatura manganese ore concentrate (Republic of Georgia) and baghouse dust from silicomanganese production were used as raw material for brex production. The chemical composition of the manganese ore concentrate and silicomanganese production baghouse dust is given in Table 25.17. The main minerals of the concentrate are pyrolusite, psilomelane and manganite. Pyrolusite from Chiatura manganese ore has a finely spherulitic (oolitic) and clastic brecciate structure. Spherulites fragments do not exceed 0.25 mm in size. Pyrolusite is partially recrystallized up to hundredths of a millimeter during grain coarsening. The Chiatura oxide concentrate softening point is 1049 °C according to the data in [56]. Eighty-five percent of baghouse dust particles are smaller than 10 μm. Primary particles have a spherical shape due to phase transitions.

Two types of mixtures from the above materials were prepared for brex making: 1—a mixture of an equal mass (50:50) of concentrate and dust and 2—a mixture of 70% concentrate and 30% dust. The granulometric composition of the second mixture is shown in Fig. 25.24.

Coke breeze was used as a reducing agent; it was provided by the owner of ferroalloy smelter. The coke breeze has the following composition ratio (%): carbon—68.72; volatiles—7.53; ash—23.75. 88.46% of coke breeze particles are smaller than 0.635 mm in size. Its moisture content is 9.86%. Three brex mixtures with low binder content were tested in the study (Table 25.18).

Table 25.17 Chemical composition of manganese ore concentrate and baghouse dust

Material	Mn	MnO	Fe ₂ O ₃	FeO	Al ₂ O ₃	SiO ₂	CaO	MgO	P
Concentrate	35.0–45.0	–	1.2–2.2	–	2.0–3.5	14.0–25.0	2.0–3.5	0.86	0.20
Baghouse dust	–	29.74–31.41	–	0.30	0.01	30.0–34.0	1.67–2.42	1.50	–

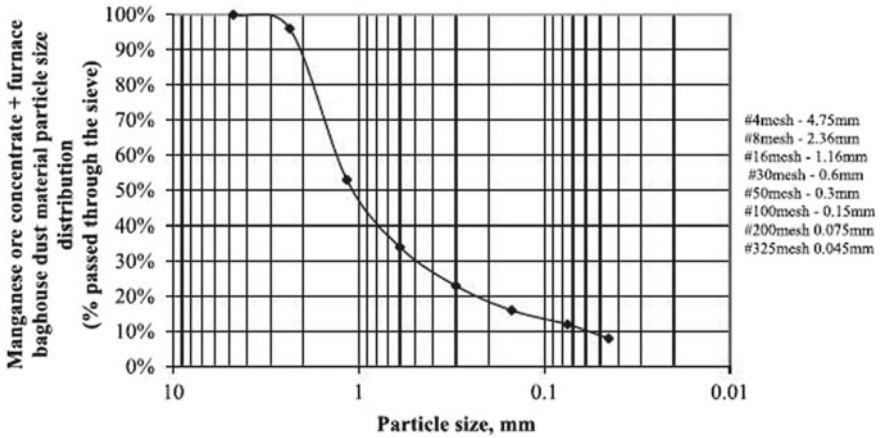


Fig. 25.24 Granulometric composition of mixture for brex production

Table 25.18 Composition of brex

Component	No. 1	No. 2	No. 3
Manganese ore concentrate	47.6	66.7	56.0
Coke breeze	—	—	15.0
Baghouse dust	47.6	28.6	24.0
Portland cement	4.8	4.7	5.0

Test samples of brex were produced using a computerized laboratory extruder that simulates the processing of a briquetted mixture in commercial even feeders, pug mills and the extruder itself. The brex had a circular cross section of 2.5 mm in diameter and 1.5–2.0 mm in length. The average moisture content of freshly formed brex was 11%. The vacuum level in the working chamber of the extruder was maintained at 38–48 mm Hg.

Due to the cylindrical shape of brex, its cold strength was determined by measuring both compressive strength and tensile splitting strength, since these types of stress would be exerted on brex during actual transport and stacking. These properties were measured using an Instron 3345 system (USA). The compressive and tensile splitting strength tests were performed using six specially prepared brex samples with a diameter of 25 mm and a length of 20 mm which were subjected to compression and tensile splitting.

Figures 25.25 and 25.26 illustrate the behavior of brex and the mechanism of brex destruction during compressive and splitting strength tests. At the initial stage (1), the elastic loading of brex shows a linear dependence between the applied force and the displacement of the active pressing surface. The beginning of the second stage is characterized by a sharp decrease in the applied force due to the formation of surface fractures. At this stage, the “near-surface” layers of the brex are destroyed and peeled (15–20% of the radius). However, the “core” (central part) of the brex continues to

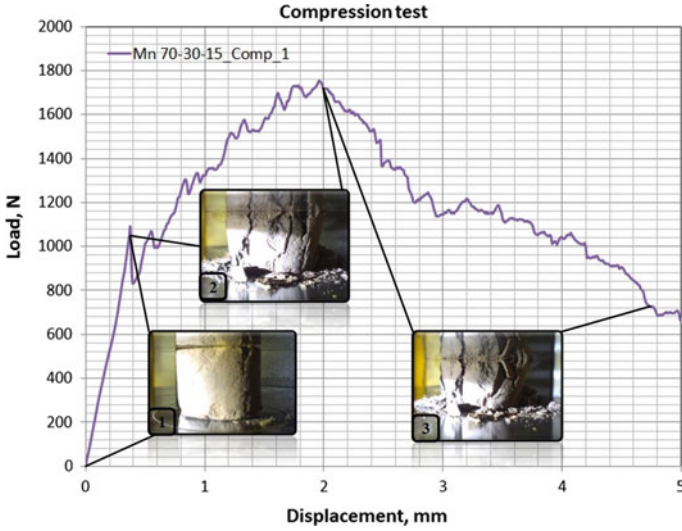


Fig. 25.25 Compression test of brex No. 3

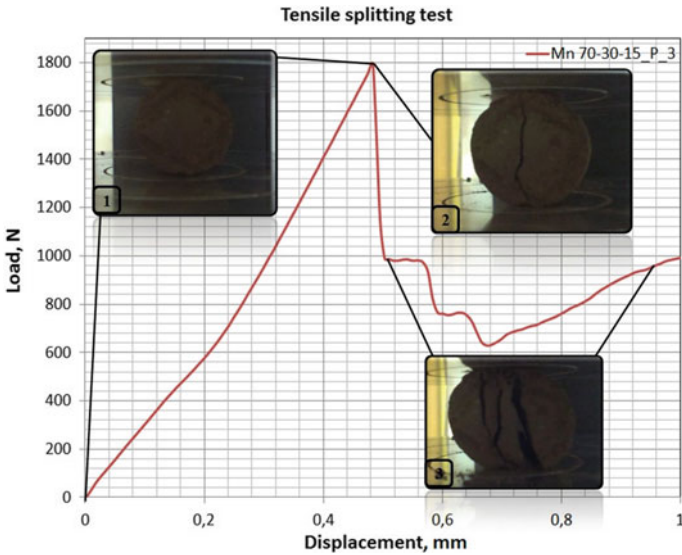


Fig. 25.26 Tensile splitting test of brex No. 3

endure the pressure, as evidenced by the core’s growth. A clear zonal structure of the brex can be observed in the radial direction. The near-surface layers of the brex have a relatively higher stiffness than its “core”. This statement is supported by the difference in slopes of the curves at Stage 1 and Stage 2.

Table 25.19 Mechanical strength of brex, kgF/cm²

Brex No.	Tensile splitting strength	Compressive strength
1	18.3	160.8
2	28.6	291.2
3	13.1	124.6

In the third stage, once the applied force reaches its maximum, the “core” of brex is destroyed with a complete strength loss.

Table 25.19 illustrates the average compressive strength and splitting strength.

Subsequently, compressive strength of samples of industrially manufactured brex No. 2 was tested by independent laboratory L. Robert Kimball & Associates, Inc (USA). The compressive strength of a sample with a diameter of 32.3 mm and a length of 57.7 mm was 206 kgF/cm². It is clear that the results obtained for compressive strength significantly exceed the compressive strength of briquettes required for electric furnaces.

Brex porosity was examined by electron microscopy using an LEO 1450 VP microscope (Carl Zeiss, Germany) with a resolution of 3.5 nm in combination with X-ray computed tomography using a Phoenix V | tome | X S 240 tomograph (General Electric, USA). The computed tomography method was used to determine the sample porosity in the pore size range above 100 μm. The electron microscopy method was used to study the porosity fraction represented by pores with sizes less than 100 μm. Interpretation of these microscopic studies was carried out using the computer program STIMAN [57]. It was found that the porosity of the brex was 18.5% (5.6% is the porosity measured by computed tomography and 12.9% by electron microscopy). Subsequently, the porosity of industrially manufactured brex with the same content of major components (with 3% Portland cement) was measured at the above-mentioned independent laboratory and amounted to 18.7%.

Thermal studies using powder samples with a mass of 50–70 mg, carried out on an STA 449 °C installation (Germany) in an argon atmosphere, in the temperature range of 20–1400 °C at a heating rate of 20°/min, allowed to determine the nature of phase transformations in brex during their heating and showed that the thermal effects on the DSC curve for brex No. 1 and No. 2 are almost identical (Fig. 25.27).

The manganite (MnO(OH)) dehydrates to form pyrolusite or β-kurnakit ($2\text{MnOOH} = \text{Mn}_2\text{O}_3 + \text{H}_2\text{O}$) in the temperature range 300–450 °C. At temperatures above 400 °C, psilomelane of manganese ore transforms to hollandite or Hausmannite. Exothermic peaks with a maximum temperature of 795.8 °C in brex No. 1 and 801.0 °C in brex No. 2 are most likely associated with the dissociation of pyrolusite and the formation of β-kurnakit which is accompanied by oxygen release and mass loss. The same peak in brex No. 3 at a temperature of 742.8 °C is not followed by a loss of mass; it can be explained by the effects of recrystallization of amorphous phases. β-kurnakit decomposes in the temperature range 900–1050 °C, and the formation of β-hausmannite takes place [58]. In the range 1080–1250 °C, β-Hausmannite is polymorphically converted to γ-Hausmannite.

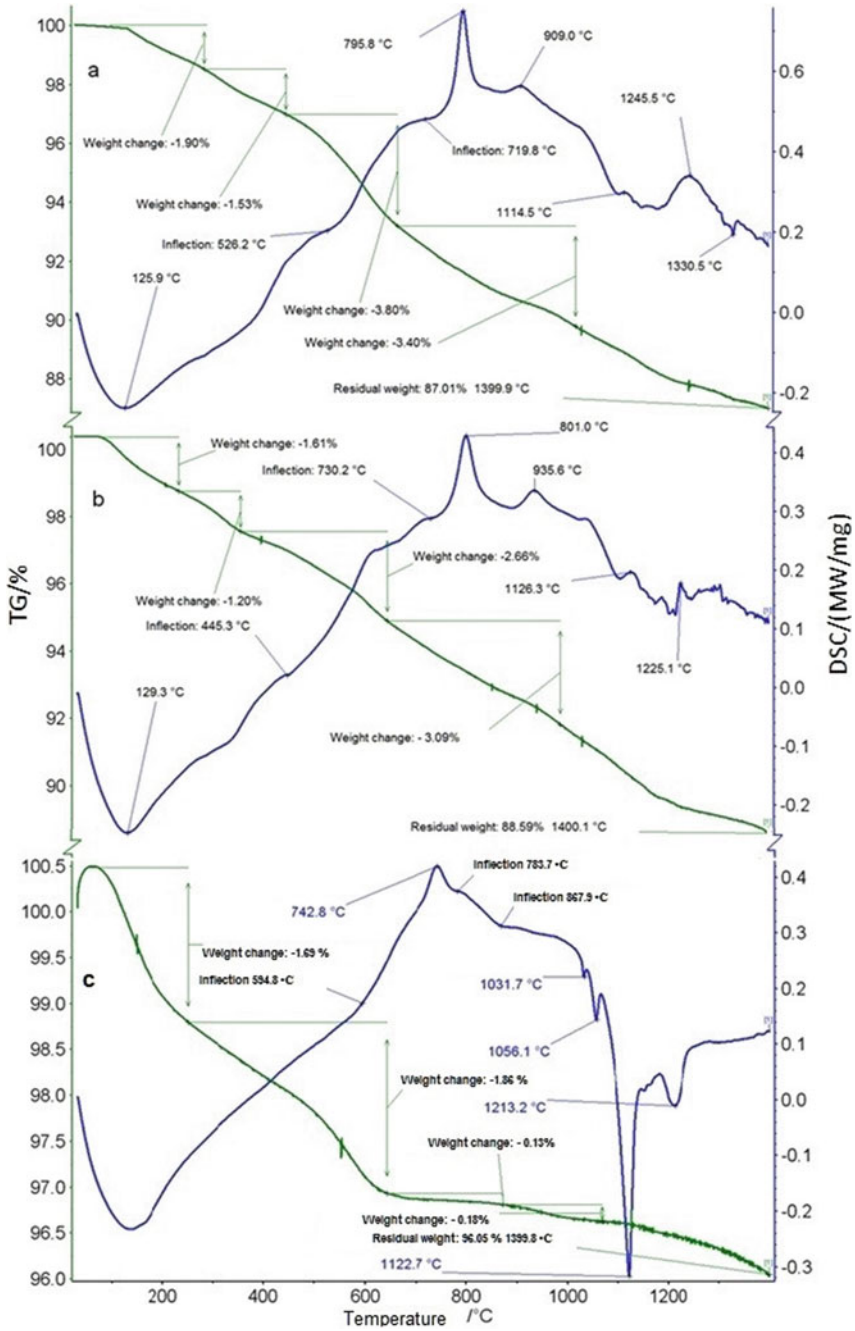


Fig. 25.27 Thermograms of the brex samples No. 1 (a), No. 2 (b), No. 3 (c) (left-hand vertical TG/%; right-hand vertical—DSC/(MW/mg))

In brex No. 3, the endothermic peak in the 150–200 °C temperature range is accompanied by mass loss due to sorption moisture removal. In the 300–500 °C temperature range, there are no pronounced endothermic peaks, but there is a loss of mass associated with the reduction of MnO_2 to Mn_2O_3 . A phase transformation of manganite (MnOOH) into kurnakit occurs in the same temperature range. The endothermic effect with a maximum at 1031.7 °C is associated with the reduction of Mn_3O_4 to MnO due to mass loss; the effect at 1056.1 °C is determined by the ferric phase change.

The endothermic peak with a maximum at 1122.7 °C is determined by forming manganese carbide Mn_3C , where carbon recovers manganese from MnO . The coke breeze in brex provides for intensive iron and manganese reduction, marked by endothermic peaks at 1122.7 °C and 1213.2 °C.

Figure 25.28 shows the microstructure of brex No. 2.

Portland cement is known to lose its binding properties at 750–900 °C. Therefore, it is important to understand what provides for the hot strength of brex at temperatures higher than the above-mentioned temperature range. Previous studies [59] explored the behavior of a pyrolusite sample of manganese concentrate from the Chiatura mine when heated in a reducing atmosphere (helium 40% and hydrogen 60%; heating at a rate of 20 °C per minute). A cubic sample measuring $5 \times 5 \times 5$ mm was observed to gradually expand by a considerable amount up to 0.8 mm; the thermal expansion

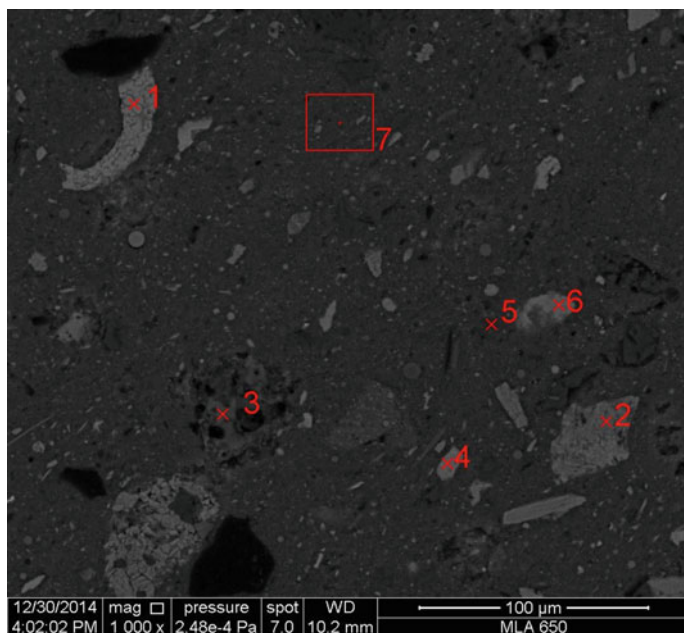


Fig. 25.28 Microstructure of brex No. 2 structure. (1—pyrolusite, 2—haussmanite, 3—diopside, 4—fayalite, 5—mullite, 6—pyrolusite, 7—solid solution of $\text{Ca}_2\text{SiO}_4\text{-Mn}_2\text{SiO}_4$)

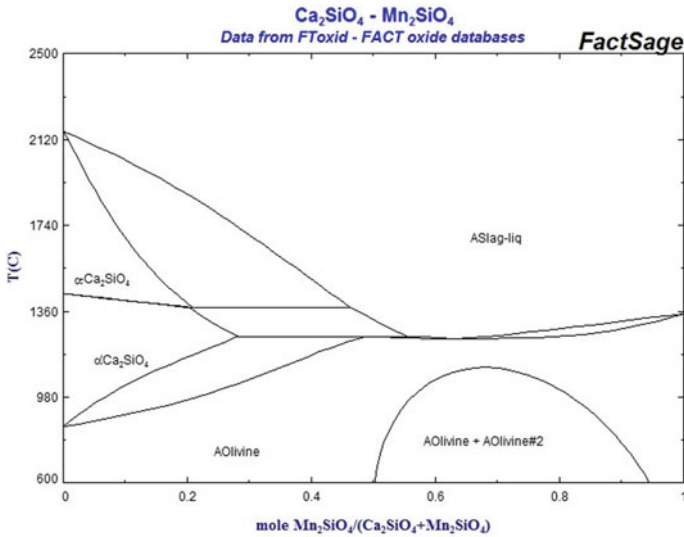


Fig. 25.29 Diagram of system $\text{Ca}_2\text{SiO}_4\text{-Mn}_2\text{SiO}_4$ [60]

was accompanied by sample cracking. Cracks were first observed at 500 °C, with the number of cracks increasing with heating. The fractures formed during the tests are characterized by a certain orientation pattern. Radial and concentric cracks are found within the spherulites. Cracks in random directions are found in the interspherulites cementing mass. Despite this fracture pattern, the sample maintained integrity at 800 °C. After that, a slow and irreversible compression process began. In our opinion, a dense silicate phase (olivine or Wollastonite) protected the sample from destruction. The formation of the phase in the indicated temperature range corresponds to the well-known phase diagrams of systems $\text{Ca}_2\text{SiO}_4\text{-Mn}_2\text{SiO}_4$ and $\text{CaSiO}_3\text{-Mn}_2\text{SiO}_3$ (Fig. 25.29 and Fig. 25.30 [60]). Manganese silicates (tephroite- Mn_2SiO_4 and rhodonite- MnSiO_3) were discovered in the intervals between the oxide phase’s grains of the Chiatura concentrate sample.

Up to 1250 °C, the strength of brex is provided by the dense structure of the mentioned silicate phases, and above this temperature two eutectics are formed in the MnO-SiO_2 system: tephroite + rhodonite + liquid (1251 °C) and tephroite + manganosite + liquid (1315 °C) which contribute to preserving the strength of the brex (Fig. 25.31), due to the appearance of a liquid binder.

An important property of brex for smelting ferroalloys in ore-smelting furnaces is the specific electric resistance. The measured specific electrical resistance of brex samples at a room temperature is given in Table 25.20.

The measuring system used in the study made it possible to investigate the dynamic pattern of brex resistance at a temperature up to 800 °C. As a result, the behavior of brex resistance was studied up to the first exothermic peak described in Fig. 25.27. It corresponds to a relatively deep brex immersion in the furnace to levels where lower

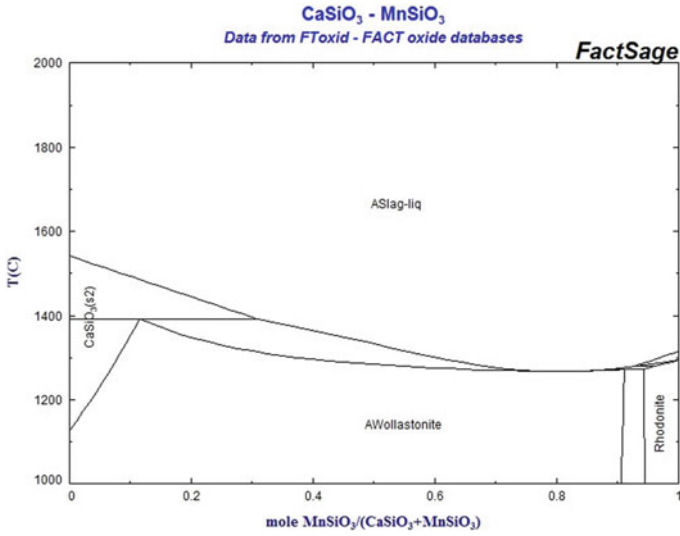


Fig. 25.30 Diagram of system $\text{CaSiO}_3\text{-MnSiO}_3$ [60]

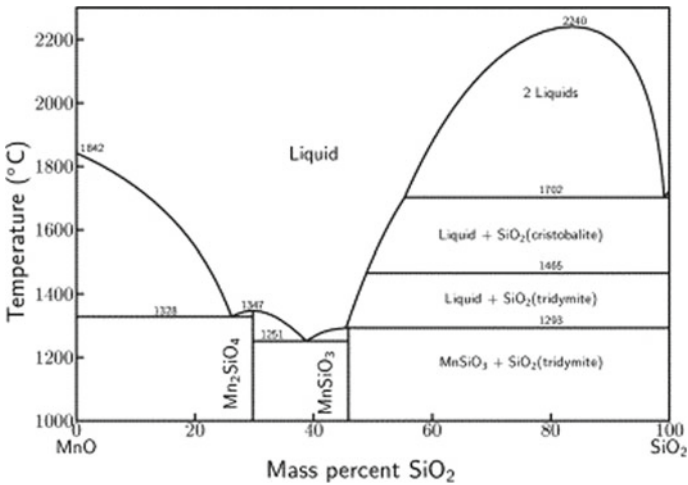


Fig. 25.31 Phase diagram of the MnO-SiO_2 system

Table 25.20 Specific electric resistance of brex No. 1–3 at room temperature

Brex, No.	ρ , MOhm-mm	
1	26.3	25.5
2	32.3	28.9
3	9.42	12.4

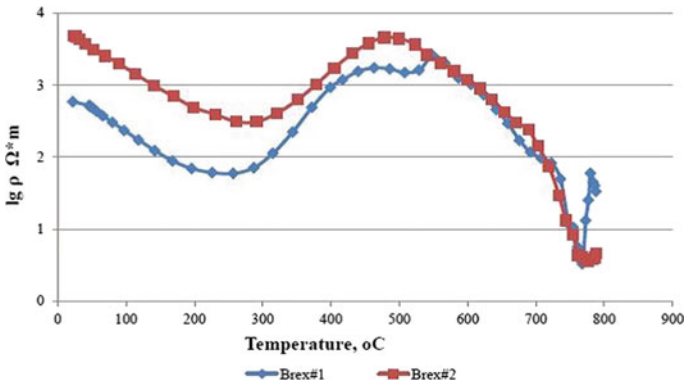


Fig. 25.32 Specific electric resistances of brex No. 1 and brex No. 2

manganese oxide is formed. Due to the low electric resistance of brex No. 3 (with 15% coke breeze in the mass of brex), which is lower than the resistance of lump manganese ore of the same deposit [61], this type of brex was excluded from further study.

Figure 25.32 shows the results of resistance measurements in brex No. 1 and brex No. 2 when heated to 800 °C.

The increase in resistivity of brex in the 300–500 °C temperature range coincides with the above-mentioned endothermic effects of mass loss, which is associated with manganite dehydration and with kurnakit formation.

The resistivity of brex No. 1 is lower than that of brex No.2 because of the higher carbon content in brex No. 1 resulting from a higher baghouse dust content that adds carbon to brex No. 1. Based on the above-mentioned conclusions regarding the physical and mechanical properties of brex, the behavior of brex during heating and measurements of the specific electrical resistivity, brex No. 2 was selected as a component of the submerged EAF charge.

25.4.4 Full-Scale Testing of Silicomanganese Smelting with Brex in the Charge of Submerged EAF

For the full-scale testing, an experimental batch of 2000 tons of brex of 1400 tons of Chiatara manganese oxide and 600 tons of aspiration dust from production of silicomanganese were manufactured. The components of the mixture were mixed in the ore yard by a front loader and fed to the extrusion line. In the manufacture of this batch, it was decided to limit the proportion of binder (Portland cement) in the charge mixture of 3%, which was sufficient to ensure the strength of brex that withstood 20 overloads on the way from the briquetting factory to the ferroalloy plant: extruder–conveyors–dump truck–piles–front loader–truck–stack at the port of loading–front

Table 25.21 Chemical composition of charge components

Material	Components composition						
	Mn	SiO ₂	CaO	MgO	Al ₂ O ₃	Fe	P
Ore-1	49.5	13.0	0.7	0.5	1.0	4.0	0.05
Ore-2	29.0	20.2	5.9	5.2	2.1	0.9	0.06
Brex	31.37	24.32	6.10	2.05	2.79	1.36	0.12
Scraps	23.3–38.6	n/a	n/a	n/a	n/a	n/a	n/a
Silicomanganese fines briquettes (vibropressed)	53	18	4	n/a	n/a	10.5	0.15

loader–bunker–grab–barge–grab at the port of discharge–bunker–conveyors–dump truck–stack in the ore yard of the ferroalloy plant wheel loader–hopper–oven. At the same time, the cumulative formation of fines (less than 6 mm) did not exceed 10%. Such a decrease in the mass content of the binder was made possible thanks to the well-known binding properties shown by dust aspiration from the production of manganese ferroalloys.

The pilot campaign was conducted in a stably operating industrial submerged EAF with a capacity of 27 MV A, with a productivity of 85 tons/day. The specific power consumption averaged 4200 kWh/t. The degree of recovery of manganese is 80%. The manganese content in waste slag is 12–14%. The chemical composition of the manganese components of the mixture is given in Table 25.21.

Scraps are the internal wastes generated while deslagging the surface of metal in a ladle, cleaning buckets and furnace notch, sorting at slag dumps and casting silicomanganese. Briquettes made from silicomanganese fines are produced by the process of vibropressing (unconditioned fines fraction 0–6 mm). To impart the necessary strength to the briquettes made from these fines, Portland cement was used (10% mass).

A preliminary calculation of the composition of the charge was carried out to achieve stable manganese content in the ore part of the charge (Table 25.22).

For the accuracy of the comparison of the results of the furnace operation with and without brex, a month-long period of furnace operation was observed. A weeklong period of the furnace operating without brex immediately preceding the beginning of the pilot period was taken as a reference.

It was decided to begin with 5% of the brex share in the ore part of the charge to get a first experience with the agglomerated burden. Over the course of three days of observation, no visible changes had been registered in the process of silicomanganese smelting; the furnace worked smoothly, with a constant and uniform current load during the period of brex use. The slight 0.3% decrease in manganese extraction during this period was due to furnace downtime associated with the taphole unit repair (1.5 h downtime). Then, for four consecutive days, the brex share in the charge was maintained at 10%. Improvement in the furnace top functioning was visually apparent. Gas flames throughout the furnace's top area confirmed an improvement

Table 25.22 Composition of the charge (net tons)

Component of the charge	Reference and full-scale trial periods						
	Reference period	1	2	3	4	5	6
Mn Ore-1	0.526 (30%)	0.525 (30%)	0.525 (30%)	0.525 (30%)	0.525 (30%)	0.525 (30%)	0.525 (30%)
Mn Ore-2	1.205 (70%)	1.120 (65%)	1.030 (60%)	0.855 (50%)	0.705 (41%)	0.600 (35%)	0.525 (30%)
Brex	–	0.087 (5%)	0.175 (10%)	0.350 (20%)	0.500 (29%)	0.605 (35%)	0.690 (40%)
Estimated weight of charge	1.730	1.732	1.730	1.730	1.730	1.730	1.740
<i>Incoming manganese with</i>							
Ore-1	0.262 (43%)	0.262 (42.6%)	0.262 (42.6%)	0.262 (42.4%)	0.262 (42.2%)	0.262 (42.1%)	0.262 (41.8%)
Ore-2	0.350 (57%)	0.325 (53%)	0.299 (48.6%)	0.224 (40.1%)	0.205 (32.8%)	0.174 (27.9%)	0.152 (24.2%)
Brex	–	0.027 (4.4%)	0.054 (8.8%)	0.109 (17.5%)	0.160 (25%)	0.188 (30%)	0.214 (34%)
Manganese charge weight	0.612	0.614	0.614	0.619	0.622	0.624	0.628
Average manganese content, %	35.4	35.5	35.6	35.8	36.0	36.1	36.1

in gas permeability of the column of the charge and the uniformity of the temperature distribution over the surface of the furnace top. Deeply submerged electrodes functioned without producing surface blowholes in the electrodes circle and in the surrounding area. No sintering in the electrodes circle was observed. During the next three days, brex share in the charge was increased up to 20%. The furnace operated smoothly, the electrodes were deeply submerged, the current load had no visible abnormalities or jolts, and the gas permeability of the charge was good for the entire area of the furnace top. Throughout the next week, the brex share of the charge was increased to 29%. The furnace worked well. An increase in the rate of the charge descent in the electrodes circle, especially during the tapping, indicates an increase in the melting rate of the charge in the active zone of the furnace. The furnace top functioned smoothly without surface blowholes with a constant load current, smooth, without bumps and drops. Melt out was good, and metal and slag were sufficiently warmed up. However, in the end of this period, there was a furnace downtime for 4 h due to reasons not related with the brex presence in the charge (electrical problem in the transformer).

The beginning of the next phase of the pilot period, when the brex share rose to 35% substituting the ore-2, was associated with a problem caused by a disruption in the taphole electrode bypass, resulting in its shortening and the deterioration of the melt output. The bulk of the slag remained in the furnace. This resulted in an increased coke rate and scraps withdrawal from the charge along with briquettes of silicomanganese fines. During this period, a deterioration in the technical and economic performance of the furnace had been registered, namely an increase in specific energy consumption and specific consumption of manganese ore raw materials, as well as a reduced extraction of manganese. To restore its normal functioning, the furnace heating rate was increased so as to warm up the slag and ensure its normal tapping.

In the final phase (week) of the pilot operation period, the furnace worked with the brex share in the charge up to 40%. The furnace operation was characterized by a good current load, top gas release was smooth, with no surface blowholes and furnace charge downsides and with a normal tapping.

As the share of brex in the ore part of the charge increased, the share of ore 2 was proportionally reduced, which is an equivalent substitute for the amount of manganese introduced, since the average manganese content in brex was 31% and in ore—29% (Tables 25.23 and 25.24).

Substitution of the essential part of manganese ore in the charge with brex based on ore fines and aspiration dust led to an improvement in the technical and economic indicators of the process as a whole. The pilot industrial campaign itself went without any visible changes in the technological process: The furnace worked smoothly, with a constant current load, the melt was produced according to the schedule, there were no significant changes in the chemical composition of the metal and slag, and the gas permeability of the furnace throat improved.

The specific energy consumption during the experimental period has significantly decreased. In the base period, the power consumption per 1 ton of alloy was 4091 kWh. When 40% of manganese-containing brex were fed into the ore part

Table 25.23 Furnace parameters during the reference and the full-scale trial period

Parameter	Reference and full-scale trial periods						
	Reference period 1	2	3	4	5	6	
Actual metal production over a period of time, t	ton	298.4	277.1	196.6	570.6	397.2	757.2
	b.t (basic ton)	300.7	285.8	199.5	584.75	393.2	767.8
Actual furnace performance, %	98.9	97.6	97.4	99.7	96.2	98.6	93.6
Power consumption, MW	3.339.27	1.078.2	1.085.4	734.7	2.120.8	1.536.3	2.821.48
Specific power consumption, kWh/b.t	3.977	3.586	3.798	3.682	3.627	3.908	3.675
	t(29%Mn)/b.t	1.106	0.933	0.892	0.714	0.635	0.492
Ore-2	t(48%Mn)/b.t	0.668	0.563	0.539	0.431	0.383	0.297
	t(49.5%Mn)/b.t	0.565	0.505	0.482	0.509	0.480	0.484
Ore-1	t(48%Mn)/b.t	0.582	0.520	0.497	0.525	0.495	0.499
	t(31.37%Mn)/b.t	0	0.077	0.164	0.273	0.387	0.605
Brex	t(48%Mn)/b.t	0	0.050	0.107	0.178	0.252	0.395
	t/b.t	1.671	1.515	1.538	1.496	1.502	1.581
The total consumption of raw manganese ore	t(48%Mn)/b.t	1.250	1.133	1.143	1.134	1.130	1.191
	Coke, t/b.t	0.446	0.339	0.420	0.405	0.395	0.413
Quartzite, t/b.t	0.419	0.499	0.524	0.465	0.529	0.456	0.475
	Silicomanganese fines briquettes t/b.t	0.158	0.082	0.103	0.092	0.120	0.094
Scrap (Mn content in scrap, %), t/b.t	0.358 (23.3)	0.601 (29.9)	0.462 (33.0)	0.477 (35.3)	0.461 (32.0)	0.455 (25.8)	0.373 (38.6)
	Electrode mass, t/b.t	0.034	0.032	0.030	0.035	0.028	0.028
Manganese extraction from the ore component, %	80.1	79.8	80.7	80.7	83.6	79.1	79.9

Table 25.24 Main components composition during the reference and pilot operation period

Phase	Main components composition								
	In metal				In furnace charge				
	Mn	Si	Fe	P	MnO	MgO	SiO ₂	CaO	Al ₂ O ₃
Base	66.64	17.71	14.06	0.127	10.50	7.38	44.28	21.43	15.29
1	66.33	16.30	14.25	0.128	12.70	7.14	45.33	20.31	13.46
2	66.90	17.69	14.18	0.098	12.89	6.52	44.78	18.67	13.80
3	66.77	16.45	14.21	0.12	11.30	6.77	44.57	19.86	15.07
4	68.02	16.02	14.01	0.14	11.79	6.39	45.11	19.42	15.13
5	65.98	15.22	14.30	0.16	15.08	5.73	46.20	26.11	15.71
6	66.08	17.07	14.25	0.18	10.8	5.17	45.30	19.83	15.35

of the charge, the specific energy consumption decreased to 3727 kWh per 1 ton of alloy.

The next positive factor of the campaign was an increase in extraction of manganese from the ore component of the charge. If in the comparative period of the furnace operation without brex, manganese extraction from the ore part of the charge averaged 80%, while using 30% of the brex in the ore part of the charge, manganese extraction reached 83.5%.

The deterioration of the manganese extraction parameters in the period preceding the final one was not related to the presence of brex in the charge and was due to the stoppage of the furnace and problems with the electrode.

The obtained results formed the basis for the design and construction of several briquetting factories based on stiff vacuum extrusion in different countries around the world. In particular, a briquette factory with a capacity of 260 thousand tons of briquettes per year was put into operation at the “Chelyabinsk Electrometallurgical Integrated Plant” (ChEMK). Brex are made from a mixture of manganese ore and baghouse dusts. The ratio of these components in the briquette charge depends on the type of imported ore fines. At 30% of the dust content in the mass of the briquette, only 1.5% of the cement by mass of the briquette is required. The share of cement increases to 3% at 15% of the content in the dust in the briquette.

25.4.5 Metallurgical Properties of Briquettes Based on Chromium-Containing Materials

The possibility of obtaining inexpensive and efficient agglomerated charge materials for smelting ferrochromium without prior calcination has always attracted ferroalloys technologists. However, cold briquetting of chromium ore fines and concentrates is not widespread and is still significantly inferior to sinter and pellet production.

Practical experience of using roller presses and vibropressing confirmed the possibility of achieving satisfactory metallurgical properties of briquettes obtained by such methods. Suffice to mention the experience of the Serov Ferroalloy Plant [48] confirmed the feasibility of replacing lumpy chromium ore with briquettes due to productivity growth (by 4%) without deterioration of the slag mode with a calm and even furnace running. The specific energy consumption (kWh/t) decreased by 1%. The decrease in chromium extraction when working on briquettes (by 2.3%) is due to the additional consumption of ore to increase the ore layer.

Also known are the successful results of the full-scale industrial testing of Globe Metallurgical Inc. [48] using briquettes made of Turkish chromite ore. A mixture of lime and molasses was used as a binder (5% by weight). The share of briquettes in the ore part of the charge reached 100%. Since 1988 in Sweden, as noted earlier, the plant for the production of briquettes by vibropressing has been successfully operating at Vargön Alloys.

However, roller briquetting is accompanied by the formation of a significant amount of waste. Achieving hot strength requires the use of significant quantities of expensive binder. Vibropressing technology also involves the heat treatment of raw briquettes and inevitably leads to the “dilution” of the charge component thus obtained due to the need to use a substantial amount of binder. A significant amount of cement binder inevitably also leads to an increase in the sulfur content in the alloy. This, in particular, caused the closure of the vibropress briquetting factory at the Serov Ferroalloy Plant.

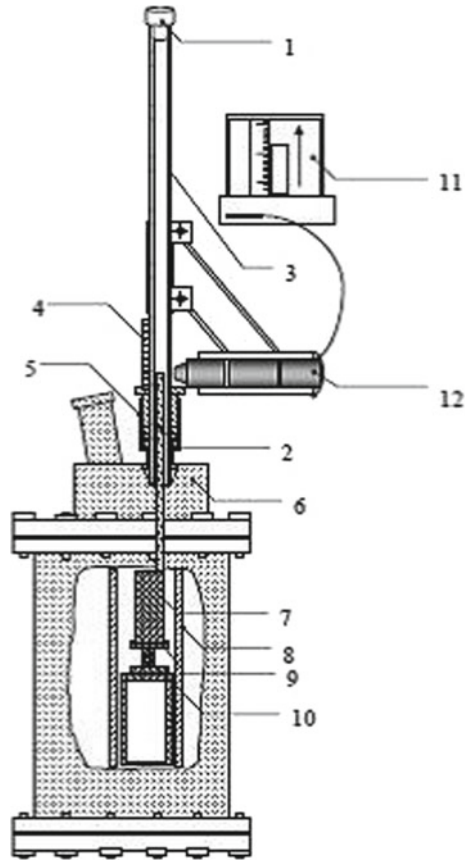
The SVE method opens up new opportunities for the widespread commercialization of cold briquetting chromium ore materials due to its higher performance, sufficiently high strength of raw briquettes and significantly lower binder content required to achieve the required level of metallurgical properties and the lack of thermal processing of raw briquettes.

In [62], the metallurgical properties of two types of briquettes made of chromium-containing materials—ore and ore-coal (including ore-coke) briquettes—were studied.

The choice of cement as a binder was also based on the results of studies of hot strength of laboratory briquettes made of chromium ore concentrate, described in [63]. The hot strength of briquettes was determined by the method of linear heating of the sample under load (2 kg) at a rate of 17 °C/min under reducing conditions. The choice of the load value corresponds to the pressure of a briquette column with a height of 2 m. Reducing conditions are provided by conducting an experiment in a stagnant furnace atmosphere of gaseous reaction products (CO) and placing the test sample of the briquette between two graphite plates, which simulates the contact of the briquette with pieces of coke in an electric furnace.

An experimental setup for determining the hot strength of briquettes based on fine-grained chromium ore when heated in a reducing atmosphere in the temperature range 20–1800 °C is shown in Fig. 25.33. Before the start of the experiment, the briquette was installed in the isothermal zone of the furnace between graphite plates. The top plate was prevented by the load and the alundum displacement indicator with a total mass of 2 kg. The furnace was closed, pumped out and filled with

Fig. 25.33 Installation diagram for determining the hot strength of briquettes in reducing conditions with a temperature change from 293 to 2073 K. 1—rubber stopper; 2—alundum index pointer; 3—transparent quartz tube; 4—ruler; 5—vacuum tight sleeve; 6—cover; 7—load weighing 2 kg; 8—graphite heater; 9—pressure graphite plates; 10—tested briquette; 11—the computer; 12—digital microscope



argon. In the course of linear heating at a rate of $17\text{ }^{\circ}\text{C}/\text{min}$, set by the furnace programmer, the gas from the furnace was vented, maintaining the pressure in the furnace equal to the atmospheric pressure. Changes in the sizes of the briquette were fixed according to the movement of the alundum pointer. To improve the accuracy of the readings, an Intel digital microscope was used, which made it possible to conduct linear movements on the computer screen with an accuracy of 0.01 mm . If the absolute value of the displacement is 1 mm (typical for the first heating period of the briquette, when the usual thermal expansion of the briquette prevails), then the relative measurement accuracy is 1% (rel.), which is sufficient for technical measurements. After the experiment, a metallographic section was prepared from the “crushed” briquette, and a metallographic analysis of the phase components formed in the briquette was performed.

Comparison of softening curves (dilatometric curve) and the results of metallographic analysis of briquettes after melting makes it possible to qualitatively compare the melting and reduction rates for a given briquette composition and thus simulate their behavior in the ore-smelting furnace. The use of the method of linear heating

under load can be illustrated by the example of briquette No. 1 from Kazakhstanian concentrate of chromium ore with cement as a binder (6% by mass) in comparison with briquette No. 2 with the addition of coke breeze (8% by weight) and with the synthetically modified liquid glass substance (Penolite) as a binder (6% of the mass) and with the briquette No. 3, which differs from the briquette No. 2 by the absence of coke in its composition.

Photos of briquettes and polished sections from such briquettes are presented in Figs. 25.34, 25.35 and 25.36. Figure 25.37 shows the softening curve of briquettes when heated under load.

Briquette No. 1 has a high final softening temperature—1620 °C, which allows intensive processes of formation of ferrochromium to develop at the places of contact of the ore briquette with carbon pressure plates. The bulk of the briquette at the end of the experiment turns into a pasty solid–liquid state. In general, it can be assumed that for this case the melting rate corresponds to the rate of reduction of the components of the briquette by carbon.

Interestingly, the smallest drops of metal are distinguishable in the body of briquette No. 1, although in this case this process does not receive development. The most likely reason for this is the transfer of the reducing agent from carbon pieces to ore grains in the form of gaseous carbon-containing molecules of the type CH_x along cracks and pores of the briquette. Such a mechanism for the carbothermic reduction of chromites was proposed in [64] to explain the results of a study on the reduction of Ural chromium ores by carbon. Creating conditions in the ore-smelting furnace for the formation of gaseous carbon-containing compounds with increased reducing ability can be a significant reserve for the intensification of reduction processes.

Adding 8% of coke to the composition of the briquette No. 2 leads to a decrease in the softening end temperature to the level of 1550 °C, i.e., less than for cement

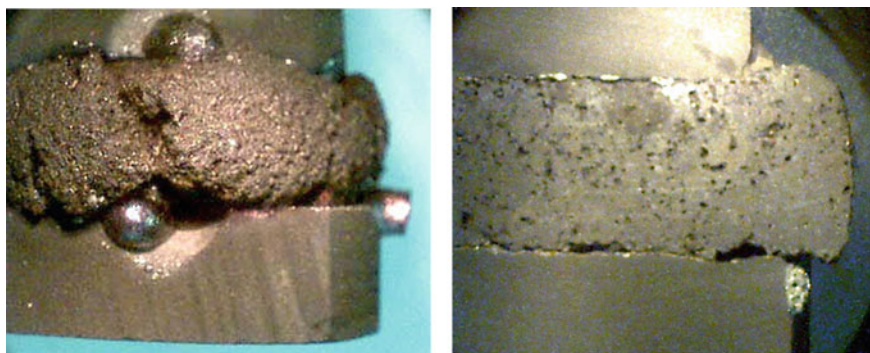


Fig. 25.34 Appearance and thin sections of briquette No. 1 with a cement binder after determining the hot strength (on the left is a briquette; on the right is a thin section, magnification 10). The composition of the briquette is Kazakhstanian chromium ore and cement grade M500 in the amount of 6% by weight of the ore, drying at room temperature for 24 h. The experimental conditions are linear heating of the sample at a rate of 17 °C/min to a temperature of 1680 °C under a load of 2 kg in a reducing atmosphere

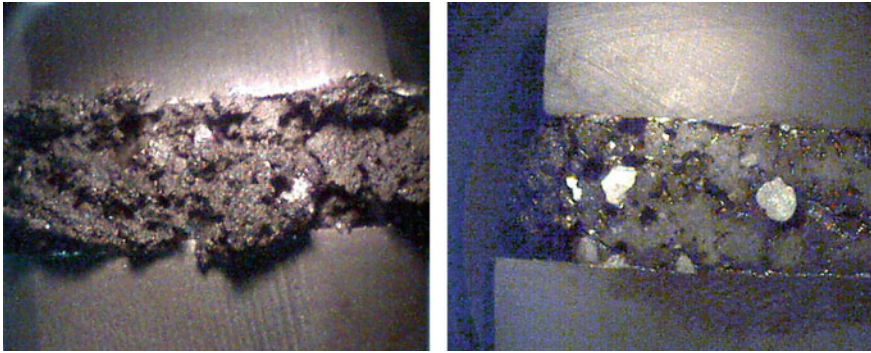


Fig. 25.35 Appearance and thin sections of ore-coke briquette No. 2 with a Penolite binder after determining the hot strength (on the left is a briquette; on the right is a thin section, magnification 10). The composition of the briquette is Kazakhstani chromium ore, and coke breeze is 8% by weight of the ore and Penolite in the amount of 6% by weight of the ore, drying at room temperature for 24 h. The experimental conditions are linear heating of the sample at a rate of 17 °C/min to a temperature of 1780 °C under a load of 2 kg in a reducing atmosphere

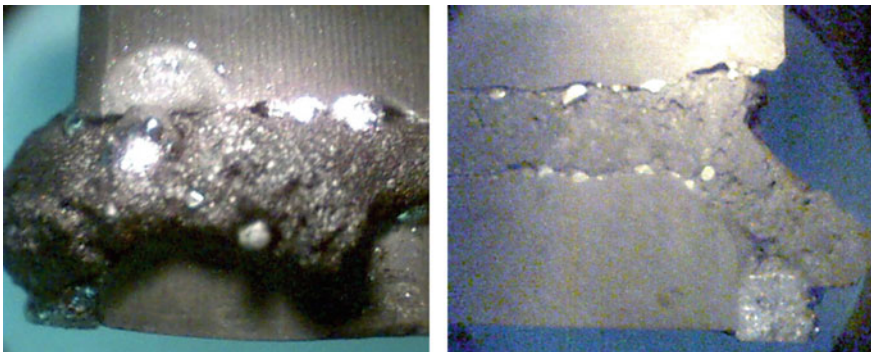


Fig. 25.36 Appearance and thin sections of briquette No. 3 with a Penolite as a binder after determining the hot strength (on the left—briquette, on the right—thin section, magnification 10). The composition of the briquette is Kazakhstani chromium ore and Penolite in the amount of 6% by weight of the ore, drying at room temperature for 24 h. Experimental conditions—linear heating of the sample at a rate of 17 °C/min to a temperature of 1780 °C under a load of 2 kg in a reducing atmosphere

bonded briquettes (1620 °C). However, the reason for the decrease in this temperature here is not the melting of the ore material, but the intensive formation of liquid metal inside the briquette. The appearance of metallic liquid in the body of the briquette leads to its weakening and crushing, although the remainder of the ore material of the briquette is predominantly in the solid state. In this case, the melting rate lags behind the rate of reduction of the components of the briquette by carbon, which allows increasing the heating rate of such a charge without disrupting the process conditions.

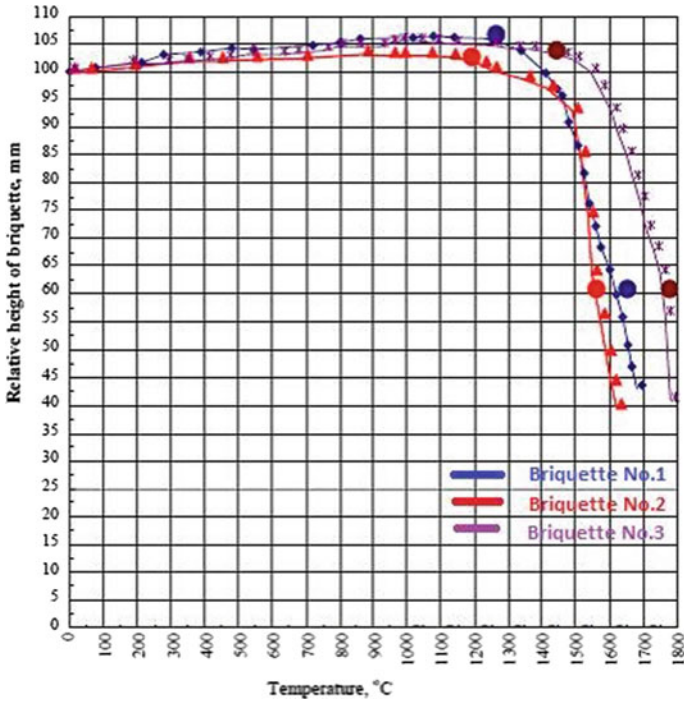


Fig. 25.37 Softening curves for briquettes No. 1–3

Briquette No. 3 shows a record of high softening end temperature of 1765 °C. At such a high temperature, there is an intensive reduction of chromic ore with carbon at the interface of briquette–graphite; there is a vigorous outflow of droplets of ferrochromium from the briquette. The remaining substance of the briquette (“slag residue”) is squeezed out under load from the pressure plates, but retains the solid–liquid state. Here, also, the melting rate corresponds to the reduction rate of the components of the briquette with carbon, but the reduction process until the softening of the briquette goes much further in terms of the amount of ferrochromium produced. This is natural, because this binder (Penolite) allows “overheating” of the briquette by more than 100 °C than the cement binder, with the corresponding larger development of reduction processes.

The addition of a carbonaceous reducing agent leads to an intensification of the reduction processes, which opens up possibilities for increasing the productivity of the electric furnace. But at the same time, the choice of the optimal content of carbon-containing reducing agent should be based on the analysis of the totality of the consequences of its introduction into the composition of the briquette, including the reduction of mechanical strength and the growth of electrical conductivity.

Based on the results of the study of hot strength of laboratory briquettes No. 1–3, the metallurgical properties of extrusion briquette (brex) made of the chromium ore fines and concentrates with the addition of coal were studied.

At the first stage, the metallurgical properties of the ore-coal briquettes of the following composition were investigated: briquette No. 4—concentrate of chromium ore (71.4%), coal (23.8%) and cement (4.8%); briquette No. 5—concentrate of chromium ore (76.2%), coal (19%) and cement (4.8%). The following average values of mechanical strength in tensile and compression tests for these briquettes were obtained: briquette No. 1—28.8 kgF/cm² and 80.56 kgF/cm², briquette No. 2—47.8 kgF/cm² and 84.6 kgF/cm², respectively.

To determine the heat resistance of briquettes, a cylindrical sample (diameter 26.4 mm) weighing 33.6 g was placed in a melt heated to a temperature of 1500 °C, which was further heated to 1650 °C after lowering the briquette into it. A sample of briquette was removed from the melt after 10 min. The mass loss of the sample of briquette No. 4 was 31.25%, and its diameter decreased to 21.5 mm (Fig. 25.38).

The dependence of the conductivity of briquette No. 4 on the temperature is shown in Fig. 25.39. It is seen that closer to 800 °C begins almost exponential growth of electrical conductivity, which can lead to the above-mentioned negative consequences in the operation of the furnace. The conductivity of such a briquette at 788 °C is almost 6 times higher than that of a briquette based on manganese ore fines and aspiration dust and 6 orders of magnitude higher than the conductivity of lumpy chromium ore [65].

The properties of chromium ore brex on a bentonite binder were also studied. The main component of brex is the gas cleaning dust of carbon ferrochromium production (97% of the mass of brex). Bentonite has been used as a plasticizer and binder, providing high impact strength. The fraction of the fine fraction (particles less than 5 mm in size) formed after four drops of brex samples onto a concrete floor from a height of 2 m did not exceed 1%.

The strength of the raw brex is also illustrated by Fig. 25.40, which shows the moment when the raw brex on the bentonite binder is squeezed out of the die of the

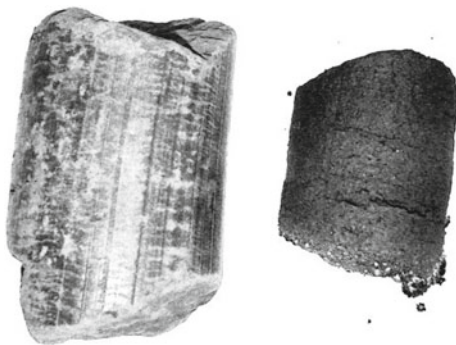


Fig. 25.38 Sample briquette No. 4 before (left) and after holding for 10 min at 1650 °C

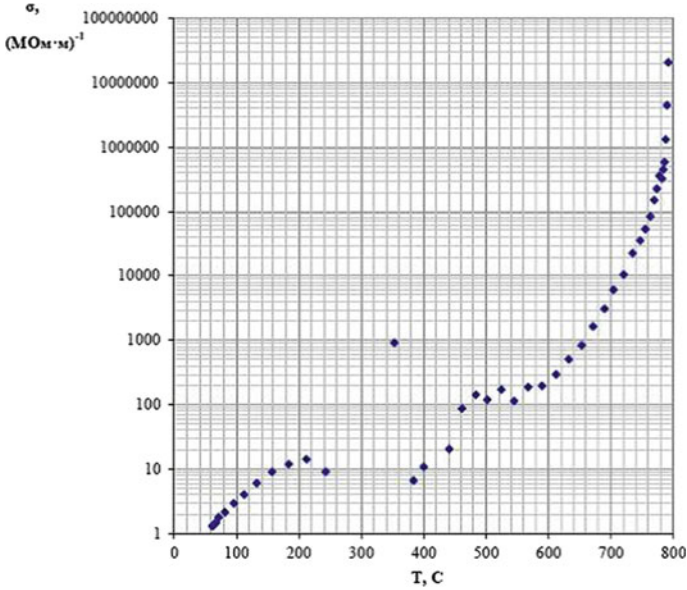


Fig. 25.39 Electrical resistivity of briquette No. 4 when heated



Fig. 25.40 Production of bentonite bonded chromium ore fines brex on a laboratory extruder

laboratory extruder. Raw brex was so strong that it easily moved the cuvette with previously made samples.

The results obtained formed the basis for designing an industrial line for the production of brex in Kazakhstan (TNK Kazchrome, Aktobe), which was commissioned in 2017 (Fig. 25.41). Currently, brex are successfully used as a component of the charge of ore-smelting furnaces for smelting ferrochromium [66].

Fig. 25.41 Industrial production of chromium-based brex at Aktobe Ferroalloy Plant



25.5 Charge Preheating

Preheating is designed to remove moisture from the charge components being loaded and to heat it as much as possible to the extent that it does not lead to igniting or oxidizing of coke. Depending on the type of smelted ferroalloys, the preheating temperature can vary from 650 to 1000 °C. Calculations show and industrial experiments confirm that preheating the charge to 800–1000 °C provides a saving of 20–25% of electricity in the production of ferroalloy, while increasing the productivity of the furnace unit.

Preheating of the feed materials may be due to the physical heat of the exhaust gases and/or their chemical potential. The charge can be heated in rotary or shaft kilns.

An example of a solution using a rotary kiln for preheating is shown in Fig. 25.42. Preheating of manganese lump ore and coke is organized in a rotary kiln with a length of 75 m diameter 3.5 m and a capacity of 36 t/h. The kiln is heated by chilled and purified furnace gas. The charge, heated in the furnace to 870 °C and partially reduced, is loaded into the receiving hopper of the melting furnace using a lift container. When transporting the mixture from a rotary kiln to a melting furnace, the temperature of

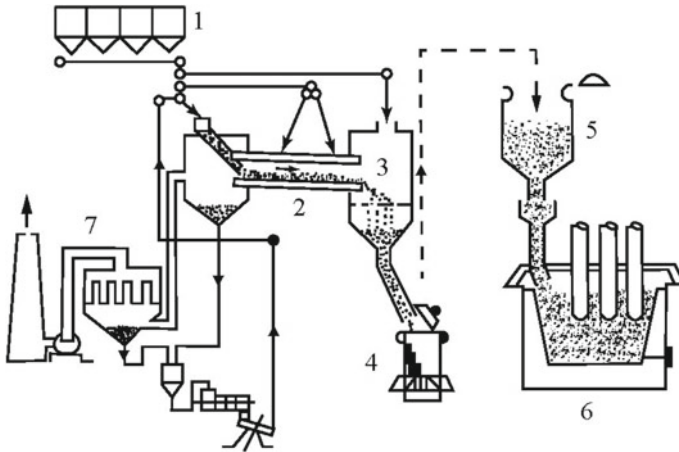


Fig. 25.42 Scheme of the ore-smelting furnace in combination with a rotary furnace for heating the charge. 1—bunker for the charge; 2—rotary kiln; 3—intermediate hopper; 4—container; 5—furnace bunker; 6—ore reduction furnace; 7—gas cleaning

the charge decreases to 630 °C. To prevent further cooling of the mixture during its movement, the intermediate transfer paths and devices are lined with refractory concrete. The decrease in the specific energy consumption by 400 kWh/t of carbon ferromanganese was achieved.

The use of shaft kilns for heating the charge was implemented in the well-known Outokumpu project for smelting carbon ferrochromium (Outokumpu Preheating Kiln—OPK™, Fig. 25.43). Prepared and metered materials are loaded into a shaft preheating kiln installed above a sealed ore-smelting furnace. The mixture is heated by burning flue gas from the furnace (80–88% CO). The heated charge along the pipes in the lower part of the preheating kiln is lowered under its own weight into the furnace for smelting carbon ferrochromium. A decrease in specific energy consumption by 10–15% and a significant reduction in the cost of ferrochromium were observed. Among other advantages of preheating in the stationary OPK™: higher FeCr production level and stable furnace operation control, elimination of reactions between water vapor and coke in the ore-smelting furnace, which leads to coke consumption minimization, simplification of pressure control in the furnace when using a dry and heated mixture.

Another example of the utilization of purified furnace exhaust gas (mainly CO gas) for preheating chromite ore is a project by Tenova Pyromet to upgrade one of Kazchrome's workshops (Akssu, Kazakhstan, Fig. 25.44, [67]) using a Multiple Preheater (MPH, [electronic]). CO gas is burned in a specially designed combustion chamber developed by Pyromet, which provides optimal mixing and control of the gas burned to produce uniform hot gas for preheating chromite ore. The modular design allows you to adapt the system to existing operations. Preheater vessels are

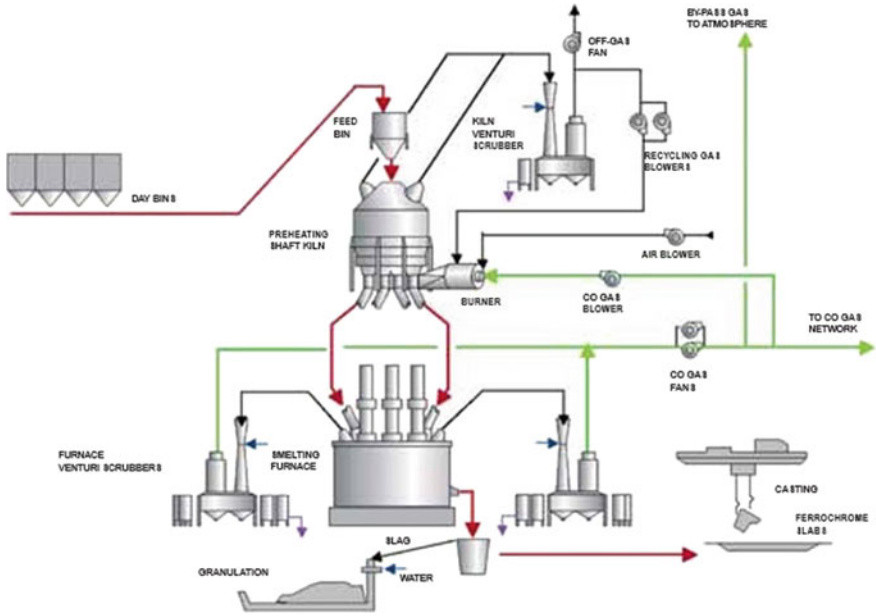


Fig. 25.43 Functional principle of preheating, smelting and gas cleaning in the Outotec ferrochromium manufacturing process

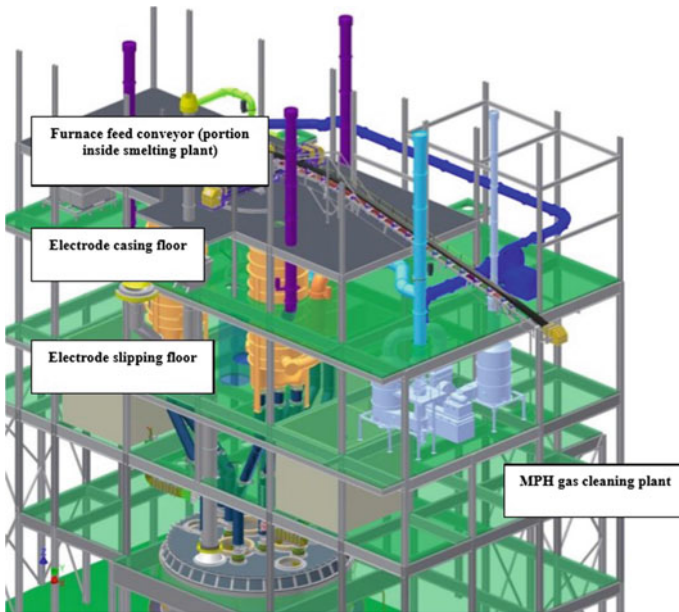


Fig. 25.44 Sectional view of Tenova Pyromet Multiple Preheater [67]

located lower in the building, reducing the load on the steel structure of the furnace. The advantages of this solution include

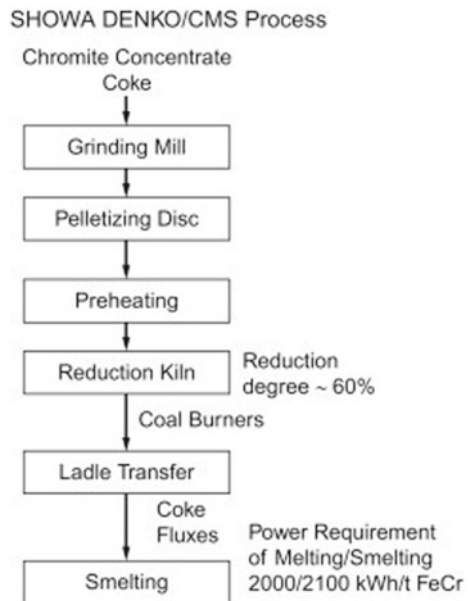
- reduction in furnace power consumption by 15%;
- reduction in volatile matter of the reductant (20%) which increases the CO content of the furnace gas;
- better ore reducibility.

25.6 Charge Prereduction

In search of ways to increase the efficiency of ferroalloy smelting processes, reduce coke consumption and power consumption, experts are increasingly turning to the method of introducing prereduced components (ore lumps, pellets, briquettes) into the charge. This direction has not yet received wide distribution, repeating in many respects the fate of the known methods of direct reduced iron (DRI) production, which at the present stage is still significantly inferior to traditional technologies.

Of the currently known methods based on preliminary reduction of the charge, the most common methods are the partial metallization of chromite and laterite nickel ores. Commercially completed prereduction projects in the ferroalloy industry include two projects using the Showa-Denko/CMS process in Japan and South Africa [68], Outokumpu’s project, and a project based on the CODIR process. Figure 25.45 shows the layout of Showa-Denko/CMI process.

Fig. 25.45 Prereduction of pellets and smelting in Showa-Denko/CMI process



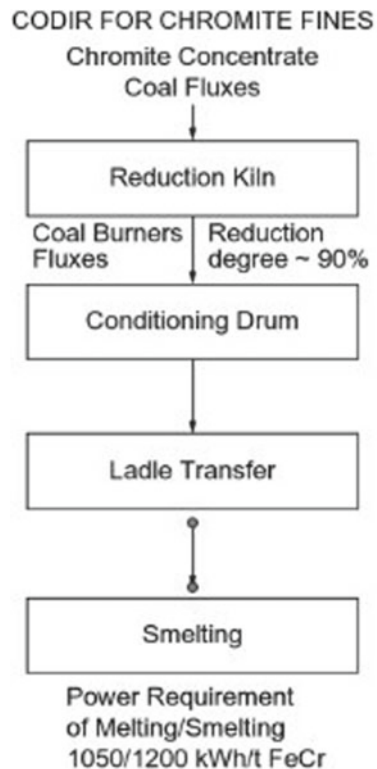
In the Outokumpu project [69–73], enriched concentrates (~44% Cr_2O_3) of chromium ore from Finnish deposits in Kemi are crushed to $-74 \mu\text{m}$, binders are added, pelletized to form pellets with a diameter of 11–13 mm, dried, prereduced in a tubular furnace at 1350–1450 °C and melted in the ore-smelting furnace. Specific energy consumption is reduced to 3000 kW/t.

In the CODIR process [72], non-agglomerated fines of chromite ore undergo preliminary reduction. Figure 25.46 shows the scheme of this process.

This process has been first tested by Krupp in 1980 s and finally commercialized by Mannesmann Demag. The fines are charged directly (without preliminary agglomeration) to rotary kiln. The reduction of chromites is achieved with the help of cheap non-coking coals. In the rotary kiln, chromite ore fines and coal react at temperature 1450 °C. Samancor (South Africa) commissioned CODIR process to produce up to 120,000 tons per year of calcined prereduced charge for electric furnace with transformer capacity 33 MV A.

Another example of the concept of preliminary reduction of chromite ores is the Premus process [73, 74]. This technology uses South African chromium ores with an average grade of 44–50% Cr_2O_3 . The technology is the production of chromium-carbon pellets, their reduction firing in a rotary tube furnace and the re-reduction of

Fig. 25.46 Prereduction of non-agglomerated fines of chromite ore in CODIR process



hot pellets in a closed ore reduction furnace with CO utilization. Due to preliminary recovery and heating in a rotary kiln, the total energy consumption in the process is 1/3 less than by traditional smelting technology, and the amount of exhaust gases is further reduced by about 1/3.

An example of a successfully implemented project for the preliminary recovery of charge materials is the RKEF process in Cerro Matoso, mentioned in Sect. 25.4, for smelting ferronickel using prereduced brex in a rotary kiln.

One of the few completed projects with preliminary reduction of manganese ores was carried out at Nippon Denko Co. Tolushima. Ltd's [75]. In this project, preliminary reduction of carbonate manganese ore in a rotary kiln is used to obtain low-phosphorus ferromanganese. Previously, for the purpose of decarbonization, firing was used at the enterprise. In addition to decarbonization, a prereduction of manganese ore took place in such a furnace. Rotary kiln is able to obtain greater reduction than a sintering machine, with the addition of a reducing agent. In other words, using the rotary kiln for prereduction would enable greater cost reduction. In addition, it turned out that the use of manganese ore thus prepared leads to a decrease in the consumption of silicomanganese used as a reducing agent.

Tube and shaft furnaces have received much greater use for roasting carbonate manganese ores, which is discussed in detail in Sect. 25.7.

The possibility of using rotary hearth furnaces (RHF) for the preliminary metallization of chromite ores was studied by Hofmann et al. [76]. Prereduction of chromium ore as a first step will significantly reduce the specific energy consumption in the subsequent electric furnace.

Preliminary reduction of iron and chromium-containing components in the pellets is carried out in a rotary bath furnace at temperatures up to 1500 °C. Coal inside the agglomerates (pellets, briquettes, brex) reacts with metal oxides and stimulates chemical reduction. The pellets in the bathtub are surrounded by CO gas, which speeds up the recovery process of the pellets (Fig. 25.47).

Based on the investigation results, it was concluded that apart from savings in electric power the use of a prereduction unit for ferroalloys production can lead to the following improvements of the overall process:

- increased smelting furnace throughput rate;
- increased chromium recovery;
- increased carbon control;
- substitution of metallurgical coke by non-coking coals.

Research on the use of rotary hearth furnaces for the partial metallization of chromium ore extrusion briquettes (brex) was carried out in 2012 (M. Kospanov, private communication). The appearance of the used brex is shown in Fig. 25.48.

A total of more than 15 tons of brex was partially metallized. The mechanical strength of the brex was sufficient for subsequent melting processes. Test results were qualified as positive. Tests have shown that energy consumption in an electric furnace can be reduced to < 50% at high metallization rates.

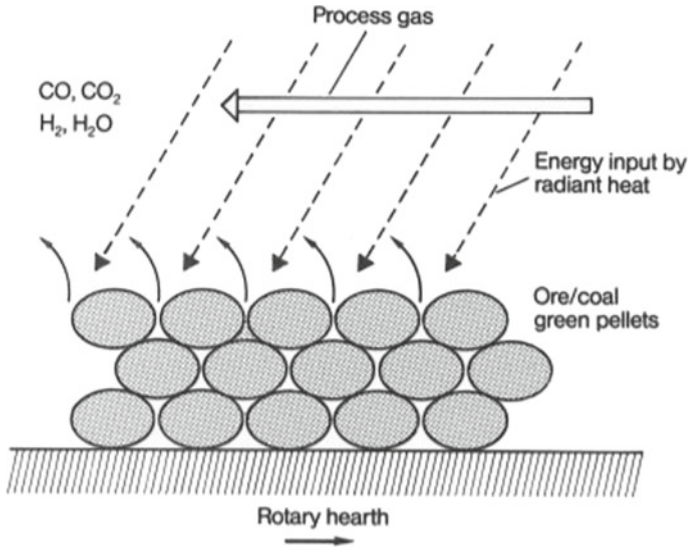


Fig. 25.47 Principle of the rotary hearth furnace [76]



Fig. 25.48 Extruded brex for pilot testing of partial metallization of chromites in RHF

25.7 Firing Carbonate Manganese Concentrates

The production of carbonate raw materials is possible in two classes: 10–0 mm and lumpy carbonate concentrate fractions of 50–10 mm. It is advisable to agglomerate the first class in a mixture with oxide concentrates, and the second one is used for

smelting manganese alloys after heat treatment (decarbonization) or without it. In all cases, heating of the material to the temperature of dissociation of carbonates and heat consumption for their decomposition is required. The use of natural carbonate ores and concentrates in an ore reduction furnace is considered economically unjustified, since the decomposition of manganese carbonates requires additional costs of coke and electricity.

Firing lumpy carbonate manganese concentrates is carried out in rotary kilns or shaft furnaces. Decarbonization and the use of a hot charge for smelting manganese alloys reduce the specific energy consumption and increase the productivity of units by 25–30%. If firing is carried out at mining and processing plants, then the costs are reduced by about 45% for the transportation of raw materials due to the removal of moisture and losses during calcination. For the production of ferromanganese, it is necessary to decarbonize the carbonate ore while maintaining the particle size distribution of the initial ore. Cracking of carbonate ore upon heating does not matter during its sintering.

According to [77], energy saving during smelting of ferromanganese is 1000 kWh, and coke consumption is reduced by 0.65 tons as a result of using calcined carbonate ore. The manganese content in the metal increases from 76 to 79%. Therefore, lumpy carbonate concentrates without firing are used for melting to a limited extent in the charge together with manganese oxide concentrate, and the fine fractions are subjected to sintering. Lumpy carbonate concentrates are used for smelting ferromanganese in blast furnaces, where firing occurs with gas passing through the charge layer. The use of lumpy non-calcined carbonate concentrates in the smelting of manganese ferroalloys, in addition to increasing the extraction of manganese in the alloy, stabilizes the electric mode and improves the yield of the charge. The cost of the alloy is reduced. Carbonates absorb the heat of the exhaust gases in the charge layer located in the loading funnel, reduce temperature and conductivity and contribute to the deep immersion of the electrodes.

Carbonate feedstock has an advantage over oxide feedstock, especially in ferromanganese smelting, since it has a natural basicity of 0.6–1.4, which eliminates limestone additives in the charge, and the melting point of carbonate concentrates is about 200 °C higher than oxide concentrates, which improves reduction process conditions.

The use of carbonate manganese raw materials for melting in an ore reduction furnace is characterized by an additional energy consumption of about 240 kWh/t of material and an increased consumption of a carbon reducing agent [78]. Pieces of carbonate concentrate are destroyed with the formation of up to 30% of fine fractions (0–8 mm), which reduces the gas permeability of the mixture.

It was established [79] that at the temperature of the first endothermic effect, not all MnCO_3 decomposed into calcium rhodochrosite and manganocalcite decomposes, but only a part of it. MnO formed upon decomposition is oxidized in air to $\gamma\text{-Mn}_2\text{O}_3$. At temperatures around 750, 850 and 900–950 °C, low-grade manganese-calcium carbonates gradually decompose. The products of their decomposition are oxidized in air and interact with the formation of CaMn_3O_7 , CaMn_2O_4 and CaMnO_3 . Compounds $\gamma\text{-Mn}_2\text{O}_3$ and CaMn_3O_7 formed during firing are unstable at high temperatures and

are reduced to Mn_3O_4 and CaMn_2O_4 . The compounds obtained by high-temperature (1000–1100 °C) oxidative calcination of carbonates are represented by marokite (CaMn_2O_4), Hausmannite (Mn_3O_4) and partially CaMnO_3 .

During the heat treatment of manganese concentrates in various gaseous media, it was shown that in the flow of reducing gases, in comparison with a neutral atmosphere, the degree and speed of the decarbonization process slightly increase. A change in reducing media (hydrogen, carbon monoxide and their mixture) practically does not affect the course of crystallochemical transformations [80, 81].

It was determined [82] that cracking of carbonate concentrates mainly ends at 550–750 °C. A further increase in temperature does not affect the final fractional composition. When heated at a speed close to an industrial electric furnace, the final fraction content of 5–0 mm does not exceed 12–14%. Unbaked carbonate concentrate has a high electrical resistance. The most noticeable difference from the usual mixture is noted up to temperatures of 800–900 °C.

It is believed [83] that structural disruption during firing with the formation of pores, cracks, ruptures and others is equally inherent in oxide and carbonate raw materials and is primarily due to the presence of hydrated components. Externally monolithic dense structure, the initial samples contain numerous multidirectional cracks of genetic origin. These include discontinuities that occur in the rock masses of sedimentary rocks during their formation (the so-called shrinkage cracks), as well as cracks caused by partial relaxation of internal stresses and the presence of impurities that deform the subcrystalline lattice. Cracking of carbonates is enhanced by the so-called perfect cleavage of carbonate crystals, i.e., the ability to split or split along certain crystallographic planes parallel to real faces. Additional pores and cracks in the samples wax during heat treatment in the temperature range from 100–800 °C. The possibility and intensity of failure are determined by the ratio of the rates of formation and « healing » of microcracks and are associated with the nature of the material and the thermomechanical parameters of plastic deformation (temperature, strain rate, type of stress state, etc.).

M.I. Gasik showed that the characteristics of the probability of destruction of a sample from carbonate raw materials depend on the rate of its heating [77]. So at a heating rate of 0; 5; 10; 15; 20; 25; 30 and 35 °C/min, the degree of destruction is 0.00; 0.00; 0.00; 0.006; 0.333; 0.905; 0.997 and 1.000, respectively. The critical heating rate is 15 °C/min, over which the proportion of destroyed samples increases. The heating rate of concentrates both in the rotary kiln (countercurrent exhaust gas temperature 420–460 °C) and on the top of the shaft furnace (420–500 °C) was comparable and quite high. A lump concentrate of a fraction of 50–5 mm is stored at a heating rate of samples up to 400–10 °C/min, from 400 to 1000 °C—15–18 °C/min. To preserve pieces of manganese ore materials during heat treatment, a moderate speed of 9–10 °C/min in the interval of intensive dehydration and loosening of the material (100–400 °C) is required.

A technology has been proposed for the preparation of carbonate manganese ores for electric smelting [84]. Manganese carbonate ore after enrichment is fired. Losses on ignition are reduced to 2.0%, and the manganese content rises to 40.3% (Table 25.25).

Table 25.25 Chemical composition of the initial and calcined carbonate manganese concentrate, %

Concentrate	MnO	CaO	MgO	SiO ₂	P	LOI	(CaO + MgO)/SiO ₂
Initial carbonate	28.0	12.0	2.1	13.0	0.23	32	1.08
Fired carbonate	40.3	17.3	3.0	18.7	0.33	2.0	1.08

By firing, a fired product with a fraction content of 5–0 mm of not more than 10.5% is obtained. Calcined carbonate manganese concentrate can be used instead of oxide manganese ores in the smelting of manganese alloys.

The firing of the concentrate is carried out by the combustion of natural gas; its consumption is 55–65 nm³ per 1 ton of calcined concentrate. The performance of the kiln for the calcined product is 25 t/h.

Heat treatment and agglomeration of the charge were carried out [85] in a tubular rotary kiln with a diameter of 1.6 m and a length of 8 m with the introduction of carbonate concentrates and a reducing agent and got cakes with impact strength of 93–95% and abrasion resistance of 11–13%, which significantly exceeds the performance for the sinter from the same mixture. A feature of the process is the complete reduction of higher manganese oxides to manganosite at a firing temperature of 1150–1250 °C, a firing duration of 40–50 min and the amount of solid carbon in the charge 12.5–25%. The technology of smelting manganese alloys using a thermally prepared and heated mixture is one of the most promising ways to increase the productivity of electric furnaces and reduce energy consumption (Sect. 26.5, [85–87]). When using calcined carbonate concentrates loaded into a furnace at 600–800 °C, extraction of manganese alloy increases by 6–9%, electric furnace productivity increases by 21–22%, and energy consumption decreases by 20–22%.

It was found that [78] at temperatures above 900 °C, the thermal dissociation of methane $\text{CH}_4 \rightarrow \text{C} + 2\text{H}_2$ and the interaction of water vapor with solid carbon by the reaction $\text{H}_2\text{O} + \text{C} \rightarrow \text{H}_2 + \text{CO}$ occur, which ensures the reduction potential of the gas phase in the material layer and prevents oxidation manganosite—the primary product of dissociation of manganocalcite.

Dephosphorization of the carbonate manganese concentrate of the Nikopol deposit was carried out by heat treatment in a rotary kiln 1.5 m long and 0.3 m in diameter. The concentrate was fired (26.3% Mn; 0.24% P; 11.15 SiO₂; 12.65% CaO; 2.12% MgO; LOI 32.1%; P/Mn = 0.00813) and was performed under various conditions. The dephosphorization process occurs with all firing options. The highest degree of dephosphorization (38.2%) of the carbonate concentrate was achieved by purging the layer of materials with a mixture of natural gas and steam in the presence of a solid carbonaceous reducing agent.

Thus, technological developments allow the efficient use of carbonate manganese concentrates in various metallurgical processes after appropriate preparation. Preheating the charge increases the transition of manganese into alloy by 6–9% with an increase in furnace productivity by 20–22%.

25.8 Wastes and by-Products Processing

In the production of ferroalloys, various wastes and by-products are generated (slag, dust and sludge, pellets and sinter fines, small fractions of crushed ferroalloys). In the ferroalloy industry, dry (open and semi-closed ore-smelting furnaces) and wet systems (closed and sealed furnaces) are used. Open and semi-closed ore-smelting furnaces are equipped with a dry gas cleaning, and closed and sealed furnaces are equipped with a wet gas cleaning.

Slags of bulk ferroalloys production processes do not subject to self-disintegration after crystallization, so lump slags do not require stabilization and use of special equipment for fine materials processing. Typical chemical composition of slags and dusts of chromium, manganese and silicon ferroalloys production [19, 77, 88–94] is given in Tables 25.26, 25.27, 25.28 and 25.29.

As a rule, high-carbon ferrochromium and ferrosilicochromium are produced in the same melting shop, and dust collection is organized simultaneously from different furnaces without separation of different types. Dusts from ferrosilicochromium furnaces differ from those smelting high-carbon ferrochromium mainly by concentration of silica. Work with fine materials is far more difficult than with lump slags. Utilization of waste gases requires the construction of additional installations and units for implementation of continual process. One of the problems of dust collection from waste gases is a difference in design of submerged electric arc furnaces (SAF): open, semi-closed, closed top and sealed type.

It is undoubtedly that the use of closed top and sealed furnaces provides the most effective dust collection from waste gases without air dilution. Nevertheless, units and technologies for collection of toxic manganese dusts from SAF producing high-carbon ferromanganese and silicomanganese have a broad distribution [95]. These technologies provide dry gas cleaning up to 8–11 mg/m³ of residual dust concentration when content of dust in gas before cleaning is ~1.15 g/m³, so bag filters efficiency exceed 99%. Use of top-closed and sealed furnaces for manganese and

Table 25.26 Chemical composition of slag of ferrosilicon production

Material	Content, % wt.										
	SiO ₂	SiO ₂ amorph.	CaO	Al ₂ O ₃	MgO	SiC	Metal*	Fe ₂ O ₃	Na ₂ O	K ₂ O	C
Ferrosilicon slag	32	–	18	16	0.8	15	15–25	–	–	–	–

Table 25.27 Chemical composition of slag of chromium ferroalloys production

Material	Content, % wt.							
	Cr ₂ O ₃	MgO	Al ₂ O ₃	SiO ₂	CaO	FeO	C	SiC
Ferrochromium-silicon slag	3.5	8	13	45	0.5	0.2	–	3
High-carbon ferrochromium slag	4.3	44.2	17.3	29.8	2.5	0.8	–	–

Table 25.28 Chemical composition of slag of manganese ferroalloys production

Material	Content, % wt.											
	MnO	Fe _{tot}	P ^a	CaO	MgO	SiO ₂	Al ₂ O ₃	S	Na ₂ O + K ₂ O	ZnO	LOI	C
High-carbon ferromanganese and silicomanganese												
Silicomanganese slag	14.2–16.8	0.15–0.20	0.012–0.014	17–18	4.5–5.5	49.0–50.0	7.0–8.0	0.8–1.3	3.3–4.5	–	–	0.2–0.4
High-carbon ferromanganese slag	15.5–18.1	0.10–0.15	0.08–0.11	35–38	3.0–4.0	34.0–36.0	4.0–5.0	0.5–0.8	2.4–3.5	–	–	0.2–0.4

^aDepends on phosphorus content in manganese raw materials

Table 25.29 Chemical composition of the dust generated during production of ferroalloys

Ferroalloy			Volume	Content, %		
	SiO ₂	CaO	MgO	Al ₂ O ₃	MnO	Cr ₂ O ₃
Ferrosilicon:						
FS90	75–90	1.0–2.0	0.5–1.0	1.0–2.0	–	–
FS75	47–90	0.8–1.1	0.2–0.3	0.4–4.0	–	–
FS45	42–90	0.2–0.4	1.3–6.5	1–7	–	–
High-carbon ferromanganese	5–33	1.5–6.0	0.5–1.5	1.5–3.0	5–20	–
Silicomanganese	30–50	0.1–3.0	1.2–3.0	2.3–3.5	10–25	–
Low-phosphorous slag	27	4–10	1.0–2.0	1.0–5.0	–	–
Silicocalcium	66–74	20–24	1.4–3.4	0.4–1.4	–	–
Ferrosilicochromium	55–64	20–37	2–8	1.3–4.0	–	3–10
Carbon ferrochromium	10–15	0.8–4.5	13–20	5–8	–	–
Low-carbon ferrochromium	1.5–3.3	36–44	7–11	3.3–4.7	–	14–25
Metallic manganese	6.6	39.2	1.8	0.34	–	–

chromium ferroalloys production is rational since it is related with decrease in oxygen partial pressure under the furnace roof and promotes less oxidation of dust particles and less generation of toxic chemical compounds with Fe, Mn and Cr [96]. Volumes of dust collection in Russian ferroalloy industry are estimated on the basis of industrial data on dust generation and collection. So, blast furnace ferromanganese production generates dust and sludge approximately 10 and 100 kg/t of alloy, respectively. High-carbon ferrochromium production in SAF generates ~50/150 kg of dust per 1 t of alloy and silicon alloys (depends on alloy grade) 60–150 kg/t. Calculated figures on dust generation in Russian ferroalloy industry are given in Table 25.30. Collected dust of high-carbon ferrochromium production has fine particle size (Tables 25.31 and 25.32) and alike slags of this alloy have high heat resistance and can be applied in refractories [97].

There are different ways for recycling of manganese dusts. One of the most advanced and environmentally friendly ways is arranged in Japan [98], where manganese dust is used in production of manganese ore pellets. These pellets are charged into SAF after preheating and prereduction in rotary kiln with waste gases.

Table 25.30 Dust and sludge generation at Russian ferroalloys industry

Alloy type	Production capacity, tpy	Dusts		Sludge		Total, tpy
		Yield, kg/t	Total, tpy	Yield, kg/t	Total, tpy	
Siliceous	566.4	120	67,968	n/a	n/a	67,968
Chromite	354.0	150	53,100	n/a	n/a	53,100
Manganese	188.8	10	1888	100	18,880	29,768
Total	1109.2		122,956		18,880	141,836

Table 25.31 Granulometric composition of gas cleaning dust at high-carbon ferrochromium production, % wt

Dust type	Fraction yield, mm						
	>2.5	1.6–2.5	1.0–1.6	0.4–1.0	0.16–0.4	0.063–0.16	<0.063
Cyclone	0.28	0.25	0.42	13.37	17.27	39.74	28.67
Bag filter	–	0.003	0.015	0.51	5.99	46.76	46.62

Table 25.32 Granulometric composition of dust (bag filters) at SAF production of high-carbon ferromanganese, % wt

Fraction yield, μm		
<1	10–40	>40
49	39	12

One of the examples of wastes recycling at the post-soviet space is the use of waste slags, dusts and sludge in manganese ferroalloys industry and production of electro-melted fluxes at Nikopol ferroalloy plant where anthropogenic materials are added into sinter charge [99] though the solution leads to increased dust generation in agglomeration process and requires additional control of dusts and gases generation and propagation in atmosphere [100]. Recycling of gas cleaning dust (20–43% Cr_2O_3) at chromium ferroalloys production can be arranged in the form of additions to chromite pellets and as a charge component at smelting of metal product of slag separation [101]. Dry gas cleaning systems are very effective from the point of view of dust collection for manganese and chromium ferroalloys production [94]. Ferrosilicon slags are completely recycled in SAF as a flux for high-carbon ferrochromium and charge chromium. Slags of ferrochromium and ferromanganese require sophisticated separation schemes due to weak magnetic properties of metal fines and can hardly be separated from slag by magnetic separation (in contrast to metal fines in steelmaking industry). Separation complex for ferroalloy slags often includes jiggling machines, classifiers and other special equipment.

Peculiar property of high-carbon ferrochromium slags is a comparatively high-melting temperature (heat resistance) which allows using them in refractories industry for production of firebricks and tapping hole mix. These materials are in demand at the same plants where they are generated [97]. One of the ways of recycling of manganese ferroalloys slags is a production of high-quality cast products with high performance characteristics from hot liquid slags for civil and industrial engineering [102]. A special attention should be paid to wastes of chromium- and manganese ores extraction and concentration processes as these tailings make a sufficient part from the volumes of crude ores. This type of materials are often of equal or higher quality by their chemical composition if compared with anthropogenic wastes of ferroalloys smelting process and, in some cases, are better than crude ores before concentration. In the world ferroalloy industry, one can find a trend for development of environmentally friendly zero-waste complex technologies, where by-products are considered as additional raw materials for ferroalloy industry and analogous areas. A

good example of complex use of chromium ores is a strategy of ferroalloy producers in South Africa where ores of Bushveld mining deposit are separated after extraction and concentration into several products. Use of these materials in ferroalloy industry varies due to chemical composition and fraction and includes smelting of both lump ores (6–150 mm and 6–25 mm) and pellets (made from fines—6 mm, with or without reductant) of different types (including Outotec process on steel belt) in SAF. Fine fractions of chromites (gravitational concentrate) can be smelted in DC electric furnaces without palletizing or sintering and with comparatively cheap coal instead of coke as a reductant. So, this technology and general approach include alternative technological processes, furnaces and auxiliary equipment that makes national ferroalloy industry more flexible.

References

1. Velichko BF, Gavrillov VA, Gasik MI et al (1996) Enrichment of manganese ores. Metallurgy of manganese of Ukraine, Kyiv, 471 p (in Russian)
2. Hooper RT (1974) The optimum utilization of raw materials in manganese smelting. In: Proceedings of the first international conference on ferroalloys (INFACON 74), Johannesburg, 22–26 Apr 1974, pp 101–105
3. Hooper RT (1978) Production and smelting of manganese sinter. In: Proceedings of the 36th electric furnace conference, pp 118–126
4. Dancoisne PL (1970) Optimum manganese ore preparation. In: Proceedings of the 28th electric furnace conference, pp 106–111
5. Olsen SE, Tangstad M, Lindstad T (2007) Production of manganese ferroalloys. SINTEF and Tapir Academic Press, Trondheim, p 247
6. Gasik MI, Lyakishev NP, Emlin BI (1988) Theory and technology of ferroalloys production. Metallurgy, Moscow, p 784 (in Russian)
7. Kisin DA, Kravchenko VA, Shilo AA et al (1969) Obtaining sinter from a mixture of Nikopol manganese concentrates. Steel 2:142–143 (in Russian)
8. Koryakova OF (1963) Sintering of manganese ores and concentrates from the Nikopol deposit. Transactions of NTO ChM, Moscow, pp 140–145 (in Russian)
9. Kutsin VS, Olshansky VI, Dedov YuB, Gasik MI, Gasik MM (2014) Smelting of ferrosilicomanganese with the use of manganese magnesium sinter. Steel 1:24–27 (in Russian)
10. Krivenko VV, Ovcharuk AN, Pereverzev AD (2004) Research and development of technology for the production of sinter, providing its physico-mechanical properties. In: Modern problems of metallurgy. vol 2. Dnipro, 272 p (in Russian)
11. Petrov AV, Kostyuk AA, Chikomasov VF et al (1985) Development of the technology for sintering manganese concentrate in a high layer. Bull Cent Res Inst Iron Metall 14(994):32–34 (in Russian)
12. Rogachev IP, Ovcharuk AN, Petrov AV et al (1985) Production technology and the quality of sinter with metal additives. In: Intensification of electroferroalloy processes and improving product quality. Dnipro, pp 16–17 (in Russian)
13. Ovcharuk AN, Ugantserovsky OG, Mironenko PF et al (1985) The use of secondary materials in the sintering of manganese. In: Intensification of electroferroalloy processes and improving product quality. Dnipro, pp 17–18 (in Russian)
14. Koval AV, Grishchenko SG, Mironenko PF et al (1999) Improvement of the production technology of manganese sinter. In: Proceedings of the international conference, Dnipro, pp 43–44 (in Russian)

15. Fedorenko IV, Kopyrin IA, Pershina RF (1981) Obtaining sinter from manganese concentrate. *Bull Cent Res Inst Iron Metall* 20(894):52–53 (in Russian)
16. Ryss MA Ferroalloy production (1985) Metallurgy, Moscow, 344 p (in Russian)
17. Zhuchkov VI, Vatolin NA, Leontiev LI et al (1994) Ural Manganese. Ores and ferroalloys. Yekaterinburg, 1994, pp 53–62 (in Russian)
18. Kashin VV, Krashennikov MV (1994) Ural manganese. Ores and ferroalloys. Yekaterinburg, 1994, pp 7–14 (in Russian)
19. Akberdin AA (2013) Agglomeration of refractory chromite ore. In: Akberdin AA, Kim AS, Akberdin RA (eds) Proceedings of INFACON XIII—the thirteenth international ferro-alloy congress. Efficient technologies in ferroalloy industry. (June 9–12, 2013 Almaty, Kazakhstan), vol I, pp 1–4
20. Khitrik SI et al (1968) Ferrochromium electrometallurgy. Metallurgy, Moscow, 148 p (in Russian)
21. Khokhlov DG et al (1965) Development of technology for agglomeration of chromite ores and concentrates. Scientific. In: Proceedings of Uralmekhanobr. Sverdlovsk: Uralmekhanobr, no 12. pp 43–45 (in Russian)
22. Banerjee GN et al (2010) Sintering studies on chromite fines and concentrates and some design aspects. *J Mines, Metals and Fuels* 58(9):251–254
23. Pietsch W (2005) Agglomeration in industry. Occurrence and applications Wiley, 375 p
24. Wegman EF (1976) Ore and concentrate tubing. Metallurgy, Moscow, 224 p (in Russian)
25. Rovensky II, Petrov A, Zhuravlev FM, Krendeleev VL (1967) Production of pellets from manganese flotation concentrates. *Steel* 7:613–616 (in Russian)
26. Petrov AV, Voskerichan NV, Berezhnoy NN (1975) Firing of pellets from manganese concentrate. *Bull Cent Res Inst Iron Metall* 4(744):26–29 (in Russian)
27. Chaychenko AA, Murakhovskiy VV, Grishchenko SG et al (1983) Metallurgy and coke chemistry. Kyiv: Tekhnika, no 81, pp 36–39 (in Russian)
28. Tskitishvili AA, Arabuli IA, Begadze LA (1986) Metallurgy of manganese. Tbilisi, pp 90–91 (in Russian)
29. Gubin GV, Petrov AV, Drozhilov LA et al (1978) Production of ferroalloys: collection no. 6. Metallurgy, Moscow, 1978, pp 46–53 (in Russian)
30. Serov GV, Mizin VG, Koshkin GA et al (1976) The use of rounded charge in the smelting of 75% ferrosilicon. *Steel* 10:913–916 (in Russian)
31. Lotosh VE (2009) Unburnt agglomeration of fine materials and minerals fines. Ekaterinburg: Philanthrop Publishing House, 525 p (in Russian)
32. Thaning G (1974) The production of cold-bonded pellets from steel mill waste. In: Ironmaking proceedings, no 33, pp 73–79
33. Doughty FTC (1975) COBO: a low-cost cold bond process. In: Proceedings of the 14th biennial conference of the IBA, Hyannis, MA, Aug 1975, pp 173–182
34. Fedorov NF (1970) On the classification of binders. *Cement*, no. 10, pp 8–9 (in Russian)
35. Svensson J (1968) The grangcold pellet process. *Steel Times* 197(5):362–364
36. Ahmed Yasser, Mohamed FM (2005) Recycling of manganese secondary raw material via cold-bond palletizing process. *La Metallurgia Italiana* 97(10):33–38
37. Tolymbekova LB (2014) Development of technology for smelting ferrosiliconmanganese from pelletized high-silicon manganese raw materials. Abstract dis. ... candidate of technical sciences. Institute of Metallurgy, Ural Branch of the Russian Academy of Sciences. Yekaterinburg, (in Russian)
38. Dwarapudi S, Tathavadkar V, Rao BC, Kumar TKS, Ghosh TK, Denys M (2013) Development of cold bonded chromite pellets for ferrochromium production in. Submerged arc furnace. *ISIJ Int* 53(1):9–17
39. Production of unbaked pellets from metallurgical wastes (1976). *Ferrous metallurgy. Bulletin*, no 5, pp 55–56 (in Russian)
40. Shchedrovitsky VY, Eliseev SB, Kopyrin IA (1986) Metallurgy of manganese. Tbilisi, pp 114–125 (in Russian)

41. Korotich VI (1978) Fundamentals of the theory and technology of preparation of raw materials for blast smelting. Metallurgy, Moscow, 208 p (in Russian)
42. Maerchak S (1982) Production of pellets. Moscow: Publishing house, Metallurgy, 232 p (in Russian)
43. Tolochko AI et al (1990) Utilization of dust and residues in ferrous metallurgy. Metallurgy, Moscow, 143 p (in Russian)
44. Khazanova TP et al (1961) Production of manganese alloys from low-grade oxide and carbonate ores. Development of the USSR ferroalloy industry. Kyiv, 122 p (in Russian)
45. Khvichia AP et al (1970) Smelting of silico-manganese from ore briquettes in a furnace with a capacity of 16.5 MV A. Steel. no 2, 138 p (in Russian)
46. Sukhorukov AI, Sosedko PM, Khitrik SI (1970) Steel. no 2, p 135 (in Russian)
47. Kozhevnikov IY, Ravich BM (1991) Agglomeration and the foundations of metallurgy. Moscow, Metallurgy, 296 p (in Russian)
48. Ravich BM (1982) The Briquetting of ores. Nedra, Moscow, 296 p (in Russian)
49. Dashevskii VY, Kashin VI, Lyakishev NP, Velitchko BF, Ishutin VI (1992) Improving the technological processes of production of manganese ferroalloys. Izvestiya VUZov. Ferrous Metallurgy, no 12, p 45 (in Russian)
50. Electronic resource. http://www.vargonalloys.se/index_eng.html
51. Electronic resource. <http://www.eurometa.fr/en/>
52. Mazmishvili SM et al (1992) Development and industrial development of technologies for producing dust briquettes and smelting manganese ferroalloys from them. Izvestiya VUZov. Ferrous Metallurgy. no 12, p 43 (In Russian)
53. BREV. Certificate of trademark (service mark) No. 498006, application No. 2012706053 of 02.03.2012. Right holder AM Bizhanov. (in Russian)
54. Duarte A, Lindquist WE (1999) Recovery of nickel laterite fines by extrusion. In: Proceedings 27th biennial conference. IBA, USA, pp 205–217
55. Bizhanov A, Kurunov I, Podgorodetskyi G, Dashevskii V, Pavlov A, Chadaeva O (2014) Extruded briquettes—new charge component for the ferroalloys production. ISIJ Int 54(10):2206–2214
56. Zhdanov AV et al (2007) Study of reducibility of manganese ore raw materials electrometallurgy. no 4, pp 32–35 (in Russian)
57. Sokolov VN, Yurkovets DI, Razgulina OV (1997) Determination of tortuosity coefficient of pore channels by computer analysis of SEM images. Proc Russ Acad Sci Phys Ser 61(10):1898–1902
58. Ivanova VP, Kasatov BK, Krasavina TN (1974) Thermal analysis of minerals and rocks. Resources Publishing House, Leningrad, 399 p (in Russian)
59. Tolstunov VL, Petrov AV (1989) Study of the processes of phase and microstructural transformations in manganese ores during their reducing heating. Izvestiya VUZov Ferrous Metall 4:9–14 (in Russian)
60. Glasser FP (1962) The ternary system CaO–MnO–SiO₂. J Am Ceram Soc 45(5):242
61. Zhdanov AV (2007) Study of electric resistance of materials and batches used for ferromanganese production. In: Zhdanov AV, Zayakin OV, Zhuchkov VI (eds) Electrometallurgy 6:24
62. Bizhanov FV, Steele RB, Podgorodetskyi GS, Kurunov IF, Dashevskii VY, Korovushkin VV (2013) Extruded briquettes (bricks) for ferroalloy production. Metallurgist 56(11–12):925–932
63. Pavlov AV et al (2000) Research of briquetting process of the fine chromium ores. In: 12th International ferroalloys conference, Helsinki, Finland, 6–9 June 2000
64. Mikhailov GG, Pashkeev IY, Senin AV et al (2001) Intensification of chromite carbothermic reduction. In: “Metallurgy and Metallurgists of the 21st Century”, international conference-debate. MISIS, Moscow, pp 83–98 (in Russian)
65. Akimov EN, Mal'kov, NV, Roschin VE (2013) The electrical conductivity of high-alumina chromic ore. Bull South Ural State Univ Ser “Metall” 13(1):186–188 (in Russian)
66. Kazchrome News (2018) Vestnik Kazchroma. 5(406):5 (in Russian)

67. Jonker AP (2015) Implementation of Tenova preheating technology at JSC Kazchrome. The fourteenth international ferroalloys congress May 31-June 4, 2015 Energy efficiency and environmental friendliness are the future of the global Ferroalloy industry Kyiv, Ukraine, pp 48–51
68. Naiker O (2007) The development and advantages of Xstrata Premus process. In: Naiker O (ed) INFACON XI—Delhi, India 2007, pp 112–119
69. Honkaniemi M (1991) The Outokumpu ferrochromium process. In: Honkaniemi M, Suvanto P (eds) UNEP industry and environmental, 1991, pp 63–66
70. Riekkola-Vanhanen M (1999) Finnish expert report on best available techniques in ferrochromium production. Marja Riekkola-Vanhanen—Helsinki, 1999, p 50
71. Neuschutz D (1992) Kinetic aspects of chromite ore reduction with coal at 1200–1550 °C. In: Neuschutz D (ed) INFACON 6, Cape Town, South Africa, 1992, pp 65–70
72. Xiao Y (2004) Solid state reduction of chromite with CO. In: Xiao Y, Schuffenecker C, Reuter M, Holappa L (eds) INFACON 6, Cape Town, South Africa, pp 26–35
73. Seetharaman S (2013) Treatise on Process Metallurgy, vol 3: industrial processes. Amsterdam, Elsevier (2013)
74. Naiker O and Riley T (2006) Xstrata Alloys in profile. In: Naiker O, Riley T (eds) South African Pyrometallurgy, S.A.I.M.M. 2006, pp 297–306
75. Yoshimura R et al (1981) Studies on the pelletizing of Chromium ores—Consideration a point of view on the properties of the raw materials. In: Yoshimura R (ed) Metallurgical research laboratory, metals and alloys division—Showa Denko K.K. Ferroalloys, vol 22, pp 14–19
76. Teguri D, Saito K and Miyauchi Y (2018) Manganese ore pre-reduction using a rotary kiln to manufacture super-low-phosphorus ferromanganese. In: Jones RT, den Hoed P, Erwee MW (eds) Infacon XV: international ferro-alloys congress, Southern African Institute of Mining and Metallurgy, Cape Town, 25–28 Feb 2018
77. Hofmann W, Vljajic T, Rath G (1989) The rotary hearth furnace direct-reduction process—a coal based route to substitute electrical energy in ferroalloy. INFACON 5—New Orleans, USA, 1989, pp 185–195
78. Gasik MI (1992) Manganese. Metallurgy, Moscow, 608 p (in Russian)
79. Kucher AG (1999) The study of physical and chemical transformations in carbogate manganese concentrates during heat treatment. In: Proceedings of the international conference, Dnipro, 1999, pp 122–126 (in Russian)
80. Lyashenko VS, Yanchuk EA, Samborskaya LE et al (1985) On the thermal transformations of calcium-manganese carbonates. In: Intensification of electroferroalloy processes and improving product quality. Dnipro 1985, p 25 (in Russian)
81. Rozhkov AD, Kamkina LV (1982) Behavior of manganese concentrates during heat treatment in various gaseous media. In: Integrated use of raw materials and secondary resources in the electrothermics of ferroalloys: abstracts of the 5th republican scientific and technical conference of ferroalloys of ukraine. Dnepropetrovsk, 1982, p 31 (in Russian)
82. Kucher AG, Stepanov OA, Mironenko PF, Rozhkov AD (1975) Study of the kinetics of thermal dissociation and reduction of carbonate manganese concentrates. Manganese metallurgy: abstracts of the All-Union meeting, Moscow, 1975, pp 23–25 (in Russian)
83. Katunin VM, Bogutsky YuM, Shchedrovitsky VYa, Kargina ZP (1985) On the use of carbonate manganese concentrate. Intensification of electroferroalloy processes and improving product quality. Dnipro 1985, p 22 (in Russian)
84. Grishchenko SG, Kargina ZP, Katunin VM, Kharchenko NI (1985) The involvement in the metallurgical redistribution of carbonate manganese ores. Bull Cent Res Inst Iron Metall 12(992):8–22 (in Russian)
85. License (1984) The technology of preparation of carbonate manganese ores for electric smelting. Bull Cent Res Inst Iron Metall 11(967):49 (in Russian)
86. Kucher AG, Shestakovsky OF, Petrov AV et al (1972) Heat treatment and agglomeration of ferromanganese charges before electric furnace melting. Metallurgy and coke chemistry. Kyiv, 1972, no 31, pp 42–44 in Russian)

87. Kucher AG, Mironenko PF, Khitrik SI, Gavrilov VG (1975) Smelting of carbon ferromanganese on thermally prepared carbonate concentrates. Technical progress of electrometallurgy of manganese and silicon alloys. Dnepropetrovsk, 1975, pp 58–60 (in Russian)
88. Kucher AG, Mironenko PF, Khitrik SI et al (1975) Development of technology for the smelting of manganese alloys using thermally prepared and hot blends. Metallurgy of manganese: abstracts of the All-Union meeting, Moscow, 1975, pp 74–77 (in Russian)
89. Yaroshenko YuG (2012) Energy- and resource-saving technologies of ferrous metallurgy. In: Yaroshenko YG, Gordon YM, Hodorovskaya IY (eds) Ekaterinburg: UIPC Ltd., 670 p (in Russian)
90. Theory and technology of electrometallurgy of ferroalloys (1999) Handbook for higher educational establishments. In: Gasik MI, Lyakishev NP (eds) SP internet engineering, 1999, 764 p (in Russian)
91. Gladkih VA (2004) Design and equipment of electric steelmaking and ferroalloy production. In: Gladkih VA, Gasik MI, Ovcharuk AN, Proydak YS (eds) Dnepropetrovsk, 736 p (in Russian)
92. Voroby'ev VP (2009) Electrothermics of reduction processes. In: Voroby'ev VP (ed) Ekaterinburg: UD of RAS, 269 p (in Russian)
93. Lyakishev NP (1999) Metallurgy of chromium. In: Lyakishev NP, Gasik MI (eds) ELIZ, 582 pp (in Russian)
94. Zubov VL (2002) Electrometallurgy of ferrosilicon. In: Zubov VL, Gasik MI (eds) Dnepropetrovsk: Sistemnie tehnologii, 704 p (in Russian)
95. Zhuchkov VI (2007) Technology of manganese ferroalloys. High-carbon ferromanganese. In: Zhuchkov VI, Smirnov LA, Zayko VP, Voronov YI (eds) Ekaterinburg: UD of RAS, vol 1, 414 p (in Russian)
96. Stalinskiy DV (2012) Cleaning of waste gases of SAF at manganese ferroalloys production. In: Stalinskiy DV, Shvets MN, Shaparenko AV, Lyzhnik GV (eds) Bulletin "Ferrous metallurgy", vol 3, pp 76–79 (in Russian)
97. Midander K (2010) Bioaccessibility of ferrochromium and ferrosilicon-chromium particles compared to pure metals and stainless steel—aspects of human exposure. In: Madander K, de Frutos A, Hedberg Y, Darrie G, Odnevall Wallinder I (eds) Proceedings of the twelfth international ferroalloys congress. Sustainable Future. (June 6–9, 2010. Helsinki, Finland), vol I, pp 43–52
98. Kascheev ID (2012) Basic characteristics of slags and dusts of ferrochromium production. Kascheev ID, Zemlyanoy KG, Dosekenov MS, Zhuchkov VI, Zayakin OV (eds) Proceedings of international congress "fundamental basics of wastes recycling technologies"—Ekaterinburg: UIPC Ltd., pp 101–104
99. Ishitobi T (2010) Operational improvements of a submerged arc furnace in Kashima works (KF-1) relined in 2006. In: Ishitobi T, Ichihara K, Homma T (eds) Proceedings of the twelfth international ferroalloys congress. Sustainable future. (June 6–9 2010. Helsinki, Finland), vol II, pp 509–515
100. Velichko BF (1991) Complex technology for recycling of waste slags, dusts and sludge at manganese ferroalloys and electrofluxes smelting. In: Velichko BF, Gasik MI, Koval' AV, Tkach GD, Poleschuk PN, Rogachev IP, Ovcharuk AN, Grishchenko SG, Ishutin VI. Steel #10:74–78 (in Russian)
101. Kutsin VS (2013) Mathematical simulation of waste gases and dusts propagation at agglomeration of manganese concentrates and ferroalloys smelting. In: Kutsin VS, Zhadanov AV, Gasik MI (eds) Proceedings of international conference "problems and outlook of mining and metallurgy industries: theory and practice"—Karaganda, HMI, pp 265–268
102. Dosekenov MS (2014) Analysis of generation and recycling of anthropogeneous wastes of ferrochromium production. In: Dosekenov MS, Samuratov EK, Nurgali NZ (eds) Proceedings of the XV international conference "Modern problems of electrometallurgy of steel"—Chelyabinsk: SUSU vol 2, pp 168–172

Chapter 26

Ferroalloys Furnaces



Ferroalloy production processes require high temperatures for their implementation and, in most cases, a concentration of heat in a limited furnace space. To the greatest extent, these conditions are met by heating devices using electric energy, called electric furnaces.

Ferroalloy furnaces belong to furnaces where carbon electrodes are current-carrying elements, and the electric circuit is closed through liquid metal and slag and through an electrically conductive charge. In turn, ferroalloy arc furnaces are subdivided into arc furnaces with a closed arc—*ore-smelting furnaces* with an arc burning in a crucible under the charge layer, and arc furnaces with an open arc or arc burning in slag are *refining furnaces*. The name of the ferroalloy furnaces is based on the technological features of the process. Ore-smelting furnaces, or as they are also called ore-reduction furnaces, are used to produce ferroalloys by the carbothermic process in a continuous way. Refining furnaces are intended for carrying out refining silicothermic processes and for producing ore-lime melts.

All industrial ferroalloy furnaces operate on alternating current. There are single-phase and three-phase furnaces. According to the number of electrodes, the furnaces are divided into single-electrode and two-electrode (single-phase) and three-electrode and six-electrode (three-phase).

According to the geometric shape, the bathtubs of ferroalloy furnaces are divided into furnaces with a round bathtub and furnaces with a rectangular bathtub. According to the design of the top of the furnace bath and the presence of the arch, the furnaces are divided into:

open—furnaces work without a roof with open top, the arc is open or burns in slag, or under a layer of a charge;

closed—furnaces work with a closed arch with a top, an arc burns under a layer of a charge that enters the furnace through funnels located around the electrodes;

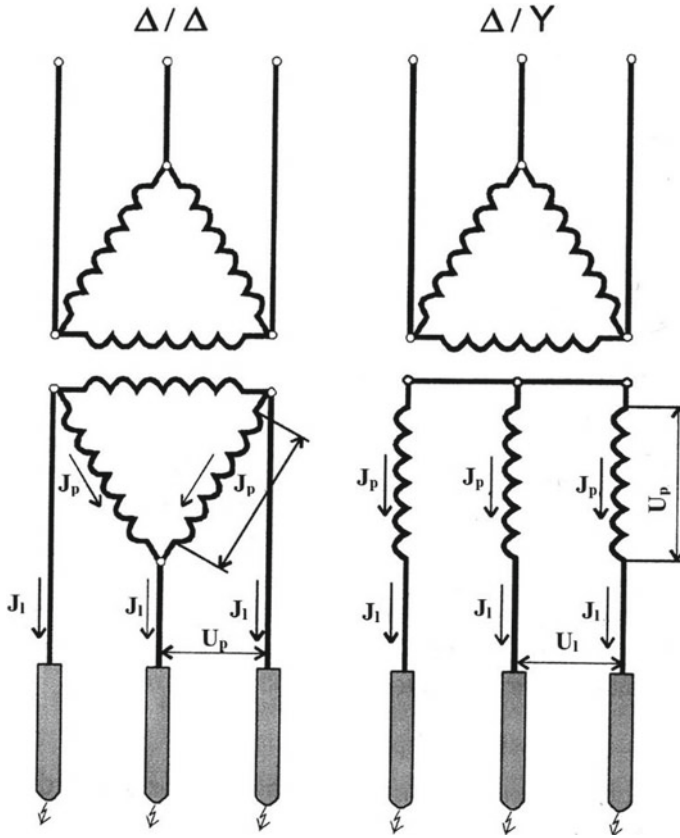


Fig. 26.1 Connection diagram of transformer windings and short-circuit design

hermetic—the furnaces work with the top, hermetically sealed arch, the arc burns under the arch of the charge, which enters with the help of pipe-chutes under the arch of the furnace.

Ferroalloy furnaces are equipped, as a rule, with installed power up to 8 MV•A with three-phase transformers, and above 8 MV•A—with three single-phase transformers. This is due to the high capacity of the furnaces reaching 115 MV•A, at which the dimensions of three-phase transformers would be very large.

There are two schemes for connecting transformer windings: *a triangle and a star*. When connected to a triangle, the beginning of one winding is connected to the end of another, and so on in a closed triangle; when connected by a star, the beginnings of all windings are connected to one point, and the ends are connected to electrodes (Fig. 26.1).

The primary windings of all transformers of ferroalloy furnaces are connected in a triangle. When connecting a triangle—a triangle (Δ/Δ), the secondary linear voltage is equal to the phase voltage, and the secondary linear current—the electrode

current is equal to the algebraic sum of the phase currents:

$$U_1 = U_p; \quad I_1 = \sqrt{3}I_p.$$

When connecting a triangle-star (Δ/Y), the secondary line current is equal to the phase current, and the linear voltage is equal to the algebraic sum of the phase voltages:

$$I_1 = I_p; \quad U_1 = \sqrt{3}U_p.$$

The electric current power does not depend on the connection scheme, as can be seen from the expressions given below:

$$\Delta/\Delta \quad P = 3U_p \cdot I_p = 3U_p \cdot I_1/\sqrt{3} = 1.73 I_1 \cdot U_1;$$

$$\Delta Y \quad P = 3U_p \cdot I_p = 3I_1 \cdot U_1/\sqrt{3} = 1.73 I_1 \cdot U_1$$

The choice of the connection circuit of the secondary windings is dictated by the requirements of the technology. In ore-smelting furnaces operating with electrodes immersed in the charge, the secondary windings are connected in a triangle, which increases the electrode current by 1.73 times and provides the necessary electrode landing depth.

In refining furnaces, depending on the technology conditions, the connection can be performed both by a star and a triangle. In furnaces smelting low-carbon ferrochromium, the secondary windings are connected by a star. In this case, an increase in the secondary voltage increases the length of the arc, which reduces the contact of the electrode with the melt, i.e., carburization of the alloy is prevented. On the contrary, when smelting silicocalcium, the secondary windings are connected in a triangle so as not to increase the secondary voltage. This is due to the fact that a high-silicon content in silicocalcium guarantees a low-carbon content, and calcium actively flies due to the high vapor pressure at process temperatures.

26.1 Electric Ore-Smelting Furnaces

Ore-smelting furnaces are designed to produce carbothermic process of silicon, manganese and chromium ferroalloys, as well as for the smelting of low-phosphorous slag in a continuous way. The power, design features and lining of the furnace are determined by the type of ferroalloy for the smelting of which they are intended.

The most characteristic features that determine the design features of the furnaces and their main working units are the shape of the bath and the shelter of the furnaces with the arch.

Round bath furnaces can be rotating and stationary. Due to the high heat intensity, as well as the large gas evolution on the top of the furnace, they are covered with arch. However, due to the specifics of the physicochemical processes that occur during the smelting of high-silicon alloys containing more than 70% Si, open furnaces or furnaces with an arch umbrella, the so-called semi-closed furnaces, are used. The designs of ore-smelting furnaces are shown in Figs. 26.2, 26.3, 26.4 and 26.5.

The furnaces are powered by a short network (Fig. 26.6).

From a transformer located in a separate room, the current through the busbar package, connected by a compensator to the low voltage terminals of the transformer and supported by the short-circuit suspensions, flows through flexible garlands to a

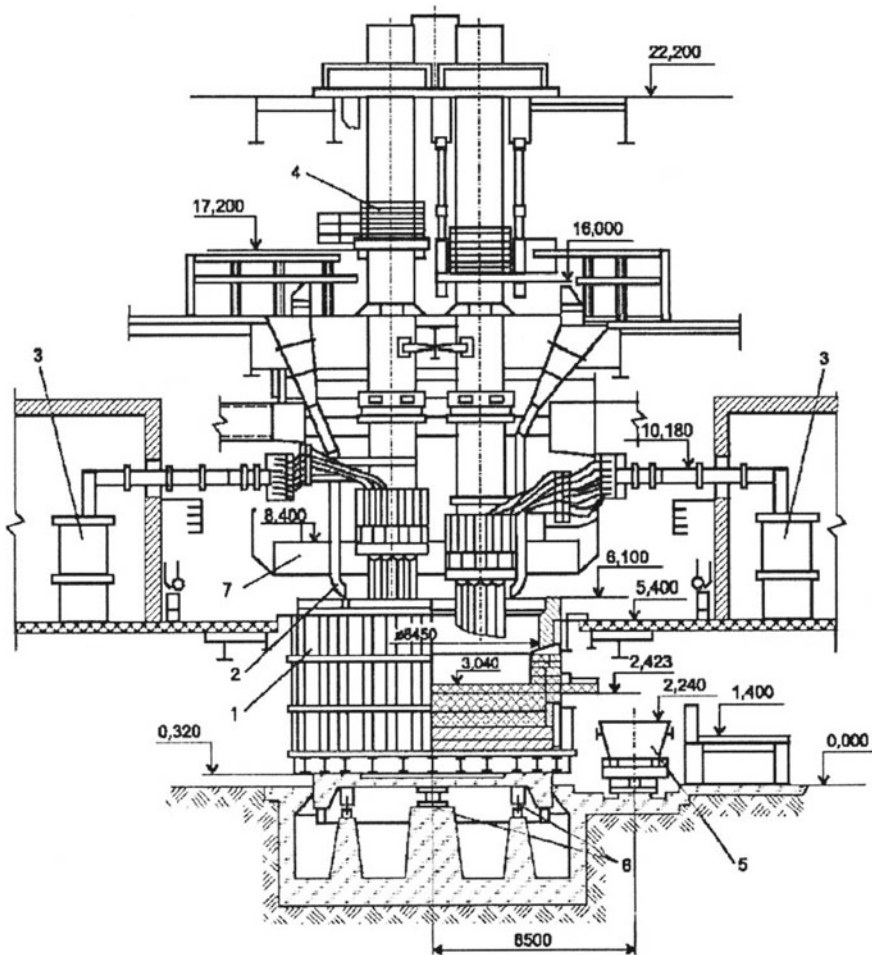


Fig. 26.2 Open ore-smelting furnace with low umbrella, 1—bath; 2—loading pipe; 3—transformer; 4—electrode bypass mechanism; 5—trolley with a bucket; 6—bath rotation mechanism; 7—arch umbrella

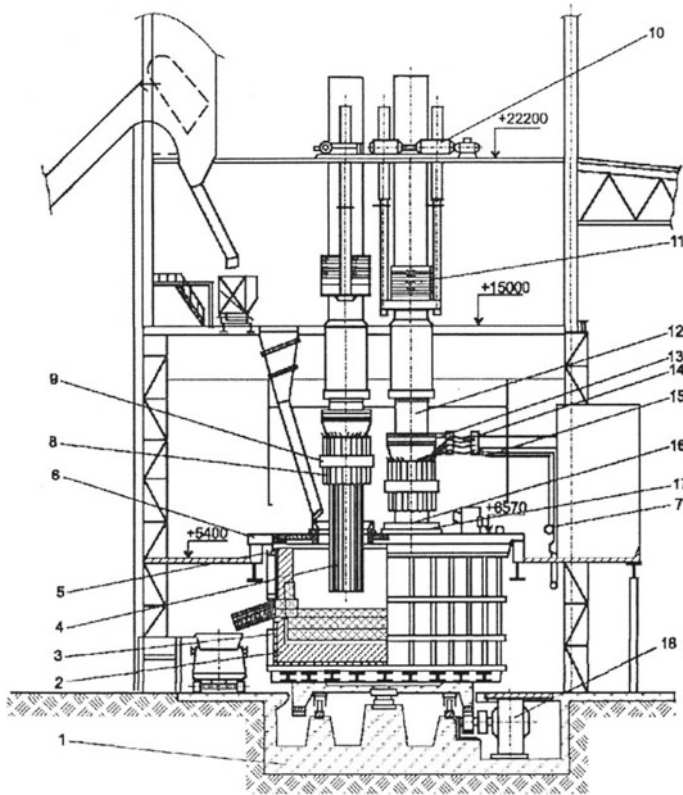


Fig. 26.3 Closed ore-smelting furnace with a capacity of 27 MV•A, 1—foundation; 2—lining; 3—furnace casing; 4—electrode; 5—sand shutter; 6—arch; 7—water cooling; 8—contact cheek; 9—pressure ring; 10—electrode lifting mechanism; 11—electrode bypass mechanism; 12—bearing cylinder; 13—traverse; 14—short network; 15—current pipes; 16—shell; 17—funnel; 18—bath rotation mechanism

movable shoe, which is suspended by traverses on the carrier cylinder. From the movable shoe, the current flows through the water-cooled copper conductive pipes to the contact cheeks, which supply power directly to the electrode (Chap. 27).

The hydraulic devices of the furnace are powered from the pump-accumulator station. The charge is loaded into the furnace bath using the loading system, which has its own design features for open, closed and sealed furnaces. An exhaust hood connected to the chimney through a gas cleaning system serves to collect and discharge the gases released from the furnace. Gases from under the roof of the furnace are sucked out by smoke exhausters and cleaned by wet gas cleaning.

Bath of Ore-smelting Furnace

The bath of a ferroalloy furnace is an internal space in which processes associated with the supply of raw materials, melting of the charge, reduction of the leading elements, the formation of ferroalloy and slag, their accumulation and separation, and

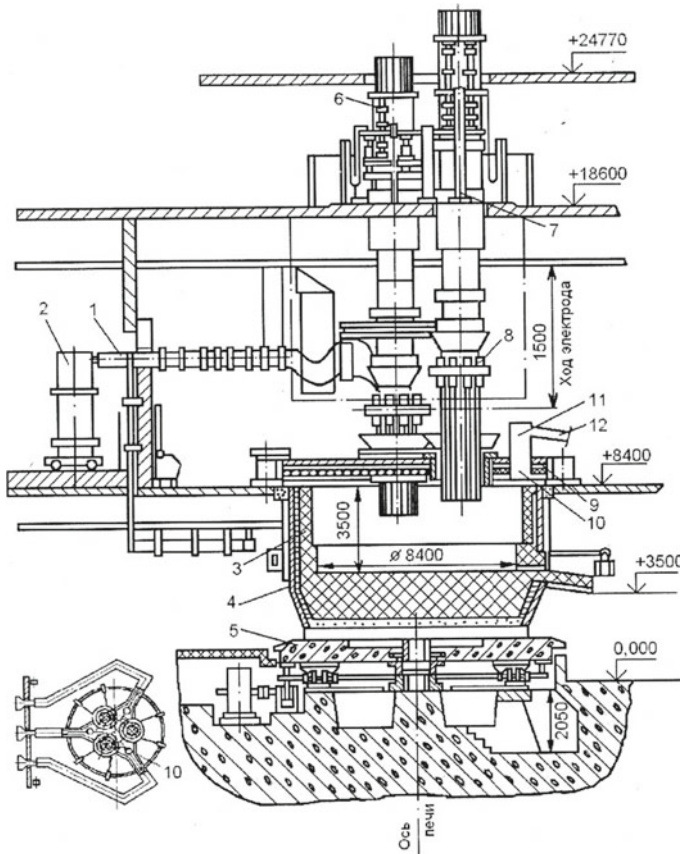


Fig. 26.4 Closed ore-smelting furnace RKZ-33M2, 1—short network; 2—transformer; 3—lining; 4—a casing; 5—rotation mechanism of the bath; 6—device for bypassing the electrodes; 7—hydraulic lift; 8—electrode holder; 9—arch; 10—openings of flues; 11—nozzle of gas vent; 12—irrigated incline duct

the release of melting products proceed. Since the processes for producing ferroalloys are realized at temperatures from 1450 to 2100 °C, the internal volume of the furnace bath is lined with refractory materials. Outside, the lining of the furnace is covered by a metal casing, which also serves to fasten and maintain the main elements of the furnace.

The design of the casing is diverse. The casing is cylindrical, oval, rectangular, cylinderconical in shape. However, there is a general requirement—the casing must be airtight to protect the lining from contact with air, to ensure the safety of the heat and electrical insulating layer. The furnace casing experiences great mechanical stresses determined by the mass of the lining, metal, slag and charge, as well as thermal loads. Therefore, the walls of the furnace casing are reinforced with horizontal and vertical stiffeners (Fig. 26.7). In many cases, the upper stiffening belt serves as a sand valve

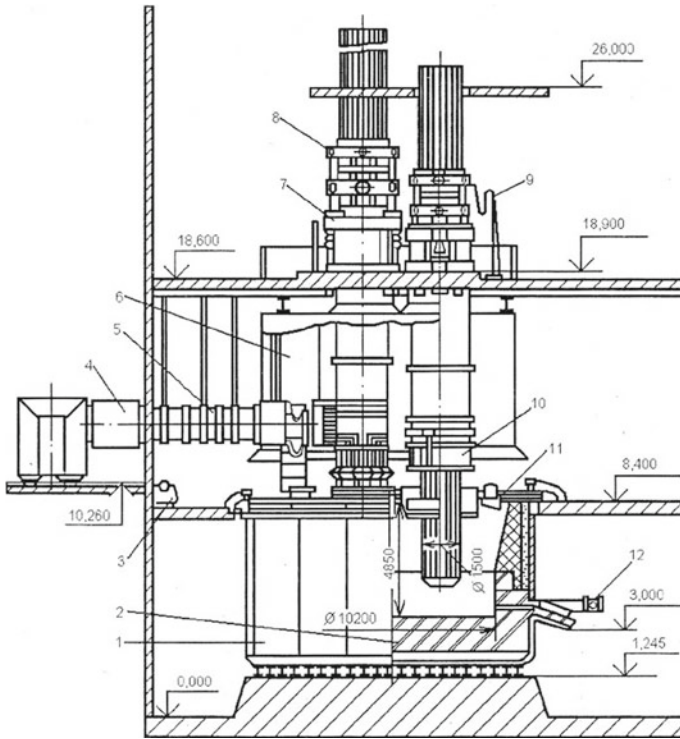


Fig. 26.5 Sealed ore-smelting furnace RKG-33M1, 1—casing of the furnace; 2—lining; 3—water cooling system; 4—compensators; 5—short network; 6—an umbrella; 7—hydraulic lift; 8—device for bypassing the electrodes; 9—hydraulic lift; 10—bearing cylinder; 11—arch; 12—installation for burning tapholes

to create a tight connection between the furnace casing and the air. The bottom of the bathtub is usually flat.

The lining of the furnace can be coal and ceramic. The hearth is the most important part of the lining, since it is constantly in contact with the metal, and sometimes slag melt. The lining of the ore-smelting furnace with a capacity of 16.5 MV•A is shown in Fig. 26.8.

Coal lining is carried out by coal blocks tightly fitted to each other. Blocks are installed on a pre-tamped layer of hearth mass; open slots are poured with resin. The lower brickwork is dry, filling the cracks between the bricks with finely ground powder of the same material as the brick. Over the entire inner surface, the casing is covered with sheet asbestos, and the gap between asbestos and brickwork is filled with sifted fireclay.

The mechanism of rotation of the bath of the ore-smelting furnace

The practice of operating round ore-smelting furnaces has shown that the rotation of the bath is advisable for smelting high-silicon ferroalloys. The mechanism of

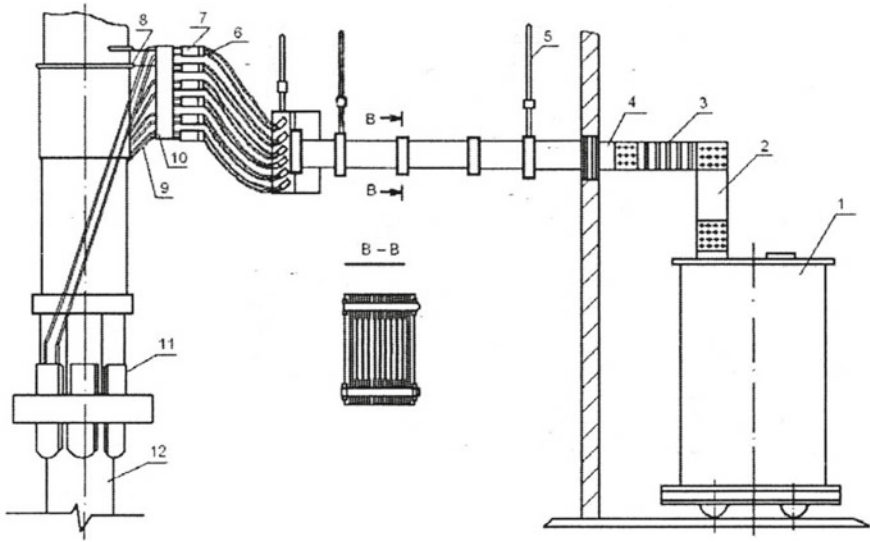


Fig. 26.6 Short network of ferroalloy electric furnace, 1—transformer; 2—output low voltage transformer; 3—compensators; 4—busbar package; 5—suspension of a short network; 6—garland; 7—movable shoe; 8—suspension; 9—current tubes; 10—traverse; 11—contact cheek; 12—electrode

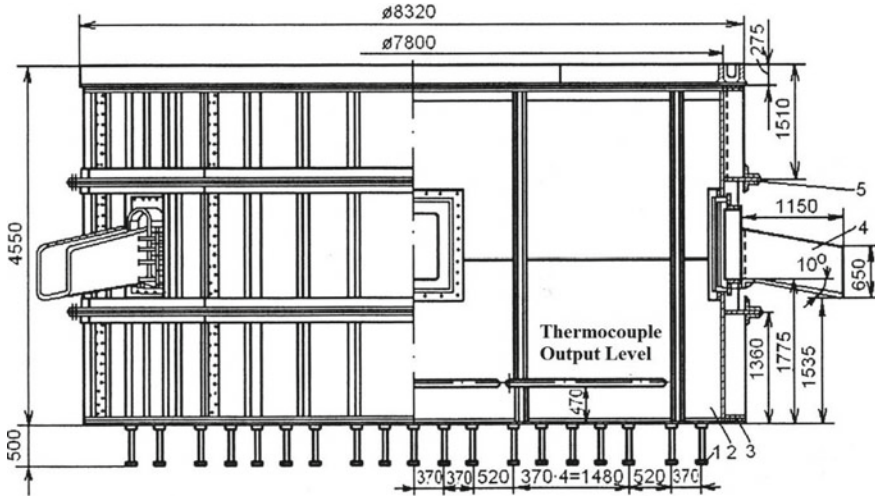


Fig. 26.7 The casing of the bath of the ore-smelting furnace with a capacity of 16.5 MV•A, 1—supporting beams; 2—a casing; 3—asbestos gasket; 4—notch; 5—stiffness belt

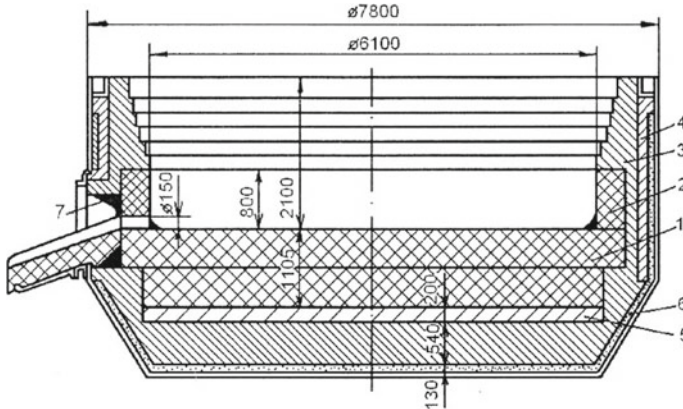


Fig. 26.8 Lining of an ore-smelting furnace with a capacity of 16.5 MV•A for smelting 45% ferrosilicon. 1—coal blocks with a cross section of 550 mm × 550 mm; 2—coal blocks with a size of 400 mm × 400 mm × 800 mm; 3—brickwork from refractory fireclay bricks; 4—a layer of thermal insulation from lightweight fireclay; 5—brickwork layer from magnesite bricks; 6—filling of fireclay; 7—rammed mass, consisting from a mixture of fireclay with carborundum on liquid glass

rotation of the furnace bath 16.5 MV•A for smelting high-silicon ferrosilicon is shown in Fig. 26.9.

Initially, it was assumed that the rotation of the furnace bath will ensure uniform wear of the lining of the walls and the hearth of the furnace, loosening the mixture and preventing its sintering on the top, eliminating local overheating and intensifying the process as a whole. However, the parallel improvement of other components of the furnace, its lining, changing the loading mode and other measures allowed to abandon the use of the rotation mechanism of the furnace bath in the smelting of almost all alloys obtained by the carbonthermic process, with the exception of ferrosilicon containing more than 70% silicon, where the gas permeability of the top and sintering of the charge have a significant impact on the technological course of the smelting and its efficiency.

Arch of the ore-smelting furnace

The furnace roof is designed to shelter the top of the furnace, reduce heat loss, reduce heat stress at the working site and improve working conditions, capture and evacuation of gases generated in the recovery processes, as well as improve the service of electrode and charge equipment. The operating experience of arch-sealed furnaces has shown their high efficiency; therefore, currently, smelting furnaces are closed by an arch, with the exception of furnaces smelting high-silicon alloys containing more than 70% silicon.

Sectional metal or concrete arches are used (flat, arched, domed, water-cooled or non-water-cooled). The most widespread are flat arches from metal water-cooled sections (Fig. 26.10).

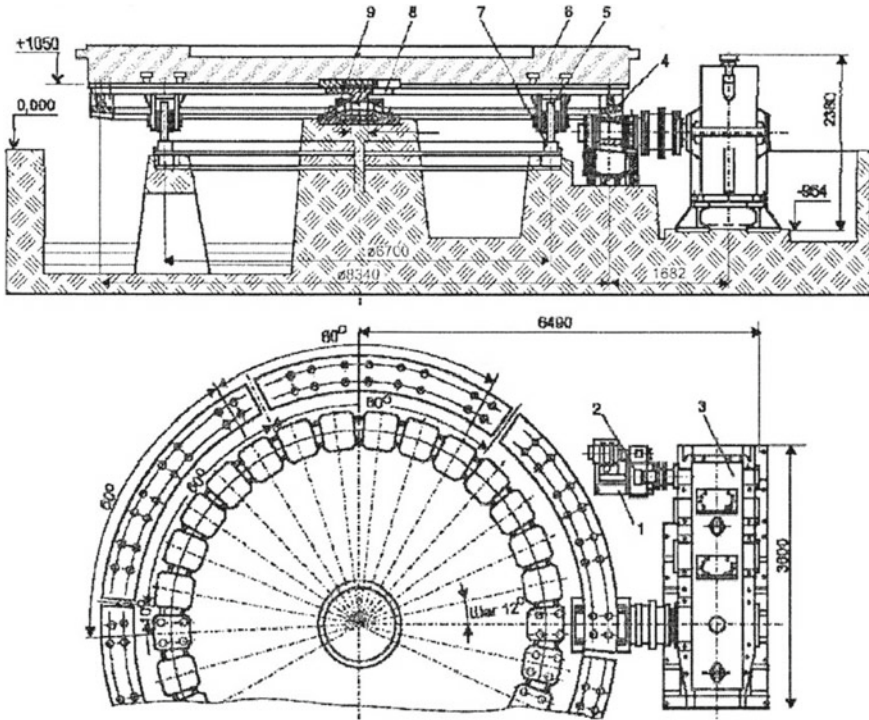


Fig. 26.9 Device for rotating the bathtub of the furnace, 1, 3—gear; 2—electric motor; 4—a gear wheel; 5—track roller; 6—concrete slab; 7—circular rail; 8—supporting pin; 9—nozzle

The arch consists of ten water-cooled sections—nine peripheral and one central, outer ring, at the bottom of which there is a knife that enters the annular channel of the furnace casing, filled with sand, which prevents air from entering the furnace space at the junction of the arch—casing of the furnace. To protect against high temperatures and aggressive gases, the metal arch below has a protective layer 50 mm thick of refractory concrete, which is reinforced with metal hooks welded from the bottom to the sections. As a filler of the refractory layer, high-alumina cement, chamotte, magnesite powder and slags of smelting low-carbon ferrochromium with the addition of a binder of liquid glass and sodium silicofluoride as a hardener are used. The top of the arch is covered with refractory bricks or poured with concrete with a layer of 50 mm to prevent a short circuit between sections through dust, mixture or tools. Concrete sections with high-alumina cement and high-temperature slag without water cooling are sometimes used.

To enter the electrodes into the furnace in the arc, there are three holes formed by the peripheral and central sections into which electrode funnels with shells are mounted, which serve to supply charge to the furnace along the gap formed between the electrode and the funnel. The size of the gap along the radius is selected by at least 4–5 values of the maximum fraction of the charge component. Funnels of several

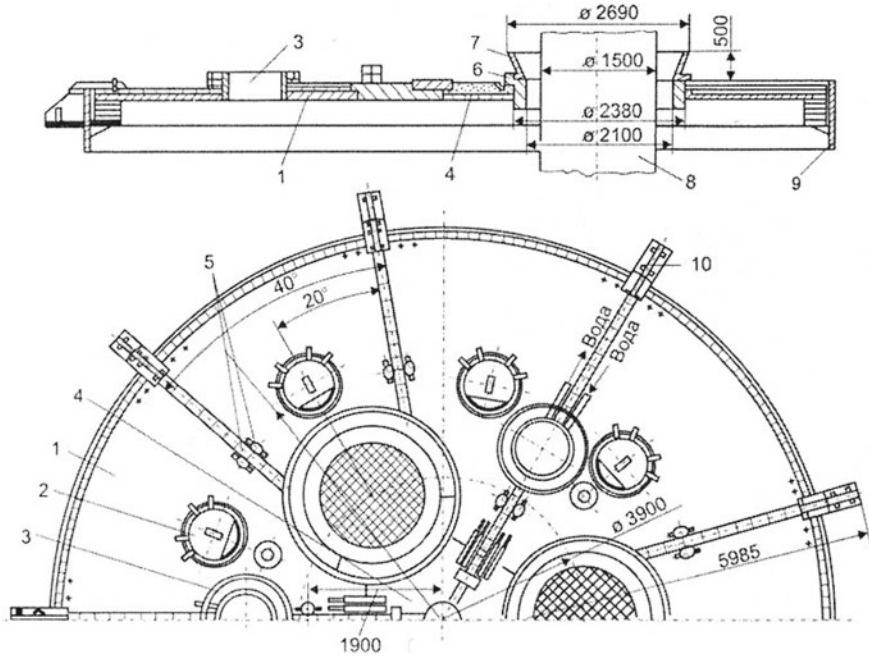


Fig. 26.10 Water-cooled arch of the furnace RKZ-33M2, 1—peripheral section; 2—explosive valve; 3—gas extraction point; 4—central section; 5—suspension of the arch; 6—funnel; 7—shell; 8—electrode; 9—ring; 10—support bracket

types are used: water-cooled copper made of refractory concrete and slags of the current production, cooled or not. To prevent accidental emissions of the charge and gases in case of violation of the technological mode of melting in closed furnaces, explosion valves are installed on the roof.

Closed furnaces are much more environmentally efficient compared to open furnaces; however, the operation of these furnaces is associated with significant emissions of the charge and gases from under the arch and the release of gas through the charge in the loading funnels. Therefore, further improvement of the design of furnaces goes along the path of their sealing.

Provision of furnaces with a charge

One of the most important stages in the production of ferroalloys by a carbothermic method by a continuous process is the preparation, dosing and feeding of charge materials into an ore-smelting furnace. Three types of preparation and feeding systems for the charge in the furnace can be distinguished:

- (1) accumulation of supplied materials in the stock of charge materials, feeding them to the hoppers of the smelting shop, periodic dosing directly in the smelting shop to each furnace separately and distribution into the pockets of the furnace;
- (2) accumulation of prepared charge materials and their periodic dosage into skips at the charge warehouse, and feeding into the melting shop is carried out using

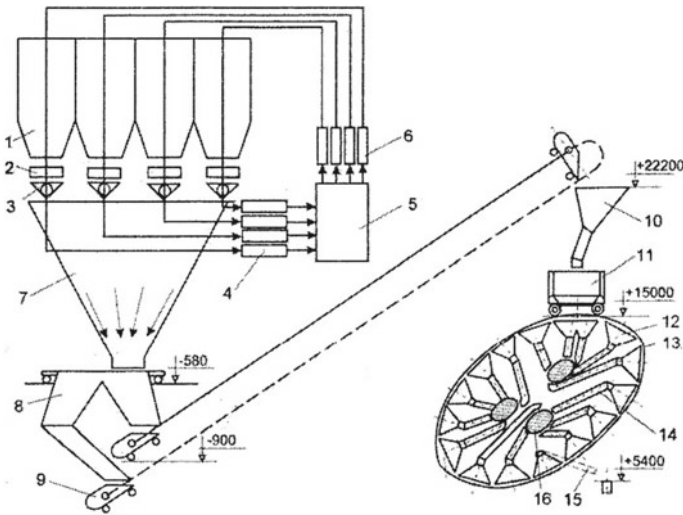


Fig. 26.11 The scheme of dosing and feeding the mixture into the furnace, 1—feed hopper; 2—electrovibration feeder; 3—strain gauge weight sensor; 4—digital weight meter; 5—software control device; 6—power unit; 7—mixing hopper; 8—guide transfer trolley; 9—skip; 10—receiving hopper of the shop; 11—distribution loading trolley; 12—stove pocket; 13—furnace top; 14—pipe-chute to the funnel; 15—pipe-chute to the site; 16—electrode with a funnel

two skip hoists along parallel lines to each furnace separately and then the charge materials are distributed over furnace pockets (Fig. 26.11); the advantage of this method is the compactness of the entire system, the close location of the charge warehouse to the melting body, the possibility of individual dosage for each furnace and the speed of adjusting the composition of the charge;

- (3) the accumulation of prepared materials in a special batching unit, and then their continuous dosage on the conveyor belts, feeding a metered charge to the intermediate hopper and distributing the metered charge over two furnaces with the shuttle reversing conveyor through the furnace pockets (Fig. 26.12).

Furnace pockets are intermediate containers that provide a supply of charge before loading it into the tubes (closed or open furnaces) or into the hopper of the filling machine (open furnaces). The scheme of loading an open furnace with charge materials using pipe-chute is shown in Fig. 26.13.

Along with the pipe-chute, the charge is loaded into an open furnace by filling machines. The filling machine FP-1 M is a self-propelled floor trolley moving along a circular rail track laid around the furnace (Fig. 26.14). The charge is loaded into the receiving hopper of the filling machine from one of the furnace pockets. From the receiving hopper, a portion of the charge with the help of a feeder enters the loading shovel, which throws the charge into the furnace under the electrodes.

Along with throw-type filling machines, a loading machine with a rotating tube is used to load the charge and process the top of open ore-smelting furnaces (Fig. 26.15). The productivity of the machine is sufficient to service one furnace with one machine.

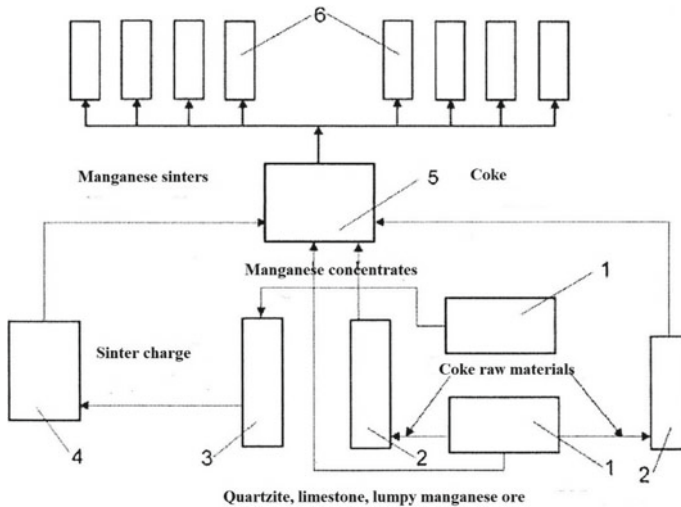


Fig. 26.12 Scheme of centralized supply of charge materials to the melting shops of the Nikopol Ferroalloy Plant, 1—raw materials warehouse; 2—building materials preparation; 3—housing charge bins; 4—sinter plant; 5—central distribution point; 6—batching departments of workshops

The mixture in the pipe moves continuously, mixes well and is poured from the end of the rotating pipe with a uniform stream. Installation at the end of the rotating pipe of the inclined trough allows you to pour the mixture in the form of a cone around the electrodes. The machine has good maneuverability, which allows you to properly fill the charge throughout the top.

26.2 Refining Electric Furnaces

Refining furnaces are designed to produce refined ferroalloys (medium-carbon and low-carbon ferromanganese, metallic manganese, medium-carbon and low-carbon ferrochromium) using a silicothermic process. A general view of refining furnaces with a capacity of 2.5 and 3.5 MV•A is shown in Figs. 26.16 and 26.17, respectively.

Refining furnaces—open type, the mixture is loaded with pipe-chutes and loading machines, furnace gases are caught by an umbrella. The furnaces are equipped with an inclined and rotating bathtub of circular cross section and three electrodes located at the vertices of an equilateral triangle. Furnaces operate in a batch mode with a periodic charge loading (for each heat) and a complete release of the products of each heat.

The furnace bath is rotated by an electromechanical drive and rollers mounted on four supporting tables. The tilt of the bath to drain the alloy is carried out by two hydraulic cylinders. The electrodes are electromechanical; electrode holders are spring-pneumatic. The electrode holder shaft is mounted on a separate foundation

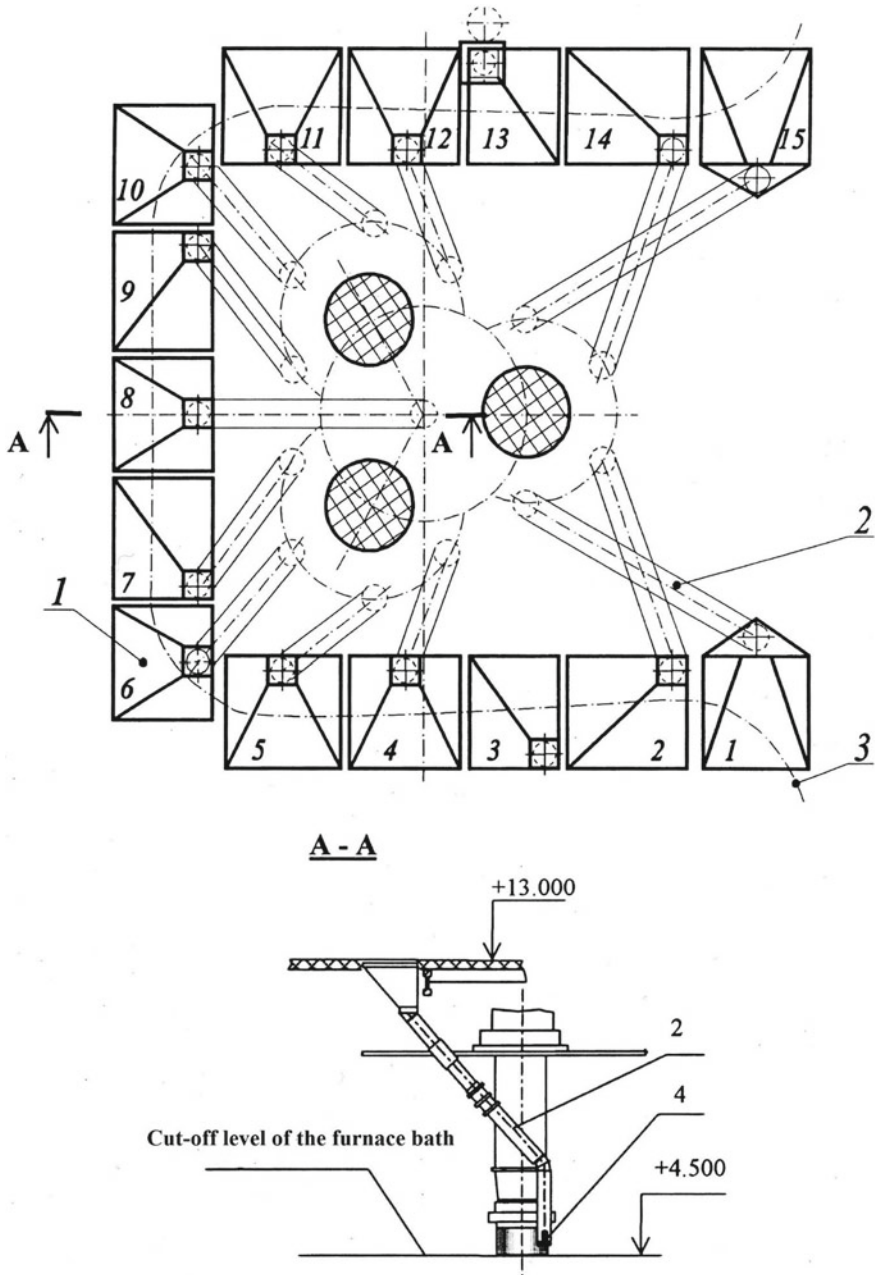


Fig. 26.13 Scheme of loading an open furnace with pipe-chute, 1—furnace pockets; 2—water-cooled shaft tubes; 3—transfer mono-rail trolleys; 4—pipe-chute protection

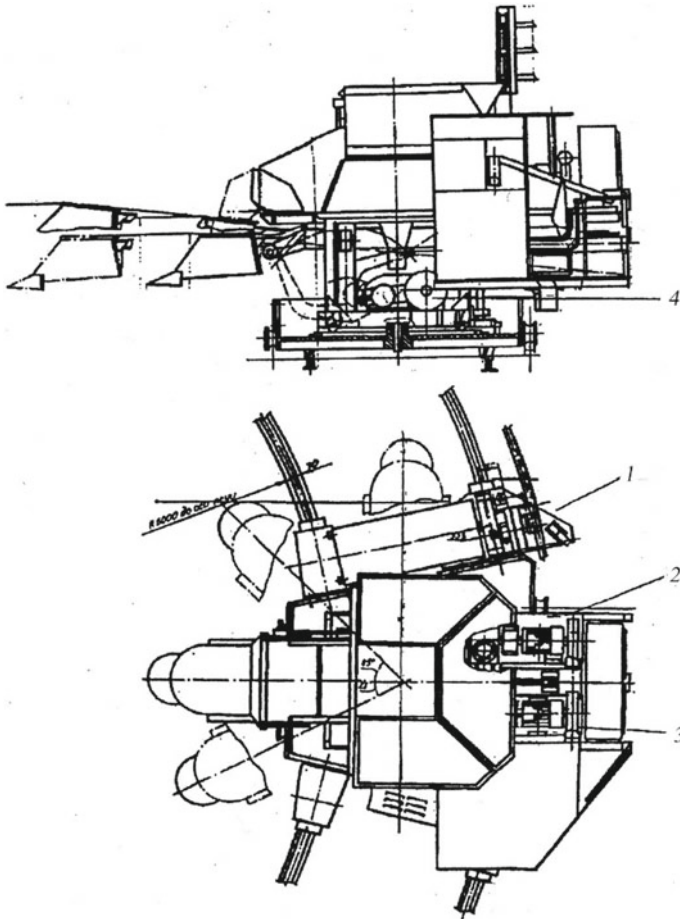


Fig. 26.14 Filling machine FP-1 M, 1—movement mechanism; 2—rotation mechanism; 3—loading mechanism; 4—throw mechanism

and does not tilt with the bathtub. The furnace lining is magnesite. The melting process is conducted with open arcs.

The main components of the refining furnace: casing, lining, bath rotation mechanism, bath tilt mechanism, hydraulic drive system, shafts for moving the electrode holders, electrode moving mechanism, electrode holders, short network, water cooling system, air duct.

For smelting metal manganese at the Zaporizhzhya Ferroalloy Plant, a refining electric furnace with a capacity of 7 MV•A (Fig. 26.18) is used, which operates in a unit with a furnace smelting low-phosphorous slag.

Converted liquid low-phosphorous slag (the main manganese-containing component) in liquid form is poured into a bathtub through a special trough. The durability

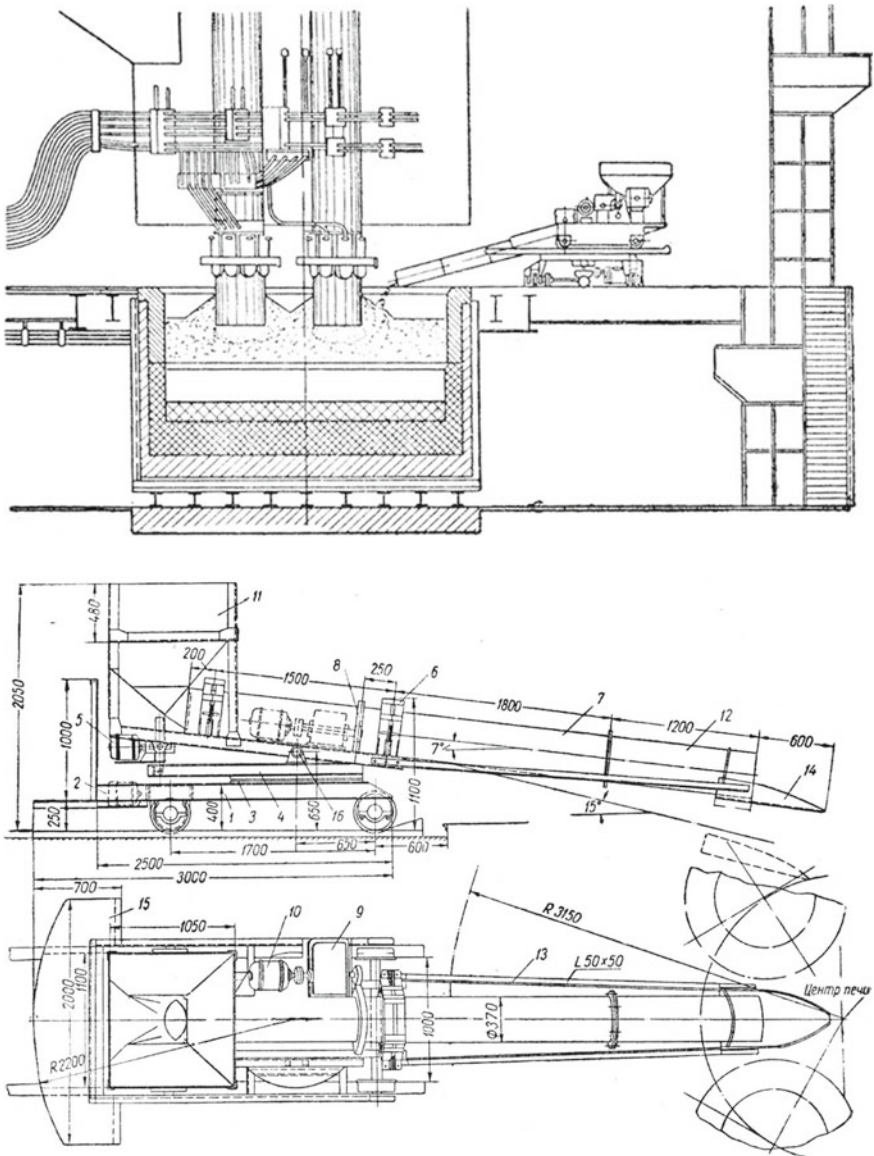


Fig. 26.15 Rotating tube-loading machine, 1—trolley frame; 2—electric motor and gear reducer; 3—ball bearing; 4—rotary frame; 5—electric motor and pipe swing mechanism; 6—pipe support; 7—pipes; 8—gear transmission; 9—gearbox rotation mechanism; 10—electric motor; 11—hopper; 12—replaceable end of the pipe; 13—frame for mounting the tray; 14—tray; 15—a platform with a railing; 16—axis of swing

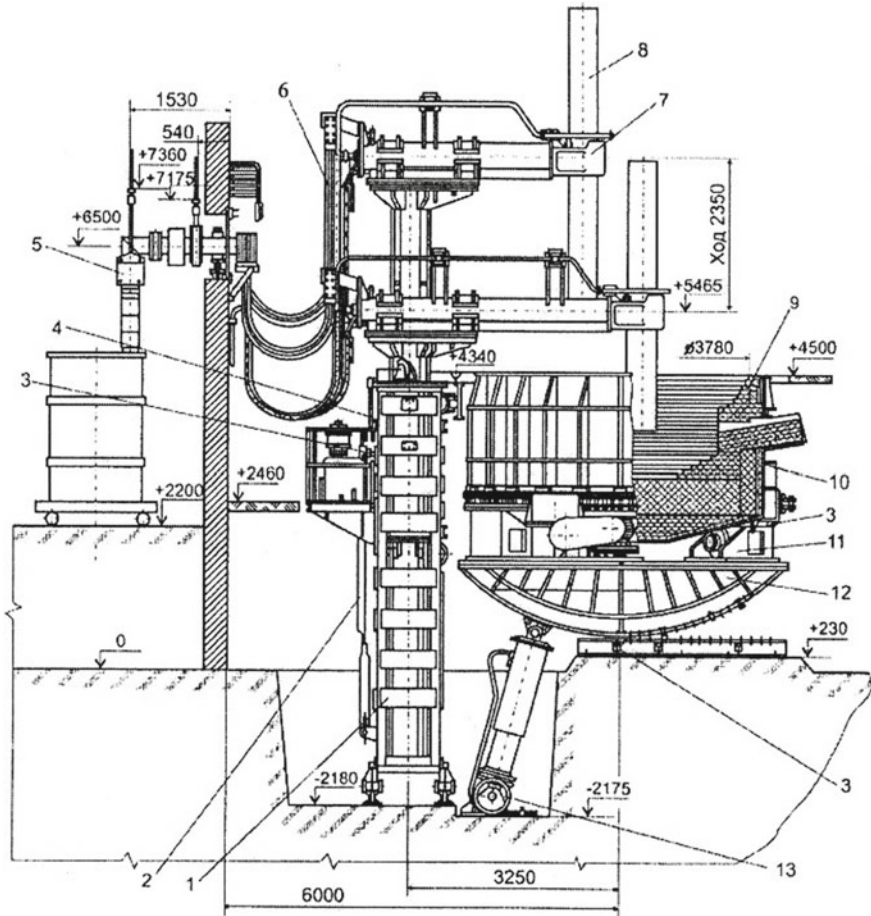


Fig. 26.16 Refining electric furnace RKO-2.5N2, 1—shaft of the mechanism for moving the electrode; 2—mechanism for moving the electrode; 3—final switch; 4—centralized lubrication; 5—short network; 6—current lead; 7—electrode holder; 8—electrode; 9—lining; 10—a casing; 11—the mechanism of rotation of the bath; 12—tilt mechanism; 13—hydraulic drive system; 14—air supply; 15—water cooling system

of the magnesite lining is 40–50 days; the duration of the bath re-lining is 3–6 days. In order to increase the productivity of the furnace unit, the refining of the furnace is carried out at a special site in the casting span. To do this, the furnace is installed on a special trolley with a carrying capacity of 150 tons, which is constantly located under the furnace. The rolling out of the furnace bath is done by a winch. In the casting span, the furnace bathtub is removed by the crane from the cradle remaining on the trolley and fed to the re-lining section, The casing of the furnace, lined earlier in this section, is mounted by a crane on a cradle located on a trolley that rolls into the furnace span

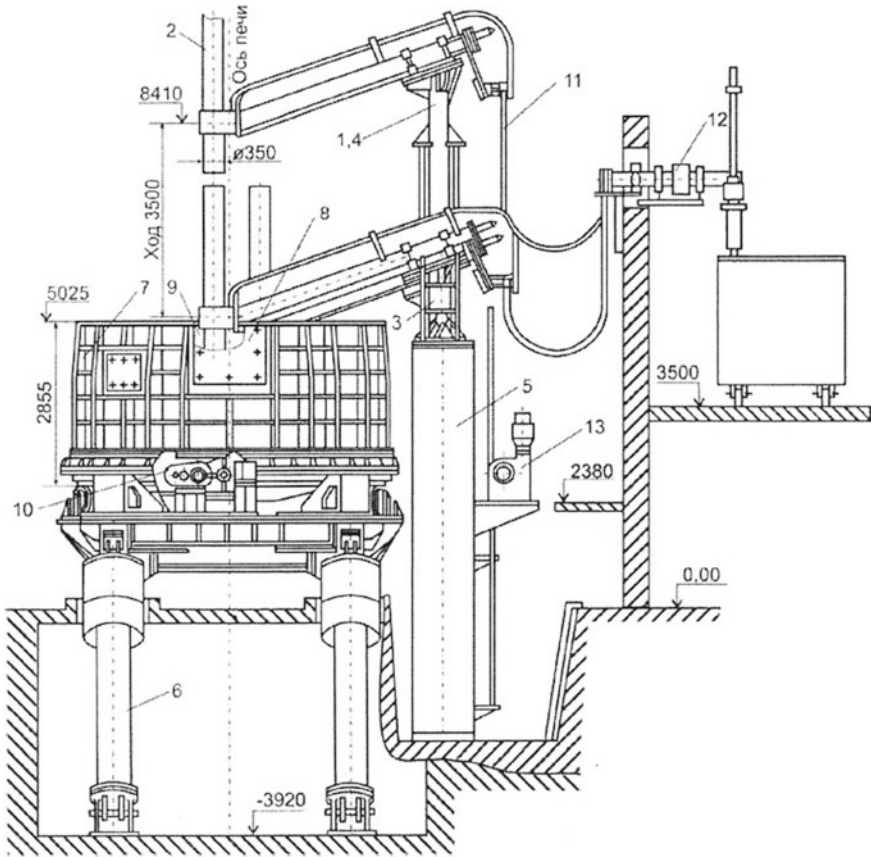


Fig. 26.17 Refining furnace RKO-3,5, 1, 3, 4—columns of the mechanism for moving the electrodes; 2—electrode; 5—shaft columns; 6—mechanism of furnace tilt; 7—a casing; 8—notch; 9—lining; 10—the mechanism of rotation of the bath; 11—flexible cable; 12—short network; 13—drive mechanism for moving the electrodes

to prepare for smelting. Such a bath replacement system can reduce downtime from 72–144 to 8–12 h and thereby significantly increase furnace productivity.

Furnace casing. The cylindrical casing with a conical bottom is welded from sheet steel and reinforced with longitudinal and transverse stiffeners. An annular metal bar is welded to the bottom, with which the casing is supported by the support rollers of the rotation mechanism. On the casing of the furnace at different heights, two notches are provided: for removing slag and discharging the metal melt.

Furnace lining. The working space of the furnace bath is lined with magnesite brick. The hearth additionally has a packed layer of magnesite powder. The heat-insulating layer of the lining is made of fireclay brick. The inner walls of the casing are lined with sheet asbestos.

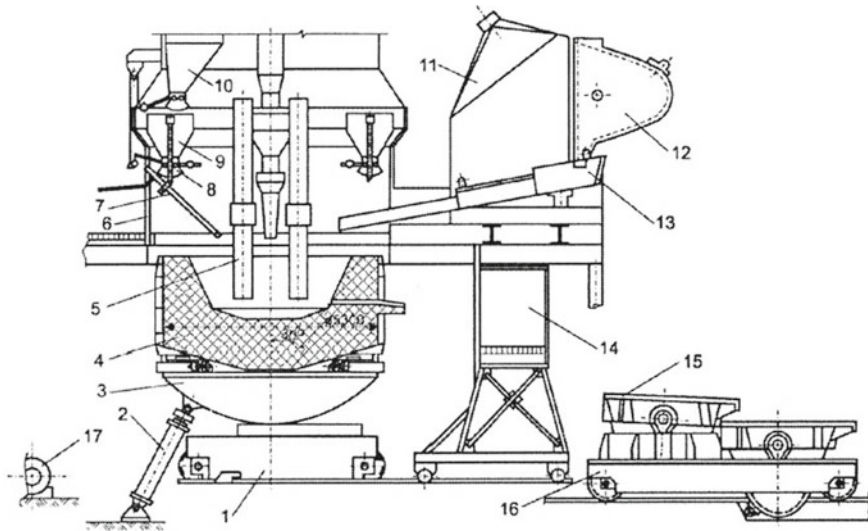


Fig. 26.18 7 MV • A refining electric furnace with draw-out bath: 1—trolley roll-out bath furnace; 2—hydraulic cylinder of the furnace tilt mechanism; 3—cradle; 4—furnace bath; 5—graphite electrodes; 6—curtains with exhaust hood; 7—loading tray; 8—shutter; 9—intermediate hopper; 10—furnace bunker; 11—a chamber with an exhaust hood; 12—ladle with low-phosphorus slag; 13—jellied trench; 14—trolley of the furnace platform; 15—metal-receiving bucket; 16—bucket trolley; 17—winch

The mechanism of rotation of the bath. The mechanism serves to periodically rotate the furnace bath in a limited sector toward the casting span in order to provide a more complete discharge of the melt and remove slag.

The mechanism of the tilt of the bath. The mechanism tilts the furnace bath to the required angle at a certain speed. The furnace tilts toward the discharge of metal and slag and toward the work platform. In contrast to electric arc furnaces, the bath of the refining furnaces is tilted without tilting the electrode holders. For this, it is necessary to increase the stroke of the electrode holders to 3–4 m.

The shaft for moving electrodes holders. The shaft is intended for installation of an electrode holder column and its movement. It consists of a welded frame on which guide rollers of racks of electrode holders and suspension blocks of counterweights are mounted. In order to displace the electrodes relative to the hearth during its surfacing with magnesite, the shaft can move along the support beams in one direction or another.

The mechanism for moving the electrodes. The mechanism consists of rack and pinion electromechanical drives and suspension of columns and balances. The movement mechanism is electromechanical or hydraulic.

Electrode holder. The electrode holder serves to supply electric current to the electrode and hold the electrode in a predetermined position without slipping between the cheeks supplying current. The electrode holder consists of a sleeve to which an electrode clip is attached via an insulating gasket. The sleeve can be attached to the

carriage, which moves along a stationary rack, or can be rigidly connected to the rack, forming a single L-shaped structure that moves all together. For refining furnaces, mechanical electrode clamps of a tick-borne or spring-hydraulic type are used.

Short network. The short network serves to supply electric current from the electric furnace transformer to the electrode holders and consists of suspended packs of copper buses, flexible current-carrying wires and compensators made of flexible copper tapes.

Water cooling system. The system provides water inlet and outlet from current-carrying pipes, bodies and hoses of electrode holders.

Air duct. The air duct is intended for supplying compressed air to the pneumatic cylinders of the electrode holders and for blowing the electrodes and electrode holder housings when the electrodes are bypassed.

Chapter 27

Self-baking Electrodes



At the end of the nineteenth century, the production of coal and graphite electrodes was started according to the Acheson method. A method of manufacturing continuous self-baking electrodes, the most widely used in ferroalloy and other ore-smelting furnaces, was developed in 1918 by the Norwegian engineer Söderberg.

Self-baking electrodes are made directly on operating ferroalloy furnaces, and their firing modes and linear consumption are strictly related to the technological parameters of smelting a particular ferroalloy. The working ends of the self-baking electrodes are constantly immersed in the mixture (in the working crucibles of the furnace bath); therefore, the carbon of the electrodes, like the coke of the mixture, is involved in the recovery processes. The electrodes are continuously consumed, and to maintain a given distance from the ends of the electrodes to the bottom of the furnace, they must be *slipped* and build up.

27.1 Self-baking Electrodes Design

The self-baking electrode consists of a steel casing and carbon electrode mass. The electrode casing is a cylinder of round (diameter up to 2000 mm) or rectangular (3200 × 850 mm) section, made of sheet steel, up to 4.5 mm thick, depending on the diameter (section) of the electrode. The casing must have sufficiently high mechanical properties at moderate and elevated temperatures, a relatively high electrical conductivity and thermal conductivity, good oxidation resistance in gaseous media at elevated temperatures. The material of the casing should not be a source of harmful impurities and should not be expensive. These requirements are met by carbon steel. The electrode mass loaded into the casing up to 300–400 °C does not lead to its carburization. Above 1000–1100 °C, a noticeable carburization of the steel casing occurs, leading to a change in its physical and mechanical properties.

In existing furnaces, the electrode casing has a height of 10–15 m. It is formed from welded Sections 1.4–1.6 m high. The casing has ribs welded to the cylindrical shell along the generatrix. The width of the ribs depends on the diameter of the casing. Holes with a diameter of 100–150 mm are punched out in the ribs, designed to ensure adhesion of the casing to the calcined electrode mass.

The mechanical equipment of self-baking electrodes includes: a device for suspending electrodes, an electrical contact assembly, a mechanism for moving electrodes, a mechanism for slipping electrodes relative to a contact assembly, electrodes cooling and blowing system.

A device for suspension and bypass of electrodes is called an electrode holder. Two types of electrode holders are used. The device of the first type is free hanging; all ore-smelting ferroalloy furnaces are equipped with it (Fig. 27.1). The device of the second type is cantilever, and it is used on refining furnaces. These furnaces typically use graphite electrodes.

In modern furnaces, the self-baking electrode is held by the electrode slipping mechanism, which is attached to the upper ring of the carrier cylinder. For the electrode slipping, a spring-hydraulic mechanism is used (Fig. 27.2).

The contact node performs the function of supplying current to the electrode. It consists of contact cheeks, a pressure ring and a mechanism for pressing the cheeks to the electrode. The electrocontact assembly is suspended from the lower ring of the carrier cylinder. The high current-loading of the cheeks, as well as the proximity of the location of this site to the furnace top, determines the difficult operating conditions. A large current flows through the contact cheeks (in the electrode with a diameter of 2000 mm, the working current reaches 150 kA), so the cheeks and pressure ring are cooled by water.

The system of blowing electrodes with air, designed to control the temperature regime of firing electrodes, includes fans, ducts and mechanisms for regulating airflow. Air is supplied into the annular gap between the electrode casing and the bearing cylinder (Fig. 27.3).

27.2 Electrode Mass

The requirements for the quality of the electrode mass are given below:

Grade	A	B	C
Ash content, %	8	9	6
Specific electrical resistivity, mOhm·m (no more)	90	150	80
Temporary resistance, MPa (no less)	1.47	1.47	1.76
Fluidity factor, relative units	2.	2.8	2.3

To obtain the electrode mass, carbon-containing materials are used: anthracite, thermoanthracite, blast furnace coke, foundry coke and binder—coal tar pitch. Along

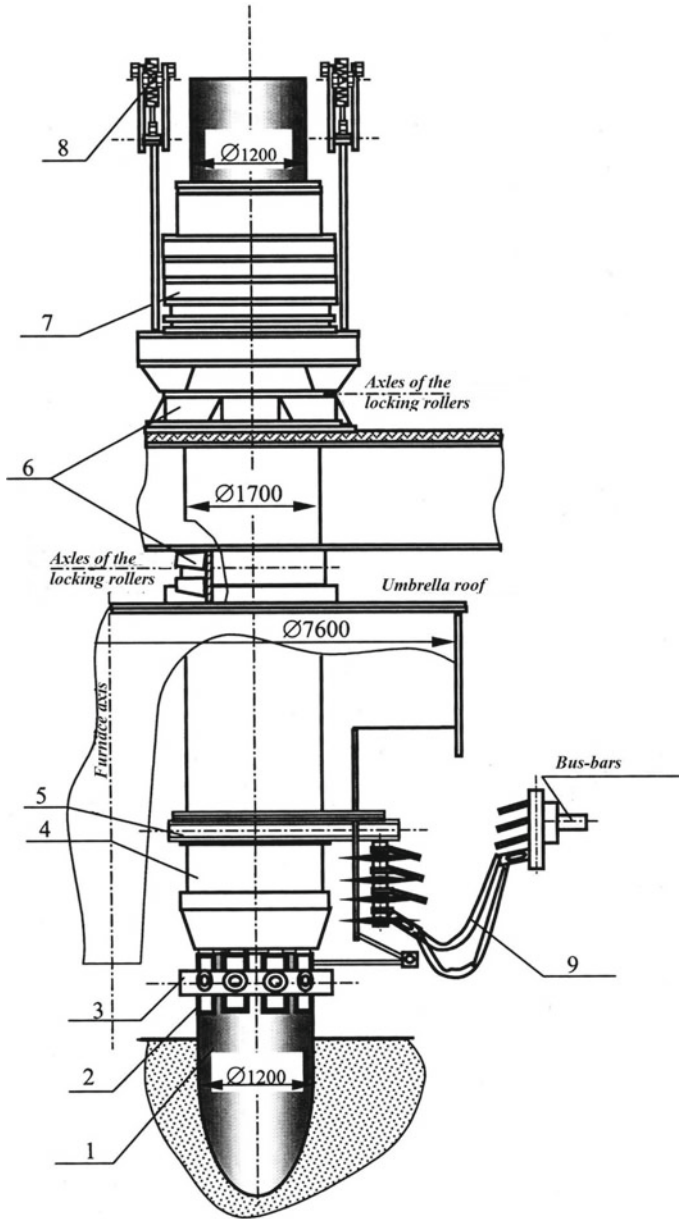


Fig. 27.1 Electrode holder, 1—electrode; 2—contact cheeks; 3—pressure ring of the electrode holder; 4—suspension casing; 5—traverse current lead; 6—upper and lower rings of fixation of the electrode; 7—pneumatic slipping; 8—electrode suspension; 9—current supply

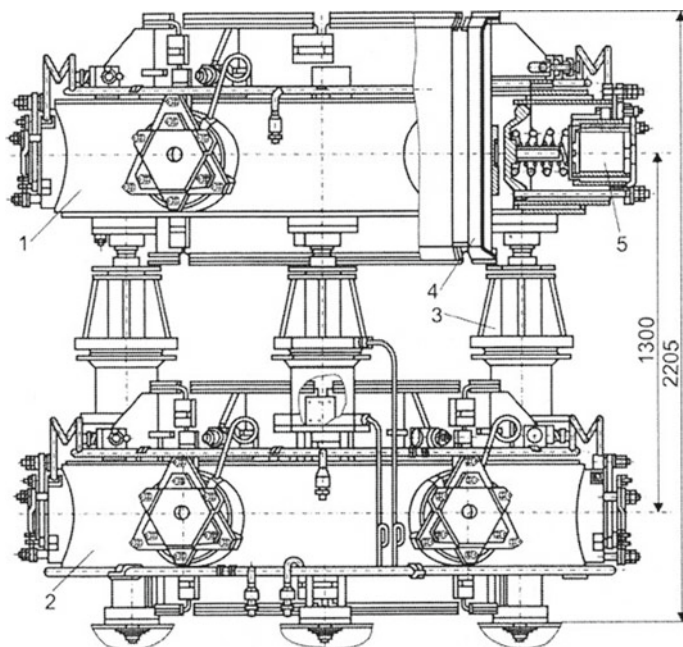


Fig. 27.2 Spring-hydraulic clamp for bypass round electrodes, 1, 2—ring; 3—hydraulic lift; 4—cheek; 5—plunger

with these materials, natural graphite, silicon carbide, graphite waste from related industries, anthracene oil, etc., can also be used. The required quality of the electrode mass can be ensured by strict adherence to the formulation, including normalized starting materials, their granulometric composition and proportion of ingredients. The formulation of the electrode mass, most often used in ferroalloy plants in the workshops of the electrode mass, is given in Table 27.1.

The production of electrode mass is organized at ferroalloy and electrode plants in specialized workshops. In the technological scheme, two streams of carbon-containing materials can be distinguished: solid materials (initial and recycled) and binders. To ensure the necessary properties and particle size distribution, solid materials are calcined, crushed, milled and sieved. For dehydration, binders are also heated. The prepared components of the mixture in accordance with a given mass recipe are dosed and mixed. Then, the electrode mass in the stream is vibro-compacted and formed into commodity briquettes.

Solid carbonaceous materials include anthracite (thermoanthracite), metallurgical coke and natural graphite. Anthracite is a coal of the last stage of the diagenesis of solid fossil fuels. The carbon content in anthracite is 91–97%, volatiles 2–8% and ash 5–7%. Thermoanthracite is obtained by calcining anthracite at 1250–1300 °C. Thermoanthracite is an important component of the electrode mass; self-baking electrodes made without thermoanthracite have low heat resistance. Thermal treatment

Fig. 27.3 Air distribution scheme in the self-baking cylinder electrode size 2800 × 650 mm of RPZ-63 furnace

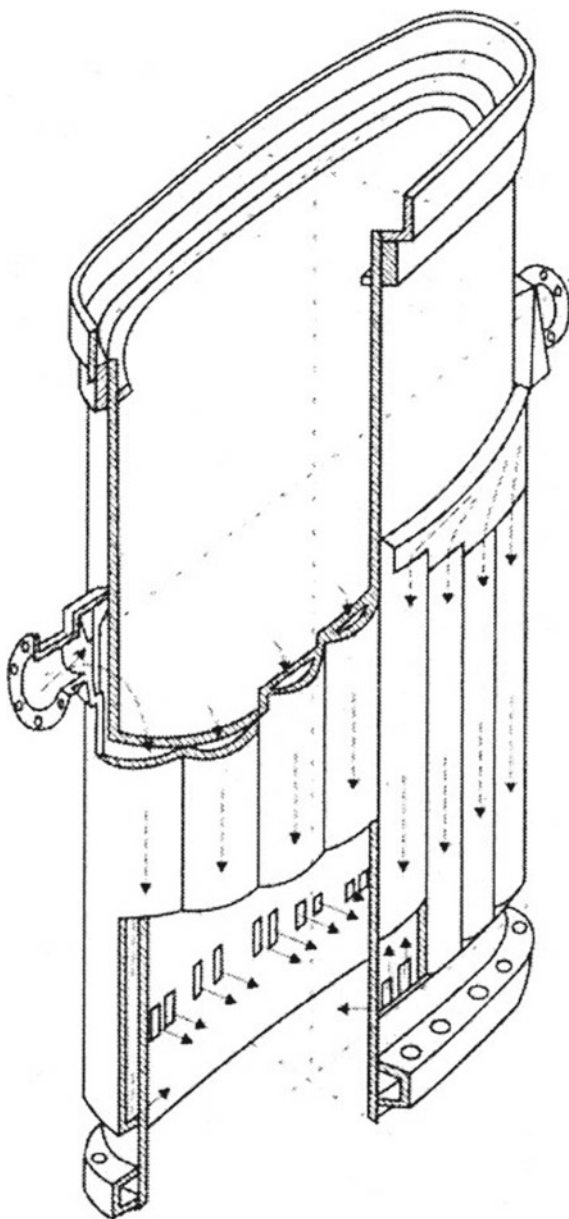


Table 27.1 Charge components, their weights and composition of the electrode mass

Component	Particles size, mm	Batch, kg	Mass fraction of components, %
Thermoanthracite	20–10	140	14
	10–4	130	13
	4–0	210	21
Coke (with grinding)	4–0	320	32
Coal pitch	–	200	20

of anthracite allows you to reduce its electrical resistivity and increase density. With the gradual heating of anthracite to 1250–1300 °C, external moisture is released (up to 105 °C), adsorbed moisture is distilled off (up to 300 °C), shrinkage, degassing, pyrolysis of hydrocarbons and decomposition of sulfur compounds occur. The most intense volatiles are released in the range of 870–970°C.

There are three types of metallurgical coke—coal coke (blast furnace, foundry), petroleum coke and pitch coke. Coal coke is produced at coke plants by coking of batch consisting of coal and, first of all, coking coals. Coke, along with anthracite, is the main component of the charge for the electrode mass. Blast furnace coke should comply with the following indicators: mass fraction of sulfur—average 1.8%, marginal 2.0%; ash content—average $\leq 9.5\%$, marginal $\leq 10.5\%$; mass fraction of working moisture—not more than 4.0%. Coal coke is also subjected to preliminary calcination at 1250–1300 °C to remove moisture and volatile substances.

Petroleum coke in the composition of the mixture to obtain the electrode mass is currently not used. It is the main component of the charge for the production of graphitized electrodes. Elemental composition, %: 90–97 C; 1.2–5 H; 0.5–1.0 S. Ash content does not exceed 0.5%. Petroleum coke is used in the production of crystalline silicon and boron carbide.

Pitch coke, like petroleum coke, is not part of the electrode mass. However, the preparation methods and its properties are of great interest for the practice of forming self-baking electrodes, since the composition of the electrode mass includes coal tar pitch as a binder, which is the feedstock for production of pitch coke at coke plants. Knowledge of the main features of the formation of solid coke in the production of pitch coke allows us to predict the properties of coke—a binder for roasting the electrode mass.

Natural graphite is introduced into the electrode mass to reduce the electrical resistivity, increase the thermal conductivity of the baked electrode. Due to the deficiency, natural graphite is used in small quantities in the electrode mass only for electrodes of large cross section.

The binder in the composition of the electrode mass should have a number of properties: soften at 60–70 °C, have the necessary complex of surface properties (surface tension, wetting), etc. The coking product of the binder (coke binder) should have optimal porosity. It is important that the coking of the binder is accompanied by small volumetric changes, and the coke residue can be well graphitized. Most fully meets these requirements, the pitch obtained from coal tar, which in small quantities

Table 27.2 Physico-chemical characteristics of coal tar pitch

Parameter	A	B	C
Softening point, °C	65–70	67–73	85–90
Mass fraction of substances, %: insoluble in toluene (α -fraction) insoluble in quinoline (α_1 fraction), no more	24–28 6	25–31 8	≥ 31 12
The yield of volatiles, %	59–63	58–62	53–57
Ash content, %, no more	0.3	0.3	0.3
Mass fraction of water in pitch, %, no more: liquid solid	0.5 4.0	0.5 4.0	0.5 4.0

can also be used in a mixture with pitch as a binder. The resin is a dark viscous liquid with a specific odor. In its composition, the resin is a mixture of aromatic compounds of naphthalene, anthracene, carbazole, phenanthrene, phenol and their derivatives.

Coal tar pitch is the main type of binder in the production of electrode mass and electrode products, the requirements for the quality of the pitch are given in Table 27.2.

The pitch of grades A and B is called medium, and grade C is called high-temperature. For the manufacture of the electrode mass, medium-temperature pitch is used. It is obtained at coke plants using the method of heat treatment of the original coal tar pitch with air supply for polycondensation of the substances contained in it with dehydrogenated oxygen. At the same time, the content of the α_2 fraction in the pitch, which has high ductility and sintering ability, increases. The necessary group composition of the pitch can also be achieved by heating it with the supply of water vapor.

In practice of the production of electrode mass, to increase its fluidity, anthracene oil is sometimes used, which is a complex mixture of high-boiling aromatic compounds (phenanthrene, anthracene, carbazole, naphthalene, etc.). The flash point of anthracene oil is 100–110 °C, ignition 145–150 °C, spontaneous combustion 530 °C; explosive temperature limits of 100 and 145 °C.

27.3 Electrode Mass Production Technology

The technological scheme for the production of electrode mass (Fig. 27.4) includes the following stages: (1) reception and storage of solid carbon-containing materials and binders; (2) pre-crushing of coke, thermoanthracite and anthracite (before calcination); (3) heat treatment (calcination) of thermoanthracite, anthracite, coke and other carbon-containing materials; (4) crushing (grinding) and sieving of heat-treated materials; (5) grinding and sieving of thermoanthracite and coke; (6) dosing of charge components in accordance with the formulation of the mass; (7) mixing solid

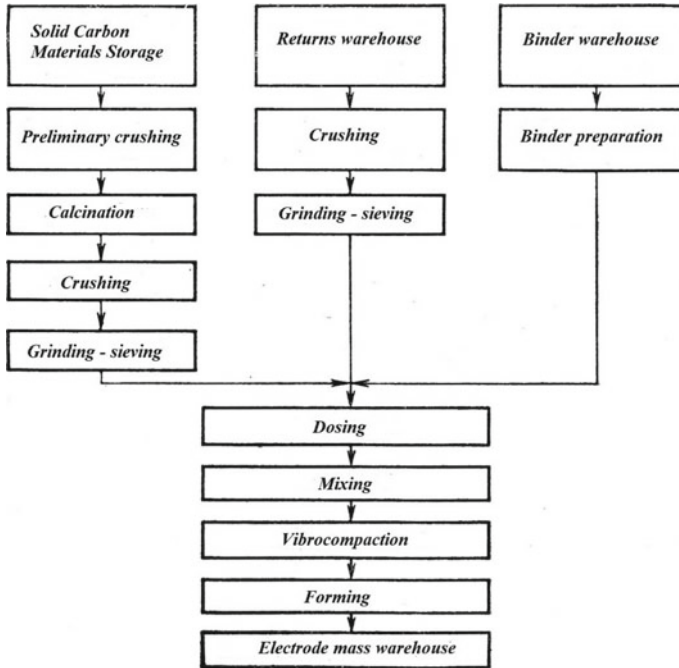


Fig. 27.4 Technological scheme of the production of electrode mass

carbonaceous materials with binders; (8) forming the electrode mass; (9) product quality control. The main technological equipment of the electrode mass workshop is shown in Fig. 27.5.

27.4 The Processes Occurring During Firing of the Electrode Mass

Blocks of finished electrode mass are periodically loaded into the casing of the electrodes. When the electrode mass is fired in the casing, volatiles are released and pyrolyzed (decomposed) with the deposition of free carbon electrode in the pores of the carbon block, which makes it less porous. Free carbon increases the strength of the electrode and reduces its electrical resistance.

In the entire temperature range of the formation and operation of the self-baking electrode, graphitization of thermoanthracite, coke, and free carbon is thermodynamically probable. Kinetically, this process is more dependent on temperature than on time. Studies of the effect of temperature on the degree of graphitization of thermoanthracite showed that with increasing temperature from 1200 to 2600 °C the interplanar spacing decreases and the size of crystallites of thermoanthracite increases.

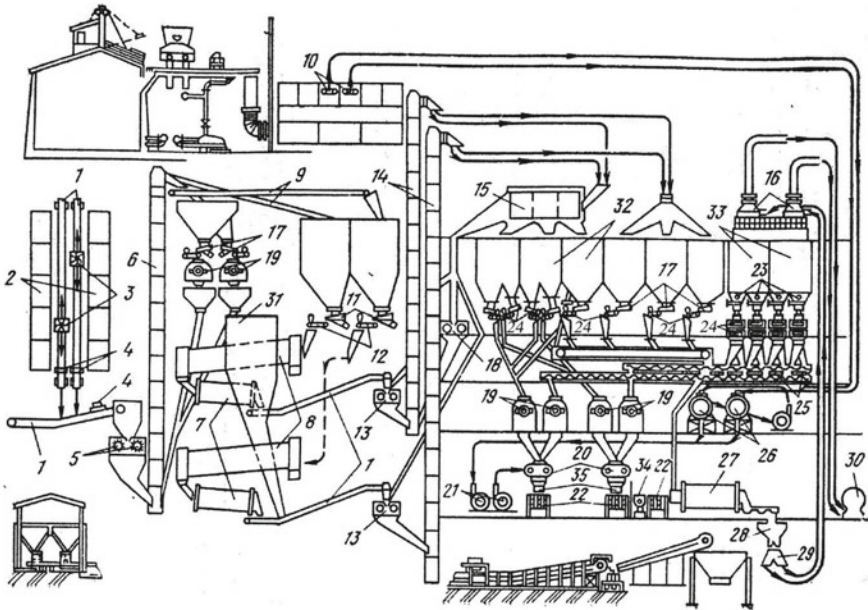


Fig. 27.5 Technological equipment of the electrode mass workshop, 1—belt conveyor; 2—coke and thermoanthracite bunker; 3—movable paddle feeders; 4—magnetic separators; 5—twin roll crusher; 6—elevator; 7, 8—rotary calcining furnaces; 9—conveyor belts; 10—pitch pumps; 11—vibratory feeders; 12—tape weight measuring instruments; 13—roll crusher; 14—elevators; 15—polygonal sieve; 16—filters with precipitant; 17—vibratory feeders; 18—crusher; 19—powder heaters; 20—mixers; 21—liquid dispensers; 22—molding machines; 23—agitators of bins for ground materials; 24—feeder and dispensers; 25—screws; 26—pitch consumables; 27—ball mill; 28—intermediate bunker; 29—combined dual nozzle; 30—a vacuum pump; 31—spare hopper calcined materials; 32—consumable bins; 33—bunker ground materials; 34—batch mixer; 35—vibrators for mass compaction

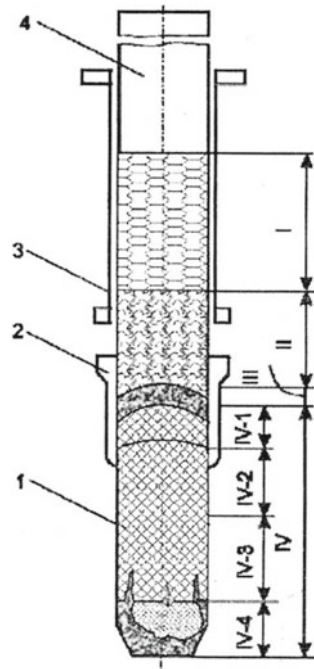
Coke, like anthracite, refers to easily graphitizable carbon-containing materials. Heating coke to 2450 °C turns it into high-density graphite (2.14 g/cm³). When heated from room temperature to high temperatures, the electrical resistance of coke decreases sharply when it reaches 800–900 °C, changes weakly in the range 900–1200 °C, and again above 1700 °C it decreases noticeably. The appearance of the graphite phase in coke having an initially amorphous structure is noted at 1400 °C and above.

At low temperatures, the electrode mass does not conduct current. As the temperature rises, the electrical resistance of the mass decreases sharply. When heated to 700 °C, the electrical resistance decreases by 30 times, however, the carbon block of the self-baking electrode, which has been fired up to 700 °C, is still characterized by a fairly high electrical resistance, the current through the calcined mass practically does not pass; all current load falls on the iron casing. When heated to 900 °C, the rate of decrease in electrical resistance slows down.

In a self-baking electrode, the temperature varies from the temperature of the environment at the top of the casing to the temperature of the electric arc at the end of the working end of the electrode. The electrode mass loaded into the casing (in pieces), as the electrode is bypassed, passes through all temperature zones, as a result of which it is coked (burned) and, under the influence of high temperatures, turns into a carbon block of the self-baking electrode. Normal operation of electrodes of this type and, consequently, of a ferroalloy furnace as a whole can be ensured only if optimal temperature conditions for firing the electrodes are created. Violation of the firing conditions of the electrode is accompanied by a disruption in its operation and sometimes leads to undesirable consequences (leakage of liquid mass to the furnace top, fire associated with mass ignition, etc.).

Several zones are distinguished by the height of the self-baking electrode (Fig. 27.6). In which, the upper part of the electrode is a casing that is not filled with electrode mass. The first zone is the zone in which the electrode mass is in lumps. As they approach the electrical contact unit, the lumps of mass are melted and form a column of liquid mass, which is released into the third zone. The boundary between the first and second zones is isotherm $65-75^{\circ}\text{C}$, since in this interval the binder (pitch) is melted, and the mass acquires a conditionally liquid state. The third zone, usually the smallest in height, but very responsible, is in a relatively narrow temperature range of $350-550^{\circ}\text{C}$. In this zone, a coke lattice of binder is formed from the pitch, which is accompanied by the release of a large amount of volatile

Fig. 27.6 Self-baking electrode zones, I—solid mass; II—liquid mass; III—zone of coke formation from the binder; IV—carbon block of the electrode (IV-1—IV-4—subzones)
1—coked electrode; 2—electrical contact node; 3—bearing cylinder; 4—the casing of the electrode, unfilled with electrode mass



substances and coking of the mass. The area of the carbon block of the electrode from 550 °C and up to its end is isolated in the fourth zone. The electrode in this zone consists of solid components cemented by coke. However, the properties of the electrode of the fourth zone differ significantly in height. In this regard, in the fourth zone, four subbands are distinguished on the basis of the properties of the carbon block fired at different temperatures and not the properties of the aggregate state of the electrode mass. The temperature ranges for the allocation of subzones are as follows: (1) 550–850 °C; (2) 850–1450 °C; (3) 1450–2500 °C; (4) 2500 °C—temperature of the electric arc.

In the electrodes of ferroalloy furnaces, the third zone (350–550 °C) should be at the level of the middle of the contact cheeks, and the temperature of the electrode at the exit from the cheeks should not exceed 900–1100 °C. The electrode must enter the contact cheeks in a ductile manner, that is, the mass must have a temperature of 150–250 °C, which ensures the necessary contact between the cheek and the electrode.

Chapter 28

Ferrous Dispersion (Atomizing)



Granular ferrous alloys obtained by dispersing melts with air and water are widely used in various industries. Powdered (spherical) ferrosilicon, containing 18% Si, is used in the enrichment industry as a weighting agent for an aqueous suspension to enrich minerals. Granular ferrosilicon is also used in the enrichment of chromium and other ores. Ferrous alloys sprayed with water are also used in powder metallurgy, in the manufacture of welding electrodes, etc. Powder ferrous alloys are necessary for the production of nitrided ferrous alloys.

In metallurgy, atomized aluminum is included in the mixture as a reducing agent.

The most important characteristics of the ferrous alloys used for dispersion are the temperature of the liquidus and solidus, as well as the viscosity at high temperatures. These, like many other properties of liquid ferrous alloys, are determined by the strength of interatomic bonds, which depend on the electronic configuration of atoms. To calculate the dispersion processes, it is important to know the change in the density of ferrous alloys at various temperatures and chemical composition. The chemical composition and temperature of the ferrous alloy also determine the viscosity and surface tension of the melt. In alloys of the Fe–Si binary system, alloys with a high silicon content have the lowest viscosity and surface tension. However, powders of high-silicon alloys cannot be used as a weighting agent for aqueous suspensions (heavy media). The presence of impurity elements (S, O, N, Al), transition metals in ferrous alloys significantly change the properties of the melts.

Many methods are known for dispersing liquid metals and ferrous alloys. Two groups of fundamentally different methods are distinguished. The essence of the methods referred to the first group, called *nozzle*, is to spray a jet of liquid ferrous alloys with an energy carrier. The second group of methods combines centrifugal *spraying* processes. Upon obtaining of dispersed ferrous alloys (e.g., ferrosilicon), nozzle methods are used with water and air as an energy carrier.

The technological scheme for producing ferrosilicon powder by dispersing liquid ferrosilicon with 15% Si is shown in the Fig. 28.1.

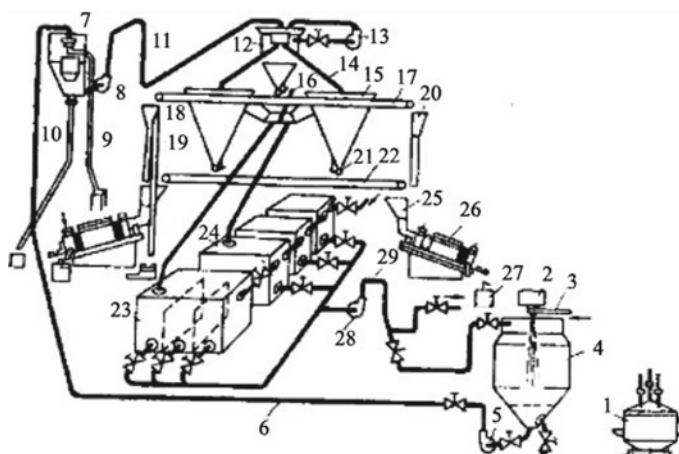


Fig. 28.1 Technological scheme of the production of powders from melts based on 15% ferrosilicon: 1—electric furnace; 2—metal receiver; 3—nozzle with a Laval nozzle; 4—dispersion chamber; 5—pump; 6—slurry pipeline; 7—a box with sand; 8—sand pump; 9—a sampler; 10—sand; 11—valve; 12—classifier small; 13—return wash pump; 14—discharge into large classifiers; 15—classifier; 16—shiber; 17—conveyor for return; 18—shutter; 19—return issue; 20—receiving device; 21—shutter classifier; 22—conveyor for powder; 23—sump tank No. 1; 24—sump tanks No. 2,3,4; 25—receiving device; 26—drying electric furnace; 27—tub for dry powder; 28—slurry pump; 29—clarified water pipeline

Table 28.1 Granulometric composition of ferrosilicon containing 14–18% Si

Grade	Fraction content %, mm					
	>0.16	<0.16	<0.071	<0.04	0.02–0.01	<0.01
FeSi15-1	≤5	≥95	≥80	≥60	≥12	≤14
FeSi15-2	≤8	≥92	≥60	≥40	≥10	≤10
FeSi15-3	≤8	≥92	≥60	≥40	—	—

The produced granular ferrosilicon is characterized by the properties shown in the Table 28.1.

The maximum silicon content in the alloy is 14–16% due to the fact that this provides sufficient magnetic permeability, density and corrosion resistance of the powder. High percent ferrosilicon compositions are non-magnetic. To obtain 15% ferrosilicon, FS45 (rarely FS65) and steel shavings are used. Slag is formed from sand and lime. The mixture is fused in steelmaking arc furnaces with an acid lining. The composition of the charge: 400 kg ferrosilicon FS45; 800 kg of steel shavings; 60 kg of sand; 20 kg of lime; 500–600 kg of granulation waste. Ferrosilicon is smelted by a batch process.

Spraying liquid ferrosilicon is made by air. The melt from the metal receiver is sprayed through the channel through an opening measuring 35–40 mm, which closes when the metal is drained from the furnace into the metal receiver with a graphite

plug. Spray air is supplied through the nozzle. After filling the metal receiver, the graphite plug is removed, the air pressure in the nozzle is increased to 2 MPa. Particles of atomized ferrosilicon fall into water with a temperature not exceeding 50 °C. Metal of one melt is sprayed in at least three doses in order to avoid overheating of the water and to prevent an explosion. The pulp, consisting of particles of atomized ferrosilicon and water, is transported by pumps to classifiers.

The classification of the powder is carried out to separate the coarse fraction from the fine and obtain powders of strictly specified fraction. Pulp initially enters the first classifier, in which part of the smallest particles is separated. Through pipelines, these particles enter two large classifiers. The powder isolated from this pulp contains granules <0.04 mm (58–65%) in size, is not sieved and is a commercial product. The second part of the powder is divided by the following classifiers. The resulting powders are fed to two drying electric furnaces. Sieving of the powder is carried out on a sieve <0.16 mm. Particles with a diameter >0.16 mm enter the hopper and return to remelting. Powder with a particle size <0.16 mm is sent to the hopper for subsequent screening and dosing to obtain marketable powder of a given size, provided for by the technical conditions.

In the production of powder ferroalloys, air control for aerosols and other hazards is mandatory. The maximum permissible aerosol concentrations are: carbon monoxide 20 mg/m³, silicon dioxide 1.0 mg/m³. Ferrosilicon granulation workshops are equipped with a gas purification system that provides suction and cleaning of dust and gas emissions to a level that meets the requirements of regulatory documents.

Melts of ferrochromium, ferromanganese and other alloys can also be dispersed. To optimize the process of smelting and dispersing these melts, a comprehensive study of the composition-temperature-property complex is necessary. From the data presented in Fig. 28.2, it follows that high-silicon melts (40–80% Cr) are characterized, in comparison with melts of the Fe–Si system, by higher values of viscosity, surface tension and have low fluidity. The physical properties of ferromanganese melts also depend on composition and temperature. For alloys of the Mn–Fe system, the maximum kinematic viscosity at 1450 and 1600 °C corresponds to the equiatomic composition. With the introduction of 1% C, the maximum viscosity at all temperatures shifts to the range of 20–30% Mn. Some conversion (foundry) ferroalloys are granulated to replace the energy-intensive crushing of lumpy ferroalloys. Foundry carbon ferrochromium, ferrosilicochromium and silicomanganese are subjected to granulation. The granulation technology of such ferroalloys is as follows. After the ferroalloy is discharged from the furnace to the ladle, the latter is fed to the granulation unit and then is drained into the receiver by a slow stream. A jet of ferroalloy (silicomanganese) flows down a long trough into a granulation tank. In this case, it is sprayed with a stream of water. The resulting ferroalloy particles enter a granulation tank filled with running water. Before the granulation, a basket is installed on the bottom of the tank for the accumulation of granular ferroalloy in it. After the liquid ferroalloy is discharged, the basket is lifted by an overhead crane and granules fall into the warehouse for use as charge components in the smelting of ferroalloys or in steel production.

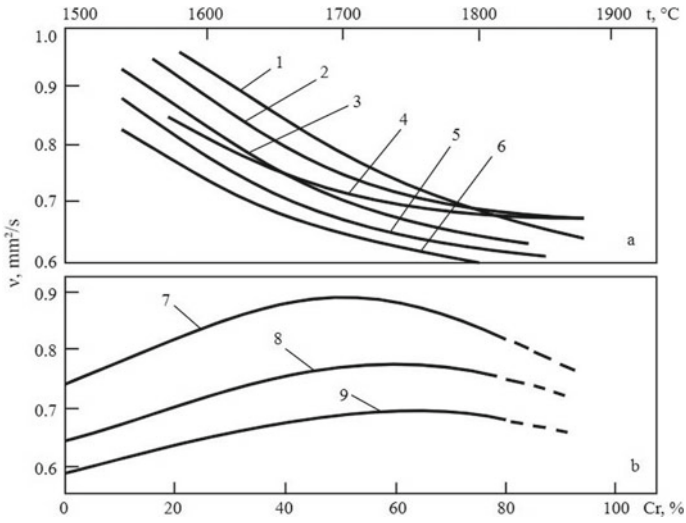


Fig. 28.2 Physical properties of the melts of the Fe-Cr system **a** polytherms; **b** isotherms of kinematic viscosity; 1-50% Cr; 3-40% Cr; 5-20% Cr; 6-Fe; 7-1000 $^{\circ}\text{C}$; 8-1700 $^{\circ}\text{C}$; 9-1800 $^{\circ}\text{C}$

Chapter 29

Environmental Protection in Ferrous Industry



29.1 Basic Principles

The main tasks of environmental protection in the process of metallurgical production are

1. continuous monitoring of the environment and pollution sources using the latest scientific and technical means in order to take the necessary measures to protect nature;
2. reducing the environmental impact of metallurgical waste. To this end, it is necessary to develop and implement technological processes, including processes for producing ferrous alloys, ensuring waste reduction, as well as their use in the actual ferrous alloy production, related industries and other industries.
3. the use of water in metallurgical technology (for cooling structural elements of electric furnaces, granulation of ferrous alloys, slags, etc.) in a closed cycle, for which purpose, it is necessary to develop and introduce highly effective treatment facilities into production.
4. the development of new methods and means of combating harmful emissions into the atmosphere, exposure to electric and magnetic fields and radiation, vibration and noise;
5. protection of fertile soils from pollution by industrial waste (slag, sewage, etc.);
6. implementation of measures for the integrated and rational use of mineral raw materials and water resources;
7. improving the forecasting of the environmental impact of metallurgical production, taking into account its possible social and economic consequences when developing projects for metallurgical units and enterprises (ferrous alloy furnaces, workshops, factories);

With the current scale of metallurgical production, the problem of protecting the environment from harmful emissions is becoming global. Emissions from ferrous metallurgy enterprises exceed 7.52%. An integrated metallurgical plant producing

10 million tons of steel annually emits 220,000 tons of dust, 50,000 tons of sulfur compounds, 250,000 tons of carbon monoxide and other substances.

29.2 Characterization of Harmful Emissions in Ferroalloy Production

The main harmful emissions from the production of ferroalloys are top gases, slag and dust formations. The quantity and composition of these by-products of ferroalloys production depend on the technology of smelting, the design of ferroalloy furnaces and also on the efficiency of treatment facilities. The largest amount of dust and gas emissions and waste slag falls on the processes associated with the use of carbon as a reducing agent.

The resulting top gases contain 70–90% carbon monoxide and other gaseous oxides (SO_2 , NO_x), a significant amount of fine dust. In small concentrations, the presence of hydrogen fluoride HF, polyaromatic hydrocarbons (PAHs), volatile organic compounds (VOCs) and heavy metals is possible (Table 29.1). The formation of PCDD/F (polychlorinated dibenzo-para-dioxins (PCDD) and polychlorinated dibenzofurans (PCDF)) in the combustion zone and in the gas treatment cooling zone (secondary synthesis) is likely for semi-open furnaces. CaF_2 fluor spar can be used as a flux in the production of ferromolybdenum, which may lead to the emission of fluorides in an amount of 150–260 mg/nm^3 .

Sources of air pollution are also furnaces for drying and firing the charge components.

Table 29.1 Emissions into the air during the production of ferroalloys, kg/t

Substance	Ferroalloy		
	Ferrosilicon	Ferrosilicon	Ferromolybdenum
SO_2	0.93–1.068	1.326–4.26	64.96–86.5
CO		2.16–9.78	93.7–135.6
NO_2	1.4–1.763	0.77–14.322	2.2–3.53
Dioxins ^a	$\leq 0.1 \text{ ng}/\text{nm}^3$	40 ng/t	n/a
PAHs ^b	n/a	0.0015	n/a
VOC ^c	n/a	0.045	n/a
Dust 20–70% SiO_2	n/a	n/d	3.7–8.6
Dust $\geq 70\%$ SiO_2	n/a	0.17–7.5	n/a
Suspended substances	0.954–1.031	n/a	n/a
Cr	0.039	n/a	n/a

^aPolychlorinated dibenzo-para-dioxins (PCDD) and polychlorinated dibenzofurans (PCDF)

^bPolyaromatic hydrocarbons (PAHs)

^cVolatile organic compounds (VOCs)

The dust released during the production of various ferroalloys consists of SiO_2 , CaO , MgO , Al_2O_3 , $\text{FeO} + \text{Fe}_2\text{O}_3$, Cr_2O_3 and other components, the content of which depends on the type of alloy and the composition of the charge. So, upon obtaining of ferrosilicon, the main component of dusts is silicon dioxide, silicocalcium—oxides of silicon and calcium. Manganese ferroalloys are characterized by the presence of manganese oxides in dust, and chromium ferroalloys are characterized by chromium oxides (Sect. 25.8).

Pollutants are also found in sublimates. Thus, in the production of ferrotungsten, in addition to the main dust emissions of oxides of silicon, calcium, manganese, iron and tungsten, sublimates contain lead, bismuth, copper, arsenic, zinc, phosphorus, sulfur, magnesium oxides and aluminum [1].

Due to the fact that the composition of the exhaust gases includes many different chemical compounds, their cleaning is associated with high costs. The cost of the gas cleaning system of a closed furnace is 10% of the cost of the entire furnace installation, and for an open furnace, the cost increases to 90% [2].

Gases from the open furnaces are captured using an umbrella located above the furnace. At the same time, together with the gases under the umbrella, air is sucked in, and the components of the gas are burned when they are mixed with oxygen. Large volumes (up to 400 thousand m^3/h) of air-gas mixture are formed with a temperature of up to 500°C and a dust content of $1\text{--}3\text{ mg/m}^3$. Gas purification from open ferroalloy furnaces is carried out in fabric filters, high-speed dust collectors with Venturi pipes and electric filters. Designs of dust and gas treatment facilities for collecting toxic manganese dust in the exhaust gases of open furnaces producing high-carbon ferromanganese and silicomanganese provide dry gas purification using bag filters to a residual dust level of less than 10 mg/m^3 with a dust content in front of bag filters 1.15 mg/m^3 (efficiency 99%) [3].

The main component of the exhaust gases from a closed furnace is CO (70–90%); a higher CO content corresponds to the smelting of silicon alloys, and a lower one corresponds to the smelting of carbon ferrochromium. In addition, the gas contains%: 2–19 CO_2 , 2–11 H_2 , 0.3–0.5 CH_4 , 0.1–4.0 N_2 , 0.2–2.0 O_2 . The combustible part of the gas is H_2 and CH_4 , in a small amount, there are SO_2 , H_2S and other components that lead to corrosion of the gas path, dust and gas purification apparatuses and sludge facilities. The temperature of undiluted gas can be from 400°C to 1150°C [2]. The dust content of the gas is $15\text{--}40\text{ mg/m}^3$, with 98% of dust particles having a size of $\leq 10\text{ }\mu\text{m}$ and 68–80% of $\leq 5\text{ }\mu\text{m}$. The bulk of the gas (up to 85%) is discharged for purification, and a small part of it falls into the workshop, which is removed through the filter.

Wet (Venturi scrubbers) and dry methods (bag filters using high-temperature resistant fabrics provide dust content of the exhaust gas less than 10 mg/m^3) are used to clean the exhaust gases of closed furnaces. Electrofilters are used less often, since the specific resistance of dry dust is more than $1011\text{ }\Omega\cdot\text{s}$. The dry cleaning method allows you to return to the production of dust carried away by gases from ferroalloy furnaces.

However, the dry method has several disadvantages: low resistance of fabric filters, high operating and capital costs. If the cost of a wet gas cleaning system of closed

furnaces is about 10% of the cost of the entire furnace installation, then the cost of a dry gas cleaning system of open furnaces is 30%.

The advantage of wet gas cleaning is that the top gas in contact with water is immediately cooled; however, this requires the creation of a local reverse cycle.

After purification, the gas is either used as fuel or emitted into the atmosphere with preliminary afterburning to carbon dioxide (CO_2), which is carried out in open furnaces. Gases from a closed ferroalloy furnace can be used as fuel and as raw materials for the chemical industry.

Wastewater. Wastewater of ferroalloy production is formed during gas purification, casting and granulation of ferroalloys and carbon production. The effluents are characterized by the presence of suspended particles, have an alkaline reaction, contain cyanides and rhodanides (effluents from gas purification of electric furnaces in the smelting of ferroalloys), in an increased amount of dry residue and phenols (effluents from the electrode mass shop), manganese, fluorine (effluents from flux-smelting production), chromium, arsenic, vanadium, nickel, etc. [3]. Wastewater is contaminated with tiny ferromagnetic suspensions. Approximately 70% of the particles contained in the wastewater of gas purification of electric furnaces are characterized by a particle size of $\leq 10 \mu\text{m}$, so this suspension is difficult to precipitate.

Ferroalloy production uses recycled water supply (85% of all used water is in circulation); at the same time, dirty water from gas flushing is also included in the circulation, it is used after clarification in horizontal, radial sedimentation tanks or in a thickener. The hydraulic load per 1 m^2 of the surface of the sump does not exceed $0.6 \text{ m}^3/\text{h}$, and the use of magnetic coagulation contributes to an increase in the specific load by $1\text{--}1.2 \text{ m}/(\text{h} \cdot \text{m}^2)$ [2]. Along with the magnetic field, flocculants additives (polyacrylamide) are introduced.

Waste and by-products. The amount and composition of waste generated during the production of ferroalloys were considered in Sect. 25.8.

The dust collected during dry cleaning of the gas leaving the ferroalloy furnaces contains non-ferrous metals that are part of the charge components for the production of ferroalloys (with a high cost of the leading component—ferrovandium, ferromolybdenum, ferroniobium), so dust and sludge (after dehydration) are recycled.

Silicon alloy dust is used in the manufacture of refractories, building materials, concrete, for the application of protective coatings on the surface of molds, as a heat-insulating material, etc.

The current slag from the production of ferroalloys after crushing and fractionation is used in road construction.

Secondary energy resources. In the composition of the exhaust gases of closed ferroalloy furnaces, carbon monoxide predominates (70–90%), and for this reason, the gas of ferroalloy furnaces is a secondary energy resource. The output of ferroalloy gas varies from 300 to $1350 \text{ m}^3/\text{t}$ of alloy.

The cleaned top gas of closed ferroalloy furnaces is a high-calorific fuel with a calorific value of $9250\text{--}10,500 \text{ kJ}/\text{m}^3$ and is used for heating boilers, lime kilns and in tube furnaces for preheating the charge.

References

1. Tuguz ShM, Schenfeld B et al (2008) Environmental aspects of the production of ferroalloys. *Steel* 7:118–119. (in Russian)
2. Bolshina EP (2012) Ecology of metallurgical production. In: Lecture course, Novotroitsk, NITU MISiS, p 155. (in Russian)
3. Zhdanov AV, Zhuchkov VI, Dashevskii VYa, Leontyev LI (2015) Wastes generation and use in ferroalloys production. In: The Fourteenth international ferroalloys congress May 31–June 4, 2015 energy efficiency and environmental friendliness are the future of the global Ferroalloy industry Kyiv, Ukraine (2015), pp 754–758. (in Russian)

Appendix A

Calculation of the Charge for Smelting High-Carbon Ferromanganese by Flux Method

Calculation of the charge was carried out for smelting high-carbon ferromanganese brand FeMn78. The composition of carbon ferromanganese, charge materials and the distribution of elements between the smelting products is given in Tables A.1, A.2, A.3 and A.4.

Smelted Ferroalloy—**High-Carbon Ferromanganese.**

The calculation is carried out per 100 kg of manganese sinter.

High-carbon ferromanganese is smelted by *flux method*.

Slag basicity adopted in this process $\text{CaO/SiO}_2 = 1.2$.

1. The amount of alloy obtained
 $49.02 \cdot 0.78 / 0.8 = 47.794$ kg,
 where 49.2—the amount of manganese in 100 kg of sinter;
 0.78—the degree of transition of manganese into metal;
 0.8—manganese content in metal.
2. The amount of carbon that should be in the alloy
 $47.794 \cdot 0.065 = 3.107$ kg,
 where 47.794—amount of alloy obtained;

Table A.1 Chemical composition of high-carbon ferromanganese, %

Mn	Fe	C	Si	P	S
80.0	12.5	6.5	1.0	0.5	0.03

Table A.2 Chemical composition of the charge materials, %

Material	Mn	Fe ₂ O ₃	P	SiO ₂	CaO	Al ₂ O ₃	MgO	S	CO ₂
Manganese sinter	49.02	1.2	0.224	17.1	4.3	2.2	1.4	0.13	–
Limestone	–	–	–	–	56.0	–	–	–	44.0
Coke breeze ash	0.17	10.4	0.347	51.4	4.0	27.9	2.5	–	–

Table A.3 Coke breeze composition, %

Material	C	S	Moisture	Volatile	Ash
Coke breeze	83.77	0.52	1.0	1.27	13.44

Table A.4 Distribution of elements between the products of melting, %

Element	Into metal	To slag	Volatile and loss
Mn	78	12	10
Fe	95	5	—
P	85	5	10
Si	10	90	—
S	2	50	48

0.065—carbon content in the alloy.

3. The amount of manganese that will turn into metal
 $49.02 \cdot 0.78 = 38.236$ kg,
 where 49.02—the amount of manganese in 100 kg of sinter;
 0.78—the degree of transition of manganese into metal.
4. The amount of manganese that will turn into gases
 $49.02 \cdot 0.10 = 4.902$ kg,
 where 0.10—the degree of transition of manganese into the gas phase.
5. Manganese reduced from MnO in total
 $38.236 + 4.902 = 43.138$ kg.
6. Oxygen bound to manganese
 $43.138 \cdot 16/55 = 12.549$ kg,
 where 16 is the atomic mass of oxygen;
 55—atomic mass of manganese.
7. Amount of iron that will recover from oxide Fe₂O₃
 $1.2 \cdot 112 \cdot 0.95/160 = 0.798$ kg,
 where 1.2 is the amount of Fe₂O₃ in 100 kg of sinter;
 112—molecular weight of iron in Fe₂O₃;
 160—molecular weight of Fe₂O₃.
8. Oxygen bound to iron
 $0.798 \cdot 48/112 = 0.342$ kg,
 where 48 is the molecular mass of oxygen in Fe₂O₃.
9. Amount of silicon recovered from SiO₂ oxide
 $17.1 \cdot 0.1 \cdot 28/60 = 0.798$ kg,
 where 17.1 is the amount of SiO₂ in 100 kg of sinter;
 0.1—the degree of transition of silicon into metal;
 28—molecular weight of silicon;
 60 is the molecular weight of SiO₂.
10. Silicon bound to oxygen
 $0.79832/28 = 0.912$ kg,

- where 32 is the molecular mass of oxygen in SiO_2 .
11. Amount of phosphorus that will pass into metal
 $0.224 \cdot 0.85 = 0.190$ kg,
 where 0.224 is the amount of phosphorus in 100 kg of sinter;
 0.85—the degree of transition of phosphorus to metal.
 12. Phosphorus will pass into gases
 $0.224 \cdot 0.1 = 0.022$ kg,
 where 0.1 is the degree of transition of phosphorus into the gas phase.
 13. Total phosphorus reduced
 $0.190 + 0.022 = 0.212$ kg.
 14. Phosphorus bound to oxygen
 $0.21280/62 = 0.274$ kg,
 where 80 is the molecular mass of oxygen in P_2O_5 ;
 62 is the molecular weight of phosphorus in P_2O_5 .
 15. Total reduced oxides contain oxygen
 $12.549 + 0.342 + 0.912 + 0.274 = 14.077$ kg.
 16. Carbon required for CO
 $14.07712/16 = 10.558$ kg,
 where 12 is the atomic mass of carbon;
 16—atomic mass of oxygen.
 17. Together with alloy's carbon, additional carbon is required
 $10.558 + 3.107 = 13.665$ kg.
 18. Sulfur will pass into metal from 100 kg of sinter
 $0.13 \cdot 0.02 = 0.0026$
 where 0.02 is the degree of transition of sulfur to metal.
 19. Pass to slag from 100 kg of sinter:
 $\text{MnO}: 49.02 \cdot 0.12 \cdot 71/55 = 7.594$ kg,
 where 49.02 is the amount of manganese in 100 kg of sinter;
 0.12—the degree of transition of manganese to slag;
 71—molecular weight of MnO;
 55—atomic mass of manganese;
 $\text{FeO}: 1.2 \cdot 0.05 \cdot 144/160 = 0.054$ kg,
 where 1.2 is the amount of Fe_2O_3 in 100 kg of sinter;
 0.05—the degree of transition of iron to slag;
 144—molecular weight of FeO in Fe_2O_3 ;
 160—molecular weight of Fe_2O_3 ;
 $\text{SiO}_2: 17.1 \cdot 0.9 = 15.390$ kg,
 where 17.1 is the amount of SiO_2 in 100 kg of sinter;
 0.9—the degree of transition of silicon into slag;
 $\text{P}_2\text{O}_5: 0.224 \cdot 0.05 \cdot 142/62 = 0.026$ kg,
 where 0.224 is the phosphorus content in 100 kg of sinter;
 0.05—the degree of transition of phosphorus to slag;
 142—molecular weight of P_2O_5 ;
 62—molecular weight of phosphorus in P_2O_5 ;
 CaO: 4.3 kg,

where 4.3 is the CaO content in 100 kg of sinter;

Al₂O₃: 2.2 kg,

where 2.2 is the Al₂O₃ content in 100 kg of sinter;

MgO: 1.4 kg,

where 1.4 is the MgO content in 100 kg of sinter;

S: $0.13 \cdot 0.5 = 0.065$ kg,

where 0.13 is the sulfur content in 100 kg of sinter;

0.5—the degree of transition of sulfur to slag.

20. Will turn sulfur into gases

$0.13 \cdot 0.48 = 0.0624$ kg,

where 0.5 is the degree of transition of sulfur to the gas phase.

21. Carbon will be required to recover oxides of Mn, Fe, Si and P from coke breeze ash

per 100 kg of coke breeze:

MnO: $(13.44 \cdot 0.17/100) \cdot 0.88 \cdot 12/55 = 0.004$ kg,

where 13.44—the amount of ash in 100 kg of coke breeze;

0.17—the manganese content in coke breeze ash;

0.88—the degree of transition of manganese into metal and into the gas phase;

12—atomic mass of carbon;

55—atomic mass of manganese;

Fe₂O₃: $(13.44 \cdot 10.04/100) \cdot 0.95 \cdot 36/160 = 0.288$ kg,

where 10.04 is the content of Fe₂O₃ in coke breeze ash;

0.95—the degree of transition of iron into metal;

36—molecular weight of carbon;

160—molecular weight of Fe₂O₃;

SiO₂: $(13.44 \cdot 51.4/100) \cdot 0.1 \cdot 24/60 = 0.276$ kg,

where 51.4 is the SiO₂ content in coke breeze ash;

0.1—the degree of transition of silicon into metal;

24—molecular weight of carbon;

60—molecular weight of SiO₂;

P₂O₅: $(13.44 \cdot 0.347/100) \cdot 0.95 \cdot 60/82 = 0.033$ kg,

where 0.347 is the phosphorus content in the coke breeze ash;

0.95—the degree of transition of phosphorus into metal and into the gas phase;

60—molecular weight of carbon;

82 is the molecular weight of phosphorus in P₂O₅.

22. In total, carbon will be required for the reduction of ash oxides in 100 kg of coke breeze

$0.004 + 0.288 + 0.276 + 0.033 = 0.601$ kg.

23. Remains active carbon in 100 kg of coke breeze

$83.77 - 0.601 = 83.169$ kg,

where 83.77 is the amount of carbon in 100 kg of coke breeze.

24. Coke breeze will be needed

$13.665/83.169 = 16.430$ kg,

where 13.665 is the amount of carbon required for the reduction of the oxides of Mn, Fe, Si and P in sinter and for carburization of metal.

25. Based on factory practice, in connection with carbon monoxide fumes at the top according to the reaction
 $C + CO_2 = 2CO$ in the interaction with CO_2 formed during the decomposition of limestone, and in the reaction $C + \frac{1}{2}O_2 = CO$ in the reaction with oxygen formed during the dissociation of higher manganese oxides, the coke weight should be increased by ~20%
 $16.430 \cdot 1.2 = 19.716$ kg.
26. The required amount of coke breeze contains ash
 $19.716 \cdot 13.44/100 = 2.650$ kg,
 where 13.44 is the ash content in coke.
27. Sulfur will pass from coke breeze to metal
 $(19.716 - 0.52/100) \cdot 0.02 = 0.002$ kg,
 where 0.52—sulfur content in coke;
 0.02—the degree of transition of sulfur to metal.
28. Sulfur will pass from coke breeze to slag
 $(19.716 - 0.52/100) \cdot 0.5 = 0.051$ kg,
 where 0.5 is the degree of transition of sulfur to slag.
29. Sulfur will evaporate from coke breeze
 $(19.716 \cdot 0.52/100) \cdot 0.48 = 0.049$ kg,
 where 0.48 is the degree of transition of sulfur to the gas phase.
30. Coke breeze will introduce volatile
 $19.716 \cdot 1.27/100 = 0.250$ kg,
 where 1.27 is the content of volatiles in coke breeze.
31. Coke breeze will bring moisture
 $19.716 \cdot 1.0/100 = 0.197$ kg,
 where 1.0 is the moisture content in coke breeze.
32. From coke breeze ash will go into metal:
 Mn: $(2.65 \cdot 0.17/100) \cdot 0.78 = 0.004$ kg,
 where 2.208 is the ash content in the required amount of coke breeze;
 0.17—the manganese content in coke breeze ash;
 0.78—the degree of transition of manganese into metal;
 Fe: $(2.65 \cdot 10.04/100) \cdot 0.95 \cdot 112/160 = 0.176$ kg,
 where 10.04 is the content of Fe_2O_3 in coke breeze ash;
 0.95—the degree of transition of iron into metal;
 112—molecular weight of iron in Fe_2O_3 ;
 160—molecular weight of Fe_2O_3 ;
 Si: $(2.65 \cdot 51.4/100) \cdot 0.1 \cdot 28/60 = 0.064$ kg,
 where 51.4 is the SiO_2 content in coke breeze ash;
 0.1—the degree of transition of silicon into metal;
 28—atomic mass of silicon in SiO_2 ;
 60—molecular weight of SiO_2 ;
 P: $(2.65 \cdot 0.347/100) \cdot 0.85 = 0.008$ kg,
 where 0.347 is the phosphorus content in the coke breeze ash;
 0.85—the degree of transition of phosphorus to metal.

33. From coke breeze ash will go to slag:
 $\text{MnO: } (2.65 \cdot 0.17/100) \cdot 0.12 \cdot 71/55 = 0.001 \text{ kg,}$
 where 0.17 is the manganese content in coke breeze ash;
 0.12—the degree of transition of manganese to slag;
 71—molecular weight of MnO;
 55—atomic mass of manganese;
 $\text{FeO: } (2.65 \cdot 10.04/100) \cdot 0.05 \cdot 144/160 = 0.012 \text{ kg,}$
 where 10.04 is the content of Fe_2O_3 in coke breeze ash;
 0.05—the degree of transition of iron to slag;
 144—molecular weight of FeO in Fe_2O_3 ;
 160—molecular weight of Fe_2O_3 ;
 $\text{SiO}_2: (2.65 \cdot 51.4/100) \cdot 0.9 = 1.225 \text{ kg,}$
 where 51.4 is the SiO_2 content in coke breeze ash;
 0.9—the degree of transition of silicon into slag;
 $\text{P}_2\text{O}_5: (2.65 \cdot 0.347/100) \cdot 0.05 \cdot 142/82 = 0.001 \text{ kg,}$
 where 0.347 is the phosphorus content in the coke breeze ash;
 0.05—the degree of transition of phosphorus to slag;
 142—molecular weight P_2O_5 ;
 82—molecular weight of phosphorus in P_2O_5 ;
 $\text{CaO: } (2.65 \cdot 4.0/100) = 0.106 \text{ kg,}$
 where 4.0 is the CaO content in the coke breeze ash;
 $\text{Al}_2\text{O}_3: (2.65 \cdot 27.9/100) = 0.739 \text{ kg,}$
 where 27.9 is the Al_2O_3 content in coke breeze ash;
 $\text{MgO: } (2.65 \cdot 2.5/100) = 0.066 \text{ kg,}$
 where 2.5 is the Al_2O_3 content in the coke breeze ash.
34. Will fly away from coke breeze ash:
 $\text{Mn: } (2.65 \cdot 0.17/100) \cdot 0.10 = 0.0004 \text{ kg,}$
 where 0.17 is the manganese content in coke breeze ash;
 0.10—the degree of transition of manganese into the gas phase;
 $\text{P: } (2.65 \cdot 0.347/100) \cdot 0.10 = 0.0008 \text{ kg,}$
 where 0.347 is the phosphorus content in the coke breeze ash;
 0.10—the degree of transition of phosphorus to slag.
35. The slag contains SiO_2 from sinter and coke breeze ash
 $15.390 + 1.225 = 16.615 \text{ kg.}$
36. With a slag basicity of $\text{CaO/SiO}_2 = 1.2$, the slag should have CaO
 $16.615 \cdot 1.2 = 19.938 \text{ kg.}$
37. Slag contains CaO from sinter and coke breeze ash
 $4.3 + 0.106 = 4.406 \text{ kg.}$
38. Need to add CaO
 $19.938 - 4.406 = 15.532 \text{ kg.}$
39. Limestone (CaCO_3) required
 $15,532 \cdot 100/56 = 27.736 \text{ kg,}$
 where 56 is the CaO content in limestone.

Table A.5 Amount and composition of the metal

Element	From ore part of charge, kg	From coke breeze, kg	From coke breeze ash, kg	From steel shavings, kg	Total	
					kg	%
Mn	38.236	–	0.004	–	38.240	79.03
Fe	0.798	–	0.176	5.0	5.974	12.35
C	–	3.107	–	–	3.107	6.42
Si	0.798	–	0.064	–	0.862	1.78
P	0.190	–	0.008	–	0.198	0.41
S	0.003	0.002	–	–	0.005	0.01
In total					48.386	100

Table A.6 Amount and composition of slag

Element	From ore part of charge, kg	From coke breeze, kg	From coke breeze ash, kg	From limestone, kg	Total	
					kg	%
MnO	7.594	–	0.001	–	7.595	15.576
FeO	0.054	–	0.012	–	0.066	0.135
SiO ₂	15.390	–	1.225	–	16.615	34.074
CaO	4.3	–	0.106	15.532	19.938	40.889
Al ₂ O ₃	2.2	–	0.739	–	2.939	6.027
MgO	1.4	–	0.066	–	1.466	3.006
P ₂ O ₅	0.026	–	0.001	–	0.027	0.055
S	0.065	0.051	–	–	0.116	0.238
In total					48.762	100

40. Limestone contains carbon
 $27.73612/100 = 3.328$ kg,
 where 12 is the carbon content of limestone.
41. The alloy contains iron from sinter and coke breeze ash
 $0.798 + 0.176 = 0.974$ kg.
42. There must be iron in the alloy
 $47.79412.5/100 = 5.974$ kg,
 where 47.794 is the amount of alloy obtained;
 12.5—iron content in the alloy.
43. Need to add steel shavings
 $5.974 - 0.974 = 5.0$ kg.

Composition of Metal and Slag

See Tables A.5 and A.6.

Slag ratio— $48.762/48.386 = 1.008$

Table A.7 Material balance of manganese

Incoming			Consumption		
Received	kg	%	Obtained	kg	%
Manganese sinter	49.02	99.99	Metal	38.2395	78.00
Coke breeze ash	0.0045	0.01	Slag	5.8825	12.00
			Volatized and lost	4.9025	10.00
Total	49.0245	100	Total	49.0245	100

Table A.8 Material balance for iron

Incoming			Consumption		
Received	kg	%	Obtained	kg	%
Manganese sinter	0.84	13.94	Metal	5.974	99.15
Steele shavings	5.0	82.98	Slag	0.0513	0.85
Coke breeze ash	0.1853	3.08			
Total	6.0253	100	Total	6.0253	100

Charge composition

sinter—100 kg;
 coke breeze, taking into account the waste of 20% on the top—19.716 kg;
 limestone—27.736 kg;
 steel shavings—5.0 kg.

Consumption of materials per 1 t of high-carbon ferromanganese

sinter—2067 kg;
 coke breeze—408 kg;
 limestone—573 kg;
 steel shavings—103 kg.

Material Balances

See Tables [A.7](#), [A.8](#), [A.9](#), [A.10](#), [A.11](#) and [A.12](#).

Table A.9 Carbon material balance

Incoming			Consumption		
Received	kg	%	Obtained	kg	%
Coke breeze	16.516	83.23	Metal	3.107	15.66
Limestone	3.328	16.77	CO from reduction of sinter oxides	10.558	53.20
			CO from reduction of coke breeze ash oxides	0.099	0.50
			CO from burning coke on the top	2.753	13.87
			CO ₂ from decomposition of limestone	3.328	16.77
Total	19.844	100	Total	19.844	100

Table A.10 Material balance for silicon

Incoming			Consumption		
Received	kg	%	Obtained	kg	%
Manganese sinter	7.980	92.62	Metal	0.862	10.00
Coke breeze ash	0.636	7.38	Slag	7.754	90.00
Total	8.616	100	Total	8.616	100

Table A.11 Material balance in phosphorus

Incoming			Consumption		
Received	kg	%	Obtained	kg	%
Manganese sinter	0.224	96.14	Metal	0.198	84.98
Coke breeze ash	0.009	3.86	Slag	0.012	5.15
			Volatized	0.023	9.87
Total	0.233	100	Total	0.233	100

Table A.12 Material balance for sulfur

Incoming			Consumption		
Received	kg	%	Obtained	kg	%
Manganese sinter	0.130	55.79	Metal	0.005	2.15
Coke breeze ash	0.103	44.21	Slag	0.116	49.79
			Volatized	0.112	48.06
Total	0.233	100	Total	0.233	100

Appendix B

Calculation of the Charge for Smelting Ferrosiliconmanganese

Calculation of the charge was carried out for smelting ferrosiliconmanganese grade SiMn17. The composition of ferrosiliconmanganese, charge materials and the distribution of elements between the smelting products is given in Tables B.1, B.2, B.3 and B.4.

Smelted Ferroalloy—**Ferrosiliconmanganese.**

The calculation is per 100 kg of manganese ore.

The amount of SiO₂ in the charge is determined from the ratio SiO₂/Mn (in the ore) = 1

1. The lack of SiO₂ in the mixture
 $25.20 - 13.32 = 11.88$ kg,
 where 25.20—the amount of manganese in 100 kg of concentrate;
 13.32—amount of SiO₂ in 100 kg of concentrate.
2. Quartzite should be added
 $11.88/0.98 = 12.12$ kg,
 where 11.88—amount of SiO₂ in added quartzite;
 0.98—SiO₂ content in quartzite.

Table B.1 Chemical composition of ferrosiliconmanganese, %

Mn	Si	Fe	C	P	S
70	17	10	2.5	0.5	0.02

Table B.2 Chemical composition of the charge materials, %

Material	Mn	Fe ₂ O ₃	P	SiO ₂	CaO	Al ₂ O ₃	MgO	S	CO ₂
Manganese concentrate	25.20	4.71	0.15	13.32	14.95	1.40	2.85	0.90	26.2
Quartzite	–	–	–	98.0	–	2.0	–	–	–
Coke breeze ash	0.17	10.04	0.347	51.4	4.0	27.9	2.5	–	–

Table B.3 Coke breeze composition, %

Material	C	S	Moisture	Volatiles	Ash
Coke breeze	83.77	0.52	1.0	1.27	13.44

Table B.4 Distribution of elements between the products of melting, %

Element	Into metal	To slag	Volatized and lost
Mn	80	10	10
Fe	95	5	—
P	85	5	10
S	1	50	49

3. Conversion of manganese to metal
 $25.20 \cdot 0.8 = 20.16$ kg,
 where 25.20 is the amount of manganese in 100 kg of concentrate;
 0.8—the degree of transition of manganese into metal.
4. Manganese transition into gases
 $25.20 \cdot 0.10 = 2.52$ kg,
 where 0.10—the degree of transition of manganese into the gas phase.
5. Total reduced manganese from MnO oxide
 $20.16 + 2.52 = 22.68$ kg.
6. Oxygen bound to manganese
 $22.68 \cdot 16/55 = 6.59$ kg,
 where 16 is the atomic mass of oxygen; 55—atomic mass of manganese.
7. The amount of alloy obtained
 $25.20 \cdot 0.8/0.7 = 28.8$ kg,
 where 25.20 is the amount of manganese in 100 kg of ore;
 0.8—the degree of transition of manganese into metal;
 0.7—manganese content in the metal.
8. There will be carbon in the alloy
 $28.8 \cdot 2/100 = 3.107$ kg,
 where 28.8 is the amount of alloy obtained;
 2—carbon content in the alloy.
9. The amount of silicon in the metal
 $28.8 \cdot 17/100 = 4.896$ kg
 where 28.8 is the amount of alloy obtained;
 17—silicon content in the alloy.
10. Silicon bound to oxygen
 $4.896 \cdot 32/28 = 5.595$ kg,
 where 4.896 is the amount of silicon in the alloy;
 32—molecular mass of oxygen in SiO₂;
 28—atomic mass of silicon.
11. Iron will be recovered from Fe₂O₃ oxide
 $4.71 \cdot 0.95 \cdot 112/160 = 3.132$ kg,

- where 4.71 is the amount of Fe_2O_3 in 100 kg of concentrate;
 0.95—the degree of transition of iron into metal;
 112—molecular weight of iron in Fe_2O_3 ;
 160—molecular weight of Fe_2O_3 .
12. Iron bound to iron
 $3.13248/112 = 1.342$ kg,
 where 48 is the molecular mass of oxygen in Fe_2O_3 .
 13. Will transfer phosphorus to metal
 $0.15 \cdot 0.85 = 0.128$ kg
 where 0.15 is the amount of phosphorus in 100 kg of concentrate;
 0.85—the degree of transition of phosphorus to metal.
 14. Phosphorus will pass into gases
 $0.15 \cdot 0.1 = 0.015$ kg
 where 0.1 is the degree of transition of phosphorus into the gas phase.
 15. Total phosphorus reduced
 $0.128 + 0.015 = 0.143$ kg.
 16. Phosphorus bound to oxygen
 $0.14380/62 = 0.185$ kg
 where 80 is the molecular mass of oxygen in P_2O_5 ;
 62 is the molecular weight of phosphorus in P_2O_5 .
 17. In total, reduced oxides contain oxygen
 $6.59 + 1.342 + 5.595 + 0.185 = 13.712$ kg.
 18. Requires carbon to form CO
 $13.712 \cdot 12/16 = 10.284$ kg,
 where 12 is the atomic mass of carbon;
 16—atomic mass of oxygen.
 19. Together with carbon alloy, carbon is required
 $10.284 + 0.576 = 10.86$ kg.
 20. Sulfur will pass into metal from 100 kg of concentrate
 $0.9 \cdot 0.01 = 0.009$ kg
 where 0.9 is the amount of sulfur in 100 kg of concentrate;
 0.01—the degree of transition of sulfur to metal.
 21. Pass to slag from 100 kg of concentrate:
 MnO: $25.2 \cdot 0.1 \cdot 71/55 = 3.2531$ kg,
 where 25.2 is the amount of manganese in 100 kg of concentrate of the second grade;
 0.1—the degree of transition of manganese to slag;
 71—molecular weight of MnO;
 55—atomic mass of manganese.
 FeO: $4.71 \cdot 0.05 \cdot 144/160 = 0.212$ kg,
 where 4.57 is the amount of Fe_2O_3 in 100 kg of concentrate;
 0.05—the degree of transition of iron to slag;
 144—molecular weight of FeO in Fe_2O_3 ;
 160—molecular weight of Fe_2O_3 ;
 SiO_2 : $25.2 - (4.896 + 5.595) = 14.709$ kg

where 25.2 is the amount of SiO_2 in the ore part of the charge (concentrate + quartzite);

4.896—reduced Si;

5.595—oxygen bound to Si.

P_2O_5 : $0.15 \cdot 0.05 \cdot 142/62 = 0.017$ kg,

where 0.15 is the phosphorus content in 100 kg of concentrate of the second grade;

0.05—the degree of transition of phosphorus to slag;

142—molecular weight of P_2O_5 ;

62—molecular weight of phosphorus in P_2O_5 ;

CaO: 14.95 kg

where 14.95 is the CaO content in 100 kg of concentrate;

Al_2O_3 : 1.40 kg,

where 1.40 is the Al_2O_3 content in 100 kg of concentrate;

MgO: 2.85 kg,

where 2.85 is the MgO content in 100 kg of concentrate;

S: $0.90 \cdot 0.5 = 0.45$ kg,

where 0.90 is the sulfur content in 100 kg of concentrate;

0.5—the degree of transition of sulfur to slag.

22. Will turn sulfur into gases

$0.90 \cdot 0.49 = 0.441$ kg,

where 0.49 is the degree of transition of sulfur to the gas phase.

23. Goes to Al_2O_3 slag from quartzite

$12.12 \cdot 2.0/100 = 0.2424$ kg,

where 12.12—the amount of added quartzite;

2.0— Al_2O_3 content in quartzite.

24. Contains carbon in 100 kg of concentrate and will transfer in the form of CO_2 to gas phase during the decomposition of carbonates of concentrate

$26.2 \cdot 12/44 = 7.145$ kg,

where 26.2 is the CO_2 content in 100 kg of concentrate;

12—atomic mass of carbon;

44 is the molecular weight of CO_2 .

25. Carbon will be required to recover oxides of Mn, Fe and P from coke breeze ash per 100 kg of coke breeze:

MnO: $(13.44 \cdot 0.17/100) \cdot 0.9 \cdot 12/55 = 0.004$ kg,

where 13.44—the amount of ash in 100 kg of coke breeze;

0.17—the manganese content in coke ash;

0.9—the degree of transition of manganese into metal and into the gas phase;

12—atomic mass of carbon;

55—atomic mass of manganese;

Fe_2O_3 : $(13.44 \cdot 10.04/100) \cdot 0.95 \cdot 36/160 = 0.288$ kg,

where 10.04 is the content of Fe_2O_3 in coke breeze ash;

0.95—the degree of transition of iron into metal;

36—molecular weight of carbon;

160—molecular weight of Fe_2O_3 ;

$$P_2O_5: (13.44 \cdot 0.347/100) \cdot 0.95 \cdot 60/82 = 0.032 \text{ kg,}$$

where 0.347 is the phosphorus content in the coke breeze ash;

0.95—the degree of transition of phosphorus into metal and into the gas phase;

60—molecular weight of carbon;

82 is the molecular weight of phosphorus in P_2O_5 .

26. In total, carbon will be required for the reduction of ash oxides in 100 kg of coke breeze
 $0.004 + 0.288 + 0.032 = 0.324 \text{ kg}$
27. Remains active carbon in 100 kg of coke breeze
 $83.77 - 0.324 = 83.446 \text{ kg,}$
 where 83.77 is the amount of carbon in 100 kg of coke breeze.
28. Coke breeze will be needed
 $10.86100/83.446 = 13.014 \text{ kg,}$
 where 10.86 is the amount of carbon required for the reduction of the oxides of Mn, Fe, Si and P ore part of the charge (concentrate + quartzite) and for carburization of metal.
29. Based on factory practice, in connection with carbon fumes of coke on the top according to the reaction $C + CO_2 = 2CO$ when interacting with CO_2 formed during the decomposition of manganese carbonate, and by the reaction $C + \frac{1}{2}O_2 = CO$ when interacting with oxygen formed during the dissociation of higher manganese oxides, increase the sample weight of coke breeze by ~15%
 $13.014 \cdot 1.15 = 14.966 \text{ kg.}$
30. The required amount of coke breeze contains carbon
 $14.966 \cdot 83.77/100 = 12.537 \text{ kg,}$
 where 83.77 is the carbon content in coke.
31. The required amount of coke breeze contains ash
 $14.966 \cdot 13.014/100 = 1.948 \text{ kg}$
 where 13.014 is the ash content in coke breeze.
32. Sulfur will pass from metal to metal
 $(14.966 \cdot 0.52/100) \cdot 0.01 = 0.0008 \text{ kg,}$
 where 0.52—sulfur content in coke breeze;
 0.01—the degree of transition of sulfur to metal.
33. Sulfur will pass from coke breeze to slag $(14.966 \cdot 0.52/100) \cdot 0.5 = 0.0389 \text{ kg,}$
 where 0.5 is the degree of transition of sulfur to slag.
34. Sulfur will evaporate from coke breeze
 $(14.966 \cdot 0.49/100) \cdot 0.49 = 0.0381 \text{ kg,}$
 where 0.49 is the degree of transition of sulfur to the gas phase.
35. Coke breeze will make volatiles
 $14.966 \cdot 1.27/100 = 0.190 \text{ kg,}$
 where 1.27 is the volatile content in coke breeze.
36. Coke breeze will bring moisture
 $14.966 \cdot 1.0/100 = 0.150 \text{ kg,}$
 where 1.0 is the moisture content in coke breeze.

37. From coke breeze ash will go into metal:
 Mn: $(1.948 \cdot 0.17/100) \cdot 0.8 = 0.0026$ kg,
 where 1.948 is the ash content in the required amount of coke breeze;
 0.17—the manganese content in coke breeze ash;
 0.8—the degree of transition of manganese into metal;
 Fe: $(1.948 \cdot 10.04/100) \cdot 0.95 \cdot 112/160 = 0.130$ kg,
 where 10.04 is the content of Fe_2O_3 in coke breeze ash;
 0.95—the degree of transition of iron into metal;
 112—molecular weight of iron in Fe_2O_3 ;
 160—molecular weight of Fe_2O_3 ;
 P: $(1.948 \cdot 0.347/100) \cdot 0.85 = 0.0057$ kg,
 where 0.347 is the phosphorus content in the coke ash;
 0.85—the degree of transition of phosphorus to metal.
38. From coke breeze ash will go to slag:
 MnO: $(1.948 \cdot 0.17/100) \cdot 0.1 \cdot 71/55 = 0.0004$ kg,
 where 0.17 is the manganese content in coke breeze ash;
 0.1—the degree of transition of manganese to slag;
 71—molecular weight of MnO;
 55—atomic mass of manganese;
 FeO: $(1.948 \cdot 10.04/100) \cdot 0.05 \cdot 144/160 = 0.0088$ kg,
 where 10.04 is the content of Fe_2O_3 in coke breeze ash;
 0.05—the degree of transition of iron to slag;
 144—molecular weight of FeO in Fe_2O_3 ;
 160—molecular weight of Fe_2O_3 ;
 SiO₂: $(1.948 \cdot 51.4/100) = 1.001$ kg,
 where 51.4 is the SiO₂ content in coke breeze ash;
 P₂O₅: $(1.948 \cdot 0.347/100) \cdot 0.05 \cdot 142/62 = 0.0008$ kg,
 where 0.347 is the phosphorus content in the coke breeze ash;
 0.05—the degree of transition of phosphorus to slag;
 142—molecular weight P₂O₅;
 62—molecular weight of phosphorus in P₂O₅;
 CaO: $(1.948 \cdot 4.0/100) = 0.078$ kg,
 where 4.0 is the CaO content in coke breeze ash;
 Al₂O₃: $(1.948 \cdot 27.9/100) = 0.543$ kg,
 where 27.9 is the Al₂O₃ content in coke breeze ash;
 MgO: $(1.948 \cdot 5/100) = 0.049$ kg,
 where 2.5 is the MgO content in coke breeze ash.
39. From the coke breeze ash will disappear:
 Mn: $(1.948 \cdot 0.17/100) \cdot 0.10 = 0.0003$ kg,
 where 0.17 is the manganese content in coke breeze ash;
 0.10—the degree of transition of manganese into the gas phase;
 P: $(1.948 \cdot 0.347/100) \cdot 0.10 = 0.0007$ kg,
 where 0.347 is the phosphorus content in the coke breeze ash;
 0.10—the degree of transition of phosphorus to slag.

Table B.5 Amount and composition of metal

Element	From concentrate and quartzite, kg	From coke breeze, kg	From coke breeze ash, kg	Total	
				kg	%
Mn	20.16	–	0.0026	20.1626	69.43
Si	4.896	–	0.130	4.896	16.86
Fe	3.132	–	–	3.262	11.24
C	–	0.576	0.0057	0.576	1.98
P	0.1275	–	–	0.1332	0.46
S	0.009	0.0008	–	0.0098	0.03
Total				29.0396	100.00

Table B.6 Amount and composition of slag

Component	From concentrate and quartzite, kg	From coke breeze, kg	From coke breeze ash, kg	Total	
				kg	%
MnO	3.2531	–	0.0004	3.2535	8.17
FeO	0.2121	–	0.0088	0.2209	0.55
SiO ₂	14.709	–	1.001	15.710	39.47
CaO	14.950	–	0.078	15.028	37.76
Al ₂ O ₃	1.6424	–	0.543	2.1854	5.49
MgO	2.8500	–	0.049	2.899	7.28
P ₂ O ₅	0.0172	–	0.0008	0.0180	0.05
S	0.4500	0.0389	–	0.4889	1.23
Total				39.8037	100.00

40. Carbon will pass in the form of CO into the gas phase from the reduction of oxides of coke breeze
 $13.014 \cdot 0.324/100 = 0.042$ kg,
 where 13.014 is the amount of coke breeze needed for the reduction of oxides of Mn, Fe and P of the ore part of the charge (concentrate + quartzite) and for carburizing the metal;
 0.324—the amount of carbon required for the reduction of oxides of Mn, Fe and P ash in 100 kg of coke breeze.
41. Carbon will pass in the form of CO into the gas phase from the combustion of coke on the top
 $(13.014 \cdot 0.15) \cdot 83.77/100 = 1.635$ kg,
 where $(13.014 \cdot 0.15)$ —the amount of coke breeze burned at the top;
 83.77—carbon content in coke breeze (Tables B.5 and B.6).

Slag ratio— $39.8046/29.0396 = 1.37$

Slag basicity— $15.028/15.710 = 0.96$

Obtained standard composition ferrosiliconmanganese grade MnC17.

Table B.7 Manganese material balance

Incoming			Consumption		
Received	kg	%	Obtained	kg	%
Concentrate	25.200	99.986	Metal	20.1626	80.00
Coke breeze ash	0.0033	0.014	Slag	2.5203	10.00
			Volatized and lost	2.5204	10.00
Total	25.2033	100	Total	25.2033	100

Table B.8 Iron material balance

Incoming			Consumption		
Received	kg	%	Obtained	kg	%
Concentrate	3.2970	95.84	Metal	3.2620	95.00
Coke breeze ash	0.1368	4.16	Slag	0.1718	5.00
Total	3.4338	100	Total	3.4338	100

Table B.9 Carbon material balance

Incoming			Consumption		
Received	kg	%	Obtained	kg	%
Coke breeze	12.537	63.70	Metal	0.576	2.93
Concentrate	7.145	36.30	CO from concentrate oxide reduction	10.284	52.25
			CO from reduction of oxides of coke breeze ash	0.042	0.21
			CO from the combustion of coke breeze on the top	1.635	8.31
			CO ₂ from the decomposition of concentrate	7.145	36.30
Total	19.682	100.00	Total	19.682	100.00

The composition of the charge:

concentrate—100 kg;
 coke—14.966 kg;
 quartzite—12.12.

Consumption of materials per 1 t of high-carbon ferromanganese:

concentrate—3443.6 kg;
 coke—515.4 kg;
 quartzite—417.4 kg (Tables B.7, B.8, B.9, B.10, B.11 and B.12.).

Table B.10 Silicon material balance

Incoming			Consumption		
Received	kg	%	Obtained	kg	%
Concentrate	6.216	50.75	Metal	4.8960	39.98
Quartzite	5.544	45.27	Slag	7.3313	60.02
Coke breeze ash	0.4673	3.98			
Total	12.2273	100	Total	12.2273	100

Table B.11 Phosphorus material balance

Incoming			Consumption		
Received	kg	%	Obtained	kg	%
Concentrate	0.150	95.54	Metal	0.1332	85.03
Coke breeze ash	0.0067	4.46	Slag	0.0078	4.97
			Volatized	0.0157	10.00
Total	0.1567	100	Total	0.1567	100

Table B.12 Sulfur material balance

Incoming			Consumption		
Received	kg	%	Obtained	kg	%
Concentrate	0.80	92.38	Metal	0.0098	1.00
Coke breeze ash	0.0778	7.62	Slag	0.4889	50.00
			Volatized	0.4791	49.00
Total	0.8778	100	Total	0.8778	100

Appendix C

The Charge Calculation for Smelting High-Carbon Ferrochromium

1. Initial Data

Chemical composition

Material	A ^c	V (LOI)	W	S	C _s	SiO ₂	Al ₂ O ₃	FeO/Fe ₂ O ₃	CaO	MgO	P ₂ O ₅	Cr ₂ O ₃	∑
Chromium ore 1		2.79	0	0.024	-	12	7.7	10.7	0.3	21.3	0.006	45	99.820
Chromium ore 2		0	0	0	0	0	0	0	0	0	0	0	0.000
Chromium ore total	-	2.790		0.024	0.000	12.000	7.700	10.700	0.300	21.300	0.006	45.000	99.820
Coal	1	1	1	1	1	1	1	1	1	1	1	1	7.000
Coke	9.88	7.77	5	31	51.35	49.5	22.8	17.9	5.38	3.48	0.94	0	100.000
Quartzite		0.29	0	0.02	0	97.9	0.89	0.63	0.21	0.04	0.02	0	100.000

Distribution of elements

Smelting products	Elements				
	Si	Cr	Fe	S	P
Alloy	5	94	97	10	80
Slag	95	6	3	30	10
Loss	0	0	0	60	10

Electrode mass consumption	0.85	
Ratio Cr/Fe	3.70	
Carbon excess ratio K_{ex}	1.1	
The share of coal in the reduced mixture by carbon	0	
SiO ₂ content in slag	30	
Ore ratio 1:2	1	0
Carbon in metal, %	8.3	

2. Charge calculation

Carbon needed to reduce 100 kg of ore

Reaction	C, kg
SiO ₂ → Si	0.240
Cr ₂ O ₃ → Cr	10.018
FeO → 2Fe	1.730
P ₂ O ₅ → 2P	0.002
Total	11.991
With K_{ex}	13.190

Carbon needed to reduce ash of 100 kg of coke

Reaction	C, kg
SiO ₂ → Si	0.098
Cr ₂ O ₃ → Cr	0.000a coke ash
Fe ₂ O ₃ → 2Fe	0.386
P ₂ O ₅ → 2P	0.035
Total	0.519
With K_{ex}	0.571

Carbon needed to reduce ash of 100 kg of coal

Reaction	C, kg
SiO ₂ → Si	0.000
Cr ₂ O ₃ → Cr	0.002
Fe ₂ O ₃ → 2Fe	0.002
P ₂ O ₅ → 2P	0.004
Total	0.008
With <i>K_{ex}</i>	0.009

Given the carburization of the metal, carbon is needed	15.716		
Coke contains active carbon, kg	50.779	Coal contains active carbon, kg	0.991
It is necessary to add per 100 kg of concentrate	30.949	kg dry coke and 0.000 kg of dry coal	
It is necessary to add per 100 kg of concentrate	32.578 kg coke and 0.000 kg coal		
From concentrate and ash of coal and coke are formed	49.032 kg of slag, which contains 26.18% SiO ₂		
To refine the slag in SiO ₂ to	30.0%	Is required	2.731 kg of quartzite

3. Amount and composition of slag

Element	Source				Total	
	Chr. ore	Quartzite	Coal	Coke	kg	%
SiO ₂	11.400	2.674	0.000	1.438	15.512	29.971
Al ₂ O ₃	7.700	0.024	0.000	0.697	8.421	16.272
Fe ₂ O ₃	0.321	0.017	0.000	0.016	0.355	0.685
CaO	0.300	0.006	0.000	0.165	0.470	0.909
MgO	21.300	0.001	0.000	0.106	21.408	41.363
Cr ₂ O ₃	2.700	0.000	0.000	0.000	2.700	5.217
S	0.007	0.001	0.000	2.878	2.886	5.576
P ₂ O ₅	0.001	0.001	0.000	0.003	0.004	0.008
Total	43.729	2.723	0.000	5.304	51.756	100.000

4. Amount and composition of metal

Element	Source			Total	
	Chr. ore	Coal	Coke	kg	%
Si	0.280	0.000	0.035	0.315	0.750
Fe	8.073	0.000	0.372	8.444	20.081
Cr	28.942	0.000	0.000	28.942	68.825
S	0.002	0.000	0.959	0.962	2.287
P	0.002	0.000	0.010	0.012	0.029
C	0.850	0.000	2.526	3.376	8.028
Total	38.149	0.000	3.902	42.052	100.000

Slag ratio: 1.231

5. Amount of gas, dust and loss

Element	Source				Total	
	Chr. ore	Quartzite	Coal	Coke	kg	%
Cr	0.000	0.000	0.000	0.000	0.000	0.000
P	0.000	0.000	0.000	0.001	0.002	0.004
S	0.014	0.000	0.000	5.757	5.771	13.684
V (LOI)	2.790	0.008	0.000	2.405	5.203	12.337
W	0.000	0.000	0.000	1.629	1.629	3.863
CO + O ₂	15.987	0.000	0.000	13.581	29.568	70.113
Total	18.792	0.008	0.000	23.372	42.172	100.000

6. Charge composition

Charge composition	400	900	1000
Chr. ore	400.00	900.00	1000.00
Coke	130.31	293.20	325.78
Coal	0.00	0.00	0.00
Quartzite	10.93	24.58	27.31
Metal yield	168.21	378.46	420.52
Slag yield	207.02	465.80	517.56

7. Material balance

Set		Obtained	
Chr. ore	100.000	Metal	42.052
Coke	32.578	Slag	51.756
Coal	0.000	Gas and loss	42.172
Quartzite	2.731		
Electrodes	0.850	Residual	0.180
Total	136.159	Total	136.159

8. Specific consumption of materials, kg/t of chromium

Chr. ore	3455.2
Coal	0.0
Coke	1125.6
Quartzite	94.4

Calculation of the heat balance for smelting high-carbon ferrochromium

1. Initial data

Metal temperature at the outlet, C	1760	Solid metal enthalpy	1150 kJ/kg	The heat content of basic oxides	
Slag temperature at the outlet, C	1830	Heat of fusion	336.5 kJ/kg	Al ₂ O ₃	326.91 kJ/mol
Flue gas temperature, C	450	Heat capacity of liquid metal	0.767 kJ/kg K	SiO ₂	125.21 kJ/mol
Thermal efficiency	0.875	Metal melting point	1660 °C	MgO	141.71 kJ/mol
Electrical efficiency	0.900			Cr ₂ O ₃	317.09 kJ/mol

2. Heat input

	kJ	kW/t	%
<i>2.1 Heat of exothermic reactions</i>	43,800	289	7.9
Carbon oxidation, C + 1/2O ₂ = CO	11,195		
Metal formation	17,519		
Fe + Si = FeSi	830		

(continued)

(continued)

	kJ	kW/t	%
$7\text{Cr} + 3\text{C} = \text{Cr}_7\text{C}_3$	16,689		
Slag formation	15,085		
$\text{MgO} + \text{Al}_2\text{O}_3 = \text{MgO}\cdot\text{Al}_2\text{O}_3$	1950		
$2\text{MgO} + \text{SiO}_2 = 2\text{MgO}\cdot\text{SiO}_2$	13,135		
<i>2.2 Electric power</i>	512,512	3385	92.1
Total	556,312	3675	100.0

3. Heat consumption

	kJ	kW	%
<i>3.1. Heat content of metal at the outlet</i>	65,735	434	11.8
<i>3.2. Heat content of slag at the outlet</i>	140,837	930	25.3
<i>3.3. Heat content of gases at the outlet</i>	18,919	125	3.4
<i>3.4. Heat of endothermic reactions</i>	261,282	1726	47.0
$\text{Cr}_2\text{O}_3 + 3\text{C} = 2\text{Cr} + 3\text{CO}$	225,348		
$\text{FeO} + \text{C} = \text{Fe} + \text{CO}$	22,332		
$\text{Fe}_2\text{O}_3 + 3\text{C} = 2\text{Fe} + 3\text{CO}$	1628		
$\text{SiO}_2 + 2\text{C} = \text{Si} + 2\text{CO}$	7776		
$\text{P}_2\text{O}_5 + 5\text{C} = 2\text{P} + 5\text{CO}$	215		
$\text{H}_2\text{O}_l = \text{H}_2\text{O}_g$	3983		
<i>3.5. Heat loss</i>	69,539	459	12.5
Total	556,312	3675	100.0

		Liquid	Commodity
Specific power consumption	kWh/t	3762	4702
	kWh/Cr	5465	6832

Recommended Bibliography

1. Baratashvili IB (1987) Theoretical foundations of dephosphorization and desulfurization of manganese and alloys based on it. Mitsniereba, Tbilisi, 158 p (in Russian)
2. Bizhanov A, Chizhikova V (2020) Agglomeration in metallurgy. Springer, Berlin 454 p
3. Bizhanov AM, Kurunov IF (2017) Extrusion briquettes (brex)—new stage in the agglomeration of raw materials for ferrous metallurgy. Metallurgizdat, Moscow, 234 p (in Russian)
4. Bizhanov AM, Zagainov SA (2020) Briquetting technologies in ferrous metallurgy. Infra-Engineering, Moscow Vologda, 256 p (in Russian)
5. Bobkova OS (1981) Silicothermal reduction of metals. Metallurgy, Moscow, 240 p (in Russian)
6. Cazenat EK, Chizhikov DM (1976) Steam pressure and composition over oxides of chemical elements. Science, Moscow, 342 p (in Russian)
7. Chernobrovin VP, Pashkov IYu, Mikhayliv GG et al (2004) Theoretical foundations of the processes of production of carbon ferrochromium from the Ural ores. Ed. SUSU, Chelyabinsk, 346 p (in Russian)
8. Chernobrovin VP, Mizin VG, Sirina TP, Dashevskii VYa (2009) Complex processing of carbonate manganese raw materials: chemistry and technology. Ed. Center of SUSU, Chelyabinsk, 294 p (in Russian)
9. Collection of scientific papers of the International Research Conference “Actual Problems and Prospects of Electrometallurgical Production: Theory and Technology, Efficiency of the Use of Mineral Resources, Ecology, Economic Aspects of the Development of Internal and Foreign Markets”, dedicated to the 100th anniversary NMetAU (DMetI) and the 75th anniversary of the Department of Electrometallurgy (1999) GNPP “System Technologies”, Dnepropetrovsk, 448 p
10. Current problems of metallurgy (2001) T. 2. Electrothermal production of ferroalloys and non-ferrous metals at the junction of the 20th and 21st centuries: results, problems, development prospects. Materials of the International Scientific and Practical Conference dedicated to the 35th anniversary of OAO NZF and the 70th anniversary of the Hero of Socialist Labor BF Velichko. GNPP “System Technologies”, Dnepropetrovsk, 303 p (in Russian)
11. Dashevskii VYa, Polulyakh LA, Travyanov AYa (2018) Phosphorus in the smelting of manganese-containing ferroalloys. Publishing house of NUST “MISiS”, Moscow, 96 p (in Russian)
12. Dashevskii VYa, Travyanov AYa, Polulyakh LA (2018) Modern methods and equipment of metallurgy and materials science. Phosphorus in the smelting of manganese-containing ferroalloys Publishing house of NUST “MISiS”, 98 p (in Russian)
13. Dashevskii VYa (2011) Physico-chemical base of the deoxidation of the ferronickel smelts. Fizmatlitz, Moscow (in Russian)

14. Durrer R, Volkert G (1976) Metallurgy of ferroalloys. Metallurgy, Moscow, 480 p
15. Earnaukhov VN, Voronov VI, Zaiko VP, Zhuchkov VI (2001) Technology of low-carbon ferrochromium. NISO UB RAS, Yekaterinburg, 481 p (in Russian)
16. Edge NI, Onishchin BP, Meisel EI (1971) Electromelting of nickel oxide ores. Metallurgy, Moscow, 248 p (in Russian)
17. Efimenko GG, Gimmelfarb AA, Levchenko VE (1981) Cast iron metallurgy. Vishcha shkola, Kyiv, 496 p (in Russian)
18. Elyutin VP, Pavlov YuA, Levin BE, Alekseev EM (1957) Production of ferroalloys. Meallurgizdat, Moscow, 436 p (in Russian)
19. Emlin BI, Gasik MI (1978) Handbook of electrothermal processes. Metallurgy, Moscow, 288 p (in Russian)
20. Ershov VA, Dantsis YaB, Zhilov GM (1978) Theoretical foundations of chemical electrothermy. Chemistry, Leningrad, 184 p (in Russian)
21. Ershov VA, Dantsis YaB, Reutovich LM (1978) Calcium carbide production. Chemistry, Leningrad, 184 p (in Russian)
22. Garmata VA, Petrunko AN, Galitsky NV et al (1983) Titanium. Metallurgy, Moscow, 559 p (in Russian)
23. Gasik MI, Ignatiev VS, Kablukovsky AF et al (1970) Gases and impurities in ferroalloys. Metallurgy, Moscow, 148 p (in Russian)
24. Gasik MI (1992) Manganese. Metallurgy, Moscow, 608 p (in Russian)
25. Gasik MI (1976) Self-baking electrodes of ore-smelting electric furnaces. Metallurgy, Moscow, 368 p (in Russian)
26. Gasik MI (1984) Electrodes of ore-smelting electric furnaces. Metallurgy, Moscow, 248 p (in Russian)
27. Gasik MI (1979) Electrothermics of manganese. Tekhnika, Kyiv, 167 p (in Russian)
28. Gasik MI, Emlin BI (1983) Electrometallurgy of ferroalloys (theory and technology). Vishcha shkola, Kyiv, 376 p (in Russian)
29. Gasik MI, Lyakishev NP (1999) Theory and technology of electrometallurgy of ferroalloys: Textbook for universities. JV Internet Engineering, Moscow, 764 p (in Russian)
30. Gasik MI, Gasik MM (2011) Electrothermics of silicon (physical chemistry and technology). NMetAU, Dnepro-Petrovsk, 487 p (in Russian)
31. Gasik MI, Ragulina RI, Lvova OK et al (1965) Production and operation of continuous self-baking electrodes and anodes. Metallurgy, Moscow, 254 p (in Russian)
32. Gasik MI, Emlin BI, Klimkovich NS, Khitrik SI (1971) Electric smelting of aluminosilicates. Metallurgy, Moscow, 304 p (in Russian)
33. Gasik LN, Ignatiev VS, Gasik MI (1975) The structure and quality of industrial ferroalloys and alloys. Technique, Kyiv, 142 p (in Russian)
34. Gasik MI, Gladkikh VA, Shifrin VM, Ignatiev VS (1987) Design of electroferroalloy workshops. Vishcha Shkola, Kyiv—Donetsk, 178 p (in Russian)
35. Gasik MI, Lyakishev NP, Emlin BI (1988) Theory and technology for the production of ferroalloys. Metallurgy, Moscow, 784 p (in Russian)
36. Gasik MI, Gantserovsky OG, Ovcharuk AN, Rogachev IP (2000) Ferroalloys of Ukraine—2000. GNPP “System Technologies”, Dnepropetrovsk, 385 p (in Russian)
37. Gavrilo VA, Gasik MI (2001) Manganese silicothermy. GNPP “System Technologies”, Dnepropetrovsk, 512 p (in Russian)
38. Gavrilo VA, Polyakov II, Polyakov OI (1996) Optimization of operating conditions of ferroalloy furnaces. Metallurgy, Moscow, 176 p (in Russian)
39. Geld PV, Baum BA, Petrushevsky MS (1973) Ferroalloy melts. Metallurgy, Moscow, 288 p (in Russian)
40. Gladkikh VA, Gasik MI, Ovcharuk AN et al. (2004) Design and equipment of electrofusion steelmaking and ferroalloy workshops. Dnepropetrovsk: Smstemnye technology. 2004.- 736 p (in Russian)
41. Gladkikh VA, Gasik MI, Ovcharuk VN, Proydak YuS (2007) Ferroalloy electric furnaces. System Technologies, Dnepropetrovsk, 259 p (in Russian)

42. Grigoryan VA, Belyanchikov LN, Stomakhin AYa (1979) Theoretical foundations of electric steelmaking processes. Metallurgy, Moscow, 256 p (in Russian)
43. Grinenko V, Polyakov OI, Gasik MI et al (2001) Chromium of Kazakhstan. Metallurgy, Moscow, 416 p (in Russian)
44. Gvelisiani GG, Baratashvili IB, Tsagareishvili DSh (1982) Thermodynamics of the interaction of manganese with phosphorus. Mitsniereba, Tbilisi, 116 p (in Russian)
45. Ignatiev VS, Medvedev IA (1978) Organization and planning of ferroalloy production. Metallurgy, Moscow, 284 p (in Russian)
46. Improving the production of ferrosilicon (1997) Collection of scientific papers of Kuznetsk Ferroalloys OJSC. Novokuznetsk, 400 p (in Russian)
47. Karimov AM (1978) Dust and gas emissions in the production of the main types of ferroalloys. Metallurgy, Moscow, 284 p (in Russian)
48. Kormilitsin SP, Tsemekhman LSh, Afanasyev SG (1976) Ferronikel refining and enrichment. Metallurgy, Moscow, 240 p (in Russian)
49. Kozhevnikov GN, Zayko VP (1980) Electrotherm of chromium alloys. Science, Moscow, 187 p (in Russian)
50. Kozhevnikov GN, Zayko VP, Ryss MA (1978) Electrothermal ligatures of alkaline earth metals with silicon. Nauka, Moscow, 224 p (in Russian)
51. Kubashevsky O (1976) State diagrams of binary systems based on iron. Directory. Metallurgy, Moscow, 184 p (in Russian)
52. Kulikov IS (1975) Deoxidation of metals. Metallurgy, Moscow, 504 p (in Russian)
53. Kurunov I, Bizhanov A (2017) Stiff extrusion briquetting in metallurgy. Springer, Berlin 169 p
54. Kutuzov SV, Gasik MI, Urazlina OYu et al (2018) Scientific foundations and technologies for the production of thermoanthracite in tubular rotary kilns and electric calcinators. ChMP "Economics", Dnepropetrovsk, 468 p (in Russian)
55. Kutuzov SV, Derkach VV, Gasik MI et al (2020) Scientific basis for the production of electrode mass and the formation of continuous self-baking electrodes of ore-smelting electric furnaces. ChMP "Economics", Dnepropetrovsk, 654 p (in Russian)
56. Leontyev LI, Vatolin NA, Shavrin SV, Shumakov N (1997) Pyrometallurgical processing of complex ores. Metallurgy, Moscow, 432 p (in Russian)
57. Linchovsky BV (1986) Thermodynamics and kinetics of the interaction of gases with liquid metals. Metallurgy, Moscow, 222 p (in Russian)
58. Lyakishev NP (ed) (1996) State diagrams of double metal systems. Mechanical Engineering, Moscow. Pastukhov EA, Vatolin NA, Lisin VL et al (2003) Diffraction studies of high-temperature melts. Ural Branch of the Russian Academy of Sciences, Yekaterinburg, 353 p (in Russian)
59. Lyakishev NP, Gasik MI (1999) Metallurgy of chromium. ELIZ, Moscow, 382 p (in Russian)
60. Lyakishev NP, Gasik MI (2005) Physicochemistry and technology of ferroalloys. ELIZ, Moscow, 448 p (in Russian)
61. Lyakishev NP, Pliner YuL, Rubinstein EA (1971) Niobium in the steel industry. Metallurgy, Moscow, 216 p (in Russian)
62. Lyakishev NP, Pliner YuL, Ignatenko GF, Lappo SI (1978) Aluminothermy. Metallurgy, Moscow, 424 p (in Russian)
63. Lyakishev NP, Tulin NA, Pliner YuL, Rubin-Matte EA (1981a) Alloying alloys and steels with niobium. Metallurgy, Moscow, 192 p (in Russian)
64. Lyakishev NP, Tulin NA, Pliner YuL (1981b) Alloying alloys and steels with niobium. Metallurgy, Moscow, 192 p (in Russian)
65. Lyakishev NP, Slotvinsky-Sidak NP, Glider YuL, Lappo SI (1983) Vanadium in the steel industry. Metallurgy, Moscow, 192 p (in Russian)
66. Lyakishev NP, Glider YuL, Lappo SI (1986) Boron containing steels and alloys. Metallurgy, Moscow, 192 p (in Russian)
67. Lyakishev NP, Gasik MI, Dashevskii VYa (2006a) Metallurgy of ferro-alloys. Part 1. Ucheba, Moscow (in Russian)

68. Lyakishev NP, Gasik MI, Dashevskii VYa (2006b) Metallurgy of ferro-alloys. Part 2. Ucheba, Moscow (in Russian)
69. Lyakishev NP, Gasik MI, Dashevskii VYa (2006c) Metallurgy of ferro-alloys. Part 3. Ucheba, Moscow (in Russian)
70. Misin VG, Rabinovich EM, Sirina TP et al (2005) Integrated processing of vanadium raw materials: chemistry and technology. NISO Ural Branch of RAS, Yekaterinburg, 416 p (in Russian)
71. Mizin VG, Serov GV (1979) Carbon reducing agents for ferroalloys. Metallurgy, Moscow, 232 p (in Russian)
72. Mizin VG, Chirkov NA et al (1992) Ferroalloys. Metallurgy, Moscow, 415 p (in Russian)
73. Monastyrsky AV, Aleksandrov AV (1979) Furnaces for the production of lime: reference. Metallurgy, Moscow, 232 p (in Russian)
74. Ostriuk PN, Gasik MI, Pirog VD (1992) Metallurgy of sponge and powder ligatures. Technique, Kyiv, 128 p (in Russian)
75. Physical chemistry and technology in metallurgy (1996). Sat scientific works, dedicated. 70th anniversary of the academician of the Russian Academy of Sciences Vatolin N.A. Ekaterinburg. UrB RAS, 306 p (in Russian)
76. Popel SI, Nikitin YuP, Barmin LA et al (1975) Interaction of molten metal with gas and slag. UPI, Sverdlovsk, 200 p (in Russian)
77. Popel SI, Sotnikov AI, Boranenko VN (1986) Theory of metallurgical processes. Metallurgy, Moscow, 455 p (in Russian)
78. Porada AN, Gasik MI (1986) Electrotherm of inorganic materials. Metallurgy, Moscow, 232 p (in Russian)
79. Povolotsky DYa, Roshchin VE, Ryss MA et al (1984) Electrometallurgy of steel and ferroalloys. Metallurgy, Moscow, 568 p (in Russian)
80. Povolotsky DYa, Roshchin VE, Malkov NV (1995) Electrometallurgy of steel and ferroalloys. Metallurgy, Moscow, 592 p (in Russian)
81. Prikhodko EV (1983) Metallochemistry of complex alloying. Metallurgy, Moscow, 184 p (in Russian)
82. Rabinovich EM, Mizin VG, Rabinovich ME et al (2005) Complex processing of vanadium raw materials: metallurgy. NISO Ural Branch of RAS, Yekaterinburg, 251 p (in Russian)
83. Ragulina RI, Emlin BI (1972) Electrotherm of silicon and silumin. Metallurgy, Moscow, 240 p (in Russian)
84. Rostovtsev ST, Gasik MI (eds) (1977) Recovery processes in the production of ferroalloys. Science, Moscow, 244 p (in Russian)
85. Rutman DS, Toropov YuS, Pliner AL et al (1985) Highly refractory materials from zirconia. Metallurgy, Moscow, 136 p (in Russian)
86. Ryss MA (1985) Ferroalloy production. Metallurgy, Moscow, 344 p
87. Seasonenko ON, Gasik MI, Polyakov OI (2011) Electrothermal metallic manganese. NMetAU, Dnepropetrovsk, 160 p (in Russian)
88. Sinyayev GB, Vatolin NA, Trusov BG, Moiseev GK (1982) The use of computers for thermodynamic calculations of metallurgical processes. Nauka, Moscow, 232 p (in Russian)
89. Ryabchikov IV, Mizin VG, Lyakishev NP, Dubrovin AS (1983) Ferroalloys with rare and alkaline earth metals. Metallurgy, Moscow, 272 p (in Russian)
90. Schedrovitsky LS (1975) Ferroalloy production in closed furnaces. Metallurgy, Moscow, 312 p (in Russian)
91. Shevchenko VF (1997) Improving workshops and equipment for ferroalloy production. Metallurgy, Moscow-Kharkov, 470 p (in Russian)
92. Snitko YuP (2000) Production of ferrosilicon. Directory. Doctor of Technical Sciences. Novokuznetsk, 426 p (in Russian)
93. Sokolov IP, Ponomarev IP, Ponomarev NL (1990) Introduction to metallurgy: a training manual for students of metallurgical and chemical-technological universities. Metallurgy, Moscow, 134 p (in Russian)

94. Svenchansky AD, Zherdev I, Kruchinin AM (1981) Electric industrial furnaces. Arc furnaces and special heating installations. Energoizdat, Moscow, 296 p (in Russian)
95. Tolstoguzov NV (1992) Theoretical foundations and technology for melting silicon and manganese alloys. Metallurgy, Moscow, 238 p (in Russian)
96. Tsvetkov YuV, Panfilov SA (1980) Low-temperature plasma in the recovery process. Science, Moscow, 360 p (in Russian)
97. Vanyukov AV et al (1993) Theory of pyrometallurgical processes. Metallurgy, Moscow, 184 p (in Russian)
98. Vaughan D, Craig J (1981) Chemistry of sulfide minerals. MIR, Moscow, 576 p (in Russian)
99. Velichko BF, Gavrilov VA, Gasik MI et al (1996) Metallurgy of manganese of Ukraine. "Technics", Kyiv, 472 p (in Russian)
100. Vertiy IG, Rozhdestvenskaya TL, Mikhailov GG et al (1994) Ferroalloys, slag, refractories: atlas of microstructures, diffraction characteristics. Metals, Chelyabinsk, 112 p (in Russian)
101. Voronov YuL, Zayko VP, Zhuchkov VI (2000) Technology of molybdenum-containing ferroalloys. Ural Branch of the Russian Academy of Sciences, Ekaterinburg, 267 p (in Russian)
102. Voronov VI, Zayko VP, Zhuchkov VI (2008) Technology of molybdenum-containing ferroalloys. NISO UB RAS, Yekaterinburg, 443 p (in Russian)
103. Utkov VA (1977) Highly basic sinter. Metallurgy, Moscow, 156 p (in Russian)
104. Yakushevich NF, Gayevsky GV (1999) The interaction of carbon with oxides of calcium, silicon and aluminum. Publishing Center, SibGIU, Novokuznetsk, 250 p (in Russian)
105. Yusfin YuS, Gimmelfarb AA, Pashkov NF (1991) New processes for the production of metals (iron metallurgy). Metallurgy, Moscow, 320 p (in Russian)
106. Zaiko VP, Zhuchkov VI, Leontyev LI et al (2004) Technology of vanadium-containing ferroalloys. "Academic Book", Moscow, 515 p (in Russian)
107. Zaiko VP, Zhuchkov VI, Drobyshevsky PA et al (2005) Technology of tungsten-containing ferroalloys. NISO UB RAS, Yekaterinburg, 557 p (in Russian)
108. Zelikman AN (1970) Molybdenum. Metallurgy, Moscow, 320 p (in Russian)
109. Zelikman AN (1986) Metallurgy of refractory and rare metals. Metallurgy, Moscow, 440 p (in Russian)
110. Zhuchkov VI, Smirnov LA, Zayko VP, Voronov VI (2007) Technology of manganese ferroalloys. Part 1. NISO UB RAS, Yekaterinburg, 415 p (in Russian)
111. Zhuchkov VI, Smirnov LA, Zayko VP, Voronov VI (2008) Technology of manganese ferroalloys. Part 2. NISO UB RAS, Yekaterinburg, 443 p (in Russian)
112. Zubilin IG, Rudyka VI, Pinchuk SI (2001) Obtaining energy reducers from coal for basic industries. KNU named after V.N. Karazin. Publishing Center, Kharkov, 351 p (in Russian)
113. Zubov VL, Gasik MI (2002) Electrometallurgy ferrosilicon (physical chemistry and technology). GNPP "System Technologies", Dnepropetrovsk, 704 p (in Russian)